

USARTL-TR-77-54A

ADA 079631

ROTORCRAFT FLIGHT SIMULATION, COMPUTER PROGRAM C81
Volume I - Engineer's Manual

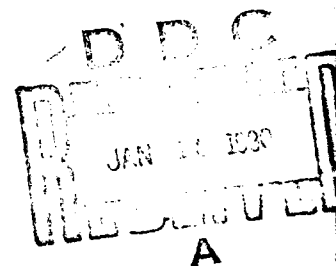
J. R. Van Gaasbeek, T. T. McLarty, S. G. Sadler
BELL HELICOPTER TEXTRON
P. O. Box 482
Fort Worth, Tex. 76101

October 1979

Final Report for Period November 1976 - August 1977

DDC FILE COPY

Approved for public release;
distribution unlimited.



Prepared for

APPLIED TECHNOLOGY LABORATORY
U. S. ARMY RESEARCH AND TECHNOLOGY LABORATORIES (AVRADCOM)
Fort Eustis, Va. 23604

80 1 21 056

APPLIED TECHNOLOGY LABORATORY POSITION STATEMENT

This report documents an engineering analysis and resulting computer programs for the evaluation of rotary-wing aircraft performance, handling qualities, rotor blade loads, maneuvering characteristics, and rotor system aeroelastic stability through application of the modal technique to the rotor blade equations of motion and stepwise integration of the time domain equations for the rotor, hub, aircraft and control system. The primary computer programs associated with the current effort are the Mykestad Program, for computing rotor blade natural frequencies and mode shapes; and the Rotorcraft Flight Simulation, Computer Program C81, for computing the wide variety of flight characteristics listed above.

The version of C81 developed under this contract is designated version AGAJ77. The immediately preceding version in the public domain is designated version AGAJ76. AGAJ77 differs from AGAJ76 in the following respects: an improved autopilot; more comprehensive elastic rotor analysis; an improved engine/governor model; an improved wake analysis; and enhanced output capabilities. While most of these improvements were successfully installed in the computer software, extensive difficulties were experienced in the implementation of the elastic rotor refinements. While the other improvements may make the AGAJ77 version preferable for many types of studies, AGAJ76 is recommended for the examination of rotor dynamics and loads. In using either program, some evaluation of the program's applicability to the problem under investigation through correlation with existing data is a judicious first step.

The Project Engineer for this contract was Mr. Edward E. Austin, Aeromechanics Technical Area, Aeronautical Technology Division.

DISCLAIMERS

The findings in this report are not to be construed as an official Department of the Army position unless so designated by other authorized documents.

When Government drawings, specifications, or other data are used for any purpose other than in connection with a definitely related Government procurement operation, the United States Government thereby incurs no responsibility nor any obligation whatsoever; and the fact that the Government may have formulated, furnished, or in any way supplied the said drawings, specifications, or other data is not to be regarded by implication or otherwise as in any manner licensing the holder or any other person or corporation, or conveying any rights or permission, to manufacture, use, or sell any patented invention that may in any way be related thereto.

Trade names cited in this report do not constitute an official endorsement or approval of the use of such commercial hardware or software.

DISPOSITION INSTRUCTIONS

Destroy this report when no longer needed. Do not return it to the originator.

UNCLASSIFIED

SECURITY CLASSIFICATION OF THIS PAGE (When Data Entered)

REPORT DOCUMENTATION PAGE		READ INSTRUCTIONS BEFORE COMPLETING FORM
1. REPORT NUMBER USARTL TR-77-54A	2. GOVT ACCESSION NO.	3. RECIPIENT'S CATALOG NUMBER (14) BH 77-699-099-062-VOL-1
4. TITLE (and Subtitle) (6) ROTORCRAFT FLIGHT SIMULATION, COMPUTER PROGRAM C81, Volume I, Engineer's Manual,	5. TYPE OF REPORT & PERIOD COVERED (9) Final Report, November 1976 - August 1977	6. PERFORMING ORG. REPORT NUMBER
7. AUTHOR(s) (10) JAMES R. Van Gaasbeek, T. T. McLarty, and S. G. Sadler	8. CONTRACT OR GRANT NUMBER(s) (15) DAAJ02-77-C-0003	
9. PERFORMING ORGANIZATION NAME AND ADDRESS Bell Helicopter Textron P. O. Box 482 Fort Worth, Texas 76101	10. PROGRAM ELEMENT, PROJECT, TASK AREA & WORK UNIT NUMBERS (16) 62209A 1L262209AH76 00 179 EK (12) pp	
11. CONTROLLING OFFICE NAME AND ADDRESS Applied Technology Laboratory, U.S. Army Research and Technology Laboratories (AVRADCOM) Fort Eustis, VA 23604	12. REPORT DATE (11) October 1979	
14. MONITORING AGENCY NAME & ADDRESS (if different from Controlling Office) (12) 392	13. NUMBER OF PAGES 390	
	15. SECURITY CLASS. (of this report) Unclassified	
	15a. DECLASSIFICATION/DOWNGRADING SCHEDULE	
16. DISTRIBUTION STATEMENT (of this Report) Approved for public release; distribution unlimited.		
17. DISTRIBUTION STATEMENT (of the abstract entered in Block 20, if different from Report)		
18. SUPPLEMENTARY NOTES Volume I of a three-volume report		
19. KEY WORDS (Continue on reverse side if necessary and identify by block number) Aerodynamics Flight Simulation Dynamics Aeroelasticity Helicopters Structural Properties Rotors Control Stability Computer Programs Numerical Analysis Wake Analysis Digital Computers Rotary Wing Aircraft		
20. ABSTRACT (Continue on reverse side if necessary and identify by block number) ★ This report consists of three volumes and documents the current version in the C81 family of rotorcraft flight simulation programs developed by Bell Helicopter Textron. This current version of the digital computer program is referred to as AGAJ77. The accompanying program for calculating fully coupled rotor blade mode shapes is called DNAM05, and the rotor wake program is called AR9102.		

DD FORM 1 JAN 73 1473

EDITION OF 1 NOV 65 IS OBSOLETE

UNCLASSIFIED

SECURITY CLASSIFICATION OF THIS PAGE (When Data Entered)

~~UNCLASSIFIED~~

SECURITY CLASSIFICATION OF THIS PAGE (When Data Entered)

20. Continued

The new or revised mathematical models or documentation incorporated into this report are listed below:

- (1) The maneuver autopilot was modified to accept four more time history commands (pitch, roll, yaw, and climb rates) in addition to the normal load factor. A digital filter is used to process the airframe response signal in order to reduce the b-per-rev component and to smooth the autopilot-generated control commands.
- (2) The effects of an offset pitch change axis have been incorporated in DNAM05 and C81.
- (3) A first-order lag has been introduced into the engine power available calculations.
- (4) The rotor-induced velocity distribution tables have been modified to be functions of advance ratio and wake-plane angle of attack. An average induced velocity table has been added to the analysis. In addition, the digital filter is used in the calculations to reduce the oscillation of the induced velocity experienced in previous versions of C81.
- (5) A rotor contour plot option has been added.
- (6) Time-history plots may now be made after time-variant trim.
- (7) The rotorcraft flightpath stability analysis (STAB) has been modified to output the numerators of more transfer functions.

The first volume, the Engineer's Manual, presents an overview of the computer program capabilities plus discussions for the background and development of the principal mathematical models in the program. The models discussed include all those currently in the program.

Volume II, the User's Manual, contains the detailed information necessary for setting up an input data deck and interpreting the computed data. Volume III, the Programmer's Manual, includes a catalog of subroutines and a discussion of programming considerations. The source tapes and related software for the computer programs documented in this report are unpublished data on file at the Applied Technology Laboratory, U. S. Army Research and Technology Laboratories (AVRADCOM), Fort Eustis, Virginia.

PREFACE

This report and its accompanying computer program were developed under Contract DAAJ02-77-C-0003 awarded in 1976 by the Eustis Directorate of the U. S. Army Air Mobility Research and Development Laboratory (USAAMRDL)*. This report supersedes all previous versions of the program and documentation, including USAAMRDL-TR-76-41A, B, C.

Technical program direction was provided by Mr. E. E. Austin of ATL. The principal Bell Helicopter personnel associated with the current contract were Messrs. J. R. Van Gaasbeek, T. T. McLarty, Dr. S. G. Sadler, and P. Y. Hsieh.

The American Helicopter Society granted permission to reprint Figure 4 from Reference 41. This article, "Flap-Lag Stability of Helicopter Rotor Blades in Forward Flight," by D. A. Peters, appeared in the JOURNAL OF THE AMERICAN HELICOPTER SOCIETY, Volume 20, Number 4, October, 1975.

14275 A
A-42 B

Approved For	
By	
Date	
Unrestricted	
Justified	
By	
Date	
Dis	
A	

*Redesignated Applied Technology Laboratory, U. S. Army Research and Technology Laboratories (AVRADCOM), effective 1 September 1977.

TABLE OF CONTENTS

	<u>Page</u>
PREFACE.....	3
LIST OF ILLUSTRATIONS.....	8
LIST OF TABLES.....	13
1.0 INTRODUCTION.....	14
1.1 BACKGROUND.....	14
1.2 DISCUSSION OF THE MOST RECENT ADDITIONS (1975-1976).....	16
1.3 DEVELOPMENT OF AGAJ77.....	17
1.4 DOCUMENTATION CONSIDERATIONS AND ORGANIZATION....	19
2.0 COMPUTER PROGRAM ORGANIZATION.....	20
2.1 MATHEMATICAL MODEL OF THE ROTORCRAFT.....	20
2.2 ROTOR ANALYSES.....	21
2.3 DETERMINATION OF THE EQUILIBRIUM FLIGHT CONDITION.....	22
2.4 FLIGHTPATH STABILITY ANALYSIS.....	23
2.5 MANEUVERS.....	24
2.6 PROGRAMMING CONSIDERATIONS.....	25
3.0 ROTOR SYSTEM MATHEMATICAL MODEL.....	26
3.1 INTRODUCTION.....	26
3.2 DYNAMICS.....	27
3.3 MODAL PYLON MODEL.....	100
3.4 AERODYNAMICS.....	112
4.0 FUSELAGE MATHEMATICAL MODEL.....	147
4.1 INTRODUCTION.....	147
4.2 DEVELOPMENT OF THE FUSELAGE MATHEMATICAL MODEL....	147
4.3 EXAMPLES OF THE FUSELAGE REPRESENTATION.....	172
4.4 AIDS TO DETERMINING THE INPUTS FOR THE FUSELAGE REPRESENTATION.....	172
5.0 AERODYNAMIC SURFACE MATHEMATICAL MODEL.....	180
5.1 INTRODUCTION.....	180
5.2 DEVELOPMENT OF THE MATHEMATICAL MODELS.....	180
5.3 EXAMPLES OF THE REPRESENTATION.....	189

TABLE OF CONTENTS - Continued

	<u>Page</u>
6.0 EXTERNAL STORES/AERODYNAMIC BRAKES MATHEMATICAL MODEL	192
6.1 GENERAL.....	192
6.2 DEVELOPMENT OF THE MATHEMATICAL MODELS.....	192
6.3 EXAMPLES OF THE STORE/BRAKE REPRESENTATION.....	198
7.0 AUXILIARY PROPULSION (JETS) MATHEMATICAL MODEL.....	213
8.0 CONTROL SYSTEM MATHEMATICAL MODEL.....	214
8.1 PRIMARY FLIGHT CONTROL SYSTEM REPRESENTATION....	214
8.2 AUTOMATIC FLIGHT CONTROLS.....	236
8.3 MANEUVER AUTOPILOT.....	240
9.0 ENGINE-GOVERNOR.....	250
9.1 CALCULATION OF MAXIMUM AVAILABLE HORSEPOWER.....	250
9.2 CALCULATION OF HORSEPOWER REQUIRED.....	252
9.3 DRIVE SYSTEM DYNAMIC EQUATIONS.....	252
10.0 TRIM PROCEDURE.....	254
10.1 GENERAL.....	254
10.2 DEFINITION OF TRIMMED FLIGHT CONDITION.....	259
10.3 METHODOLOGY OF THE TRIM PROCEDURE.....	261
10.4 ROTOR-ONLY TRIM PROCEDURE.....	270
11.0 ROTORCRAFT STABILITY ANALYSIS.....	272
11.1 INTRODUCTION.....	272
11.2 STABILITY ANALYSIS EQUATIONS.....	272
11.3 AUXILIARY EQUATIONS.....	275
11.4 INDEXED NOTATION.....	276
11.5 THE EIGENVALUE SOLUTION.....	279
11.6 EVALUATION OF THE PARTIAL DERIVATIVES.....	282
11.7 CONTROL POWER DERIVATIVES AND TRANSFER FUNCTIONS.....	291
11.8 THE OUTPUT.....	292
12.0 MANEUVER SIMULATION.....	293
12.1 INTRODUCTION.....	293
12.2 EVALUATION OF TECHNIQUES OF NUMERICAL INTEGRATION.....	294
12.3 CURRENT PROGRAM OPTIONS.....	301

TABLE OF CONTENTS - Concluded

	<u>Page</u>
13.0 COUPLED ROTOR STABILITY ANALYSIS.....	303
13.1 GENERAL.....	303
13.2 STUDY OF FLOQUET TECHNIQUE.....	304
13.3 THE MOVING BLOCK FAST FOURIER TRANSFORM.....	308
13.4 PRONY'S METHOD CURVE FIT.....	308
13.5 MANEUVER PERTURBATIONS.....	313
13.6 DEMONSTRATION OF ROTOR STABILITY ANALYSES.....	314
14.0 CONCLUSIONS AND RECOMMENDATIONS.....	328
15.0 REFERENCES.....	330
16.0 BIBLIOGRAPHY.....	334
APPENDIX A - ROTOR DIFFERENTIAL EQUATIONS.....	335
APPENDIX B - EULER ANGLE TRANSFORMATION.....	367
APPENDIX C - USE OF MANEUVER PERTURBATION OPTION IN C81...	370
LIST OF SYMBOLS.....	373

LIST OF ILLUSTRATIONS

<u>Figure</u>		<u>Page</u>
1	Typical Blade Element as Modeled in DNAM05.....	32
2	Inertia Transfer Functions for DNAM05.....	36
3	Local Deformed Blade Element System Stress Resultant and Elastic Axis Offset Notation.....	39
4	Local Blade Element Stress Resultants.....	41
5	Flexibility Transfer Functions for DNAM05.....	53
6	Pitch-Horn and Control System Model for DNAM05...	70
7	Schematic of Skewed Flapping Hinge Leading to Pitch-Flap Coupling.....	72
8	Kinematic Coupling through Skewed Hinges.....	73
9	Calculation of Coriolis Acceleration.....	81
10	Schematic Diagram of Flapping Spring and Stops...	84
11	Flapping Moment Functions for Spring and Stops...	84
12	Schematic of Lag Hinge with Spring and Damper....	87
13	Response of Four-Bladed Gimbale Rotor to Harmonic Forcing Functions.....	91
14	Guide for Selection of Blade Mode Types to Simulate Various Hub Types.....	93
15	Top View of Rotor Hub, Indicating Pylon Motion...	103
16	Flow Chart for Sequence of Calculations with Modal Pylon Equations.....	113
17	Flow Chart for Rotor Aerodynamic Logic.....	115
18	Flow Chart of Induced Velocity Calculations.....	119
19	Wake-Plane Angle of Attack and Flapping Angles...	123
20	Wake-Plane Phase Angle.....	124

LIST OF ILLUSTRATIONS - Continued

<u>Figure</u>		<u>Page</u>
21	Reference Axis System for Blade Aerodynamics.....	128
22	Effect of Yawed Flow on Lift Coefficient.....	130
23	Flow Chart for Steady State Pitching Moment Calculation.....	132
24	Determination of Steady State Pitching Moment Coefficient.....	133
25	Effect of Tip Sweep.....	135
26	Definition of Aerodynamic Angles in a Wind Tunnel	151
27	Orientation of Flightpath in Ground Reference....	151
28	Euler Angles from Ground to Body Reference.....	152
29	Aerodynamic Angles in Body Reference.....	152
30	Aerodynamic Pitch Angle in Sideward Flight.....	154
31	Sketch of Fuselage Drag as a Function of θ_w and ψ_w	159
32	Phasing of Fuselage NAE and HAE Models.....	171
33	Examples of Fuselage Aerodynamic Representation at Large Angles for a Medium Utility Helicopter..	173
34	Flow Chart for Flow Field Model.....	183
35	Relationship of Body and Aerodynamic Surface Reference Systems.....	187
36	Comparison of Test and Simulation Data for the Bell Model 533.....	190
37	Time History of Dive Brake Application on a Bell Model 309.....	201
38	Time History of an External Store Drop from a Bell Model 209 (SCAS Off).....	205

LIST OF ILLUSTRATIONS - Continued

<u>Figure</u>		<u>Page</u>
39	Time History of an External Store Drop from a Bell Model 209 (SCAS On).....	208
40	Schematic Diagram of Flight Control System.....	217
41	Schematic Diagram of Aerodynamic Surface and Jet Control Systems.....	219
42	Control System Schematic for Simple Single-Main-Rotor Helicopter.....	220
43	Schematic Diagram of Control Coupling/Mixing Box.	222
44	Model for Swashplate in the Nonrotating System...	224
45	Rotating Control Linkages.....	228
46	Blade Feathering Angle.....	230
47	Aerodynamic Surface Control Linkages.....	237
48	Schematic Diagram of SCAS.....	238
49	Magnitude and Time Lag Characteristics of a Three-Pole Butterworth Filter with a 5-Hertz Break Frequency.....	242
50	Maneuver Autopilot Roll Channel Flow Chart.....	245
51	Maneuver Autopilot Pitch Channel Flow Chart.....	246
52	Maneuver Autopilot Rate-of-Climb Channel Flow Chart.....	248
53	Straight-Line Definition of Engine Power Available Curve.....	251
54	Flow Chart of Trim Procedure.....	255
55	Flow Chart of Partial Derivative Matrix Computation.....	256
56	Flow Chart of Time-Variant Rotor Trim.....	257
57	Flow Chart of Rotor Force and Moment Computations During Trim Procedure.....	258

LIST OF ILLUSTRATIONS - Continued

<u>Figure</u>		<u>Page</u>
58	Algebraic Formulation of Trim Procedure.....	264
59	Elastic Trim Technique.....	266
60	Inertial Matrix.....	288
61	Damping Matrix.....	289
62	Stiffness Matrix.....	290
63	Forcing Functions Used in Study of Techniques....	295
64	SIMFLO Time History with Dominant One-Per-Rev....	307
65	SIMFLO Time History Showing Several Harmonic Components.....	309
66	Huey Cobra Time History for Pylon Mode One, Unperturbed.....	315
67	Huey Cobra Time History for Pylon Mode One, Perturbed.....	316
68	Huey Cobra Time History for Pylon Mode Two, Unperturbed.....	317
69	Huey Cobra Time History for Pylon Mode Two, Perturbed.....	318
70	Huey Cobra Time History for Pylon Mode Three, Unperturbed.....	319
71	Huey Cobra Time History for Pylon Mode Three, Perturbed.....	320
72	Huey Cobra Pylon Mode One Stability Results.....	321
73	Huey Cobra Pylon Mode Two Stability Results.....	322
74	Huey Cobra Pylon Mode Three Stability Results....	323
75	Comparison of Stability Results for Simple Check Case.....	325
A-1	Undisplaced Blade Coordinate System.....	336

LIST OF ILLUSTRATIONS - Concluded

<u>Figure</u>		<u>Page</u>
A-2	Displaced Blade Coordinate System.....	336
A-3	Transformation to x, y, z Coordinates.....	345
A-4	Equilibrium of Forces and Moments.....	347
B-1	General Euler Angle Transformation Matrix.....	369

LIST OF TABLES

<u>Table</u>		<u>Page</u>
1	Blade Boundary Conditions in DNAM05.....	67
2	Blade Boundary Conditions at Root.....	89
3	Blade Boundary Conditions and Mode Types for Hingeless or Articulated Hubs.....	89
4	Blade Boundary Conditions and Mode Types for Gimbaled or Teetering Hubs.....	92
5	Fuselage/Aerodynamic Surface Analogy.....	157
6	High Angle Equations for Fuselage Aerodynamic Forces and Moments.....	160
7	Nominal Angle Equations for Longitudinal Aerodynamic Forces and Moments.....	166
8	Nominal Angle Equations for Lateral-Directional Aerodynamic Forces and Moments.....	167
9	Effect of Deleting Terms from Baseline Equation on Accuracy of Curve Fits.....	168
10	Examples of Fuselage Aerodynamic Representation at Small Angles for a Light Commercial Helicopter.....	175
11	Equations for Recalculation of Weight, Center of Gravity, and Inertias.....	199
12	Definition of Trim Condition.....	260
13	Independent Trim Variables.....	260
14	Stability Analysis Equations.....	273
15	Prony's Method Test Cases.....	311
16	Prony's Method Results for Time History.....	312

1. INTRODUCTION

1.1 BACKGROUND

Bell Helicopter Textron began development of a rotorcraft flight simulation program for digital computers in 1963. The original program was identified as C81. This identification has since become the family name for several different versions developed over the years. To minimize confusion as to which version of the program is being referred to, the more recent versions of C81 have been identified by four letters and the year in which they became production programs; e.g., AGAJ74 was developed in 1974. This report documents the current version of C81, AGAJ77.

The early history and basic analysis of C81 are given in Reference 1. The simulation for that study included a rigid body fuselage in three dimensions, coupled with two rotors, for a total of eleven degrees of freedom. The eleven degrees of freedom were:

Six rigid body for the rotorcraft

Longitudinal and lateral flapping for each rotor

Rotor-engine torsional system

A variety of maneuvers were simulated by modeling control motions and external disturbances such as gusts. The program used a quasi-static rotor analysis. Aeroelastic feedback was represented by iteration through a rotor blade dynamic analysis.

The stop-fold rotor simulation study reported in Reference 2 delineates later additions to the program. The resulting computer program (ASAJ01) contained an uncoupled stability analysis which used the trim solutions and partial derivative computations available in the earlier version. Provisions were

¹Harvey, K. W., Blankenship, B. L., and Drees, J. M., ANALYTICAL STUDY OF HELICOPTER GUST RESPONSE AT HIGH FORWARD SPEED, Bell Helicopter Company; USAAVLABS Technical Report 69-1, U. S. Army Aviation Materiel Laboratories, Fort Eustis, Virginia, September 1969, AD862594.

²Livingston, C. L., Bird, B. J., and McLarty, T. T., A STABILITY AND CONTROL PREDICTION METHOD FOR HELICOPTER AND STOPPABLE ROTOR AIRCRAFT, Volumes I - IV, Bell Helicopter Company; Technical Report AFFDL-TR-69-123, Air Force Flight Dynamics Laboratory, Air Force Systems Command, Wright-Patterson AFB, Ohio, 1970.

made to compute stability roots during maneuvers as well as at the trim point. The rotor mathematical model was modified to include the stop-fold rotor capability. Both the tilt-forward-trail-aft and horizontal-stop-fold configurations were included. The rotor analysis in ASAJ01 was time-variant, but did not contain aeroelastic effects.

The next major expansion of the mathematical model was performed under Contract DAAJO2-70-C-0063, awarded by the Eustis Directorate of the U. S. Army Air Mobility Research and Development Laboratory (USAAMRDL). This, the AGAJ71 version of the program, included the addition of a time-variant aeroelastic rotor analysis (TVAR) and an unsteady rotor aerodynamic model. The TVAR allowed calculation of time histories of the deflection, bending moment, and aerodynamic loading along each rotor blade.

The unsteady aerodynamic analysis computed increments to the lift, drag, and pitching moment aerodynamic coefficients in both stalled and unstalled flow as functions of blade bending and pitching velocities and accelerations. Subsequently, under USAAMRDL Contract DAAJO2-71-X-0045, a second mathematical model for unsteady rotor aerodynamics was developed and incorporated in the trim portion of AGAJ71.

Two undocumented versions of the AGAJ72 program were delivered to the Eustis Directorate of USAAMRDL. The first AGAJ72 version included many refinements to the AGAJ71 version: rotor pylon degrees of freedom and an automatic control-stability package consisting of a Stability and Control Augmentation System (SCAS), an Automatic Pilot Simulator (APS), and an expanded airframe stability analysis subroutine. The second version, developed under Contract DAAJO2-72-C-0086, included two major additions: an alternate trim procedure and expanded data printout. These two features were primarily incorporated to increase the versatility of the program in simulating wind tunnel tests. The alternate trim procedure provided for locking the rotor flapping angles at their input values and then iterating on control positions to trim the rotor. The additional printout (the optional trim page) provided data in a form that was most useful when correlating with wind tunnel data (e.g., dimensional and nondimensional force and moment data, a summary of rotor parameters, and test conditions).

Under USAAMRDL Contract DAAJO2-72-C-0098, improvements to all aerodynamic representations in the program were developed. Specifically, the following aerodynamic-related modifications and additions were made to the program:

- (1) A more accurate and complete representation of fuselage aerodynamic forces and moments.

- (2) A single generalized representation for up to five aerodynamic surfaces with control surfaces (one wing and four stabilizing surfaces).
- (3) The capability of representing external stores and/or aerodynamic brakes.
- (4) The capability of representing up to five different airfoils along the span of the rotor blades.
- (5) The capability of representing the induced velocity distribution across the rotor disc as a Fourier series that is a function of advance ratio, inflow ratio, blade station, and blade azimuth.
- (6) The capability of representing the rotor wake at each aerodynamic surface as a Fourier series that is a function of rotor advance ratio, inflow ratio, and blade azimuth.

In addition to the above six tasks, the following features were also incorporated:

- (7) An alternate method for numerically integrating the rotorcraft equations of motion in maneuvers. (This method has since proved to be impractical and has been deleted from the program).
- (8) The unsteady aerodynamic model developed under Contract DAAJO2-71-C-0045, modified to work in maneuver as well as trim.

In the process of incorporating these eight features, the input format to the program was significantly revised to facilitate use of the increased versatility of the program. The benefits of the current aerodynamic representations are discussed below.

1.2 DISCUSSION OF THE MOST RECENT ADDITIONS (1975-1976)

The AGAJ76 version of C81 was developed under Contract DAAJO2-75-C-0025 for the Eustis Directorate of USAAMRDL. The following improvements in the analysis, program family, and documentation were made during this contract:

- (1) A study was made of the rotor stability analysis techniques that might be applied to C81. The Moving Block Fast Fourier Transform and Prony's method were selected and implemented in C81.

- (2) The rotor blade natural frequency program, DN9100, was provided and documented as part of the C81 program family.
- (3) The complete documentation of the rotor dynamics equations was provided for the calculation of the normal modes in DN9100 and the application of the modal analysis in C81.
- (4) Improvements were made to the hub geometry model, which allow the user to more accurately describe any rotor system.
- (5) In order to improve the calculation of rotor bending moments, the option was added for C81 to accept up to 11 normal modes for one rotor (with a limit of 12). Also, more data is transferred from the rotor frequency program (DN9100) to C81 so that a consistent set of modes and coefficients is used.
- (6) The pylon equations were reformulated in a modal form, with four modes, in order to provide completely general motion at the top of the rotor mast.
- (7) The control system was expanded to include any type of swashplate or control phasing. Also the control coupling options were increased to allow any control stick to operate any combination of rotor control functions.
- (8) The number and spacing of rotor blade segments were made variable in order to improve the modeling capability and also to reduce computer run time.
- (9) In connection with the rotor stability study, an option was added to perturb the dependent variables that are integrated during a maneuver. For example, a small change may be made to one rotor collective mode without making any control inputs or disturbing any other system degree of freedom.

1.3 DEVELOPMENT OF AGAJ77

The United States Army Air Mobility Research and Development Laboratory contracted with Bell Helicopter Textron in the summer of 1976 to modify the Rotorcraft Flight Simulation Program C81 and its attendant programs (the Rotor Frequency Program DNAM05 and the Rotor Wake Program AR9101) to provide several new features in the analysis and to make the program easier to use. The improved version of C81, AGAJ77, includes:

- (1) An improved autopilot, with a numerical filter on the airframe response inputs and four new command signals that the autopilot may act upon. The five command signals are:

- (a) roll rate (p-tracker)
- (b) pitch rate (q-tracker)
- (c) yaw rate (r-tracker)
- (d) normal load factor (g-tracker; in AGAJ76)
- (e) rate of climb (RC-tracker)

The improved autopilot model is described in Section 8.2.

- (2) An improved elastic rotor analysis, which includes the effects of inplane and out-of-plane offsets and sweep and precone of the feathering axis in DNAM05 and in C81. See Section 3.2.7.
- (3) An improved engine-governor model which provides a first-order differential equation for the available horsepower during a maneuver simulation. See Section 9.
- (4) An improved wake analysis, in which the filtered rotor thrust is used to compute the average induced velocity if a rotor-induced velocity table is not used. When it is used, the table is bivariate in advance ratio and wake-plane angle of attack (instead of inflow ratio) at any given radius. Again, the filter is used to smooth the inputs to the model. See Section 3.4.2.
- (5) The capability to plot time histories of rotor response after a time-variant trim. This feature uses some of the code in the maneuver-perturbation analysis of AGAJ76.
- (6) The ability to contour-plot up to 30 rotor variables, either from trim or maneuver.

C81 has ceased to be a single program. With the completion of Contract DAAJ02-75-C-0025, DN9100 became available to provide rotor frequencies and mode shapes for input to C81 with a minimum of manipulation. Under the current contract, an additional

program, the Rotor Wake Program AR9102, became available to produce the rotor-induced velocity tables for input to C81. The analysis embodied in this program is discussed in Section 7.2 of Volume II and in Reference 3.

1.4 DOCUMENTATION CONSIDERATIONS AND ORGANIZATION

This report has been prepared under Contract DAAJ02-77-C-0003 awarded by the Eustis Directorate of USAAMRDL. It was based on USAAMRDL-TR-76-41A (Reference 4) with revisions made only as needed to reflect improvements in the analysis and input format. This policy was followed to make the transition from AGAJ76 as easy as possible for the user.

This volume of the report, Volume I, has been prepared to document those analyses which are important to understanding the program but not necessary for its execution, to provide background information and the rationale for selecting certain mathematical models over other models, and to suggest areas in which further development of the program is warranted.

Volume II, the User's Manual, provides the information necessary to set up a data deck to successfully execute the simulation, and to interpret the results. Volume III, the Programmer's Manual, contains the information required for setting up the program on the user's computer; brief descriptions of the sub-routines are included.

³Crimi, P. THEORETICAL PREDICTION OF THE FLOW IN THE WAKE OF A HELICOPTER ROTOR, Cornell Aeronautical Laboratory Report BB-1994-S-1, Buffalo, New York, September 1965, AD 629782.

⁴McLarty, Tyce T., Van Gaasbeek, James R., and Hsieh, P. Y. ROTORCRAFT FLIGHT SIMULATION WITH COUPLED ROTOR AEROELASTIC STABILITY ANALYSIS, Volumes I - III, Bell Helicopter Textron; USAAMRDL Technical Reports, 76-41A, 76-41B and 76-41C, Eustis Directorate, U. S. Army Air Mobility Research and Development Laboratory, Fort Eustis, Virginia, May 1977, AD A042462 (TR 76-41A only).

2. COMPUTER PROGRAM ORGANIZATION

The logic of the computer program is organized into three major operations: determination of an equilibrium flight condition, computation of the time history of a prescribed maneuver, and stability analysis. The heart of each operation is the mathematical model of the rotorcraft. The following five subsections present general discussions of the rotorcraft model, the rotor analyses available, and each of the three major operations. Although the general organization of the program is essentially the same as documented in Reference 4, several models and operations in the program have been expanded or revised since the publication of that report.

2.1 MATHEMATICAL MODEL OF THE ROTORCRAFT

The mathematical model of the rotorcraft provides for detailed simulation of the following rotorcraft configurations: single main rotor, tandem rotors, and side-by-side (or tilting prop) rotors. The model is broken down into the following major components, each of which is discussed in detail in the indicated section:

- (1) Rotors (maximum of two, each with up to seven blades); Section 3
- (2) Fuselage (valid in all flight regimes); Section 4
- (3) Aerodynamic surfaces (one wing and up to four stabilizing surfaces); Section 5
- (4) External stores or aerodynamic brakes (any combination of up to four stores and brakes); Section 6
- (5) Auxiliary propulsion (up to two jet thrust vectors); Section 7
- (6) Control system (including control of each rotor, aerodynamic surface, and jet) plus a Stability and Control Augmentation System and Automatic Pilot Simulator; Section 8
- (7) Engine-governor system, including a table look-up procedure for computing the available horsepower; Section 9

Since each model is general enough to be adapted to any one of the three rotorcraft configurations, each can provide very detailed simulation of any one configuration.

2.2 ROTOR ANALYSES

Two independent and mutually exclusive rotor analyses are programmed into C81: quasi-static and time-variant. When development of C81 began in the early sixties, the entire program was predicated on the quasi-static rotor analysis. As part of the contract documented in Reference 2, the time-variant rigid blade rotor analysis was added as an option. Subsequently, under Contract DAAJO2-70-C-0063, an aeroelastic blade representation based on the modal technique was added for use with both types of rotor analyses. Definitions of these two rotor analyses are given below:

2.2.1 Quasi-Static Rotor Analysis

The quasi-static rotor analysis is frequently called the "Frisbee" analysis. This nickname evolved from the fact that quasi-static rotor is somewhat analogous to a rotating disc which generates dynamic and aerodynamic forces and moments, like a Frisbee. A more mathematical definition of the quasi-static analyses is that at any instant in time the frequency of rotor flapping is exactly one per revolution (1-per-rev). This situation requires that the path of each blade tip during one rotor revolution defines a single plane, or disc. Since the locus of the blade tips defines a plane, the orientation of the rotor disc with respect to the rotor shaft can then be defined by the longitudinal and lateral flapping angles. These flapping angles are the dependent variables in the equations of motion of the rotor, and coning is neglected. Note that the quasi-static analysis does not require that the blades be rigid, but does require that the frequency of any elastic displacements be at 1-per-rev. Hence, the quasi-static rotor analysis is best suited to teetering or gimbaled rotor systems where the dominant blade motions are at 1-per-rev and where, for most performance and flying qualities investigations, other flapping frequencies can be neglected. However, the analysis is also suitable for first-order approximations of rigid rotors and articulated rotors using the first out-of-plane mode.

The major limitation of the quasi-static analysis is that only the 1-per-rev component of the blade response is calculated. The steady component of the blade response is also calculated for elastic modes other than the first. Consequently, accurate computation of blade loads is not possible. Blade load calculations and printout are bypassed whenever the quasi-static rotor analysis is used.

Computationally, any rotor which uses the quasi-static analysis is in effect modeled as a 12-bladed rotor at each time

(computation) point. The input or computed pair of flapping angles are used to define the orientation of a single representative blade at each of 12 equally spaced azimuth angles (30-degree increments). The dynamic and aerodynamic forces and moments are then calculated at each blade station for each azimuth, numerically integrated, and multiplied by the ratio of the actual number of blades to the 12 blades of the computational rotor.

In this analysis, individual blade azimuth is irrelevant and the rotor forces and moments transmitted to the airframe are equivalent to time-averaged quantities.

2.2.2 Time-Variant Rotor Analysis

The time-variant rotor analysis is predicated on the modal technique of representing rotor blade dynamics. It is this technique, described in detail in Section 3.2, which permits the simulation of an aeroelastic rotor (i.e., a rotor where the shape and motion of each blade at any instant in time is a function of the aerodynamic loading and the elastic properties of the blade). In the time-variant rotor analysis, each blade is free to respond to aerodynamic and dynamic forces and moments of all frequencies, not just 1-per-rev, at each instant in time. Since the blades are free to respond to all frequencies, the concept of a tip-path plane and its associated longitudinal and lateral flapping angles used in the quasi-static analysis is not meaningful in the time-variant analysis. The meaningful parameters are the angle between the hub and mast plus the inplane, out-of-plane, and torsional displacements, velocities, and accelerations along the span of each blade.

The time-variant analysis is suitable for all types of rotors and should be used whenever possible, particularly for rigid or articulated rotors. It must be used when blade load data are desired.

Computationally, the forces and moments acting on each segment of each individual blade at its instantaneous position are calculated at each time point in the time-variant analysis. The resulting accelerations and current velocities are then numerically integrated to determine the velocities and displacements of each segment of each individual blade at the next time point (azimuth position).

2.3 DETERMINATION OF THE EQUILIBRIUM FLIGHT CONDITION

The technique used to determine the equilibrium, or trimmed, flight condition in C81 is an enlargement of the technique

described in Reference 2. The additional considerations are those required to represent the steady state solution of the elastic rotor equations and the elastic pylon equations. The technique which had previously been used to trim the rigid blade has been modified to apply to any blade mode that has a natural frequency at or near 1-per-rev.

The standard trim procedure determines the following quantities at each iteration: pilot control positions, angular orientation of the aircraft in space, and a harmonic analysis through 1-per-rev of the following quantities: participation factor for each mode (maximum of 12) for each blade for each rotor and four modes of pylon motion for each rotor. The effects of the elastic blade and pylon motions are included in the overall trim procedure to solve for a coupled aeroelastic trim solution.

In addition, this standard trim procedure has been modified so that the user can delete the airframe from the procedure and trim an isolated rotor (a wind tunnel simulation). This added path through the trim procedure allows the user two alternatives: to command the rotor feathering angles and trim the rotor by iterating on flapping angles, or to command the flapping angles and iterate on the feathering angles. The mathematical techniques used in the standard and alternate trim procedures are discussed in Section 10.

2.4 FLIGHTPATH STABILITY ANALYSIS

The stability analysis in this program is the same as that presented in Reference 4. In this stability analysis, the following 18 equations of motion can be considered:

- (1) Six rigid body (total rotorcraft)
- (2) Four pylon modes for two rotors
- (3) Longitudinal and lateral flapping for two rotors

The analysis may be performed for the trimmed flight condition or at specified times during a maneuver. The three stability matrices generated by the analysis can then be punched on cards for additional analysis external to C81.

The derivation of the current stability analysis is predicated on a quasi-static rotor analysis, and is not compatible with the time-variant rotor analysis. Hence, only the 1-per-rev response of elastic blades is included in this analysis (and the steady component of elastic modes other than the first). The

complete equations of motion and the numerical techniques associated with the stability analysis are contained in Section 11.

The maneuver perturbation option provides a special method for checking rotorcraft stability. A prescribed disturbance may be introduced without the extraneous effects of control motions or wind gusts. If a null aerodynamic table is used, dynamic behavior in a vacuum may also be studied by this method.

2.5 MANEUVERS

Compared to the version of C81 documented in Reference 4, the capabilities of the program for computing the time history of a maneuver have been greatly enhanced. The current fully coupled analysis includes the user options of quasi-static or time-variant rotor analyses, rigid or aeroelastic blades, and more than 30 variations of control positions, control mechanisms, rotorcraft configurations, etc. The improved and extended pilot simulation makes it much easier to obtain a desired maneuver profile.

The program includes five options for reducing the data generated by the maneuver portion of the program. These options include plotting, Moving Block Fast Fourier Transform, Prony's method curve fit, harmonic analysis, and vector analysis. Each set of reduced data may be output on the printer or on a CALCOMP plotter. The data that may be reduced consist of every parameter printed as part of the maneuver time history plus detailed rotor loads and elastic response data, for a total of more than 2300 variables. These 2300 variables may also be stored on magnetic tape and reloaded at a later date for additional analysis.

In addition, up to 30 variables may be contour plotted for each rotor trim and at predetermined time points during maneuver.

Another feature of the maneuver portion of the program is the restart capability, which permits a long continuous run to be made in several passes. This procedure causes each item on the output page and many intermediate variables to be written on a magnetic tape, which is saved. Then on subsequent runs, the start time can be any point on the saved tape. In addition, the maneuver card can be changed on each run.

2.6 PROGRAMMING CONSIDERATIONS

The current program includes a program logic group as the first group of input data. This group allows the user many options as to the data to be read in and the analyses to be performed. In view of the large number of cards required to use every capability of the mathematical models, these logic controls can greatly reduce the size of a deck when a particular option is not to be used.

The contractor's version of the program includes a data library that permits the storage of complete rotorcraft configurations or individual components (input groups) on magnetic disk. These data may then be called from storage by the first card of each input group. This feature greatly reduces the number of cards that must be included in the input deck and assures consistency in at least the initial input data when many users are making runs with the same configuration. Any parameter in most of the groups stored in the library may be changed during read-in if the user so desires.

3.0 ROTOR SYSTEM MATHEMATICAL MODEL

3.1 INTRODUCTION

The Rotorcraft Flight Simulation Program uses the identical mathematical model for both rotors. The only major restrictions on the currently programmed model are that for a given rotor the number of blades must be between two and seven inclusive, the physical properties of each blade must be identical, and rigid body feathering axes of the blades must be equally spaced around the rotor azimuth.

Some of the most useful features of the model are the options for inputting any of the following blade properties as distributions along the span of the blade rather than as single values: twist, chord, airfoil section, aerodynamic reference center location, mass, mass moments of inertia, center of gravity location, and elasticity (aeroelastic mode shapes). These distributions contain data either for a maximum of 20 blade segments or at 21 radial stations. Other blade parameters in the model include tip sweep, hub drag, precone angle, prelag angle, pitch change axis offset, a lead-lag damper, flapping restraint and stops, and pitch-flap coupling. The possible configurations for the rotor hub model include teetering (or gimbaled), articulated, and rigid. Also, undersling, the vertical distance between the flapping and feathering axes, may be simulated for teetering or gimbaled rotors.

Each rotor shaft (mast) may be given any desired orientation with respect to the airframe. In addition, a nonisotropic dynamic pylon model is included to simulate the mounting of the transmission/rotor shaft or gearbox/shaft system to the airframe. Up to four modal equations may be used to represent the rotor support system including the user's choice of mast windup, pylon motion, or flexible fuselage modes.

The above model features relate primarily to the physical properties of the rotor systems and, hence, are used in the dynamic analysis of the rotor. The model also includes a detailed aerodynamic analysis. This analysis is divided into two subanalyses: steady state and unsteady aerodynamics. The steady state aerodynamics are determined from sets of either equations or data tables. The choice of equations or tables is a user option. The option may be exercised for either an entire blade or each of the blade segments.

The user also has the option of using either an equation or a data table for computing the induced velocity distribution over the rotor disc. The table contains coefficients of a Fourier-series curve fit of wake data computed external to C81.

The table is tri-variant with arguments of advance ratio, rotor angle of attack, and blade station. The aerodynamic analysis also includes two methods for computing increments to the steady state aerodynamic coefficients due to time derivatives of the blade angle of attack. These methods, referred to as the BUNS and UNSAN unsteady aerodynamic options, and their accompanying models for yawed flow are independent and mutually exclusive. That is, the user may activate either the BUNS or UNSAN option with or without its respective yawed flow models; alternatively, both unsteady models can be deactivated, and one or none of the yawed flow models can be activated.

This section of the report contains the dynamic and aerodynamic analyses incorporated into the rotor mathematical model. The next subsection discusses the dynamic analysis including the calculation of the natural frequencies and mode shapes as well as the modal response analysis. Following the discussion of the dynamics, the aerodynamic analysis is presented, with emphasis on the procedure for computing the angles of attack, Mach number, and dimensional forces and moments at a blade station and on the two models for unsteady aerodynamic effects. The model for calculating the steady state coefficients is discussed in detail in Section 3.9 of Volume II; only selected information is repeated or expanded on in this volume.

3.2 DYNAMICS

3.2.1 General

The development of a comprehensive program such as C81 may be viewed as a three-step process.

(1) Aeroelastic Rotor Analysis

- (a) Derivation of differential equations of motion
- (b) Solution technique for differential equations of motion

(2) Helicopter Flight Simulation

- (a) Representation of gross helicopter behavior
- (b) Determination of equilibrium flight conditions
- (c) Ability to integrate numerically equations of motion

(3) Interface Between Rotor Analysis and Flight Simulation

- (a) Effect of rotor behavior on helicopter behavior
- (b) Effect of helicopter behavior on rotor behavior

The standard reference for the differential equations of motion of a helicopter rotor blade is NACA Report 1346 by Houbolt and Brooks (Reference 5). The C81 rotor analysis was actually developed without reference to the equations of Houbolt and Brooks (H&B). This report will present a development that closely parallels H&B, removing some of their simplifying assumptions and using the coordinate systems peculiar to C81. The analysis actually used in the rotor frequency program DN9100 and C81 will then be documented relative to the complete differential equations. Following this, the external effects that are not covered by the differential equations are discussed. These include the following items:

- (1) Alternate load path provided by pitch horn/pitch link
- (2) Special geometric constraints that may be introduced by hinges on the blade
- (3) Moment caused by hub springs
- (4) Effects of flapping stops
- (5) Treatment of viscous dampers
- (6) Rotor blade boundary conditions and selection of blade-mode types
- (7) Combination of blade modes to form rotor modes

3.2.2 Coordinate Systems Used

The C81 dynamic analysis uses five coordinate systems to describe the behavior of the various rotorcraft components. The systems will be described here, and the generalized transformation used to get from one system to another will be described in Appendix B.

- (1) Ground Reference - The ground reference system is taken to be the inertial reference system. Variables associated with the ground reference system will be denoted by the subscript or superscript g . The x_g axis is pointed north; y_g axis, east; and z_g axis, down.
- (2) Fuselage Reference - The fuselage coordinate system is centered at the fuselage center of gravity. Fuselage variables are denoted by the letter f . The x_f axis is forward; y_f , to the right; and z_f , down.

⁵Houbolt, John C., and Brooks, George W., DIFFERENTIAL EQUATIONS OF MOTION FOR COMBINED FLAPWISE BENDING, CHORDWISE BENDING AND TORSION OF TWISTED NONUNIFORM ROTOR BLADES, NACA Report 1346, 1958.

- (3) Mast Reference - The mast reference system is centered at the rotor flapping hinge or at the intersection of the blade radial axes if there is no single flapping hinge. This system does not rotate with the rotor. Mast referenced quantities will be identified by the letter m. The orientation of the mast reference system for zero mast tilt angles and no pylon motion has the x_m , y_m , and z_m axes parallel to the x_f , y_f , and z_f axes, respectively, and in the same directions. The mast reference system moves with the longitudinal and lateral mast tilt angles and with any angles introduced by pylon motion.
- (4) Hub Reference - The hub coordinate system is a rotating coordinate system that shares the same origin as the mast reference system. The letter h is used to indicate variables associated with the hub reference system. The y_h axis extends radially outward from the center of rotation along the blade of interest. The z_h axis is generally parallel to the z_m axis but directed upward rather than downward. The z_h axis is tilted by any flapping motion of the hub at the center of rotation. The x_h axis is directed as required to make a right-handed coordinate system. For the main rotor of an American helicopter, this is generally toward the trailing edge of the blade. For the tail rotor analysis, x_h is positive toward the trailing edge, forming a left-handed coordinate system. The hub coordinate system experiences motion due to flapping of the hub relative to the mast caused by cyclic rotor modes and due to "mast wind-up" which is reflected in the collective rotor modes rather than pylon modes. A description of cyclic and collective modes is found in Section 3.2.10.
- (5) Blade Reference - The origin of the blade coordinate system is at the inboard end of the feathering bearings. Variables associated with the blade reference are marked with the subscript b. The x_b axis is aft, parallel to the major principal axis of inertia. The y_b axis is aligned with the feathering bearings. The z_b axis is upward, parallel

to the minor principal axis of inertia. The need for this coordinate system is to account for the flap, lag, and twisting motion of the pitch change axis. Therefore in the case of rotors without feathering bearings, the origin of the blade coordinate system is at the radius where the pitch horn or other pitch mechanism applies the feathering control to the blade.

3.2.3 Development of Rotor Differential Equations

The rotor differential equations of motion are developed from first principles in a manner similar to H&B (Appendix A). The assumptions made in this development that are different from those of H&B include the following:

- (1) Rotor blade cross sections are not symmetric.
- (2) The elastic axis is not a straight line.
- (3) Structural principal axes and mass principal axes are not parallel.
- (4) The effects of the linear and angular velocities and accelerations of the rotor hub are included.
- (5) The effects of blade feathering motion are included.

The H&B assumptions that remain in the analysis of this report are as follows:

- (1) The elastic twist is assumed to be a small angle.
- (2) Shear deformation is neglected.
- (3) No plastic deformation occurs.

Not all of the terms in the differential equations appear explicitly in C81 and DNAM05. In general, the linear mass terms and the linear spring terms are included in DNAM05; nonlinear terms and terms associated with hub motion are in C81. The linear mass terms are any linear terms involving second time derivatives of the independent variables. The linear spring terms are linear terms involving only displacements of the independent variables.

3.2.3.1 Calculation of Rotor Blade Natural Frequencies and Modes - DNAM05

For the finite element model used in DNAM05, the spring and mass terms may be treated separately. In DNAM05 the rotor

blade is represented by a series of lumped, inflexible inertias connected by untwisted, massless, elastic beams. The built-in twist of the blades is made incrementally at the blade stations where the inertias are located. The DNAM05 program uses a state vector and transfer function type of solution as developed by Dr. Nils Myklestad (Reference 6).

The state vector consists of two linear displacements, the three angular rotations, and the shears and moments which correspond to these displacements. The radial extension of the blade is neglected.

In the description of the analysis, it is convenient to treat the transfer functions in matrix form even though it is inefficient to use this form in the computer program. A typical blade segment, i , is shown in Figure 1 in its undeformed position. Both the elastic element and the three-dimensional inertia dumbbell are shown. The transfer matrix equation for this segment may be written as

$$\{s_i\} = [m_i][f_i]\{s_{i+1}\} \quad (1)$$

where

$\{s_i\}$ is the state vector at station i .

$[m_i]$ is the transfer matrix across the inertia dumbbell.

$[f_i]$ is the transfer matrix across the elastic element of length L_i .

The state vector $\{s_i\}$ consists of the following variables:

u_i = inplane displacement

w_i = out-of-plane displacement

u'_i = inplane slope

w'_i = out-of-plane slope

V_{x_i} = inplane shear

V_{z_i} = out-of-plane shear

M_{x_i} = out-of-plane moment

M_{z_i} = inplane moment (right-hand moment about negative z_h axis)

⁶Myklestad, N. O., FUNDAMENTALS OF VIBRATION ANALYSIS, New York, N.Y., McGraw-Hill, 1956, pp. 237-247.

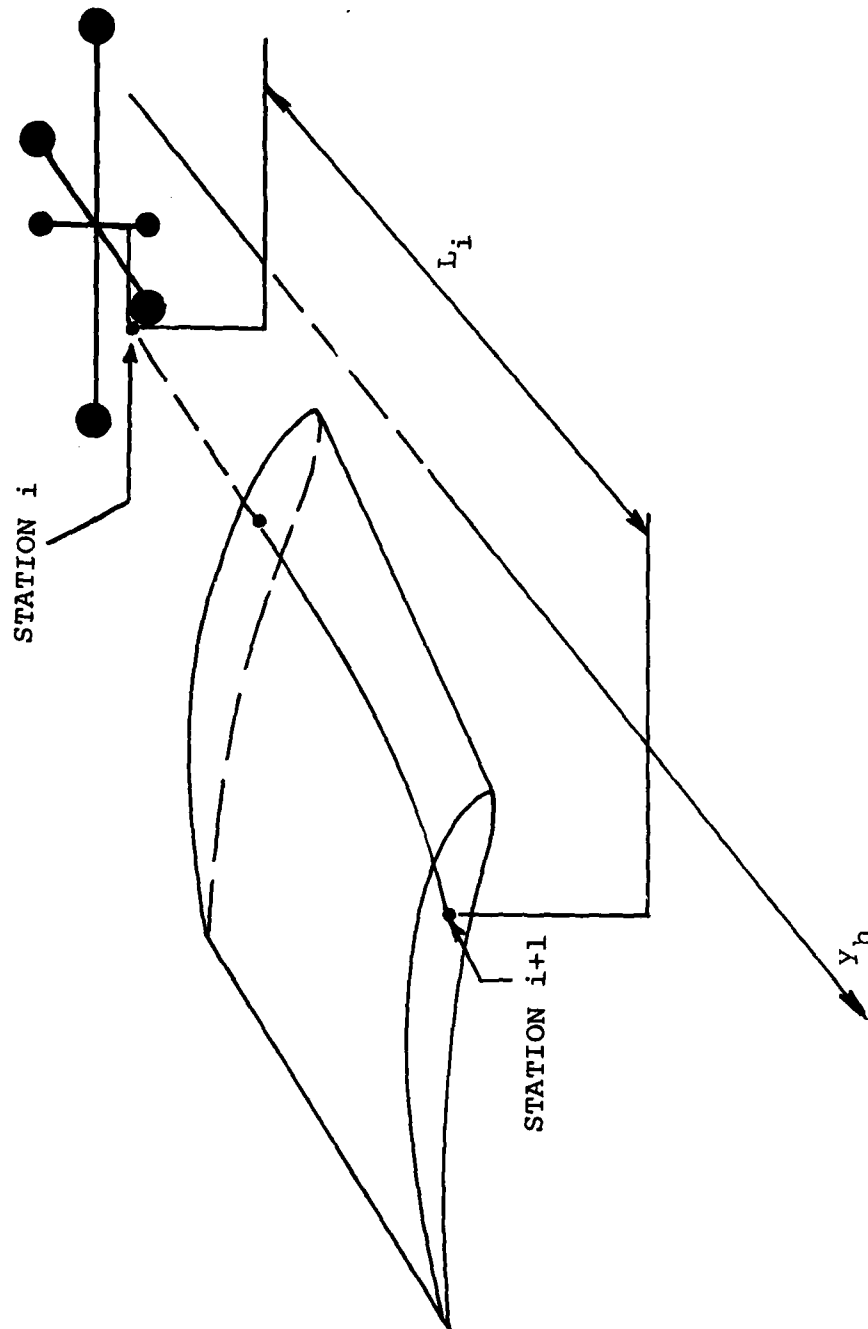


Figure 1. Typical Blade Element as Modeled in DNAM05.

ϕ_i = torsional deflection about y axis

M_{y_i} = torsional moment about y axis

Equation (1) is written so that the state is found at the in-board end of the segment in terms of the outboard end. This is done because it is more convenient to start at the tip of the blade, where the boundary conditions are always the same, and progress toward the center of rotation, where various sets of boundary conditions may be applied according to the type of rotor being modeled. It should also be noted that $[m_i]$ is comprised of the inertia of the half segments on either side of station i .

The inertia transfer function is generated by application of Equations (A-58), (A-59), (A-60), (A-64), (A-65), and (A-66), as well as the continuity of displacements and slopes. When the simplifications stated in the first paragraph of this section and the last paragraph of the previous section are made, these equations take the following form:

$$F_x = -m[(\ddot{u} - u \Omega_{bz}^2) + (\phi \Omega_{bz}^2 - \ddot{\phi})(e_{mC} \sin \theta_s - e_{mB} \cos \theta_s) - \Omega_{bz}^2 (e_{mB} \sin \theta_s + e_{mC} \cos \theta_s)] \quad (2)$$

$$F_y = m[(\ddot{u}' - u' \Omega_{bz}^2)(e_{mB} \sin \theta_s + e_{mC} \cos \theta_s) + (\ddot{w}' - w' \Omega_{bz}^2)(e_{mB} \cos \theta_s - e_{mC} \sin \theta_s) + y \Omega_{bz}^2] \quad (3)$$

$$F_z = -m[\ddot{w} - \ddot{\phi}(e_{mC} \cos \theta_s + e_{mB} \sin \theta_s)] \quad (4)$$

$$\begin{aligned} Q_x = & (\ddot{u}' - u' \Omega_{bz}^2)[\sin \theta_s \cos \theta_s (I_{\eta\eta} - I_{\zeta\zeta}) \\ & - I_{\eta\zeta}(\cos^2 \theta_s - \sin^2 \theta_s)] \\ & + (\ddot{w}' - w' \Omega_{bz}^2)[-I_{\eta\eta} \sin^2 \theta_s - I_{\zeta\zeta} \cos^2 \theta_s \\ & + 2 I_{\eta\zeta} \sin \theta_s \cos \theta_s] + m y \Omega_{bz}^2 [\phi(e_{mC} \cos \theta_s \\ & + e_{mB} \sin \theta_s) + (e_{mC} \sin \theta_s - e_{mB} \cos \theta_s)] \end{aligned}$$

$$\begin{aligned}
& - \phi u' \Omega_{bz}^2 [(I_{\eta\eta} - I_{\zeta\zeta})(\cos^2 \theta_s - \sin^2 \theta_s) \\
& + 4 I_{\eta\zeta} \sin \theta_s \cos \theta_s] \\
& + 2 \phi w' \Omega_{bz}^2 [(I_{\eta\eta} - I_{\zeta\zeta}) \sin \theta_s \cos \theta_s \\
& - I_{\eta\zeta} (\cos^2 \theta_s - \sin^2 \theta_s)]
\end{aligned} \tag{5}$$

$$\begin{aligned}
Q_y = & m \dot{w} (e_{mC} \cos \theta_s + e_{mB} \sin \theta_s) \\
& + m(\ddot{u} - u \Omega_{bz}^2)(e_{mC} \sin \theta_s - e_{mB} \cos \theta_s) \\
& - \phi (I_{\eta\eta} + I_{\zeta\zeta}) - \phi \Omega_{bz}^2 [(\cos^2 \theta_s \\
& - \sin^2 \theta_s)(I_{\eta\eta} - I_{\zeta\zeta}) + 2 I_{\eta\zeta} \cos \theta_s \sin \theta_s] \\
& - \Omega_{bz}^2 [(I_{\eta\eta} - I_{\zeta\zeta}) \sin \theta_s \cos \theta_s \\
& + I_{\eta\zeta} (\sin^2 \theta_s - \cos^2 \theta_s)] \\
& - \phi u \Omega_{bz}^2 m (e_{mC} \cos \theta_s + e_{mB} \sin \theta_s)
\end{aligned} \tag{6}$$

$$\begin{aligned}
Q_z = & m y \Omega_{bz}^2 [-\phi (e_{mC} \sin \theta_s - e_{mB} \cos \theta_s) \\
& + (e_{mC} \cos \theta_s + e_{mB} \sin \theta_s)] + \ddot{u}' [I_{\eta\eta} \cos^2 \theta_s \\
& + I_{\zeta\zeta} \sin^2 \theta_s + 2 I_{\eta\zeta} \cos \theta_s \sin \theta_s] \\
& + \dot{w}' [\cos \theta_s \sin \theta_s (I_{\zeta\zeta} - I_{\eta\eta}) \\
& + I_{\eta\zeta} (\cos^2 \theta_s - \sin^2 \theta_s)] \\
& + 2 \phi u' \Omega_{bz}^2 [(I_{\eta\eta} - I_{\zeta\zeta}) \sin \theta_s \cos \theta_s \\
& - I_{\eta\zeta} (\cos^2 \theta_s - \sin^2 \theta_s)] \\
& + \phi w' \Omega_{bz}^2 [(I_{\eta\eta} - I_{\zeta\zeta})(\cos^2 \theta_s - \sin^2 \theta_s) \\
& + 4 I_{\eta\zeta} \sin \theta_s \cos \theta_s]
\end{aligned} \tag{7}$$

Since F_x , F_y , and F_z are the forces per unit length along the radius and Q_x , Q_y , and Q_z are the moments per unit length, Equations (2) through (7) give directly the changes in shear and moment across a lumped inertia if changes are in terms of segment mass and segment inertias.

In order to model rotor built-in precone, prelag, and offsets of the pitch change axis from a radial axis, u , w , u' , and w' are considered to have steady values as well as vibratory. The steady components are marked with a bar (as in \bar{u}) in the equations which follow.

In order to simplify the notation, it is understood that the transfer functions are developed for the i th segment. All of the properties and characteristics of the segment could be written with an i subscript; the subscript is omitted. Also, the state at the inboard side of the lumped inertia will be denoted by the subscript i ; the outboard side of the lumped inertia or the inboard side of the elastic element, by j ; and the outboard side of the elastic element by $i+1$. At this point harmonic motion at the frequency ω is assumed, so that the substitution.

$$\ddot{u} = -\omega^2 u \quad (8)$$

for each independent variable can be made. By applying the continuity of slopes and displacements from j to i , the transfer function from j to i may then be written by inspection.

$$\{s_i\} = [m_i]\{s_j\} \quad (9)$$

The inertia transfer functions are given in Figure 2. Note that the s subscript used to distinguish between the structural and inertial axes has been deleted. The steady shears and moments shown in Figure 2 are used in the development of the elastic element transfer functions below.

Additional Symbols

$$e_x = e_{mC} \cos \theta + e_{mB} \sin \theta$$

$$e_z = -e_{mC} \sin \theta + e_{mB} \cos \theta$$

$$C_1 = \cos \theta$$

$$C_2 = \cos^2 \theta$$

$$S_1 = \sin \theta$$

$$S_2 = \sin^2 \theta$$

Continuity Equations

$$u_i = u_j$$

$$w_i = w_j$$

$$u'_i = u'_j$$

$$w'_i = w'_j$$

$$\phi_i = \phi_j$$

Shear Equations

$$V_{x_i} = V_{x_j} + m(\omega^2 + \Omega^2) u_j + m(\omega^2 + \Omega^2) e_z \phi_j$$

$$V_{z_i} = V_{z_j} + m\omega^2 w_j - m\omega^2 e_x \phi_j$$

Moment Equations

$$\begin{aligned} M_{x_i} = M_{x_j} &- (\omega^2 + \Omega^2)(S_1 C_1 \{I_{\eta\eta} - I_{\xi\xi}\} - \{C_2 - S_2\} I_{\eta\xi}) u'_j \\ &+ (\omega^2 + \Omega^2)(S_2 I_{\eta\eta} + C_2 I_{\xi\xi} + 2S_1 C_1 I_{\eta\xi}) w'_j \\ &+ m\gamma\Omega^2 e_x \phi_j \end{aligned}$$

Figure 2. Inertia Transfer Functions for DNAM05.

$$\begin{aligned}
M_{Y_i} &= M_{Y_j} + m(\omega^2 + \Omega^2) e_z u_j + m\omega^2 e_x w_j + [-\omega^2(I_{\eta\eta} + I_{\zeta\zeta}) \\
&\quad + \Omega^2 \{C_2 - S_2\}\{I_{\eta\eta} - I_{\zeta\zeta}\} + 2I_{\eta\zeta} S_1 C_1) \\
&\quad - \bar{u}_j \Omega^2 m e_x] \phi_j \\
M_{Z_i} &= M_{Z_j} - (\omega^2 + \Omega^2) (I_{\eta\eta} C_2 + I_{\zeta\zeta} S_2 + 2S_1 C_1 I_{\eta\zeta}) u_j \\
&\quad + (\omega^2 + \Omega^2) (S_1 C_1 \{I_{\eta\eta} - I_{\zeta\zeta}\} - I_{\eta\zeta} \{C_2 - S_2\}) w_j \\
&\quad + m y \Omega^2 e_z \phi_j
\end{aligned}$$

Steady Shears and Moments (Indicated by bar -.)

$$\begin{aligned}
\bar{V}_{x_i} &= m\Omega^2 e_x + \bar{V}_{x_j} \\
\bar{V}_{y_i} &= m y \Omega^2 + \bar{V}_{y_j} \\
\bar{V}_{z_i} &= 0 \\
\bar{M}_{x_i} &= -m y \Omega^2 e_z + \bar{M}_{x_j} \\
\bar{M}_{y_i} &= \Omega^2 (S_1 C_1 \{I_{\eta\eta} - I_{\zeta\zeta}\} - I_{\eta\zeta} \{C_2 - S_2\}) + \bar{M}_{y_j} \\
\bar{M}_{z_i} &= -m y \Omega^2 e_x + \bar{M}_{z_j} - \Omega^2 \bar{u}' (I_{\eta\eta} C_2 + I_{\zeta\zeta} S_2 + 2I_{\eta\zeta} S_1 C_1) \\
&\quad - \Omega^2 \bar{w}' [(I_{\eta\eta} - I_{\zeta\zeta}) S_1 C_1 - I_{\eta\zeta} (C_2 - S_2)]
\end{aligned}$$

Figure 2. Concluded.

Next is shown the development of a transfer function for a uniform, massless elastic field with large steady stress resultants and corresponding twist and bending slopes in summary form. The governing differential equations are given in terms of both local deformed blade element stress resultants, and in terms of stress resultants in a local blade element reference coordinate system. A linearized form of the differential equations is given, with the differential equations written in matrix form as a set of first-order constant coefficient equations, in the local blade element reference coordinate system. Methods of solution are discussed briefly, and an approach is taken which solves for the usual beam and centrifugal stiffening in an exact manner, presents a closed form but infinite series solution for the smaller (with respect to the centrifugal load stress resultant) steady stress resultant and steady twist and bending slope effects and uses a first term approximation to the infinite series. (Higher degree approximation could be developed but the implementation would most likely be done by matrix operations, within the computer program.) The resulting solution is transformed to the blade reference system, for a transfer process from the tip toward the hub.

It is most convenient to write the relationship between stress resultants and slopes, all measured in a reference system with deflections in a local undeformed blade element coordinate system and stress resultants in a local deformed blade element coordinate system. These are obtained by setting θ_x to zero in equations A-17, A-32, and A-34.

$$T = EA (v' - e_{AC} u'' - e_{AB} w'') \quad (10)$$

$$M_B = EI_B w'' - e_{AB} T \quad (11)$$

$$M_C = EI_C u'' - e_{AC} T \quad (12)$$

$$Q = (GJ + Tk_A^2) \phi' \quad (13)$$

where the shear center is taken to be the local reference coordinate axis, and the tensile axis (centroid of EA) as located by e_{AB} and e_{AC} are shown in Figure 3. Shear center offsets from the rotor blade reference system, the pitch change axis (PCA) will be accounted for later, as will misalignments between the local element's principal elastic axis and the pitch change axis.

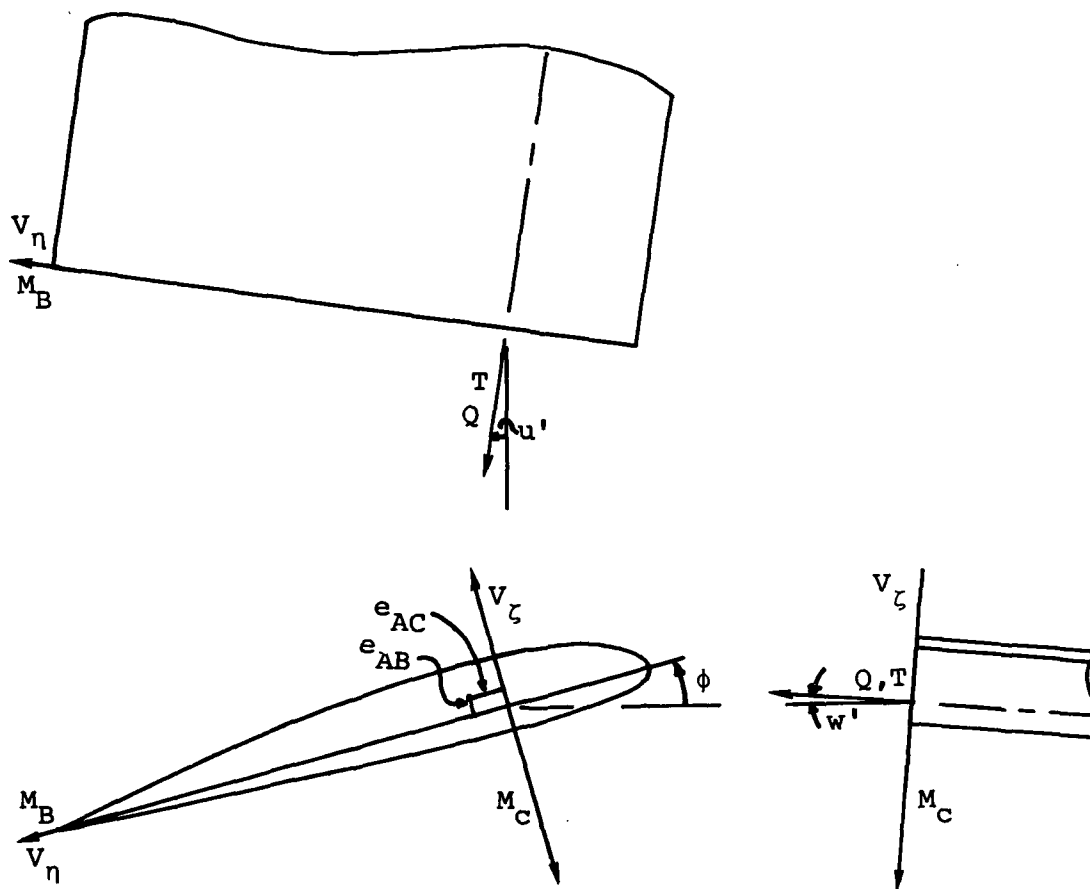


Figure 3. Local Deformed Blade Element System Stress Resultant and Elastic Axis Offset Notation.

The geometrical relationships between bending slopes and deflections are given by definition as

$$\frac{\partial w}{\partial y} = w' \quad (14)$$

and

$$\frac{\partial u}{\partial y} = u' \quad (15)$$

Equations A-67 and A-68 for equilibrium of forces and moments may be written in derivative form as

$$\left. \begin{aligned} \frac{\partial V_x}{\partial y} + F_x &= 0 \\ \frac{\partial V_y}{\partial y} + F_y &= 0 \\ \frac{\partial V_z}{\partial y} + F_z &= 0 \end{aligned} \right\} \quad (16)$$

$$\left. \begin{aligned} \frac{\partial M_x}{\partial y} &= -V_z \left(1 + \frac{\partial v}{\partial y}\right) + V_y \frac{\partial w}{\partial y} - Q_x \\ \frac{\partial M_y}{\partial y} &= -V_x \frac{\partial w}{\partial y} + V_z \frac{\partial u}{\partial y} - Q_y \\ \frac{\partial M_z}{\partial y} &= -V_x \left(1 + \frac{\partial v}{\partial y}\right) + V_y \frac{\partial u}{\partial y} + Q_z \end{aligned} \right\} \quad (17)$$

Equations (10) through (17) contain terms for stress resultants in two different coordinate systems; equations (10) through (13) contain stress resultants in the local deformed blade element system, and equations (16) and (17) contain stress resultants in a local blade element coordinate system. This local blade element coordinate system differs from the blade coordinate system defined in Section 3.2.3 by the rotation about the y-axis, of magnitude θ_s . The equations in this section were developed by transforming equations (10) through (13) to the local blade element system, and solving the differential equations in that system. Equations for the blade reference system were defined by appropriate finite magnitude angular rotation about the y-axis. The local deformed blade element stress resultants are as shown in Figure 3, and the local blade element stress resultants are shown in Figure 4.

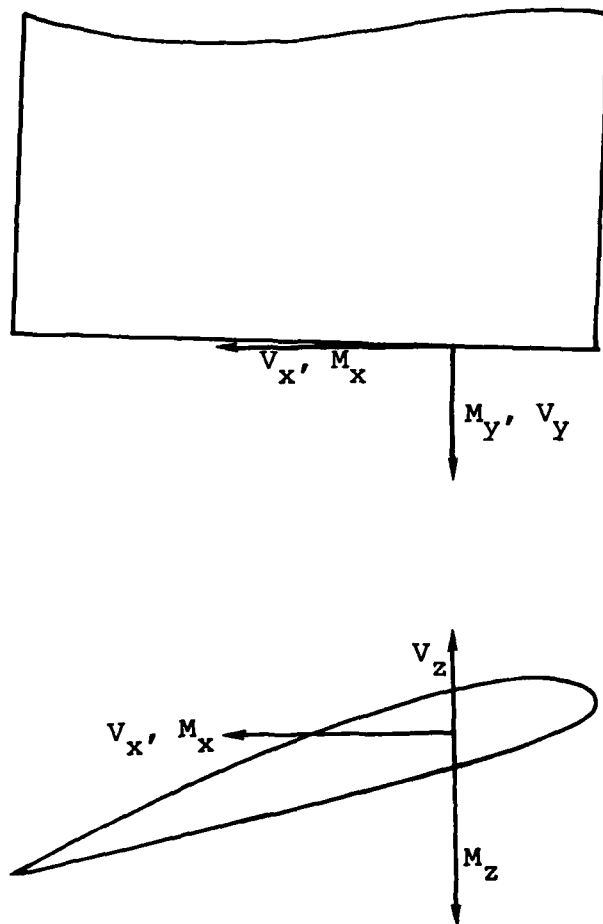


Figure 4. Local Blade Element Stress Resultants.

Elimination of u'' and w'' from Equation (10) by using Equations (11) and (12), and transformation of the stress resultants to the local blade element coordinate system by the transformations

$$\begin{Bmatrix} v_\eta \\ T \\ v_\zeta \end{Bmatrix} = \begin{bmatrix} 1 & -u' & -\phi \\ u' & 1 & +w' \\ \phi & -w' & 1 \end{bmatrix} \begin{Bmatrix} v_x \\ v_y \\ v_z \end{Bmatrix} \quad (18)$$

and

$$\begin{Bmatrix} M_B \\ Q \\ M_C \end{Bmatrix} = \begin{bmatrix} 1 & -u' & \phi \\ u' & 1 & -w' \\ -\phi & w' & 1 \end{bmatrix} \begin{Bmatrix} M_x \\ M_y \\ M_z \end{Bmatrix} \quad (19)$$

leads to the following nonlinear first-order equations

$$\frac{\partial u'}{\partial y} = \frac{1}{EI_C} \left(-\phi M_x + w' M_y + M_z + e_{AC} (u' v_x + v_y + w' v_z) \right) \quad (20)$$

$$\begin{aligned} \frac{\partial v}{\partial y} = & \left(\frac{1}{EA} + \frac{e_{AC}^2}{EI_C} + \frac{e_{AB}^2}{EI_B} \right) (u' v_x + v_y + w' v_z) \\ & + \frac{e_{AB}}{EI_B} (M_x - u' M_y + \phi M_z) \\ & + \frac{e_{AC}}{EI_C} (-\phi M_x + w' M_y + M_z) \end{aligned} \quad (21)$$

$$\frac{\partial w'}{\partial y} = \frac{1}{EI_B} \left(M_x - u' M_y + \phi M_z + e_{AB} (u' v_x + v_y + w' v_z) \right) \quad (22)$$

$$\frac{\partial \phi}{\partial y} = \left(\frac{1}{GJ + (u' v_x + v_y + w' v_z) k_A^2} \right) (u' M_x + M_y - w' M_z) \quad (23)$$

Equations (14) through (16) are linear, and the remaining equations may be linearized by assuming that the unsteady portion of the stress resultants, slopes, and displacements are small with respect to the steady portion, and that product terms involving unsteady portions are negligible. The steady terms are denoted by a bar over the variable. (It is assumed that a solution of the nonlinear steady equations is known; in practice the solution for steady terms may also depend upon linearizations or other approximations). If only first degree terms in the steady stress resultants and slopes are retained, the following equations result

$$\begin{aligned}
 \frac{\partial v}{\partial y} = & \left[\frac{1}{EA} + \frac{e_{AB}^2}{EI_B} + \frac{e_{AC}^2}{EI_C} \right] v_Y + \left[\frac{e_{AB}}{EI_B} \bar{M}_Z - \frac{e_{AC}}{EI_C} \bar{M}_X \right] \phi \\
 & + \left[\frac{e_{AC}}{EI_C} \bar{w}' - \frac{e_{AB}}{EI_B} \bar{u}' \right] M_Y + \left[\left(\frac{1}{EA} + \frac{e_{AB}^2}{EI_B} + \frac{e_{AC}^2}{EI_C} \right) \bar{v}_X \right. \\
 & - \frac{e_{AB}}{EI_B} \bar{M}_Y u' + \left. \left[\frac{e_{AB}}{EI_B} \bar{\phi} + \frac{e_{AC}}{EI_C} \right] M_Z \right. \\
 & + \left[\left(\frac{1}{EA} + \frac{e_{AB}^2}{EI_B} + \frac{e_{AC}^2}{EI_C} \right) \bar{u}' \right] v_X + \left[\frac{e_{AC}}{EI_C} \bar{M}_Y \right. \\
 & + \left. \left(\frac{1}{EA} + \frac{e_{AB}^2}{EI_B} + \frac{e_{AC}^2}{EI_C} \right) \bar{v}_Z w' + \left[\frac{e_{AB}}{EI_B} - \frac{e_{AC}}{EI_C} \bar{\phi} \right] M_X \right. \\
 & + \left. \left[\left(\frac{1}{EA} + \frac{e_{AB}^2}{EI_B} + \frac{e_{AC}^2}{EI_C} \right) \bar{w}' \right] v_Z \right] \quad (24)
 \end{aligned}$$

$$\begin{aligned}
 \frac{\partial u'}{\partial y} = & \left[\frac{e_{AC}}{EI_C} \right] v_Y - \left[\frac{\bar{M}_X}{EI_C} \right] \phi + \left[\frac{w'}{EI_C} \right] M_Y + \left[\frac{e_{AC}}{EI_C} v_X \right] u' \\
 & + \left[\frac{1}{EI_C} \right] M_Z + \left[\frac{e_{AC}}{EI_C} \bar{u}' \right] v_X + \left[\frac{\bar{M}_Y + e_{AC} \bar{v}_Z}{EI_C} \right] w'
 \end{aligned}$$

$$- \left[\frac{\bar{\phi}}{EI_C} \right] M_x + \left[\frac{e_{AC}}{EI_C} w' \right] v_z \quad (25)$$

$$\begin{aligned} \frac{\partial w'}{\partial y} = & \left[\frac{e_{AB}}{EI_B} \right] v_y + \left[\frac{\bar{M}_z}{EI_B} \right] \phi - \left[\frac{\bar{u}'}{EI_B} \right] M_y + \left[\frac{e_{AB} \bar{v}_x - \bar{M}_y}{EI_B} \right] u' \\ & + \left[\frac{\bar{\phi}}{EI_B} \right] M_z + \left[\frac{e_{AB}}{EI_B} \bar{u}' \right] v_x + \left[\frac{e_{AB}}{EI_B} \bar{v}_z \right] w' \\ & + \left[\frac{1}{EI_B} \right] M_x + \left[\frac{e_{AB}}{EI_B} \bar{w}' \right] v_z \end{aligned} \quad (26)$$

$$\begin{aligned} \frac{\partial \phi}{\partial y} = \frac{1}{GJ_T} \left[- \left(\frac{\bar{M}_y k_A^2}{GJ_T} \right) v_y + M_y + \bar{M}_x u' - \bar{w}' M_z \right. \\ \left. - \bar{M}_z w' + \bar{u}' M_x \right] \end{aligned} \quad (27)$$

$$\text{where } GJ_T = GJ + \bar{v}_y k_A^2$$

$$\begin{aligned} \frac{\partial M_x}{\partial y} = & \left[\bar{w}' - \left(\frac{1}{EA} + \frac{e_{AB}^2}{EI_B} + \frac{e_{AC}^2}{EI_C} \right) \bar{v}_z \right] v_y - \left[\frac{e_{AC}}{EI_C} \bar{v}_z \right] M_z + [\bar{v}_y] w' \\ & - \left[\frac{e_{AB}}{EI_B} \bar{v}_z \right] M_x - \left[1 + \left(\frac{1}{EA} + \frac{e_{AB}^2}{EI_B} + \frac{e_{AC}^2}{EI_C} \right) \bar{v}_y \right. \\ & \left. + \frac{e_{AB}}{EI_B} \bar{M}_x + \frac{e_{AC}}{EI_C} \bar{M}_z \right] v_z \end{aligned} \quad (28)$$

$$\frac{\partial M_y}{\partial y} = \bar{v}_z u' + \bar{u}' v_z - \bar{v}_x w' - \bar{w}' v_x \quad (29)$$

$$\begin{aligned}
\frac{\partial M_z}{\partial y} = & \left[\bar{u}' - \left(\frac{1}{EA} + \frac{e_{AB}^2}{EI_B} + \frac{e_{AC}^2}{EI_C} \right) \bar{v}_x \right] v_y - \left[\frac{e_{AC}}{EI_C} \bar{v}_x \right] M_z + \left[\bar{v}_y \right] u' \\
& - \left[\frac{e_{AB}}{EI_B} \bar{v}_x \right] M_x - \left[1 + \left(\frac{1}{EA} + \frac{e_{AB}^2}{EI_B} + \frac{e_{AC}^2}{EI_C} \right) \bar{v}_y \right. \\
& \left. + \frac{e_{AB}}{EI_B} \bar{M}_x + \frac{e_{AC}}{EI_C} \bar{M}_z \right] v_x
\end{aligned} \tag{30}$$

Equations (14) through (16) and (24) through (30) form an (approximate) set of linear first order equations with constant coefficients which may be used to develop a transfer function for an elastic field with noncoincident elastic and neutral axes and with large steady stress resultants and elastic deflections.

Some comments concerning the approximation to Equation (23) by Equation (27) are appropriate, with respect to the denominator term in Equation (23). This factor may be approximated as

$$\begin{aligned}
\frac{1}{GJ + (u'v_x + v_y + w'v_z) k_A^2} &= \left(\frac{1}{GJ + \bar{v}_y k_A^2} \right) \\
&\quad \left(1 - \frac{(u'v_x + \bar{v}_y - w'v_z) k_A^2}{GJ + \bar{v}_y k_A^2} \right)
\end{aligned}$$

where \bar{v}_y is the unsteady part of v_y . This is a first-term approximation to an infinite series expansion. The term $\bar{v}_y k_A^2$ was retained in the denominator since it is always combined with GJ , and so an effective GJ , including this term, may be defined for any rotor, by the user-defined input value of GJ_T . The factor GJ_T is used to remind users that, when not negligible with respect to GJ , the $\bar{v}_y k_A^2$ term must be included. Then, in the evaluation of the product of these terms with the numerator of Equation (23), the only term retained is $(\bar{v}_y k_A^2 / GJ_T) \bar{M}_y$.

Solution of this set of equations by the Cayley-Hamilton Theorem is impractical due to the high degree polynomial which would have to be solved for the characteristics, and other methods for obtaining an exact closed form solution are also impacted by the high amount of coupling between equations. An approximate solution may be obtained by using the infinite series expansion for the transfer matrix [U], in terms of the matrix [A], of the form

$$[U] = e^{[A]} = [I] + [A] + [A]^2/2! + [A]^3/3! + \dots \quad (31)$$

where [A] is defined from the first order differential equations when written in matrix form as

$$\frac{\partial}{\partial y} Z = [D] Z \quad (32)$$

according to

$$[A] = L [D] \quad (33)$$

where L is the section length over which the transfer is performed. It is convenient to define the complete state vector, Z, as

$$Z = \{v \quad v_y \quad \phi \quad M_y \quad u \quad u' \quad M_z \quad v_x \quad w \quad w' \quad M_x \quad v_z\} \quad (34)$$

Note that Z includes the radial displacement and shear which the s_i state vector does not. It is also convenient to write [A] as the sum of two matrices,

$$[A] = [\alpha] + [\delta] \quad (35)$$

where $[\alpha]$ contains no steady stress resultants and slopes except \bar{v}_y , and $[\delta]$ contains only terms involving the other steady stress resultants and steady slopes. Thus, $[\alpha]$ and $[\delta]$ may be written in the forms

and

$$[\delta] = \begin{bmatrix} 0 & 0 & t_5 \bar{M}_z - t_6 \bar{M}_x & t_6 \bar{w}' - t_5 \bar{u}' & 0 & t_2 \bar{V}_x - t_5 \bar{M}_y & t_5 \bar{\phi} & t_2 \bar{u}' & 0 & t_6 \bar{M}_z + t_2 \bar{V}_z & -t_6 \bar{\phi} & +t_2 \bar{w}' \\ 0 & 0 & 0 & 0 & 0 & 0 & 0 & 0 & 0 & 0 & 0 & 0 \\ 0 & t_{10} & 0 & 0 & 0 & t_9 \bar{M}_x & -t_9 \bar{w}' & 0 & 0 & -t_9 \bar{M}_z & t_9 \bar{u}' & 0 \\ 0 & 0 & 0 & 0 & 0 & \bar{V}_z L & 0 & -\bar{w}' L & 0 & -\bar{V}_x L & 0 & \bar{u}' L \\ 0 & 0 & 0 & 0 & 0 & 0 & 0 & 0 & 0 & 0 & 0 & 0 \\ 0 & 0 & -t_8 \bar{M}_x & t_8 \bar{w}' & 0 & t_6 \bar{V}_x & 0 & t_6 \bar{u}' & 0 & t_8 \bar{M}_y + t_6 \bar{V}_z & -t_8 \bar{\phi} & +t_6 \bar{w}' \\ 0 & L \bar{u}' - t_2 \bar{V}_x & 0 & 0 & 0 & 0 & 0 & -t_6 \bar{V}_x & -t_1 & 0 & -t_5 \bar{V}_x & 0 \\ 0 & 0 & 0 & 0 & 0 & 0 & 0 & 0 & 0 & 0 & 0 & 0 \\ 0 & 0 & 0 & 0 & 0 & 0 & 0 & 0 & 0 & 0 & 0 & 0 \\ 0 & 0 & t_7 \bar{M}_z & -t_7 \bar{u}' & 0 & t_5 \bar{V}_x - t_7 \bar{M}_y & t_7 \bar{\phi} & t_5 \bar{u}' & 0 & +t_5 \bar{V}_z & 0 & +t_5 \bar{w}' \\ 0 & L \bar{w}' - t_2 \bar{V}_z & 0 & 0 & 0 & 0 & -t_6 \bar{V}_z & 0 & 0 & 0 & -t_5 \bar{V}_z & -t_1 \\ 0 & 0 & 0 & 0 & 0 & 0 & 0 & 0 & 0 & 0 & 0 & 0 \end{bmatrix} \quad (37)$$

where

$$\begin{aligned}
 t_1 &= t_5 \bar{M}_x + t_6 \bar{M}_x \\
 t_2 &= L \left(\frac{1}{EA} + \frac{e_{AB}^2}{EI_B} + \frac{e_{AC}^2}{EI_C} \right) \\
 t_3 &= t_2/L \\
 t_4 &= L(1 + t_3 \bar{V}_y) \\
 t_5 &= \frac{Le_{AB}}{EI_B} \\
 t_6 &= \frac{Le_{AC}}{EI_C} \\
 t_7 &= L/EI_B \\
 t_8 &= L/EI_C \\
 t_9 &= L/GJ_T \\
 t_{10} &= t_9 (\bar{M}_y k_A^2 / GJ_T) \\
 GJ_T &= GJ + \bar{V}_y k_A^2
 \end{aligned}
 \tag{38}$$

Substitution of Equation (30) into Equation (26) yeilds

$$[U] = [I] + [\alpha] + [\delta] + \left\{ [\alpha]^2 + 2[\alpha][\delta] + [\delta]^2 \right\} / 2! + \dots$$

which may also be written as

$$\begin{aligned}
 [U] &= e^{[A]} = e^{[\alpha] + [\delta]} = e^{[\alpha]} e^{[\delta]} \\
 &= \{ [I] + [\alpha] + [\alpha]^2/2! + \dots \} \\
 &\quad \{ [I] + [\delta] + [\delta]^2/2! + \dots \}
 \end{aligned}
 \tag{39}$$

Now for a transfer function which performs a transfer in the opposite direction as the (+) y-axis, the basic transfer function, [u] is given by

$$\begin{aligned}
 [u] &= e^{-[D]L} = e^{-[A]} = [I] - [A] + [A]^2/2! \\
 &\quad - [A]^3/3! + \dots
 \end{aligned}
 \tag{40}$$

which, in terms of $[\alpha]$ and $[\delta]$, may be written as

$$[u] = [I] - [\alpha] - [\delta] + \{[\alpha]^2 + [\alpha][\delta] + [\delta][\alpha] + [\delta]^2\} / 2! - \dots \quad (41)$$

The portion of $[u]$ which is independent of $[\delta]$ then may be written as $[\hat{U}]$.

The first few terms dependent upon $[\delta]$ plus $[\hat{U}]$, yield $[\hat{u}]$, where

$$[\hat{u}] = [\hat{U}] - [\delta] + \{[\alpha][\delta] + [\delta][\alpha]\} / 2! \quad (42)$$

Then for a system which has an offset with magnitudes s_C and s_B in the x-direction and z-direction, respectively, with no flexibility in the offset and with a cancelling offset at the other end, the transfer including the offsets may be written in the form

$$[V] = [R]^{-1} [\hat{u}] [R] \quad (43)$$

where $[R]$ is a rigid offset transfer matrix, given by

$$[R] = \begin{bmatrix} 1 & 0 & 0 & 0 & 0 & -s_C & 0 & 0 & 0 & -s_B & 0 & 0 \\ 0 & 1 & 0 & 0 & 0 & 0 & 0 & 0 & 0 & 0 & 0 & 0 \\ 0 & 0 & 1 & 0 & 0 & 0 & 0 & 0 & 0 & 0 & 0 & 0 \\ 0 & 0 & 0 & 1 & 0 & 0 & 0 & -s_B & 0 & 0 & 0 & s_C \\ 0 & 0 & s_B & 0 & 1 & 0 & 0 & 0 & 0 & 0 & 0 & 0 \\ 0 & 0 & 0 & 0 & 0 & 1 & 0 & 0 & 0 & 0 & 0 & 0 \\ 0 & s_C & 0 & 0 & 0 & 0 & 1 & 0 & 0 & 0 & 0 & 0 \\ 0 & 0 & 0 & 0 & 0 & 0 & 0 & 1 & 0 & 0 & 0 & 0 \\ 0 & 0 & -s_C & 0 & 0 & 0 & 0 & 0 & 1 & 0 & 0 & 0 \\ 0 & 0 & 0 & 0 & 0 & 0 & 0 & 0 & 0 & 1 & 0 & 0 \\ 0 & s_B & 0 & 0 & 0 & 0 & 0 & 0 & 0 & 0 & 1 & 0 \\ 0 & 0 & 0 & 0 & 0 & 0 & 0 & 0 & 0 & 0 & 0 & 1 \end{bmatrix} \quad (44)$$

If this transfer function, $[V]$, is subpartitioned as 4x4 submatrices and written as

$$[V] = \begin{bmatrix} v_1^1 & v_1^2 & v_1^3 \\ v_2^1 & v_2^2 & v_2^3 \\ v_3^1 & v_3^2 & v_3^3 \end{bmatrix} \quad (45)$$

then the final transformation, which accounts for the angle between the local blade element principal elastic axes and the reference pitch change axis, to give the total elastic field transfer matrix, $[U]$, is given by

$$[U] = [\theta]^{-1}[V][\theta] \quad (46)$$

with $[\theta]$ in subpartitioned form given by

$$[\theta] = \begin{bmatrix} I & O & O \\ O & C & -S \\ O & S & C \end{bmatrix} \quad (47)$$

where $C = \cos\theta [I]$

$S = \sin\theta [I]$

θ is + for positive rotation about the y_b axis from PCA to local blade element system, and $[I]$ is a unit matrix,

Then

$$[U] = \begin{bmatrix} v_1^1 & C_1 v_1^2 + S_1 v_1^3 & C_1 v_1^3 - S_1 v_1^2 \\ C_1 v_2^1 + S_1 v_3^1 & C_2 v_2^2 + C_1 S_1 (v_2^3 + v_3^2) + S_2 v_3^3 & C_2 v_2^3 + C_1 S_1 (v_3^3 - v_2^2) - S_2 v_3^2 \\ C_1 v_3^1 - S_1 v_2^1 & C_2 v_3^2 + C_1 S_1 (v_3^3 - v_2^2) - S_2 v_2^3 & C_2 v_3^3 - C_1 S_1 (v_2^3 + v_3^2) + S_2 v_2^2 \end{bmatrix} \quad (48)$$

The transformations which account for the shear center offset and the angle between the local blade element system and the pitch change axis system have the same form for transfer from outboard-to-inboard as for transfers from inboard-to-outboard. Since the transformation from the local blade element system, lbe, to the pitch change axis system are given by

$$\begin{aligned}\bar{Z}_{PCA} &= [\theta]^{-1} [R]^{-1} \bar{Z}_{lbe} \\ (\text{or } \bar{Z}_{lbe} &= [\theta][R] \bar{Z}_{PCA})\end{aligned}\quad (49)$$

and all barred quantities above are in the lbe system, the final expressions require that the appropriate transformations be made, as given by

$$\begin{aligned}\bar{u}'_{lbe} &= C_1 \bar{u}'_{PCA} - S_1 \bar{w}'_{PCA} \\ \bar{w}'_{lbe} &= C_1 \bar{w}'_{PCA} + S_1 \bar{u}'_{PCA} \\ \bar{v}_{x_{lbe}} &= C_1 \bar{v}_{x_{PCA}} - S_1 \bar{v}_{z_{PCA}} \\ \bar{v}_{z_{lbe}} &= C_1 \bar{v}_{z_{PCA}} + S_1 \bar{v}_{x_{PCA}} \\ \bar{M}_{y_{lbe}} &= \bar{M}_{y_{PCA}} - s_B \bar{v}_{x_{PCA}} + s_C \bar{v}_{z_{PCA}} \\ \bar{M}_{x_{lbe}} &= C_1 (\bar{M}_{x_{PCA}} + s_B \bar{v}_{y_{PCA}}) + S_1 (\bar{M}_{z_{PCA}} + s_C \bar{v}_{y_{PCA}}) \\ \bar{M}_{z_{lbe}} &= C_1 (\bar{M}_{z_{PCA}} + s_C \bar{v}_{y_{PCA}}) - S_1 (\bar{M}_{x_{PCA}} + s_B \bar{v}_{y_{PCA}})\end{aligned}\quad (50)$$

After completing the transformation to the pitch change axis system, and with some rearranging of terms, the elastic field transformation for outboard-to-inboard transfer (and for shear center offset and pitch angle misalignment) is given by the equations of Figure 5. This figure then defines the final transfer function for an elastic element, f_i .

Additional Symbols

$$s_x = C_1 s_c + S_1 s_B$$

$$s_z = C_1 s_B - S_1 s_c$$

$$t_x = S_1 t_5 + C_1 t_6$$

$$t_z = C_1 t_5 - S_1 t_6$$

$$\gamma_C^2 = \bar{v}_Y L t_8$$

$$\gamma_B^2 = \bar{v}_Y L t_7$$

$$C_{1B} = \cosh \gamma_B$$

$$C_{1C} = \cosh \gamma_C$$

$$S_{1B} = \frac{\sinh \gamma_B}{\gamma_B}$$

$$S_{1C} = \frac{\sinh \gamma_C}{\gamma_C}$$

$$C_{2B} = \frac{C_{1B} - 1}{\gamma_B^2}$$

$$C_{2C} = \frac{C_{1C} - 1}{\gamma_C^2}$$

$$S_{2B} = \frac{S_{1B} - 1}{\gamma_B^2}$$

$$S_{2C} = \frac{S_{1C} - 1}{\gamma_C^2}$$

Figure 5. Flexibility Transfer Functions
for DNAM05.

$$B_B = \frac{L}{GA_{VB}} - L t_4 t_7 S_{2B}$$

$$B_C = \frac{L}{GA_{VC}} - L t_4 t_8 S_{2C}$$

where

GA_{VB} = effective shear stiffness in the beamwise direction

GA_{VC} = effective shear stiffness in the chordwise direction

$$A_1 = C_2 t_8 + S_2 t_7$$

$$A_2 = C_2 t_7 + S_2 t_8$$

$$A_3 = C_1 S_1 (t_7 - t_8)$$

Transfer Functions

$$\begin{aligned} \phi_j = & \phi_{i+1} - \left(\frac{L}{GJ_T} \right) M_{y_{i+1}} \\ & - \frac{L}{GJ_T} \left[\bar{v}_y s_B + \bar{m}_x + \frac{L}{2} \left(\bar{v}_y \bar{w}' - \bar{v}_z \right) \right] u'_{i+1} \\ & + \frac{L}{GJ_T} \left\{ \bar{w}' + \frac{1}{2} \left[A_1 (\bar{m}_x + \bar{v}_y s_B) - A_3 (\bar{m}_z + \bar{v}_y s_C) \right] \right\} M_{z_{i+1}} \\ & + \frac{L}{GJ_T} \left[s_z + \frac{t_2 \bar{v}_y}{2} \bar{w}' \right] v_{x_{i+1}} \\ & + \frac{L}{GJ_T} \left[\bar{v}_y s_C + \bar{m}_z + \frac{L}{2} (\bar{v}_y \bar{u}' - \bar{v}_x) \right] w'_{i+1} + \frac{L}{GJ_T} \left\{ -\bar{u}' \right. \\ & \left. - \frac{1}{2} \left[A_2 (\bar{m}_z + \bar{v}_y s_C) - A_3 (\bar{m}_x + \bar{v}_y s_B) \right] \right\} M_{x_{i+1}} \\ & - \frac{L}{GJ_T} \left(s_x + \frac{t_2 \bar{v}_y}{2} \bar{u}' \right) v_{z_{i+1}} \end{aligned}$$

Figure 5. Continued

$$\begin{aligned}
M_{Yj} &= M_{Yi+1} - (L\bar{V}_Z) u'_{i+1} \\
&+ \frac{L}{2} \left[A_1 \bar{V}_Z - A_3 \bar{V}_X \right] M_{Zi+1} \\
&+ (L\bar{w}') V_{Xi+1} + (L\bar{V}_X) w'_{i+1} \\
&- \frac{L}{2} \left[A_2 \bar{V}_X - A_3 \bar{V}_Z \right] M_{Xi+1} \\
&- (L\bar{u}') V_{Zi+1}
\end{aligned}$$

$$V_{Xj} = V_{Xi+1}$$

$$V_{Zj} = V_{Zi+1}$$

$$\begin{aligned}
u_j &= -\frac{L}{2} \left[A_1 (\bar{M}_X + \bar{V}_Y s_B) - A_3 (\bar{M}_Z + \bar{V}_Y s_C) \right] \phi_{i+1} \\
&+ \left\{ \frac{L}{GJ_T} s_Z + \frac{L}{2} [A_1 \bar{w}' - A_3 \bar{u}'] \right\} M_{Yi+1} + u_{i+1} \\
&+ \left\{ -L (C_2 s_{1C} + s_2 s_{1B}) + \frac{L}{GJ_T} s_Z (\bar{M}_X + s_B \bar{V}_Y) \right. \\
&- \frac{L}{2} A_3 (\bar{M}_Y + s_C \bar{V}_Z - s_B \bar{V}_X) \\
&+ \left. \frac{L^2}{2GJ_T} s_Z (\bar{V}_Y \bar{w}' - \bar{V}_Z) + \frac{L}{2} t_X \bar{V}_X \right\} u'_{i+1} \\
&+ L(C_2 t_8 C_{2C} + s_2 t_7 C_{2B}) + \left[\frac{L}{2} A_3 \right] \bar{\phi}
\end{aligned}$$

Figure 5. Continued.

$$\begin{aligned}
& - \left(\frac{L}{GJ_T} s_z \right) \bar{w}' - \frac{L}{2GJ_T} s_z [A_1 (\bar{M}_x + \bar{V}_y s_B) \\
& - A_3 (\bar{M}_z + \bar{V}_y s_C)] \} M_{z_{i+1}} \\
& + \left\{ - (C_2 B_C + s_2 B_B) - \frac{L}{GJ_T} s_z^2 \right. \\
& - \frac{L}{2} s_z [A_1 + \frac{L}{GJ_T} t_3 \bar{V}_y] \bar{w}' \\
& + \frac{L}{2} [s_z A_3 + t_x] \bar{u}' \} V_{x_{i+1}} \\
& + \left\{ L C_1 s_1 (s_{1C} - s_{1B}) - \frac{L^2}{2GJ_T} A_3 (\bar{V}_y \bar{u}' - \bar{V}_x) \right. \\
& + \frac{L}{2} A_1 (\bar{M}_y + s_C \bar{V}_z - s_B \bar{V}_x) \\
& - \frac{L}{GJ_T} s_z (\bar{M}_z + s_C \bar{V}_y) - \frac{L}{2} t_x \bar{V}_z \} w'_{i+1} \\
& + \{ L C_1 s_1 (t_7 C_{2B} - t_8 C_{2C}) \\
& - \frac{L}{2} A_1 \bar{\phi} + \left(\frac{L s_z}{GJ_T} \right) \bar{u}' \\
& + \frac{L s_z}{2GJ_T} [- A_3 (\bar{M}_x + \bar{V}_y s_B) + A_2 (\bar{M}_z + \bar{V}_y s_C)] \} M_{x_{i+1}} \\
& + \left\{ C_1 s_1 (B_C - B_B) + \frac{L s_x s_z}{GJ_T} + \frac{L}{2} [- A_3 s_x + \frac{t_3 \bar{V}_y s_z}{GJ_T}] \right. \\
& \left. \bar{u}' + \frac{L}{2} [t_x + s_x A_1] \bar{w}' \right\} V_{z_{i+1}}
\end{aligned}$$

Figure 5. Continued.

$$\begin{aligned}
u'_j = & \left\{ \bar{v}_y [s_B A_1 - s_C A_3] + (A_1 \bar{m}_x - A_3 \bar{m}_z) \right\} \phi_{i+1} \\
& + \left\{ \frac{\bar{v}_y L}{2GJ_T} [s_B A_1 - s_C A_3] - A_1 \left(\bar{w}' + \frac{L}{2GJ_T} \bar{m}_x \right) \right. \\
& + \left. A_3 \left(\bar{u}' + \frac{L}{2GJ_T} \bar{m}_z \right) \right\} M_{Y_{i+1}} \\
& + \left\{ C_2 C_{1C} + S_2 C_{1B} + A_3 \left(\bar{m}_y + \frac{\bar{v}_y L}{2} \bar{\phi} \right) \right. \\
& - \left. [t_x + s_B A_3] \bar{v}_x + s_C A_3 \bar{v}_z \right\} u'_{i+1} \\
& + \left\{ -(C_2 t_8 S_{1C} + S_2 t_7 S_{1B}) - A_3 \bar{\phi} \right\} M_{Z_{i+1}} \\
& + \left\{ -L(1 + t_3 \bar{v}_y) (C_2 t_8 C_{2C} + S_2 t_7 C_{2B}) \right. \\
& + \frac{\bar{v}_y}{2} [-A_1 (s_B t_z + s_C t_x) + \frac{L s_z}{GJ_T} (s_B A_1 - s_C A_1)] \\
& - \left[\frac{L(1 + t_3 \bar{v}_y)}{2} A_3 \right] \bar{\phi} - [t_x + s_z A_3] \bar{u}' \\
& + s_z A_1 \bar{w}' + \frac{1}{2} \left(\frac{L s_z}{GJ_T} - t_z \right) A_1 \bar{m}_x
\end{aligned}$$

Figure 5. Continued.

$$\begin{aligned}
& + \frac{1}{2} \left[-t_x A_1 - \frac{Ls_z}{GJ_T} A_3 \right] \bar{M}_z \left\{ v_{x_{i+1}} \right. \\
& + \left\{ C_1 S_1 (C_{1B} - C_{1C}) - A_1 \left(\frac{\bar{v}_Y L}{2} \bar{\phi} + \bar{M}_Y - s_B \bar{v}_x \right) \right. \\
& - \left. \left[t_x + s_C A_1 \right] \bar{v}_z \right\} w'_{i+1} \\
& + \left\{ C_1 S_1 (t_8 s_{1C} - t_7 s_{1B}) + A_1 \bar{\phi} \right. \\
& + \frac{1}{2} (t_7 t_8) (\bar{M}_Y - s_B \bar{v}_x + s_C \bar{v}_z) \\
& + \frac{1}{2} \left[-(C_1 t_5 t_8 - s_1 t_6 t_7) \bar{v}_x + (C_1 t_6 t_7 + s_1 t_5 t_8) \bar{v}_z \right] \left\{ M_{x_{i+1}} \right. \\
& + \left\{ L C_1 S_1 (1 + t_3 \bar{v}_Y) (t_8 C_{2C} - t_7 C_{2B}) \right. \\
& + \frac{\bar{v}_Y}{2} \left[-A_3 \left(s_B t_z + s_C t_x - \frac{Ls_x s_C}{GJ_T} \right) \right. \\
& - \left(\frac{Ls_x}{GJ_T} \right) s_B A_1 + \frac{1}{2} L (1 + t_3 \bar{v}_Y) A_1 \left. \right] \bar{\phi} \\
& + A_3 s_x \bar{u}' - \left[t_x + A_1 s_x \right] \bar{w}' \\
& + \frac{1}{2} \left[-t_z A_3 - \frac{Ls_x}{GJ_T} A_1 \right] \bar{M}_x \\
& + \frac{1}{2} \left[\left(t_x - \frac{Ls_x}{GJ_T} \right) A_3 \right] \bar{M}_z \left\{ v_{z_{i+1}} \right.
\end{aligned}$$

Figure 5. Continued.

$$\begin{aligned}
M_{z_j} = & - \frac{\bar{V}_Y L}{2} \left\{ \bar{V}_Y [A_1 s_B - s_C A_3] - A_1 \bar{M}_X - A_3 \bar{M}_Z \right\} \phi_{i+1} \\
& + \frac{\bar{V}_Y L}{2} \left\{ -A_3 \bar{u}' + A_1 \bar{w}' \right\} M_{y_{i+1}} \\
& - \bar{V}_Y L \left\{ (C_2 s_{1C} + s_2 s_{1B}) \right. \\
& + \frac{A_3}{2} (\bar{M}_Y - s_B \bar{V}_X + s_C \bar{V}_Z) \left. \right\} u'_{i+1} \\
& + \left\{ C_2 C_{1C} + s_2 C_{1B} + \frac{\bar{V}_Y L}{2} [A_3 \bar{\phi} + t_X \bar{V}_X] \right\} M_{z_{i+1}} \\
& + \left\{ L(1 + t_3 \bar{V}_Y)(C_2 s_{1C} + s_2 s_{1B}) + \bar{V}_Y [s_B t_Z + s_C t_X] \right. \\
& + \frac{\bar{V}_Y L}{2} \left[(t_X + A_3 s_Z) \bar{u}' - s_Z A_1 \bar{w}' \right] \\
& + t_Z \bar{M}_X + t_X \bar{M}_Z + \frac{L}{2} t_X \bar{V}_X \left. \right\} v_{x_{i+1}} \\
& + \bar{V}_Y L \left\{ C_1 s_1 (s_{1C} - s_{1B}) + \frac{1}{2} (-t_Z \bar{V}_X + t_X \bar{V}_Z) \right. \\
& + \frac{1}{2} A_1 (\bar{M}_Y - s_B \bar{V}_X + s_C \bar{V}_Z) \left. \right\} w'_{i+1}
\end{aligned}$$

Figure 5. Continued.

$$\begin{aligned}
& + \left\{ c_1 s_1 (c_{1B} - c_{1C}) - \frac{\bar{v}_y L}{2} A_2 \bar{\phi} + t_z \bar{v}_x \right\} M_{x_{i+1}} \\
& + \left\{ L(1 + t_3 \bar{v}_y) c_1 s_1 (s_{1B} - s_{1C}) + \frac{\bar{v}_y L}{2} \left[-s_x A_3 \bar{u}' \right. \right. \\
& + \left. \left. (t_x + A_1 s_x) \bar{w}' \right] + \left(\frac{L t_z}{2} \right) \bar{v}_x \right\} v_{z_{i+1}} \\
w_j = & \frac{L}{2} \left\{ -A_3 (\bar{M}_x + \bar{v}_y s_B) + A_2 (\bar{M}_z + \bar{v}_y s_C) \right\} \phi_{i+1} \\
& + \left\{ -\frac{L}{GJ_T} s_x - \frac{L}{2} \left[A_2 \bar{u}' - A_3 \bar{w}' \right] \right\} M_{y_{i+1}} \\
& + \left\{ L c_1 s_1 (s_{1C} - s_{1B}) - \frac{\bar{v}_y L s_B s_x}{GJ_T} - \left(\frac{\bar{v}_y L^2 s_x}{2GJ_T} \right) \bar{w}' \right. \\
& + \frac{L}{2} A_2 \bar{M}_y - (t_9 s_x) \bar{M}_x + \frac{L}{2} \left[t_z + s_B A_2 \right] \bar{v}_x \\
& + \left. \frac{L}{2} \left[\frac{L s_x}{GJ_T} - s_C A_2 \right] \bar{v}_z \right\} u'_{i+1} \\
& + \left\{ L c_1 s_1 (t_7 c_{2B} - t_8 c_{2C}) \right.
\end{aligned}$$

Figure 5. Continued.

$$\begin{aligned}
& + \frac{L}{2} A_2 \bar{\phi} + \frac{L s_x}{G J_T} \bar{w}' \\
& + \frac{L s_x}{2 G J_T} \left[A_1 (\bar{M}_x + \bar{V}_y s_B) - A_3 (\bar{M}_z + \bar{V}_y s_C) \right] \left\{ M_{z_{i+1}} \right. \\
& + C_1 s_1 (B_C - B_B) + \frac{L}{G J_T} \left[(C_2 - s_2) s_B s_C + C_1 s_1 (s_B^2 - s_C^2) \right] \\
& + \frac{L}{2} \left[t_z - s_z A_2 \right] \bar{u}' \\
& + \frac{1}{2} \left[- L s_z A_3 + \frac{t_3 \bar{V}_y L s_x}{G J_T} \right] \bar{w}' \left\{ V_{x_{i+1}} + w_{i+1} \right. \\
& + \left\{ -L(C_2 s_{1B} + s_2 s_{1C}) + \frac{\bar{V}_y L s_x s_C}{G J_T} \right. \\
& + \frac{L s_x}{2 G J_T} (L \bar{V}_y \bar{u}' + 2 \bar{M}_z - L \bar{V}_x) \\
& + \frac{L}{2} A_3 (\bar{M}_y - s_B \bar{V}_x + s_C \bar{V}_z) + \frac{L t_2}{2} \bar{V}_z \left\{ w'_{i+1} \right. \\
& + \left\{ L(C_2 t_7 C_{2B} + s_2 t_8 C_{2C}) \right. \\
& - \frac{\bar{V}_y L s_x}{2 G J_T} \left[s_C A_2 - s_B A_3 \right]
\end{aligned}$$

Figure 5. Continued.

$$\begin{aligned}
& - \frac{A_3}{2} (L\bar{\phi} + \frac{Ls_x}{GJ_T} \bar{M}_x) \\
& - \frac{L}{GJ_T} s_x \left[\bar{u}' + \frac{1}{2} A_2 \right] \left\{ M_{x_{i+1}} \right. \\
& + \left\{ -(C_2 B_B + s_2 B_C) - \frac{Ls_x^2}{GJ_T} \right. \\
& + \frac{1}{2} \left[-s_x L A_2 + \frac{t_3 \bar{V}_Y L}{GJ_T} \right] \bar{u}' \\
& + \frac{L}{2} \left[t_z + A_3 s_x \right] \bar{w}' \left. \right\} V_{z_{i+1}} \\
w_j' = & \left\{ -\bar{V}_Y \left[s_C A_2 - A_3 s_B \right] + A_3 \bar{M}_x - A_2 \bar{M}_z \right\} \phi_{i+1} \\
& + \left\{ A_2 \left[\bar{u}' + \frac{L}{2GJ_T} (\bar{M}_z + \bar{V}_Y s_C) \right] \right. \\
& - A_3 \left[\bar{w}' + \frac{L}{2GJ_T} (\bar{M}_x + \bar{V}_Y s_B) \right] \left. \right\} M_{y_{i+1}} \\
& + \left\{ c_1 s_1 (c_{1B} - c_{1C}) + A_2 \left(\frac{\bar{V}_Y L}{2} \bar{\phi} \right. \right. \\
& + \bar{M}_Y - s_B \bar{V}_X + s_C \bar{V}_Z \left. \right) - t_z \bar{V}_X \left. \right\} u'_{i+1} \\
& + c_1 s_1 (t_8 s_{1C} - t_7 s_{1B}) - A_2 \bar{\phi} \\
& - \frac{1}{2} t_7 t_8 (\bar{M}_Y - s_B \bar{V}_X + s_C \bar{V}_Z)
\end{aligned}$$

Figure 5. Continued.

$$\begin{aligned}
& + \frac{1}{2} \left[(C_1 t_5 t_8 - s_1 t_6 t_7) \bar{V}_x - (C_1 t_6 t_7 + s_1 t_5 t_8) \bar{V}_z \right] \} M_{z_{i+1}} \\
& + \left\{ L(1 + t_3 \bar{V}_y) C_1 S_1 (t_8 C_{2C} - t_7 C_{2B}) \right. \\
& - \frac{\bar{V}_y}{2} \left[\frac{L s_z}{GJ_T} (s_C A_2 - s_B A_3) + A_3 (s_B t_z + s_C t_x) \right] \\
& - \frac{L(1 + t_3 \bar{V}_y)}{2} A_2 \bar{\phi} - [t_z - s_z A_2] \bar{u}' \\
& + s_z A_3 \left(\bar{w}' + \frac{L}{2GJ_T} \bar{M}_x \right) \\
& - \frac{t_z}{2} A_3 \bar{M}_x + \frac{1}{2} \left[-\frac{L s_z}{GJ_T} A_2 - t_x A_3 \right] \bar{M}_z \} V_{x_{i+1}} \\
& + \left\{ C_2 C_{1B} + S_2 C_{1C} - A_3 \left(\frac{\bar{V}_y L}{2} \bar{\phi} + \bar{M}_y - s_B \bar{V}_x + s_C \bar{V}_z \right) \right. \\
& - t_z \bar{V}_z \} w'_{i+1} \\
& + \left\{ -(C_2 t_7 s_{1B} + S_2 t_8 s_{1C}) + A_3 \bar{\phi} \right\} M_{x_{i+1}} \\
& + \left\{ -L(1 + t_3 \bar{V}_y) (C_2 t_7 C_{2B} + S_2 t_8 C_{2C}) \right. \\
& + \frac{\bar{V}_y}{2} \left[\frac{L s_x}{GJ_T} (s_C A_2 - s_B A_3) \right. \\
& - (C_2 t_7 + S_2 t_8) (s_B t_z + s_C t_x) \left. \right] \\
& + L(1 + t_3 \bar{V}_y) A_3 \bar{\phi}
\end{aligned}$$

Figure 5. Continued

$$\begin{aligned}
& + A_2 \left[s_x \bar{u}' - \frac{t_z}{2} \bar{M}_x + \frac{1}{2} \left(\frac{L s_x}{G J_T} - t_x \right) \bar{M}_z \right] \\
& + s_x A_3 \left[-\bar{w}' - \frac{L}{2 G J_T} \bar{M}_x \right] - t_z \bar{w}' \left\{ v_{z_{i+1}} \right. \\
M_{x_j} = & \frac{\bar{v}_y L}{2} \left\{ A_2 (\bar{v}_y s_C + \bar{M}_z) \right. \\
& - A_3 (\bar{v}_y s_B + \bar{M}_x) \left. \right\} \bar{\phi}_{i+1} \\
& - \frac{\bar{v}_y L}{2} \left\{ A_2 \bar{u}' - A_3 \bar{w}' \right\} M_{y_{i+1}} \\
& + \frac{\bar{v}_y L}{2} \left\{ 2 L C_1 s_1 (s_{1C} - s_{1B}) - A_2 (\bar{M}_y - s_B \bar{v}_x + s_C \bar{v}_z) \right. \\
& + t_z \bar{v}_x - t_x \bar{v}_z \left. \right\} u'_{i+1} \\
& + \left\{ C_1 s_1 (C_{1B} - C_{1C}) + \frac{\bar{v}_y L}{2} A_2 \bar{\phi} + t_x \bar{v}_z \right\} M_{z_{i+1}} \\
& + \left\{ L(1 + t_3 \bar{v}_y) C_1 s_1 (s_{1B} - s_{1C}) \right. \\
& + \frac{\bar{v}_y L}{2} \left[(t_z + s_z A_2) \bar{u}' - s_z A_3 \bar{w}' \right] \\
& + \left(\frac{L(1 + t_3 \bar{v}_y) t_x}{2} \right) \bar{v}_z \left\{ v_{x_{i+1}} + \bar{v}_y L \left\{ (C_2 s_{1B} + s_2 s_{1C}) \right. \right.
\end{aligned}$$

Figure 5. Continued.

$$\begin{aligned}
& + \frac{1}{2} A_3 (\bar{M}_Y - s_B \bar{V}_X + s_C \bar{V}_Z) \Big\} w'_{i+1} \\
& + \left\{ C_2 C_{1B} + s_2 C_{1C} - \frac{\bar{V}_Y L}{2} A_3 \bar{\phi} + t_z \bar{V}_Z \right\} M_{x_{i+1}} \\
& + \left\{ L(1 + t_3 \bar{V}_Y)(C_2 s_{1B} + s_2 s_{1C}) + \bar{V}_Y (s_B t_z + s_C t_B) \right. \\
& - \frac{\bar{V}_Y L s_X}{2} A_2 \bar{u}' + \frac{\bar{V}_Y L}{2} [t_z + s_X A_3] \bar{w}' + t_z \bar{M}_X + t_X \bar{M}_Z \\
& \left. + \frac{L(1 + t_3 \bar{V}_Y)}{2} t_z \bar{V}_Z \right\} v_{z_{i+1}}
\end{aligned}$$

Figure 5. Concluded

The m_i and f_i operations are in fact separated within the computer program, so this development is essentially complete. It should be noted that for the natural frequency calculation all of the purely steady effects are deleted.

In the application of the state-vector/transfer function technique, five separate state vectors are assumed at the blade tip. Then the m_i and f_i functions are applied sequentially into the center of rotation for an assumed vibration frequency, ω . At the center of rotation, five boundary conditions are always known. Either slopes, moments, or displacements are zero for various hub types. Using the equations for the known boundary conditions and the five functions for blade tip conditions, a set of five equations in five unknowns may be written. When ω is a natural frequency of the system, all of the boundary conditions are satisfied, and the determinant of the five equations goes to zero. Locating the correct values of ω is a numerical analysis problem which will not be dealt with here. When a zero determinant is found, DNAM05 assumes there is a unit out-of-plane deflection at the blade tip and uses this fact to solve for the weighting factors on the other tip conditions for calculation of the blade mode shapes. The term "mode shapes" is here defined to include the distributions of shears and moments as well as the blade deflections. The problem of creating rotor modes from the calculated blade modes will be discussed in Section 3.2.11.

In addition to the beam elements modeled in DNAM05, there are three other types of transfer functions which need to be understood. These are the hub impedance model, the pitch horn model, and the blade hinge model.

The hub impedance model is used to include the effects of an isotropic support system in the blade modes. For collective modes, out-of-plane motion is restrained by one input spring constant and one input mass, and inplane slope changes are opposed by a torsion spring. For cyclic modes, the inplane motion is restrained by one input spring and one input mass. The boundary conditions for these cases are then modified so that a known boundary condition for the impedance is satisfied rather than the boundary conditions at the center of rotation. The boundary conditions for all modes are shown in Table 1.

The torsional boundary condition for all modes is

$$\phi = 0 \text{ at the center of rotation.}$$

TABLE 1. BLADE BOUNDARY CONDITIONS IN DNAM05.

<u>Mode Type</u>	<u>Out-of-Plane Boundary Condition</u>	<u>Inplane Boundary Condition</u>
Collective	$w' = 0$ $w = \frac{V_z}{\frac{20 * 10^6}{R * VSOFT} - \omega^2} \frac{VMASS * NB}{386.4}$	$M_z = -u' * TORSO * 10^6$ $u = 0$
Cyclic	$M_x = k_\beta w'$ $w = 0$	$u' = 0$ $u = \frac{V_x}{\frac{20 * 10^6}{R * HSOFT} - \omega^2} \frac{HMASS * NB}{386.4}$
Scissor (Reactionless)	$w' = 0$ $w = 0$	$u' = 0$ $u = 0$

In the boundary conditions in Table 1,

VSOFT is the out-of-plane restraint elasticity

VMASS is the effective hub mass in the out-of-plane direction, per blade

HSOFT is the inplane restraint elasticity

HMASS is the effective hub mass in the inplane direction, per blade

TORSO is the effective spring rate of the mast/engine system in inch-pounds per radian

NB is the number of blades

R is the blade radius in inches

and k_{β} is the blade flapping spring constant per blade.

Also let

k_{op} = the apparent spring rate of the out-of-plane support system in pounds per inch

M_{op} = the apparent mass of the out-of-plane support system in pounds mass

k_{ip} = the apparent spring rate of the inplane support system as seen in the rotating coordinate system in pounds per inch

M_{ip} = the apparent mass of the inplane support system as seen in the rotating coordinate system in pounds mass

then the inputs to DNAM05 for the hub impedance are

$$\left. \begin{aligned} VSOFT &= \frac{20 * 10^6}{R * k_{op}} \\ VMASS &= \frac{M_{op}}{NB} \\ HSOFT &= \frac{20 * 10^6}{R * k_{ip}} \\ HMASS &= \frac{M_{ip}}{NB} \end{aligned} \right\} \quad (51)$$

The pitch horn model used in DNAM05 is shown schematically in Figure 6. The pitch horn is attached at the blade station J. The pitch horn runs from point J to c to b and the control system is represented by the spring, K, from b to a. The pitch horn is assumed to be rigid. The net transfer functions from J to a or b are

$$\left. \begin{aligned} z_a &= z_J + \phi_J d_c - w_J' d_b - V_{zJ}/K \\ M_{yb} &= M_{yJ} - V_{zJ} d_c \\ M_{xb} &= M_{xJ} + V_{zJ} d_b \end{aligned} \right\} \quad (52)$$

The boundary condition at points a and b are known because a is a fixed point and b is a pin joint.

$$\left. \begin{aligned} z_a &= 0 \\ M_{yb} &= 0 \\ M_{xb} &= 0 \end{aligned} \right\} \quad (53)$$

When these boundary conditions are applied to Equation (52), the transfer functions may be solved for the shear and moments which are applied to the blade by the pitch horn in terms of the angles and displacements.

$$\left. \begin{aligned} V_{zJ} &= K(z_J + \phi_J d_c - w_J' d_b) \\ M_{yJ} &= V_{zJ} d_c \\ M_{xJ} &= -V_{zJ} d_b \end{aligned} \right\} \quad (54)$$

These are not the total shear and moment values. They are simply increments which must be added to the shear and moments already carried by the blade. Note that K is a linear spring rate in pounds per inch. The equivalent torsional spring, which is input to DNAM05, is

$$CK = K d_c^2 \quad (55)$$

If very large values of CK or K are used, the equations above may lead to numerical instabilities. However, no problems have been experienced using realistic values or even 10 times a realistic value.

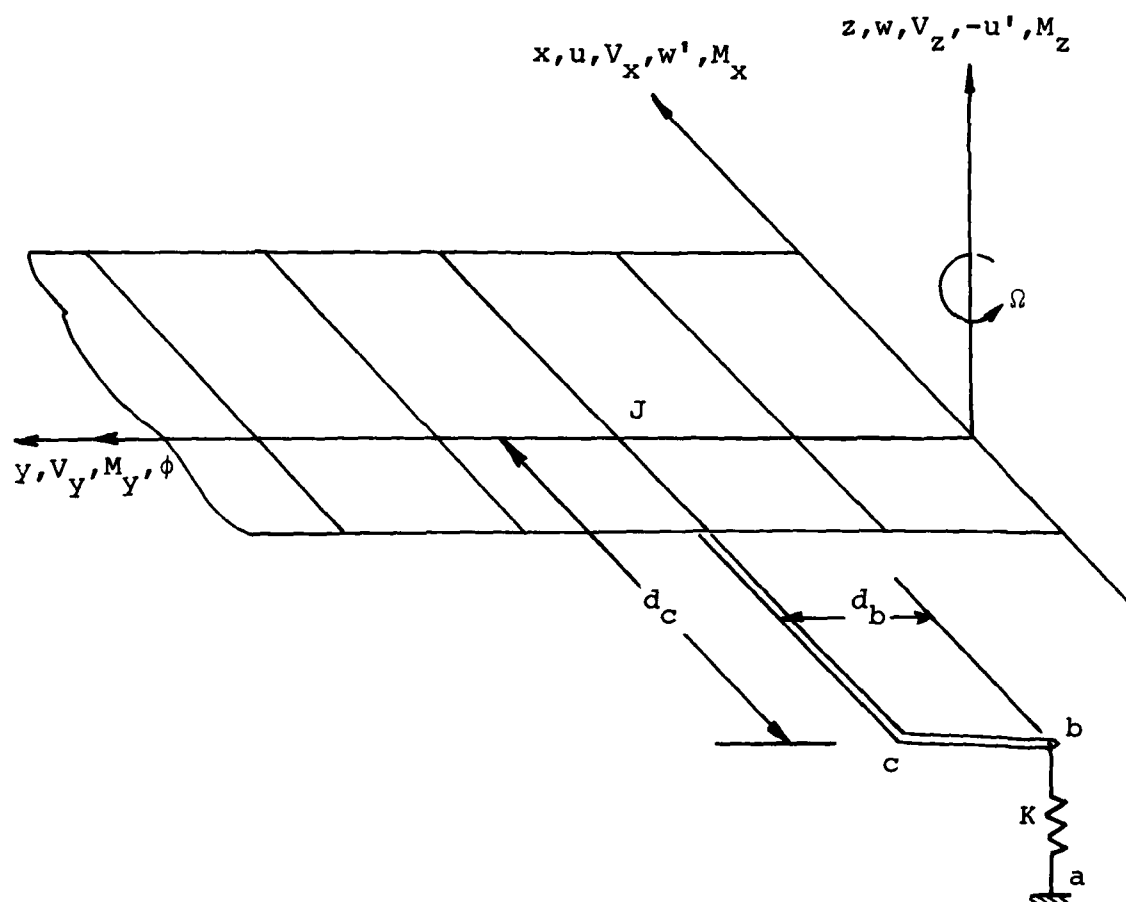


Figure 6. Pitch-Horn and Control System Model for DNAM05.

Three separate hinge angles are allowed in DNAM05 to provide for pitch-flap coupling, pitch-lag coupling, and flap-lag coupling. A hinge is modeled in the program if the user inputs a zero stiffness either beamwise or chordwise. The hinge model has very low resistance for angular motion due to applied moments and very high resistance to other types of motion. This provides a very good model of a hinge located at the outboard end of the selected segment. When a hinge is skewed with respect to its usual orientation, two additional steps are added to the transfer process from tip to root. At the outboard end of the segment a coordinate transformation through the skew angle is made for the variables affected. The usual transfer equations are applied to find the state at the inboard end of the segment, and then the reverse coordinate transformation is used to get all variables aligned with the blade coordinate system.

A schematic of a skewed flapping hinge is shown in Figure 7. The angle, γ , shown will give leading-edge-down pitch with up flapping. Looking at the top sketch in Figure 8, it is easy to write the transformation from the blade axis to the hinge axis. The out-of-plane slope and moment as well as the twist and twisting moment are modified.

$$\left. \begin{aligned} \phi_h &= w' \sin \gamma + \phi \cos \gamma \\ w'_h &= w' \cos \gamma - \phi \sin \gamma \\ M_{yh} &= M_x \sin \gamma + M_y \cos \gamma \\ M_{xh} &= M_x \sin \gamma - M_y \cos \gamma \end{aligned} \right\} \quad (56)$$

Note that pitch-flap coupling and pitch-cone coupling may also arise from the pitch horn geometry and blade bending. For the lag hinge the α_1 and α_3 rotations are performed in that sequence. The sequence may only be of interest for large values of α_1 or α_3 . The α_1 rotation couples out-of-plane slopes to inplane slopes.

$$\left. \begin{aligned} w'_h &= w' \cos \alpha_1 - u' \sin \alpha_1 \\ u'_h &= w' \sin \alpha_1 + u' \cos \alpha_1 \\ M_{xh} &= M_x \cos \alpha_1 + M_z \sin \alpha_1 \\ M_{zh} &= -M_x \sin \alpha_1 + M_z \cos \alpha_1 \end{aligned} \right\} \quad (57)$$

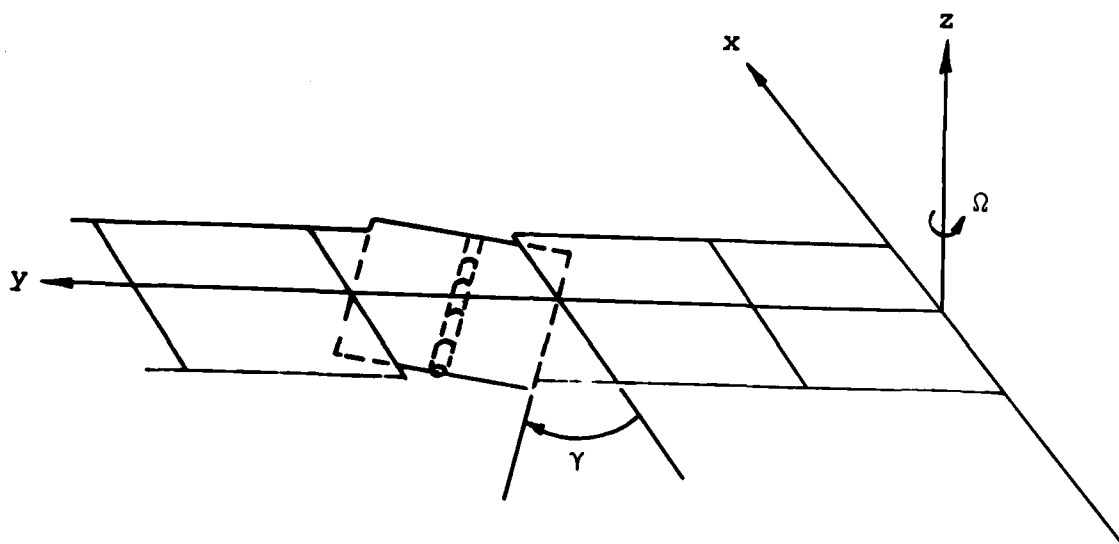


Figure 7. Schematic of Skewed Flapping Hinge Leading to Pitch-Flap Coupling.

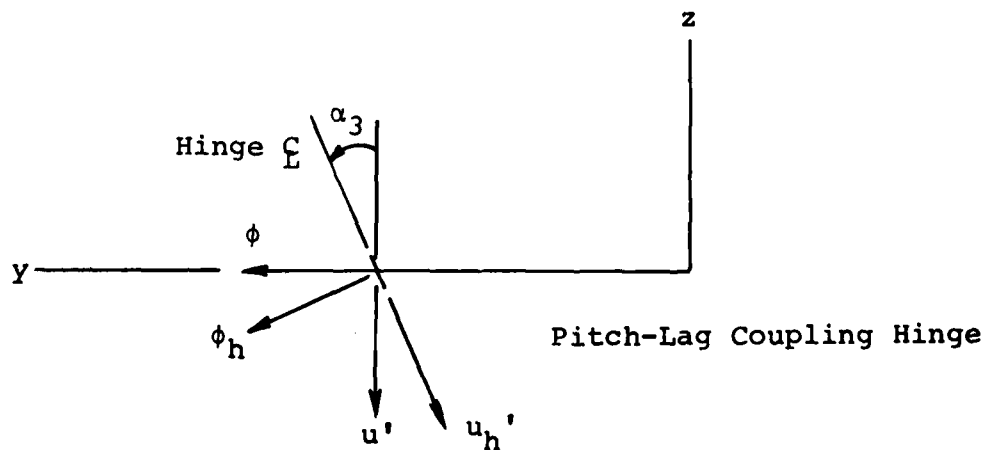
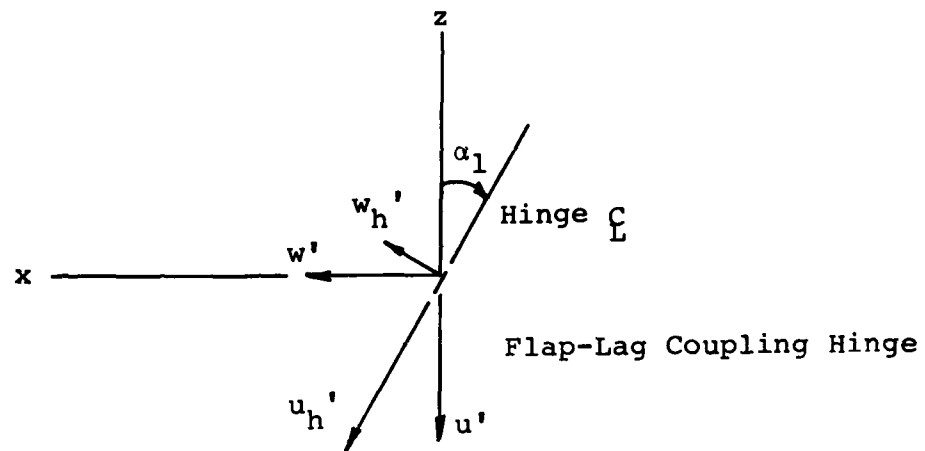
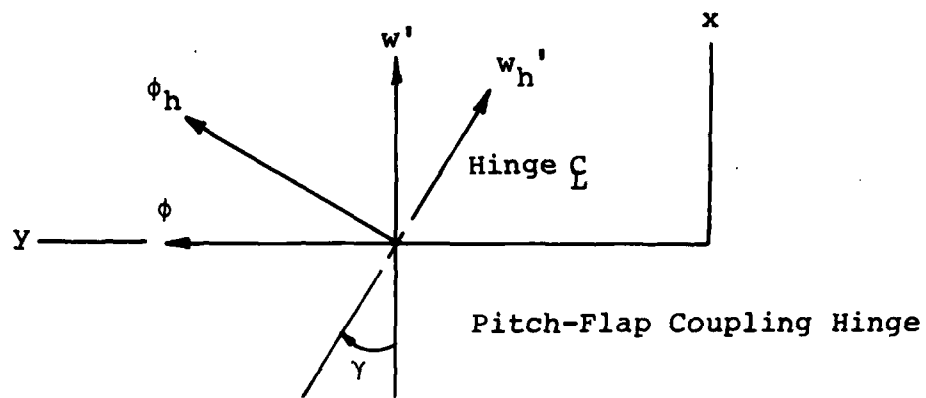


Figure 8. Kinematic Coupling Through Skewed Hinges.

The α_3 rotation couples twisting motion to the inplane slope.

$$\left. \begin{aligned} u'_h &= -\phi \sin \alpha_3 + u' \cos \alpha_3 \\ \phi_h &= \phi \cos \alpha_3 + u' \sin \alpha_3 \\ M_{zh} &= M_z \cos \alpha_3 + M_y \sin \alpha_3 \\ M_{yh} &= -M_z \sin \alpha_3 + M_y \cos \alpha_3 \end{aligned} \right\} \quad (58)$$

All of the elastic terms and the linear inertial terms in the differential equations are then used in the calculation of the rotor blade natural frequencies and mode shapes. The additional inertia terms included in C81 and those neglected will be discussed in Section 3.2.6.

3.2.5 Application of Modal Technique

The Rotorcraft Flight Simulation Program C81 includes a time-variant aeroelastic rotor representation based on the modal technique with the provision that the blade natural frequencies, mode shapes, and associated coefficients will be supplied as input data. It is important to note that any assumptions made in the derivation and the calculation of the mode shapes will be applicable to the entire analysis. For this reason it is advisable to use modes in C81 which were obtained from DNAM05, since the two programs have been developed to be compatible.

To implement the modal technique in the computer program, the following assumptions have been made:

- (1) The blade is divided into the same radial segments for both aerodynamic and dynamic calculations.
- (2) Each of the segment faces has three degrees of freedom: out-of-plane (w), inplane (u), and angular orientation of the chordline about the y axis (ϕ).
- (3) The user will supply the normal modes that describe u , w , and ϕ for each of the segment faces for each mode (obtainable from DNAM05).
- (4) Linear interpolation can be used to define the mode shapes between the two adjacent faces.
- (5) The maximum number of segments per blade is 20.
- (6) The maximum number of blades per rotor is seven.

(7) The maximum number of input modes per rotor is 11 with a total limit of 12 modes between the two rotors.

(8) The maximum number of rotors is two.

As indicated, the program is structured to handle fully coupled mode shapes, which means that all of the linear terms which couple out-of-plane, inplane, and torsional motion must be included in the calculation of the modes as they are in DNAM05.

The mode shapes have several important attributes:

- (1) Each one is a solution to the coupled differential equations of free vibration of the total system, obtained by deleting all velocity-dependent and all nonlinear terms.
- (2) Associated with each mode there is a natural frequency, ω_n .
- (3) Each mode shape must satisfy a set of physical boundary conditions that could exist on the blade.
- (4) The collection of mode shapes forms an orthogonal set of functions.

This set of attributes makes possible the modal method of structural analysis. The boundary conditions are a function of the hub type and must describe the physical constraints for the inplane, out-of-plane, and torsional behavior at the hub. To simplify the discussion, all modes will be arbitrarily labeled either cyclic, collective, or scissor. These definitions and the selection of blade mode type are discussed in more detail in Section 3.2.10.

Oette (Reference 7) shows how the separation-of-variables technique can be applied to the H&B equations; the same applies to the equations developed in Appendix A. If the independent variables are time, t , and radial location along the blade, y , then it is possible to write

$$\begin{pmatrix} u(y,t) \\ w(y,t) \\ \phi(y,t) \end{pmatrix} = \sum_{n=1}^{NM} \begin{pmatrix} u_n(y) \\ w_n(y) \\ \phi_n(y) \end{pmatrix} \delta_n(t) \quad (59)$$

where u , w , and ϕ are the total elastic deformation of the blade which vary with both y and t ; u_n , w_n , and ϕ_n are the components of the n th mode shape which are only functions of y ; and δ_n is the participation factor or generalized coordinate for the n th mode which is only a function of time. If we also let

F_u = the externally applied inplane force

F_w = the externally applied out-of-plane force

M_ϕ = the externally applied twisting moment

Oette demonstrates that

$$\ddot{\delta}_n + \omega_n^2 \delta_n = \frac{\int_0^R (F_u u_n + F_w w_n + M_\phi \phi_n) dy}{I_n} \quad (60)$$

where

I_n is the generalized inertia of the n th mode.

For small amounts of viscous damping, ζ_n , Equation (60) can be written

$$\ddot{\delta}_n + 2 \zeta_n \omega_n \dot{\delta}_n + \omega_n^2 \delta_n = \frac{F_n}{I_n} \quad (61)$$

⁷Oette, H., BERECHNUNG DER SCHLAGBIEGE-, SCHWENKBIEGE-UND TORSIONSSCHWINGUNGEN VON ROTORBLÄTTERN MIT GEKOPPELTEN EIGENFORMEN UND - FREQUENZEN, Deutsche Luft-und Raumfahrt, DLR - Forschungsbericht 71-108, 1971.

where F_n is shown in Equation (60). There will be an equation of the above type for each mode included in the response analysis. The set of modal equations is sufficient to describe the time-variant aeroelastic response of a rotor blade because: (a) the linear effects of the blade's mass, elastic, and geometric properties are included in the natural frequencies and mode shapes, and (b) the aerodynamic and aeroelastic effects are included in F_n . As indicated by Oette, dynamics terms which were deleted from the calculation of the blade natural frequencies and mode shapes should be included in F_n . This refers to terms arising from the angular rates and accelerations of the rotor reference system, the linear accelerations of the rotor hub, and such nonlinear terms as the Coriolis accelerations.

The generalized inertia, I_n , is one of the primary characteristics of a blade mode, so it has been made an input to C81 along with the mode shape and frequency. The generalized inertia definition found in Oette includes the effect of a chordwise offset of the center of gravity, e_{mC} . When the effect of a beamwise offset of the center of gravity, e_{mB} , is also included, the following expression is found

$$I_n = \int_0^R \{ m[u_n^2 + w_n^2 - 2 u_n \phi_n (e_{mC} \sin \theta_p + e_{mB} \cos \theta_p) - 2 w_n \phi_n (e_{mC} \cos \theta_p - e_{mB} \sin \theta_p)] + [I_{\eta\eta} + I_{\xi\xi}] \phi_n^2 \} dx \quad (62)$$

where

θ_p is the local blade geometric pitch and the other θ_p variables are as defined in Appendix A.

The term F_n is described as the virtual work done by all of the externally applied aerodynamic forces and inertia forces, if these forces were to act through a virtual displacement equal to the input mode shapes. It is convenient to write F_n as separate sums of aerodynamic terms and inertial terms.ⁿ

$$\begin{aligned}
 F_u &= A_u + I_u \\
 F_w &= A_w + I_w \\
 M_\phi &= A_\phi + I_\phi
 \end{aligned}
 \quad \left. \vphantom{\begin{aligned} F_u &= A_u + I_u \\ F_w &= A_w + I_w \\ M_\phi &= A_\phi + I_\phi \end{aligned}} \right\} \quad (63)$$

where

A_u , A_w , and A_ϕ are the results of the aerodynamic loading which is defined in Section 3.4.

I_u , I_w , and I_ϕ are the result of the inertial loading, and externally applied mechanical forces produced by the precone effect, the flapping spring, the flapping stop, and the lead-lag damper.

The total velocity or acceleration of some station along the blade (within the blade coordinate system) is frequently required in the analysis. These are simply obtained by differentiating Equation (59) with respect to time.

$$\begin{aligned}
 \dot{u}(y,t) &= \sum_{i=1}^{NM} u_n(y) \dot{\delta}_n(t) \\
 \dot{w}(y,t) &= \sum_{i=1}^{NM} w_n(y) \dot{\delta}_n(t) \\
 \dot{\phi}(y,t) &= \sum_{i=1}^{NM} \phi_n(y) \dot{\delta}_n(t)
 \end{aligned}
 \quad \left. \vphantom{\begin{aligned} \dot{u}(y,t) &= \sum_{i=1}^{NM} u_n(y) \dot{\delta}_n(t) \\ \dot{w}(y,t) &= \sum_{i=1}^{NM} w_n(y) \dot{\delta}_n(t) \\ \dot{\phi}(y,t) &= \sum_{i=1}^{NM} \phi_n(y) \dot{\delta}_n(t) \end{aligned}} \right\} \quad (64)$$

$$\begin{aligned}
 \ddot{u}(y,t) &= \sum_{i=1}^{NM} u_n(y) \ddot{\delta}_n(t) \\
 \ddot{w}(y,t) &= \sum_{n=1}^{NM} w_n(y) \ddot{\delta}_n(t) \\
 \ddot{\phi}(y,t) &= \sum_{i=1}^{NM} \phi_n(y) \ddot{\delta}_n(t)
 \end{aligned}
 \quad \left. \vphantom{\begin{aligned} \ddot{u}(y,t) &= \sum_{i=1}^{NM} u_n(y) \ddot{\delta}_n(t) \\ \ddot{w}(y,t) &= \sum_{n=1}^{NM} w_n(y) \ddot{\delta}_n(t) \\ \ddot{\phi}(y,t) &= \sum_{i=1}^{NM} \phi_n(y) \ddot{\delta}_n(t) \end{aligned}} \right\} \quad (65)$$

3.2.6 Rotor Inertia Loads Included in C81

For a completely exhaustive analysis, all of the terms shown in Equations (A-58) through (A-66) should be included. However, many of these terms are not necessary to obtain a reasonably accurate simulation. The terms are grouped in the following categories:

- (1) Included in the calculation of the blade natural frequencies and modes;
- (2) Included in the externally applied forcing function; or
- (3) Assumed to be small in comparison with other terms present and thus neglected.

In connection with the third category, two points should be kept in mind. First, there is no point including a term which has a 2-percent effect when the input data are not known to within 5 percent. Second, the terms which may be negligible on the rotor designs of today may be important for future designs.

A large number of the terms in all of the inertia force equations are a function of the cg offsets. Historically, these have been rather small effects and have been neglected in C81. In recent years, it was found that the cg offsets on newer rotor designs had a significant effect on frequency placement and mode shape coupling. In view of this, the steady and nonlinear effects of the cg offsets have been included in C81. The cg offsets are included with the mass and mode shape data punched out by DNAM05 for input to C81 to ensure that a consistent set of data is used.

One type of inertia loading that has been neglected in C81 is the discrete out-of-plane and inplane moments, Q_z and Q_x . Those terms not included in the natural frequency analysis are assumed to be small in comparison to the moments arising from the applied forces. It is also assumed that the product of any blade displacement and a fuselage rate is small compared to the other terms. Equations (A-58), (A-59), (A-60), and (A-65) are then reduced to the following form:

$$\begin{aligned}
I_u = F_x &= -m[\ddot{R}_{bx} - 2 \Omega_{bz} \dot{v} - \dot{\Omega}_{bz} y + 2 \Omega_{by} \dot{w} \\
&\quad - u(\Omega_{by}^2 + \Omega_{bz}^2) + y \Omega_{by} \Omega_{bx} + w \Omega_{bx} \Omega_{bz} + \dot{\Omega}_{by} w \\
&\quad - e_x(\dot{\phi}^2 + \Omega_{by}^2 + \Omega_{bz}^2 + 2 \Omega_{by} \dot{\phi}) \\
&\quad - e_z(\Omega_{bx} \Omega_{bz} + \dot{\Omega}_{by})] \\
F_y &= -m[\ddot{R}_{by} + 2 \Omega_{bz} \dot{u} + w \Omega_{by} \Omega_{bz} + u \dot{\Omega}_{bz} \\
&\quad - y(\Omega_{bx}^2 + \Omega_{bz}^2) - 2 \Omega_{bx} \dot{w} + e_x(\dot{\Omega}_{bz} + \Omega_{by} \Omega_{bx} \\
&\quad + u' \{\Omega_{bz}^2 + \Omega_{bx}^2\}) + e_z(\Omega_{by} \Omega_{bz} + w' \{\Omega_{bz}^2 + \Omega_{bx}^2\} \\
&\quad + 2 \Omega_{bz} \dot{\phi} - \dot{\Omega}_{bx})] \\
I_w = F_z &= -m[\ddot{R}_{bz} + y(\Omega_{by} \Omega_{bz} + \dot{\Omega}_{bx}) - u(\dot{\Omega}_{by} - \Omega_{bx} \Omega_{bz}) \\
&\quad - w(\Omega_{bx}^2 + \Omega_{by}^2) + 2 \Omega_{bx} \dot{v} - 2 \Omega_{by} \dot{u} + e_x(\dot{\Omega}_{by} + \Omega_{bx} \Omega_{bz}) \\
&\quad - e_z(\dot{\phi}^2 + \Omega_{bx}^2 + \Omega_{by}^2)] \\
I_\phi = Q_y &= m[e_x(\ddot{R}_{bz} - u\{\dot{\Omega}_{by} - \Omega_{bx} \Omega_{bz}\} + y\{\Omega_{by} \Omega_{bz} + \dot{\Omega}_{bx}\} \\
&\quad - w\{\Omega_{by}^2 + \Omega_{bx}^2\} + e_z(\ddot{R}_{bx} - u\{\Omega_{by}^2 + \Omega_{bz}^2\} + y \Omega_{by} \Omega_{bx} \\
&\quad + w \Omega_{bx} \Omega_{bz})) - \dot{\Omega}_{by} (I_{\eta\eta} + I_{\zeta\zeta}) - (\Omega_{bz}^2 - \Omega_{bx}^2) \\
&\quad (\{I_{\eta\eta} - I_{\zeta\zeta}\} \sin \theta \cos \theta - I_{\eta\zeta} \cos 2\theta) \\
&\quad + \Omega_{bx} \Omega_{bz} (\{I_{\eta\eta} - I_{\zeta\zeta}\} \cos 2\theta + 2I_{\eta\zeta} \sin 2\theta)
\end{aligned} \tag{66}$$

It should be noted that the displacements and slopes at the feathering bearings are included in the mode shape inputs so that the values of u , u' , w , w' , etc., may be calculated relative to the blade reference system as called for by the development in Appendix A.

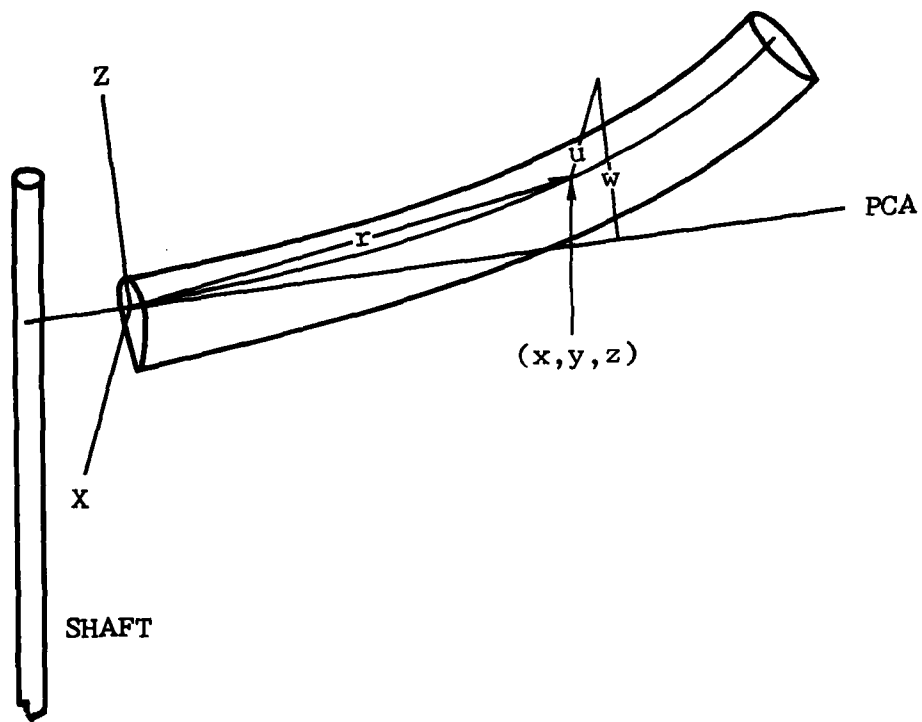


Figure 9. Calculation of Coriolis Acceleration.

Note also that some of the terms shown in Equations (66) were previously included in the equations for the frequency analysis. For these terms a difference is calculated in C81 between the current instantaneous value and the reference value used for the calculation of the modes.

Without explanation it will be stated that one nonlinear term in the strain equation arising in the torsional moment due to the change in direction of the beamwise and chordwise moments has been retained. In Reference 8, Mil gives some insight into the occurrence of this term. He also concluded that this term is quite small in all cases, which agrees with the experience in C81. Nevertheless, the term has been included and is of the form

$$\bar{Q} = \frac{dQ}{dy} = -M_B u'' + M_C w'' \quad (67)$$

The bending moments are calculated using the input bending moment coefficients and the second derivatives are approximated by numerically differentiating the displacement functions.

The treatment of the Coriolis force appearing in the F_x equation of Equations (66) should be dealt with in some detail. It is assumed that the blade is inextensible, but a term involving \dot{v} has been included. This is because geometric considerations can cause significant variations in \dot{v} even though v itself is small. Large forces can then be generated when \dot{v} is multiplied by $2 \Omega_{bz}$. To understand the geometry involved, refer to Figure 9 where

$$r^2 = x^2 + y^2 + z^2 \quad (68)$$

for the blade station shown. It is assumed that the primary source of the Coriolis force is from the first out-of-plane and first inplane modes so that r may be treated as a constant. Substituting the geometric and elastic displacements of the point, Equation 68 becomes

$$r^2 = (u)^2 + (y + v)^2 + (w)^2 \quad (69)$$

Equation (69) can be differentiated with respect to time and then solved for \dot{v} to give the net acceleration term.

*Mil, M. L., et al., HELICOPTERS: CALCULATION AND DESIGN, NASA TTF-494, 1967.

$$-2 \Omega_{bz} \dot{v} = \frac{2 \Omega_{bz} [(u) \dot{u} + (w) \dot{w}]}{y} \quad (70)$$

This term is usually referred to as the Coriolis acceleration. The location of the axis of constant rotational speed has a significant effect on the Coriolis acceleration term. If the inertia of the rotor is large in comparison to the mast stiffness, and the rotor is free to flap, then the axis of constant rpm will be perpendicular to the tip path plane. Also, if any mast bending takes place it tends to move the axis of constant rpm so as to relieve the Coriolis loads. These conditions are approximated by removing the rigid blade component, if any, from w and \dot{w} prior to calculating the Coriolis term. It has been found that improved correlation is obtained when a hingeless rotor is treated as a gimbaled rotor with the mast bending stiffness acting as a flapping spring. This was true even for a very stiff mast.

It should be pointed out that the terms in Q_y are not duplications of terms in the frequency analysis because the cyclic feathering is not present in the frequency analysis, and the propeller moment due to geometric pitch setting is a "steady" term, not an elastic one. The F_y equation was included in Equation (66) because, even though the blade is inextensible, these changes in centrifugal force are felt at the center of rotation as net shears which force the pylon equations. See Section 3.3 for the complete discussion.

3.2.7 Preload Due to Precone, Prelag and Pitch Change Axis Offsets

The vibratory portion of the effects of precone, prelag, and pitch change axis offset are included in the DNAM05 analysis. The effects of the steady centrifugal force acting through these angles and offsets must be considered as a steady external force to the modal equations. These effects are calculated as a part of the inertia loads represented by Equations (66).

3.2.8 Flapping Springs, Flapping Stops, and Lead-Lag Dampers

Some rotor configurations can be equipped with hardware that generates mechanical forces which must be considered in an elastic rotor analysis. Among these items are flapping springs, flapping stops, and lead-lag dampers. To consider the first two items, refer to Figures 10 and 11. The following variables are defined:

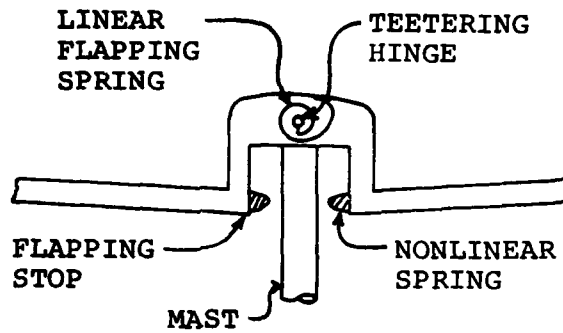


Figure 10. Schematic Diagram of Flapping Springs and Stops.

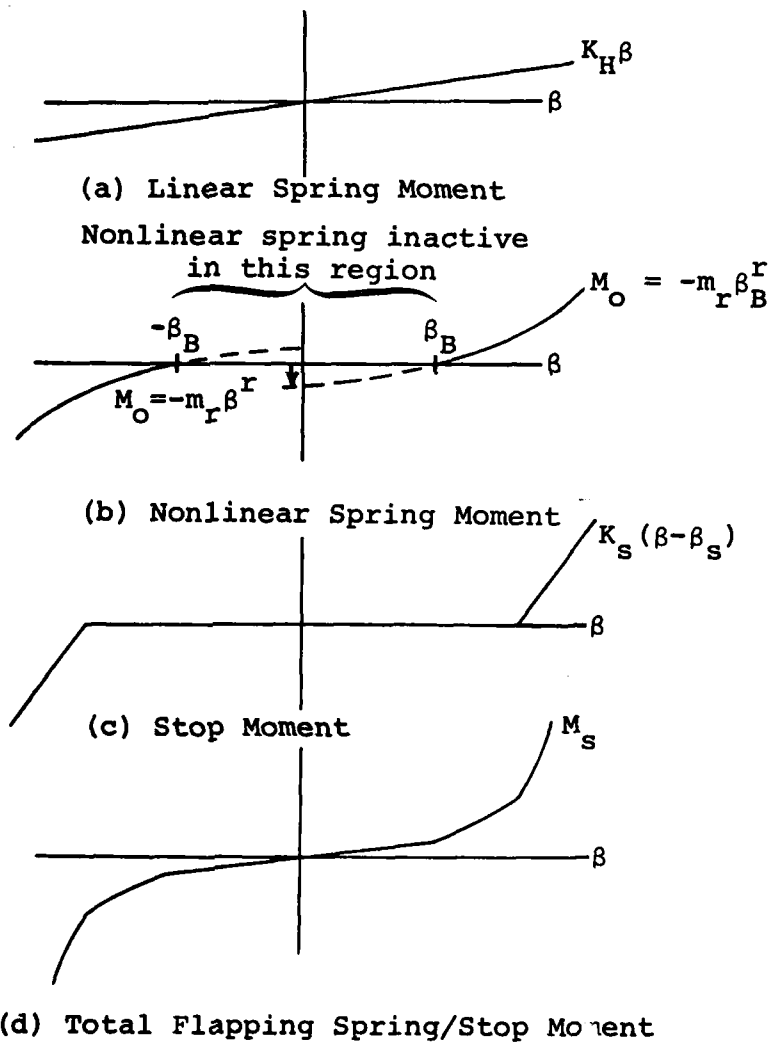


Figure 11. Flapping Moment Functions for Springs and Stops.

β = blade root flapping angle - defined by a straight line through the displaced positions of the inboard two blade stations and the z_h axis.

β_n = slope w' at the hub for the n th mode

M_s = moment transmitted to the top of the mast by flapping springs and flapping stops

K_H = linear flapping spring rate (for teetering or gimbaled rotor)

m_r = nonlinear flapping spring coefficient

r = order of spring nonlinearity - need not be an integer

β_B = flapping angle where nonlinearity begins

$M_O = -m_r \beta_B^r$

K_s = linear spring rate of the flapping stop

β_s = value of β where blade contacts the flapping stops

Figure 10 shows one possible arrangement which would have all three types of flapping springs. The linear spring represents a hub restraint used to provide control power at all flight conditions. The nonlinear spring with some clearance may represent a soft flapping stop. Then the flapping stop spring would be the hard flapping limit. The curves in Figure 11 show how each of these flapping restraints contribute to M_s .

The moment from the linear flapping spring is

$$M_H = K_H \beta \quad (71)$$

The moment contribution from the nonlinear flapping spring is zero as long as the magnitude of β is less than β_B . For larger values

$$M_r = M_O + m_r \beta^r \quad \text{for } |\beta| > \beta_B \quad (72)$$

The moment from the flapping stops is also zero as long as the flapping is less than the limiting value, β_s .

$$M_{STOP} = K_s (\beta - \beta_s) \quad \text{for } |\beta| > \beta_s \quad (73)$$

The net hub restraint moment, M_s , is then the sum of M_H , M_r , and M_{STOP} . Note that all spring rates are input on a per blade basis. Also consider that the nonlinear spring and the flapping stops are symmetrical models with the up-stop and down-stop clearances being equal.

Figure 11(d) is a plot of M_s based on Equations (71), (72), and (73). The same moment is used to calculate the effect of the spring or stops on the rotor modes. An increment ΔF_n is added to the forcing function F_n ,

$$\Delta F_n = -M_s \beta_n \quad (74)$$

Note that because the equations for flapping springs and stops are a function of the flapping angle at the center of rotation, these representations only apply to gimbaled or teetering rotors.

Lead-lag springs, k_L , and dampers, C_L , are treated as angular restraints operating on a total lag angle and velocity, u_h' and \dot{u}_h' , determined from the modal participation factors and an input lag angle for each mode at the hinge location, u_n' .

A schematic of this arrangement is shown in Figure 12. The net angular displacement and velocity are given by

$$u_h' = \sum_{n=1}^{NM} \delta_n(t) u_n' \quad (75)$$

$$\dot{u}_h' = \sum_{i=1}^{NM} \dot{\delta}_n(t) u_n' \quad (76)$$

The angle times the spring rate and the velocity times the damping rate produce additional moments at the hinge point. These moments are multiplied by the lag angle component of each mode to give an increment to the forcing function ΔF_n ,

$$\Delta F_n = u_n' [C_L \dot{u}_h' + k_L u_h'] \quad (77)$$

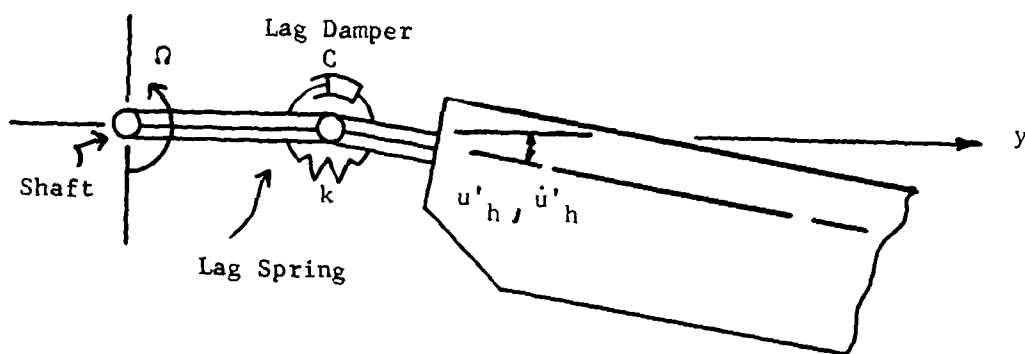


Figure 12. Schematic of Lag Hinge with Spring and Damper.

3.2.9 Rotor Bending Moments

Each normal mode of the rotor has associated with it characteristic distributions of shear and bending moment. These characteristics are just as much a part of the mode shape as the displacement functions that are normally called the mode shape. These shear and moment coefficients may be combined in the same way that the displacement functions are. Let

$VBM(y,t)$ = total out-of-plane bending moment at station y at time t

$CVBM_n(y)$ = coefficient for out-of-plane bending moment at station y for mode n

Then the total out-of-plane bending moment may be written

$$VBM(y,t) = \sum_{i=1}^{NM} CVBM_n(y) \delta_n(t) \quad (78)$$

Similar expressions may be written for inplane bending moment, torsional moment, out-of-plane shear, inplane shear, and pitch link load. All of these equations are simply obtained by the application of the principal of superposition. The fact that the shear and moment coefficients are now input to C81 ensures that the moment calculations are significantly better than early versions of the aeroelastic rotor analysis.

3.2.10 Blade Mode Type Selection

The rotor hub has the ability to act as an attenuator, filter, or amplifier with reference to the transmissibility of the externally applied loads. Gessow and Myers (Reference 9) show the response of various hub configurations to forces with various harmonic excitation frequencies. This unique behavior of the rotor hub can be related to the behavior of the mode shapes used to describe the total rotor system. The boundary conditions used to calculate and describe the blade modes are given in Table 2. These boundary conditions may be modified slightly as discussed in Section 3.2.4.

⁹Gessow, Alfred and Myers, Garry C., Jr., AERODYNAMICS OF THE HELICOPTER, New York, N.Y., The Macmillan Company, pp. 309-317.

TABLE 2. BLADE BOUNDARY CONDITIONS AT ROOT

<u>Mode Type</u>	<u>Out-of-Plane</u>	<u>Inplane</u>	<u>Torsion</u>
Collective	Cantilever	Pinned	Cantilever
Cyclic	Pinned	Cantilever	Cantilever
Scissor	Cantilever	Cantilever	Cantilever

The proper selection of which blade mode types (cyclic, collective, or scissor) should be used is essential to an accurate rotor simulation. The purpose of this section is to describe the technique used to ascertain which mode types should be used to represent various hub types. The next section describes how the input blade modes are combined into rotor modes which are used in the computer program.

The first step in selecting which type of blade modes--collective, cyclic, or scissor--should be used in the rotor simulation is to define the hub boundary conditions that can exist for each blade. The hub boundary conditions are a function of the type of hub--gimbaled, teetering, hingeless, or articulated. For the latter two--hingeless or articulated--each blade's behavior is independent of any other blade's behavior. However, for the gimbaled or teetering hub there is moment carry over across the hub, so it is possible for any one blade to affect the behavior of the other blades.

The hub boundary conditions for a rotor blade must include the out-of-plane, inplane, and torsional end restraint. The out-of-plane boundary condition for all blades on a hingeless or rigid hub is cantilever; i.e., out-of-plane slope is zero. See Table 3 for these boundary conditions and their corresponding mode types.

TABLE 3. BLADE BOUNDARY CONDITIONS AND MODE TYPES FOR HINGELESS OR ARTICULATED HUBS

<u>Mast Torsional Stiffness</u>	<u>Boundary Condition</u>			<u>Blade Mode Type</u>
	<u>Inplane</u>	<u>Out-of-Plane</u>	<u>Torsional</u>	
Zero	Pinned	Cantilever	Cantilever	Collective
Nonzero	Cantilever	Cantilever	Cantilever	Scissor

The selection of mode types for hubs with moment carry over, i.e., teetering or gimbale, is somewhat more difficult than for the hingeless or articulated hubs. The first step is to determine the actual boundary conditions that are compatible with the blade's response to integer-per-rev harmonic forcing functions. The four-bladed gimbale rotor displays all the possible characteristics of the hubs with moment carry over, and will therefore be used as an example. Let it be assumed that positive out-of-plane bending (compression in top of blade) is accompanied by positive inplane bending (tension in leading edge). Figure 13 shows that for the 0 or 4-per-rev response, each blade tip moves up and aft. Thus, the out-of-plane boundary condition is cantilever. The inplane boundary condition depends on the mast torsional stiffness. For zero mast torsional stiffness, the inplane boundary conditions would be pinned, which would require the use of collective blade modes. For the nonzero mast torsional stiffness, the scissor blade modes would be used to describe the response at 0 or 4-per-rev. The 1-per-rev and 3-per-rev are very similar. In both cases, the out-of-plane boundary condition is pinned and the inplane is cantilever, regardless of the mast torsional stiffness. For the 2-per-rev blade response, blades 1 and 3 move up and aft; blades 2 and 4 move down and forward. The out-of-plane boundary condition is cantilever (the out-of-plane slope is zero). The hub inplane 2-per-rev moment produced by blade 1 is equal and opposite to that produced by blade 2; likewise for blades 3 and 4. (Thus, the total hub moment from the four blades is zero so that there is no hub moment tending to windup the mast regardless of the mast torsional stiffness.) This condition is compatible with the cantilever inplane boundary condition.

The procedure described for the four-bladed gimbale rotor can be applied to any rotor system with moment carry over. The resulting blade boundary conditions associated with any integer-per-rev response n , for any number of blades b , and the corresponding mode types are summarized in Table 4.

The order in which the mode shapes are arranged in the input data in terms of natural frequencies (ascending or descending) is unimportant except for one condition: the mode shape that has a natural frequency closest to 1-per-rev must be the first input mode shape. It is not required that the mode shapes have adjoining frequencies; i.e., certain mode shapes can be replaced with mode shapes with higher natural frequencies. Once the natural frequencies and their corresponding mode shapes are known, the only other modal input required is the structural damping coefficient, which is normally taken to be approximately 2 percent critical for all modes except the rigid body mode for which it is zero. A flow chart for selecting the proper blade modes to simulate any conventional hub is shown in Figure 14.

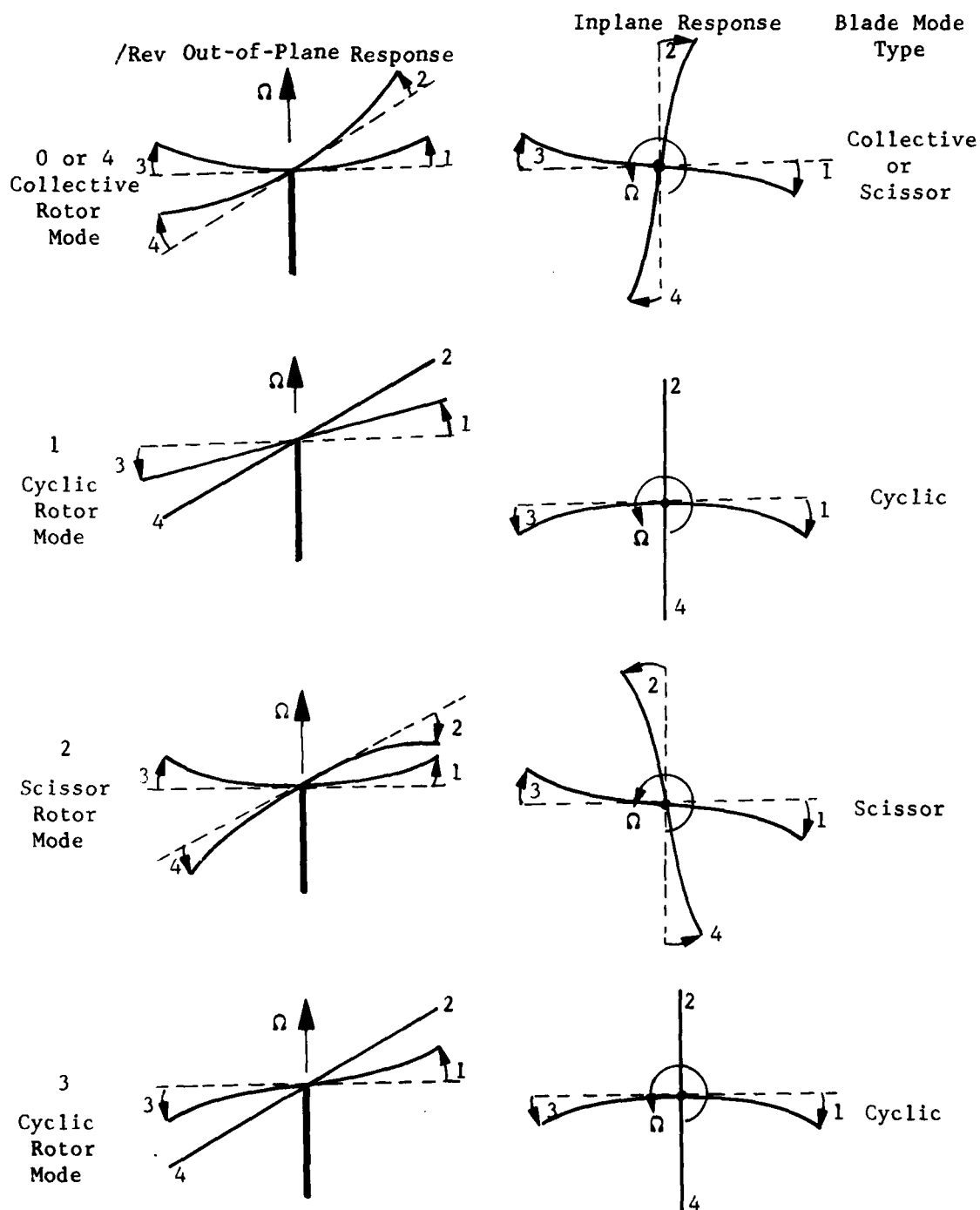


Figure 13. Response of 4-Bladed Gimbaled Rotor to Harmonic Forcing Functions.

TABLE 4. BLADE BOUNDARY CONDITIONS AND MODE TYPES
FOR GIMBALED OR TEETERING HUBS

<u>Mast Torsional Stiffness</u>	<u>Harmonic Per Rev</u>	<u>Boundary Condition</u>			<u>Blade Mode Type</u>
		<u>Inplane</u>	<u>Out-of-Plane</u>	<u>Torsional</u>	
Zero	nb	Pinned	Cantilever	Cantilever	Collective
	b(n-1/2)	Cantilever	Cantilever	Cantilever	Scissor*
	all other	Cantilever	Pinned	Cantilever	Cyclic
Nonzero	nb	Cantilever	Cantilever	Cantilever	Scissor
	b(n-1/2)	Cantilever	Cantilever	Cantilever	Scissor*
	all other	Cantilever	Pinned	Cantilever	Cyclic

n = integer-per-rev response

b = number of blades

*Only meaningful for gimbaled
rotor systems with four or
six blades.

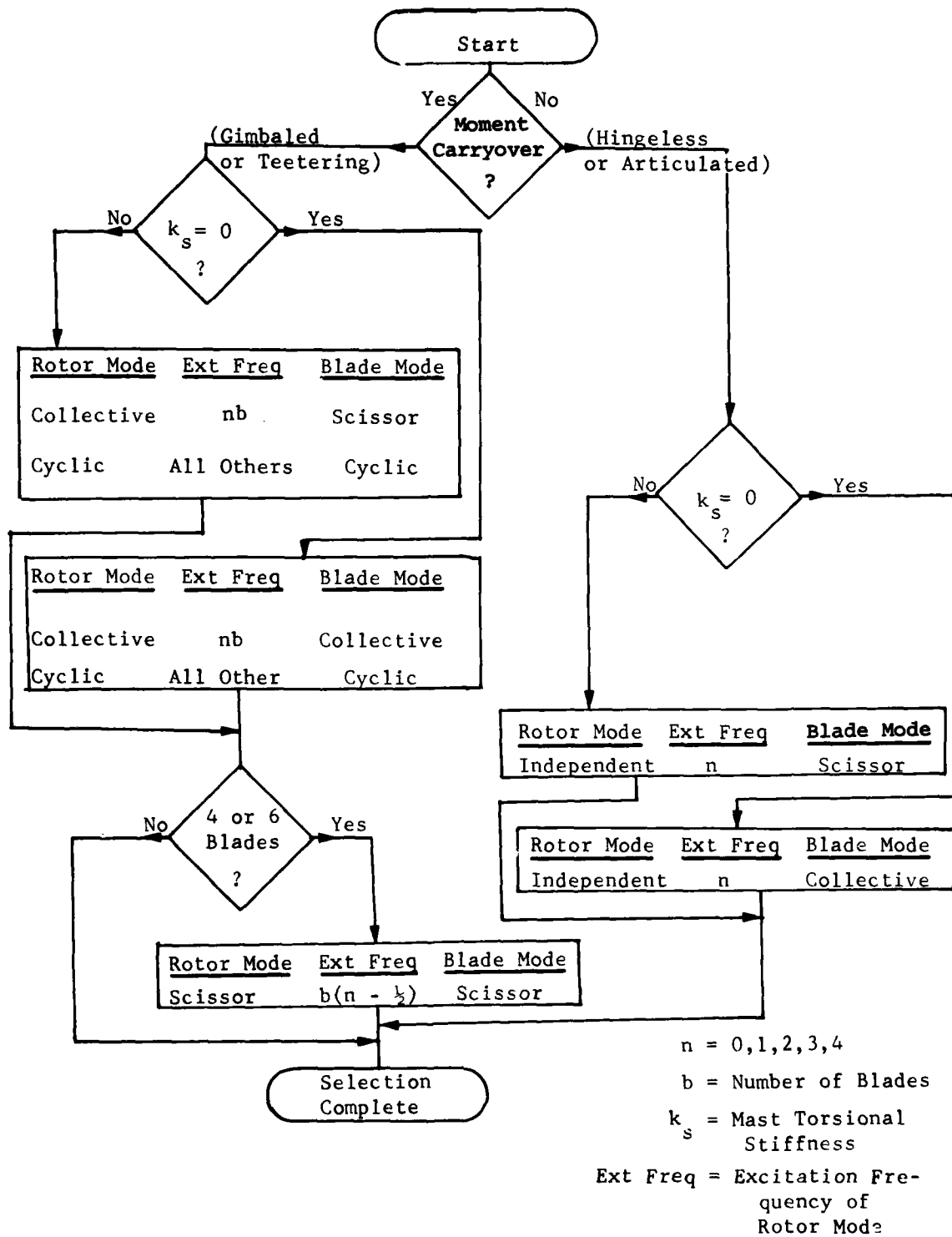


Figure 14. Guide for Selection of Blade Mode Types to Simulate Various Hub Types.

Based on these input blade modes, the computer program must have a logic network to combine the blade modes in the proper manner. The logic network will be described in the next section.

3.2.11 Hub Transfer Coefficient Matrix

The approach of the modal technique is sufficiently general to handle any particular combination of hub type and/or number of blades. The principal problems arise from the fact that the normal modes of vibration and the natural frequencies are calculated for the individual blades, while the modal equations are written for rotor modes. Some blade modes can be combined to form a rotor mode that can be described by one equation. Consider a collective blade mode for a gimbaled rotor where all blades go up and down together. Other blade modes are combined to form a rotor mode that requires two independent modal equations to define its position. Consider a cyclic blade mode for a gimbaled rotor which could move about two perpendicular axes (fore-and-aft flapping and lateral flapping).

The number of independent rotor modal equations required to describe a given blade mode is as follows: for all rotors where there is moment carry over at the hub, two equations are required to describe each cyclic mode and one equation to describe each collective or scissor mode; for all rotors where there is no moment carry over at the hub, one independent equation must be written for each mode for each blade. Thus, the total number of independent equations required to describe any combination of hub type and number of blades is difficult to express in general terms. It can be shown, however, that the number of dependent equations is b times NM where there are b blades and NM is the number of input mode shapes. These dependent equations can be used to describe all conventional hub types (hingeless, articulated, gimbaled, or teetering) for any number of blades. It is required that each input blade mode shape be designated as to whether it is to be formed into independent, cyclic, collective, or scissor rotor mode shapes. The independent rotor modes are associated with those rotor hubs without carry over, and are thus capable of responding at all integer multiples of the rotor speed. The cyclic, collective, and scissor rotor modes are associated with hubs with moment carry-over. Collective rotor modes respond at nb/rev ; scissor rotor modes respond at $b(n-1/2)/\text{rev}$; and cyclic rotor modes respond at all other harmonics where b is the number of blades, and n can be any nonnegative integer. Scissor rotor modes are associated with gimbaled hubs only with four or six blades.

The Hub Transfer Coefficient (HTC) matrix is used to represent the interdependency of hub type and mode type. The HTC matrix

will be derived for several different combinations. For each case, the input mode shape will be $MS(y)$, the generalized inertia of one blade will be I_n , and the externally applied loads on blade j will be $A_j(y)$, with components F_{u_j} , F_{w_j} , and M_{ϕ_j} as given by Equation (31).

The first case will be the cyclic mode for a four-bladed gimbaled rotor. From the input blade mode shape $MS(y)$, two independent rotor modes can be written:

<u>MODE SHAPE</u>				
<u>Mode No.</u>	<u>Blade 1</u>	<u>Blade 2</u>	<u>Blade 3</u>	<u>Blade 4</u>
1	$MS(y)$	0	$-MS(y)$	0
2	0	$MS(y)$	0	$-MS(y)$

The inertia of each mode would be $2 I_n$. The virtual work done by the externally applied air loads acting through the n th mode shape would be for the first independent rotor mode:

$$\begin{aligned}
 W_1 = \int_0^R \{ & [F_{u_1}(y) \cdot u_n(y) + F_{w_1}(y) \cdot w_n(y) \\
 & + M_{\phi_1}(y) \cdot \phi_n(y)] - [F_{u_3}(y) \cdot u_n(y) \\
 & + F_{w_3}(y) \cdot w_n(y) + M_{\phi_3}(y) \cdot \phi_n(y)] \} dy \quad (79)
 \end{aligned}$$

or

$$W_1 = \int_0^R [MS_n(y) \cdot A_1(y) - MS_n(y) \cdot A_3(y)] dy \quad (80)$$

and for the second rotor mode

$$W_2 = \int_0^R [MS_n(y) \cdot A_2(y) - MS_n(y) \cdot A_4(y)] dy \quad (81)$$

and the two independent modal equations (one for each mode) would be

$$\ddot{\varepsilon}_1 + 2 \zeta \omega_n \dot{\varepsilon}_1 + \omega_n^2 \varepsilon_1 = \frac{W_1}{2 I_n}$$

$$= \frac{\int_0^R \{MS(y) \cdot A_1(y) - MS(y) \cdot A_3(y)\} dy}{2 I_n} \quad (82)$$

and

$$\ddot{\varepsilon}_2 + 2 \zeta \omega_n \dot{\varepsilon}_2 + \omega_n^2 \varepsilon_2 = \frac{W_2}{2 I_n}$$

$$= \frac{\int_0^R \{MS(y) \cdot A_2(y) - MS(y) \cdot A_4(y)\} dy}{2 I_n} \quad (83)$$

If ε_1 and ε_2 are independent generalized coordinates, the $\delta_1, \delta_2, \delta_3, \delta_4$ are localized dependent blade coordinates such that

$$\begin{aligned} \delta_1 &= \varepsilon_1 & \delta_3 &= -\varepsilon_1 & \delta_2 &= \varepsilon_2 & \delta_4 &= -\varepsilon_2 \\ \dot{\delta}_1 &= \dot{\varepsilon}_1 & \dot{\delta}_3 &= -\dot{\varepsilon}_1 & \dot{\delta}_2 &= \dot{\varepsilon}_2 & \dot{\delta}_4 &= -\dot{\varepsilon}_2 \\ \ddot{\delta}_1 &= \ddot{\varepsilon}_1 & \ddot{\delta}_3 &= -\ddot{\varepsilon}_1 & \ddot{\delta}_2 &= \ddot{\varepsilon}_2 & \ddot{\delta}_4 &= -\ddot{\varepsilon}_2 \end{aligned} \quad (84)$$

It then becomes possible to write four dependent equations of motion.

$$\ddot{\delta}_j + 2 \zeta \omega_n \dot{\delta}_j + \omega_n^2 \delta_j = F_j \quad \text{for } j = 1 \text{ to } 4 \quad (85)$$

where F_j is written as

$$\begin{Bmatrix} F_1 \\ F_2 \\ F_3 \\ F_4 \end{Bmatrix} = \frac{1}{2 I_n} \begin{bmatrix} 1 & 0 & -1 & 0 \\ 0 & 1 & 0 & -1 \\ -1 & 0 & 1 & 0 \\ 0 & -1 & 0 & 1 \end{bmatrix} \begin{Bmatrix} W_1 \\ W_2 \\ W_3 \\ W_4 \end{Bmatrix} \quad (86)$$

where W_i is the work done by the air loads on blade i , acting through the input blade mode shape.

For a cyclic blade mode shape for a three-bladed rotor, Equation (60) would have the following form for a gimbaled rotor:

$$\begin{Bmatrix} F_1 \\ F_2 \\ F_3 \end{Bmatrix} = \frac{1}{3 I_n} \begin{bmatrix} 1 & -\frac{1}{2} & -\frac{1}{2} \\ -\frac{1}{2} & 1 & -\frac{1}{2} \\ -\frac{1}{2} & -\frac{1}{2} & 1 \end{bmatrix} \begin{Bmatrix} w_1 \\ w_2 \\ w_3 \end{Bmatrix} \quad (87)$$

and for a teetering hub the cyclic blade mode would be described

$$\begin{Bmatrix} F_1 \\ F_2 \end{Bmatrix} = \frac{1}{2 I_n} \begin{bmatrix} 1 & -1 \\ -1 & 1 \end{bmatrix} \begin{Bmatrix} w_1 \\ w_2 \end{Bmatrix} \quad (88)$$

For any cyclic mode for any number of blades,

$$HTC(i,j) = \cos [\psi(i) - \psi(j)] \quad (89)$$

which gives the effect of blade i on blade j.

The second example will be the collective mode for a four-bladed gimbaled rotor. The one independent mode would be

<u>Mode No.</u>	<u>Blade 1</u>	<u>Blade 2</u>	<u>Blade 3</u>	<u>Blade 4</u>
1	MS(y)	MS(y)	MS(y)	MS(y)

The forcing function for the independent equation would be

$$F_1 = \int_0^R [MS(y) \cdot A_1(y) + MS(y) \cdot A_2(y) + MS(y) \cdot A_3(y) + MS(y) \cdot A_4(y)] dy \quad (90)$$

and the equation of motion would be

$$\ddot{\varepsilon}_1 + 2 \zeta \omega_n \dot{\varepsilon}_1 + \omega_n^2 \varepsilon_1 = \frac{F_1}{4 I_n} \quad (91)$$

Since $\delta_1 = \delta_2 = \delta_3 = \delta_4 = \varepsilon_1$, it becomes possible to write four dependent equations as

$$\ddot{\delta}_j + 2 \omega_n \zeta \dot{\delta}_j + \omega_n^2 \delta_j = F_j \quad (92)$$

where

$$\begin{pmatrix} F_1 \\ F_2 \\ F_3 \\ F_4 \end{pmatrix} = \frac{1}{4 I_n} \begin{bmatrix} 1 & 1 & 1 & 1 \\ 1 & 1 & 1 & 1 \\ 1 & 1 & 1 & 1 \\ 1 & 1 & 1 & 1 \end{bmatrix} \begin{pmatrix} W_1 \\ W_2 \\ W_3 \\ W_4 \end{pmatrix} \quad (93)$$

Thus, for a collective mode for a gimbaled rotor,

$$HTC(i,j) = \cos [NB(\psi(i) - \psi(j))] \quad (94)$$

where NB is the number of blades.

The third case is that of a scissor mode for a four-bladed gimbaled rotor. The rotor mode for a scissor mode would be

<u>Mode No.</u>	<u>Blade 1</u>	<u>Blade 2</u>	<u>Blade 3</u>	<u>Blade 4</u>
1	MS(y)	-MS(y)	MS(y)	-MS(y)

and the forcing function for the independent rotor modal equation would be

$$F_1 = \int_0^R [MS(y) \cdot A_1(y) - MS(y) \cdot A_2(y) + MS(y) \cdot A_3(y) - MS(y) \cdot A_4(y)] dy \quad (95)$$

The localized blade coordinates would be

$$\delta_1 = \delta_3 = \varepsilon \quad \delta_2 = \delta_4 = -\varepsilon \quad (96)$$

The four dependent equations could be written

$$\ddot{\delta}_j + 2 \zeta \omega_n \dot{\delta}_j + \omega_n^2 \delta_j = \frac{F_j}{4 I_n} \quad (97)$$

where

$$\begin{Bmatrix} F_1 \\ F_2 \\ F_3 \\ F_4 \end{Bmatrix} = \frac{1}{4 I_n} \begin{bmatrix} 1 & -1 & 1 & -1 \\ -1 & 1 & -1 & 1 \\ 1 & -1 & 1 & -1 \\ -1 & 1 & -1 & 1 \end{bmatrix} \begin{Bmatrix} w_1 \\ w_2 \\ w_3 \\ w_4 \end{Bmatrix} \quad (98)$$

which leads to the conclusion

$$HTC(i,j) = \cos [NB/2(\psi(i) - \psi(j))] \quad (99)$$

The only hub type remaining is that where there is no moment carry over at the hub, i.e., rigid or articulated. For this type of rotor, the response of blade i is not related dynamically to the loads on blade j . Therefore, the hub transfer coefficient matrix would have the following form:

$$HTC(k,j) = \begin{cases} i & \text{for } i = j \\ 0 & \text{for } i \neq j \end{cases} \quad (100)$$

Equations (90), (95), (100) and (101) can be brought together in the following form:

$$HTC(i,j) = \begin{cases} \cos [\psi(i) - \psi(j)] & \text{cyclic} \\ \cos [NB/2(\psi(i) - \psi(j))] & \text{scissor} \\ \cos [NB(\psi(i) - \psi(j))] & \text{collective} \\ i \text{ or } 0 & \text{articulated or hingless} \end{cases} \begin{matrix} \text{teetering} \\ \text{or} \\ \text{gimbaled} \end{matrix} \quad (101)$$

which defines the dynamic effects of blade i on blade j for each mode type. The computer program has been written to consider up to six mode shapes and up to seven blades. The HTC matrix is therefore $7 \times 7 \times 6$.

3.2.12 Cyclic Detuning

The rotor blade natural frequencies and mode shapes are a function of the rotor speed and hub geometric pitch. Previous versions of the digital program have been structured to accept as input the mode shapes and natural frequencies at one combination of rotor speed and hub geometric pitch. This limiting assumption is modified by including the effects of cyclic

detuning in the following manner: The blade natural frequencies and mode shapes are calculated at three values of collective pitch (low, mid, high) and three values of rotor speed (low, mid, high). The mode shapes at the mid collective pitch and mid rotor speed are assumed to represent the mode shape at all combinations of pitch and rotor speed.

Four values of the natural frequencies for mode shape are input data. The four values of ω_n are obtained from the extreme combinations of rotor speed and collective pitch (low rotor speed in combination with low collective pitch and high collective pitch, etc.). The increments on rotor speed and collective pitch used in calculating the mode shapes and natural frequencies are also required input data.

The previous section (Hub Transfer Coefficient Matrix) has shown that for each blade, for each input mode shape there is an equation of the form

$$\ddot{\delta}_j + 2 \zeta \omega_n \dot{\delta}_j + \omega_n^2 \delta_j = F_j \quad (102)$$

For each blade an instantaneous value of rotor speed and hub geometric pitch (collective plus cyclic pitch) is known, which permits bivariant interpolation to calculate an instantaneous value of the natural frequency from the input data.

3.3 MODAL PYLON MODEL

The behavior of an elastic rotor may be highly dependent on the dynamic characteristics of the rotor-fuselage interface. Because of this, a good deal of effort has been expended to develop in C81 a general dynamic model of this rotor-fuselage interface, which we have termed the pylon equations. There are four pylon equations in modal form for each of the two rotors in C81. Each of these modes has three linear displacements, three angular rotations (longitudinal cyclic, lateral cyclic, and collective blade feathering) as part of the mode shape, as well as a natural frequency, generalized inertia, and damping ratio.

The modal form for the pylon equations was selected in order to provide general motion at the rotor hub with a minimum number of additional equations. More importantly, the modal form allows the use of modes based on very complex and detailed structural models of the fuselage or support system which may be obtained from structural analysis programs such as NASTRAN. The modal form may also be used easily for parametric studies during the design process. As a special convenience, the option has

been provided to use modes which were calculated either with no rotor mass included or with the full rotor mass included as a point mass. The initial analysis will be shown for modes without rotor mass. The corrections necessary to use modes with rotor mass will be shown later.

The equation of motion for the j th pylon mode is

$$\ddot{p}_j + 2 \zeta_j \omega_j \dot{p}_j + \omega_j^2 p_j = F_j/GI_j \quad (103)$$

where

- p_j is the generalized coordinate for the j th mode,
- ω_j is the input natural frequency of the j th mode,
- ζ_j is the input damping ratio for the j th mode,
- GI_j is the input generalized inertia for the j th mode, and
- F_j is the modal forcing function for the j th mode, which will be defined later.

The j th pylon mode will be in terms of the following displacements at the top of the rotor mast but in fuselage reference:

- x_j in the x_f direction
- y_j in the y_f direction
- z_j in the z_f direction
- θ_{xj} about the x_f axis
- θ_{yj} about the y_f axis
- θ_{zj} about the z_f axis

An equivalent mode shape may also be defined in the mast coordinate system by use of the $T_{m/f}$ transformation matrix

$$(x_{mj}, y_{mj}, z_{mj}) = [T_{m/f}](x_j, y_j, z_j) \quad (104)$$

$$(\theta_{xmj}, \theta_{ymj}, \theta_{zmj}) = [T_{m/f}](\theta_{xj}, \theta_{yj}, \theta_{zj}) \quad (105)$$

Then the modal forcing function may be defined

$$\begin{aligned}
 F_j = & x_{mj} V_{mx} + y_{mj} V_{my} + z_{mj} V_{mz} + \theta_{mxj} M_{mx} \\
 & + \theta_{myj} M_{my} + \theta_{mzj} M_{mz} + x_{mj} F_{mx} \\
 & + y_{mj} F_{my} + z_{mj} F_{mz}
 \end{aligned} \tag{106}$$

where

V_{mx}, V_{my}, V_{mz} are the three components of shear at the top of the mast,

M_{mx}, M_{my}, M_{mz} are the three components of moment at the top of the mast, and

F_{mx}, F_{my}, F_{mz} are the three components of force which arise from the translation of the rotor mass and were not included in either the rotor or pylon natural frequency calculations.

A similar expression for F_j may be written with all of the variables in fuselage reference.

Next, an expression for the inertia loads F_{mx}, F_{my} , and F_{mz} will be developed. In treating the inertia loads on the rotor caused by pylon motion and how they feed back into the pylon, it is necessary to look closely at the difference between radial and transverse motion. A top view of the pylon is shown in Figure 15. The linear acceleration components for the rotor hub are

$$\begin{aligned}
 (a_{xm}, a_{ym}, a_{zm}) = & \sum_{n=1}^{NP} p_j (x_{mj}, y_{mj}, z_{mj}) \\
 & + (\ddot{x}_m, \ddot{y}_m, \ddot{z}_m)
 \end{aligned} \tag{107}$$

where

NP is the number of pylon modes used, and

$(\ddot{x}_m, \ddot{y}_m, \ddot{z}_m)$ are the mast reference components of acceleration caused by motion of the rigid fuselage.

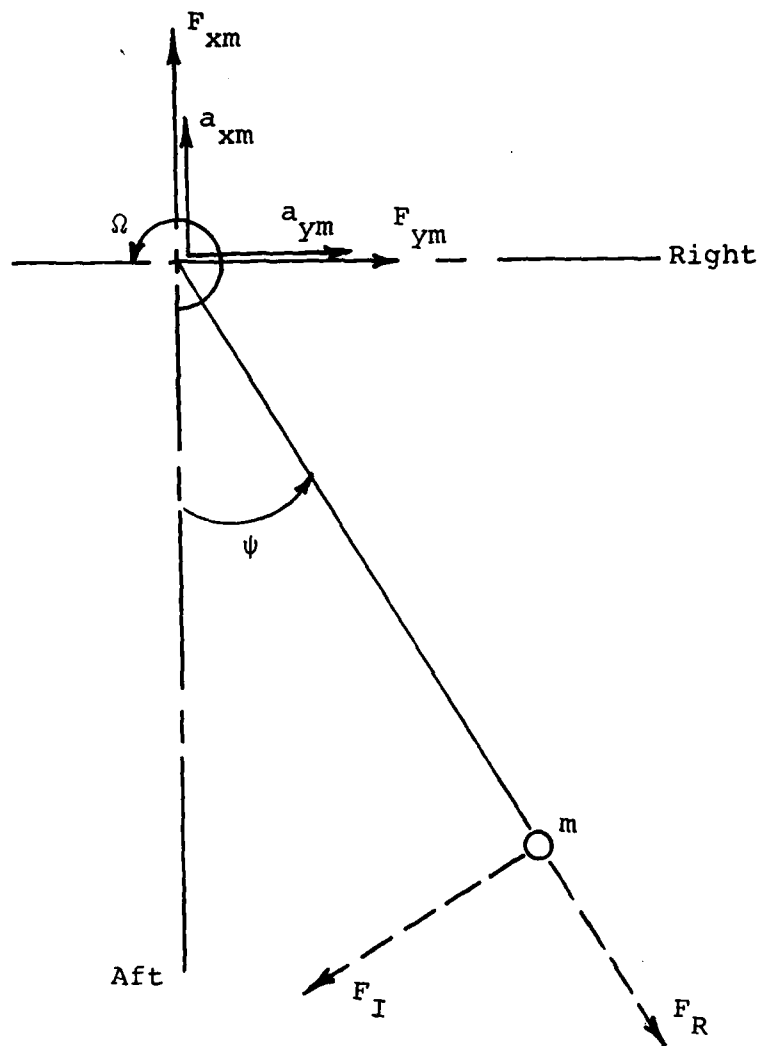


Figure 15. Top View of Rotor Hub, Indicating Pylon Motion.

The inplane hub accelerations, a_{xm} and a_{ym} , will produce the inertial forces on the blade mass particle, m , as shown by the dotted arrows in Figure 15.

The inplane inertial force perpendicular to the blade is

$$F_I = m(a_{xm} \sin \psi + a_{ym} \cos \psi) \quad (108)$$

where

ψ is the azimuth location of the blade in question.

For an elastic rotor simulation, F_I is included in the external forces applied to the elastic modes. For a nonelastic rotor (one mode), F_I is transmitted directly to the rotor hub.

The radial inertia force is not felt by the rotor modes and thus must be transmitted to the rotor hub regardless of which rotor model is used.

$$F_R = m(a_{xm} \cos \psi - a_{ym} \sin \psi) \quad (109)$$

F_I and F_R are integrated along a blade and summed over all the blades to give

$$F_{xm} = \sum_{i=1}^{NB} \int_0^R -F_I \sin \psi_i - F_R \cos \psi_i \quad (110)$$

$$F_{ym} = \sum_{i=1}^{NB} \int_0^R -F_I \cos \psi_i + F_R \sin \psi_i \quad (111)$$

For an elastic rotor, the F_I terms must be omitted, so two different expressions are obtained, depending on the rotor model.

Elastic Rotor Inertia Forces

$$\begin{aligned} F_{xm} = & -M_B \sum_{i=1}^{NM} \sum_{j=1}^{NP} \ddot{p}_j (x_{mj} \cos^2 \psi_i \\ & - y_{mj} \cos \psi_i \sin \psi_i) - M_B \sum_{i=1}^{NB} \ddot{x}_m \cos^2 \psi_i \\ & - \ddot{y}_m \cos \psi_i \sin \psi_i \end{aligned} \quad (112)$$

$$\begin{aligned}
F_{ym} = M_B \sum_{i=1}^{NB} \sum_{j=1}^{NP} \ddot{p}_j (\dot{x}_{mj} \cos \psi_i \sin \psi_i \\
- y_{mj} \sin^2 \psi_i) + M_B \sum_{i=1}^{NB} (\ddot{x}_m \cos \psi_i \sin \psi_i \\
- \ddot{y}_m \sin^2 \psi_i)
\end{aligned} \quad (113)$$

where

$$M_B = \int_0^R dm = \text{total mass of one blade.}$$

For more than two matching blades ($NB > 2$) these expressions simplify to

$$F_{xm} = -\frac{NB}{2} M_B (\ddot{x}_m + \sum_{j=1}^{NP} \ddot{p}_j x_{mj}) \quad (114)$$

$$F_{ym} = -\frac{NB}{2} M_B (\ddot{y}_m + \sum_{j=1}^{NP} \ddot{p}_j y_{mj}) \quad (115)$$

For a two-bladed rotor the summations may be written in terms of $\psi = \psi_1$.

$$\begin{aligned}
F_{xm} = -2 M_B [(\ddot{x}_m \cos^2 \psi - \ddot{y}_m \cos \psi \sin \psi) \\
+ \sum_{j=1}^{NP} \ddot{p}_j (x_{mj} \cos^2 \psi - y_{mj} \cos \psi \sin \psi)]
\end{aligned} \quad (116)$$

$$\begin{aligned}
F_{ym} = 2 M_B [(\ddot{x}_m \cos \psi \sin \psi - \ddot{y}_m \sin^2 \psi) \\
+ \sum_{j=1}^{NP} \ddot{p}_j (x_{mj} \cos \psi \sin \psi - y_{mj} \sin^2 \psi)]
\end{aligned} \quad (117)$$

Nonelastic Rotor Inertia Loads

For a nonelastic rotor all of the inertia loads are transmitted to the hub.

$$\begin{aligned}
 F_{xm} = & -M_B \sum_{i=1}^{NB} \{ (\ddot{x}_m \cos^2 \psi_i - \ddot{y}_m \cos \psi_i \sin \psi_i \\
 & + \ddot{x}_m \sin^2 \psi_i + \ddot{y}_m \cos \psi_i \sin \psi_i) \\
 & + \sum_{j=1}^{NP} p_j (x_{mj} \sin^2 \psi_i + y_{mj} \cos \psi_i \sin \psi_i \\
 & + x_{mj} \cos^2 \psi_i - y_{mj} \cos \psi_i \sin \psi_i) \} \quad (118)
 \end{aligned}$$

$$\begin{aligned}
 F_{ym} = & M_B \sum_{i=1}^{NB} \{ (-\ddot{x}_m \cos \psi_i \sin \psi_i - \ddot{y}_m \cos^2 \psi_i \\
 & + \ddot{x}_m \cos \psi_i \sin \psi_i - \ddot{y}_m \sin^2 \psi_i) \\
 & + \sum_{j=1}^{NP} p_j (-x_{mj} \cos \psi_i \sin \psi_i - y_{mj} \cos^2 \psi_i \\
 & + x_{mj} \cos \psi_i \sin \psi_i - y_{mj} \sin^2 \psi_i) \} \quad (119)
 \end{aligned}$$

For any number of blades these expressions reduce to

$$F_{xm} = -M_B \left(\ddot{x}_m + \sum_{j=1}^{NP} p_j x_{mj} \right) \quad (120)$$

$$F_{ym} = -M_B \left(\ddot{y}_m + \sum_{j=1}^{NP} p_j y_{mj} \right) \quad (121)$$

The out-of-plane inertial loading arising from a_{zm} must also be considered. For an elastic rotor, a distributed inertia load is obtained as part of the rotor forcing function. The inertia load then reaches the rotor hub as a part of the rotor shear force.

For a nonelastic rotor, the out-of-plane inertia load is transmitted to the hub so that

$$F_{zm} = -NB M_B (\ddot{z}_m + \sum_{j=1}^{NP} \ddot{p}_j z_{mj}) \quad (122)$$

This means that the entire rotor mass is being accelerated.

The inertia forces on the rotor caused by angular velocities and angular accelerations of the fuselage and pylon are included in the rotor forcing function for either an elastic or a non-elastic rotor. These effects are transmitted to the pylon by means of the net beamwise bending moment or the flapping spring moment of the rotor hub.

Let

$$F_{oj} = x_{mj} V_{mx} + y_{mj} V_{my} + z_{mj} V_{mz} \\ + \theta_{mxj} M_{mx} + \theta_{myj} M_{my} + \theta_{mzj} M_m \quad (123)$$

The calculation of the shear forces and moments is described in Section 3.2.9. Now the equations of motion for pylon modes calculated without rotor mass can be written.

For a nonelastic rotor

$$\ddot{p}_j + \left(\frac{NB M_B}{GI_j} \sum_{i=1}^{NP} \ddot{p}_i x_{mi} \right) x_{mj} \\ + \left(\frac{NB M_B}{GI_j} \sum_{i=1}^{NP} \ddot{p}_i y_{mi} \right) y_{mj} \\ + \left(\frac{NB M_B}{GI_j} \sum_{i=1}^{NP} \ddot{p}_i z_{mi} \right) z_{mj} + 2 \zeta_j \omega_j \dot{p}_j + \omega_j^2 p_j \\ = \frac{F_{oj}}{GI_j} - \frac{NB M_B}{GI_j} (\ddot{x}_m x_{mj} + \ddot{y}_m y_{mj} + \ddot{z}_m z_{mj}) \quad (124)$$

or with a more simplified form on the left-hand side

$$\begin{aligned}
 & \ddot{p}_j \left(1 + \frac{NB M_B}{GI_j} [x_{mj}^2 + y_{mj}^2 + z_{mj}^2] \right) \\
 & + \frac{NB M_B}{GI_j} \sum_{i \neq j} \ddot{p}_i [x_{mi} x_{mj} + y_{mi} y_{mj} + z_{mi} z_{mj}] \\
 & + 2 \zeta_j \omega_j \dot{p}_j + \omega_j^2 p_j \\
 & = \frac{F_{Oj}}{GI_j} - \frac{NB M_B}{GI_j} [\ddot{x}_m x_{mj} + \ddot{y}_m y_{mj} + \ddot{z}_m z_{mj}] \quad (125)
 \end{aligned}$$

For an elastic rotor the difference between two-bladed and multibladed rotors must be distinguished. The multibladed rotor has a fairly simple form for the equation because of symmetry. The pylon equation for a multibladed elastic rotor is

$$\begin{aligned}
 & \ddot{p}_j + \frac{NB M_B}{2 GI_j} \sum_{i=1}^{NP} \ddot{p}_i [x_{mi} x_{mj} + y_{mi} y_{mj}] \\
 & + 2 \zeta_j \omega_j \dot{p}_j + \omega_j^2 p_j \\
 & = \frac{F_{Oj}}{GI_j} - \frac{NB M_B}{2 GI_j} [\ddot{x}_m x_{mj} + \ddot{y}_m y_{mj}] \quad (126)
 \end{aligned}$$

For a two-bladed elastic rotor the pylon equation of motion is

$$\begin{aligned}
 & \ddot{p}_j + \frac{2 M_B}{GI_j} \sum_{i=1}^{NP} \ddot{p}_i [x_{mi} x_{mj} \cos^2 \psi + y_{mi} y_{mj} \sin^2 \psi \\
 & - \cos \psi \sin \psi (y_{mi} x_{mj} + x_{mi} y_{mj})] + 2 \zeta_j \omega_j \dot{p}_j \\
 & + \omega_j^2 p_j \\
 & = \frac{F_{Oj}}{GI_j} - \frac{2 M_B}{GI_j} [\ddot{x}_m x_{mj} \cos^2 \psi + \ddot{y}_m y_{mj} \sin^2 \psi \\
 & - \cos \psi \sin \psi (\ddot{y}_m x_{mj} + \ddot{x}_m y_{mj})] \quad (127)
 \end{aligned}$$

Modifications for Modes with Rotor Mass

Because of orthogonality conditions, the pylon equation for the nonelastic rotor must reduce to the simplest modal equation (with $F_{xm} = F_{ym} = F_{zm} = 0$) for pylon modes calculated with the rotor mass on. For this case the equation of motion is

$$\ddot{p}_j + 2 \zeta_j \omega_j \dot{p}_j + \omega_j^2 p_j = \frac{F_{oj}}{GI_j} \quad (128)$$

By a comparison of Equations (125) and (128) the effects of modes with rotor mass may be determined. The values ω_j , ζ_j , etc., will be different for the two cases.

In order to distinguish the variables associated with pylon modes calculated with rotor mass, all of these variables will be written with a bar above them.

Assume that you can start with Equation (128) for modes with rotor mass and reduce it to the same equation as Equation (125) by treating the rotor mass as a negative mass affected by all translational accelerations. These inertia forces, in mast reference will be

$$(\bar{F}_{xm}, \bar{F}_{ym}, \bar{F}_{zm})$$

By observing the results for the nonelastic rotor we obtain

$$\bar{F}_{xm} = NB M_B \left(\sum_{j=1}^{NP} \ddot{p}_j x_{mj} + \ddot{x}_m \right) \quad (129)$$

$$\bar{F}_{ym} = NB M_B \left(\sum_{j=1}^{NP} \ddot{p}_j y_{mj} + \ddot{y}_m \right) \quad (130)$$

$$\bar{F}_{zm} = NB M_B \left(\sum_{j=1}^{NP} \ddot{p}_j z_{mj} + \ddot{z}_m \right) \quad (131)$$

These forces due to the negative mass modify the three forms of the equations. An additional generalized force is added to each equation as follows:

$$\begin{aligned} \bar{F}_j = \frac{NB M_B}{GI_j} & \left(\sum_{i=1}^{NP} \ddot{p}_i (x_{mi} x_{mj} + y_{mi} y_{mj} + z_{mi} z_{mj}) \right. \\ & \left. + (\ddot{x}_m x_{mj} + \ddot{y}_m y_{mj} + \ddot{z}_m z_{mj}) \right) \end{aligned} \quad (132)$$

where the first term will be transferred to the left side of the equation and the second will remain on the right side.

For pylon modes with rotor mass the resulting three equations are given below.

Pylon Modes with Rotor Mass - Nonelastic Rotor

$$\ddot{p}_j + 2 \zeta_j \omega_j \dot{p}_j + \omega_j^2 p_j = \frac{F_{oj}}{GI_j} \quad (133)$$

Pylon Modes with Rotor Mass - Multibladed Elastic Rotor

$$\begin{aligned} \ddot{p}_j - \frac{NB M_B}{2 GI_j} \sum_{i=1}^{NP} \ddot{p}_i [x_{mi} x_{mj} + y_{mi} y_{mj} + 2 z_{mi} z_{mj}] \\ + 2 \zeta_j \omega_j \dot{p}_j + \omega_j^2 p_j \\ = \frac{F_{oj}}{GI_j} + \frac{NB M_B}{2 GI_j} [\ddot{x}_m x_{mj} + \ddot{y}_m y_{mj} + 2 \ddot{z}_m z_{mj}] \end{aligned} \quad (134)$$

Pylon Modes with Rotor Mass - Two-Bladed Elastic Rotor

$$\begin{aligned} \ddot{p}_j + \frac{NB M_B}{GI_j} \sum_{i=1}^{NP} \ddot{p}_i [x_{mi} x_{mj} (\cos^2 \psi - 1) \\ + y_{mi} y_{mj} (\sin^2 \psi - 1) - z_{mi} z_{mj} \\ - \cos \psi \sin \psi (y_{mi} x_{mj} + x_{mi} y_{mj})] \\ + 2 \zeta_j \omega_j \dot{p}_j + \omega_j^2 p_j \\ = \frac{F_{oj}}{GI_j} - \frac{NB M_B}{GI_j} \ddot{x}_m x_{mi} (\cos^2 \psi - 1) \\ + \ddot{y}_m y_{mj} (\sin^2 \psi - 1) - \ddot{z}_m z_{mj} \\ - \cos \psi \sin \psi (\ddot{y}_m x_{mj} + \ddot{x}_m y_{mj}) \end{aligned} \quad (135)$$

The sequence of calculations is important in order to achieve a consistent set of equations. The values needed to solve the pylon equations are

- (1) Aerodynamic loading
- (2) Rotor blade coordinate displacements for shear and moment evaluation
- (3) Fuselage accelerations

The values needed to solve the rotor equations are

- (1) Aerodynamic loading
- (2) Pylon accelerations
- (3) Fuselage accelerations

The values needed to find the fuselage accelerations are

- (1) Aerodynamic loading
- (2) Blade coordinate displacements for shears and moments

By inspection of these requirements, the following sequence of calculations was developed to provide a consistent set of equations without a simultaneous solution of the full set of equations.

- (1) Find aerodynamic loading for rotors, empennage, and fuselage. These loads depend only on displacements and velocities except for unsteady aerodynamic terms. We have already dealt with that problem by use of extrapolation.
- (2) Compute that portion of rotor forcing functions not dependent on fuselage or pylon accelerations.
- (3) Solve for the rigid body fuselage accelerations.
- (4) Solve for the accelerations of the pylon generalized coordinates. In general this requires a simultaneous solution for all pylon generalized accelerations.
- (5) Add the inertia loads caused by fuselage and pylon motion to the rotor forcing functions.
- (6) Solve for accelerations of rotor participation factors.

A flow chart showing how this sequence is applied in C81 is shown in Figure 16.

Use of Control Coupling Inputs

If no control coupling inputs are made with a pylon mode, the swashplate is assumed to move with the pylon. That is, the control plane angle of attack will change by the same amount as the total pylon angle. In order to modify this behavior, coupling inputs are provided for rotor collective pitch, longitudinal cyclic pitch, and lateral cyclic pitch. There is a set of control inputs for each mode as they are considered to be part of the mode shape. Three control increments are calculated for each rotor and added to the control system as shown in Figure 40. The control increments are

$$\Delta\theta_o = \sum_{j=1}^{NP} p_j \Delta\theta_{oj} \quad (136)$$

$$\Delta B_1 = \sum_{j=1}^{NP} p_j \Delta B_{1j} \quad (137)$$

$$\Delta A_1 = \sum_{j=1}^{NP} p_j \Delta A_{1j} \quad (138)$$

3.4 AERODYNAMICS

3.4.1 General

The detailed representation of rotor dynamics can be most effective when used with a similarly refined analysis of aerodynamic effects. Early versions of C81 dealt mainly with steady state aerodynamics. Tip vortex effects, lift variation time lag, and radial flow were also included. C81 now includes the aerodynamic features described in Reference 2, and in addition, two procedures for evaluating the first-order effects of unsteady aerodynamics. These features allow the interaction of the blade rigid body and elastic motions and the aerodynamic forces acting thereon, which is essential for the study of aeroelastic response phenomena.

The steady, as well as unsteady, aerodynamic model is also improved by accounting for the effect of the angle between the resultant wind velocity and the blade leading edge. This angle can be modified by a sweep angle built into the blade tip.

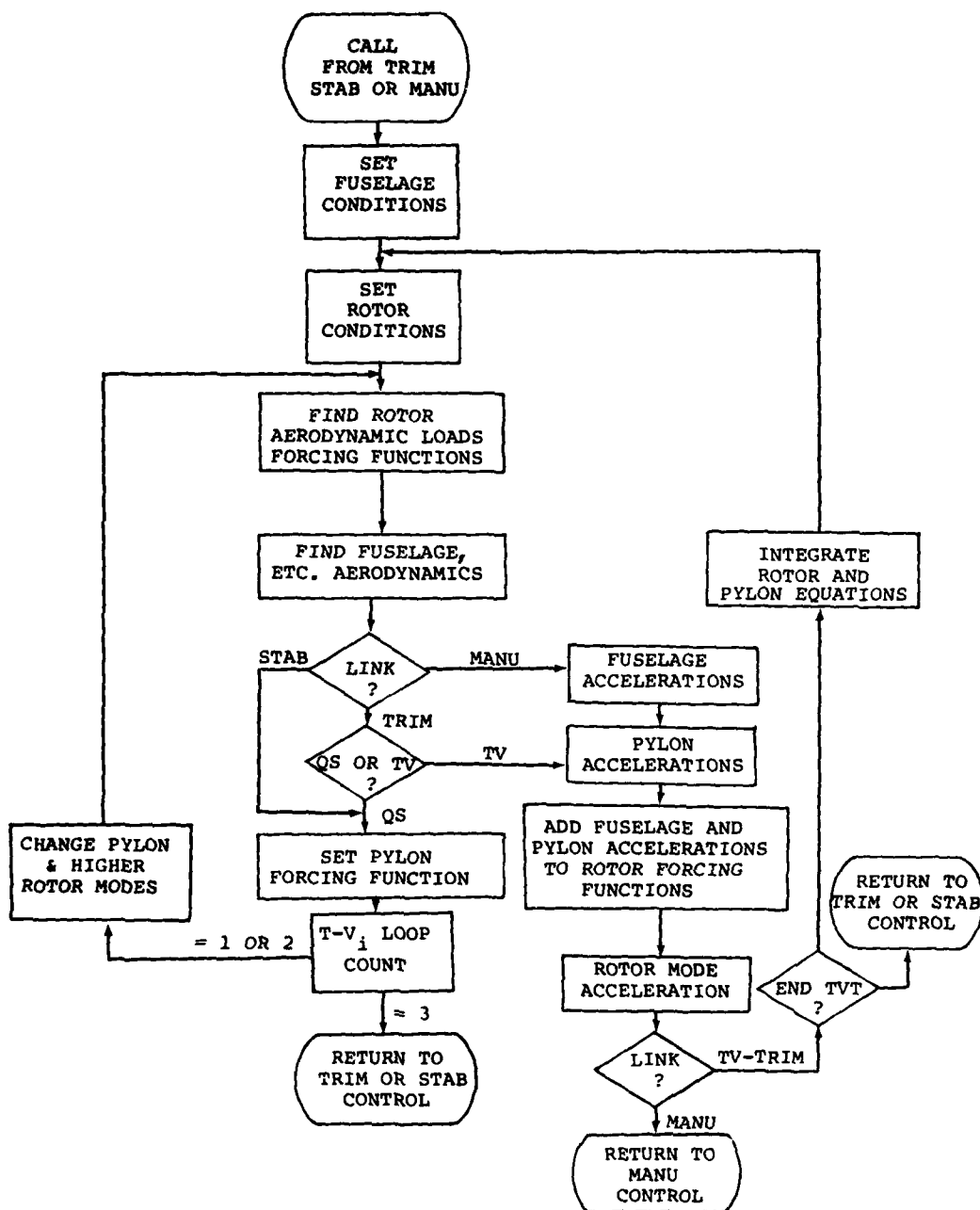


Figure 16. Flow Chart for Sequence of Calculations with Modal Pylon Equations.

Figure 17 shows the organization of the rotor aerodynamic analysis and the possible computational paths. The rotor aerodynamic analysis is the same as that discussed in Reference 4.

3.4.2 Induced Velocity Analysis

The analysis, which determines the magnitude and direction of the rotor induced velocity, v_i , assumes that the vector is always parallel to the rotor resultant force vector. Therefore, in the following discussion, the vector notation is dropped and the quantity v_i is the magnitude of the local induced velocity.

This quantity is defined as

$$v_i = \bar{v}_i F_N \quad (139)$$

where

\bar{v}_i = the nominal value of v_i across the rotor disc
(the average v_i is 8/9 of \bar{v}_i)

F_N = a function for the value of v_i normalized by \bar{v}_i

Both \bar{v}_i and F_N are either determined internally by C81 or are input in tabular form as functions of μ and α_{WP} (the wake-plane angle of attack, where the wake plane is that plane perpendicular to the resultant force vector).

If the rotor induced velocity table is not being used, then

$$F_N = \frac{4}{3} \times [1 + f_1(\mu) \cos \psi] + f_2(x, \psi) f_1(\mu) K_{27} \sqrt{-0.5 v_N^2 + \sqrt{0.25 v_N^4 + (\bar{v}_i)_N^2}} \quad (140)$$

where

v_i is the local induced velocity

\bar{v}_i is the nominal induced velocity across the rotor disc

x is nondimensional blade station (0 = root, 1 = tip)

ψ is the blade azimuth angle relative to the freestream velocity vector

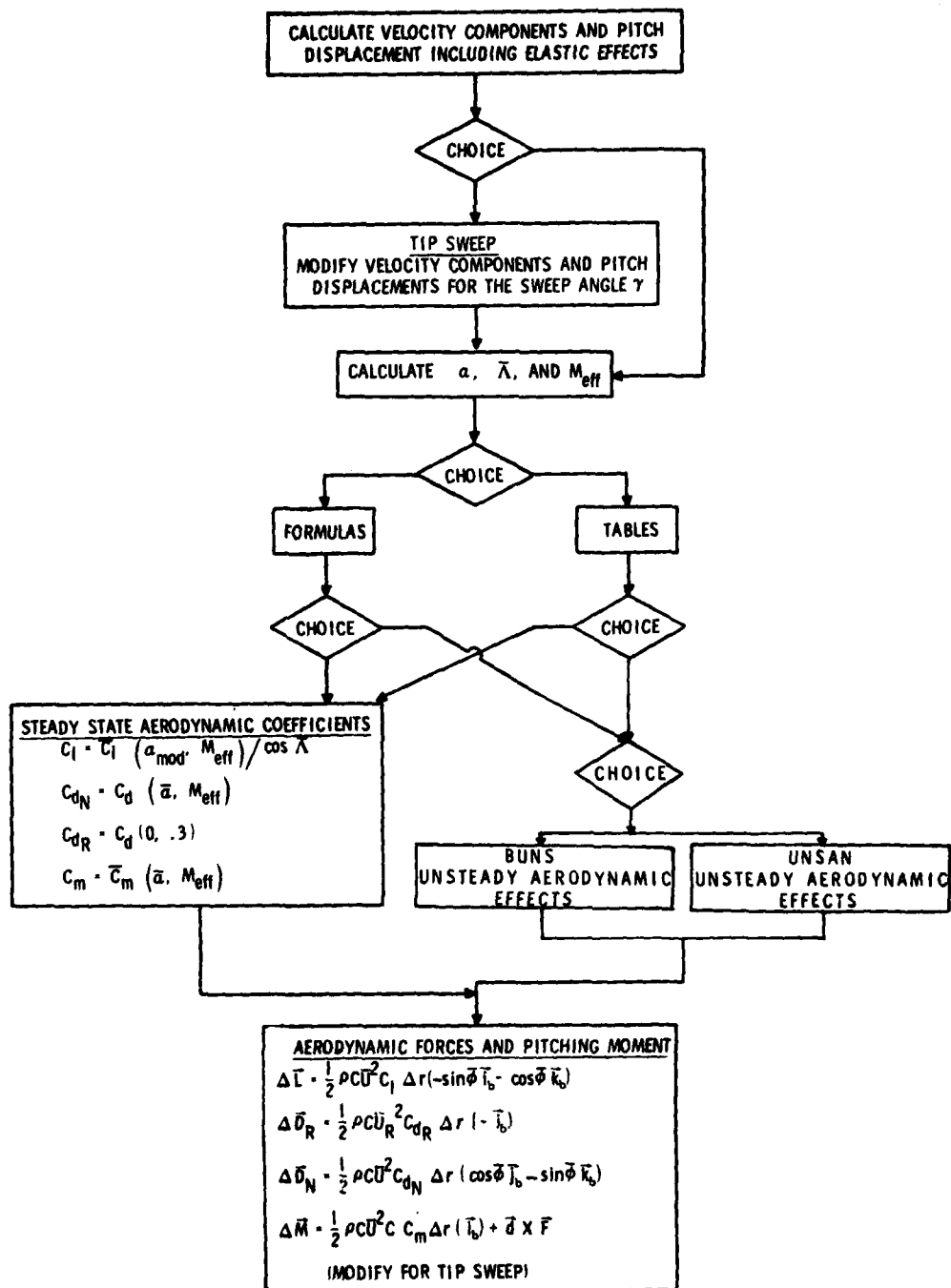


Figure 17. Flow Chart for Rotor Aerodynamic Logic.

K_{27} is the coefficient for tip vortex effect (See Volume II Section 3.9.2)

V_N is the flightpath airspeed in ft/sec divided by 1.0 ft/sec

$(\bar{V}_i)_N$ is \bar{V}_i in ft/sec divided by 1.0 ft/sec

The two functions, f_1 and f_2 , are defined as follows:

$$f_1(\mu) = \begin{cases} 0.5 & \text{if } \Omega < 1 \text{ rad/sec} \\ 11.25 \mu, & \text{if } \Omega \geq 1 \text{ and } \mu < 0.1067 \\ 1.36 - 1.5 \mu, & \text{if } \Omega \geq 1 \text{ and } 0.1067 \leq \mu < 0.5733 \\ 0.5, & \text{if } \Omega \geq 1 \text{ and } \mu \geq 0.573 \end{cases} \quad (141)$$

$$f_2(x, \psi) = \begin{cases} 0.0, & \text{if } (x < .7) \\ & \text{or } (105^\circ < \psi < 255^\circ) \\ & \text{or } (315^\circ < \psi < 360^\circ) \\ & \text{or } (0^\circ < \psi < 45^\circ) \\ \sin[6(\psi - 45^\circ)], & \text{if } (x \geq 0.7) \text{ and} \\ & \text{if } [(45^\circ \leq \psi \leq 105^\circ) \\ & \text{or } (255^\circ \leq \psi \leq 315^\circ)] \end{cases} \quad (142)$$

The f_2 function is intended to account for the effect of tip vortex-blade interaction during transition. The effect may be deleted by setting K_{27} equal to zero.

The method of computing the average induced velocity is derived from momentum theory, and is described in Reference 10 and 11. After converting to the nomenclature and sign

¹⁰Livingston, C. L., ROTOR INDUCED VELOCITY, Bell Helicopter Company Inter-Office Memo 81:CLL:am-838, October 7, 1966.

conventions of this report, the following definitions are made for the nominal advance ratio, $\bar{\mu}$, nominal induced inflow ratio, $\bar{\lambda}_i$, and nominal inflow ratio, $\bar{\lambda}$.

$$\bar{\mu} = v_h / \Omega R \quad (143)$$

$$\bar{\lambda}_i = \bar{v}_i / \Omega R \quad (144)$$

$$\begin{aligned} \bar{\lambda} &= (v_z - \bar{v}_i) / \Omega R \\ &= v_z / \Omega R - \bar{\lambda}_i \end{aligned} \quad (145)$$

where

v_h is the magnitude of the component of the free-stream velocity at the hub in the plane perpendicular to the rotor shaft (always positive)

v_z is the component of the free-stream velocity along the centerline of the rotor shaft (positive up)

The expression for \bar{v}_i is then

$$\begin{aligned} \bar{v}_i &= \bar{\lambda}_i (\Omega R) \\ &= \frac{C_B (\Omega R)}{\sqrt{0.866 \bar{\lambda}^2 + \bar{\mu}^2} + \frac{0.6 |C_B|^{1.5} (|C_B| + 8 |\bar{\lambda}| \bar{\lambda} / 3)}{(C_B + 8 \bar{\lambda}^2)(C_B + 8 \bar{\mu}^2)}} \end{aligned} \quad (146)$$

The factor C_B is the thrust coefficient corrected for tip loss and hub extent:

$$\begin{aligned} C_B &= C_T / 2(B^2 - X_h^2) \\ &= T / [2\rho \pi R^2 (\Omega R)^2 (B^2 - X_h^2)] \end{aligned} \quad (147)$$

¹¹Drees, J. M., A THEORY OF AIRFLOW THROUGH ROTORS AND ITS APPLICATIONS TO SOME HELICOPTER PROBLEMS, The Journal of The Helicopter Society of Great Britain, Vol. 3, No. 2, 1949, pp. 79-104.

where

T is thrust

ρ is air density

R is rotor radius

X_h is the hub extent divided by the rotor radius

B is the tip-loss factor

T is the average thrust for an inelastic rotor and the filtered thrust for an elastic rotor. The numerical filter used in C81 is described in Section 8.3.1.

The user may input a tip-loss factor, B, or by inputting zero, use the default expression

$$B = 1 - \frac{\sqrt{2C_T}}{b} \quad (148)$$

where b is the number of blades.

Equation (146) cannot be solved in closed form since $\bar{\lambda}$ is a function of \bar{V}_i , so the equation is solved by iteration in subroutine VIND. The flow chart of the subroutine is shown in Figure 18. The equation for VIR corresponds to Equation (146) except that the numerator and denominator have both been multiplied by ΩR so that the units of all the terms in the equation are in powers of feet per second rather than being nondimensional.

When the center of gravity of the rotorcraft is between one-fourth and one rotor diameter above the ground and the airspeed is less than 30 feet per second, \bar{V}_i is corrected in subroutine VIND for ground effect. The correction is

$$(\bar{V}_i)_{IGE} = (\bar{V}_i)_{OGE} [1 + (G - 1)\{(V - 30)/30\}^2] \quad (149)$$

where

$(\bar{V}_i)_{OGE}$ is the value of \bar{V}_i from iterative solution of Equation (146), i.e., out-of-ground effect

G is 0.25 plus the altitude of the cg divided by the rotor diameter, and

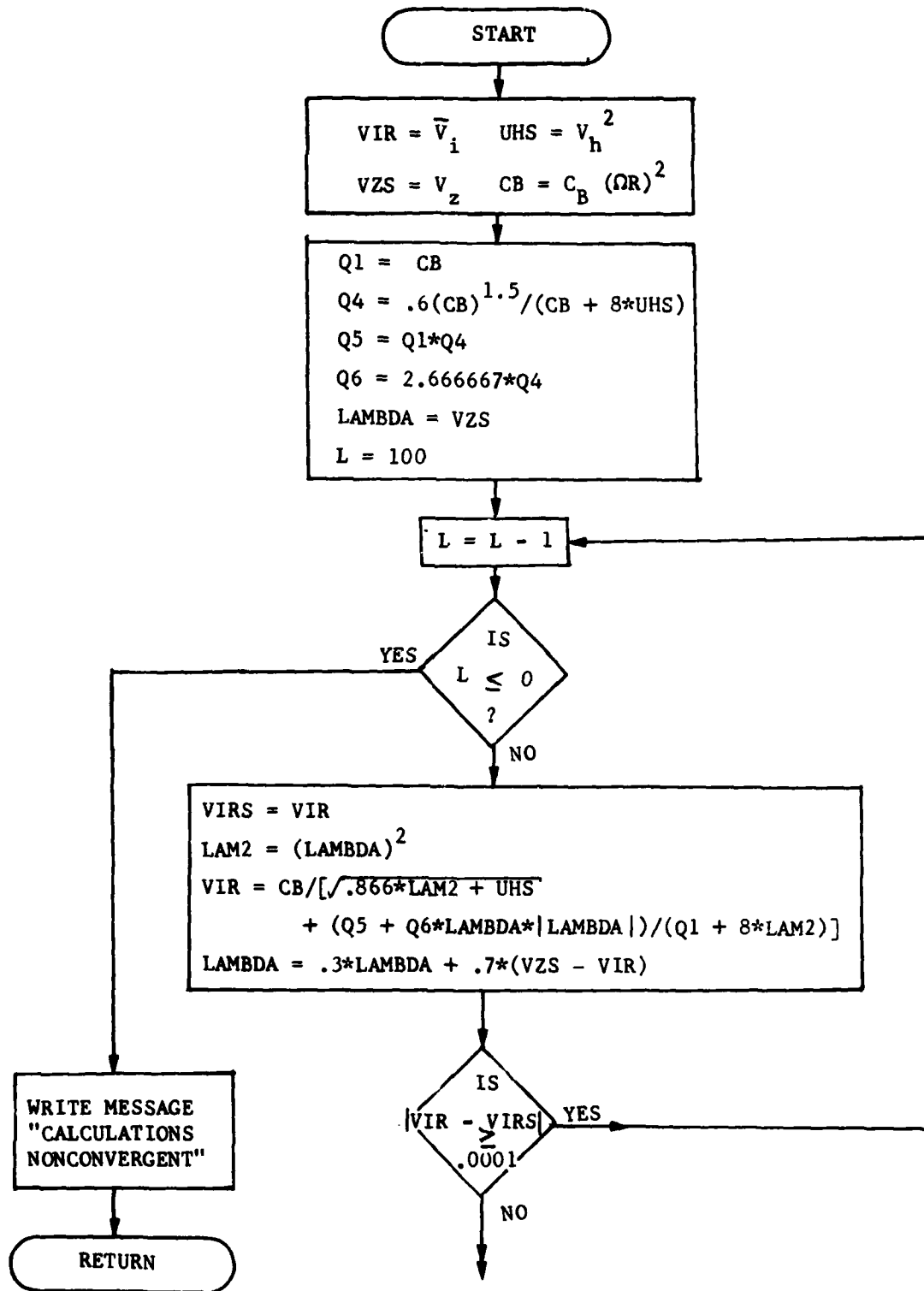


Figure 18. Flow Chart of Induced Velocity Calculations.

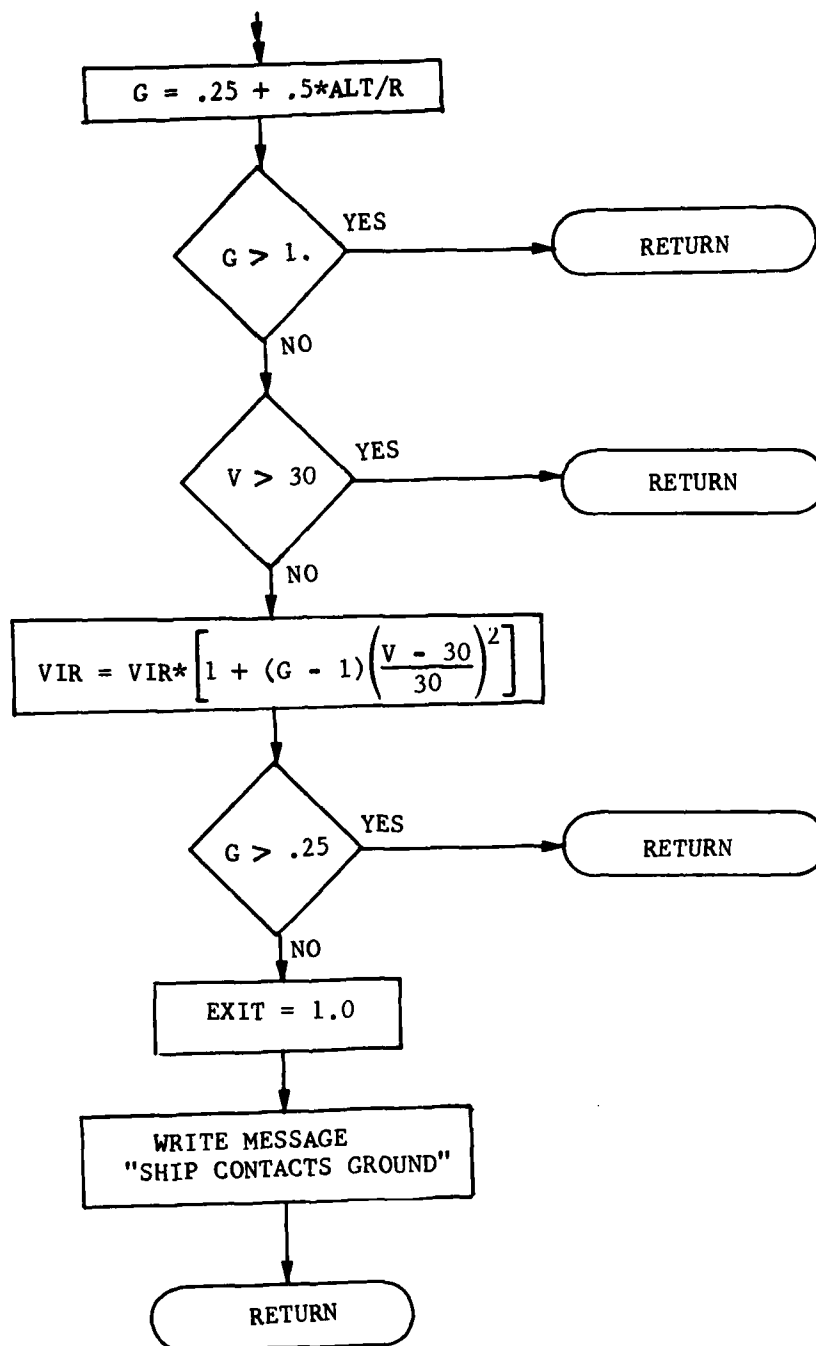


Figure 18. Concluded.

V is the flight path velocity in feet per second

If the value of G drops below 0.25 the rotorcraft is assumed to have contacted the ground, and the computer run terminates.

The user may input rotor induced velocity distribution and average induced velocity tables instead of using the C81-calculated values for F_N and \bar{V}_i , respectively. These two tables are bivariate in μ and α_{WP} , and are assumed to have been calculated at a reference value of the resultant force, F_R . The advance ratio, μ , is based upon the total free-stream velocity, and α_{WP} is the angle-of-attack of the wake plane, which is that plane perpendicular to the resultant force. The assumption is made that the total momentum induced velocity will be parallel to the resultant force, i.e., perpendicular to the wake plane. This assumes that the radial and swirl components are negligible. Defining the set of unit vectors \bar{i} , \bar{j} , and \bar{k} , which are in a new shaft axis coordinate system, then the resultant force and velocity vectors are

$$\bar{F} = H \bar{i} + Y \bar{j} + T \bar{k} \quad (150a)$$

$$\bar{U} = U \bar{i} + V \bar{j} + W \bar{k} \quad (150b)$$

for rotor 1. Since rotor 2 is left-handed, the \bar{j} component of both vectors should have a minus sign for this rotor.

The shaft axis force components of the resultant force vector are average values for a quasi-static rotor and filtered values for a time-variant rotor.

The dot product of these two vectors yields

$$\bar{F} \cdot \bar{U} = |\bar{F}| |\bar{U}| \cos \alpha' = HU + YV + TW \quad (151)$$

where α' is the smallest angle between the two vectors. The wake-plane angle of attack, α_{WP} , equals $90 - \alpha'$. Since

$$\cos \alpha' = \sin (90 - \alpha') = \sin \alpha_{WP} \quad (152)$$

Then

$$\alpha_{WP} = \sin^{-1} \left(\frac{HU + YV + TW}{\sqrt{H^2 + Y^2 + T^2} \sqrt{U^2 + V^2 + W^2}} \right) \quad (153)$$

In like manner, the wake-plane flapping angles, with respect to the mast, can also be defined by using the dot product, yielding

$$a_{1_{WP}} = \sin^{-1} \frac{H}{H^2 + T^2} \quad (154a)$$

$$b_{1_{WP}} = \sin^{-1} \frac{Y}{Y^2 + T^2} \quad (154b)$$

Figure 19 defines these three angles, while Figure 20 shows the wake-plane phase angle, ϕ_{WP} , and the two auxiliary vectors used to calculate it.

The phase angle is a sideslip angle in the wake plane, and is used to orient the zero wake azimuth position relative to the zero azimuth position of the rotor. The zero azimuth wake position is the position defined by the projection of the velocity vector in the wake phase. Since \bar{F} is perpendicular to the wake plane, and the projection of \bar{U} is in the wake plane, $\bar{B} = \bar{F} \times \bar{U}$, must lie in the wake plane at an angle of 90° to \bar{U} . The cross product is

$$\bar{B} = \bar{F} \times \bar{U} = (YW - TV)\bar{i} - (HW - TU)\bar{j} + (HV - YU)\bar{k} \quad (155)$$

The unit vector defining the intersection of the wake plane and the plane of zero rotor azimuth is \bar{A} .

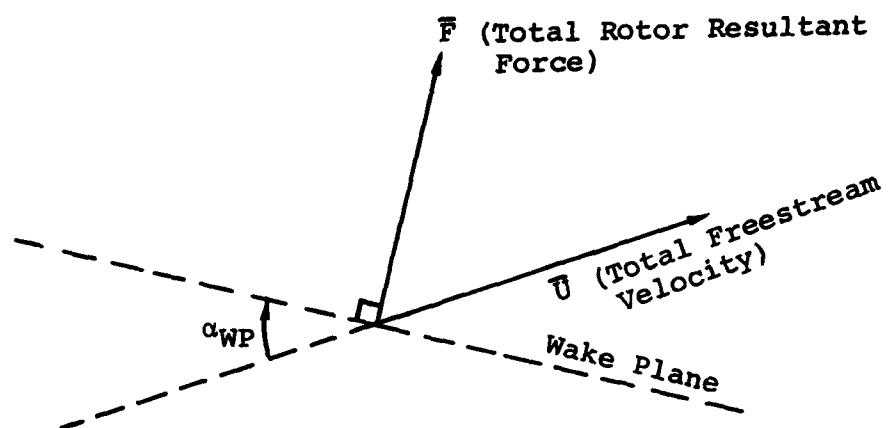
$$\bar{A} = \cos(a_{1_{WP}})\bar{i} - \sin(a_{1_{WP}})\bar{k} \quad (156)$$

and

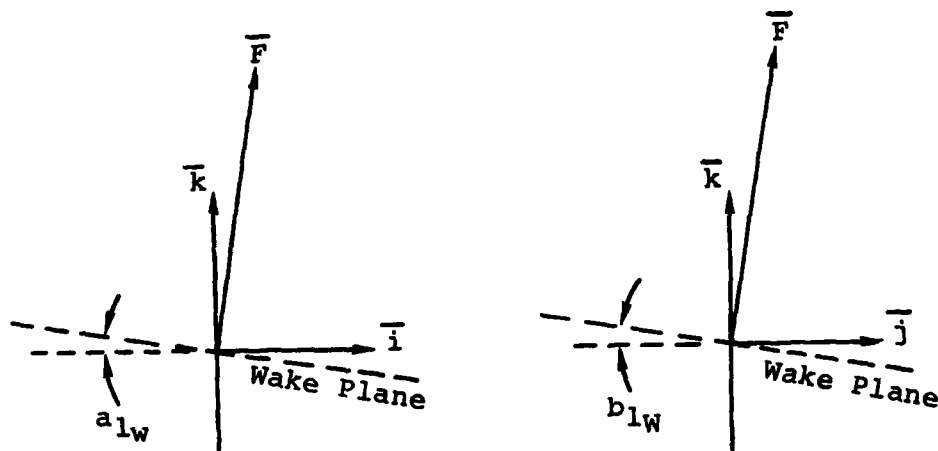
$$\begin{aligned} \bar{A} \cdot \bar{B} &= A B \cos \phi' = (YW - TV) \cos(a_{1_{WP}}) \\ &\quad + (YU - HV) \sin(a_{1_{WP}}) \end{aligned} \quad (157)$$

Since $\bar{A} = 1$ by definition, and $\phi_{WP} = 90 - \phi'$

$$\phi_{WP} = \sin^{-1} \left(\frac{(YW - TV) \cos(a_{1_{WP}}) + (YU - HV) \sin(a_{1_{WP}})}{\sqrt{(YW - TV)^2 + (HW - TU)^2 + (HV - YU)^2}} \right) \quad (158)$$



(a) Wake-Plane Complex Angle of Attack, α_{wp}



(b) Wake-Plane Longitudinal Flapping Angle, a_{1w}

(c) Wake-Plane Lateral Flapping Angle, b_{1w}

Figure 19. Wake-Plane Angle of Attack and Flapping Angles.

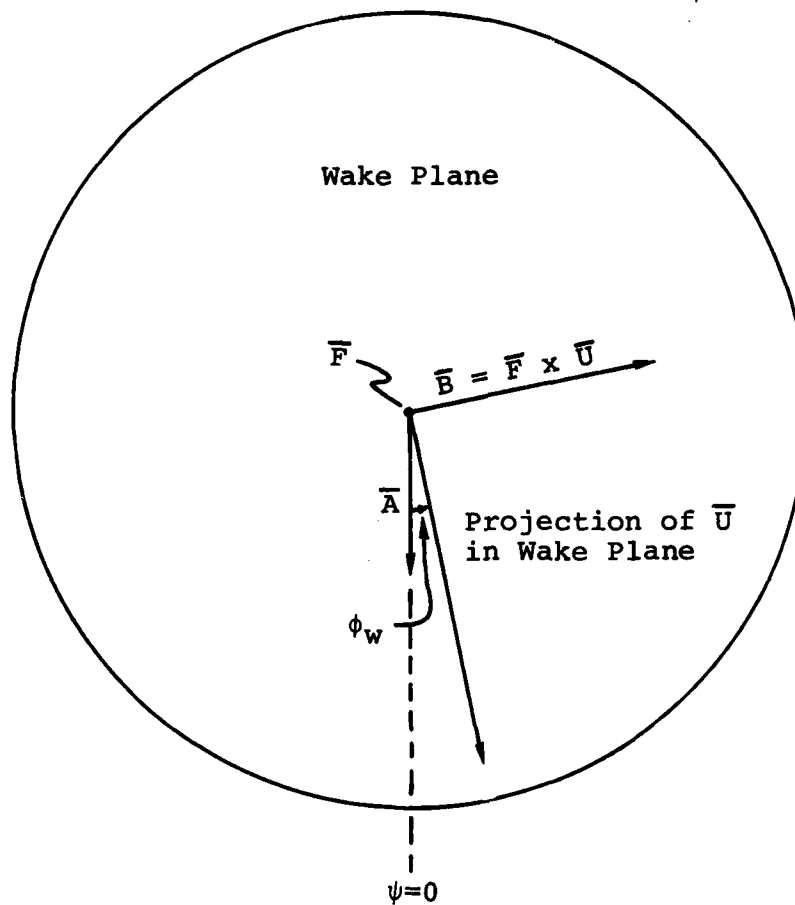


Figure 20. Wake-Plane Phase Angle.

Once \bar{F} and α_{WP} have been computed at a given instant in the calculations, either trim or maneuver, the values of μ and α_{WP} are used to interpolate the harmonic coefficients of the rotor induced velocity and the average induced velocity from the input tables. Defining the harmonic coefficients to be

$$\begin{aligned}\eta_{\sin}(r, n) &= \text{sine component of } n^{\text{th}} \text{ harmonic at radius } r \\ \eta_{\cos}(r, n) &= \text{cosine component of } n^{\text{th}} \text{ harmonic at radius } r\end{aligned}$$

then the value of the distribution function at a particular azimuth and radius is

$$\begin{aligned}F_N(r, \psi) = \sum_{n=0}^{N=NHARM} \{ &\eta_{\sin}(r, n) \sin(n\psi - \phi_{WP}) \\ &+ \eta_{\cos}(r, n) \cos(n\psi - \phi_{WP}) \} \quad (159)\end{aligned}$$

where NHARM is the number of harmonics used in the model.

The average induced velocity interpolated from the table is modified to account for any difference between the average or filtered resultant force computed by C81 at this instant and the reference value used to generate the table. The instantaneous average induced velocity is

$$(\bar{v}_{i_{\text{inst}}}) = \left\{ \frac{\bar{v}_{i_{\text{avC81}}}(F_{C81})}{\bar{v}_{i_{\text{avC81}}}(F_R)} + 0.0763 \left(1 - \frac{F_{C81}}{F_R}\right) \right\} \bar{v}_i(\mu, \alpha_{WP}) \quad (160)$$

in which

$\bar{v}_{i_{\text{avC81}}}(F_{C81})$ is the average induced velocity computed by subroutine VIND for the instantaneous average or filtered value of resultant force computed by C81

$\bar{v}_{i_{\text{avC81}}}(F_R)$ is the average induced velocity computed by subroutine VIND for the reference resultant force for which the tables were computed

F_{C81} is the instantaneous average or filtered resultant force computed by C81

F_R is the reference resultant force at which the tables were computed

$\bar{V}_i(\mu, \alpha_{WP})$ is the average induced velocity interpolated from the input table

This expression has been derived empirically from AR9102 runs. It should be noted that the tables input to C81 should be based on a resultant force roughly equivalent to the resultant force computed in C81.

The instantaneous induced velocity at a given radius and azimuth is

$$\bar{V}_i(r, \psi) = (\bar{V}_{i_{inst}}) F_N(r, \psi) \quad (161)$$

3.4.3 Blade Reference Velocities

The reference axis system used for blade aerodynamics is the blade reference system described in Appendix A. We will express the relative wind approaching point p on the blade as

$$\bar{V}_p = U_T \bar{i}_b + U_R \bar{j}_b - U_p \bar{k}_b \quad (162)$$

The axis systems and wind velocity components are shown in Figure 21. In the determination of angle of attack and dynamic pressure $\dot{Z} \cos \beta$ and $\ddot{Z} \cos \beta$ are assumed equal to \dot{Z} and \ddot{Z} . The angle from the blade xy-plane to the section reference line is θ_f , and the angle from the blade xy-plane to $(U_T \bar{i}_b - U_p \bar{k}_b)$ is ϕ_A .

Let

$$U^2 = U_T^2 + U_p^2 \quad (163)$$

Then the dynamic pressure is

$$q = \frac{1}{2} \rho U^2 \quad (164)$$

The inflow angle is

$$\phi_A = \tan^{-1} \frac{U_p}{U_T} \quad (165)$$

and the angle of attack is

$$\alpha = \theta_f + \phi_A + \phi \quad (166)$$

The calculation of θ_f is described in Section 8. The elastic twist, ϕ , is obtained from the blade modal equations. The net geometric angular velocities and accelerations are given by

$$\dot{\theta} = \dot{\theta}_f + \dot{\phi} \quad (167)$$

$$\ddot{\theta} = \ddot{\theta}_f + \ddot{\phi} \quad (168)$$

Also

$$\dot{\alpha} = \dot{\theta} + \dot{\phi}_A \quad (169)$$

3.4.4 Steady State Aerodynamic Coefficients

3.4.4.1 Lift and Drag Coefficients

The methods for calculating C_l , C_d , and C_m for steady state assumptions are discussed in Reference 4. Formulas or tables can be used for these evaluations. Aerodynamic data tables for C_l , C_d , and C_m may be supplied by the user, or a set of NACA 0012 airfoil data tables is available as compiled data.

Usually the blade aerodynamics are defined in a plane perpendicular to the leading edge. However, investigators have found that the angle in the xy-plane between the wind vector and the leading edge of the blade, the yawed flow angle, Λ , influences the aerodynamics forces generated. From Figure 21,

$$\Lambda = \tan^{-1} \frac{U_R}{U_T} \quad (170)$$

¹²Harris, F. D., Tarzanin, F. J., Jr., and Fisher, R. D. Jr., ROTOR HIGH SPEED PERFORMANCE, THEORY VS. TEST, Journal of the American Helicopter Society, Volume 15, No. 3, July 1970, pp. 35-44.

¹³Hoerner, Signard F., FLUID-DYNAMIC DRAG, New York, N.Y., Published by the author, 1958, pp. 15-20 to 15-24.

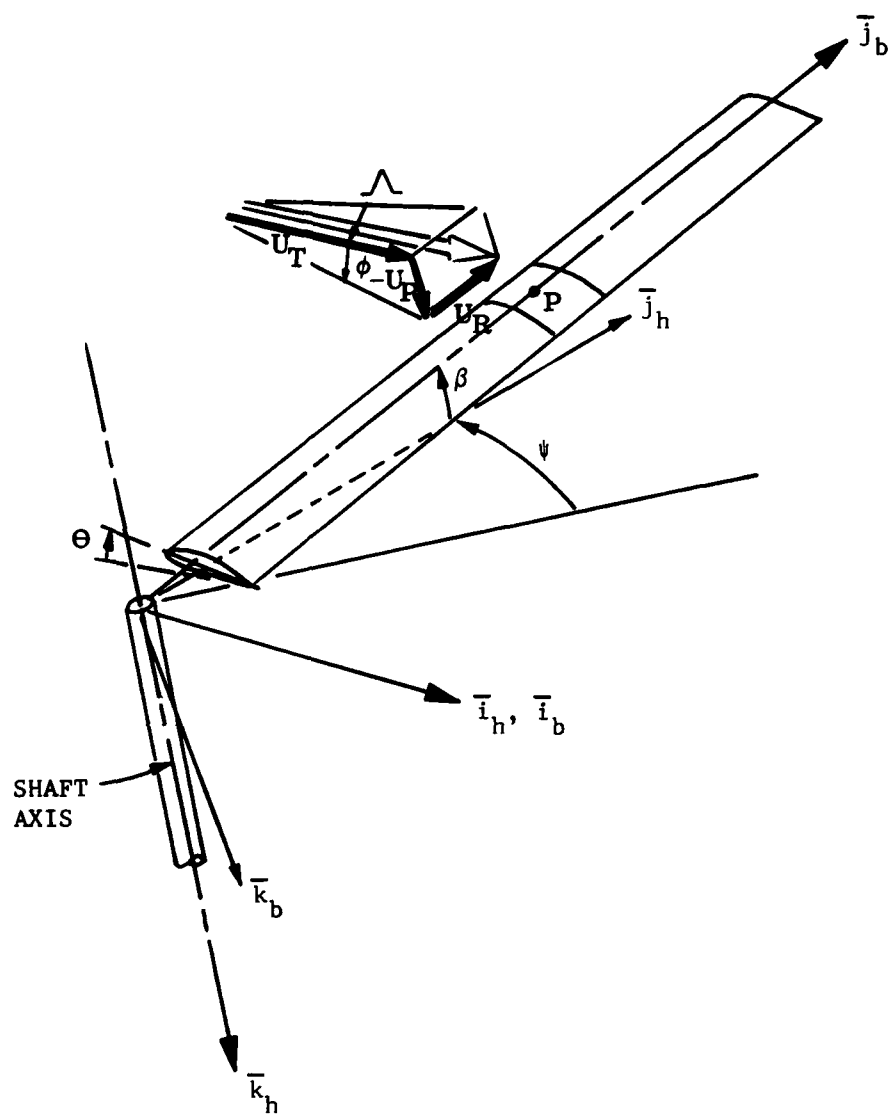


Figure 21. Reference Axis System for Blade Aerodynamics.

Harris's development (Reference 12) suggests that the influence of yawed flow be included in all aspects of the steady state lift determination. Hoerner, in Reference 13, emphasizes the need for varying the effective Mach number with Λ to improve correlation with test data. A modified angle of attack and a three-dimensional effective Mach number are calculated as follows for $\alpha < 30^\circ$:

$$\bar{\Lambda} = \text{sign}(\Lambda) \cdot \min \left\{ \begin{array}{l} \Lambda \\ 60^\circ \end{array} \right\} \quad (171)$$

$$\alpha_{\text{mod}} = \alpha \cos \bar{\Lambda} \quad (172)$$

$$M_{\text{eff}} = \frac{U_R^2 + U_T^2 + U_P^2}{v_{\text{sound}}} (\cos q_1 \bar{\Lambda})^{q_2} \quad (173)$$

Hoerner's results can be closely approximated by taking $q_1 = 0.2$, $q_2 = 1$ or $q_1 = 1$, $q_2 = 0.5$; both q_1 and q_2 are inputs to the program. The steady state lift coefficient is

$$C_{1s} = C_1(\alpha_{\text{mod}}, M_{\text{eff}}) / \cos \bar{\Lambda}, \quad (174)$$

whether formulas or tables are used. For α below stall, Λ is effective only to the extent of lowering the Mach number. When α is above stall, the yawed flow consideration can delay loss of lift as illustrated in Figure 22.

The steady state drag calculation has been modified only by the inclusion of radial flow and the use of M_{eff} . According to Harris (Reference 12),

"skin friction drag force should be calculated in the direction of the resultant velocity."

This is accomplished by computing, in addition to the conventional drag normal to the blade axis, a frictional drag along the blade based on U_R . The drag coefficient appropriate for this effect is the steady state value

$$C_{dR} = C_d(\alpha = 0, M = .3) \quad (175)$$

Harris's requirement that "Pressure drag force is then calculated only in the blade element plane normal to the blade span axis" is also satisfied by using

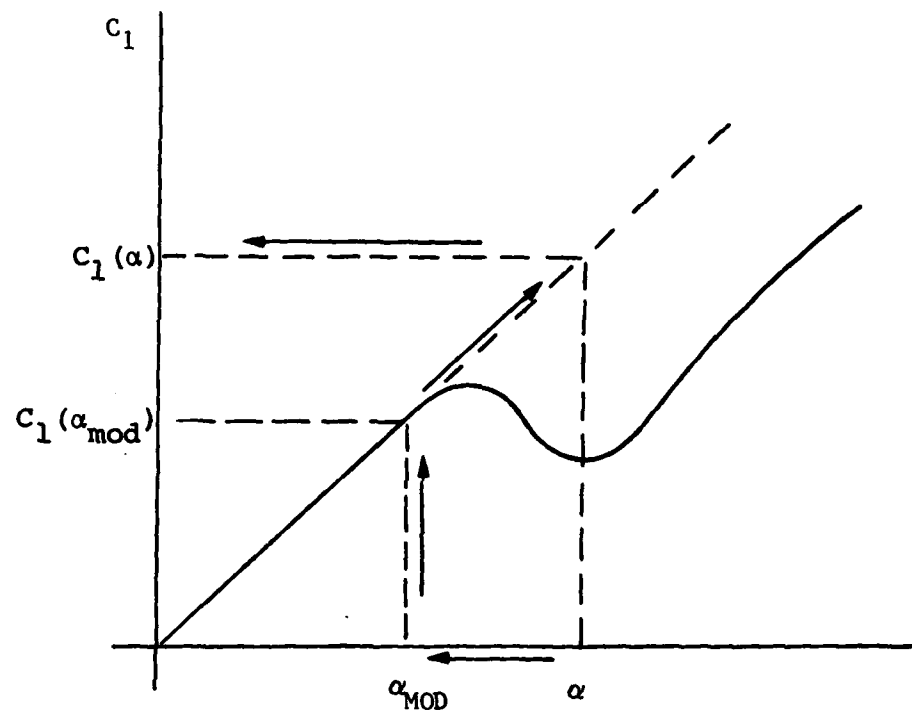


Figure 22. Effect of Yawed Flow on Lift Coefficient.

$$C_{d_N} = C_d(\alpha, M_{eff}) \quad (176)$$

3.4.4.2 Pitching Moment Coefficient

The method of calculating pitching moment coefficient is indicated in Figure 23. The C_m coefficient depends on the angle of attack, α , the effective Mach number, M_{eff} , and input constants. The inputs A_1 , A_2 , and A_3 are coefficients for a quadratic function of $|\alpha|$ determining the corresponding value of Mach number at which the C_m curve breaks sharply away from an input constant value, A_4 . For $|\alpha| < 90^\circ$, the first series of calculations and tests is to determine the relative size of α ; the angle of attack, α_B , corresponding to M_{eff} on the "break" curve; and A_5 , a critical value of angle of attack which is independent of Mach number (Figure 24, (a) and (b)). The evaluation of C_m is different for $|\alpha| \leq \alpha_B$, $\alpha_B < |\alpha| \leq A_5$ and $A_5 < |\alpha|$.

For $|\alpha|$ less than α_B ,

$$C_m = A_4 \quad (177)$$

For $|\alpha|$ between α_B and A_5 , a slope, \bar{d} , is computed for the C_m line between α_B and A_5 . This slope depends on M_{eff} and an input critical value, A_3 , as shown in Figure 24(c). The pitching moment coefficient is calculated from

$$C_m = \bar{d}(\alpha - \alpha_B)(\text{sign } \alpha) + A_4 \quad (178)$$

If α is greater than A_5 , a second slope, included in the program, is used. In this case,

$$C_m = [\bar{d}(A_5 - \alpha_B) - .00646(\alpha - A_5)](\text{sign } \alpha) + A_4 \quad (179)$$

For $\alpha > 90^\circ$, the aerodynamic center is assumed to be located at the 0.75 chord rather than at the 0.25 chord. The pitching moment about the blade reference axis (assumed to be at the 0.25 chord) is in this case mainly due to lift and drag forces.

Hence,

$$C_m = -.5(C_l \cos \alpha + C_d \sin \alpha) + A_4 \quad (180)$$

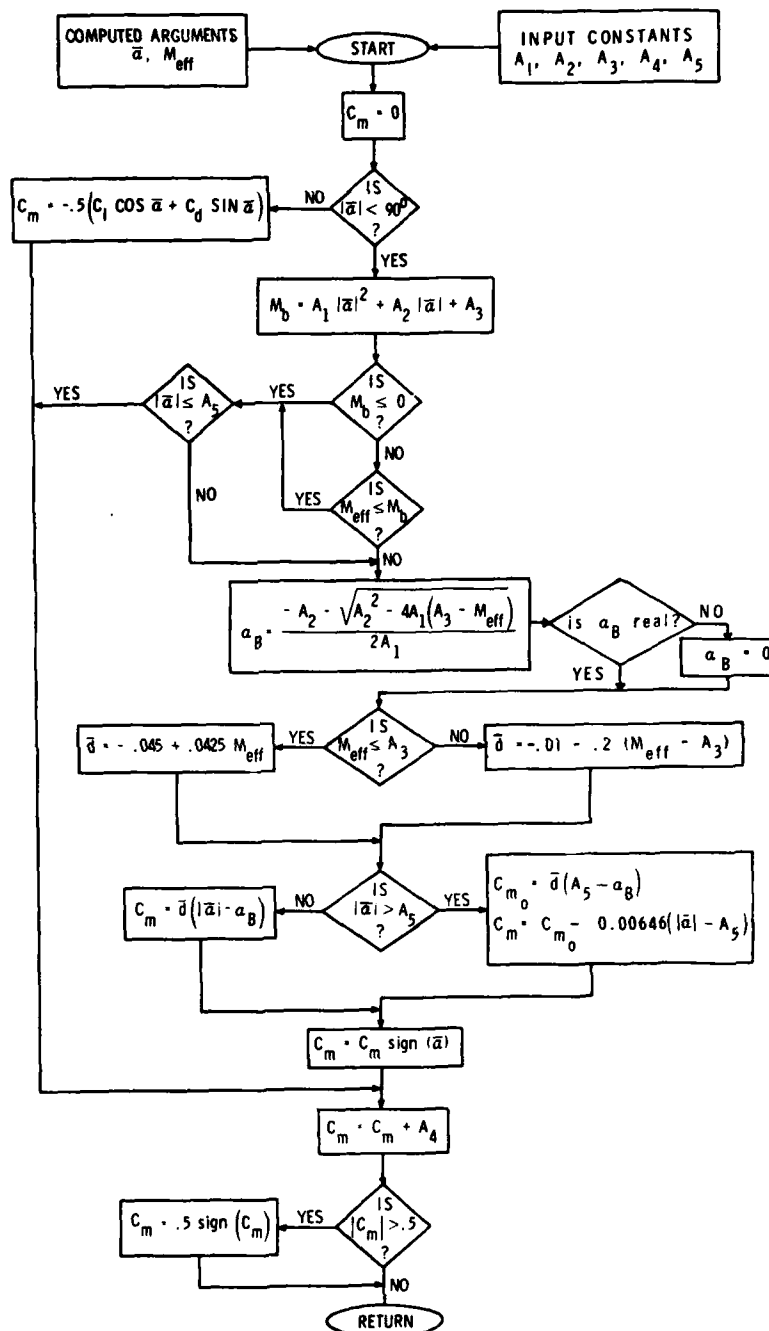
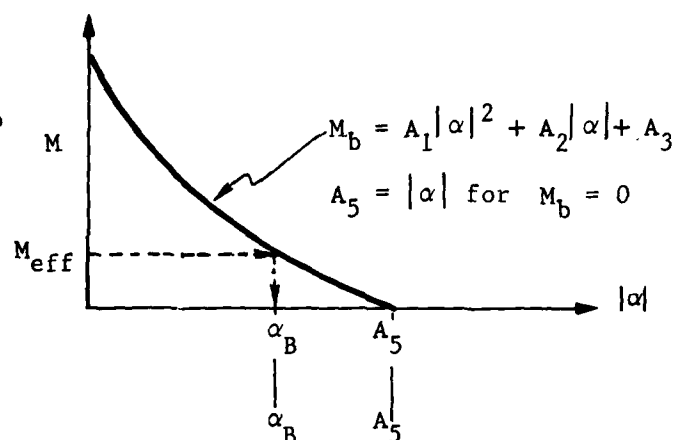
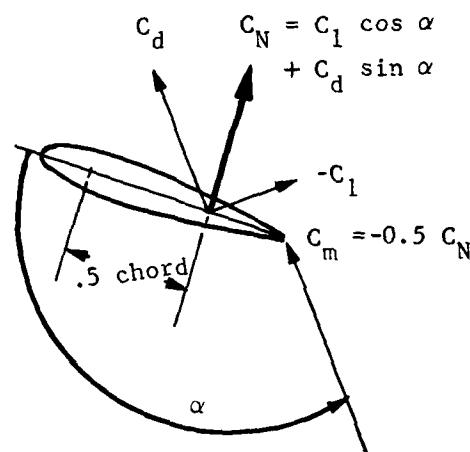
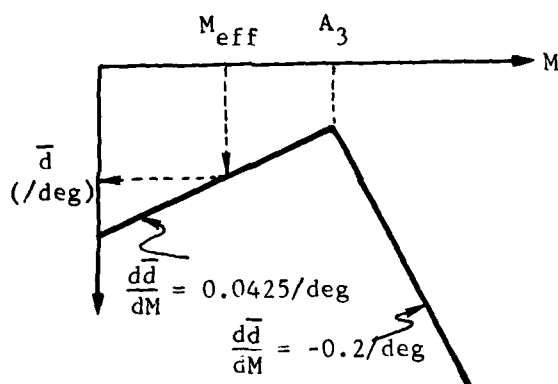
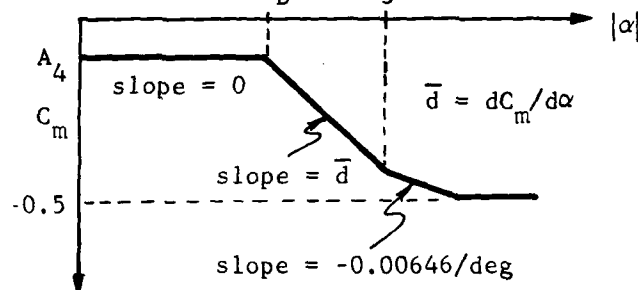


Figure 23. Flow Chart for Steady State Pitching Moment Calculation.

- (a) If $|\alpha| < 90^\circ$, determine α_B and A_5 from equation for M_b and value of M_{eff} ; otherwise go to (d) to determine normal force (C_N).



- (b) If $|\alpha| \leq \alpha_B$, set $C_m = A_4$; otherwise go to (c) to determine the value of \bar{d} .



- (c) Determine value of \bar{d} as a function of M_{eff} ; note that \bar{d} is a slope and $d\bar{d}/dM$ is the rate of change of a slope.

- (d) If $|\alpha| \geq 90^\circ$, lift and drag act at 75% chord, and hence contribute to pitching moment.

Figure 24. Determination of Steady State Pitching Moment Coefficient.

The relationships of the blade profile and the aerodynamic vectors are shown in Figure 24(d). As shown in the flow diagram (Figure 23), the magnitude of C_m is limited to 0.5 in any case.

3.4.4.3 Tip Sweep Effect

Tip sweep affects the aerodynamic forces on the tip segment of the blade. For a sweep angle γ (Figure 25), velocities and angle-of-attack components are modified as follows:

$$\bar{U}_R = U_R \cos \gamma + U_T \sin \gamma \quad (181)$$

$$\bar{U}_T = U_T \cos \gamma - U_R \sin \gamma \quad (182)$$

$$\bar{U} = \bar{U}_T^2 + \bar{U}_P^2 \quad (183)$$

$$\bar{q} = \frac{1}{2} \rho \bar{U}^2 \quad (184)$$

Then the revised inflow angle and angle of attack are

$$\bar{\phi}_A = \tan^{-1} \frac{U_P}{\bar{U}_T} \quad (185)$$

$$\bar{\theta} = \theta \cos \gamma \quad (186)$$

$$\bar{\alpha} = \bar{\theta} + \bar{\phi}_A \quad (187)$$

and

$$\bar{\lambda} = \tan^{-1} \frac{U_R}{\bar{U}_T} \quad (188)$$

3.4.4.4 Aerodynamic Forces and Moments

Aerodynamic forces and moments at a representative blade segment are then

Lift:

$$\Delta L = \frac{1}{2} \rho c U^2 \Delta r (-C_{d_N} \sin \phi_A - C_l \cos \phi_A) \quad (189)$$

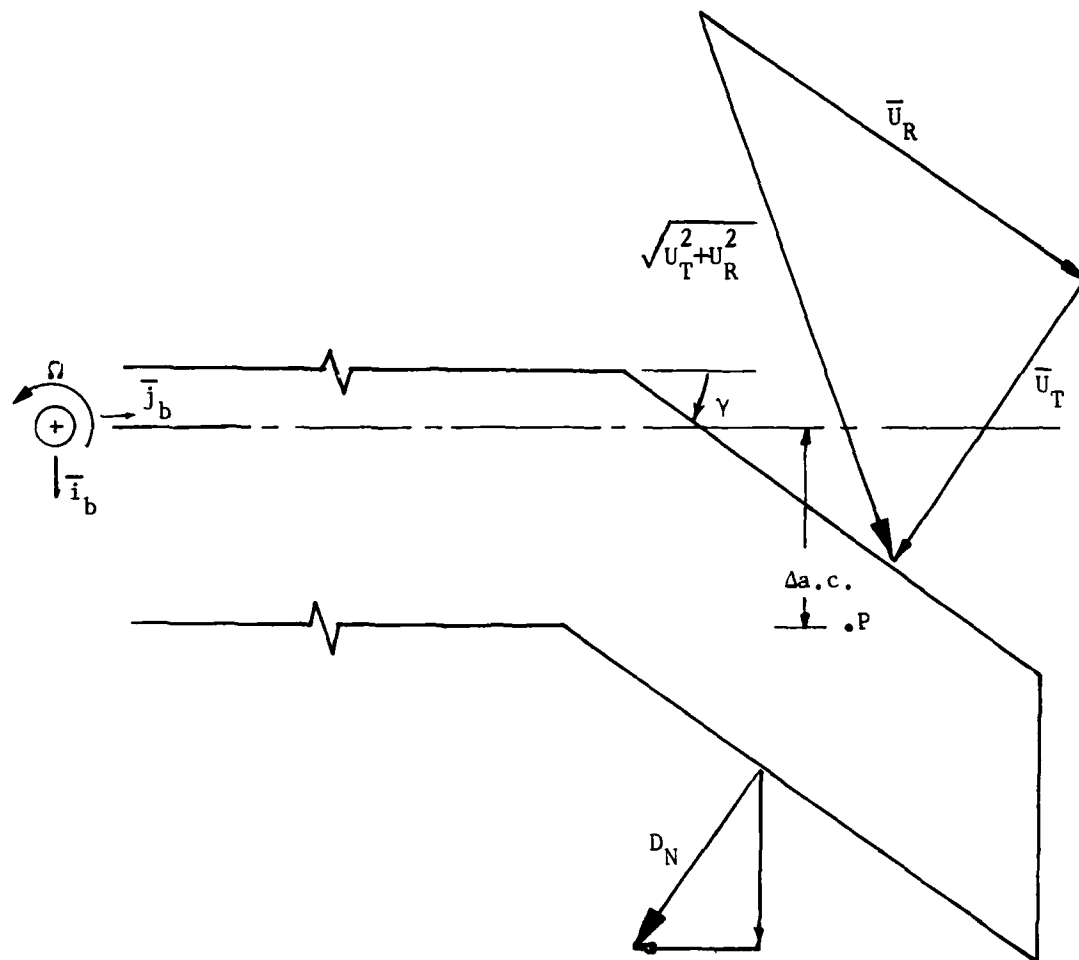


Figure 25. Effect of Tip Sweep.

Radial Component of Drag:

$$\Delta D_R = \frac{1}{2} \rho c U^2 C_{d_R} \Delta r \quad (190)$$

Normal Component of Drag:

$$\Delta D = \frac{1}{2} \rho c U^2 \Delta r (C_{d_N} \cos \phi_A - C_l \sin \phi_A) \quad (191)$$

Pitching Moment:

$$\Delta M = \left\{ \frac{1}{2} \rho c U^2 (c C_m) \Delta r \right\} + (\Delta a.c.) \Delta L \quad (192)$$

where

$\Delta a.c.$ is positive if the aerodynamic center is ahead of the reference axis.

At the blade tip, \bar{U} and $\bar{\phi}$ replace U and ϕ in the calculations. Also, the normal component of drag ΔD_N has components in the blade axis system defined by

$$\begin{aligned} \Delta D_{N_{tip}} = \frac{1}{2} \rho c \bar{U}^2 C_d \Delta r & (-\sin \gamma \cos \bar{\phi}_A \\ & + \cos \gamma \cos \bar{\phi}_A + \sin \bar{\phi}_A) \end{aligned} \quad (193)$$

The $\Delta a.c.$ shown for the tip (see Figure 25) may be input for any or all blade stations.

The radial component of drag at the tip is taken in the same direction as for the rest of the blade.

3.4.5 Unsteady Aerodynamics

The following two sections are discussions of the BUNS and UNSAN unsteady aerodynamic options. The two mathematical models were developed under separate contracts with the Eustis Directorate of USAAMRDL.

3.4.5.1 BUNS Unsteady Aerodynamic Model

As previously mentioned, the additional velocities due to flexible blade dynamics can be included in computing the angle

of attack, Mach number, and dynamic pressure at a point on the blade. The major modification to the aerodynamic simulation of Reference 2, done as a part of Contract DAAJ02-70-C-0063, was the consideration of unsteady effects.

Several investigators have discussed the importance of unsteady aerodynamics on rotary-wing aircraft. Loewy and also Timman and Van de Vooren (References 14 and 15) have shown that special circulatory terms are significant in hover flight, but conservative results are obtained by neglecting them (Drees, Reference 16). On the other hand, according to Carta (Reference 17) and Harris (Reference 12), the nonsteady air loads can assume a major role in blade aeroelastic response and can produce stall flutter.

One of the major difficulties in implementing these aerodynamic refinements is the lack of meaningful measured values over the full range of angles of attack and yaw angles that are applicable for the rotating blade. In particular, the wind tunnel data are presented in terms of angle-of-attack rates and acceleration due to rotation about the pitch-change axis ($\dot{\theta}$, $\ddot{\theta}$).

Rotation about the shaft also results in inflow angle rates and acceleration, $\dot{\phi}$, $\ddot{\phi}$; however, the damping and inertial effects from these rates are not the same as from pitch-change rates. Simplification of the problem is unavoidable due to the lack of data. It is therefore appropriate in the calculation of unsteady aerodynamics to use $\dot{\theta}$ and $\ddot{\theta}$ in terms related to blade motion only and $\dot{\alpha}$ in terms pertaining to stall hysteresis. The variables $\dot{\theta}$ and $\ddot{\theta}$ include changing geometric pitch due to cyclic variations, control motions, and elastic blade torsion.

¹⁴Loewy, R. G., A TWO-DIMENSIONAL APPROXIMATION TO THE UNSTEADY AERODYNAMICS OF ROTARY WINGS, Journal of the Aeronautical Sciences, 24(2) January 1957, pp. 81-92.

¹⁵Timman, R., and Van De Vooren, A. I., FLUTTER OF A HELICOPTER ROTOR ROTATING IN ITS OWN WAKE, Journal of the Aeronautical Sciences, 24(9) September 1957, pp. 694-702.

¹⁶Drees, J. M., AEROELASTIC ROTOR PHENOMENA AND NONSTEADY ROTOR AERODYNAMICS, Annals of the New York Academy of Sciences, Volume 154, Article 2., 1968, pp. 481-504.

¹⁷Carta, F. O., Casellini, L. M., Arcidiacono, P. J., and Elman, H. L., ANALYTICAL STUDY OF HELICOPTER ROTOR STALL FLUTTER, paper presented at the 26th Annual National Forum of the American Helicopter Society, Washington, D.C., 1970.

The remaining consideration is the blade section linear acceleration. The principal effect is due to the component normal to the blade xy-plane (the heaving acceleration) and is represented as the sum of the rigid body and elastic accelerations (Z). The linear accelerations in the xy-plane are not considered in the aerodynamics.

The computer program allows the user the option of including or omitting the unsteady aerodynamic effects. The flow diagram in Figure 15 indicates optional paths of calculation. The application of the unsteady effects to the calculation of incremental aerodynamic coefficients in stalled or unstalled flow is discussed in the following sections.

3.4.5.1.1 Pitching Moment

The aerodynamic pitching moment for steady-state assumptions has first been obtained from data tables or from formulas. Unsteady effects that include pitching velocity and acceleration of the section, both elastic and rigid body, can now be determined. The technique developed by Carta, et al. (References 17 and 18) is based on data for a two-dimensional airfoil executing forced, sinusoidal motion.

The analytical background for the theory of unsteady aerodynamics used by Carta is found in Bisplinghoff (Reference 19), and a similar discussion is given by Scanlan and Rosenbaum (Reference 20). The basic development is referred to a point aft of the quarter chord, so that equations for both the normal force and the pitching moment are usually presented and, subsequently, the reference is shifted to the quarter chord. Carta's work is unique in the development of tables based on measured data and theoretical considerations.

It was assumed in Carta's method that "the sinusoidal data could be generalized, through crossplots, to functions of instantaneous angle of attack, angular velocity parameter A, and angular

¹⁸Arcidiacono, P. J., Carta, F. O., Casellini, L. M., and Elman, H. L., INVESTIGATION OF HELICOPTER CONTROL LOADS INDUCED BY STALL FLUTTER, Sikorski Aircraft, USAAVLABS Technical Report 70-2, U.S. Army Aviation Material Laboratories, Fort Eustis, Virginia, March 1970, AD869823.

¹⁹Bisplinghoff, R. L., Ashley, H., and Halfman, R. L., AERO-ELASTICITY, Cambridge, Massachusetts, Addison-Wesley Publishing Company, 1955, pp. 380-420.

²⁰Scanlan, R. H., and Rosenbaum, R., AIRCRAFT VIBRATION AND FLUTTER, New York, N.Y., The Macmillan Company, 1951, pp. 382-408.

acceleration parameter B for a given Mach number." In the considerations which follow, the parameters A and B are defined as

$$A = \left(\frac{c}{2U} \right) \dot{\alpha} \quad (194)$$

$$B = \left(\frac{c}{2U} \right)^2 \ddot{\theta} \quad (195)$$

where c is the chord length and U is the net wind velocity perpendicular to the airfoil leading edge. The actual A-B tables are listed in Reference 18, and are based on data from a differential pressure transducer mounted on a 2-foot-chord NACA 0012 airfoil. The steady-state content in the tables is removed by requiring $\Delta C_m = 0$ when $A = B = 0$. Thus, at each α the original tabular value at $A = B = 0$ was subtracted from all entries for that α . The resulting adjusted Carta tables are included in the C81 program. The effect of Mach number on the stall point is discussed by Carta (Reference 18) and the variation represented for the NACA 0012 airfoil. This stall point variation is included by computing a shift in the angle-of-attack argument before entering the adjusted A-B tables, as follows:

$$\alpha_{\text{Carta}} = |\alpha| \quad \text{for } M_{\text{eff}} \leq .2 \quad (196)$$

$$\alpha_{\text{Carta}} = |\alpha| \frac{13.5}{13.5 - 16.25(M_{\text{eff}} - .2)} \quad \text{for } .2 \leq M_{\text{eff}} < .6 \quad (197)$$

$$\alpha_{\text{Carta}} = |\alpha| \quad 1.93 \quad \text{for } M_{\text{eff}} \geq .6 \quad (198)$$

A value $\Delta C_m(\alpha_{\text{Carta}})$ is computed by interpolation from the adjusted A-B tables. The effect of Mach number is again applied by dividing this value by N where

$$N = \sqrt{1 - M_{\text{eff}}^2} \quad \text{for } M_{\text{eff}} < .6 \quad (199)$$

$$N = .8 \quad \text{for } M_{\text{eff}} \geq .6 \quad (200)$$

Thus

$$\Delta C_m = (\text{sign } \alpha) \Delta C_m(\alpha_{\text{Carta}})/N \quad (201)$$

and

$$C_m = C_m(\text{steady state}) + \Delta C_m \quad (202)$$

3.4.5.1.2 Lift Coefficient

The aerodynamic lift coefficient computed for steady state can be augmented to represent unsteady effects. The effect of the unsteady terms on lift is defined separately for stalled and unstalled regions. In the derivation of the following equations, the slope of the lift curve is assumed to be 2. The basic equation for unstalled, unsteady lift effects is, in the notation of Scanlan and Rosenbaum (Reference 20),

$$L' = \rho \pi b^3 \left(-\frac{\ddot{h}}{b} - \frac{2v}{b} C(k) \frac{\dot{h}}{b} + a \ddot{\alpha} + \left[2\left(a - \frac{1}{2}\right)C(k) - 1 \right] \frac{v}{b} \dot{\alpha} - \frac{2v^2}{b^2} C(k) \alpha \right) \quad (203)$$

where

L' is the lift per span, positive down

α is the angle of attack, excluding the effect of vertical velocity

b is the semichord

a is the distance from the midchord to the elastic axis, divided by the semichord

$C(k) = F(k) + i G(k)$ is the circulation function

$k = b\omega/v$, where ω is the frequency of oscillation

\dot{h} and \ddot{h} are respectively the vertical velocity and acceleration, positive down

v is the resultant wind velocity

In this analysis, circulation effects are simplified by assuming that k is small; that is, $\omega \ll v/b$. The following approximations are then made:

$$F(k) = 1, G(k) = 0 \quad (204)$$

Equation (203) may be rewritten with the sign convention for lift changed to positive up, h and \dot{h} replaced by $-Z$ and $-\dot{Z}$, v replaced by U , and both sides divided by the product of the chord length and the dynamic pressure, thus:

$$\frac{\Delta L}{(2b) \frac{1}{2} \rho U^2 \Delta r} = 2 \left[-\frac{b \ddot{Z}}{2 U^2} - \frac{\dot{Z}}{U} - \frac{a b^2}{2 U^2} \ddot{\alpha} - \frac{b}{U} a - \frac{1}{2} \dot{\alpha} + \frac{b}{2 U} \dot{\alpha} + \alpha \right] \quad (205)$$

The first term on the right side of Equation (205) accounts for the inertia force generated by the vertical acceleration imparted to a cylindrical volume of air with the blade chord as a diameter. The sum of the second and last terms in the brackets

$$-\frac{\dot{Z}}{U} + \alpha$$

corresponds to the angle of attack used in the steady state aerodynamic evaluation. For the rigid body mode, $-\dot{Z}/(U)$ is the contribution to angle of attack from the flapping velocity.

The third term accounts for the effect of the inertia of the cylinder of air that moves when the blade pitches. This effect should include only the pitching acceleration $\ddot{\theta}$. The fourth term is the effect of blade pitching velocity on the angle of attack and should include only the pitch rate $\dot{\theta}$. The fifth term is interpreted as a damping term based on the total angle-of-attack change rate, $\dot{\alpha}$.

Thus, the lift coefficient increment due to unsteady aerodynamics can be expressed in conventional helicopter notation:

$$\Delta C_1 = 2 \left[-\frac{b \ddot{Z}}{2 U^2} - \frac{a b^2 \ddot{\theta}}{2 U^2} - \left(a - \frac{1}{2} \right) \frac{b \dot{\theta}}{U} + \frac{b \dot{\alpha}}{2 U} \right] \quad (206)$$

If the pitch axis (or elastic axis) is assumed to be at the quarter chord, the value of a in Equation (194) is $-1/2$.

Stall hysteresis due to variation in lift with blade pitch rate is discussed by Harris (Reference 12). This dynamic stall effect is included in the following manner.

For $\alpha_{mod} > (C_{l_{max}})/\underline{a}$, use Equation (5) of Reference 12 to obtain

$$\Delta \alpha = 61.5 \ln(.6/MM) \sqrt{|\dot{\alpha} b/U|} \quad (207)$$

where

\underline{a} is the lift curve slope, and

$$MM = \begin{cases} 0.3 & \text{for } M_{eff} < 0.3 \\ M_{eff} & \text{for } 0.3 < M_{eff} < 0.6 \\ 0.6 & \text{for } M_{eff} > 0.6 \end{cases}$$

Then

$$\alpha_{RL} = \alpha_{mod} - (\text{sign } \dot{\alpha}) \text{Min} \left\{ \begin{array}{l} \Delta \alpha \\ |.2 \alpha_{mod}| \end{array} \right\} \quad (208)$$

If $\alpha_{mod} \leq (C_{l_{max}})/\underline{a}$, $\alpha_{RL} = \alpha_{mod}$.

Then obtain a lift coefficient from the tables or formulas for steady state using α_{RL} and M_{eff} as arguments. Recalling that $\alpha_{mod} = \alpha \cos \bar{\Lambda}$, the final value of lift coefficient is given by

$$C_{l_T} = C_l(\alpha_{RL}, M_{eff}) \cdot \frac{\alpha}{\alpha_{RL}} + \Delta C_l \quad (209)$$

3.4.5.1.3 Drag Coefficient

Unsteady effects on the aerodynamic drag coefficient are handled as suggested in Reference 12. Harris states, "To account for unsteady aerodynamic effect on pressure drag, the two-dimensional drag coefficient data was used, but at α_{ref} ."

Therefore, for the drag coefficient determining drag force normal to the leading edge,

$$\alpha_{RD} = \alpha - (\text{sign } \dot{\alpha}) \text{Min} \left\{ \begin{array}{l} \Delta \alpha \\ |.2 \alpha| \end{array} \right\} \quad (210)$$

and

$$C_{d_N} = C_d(\alpha_{RD}, M_{eff}) \quad (211)$$

3.4.5.2 UNSAN Unsteady Aerodynamic Model

An alternate procedure for including unsteady aerodynamics is provided in C81. The analytical development was done under Contract DAAJ02-71-C-0045 and is presented in Reference 21.

The analysis for UNSAN may be considered to start with Equations (3) and (4) of Reference 21 which give the lift and moment, per unit span. The lift expression is the same as Equation (203), Section 3.4.5.1.2.

The terms in Equations (3) and (4), Reference 21, involving the Theodorsen function can be considered as the expression

$$E = C(k) \left[\theta_v + \frac{\dot{h}_v}{V} + d \frac{\dot{\theta}_v}{V} \right] \quad (212)$$

where the subscript v indicates the vibratory part of the variable and

$$d = c(3/4 - PA) = 1/2 c(1/2 - a) \quad (213)$$

where $PA = (a + 1)/2$

Assuming simple harmonic motion for θ_v and h_v (see Equations (9) and (1) of Reference 21), appropriate substitutions give

$$E = F(k) \left[\theta_v + \frac{\dot{h}_v}{V} + d \frac{\dot{\theta}_v}{V} \right] + i G(k) \left[-i \frac{\dot{\theta}_v}{\omega} - i \frac{\dot{h}_v}{\omega V} + i \omega d \frac{\theta_v}{V} \right] \quad (214)$$

²¹Gormont, R. E., A MATHEMATICAL MODEL OF UNSTEADY AERODYNAMICS AND RADIAL FLOW FOR APPLICATION TO HELICOPTER ROTORS, Boeing-Vertol, USAAMRDL Technical Report 72-67, Eustis Directorate, U.S. Army Air Mobility Research and Development Laboratory, Fort Eustis, Virginia, May 1973, AD767240.

so that the imaginary unit is eliminated and

$$E = (F - \frac{w}{V} \frac{d}{V} G) \theta_v + \frac{F}{V} \dot{h}_v + \frac{G}{w V} \ddot{h}_v + (\frac{d}{V} F + \frac{G}{w}) \dot{\theta}_v \quad (215)$$

The contributions to blade pitch velocity and acceleration from flapping and flapping rate, $\Omega \beta$ and $\Omega \dot{\beta}$, are added, w is replaced by Ω , and an equivalent angle of attack is given as

$$\begin{aligned} \alpha_{\text{EQU}} = & \theta_o + (F - c(3/4 - PA) \frac{G}{V} \Omega) \theta_v \\ & + \tan^{-1} \left(\left[F \dot{h}_v + \dot{h}_o + \frac{G}{\Omega} \ddot{h}_v + c(3/4 - PA) \Omega \beta_o \right. \right. \\ & \left. \left. + (c(3/4 - PA) F + \frac{G}{\Omega} V) (\dot{\theta}_v + \Omega \beta_v) \right] / U_T \right) \end{aligned} \quad (216)$$

Equation (216) is identical to equation (31) in Reference 21.

The aerodynamic coefficients (C_l , C_d , and C_m) are obtained as functions of α_{EQU} and Mach number from formulas or tables as in the steady state case. Other terms involving the vibratory variables are included separately and the expressions for aerodynamic lift, drag, and moment are given in Equation (32) of Reference 21.

In order to interface this procedure with the C81 calculations, some practical means of separating the vibratory part from the total \dot{h} , θ , and β was needed. One requirement was that the routine be operable in the maneuver section.

Since \dot{h} as given by Equation (24) of Reference 21 is just U_p , Equation (26) of that reference can be expressed as

$$\dot{h}_o = V_{\text{FLT}} \sin \alpha_s - v_{Z(o)} - (\text{rate of climb}) \quad (217)$$

where \dot{h}_o is the "steady" part of \dot{h} and is available in C81.

The pitch angle, θ , and the flapping angle, β , at a blade segment are computed in the maneuver section of C81 but are not separated into steady and vibratory parts. The following assumptions (not in Reference 21) are made to implement the C81 programming:

θ_o is the collective pitch at the segment (includes built-in twist)

β_o is the precone angle

These assumptions omit steady elastic pitch deflection and steady out-of-plane bending but retain the principal contributions to θ_o and β_o .

Then

$$\dot{h}_v = \dot{h} - \dot{h}_o \quad (218)$$

$$\dot{\theta}_v = \dot{\theta} - \dot{\theta}_o \quad (219)$$

$$\dot{\beta}_v = \dot{\beta} - \dot{\beta}_o \quad (220)$$

The derivatives required are \ddot{h}_v , $\dot{\theta}_v$, $\ddot{\theta}_v$, and $\dot{\beta}$ for the basic unsteady coefficients and $\dot{\alpha}$ for stall hysteresis effects. Rather than attempt analytical derivatives, the rates are computed numerically using the formula

$$p_n^{(r)} = \frac{1}{\Delta t^r} (1 + \frac{1}{2} \nabla + \frac{1}{3} \nabla^2 + \dots)^r \nabla^r p_n \quad (221)$$

from Reference 22.

A further modification to the analysis of Reference 21 was made by providing an input, Ω_k , for computing the reduced frequency as

$$k = \frac{c \Omega_k}{2 V} \quad (222)$$

By this means the sensitivity of blade response to this part of the analysis can be investigated.

Stall hysteresis representation described in Reference 21 was retained without change. The starting equation, Equation (39) from Reference 21, corresponds to Equation (207), but UNSAN

²²Hildebrand, F. B., INTRODUCTION TO NUMERICAL ANALYSIS, New York, McGraw-Hill, 1956, pp. 134-135.

includes expanded procedures for determining the change in angle of attack for dynamic stall for C_l and for C_m (not necessarily the same).

Effects of radial flow in Reference 21 are also retained in UNSAN. These effects are similar to the radial flow considerations in BUNS. The equations for Λ are the same (Equation (53) in Reference 21 and Equation (170) in this report). A radial component of drag due to skin friction is included; see Equation (58) in Reference 21 and Equation (175). Compare Equation (75) in Reference 21 and Equation (174) in this report for the effect of Λ on the lift coefficient.

4. FUSELAGE MATHEMATICAL MODEL

4.1 INTRODUCTION

Over the past two decades, the maximum airspeeds of pure helicopters have increased twofold or more in all flight regimes (forward, rearward, lateral, and vertical). In addition, the maximum forward airspeed for composite or compound rotorcraft has increased to 300 knots or more. Consequently, the aerodynamic representation of the fuselage was improved under contract in 1973.

This section of the report documents the background and development of the fuselage mathematical model that is currently incorporated in C81. It also contains figures and tables that compare the current mathematical model to wind tunnel test data.

4.2 DEVELOPMENT OF THE FUSELAGE MATHEMATICAL MODEL

4.2.1 Background

The primary goals in the development of the current C81 representation of the fuselage aerodynamic forces and moments were to provide a mathematical model that would:

- (1) Be valid at all orientations of the fuselage with respect to the wind, with particular emphasis on simulation of the forces and moments at the nominal forward flight aerodynamic angles and of the effects of aerodynamic coupling, i.e., variation of longitudinal forces and moments with sideslip, and lateral-directional forces and moments with angle of attack.
- (2) Take maximum advantage of the availability of wind tunnel data without sacrificing or compromising the capability of inputting analytical estimates of such data.

Since the current version of the program has the capability of simulating the aerodynamic forces and moments on a wing, four stabilizing surfaces, four external stores or aerodynamic brakes, and two pylons, the fuselage representation was developed for simulating the basic fuselage only. The landing gear or skid was the only component other than the basic airframe that was considered part of the fuselage in the development of

the model. This assumption eliminates the necessity of simulating in the fuselage representation the sharp stall characteristics associated with aerodynamic surfaces.

In the formulation of the current fuselage model, three separate approaches were considered for its general form:

- (1) Equations only
- (2) Data tables only
- (3) A combination of equations and tables

It was concluded that equations were the best approach for the following reasons:

- (1) Equations are better suited than data tables to configurations where little or no test data are available and analytical or empirical predictions of the aerodynamic characteristics must be made.
- (2) Parametric studies of changes in fuselage aerodynamic characteristics can be made more easily by changing coefficients of an equation than by modifying entries in a data table.
- (3) To provide adequate tabular representation at all aerodynamic angles, it was estimated that each of the six necessary tables should be permitted at least 500 and preferably up to 1000 or 1200 entries; this would be in addition to the more than 10,000 entries allocated for the rotor airfoil data tables.
- (4) Using the method of least-squared errors, equations of order three or less can fit most test data with a root-mean-squared error per point which is well within the accuracy of the test data.
- (5) Since test data are frequently not recorded as systematically as is required for the type of table and table interpolation routine in C81, data must be plotted and/or fitted to obtain all necessary entries for such tables. If a plot or fit step is required to construct the tables, little is gained by the use of tables.
- (6) A table interpolation routine that could directly use the standard type of test data (sweeps of one angle with the other fixed) would increase run time and storage requirements for the fuselage representation.

The new representation of the fuselage is divided into two independent models and a third model which is dependent on the other two. The first model consists of six independent equations for the forces and moments, where each equation is a function of both the aerodynamic pitch and yaw angles. This model, referred to as the Nominal Angle Equation (NAE) model is intended to simulate the forces and moments at aerodynamic angles less than approximately 15 to 25 degrees in magnitude; i.e., the angles where the majority of flight occurs and for which test data are most commonly available.

The second model also consists of six independent equations and is referred to as the High Angle Equation (HAE) model. This model cannot fit test data as accurately as the NAE model, but does provide more than adequate simulation of force and moment data throughout the range of aerodynamic angles, i.e., pitch between ± 90 degrees and yaw between ± 180 degrees. The intent of this model is to follow very closely the force and moment data trends at the large angles encountered in low-speed flight (rearward, sideward, and vertical) and those which could occur after major system failures.

The third, or dependent, model provides a smooth transition between the NAE and HAE models. It, in effect, phases out one set of equations while phasing in the other set. The user may specify the angles where phasing starts and stops.

4.2.2 Choice of Reference Systems and Definitions of Angles

Choosing the equations-only approach for the general form of the current representation made it advisable to restrict the inputs to those from one specific reference system. Although it is desirable to permit the inputs to be in any conventional reference system (i.e., wind, stability, or body), doing so requires a separate representation for data from each reference system. The requirement of separate representations comes about because the generalized shapes of the force and moment curves at large angles are strongly affected by reference system. For example, in sideward flight, wind reference drag is large and side force is near zero, while for the same condition body reference drag, or axial force, is near zero and side force equals the wind reference drag. Rather than programming three separate representations, when only one would be used at any one time, the representation for wind reference data was implemented for the following reasons:

- (1) Wind reference data are consistent with previous versions of the program, which makes conversion to the current version easier.

- (2) Wind reference data are readily available from the pyramidal-type balance systems used at most low-speed wind tunnels, or may be obtained by a simple transformation from other reference systems.
- (3) The trends of wind reference fuselage forces and moments relate easily to similar data for airfoils making interpretation of wind reference inputs somewhat easier than those in other reference systems.

In the following discussion of definitions of angles and reference systems, Figures 26, 27, 28, and 29 will help visualization of the relationships involved. The orientation, or aerodynamic, angles used in the fuselage representation were defined to be consistent with wind tunnel data. That is, the orientation of the body reference system with respect to the wind reference system is defined by two ordered rotations: yaw followed by pitch, where yaw angle (ψ_w) is defined to be between ± 180 degrees and pitch angle (θ_w) to be between ± 90 degrees. See Figure 26. However, this definition creates a problem in a simulation such as C81 where the wind and fuselage are each oriented with respect to the ground, and the orientation of the fuselage with respect to the wind is not explicitly defined. Specifically, in C81 the orientation of the flightpath (a vector) is defined by the vector sum of forward, lateral, and vertical velocities (V_w , V_y , and V_z respectively) of the rotorcraft cg in ground reference. See Figure 27. On the other hand, the orientation of the fuselage (body reference system) is defined by three ordered rotations (Euler angles) from ground reference. Although the flightpath (wind vector) corresponds to the X axis of the wind reference system, there are no parameters which directly define the orientation of the wind Y and Z axes about this X axis. Since the wind reference orientation is not completely defined, the body reference cannot be directly oriented with respect to it as in the wind tunnel.

The solution to this problem is to use the Euler angles (ψ , θ , and ϕ) that orient the body reference system with respect to the ground to resolve the three ground reference velocities into body reference. See Figure 28. The results of the resolution are the body reference X, Y, and Z velocities (u , v , and w respectively). These body velocities can then be defined as the components of the flightpath velocity (V) in a reference system which has been yawed ψ_w degrees, then pitched θ_w degrees with respect to the wind vector. See Figure 29. From this definition,

$$u = V \cos \psi_w \cos \theta_w \quad (223)$$

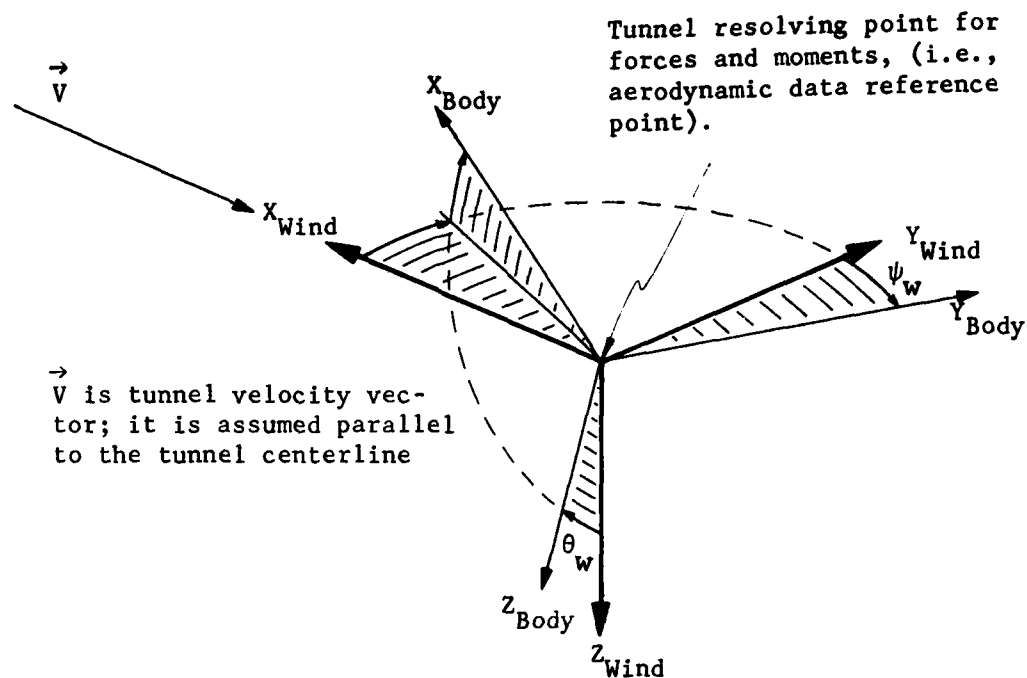


Figure 26. Definition of Aerodynamic Angles in a Wind Tunnel.

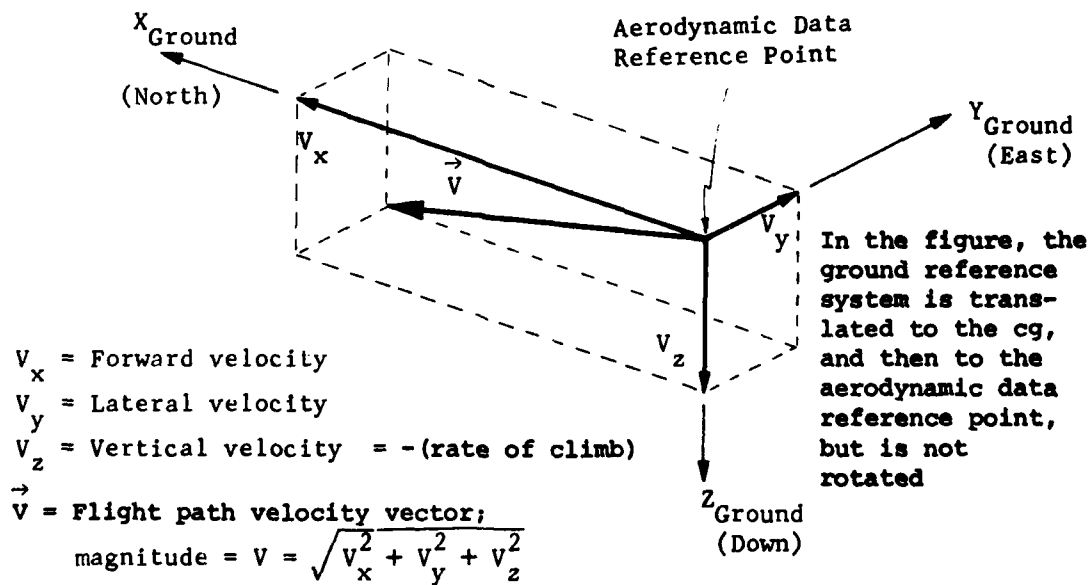


Figure 27. Orientation of Flight Path in Ground Reference.

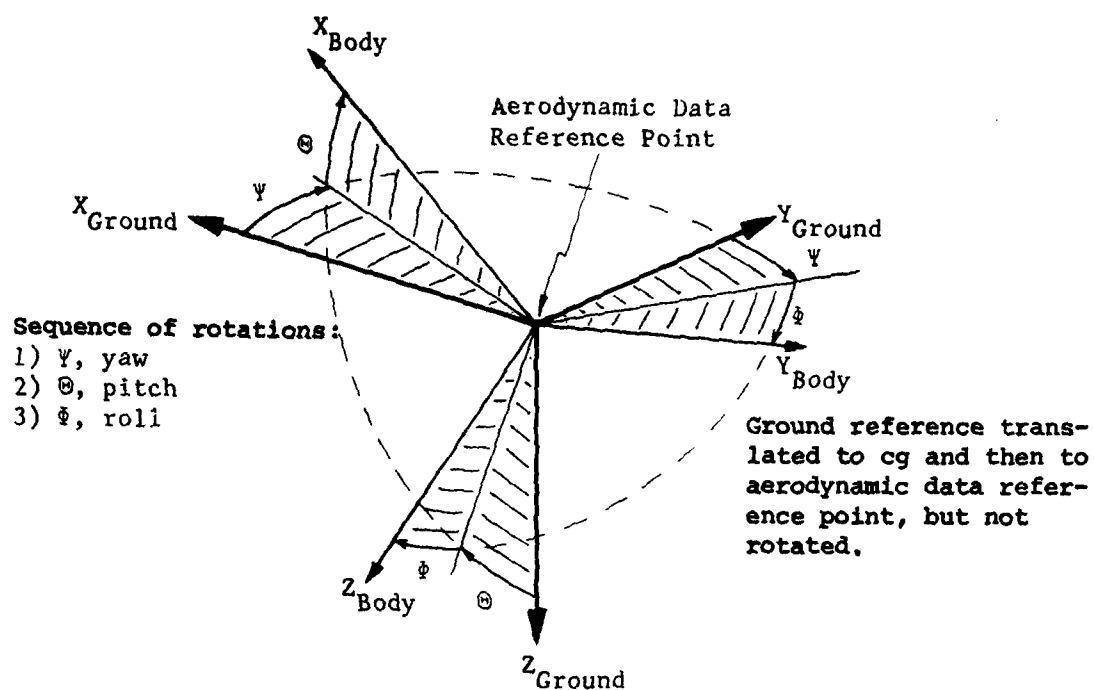


Figure 28. Euler Angles From Ground to Body Reference.

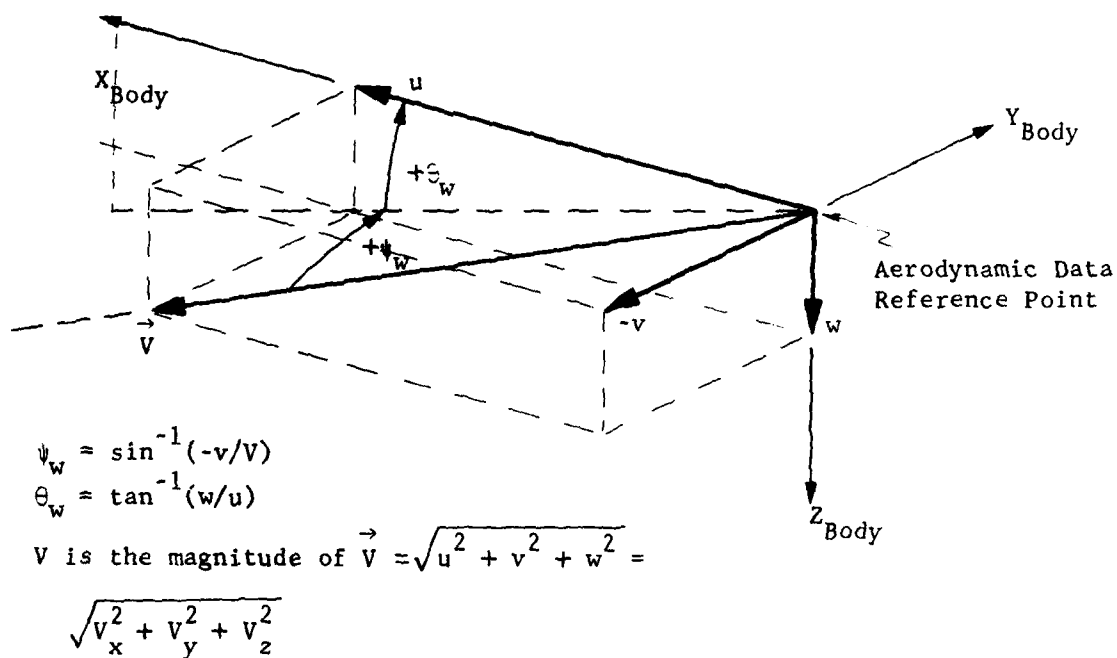


Figure 29. Aerodynamic Angles in Body Reference.

$$v = -V \sin \psi_w \quad (224)$$

$$w = V \cos \psi_x \sin \theta_w \quad (225)$$

Since the reference system of u , v , and w is the body, ordered rotations of $-\theta_w$ degrees pitch, then $-\psi_w$ degrees yaw define the orientation of the wind reference system with respect to the body. Therefore, the angles ψ_w and θ_w respectively are identical to the conventional wind tunnel yaw and pitch angles shown in Figure 26 and are termed the aerodynamic yaw and pitch angles.

From Equations (223), (224), and (225), these aerodynamic angles can be defined as functions of the flight path velocity and its body reference components.

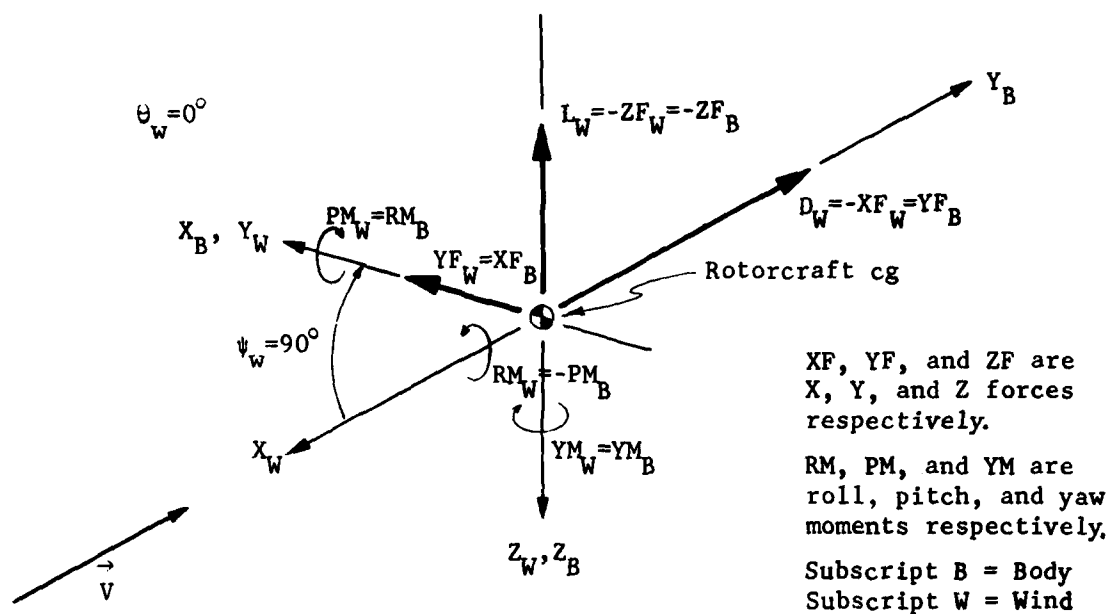
$$\psi_w = \sin^{-1}(-v/V) \quad (226)$$

$$\theta_w = \tan^{-1}(w/u) \quad (227)$$

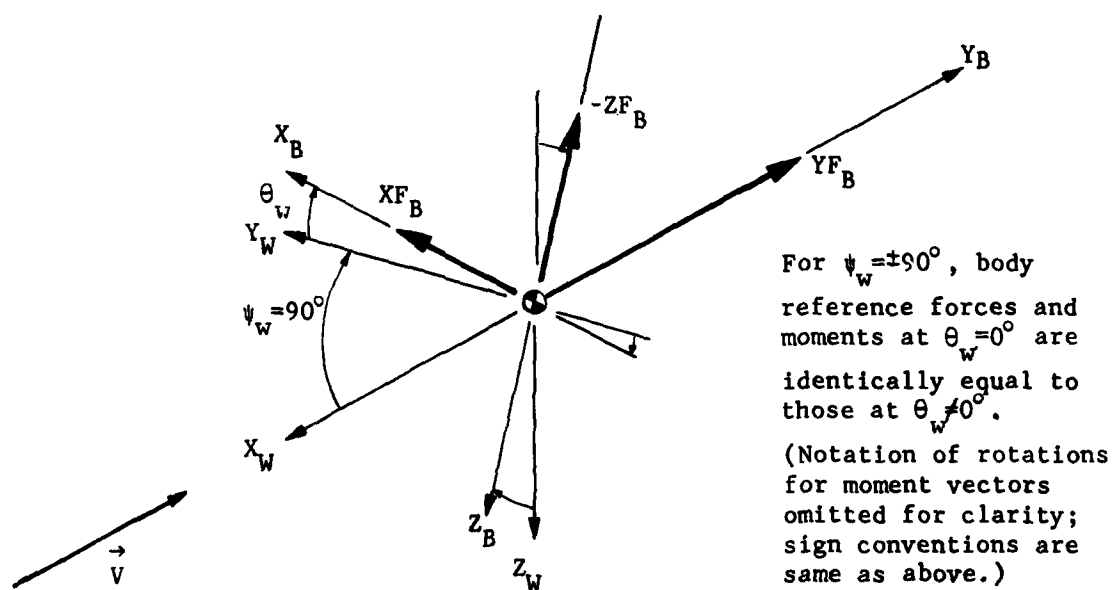
These two angles are then the two independent variables in the wind reference equations for fuselage aerodynamic forces and moments. They also serve as the rotation angles for resolving the wind reference data into the body reference system, where C81 performs its final force and moment summations.

However, note that if $V=0$, both ψ_w and θ_w are independent. Similarly, if $u = w = 0$, θ_w is indeterminant. If $V = 0$, the indeterminacy is simply resolved by defining ψ_w and θ_w to be zero, since all aerodynamic forces and moments are zero at zero velocity.

If $u = w = 0$, while $V \neq 0$ (i.e., $\psi_w = \pm 90$ degrees), it may be physically possible to pitch the wind tunnel model, but the angle cannot be defined by Equation (227). However, considering how the parameter θ_w is used in C81, it can be defined to be zero regardless of the value in the tunnel. To understand this definition, consider the forces and moments acting on a wind tunnel model which is yawed 90 degrees but not pitched, as shown in Figure 30. If the model is subsequently pitched, the drag in wind reference (Y-force in body reference) remains constant, but the other wind reference forces and moments do not. However, in the body reference system, the forces and moments are not a function of θ_w . Therefore, by defining $\theta_w = 0$ when $\psi_w = \pm 90$ degrees, the wind reference data can be resolved to body reference with a single yaw rotation and used as body reference data independently of the wind tunnel pitch angle. Since



(a) Aerodynamic Pitch Angle Equal to Zero.



(b) Aerodynamic Pitch Angle Not Equal to Zero.

Figure 30. Aerodynamic Pitch Angle in Sideward Flight.

the body reference is the system in which the data are needed for the final summation, this definition for θ_w provides the necessary results.

The interesting, if not obvious, implication of the above discussion is that aerodynamic forces and moments are dependent only on the orientation of the flightpath with respect to the fuselage and independent of the orientation of the flightpath with respect to the ground.

In its developed and programmed form, the equations of the representation of fuselage aerodynamics are actually functions of sines and cosines of ψ_w and θ_w rather than the angles themselves. Consequently, the sinusoids are defined by the velocity ratios implied by Equations (226) and (227) with the restriction that the inverse of $\sin \theta_w$ and $\cos \theta_w$ do not exceed ± 90 degrees and the inverse of $\sin \psi_w$ and $\cos \psi_w$ do not exceed ± 180 degrees.

$$\sin \theta_w = w / \text{sign}(u) \sqrt{u^2 + w^2} \quad (228)$$

$$\cos \theta_w = |u| / \sqrt{u^2 + w^2} \quad (229)$$

$$\sin \psi_w = -v/V \quad (230)$$

$$\cos \psi_w = (\text{sign}(u) \sqrt{u^2 + w^2}) / V \quad (231)$$

It should be noted that ψ_w is not the traditional sideslip angle, β . Sideslip is defined as

$$\beta = \tan^{-1} (v/u), \quad (232)$$

and an alternate definition of ψ_w is

$$\psi_w = \tan^{-1} (-v / \text{sign}(u) \sqrt{u^2 + w^2}) \quad (233)$$

Equating v in the two equations yields

$$\tan \beta = -\tan \psi_w / \cos \theta_w \quad (234)$$

Hence for small pitch angles, $\cos \theta_w \cong 1$ and

$$\beta = -\psi_w, \quad (235)$$

but at large values of θ_w , the magnitudes of β and ψ_w are not interchangeable.

4.2.3 High Angle Equation Model; The Airfoil Analogy

Since one of the primary goals in the development of the new fuselage representation was a model that would be valid at all aerodynamic angles, the first efforts for the task were directed toward a single set of equations which would accomplish this goal as well as the others. A literature search uncovered no simple analytical methods for predicting the force and moment characteristics of generalized bodies at large aerodynamic angles. Methods which are available, such as using bound vortices, would be very time consuming if programmed, approximate even if the flow were potential, and prohibitively complex following separation or stall, all due primarily to the nonuniform shape of rotorcraft fuselages. Also, test data for bodies at large angles were very limited. Consequently, the mathematical model for large angles, the High Angle Equation (HAE) model, was derived by comparing fuselages and aerodynamic surfaces with what was termed the airfoil analogy, and then supporting the conclusions with the limited test data available.

The initial step in the airfoil analogy was to consider the fuselage as a special case of an aerodynamic surface. The geometry of conventional aerodynamic surfaces is described by parameters such as aspect ratio, taper ratio, sweep angle, thickness-chord ratio, twist, and airfoil sections. Of these parameters, aspect ratio and thickness-chord ratio have strong analogies when considering the fuselage shape. The conventional aspect ratio is defined by b^2/S (b = span, S = planform area), while the thickness-chord ratio is t/c (t = maximum thickness of airfoil, c = mean chord of airfoil). For a fuselage, the analogous parameters are not single valued. They depend on the orientation of the fuselage with respect to the wind. The fuselage parameters that can be related to the surface parameters of span, area, chord, and thickness are listed in Table 5 for forward, sideward, and vertical flight. Based on the normal relationships of the fuselage parameters, the magnitude of the fuselage aspect and thickness-chord ratios can then be estimated as shown in Table 5. From this table, the following conclusions can be drawn:

- (1) In forward or rearward flight, a fuselage is analogous to an aerodynamic surface with a relatively low aspect ratio, i.e., less than unity, and a moderate thickness-chord ratio, i.e., 0.1 to 0.3.
- (2) In sideward or vertical flight, a fuselage is analogous to an aerodynamic surface with a very high thickness-chord ratio, i.e., unity or greater.

TABLE 5. FUSELAGE/AERODYNAMIC SURFACE ANALOGY

AERODYNAMIC SURFACE PARAMETER	FUSELAGE PARAMETER WHICH IS ANALOGOUS TO THE AERODYNAMIC SURFACE PARAMETER				
	FLIGHT REGIME AND REFERENCE ORIENTATION				
	Forward/Rearward Flight ($\theta_w = 0, \psi_w = 0, \pm 180$)		Sideward* Flight ($\theta_w = 0, \psi_w = \pm 90$)		Vertical Flight ($\theta_w = \pm 90, \psi_w = 0$)
	Pitch	Yaw	Yaw	Pitch	Yaw
Chord, c	Length	Length	Width	Height	Height
Thickness, t	Height	Width	Length	Length	Width
Span, b	Width	Height	Height	Width	Length
Plane of Reference Area, S**	X-Y Plane	X-Z Plane	Y-Z Plane	Y-Z Plane	X-Y Plane
Aspect Ratio, A ($=b^2/S$)	$\frac{(\text{Width})^2}{\text{X-Y Area}}$	$\frac{(\text{Height})^2}{\text{X-Z Area}}$	$\frac{(\text{Height})^2}{\text{Y-Z Area}}$	$\frac{(\text{Width})^2}{\text{Y-Z Area}}$	$\frac{(\text{Length})^2}{\text{X-Y Area}}$
Typical Value	<0.5	<0.5	1	<2	>2 <10
Thickness/Chord Ratio, t/c	$\frac{\text{Height}}{\text{Length}}$	$\frac{\text{Width}}{\text{Length}}$	$\frac{\text{Length}}{\text{Width}}$	$\frac{\text{Length}}{\text{Height}}$	$\frac{\text{Height}}{\text{Width}}$
Typical Value	>0.1 <0.5	>0.1 <0.5	>2 <10	>2 <10	1
<p>* In sideward flight ($\psi_w = \pm 90$), the equation for $\theta_w (= \tan^{-1} w/u)$ cannot define the angle. Hence, analogies with respect to the wind axis cannot be made. However, body axis forces and moments in sideward flight are independent of θ_w, so θ_w can be defined to be zero.</p> <p>** The reference area of a surface is its planform. Reference area for a fuselage is the area projected on a body plane.</p>					

These conclusions imply a third:

- (3) One type of model would be best for one of the flight regimes and a different one for the other.

A decision on whether to pursue this implication further was postponed until the HAE model was completed and could be compared to test data.

Using the above analogy and some limited aerodynamic surface test data, the shape of each fuselage force and moment curve was sketched for full-range yaw sweeps at constant pitch and full-range pitch sweeps at constant yaw.

The sets of sketches for each force or moment were then combined into a single three-dimensional sketch where the force or moment was plotted vertically (Z axis) as a function of the pitch and yaw angle (X and Y axes). Next, the lines of force or moment were faired together to form a surface above the X-Y plane. Figure 31 is an example of this technique for the drag of an arbitrary fuselage shape.

The dominant feature of Figure 31 and similar sketches is that vertical sections intersect the surface in lines which are periodic and very sinusoidal in appearance. Based on the shapes of these intersections, equations were constructed as sinusoidal functions of integer multiples of θ_w and ψ_w to provide smooth transition between all combinations of θ_w and ψ_w . The periodic nature of the equations established the coefficients as the values of the forces or moments at integer multiples of 45 degrees.

Data from large angle wind tunnel tests of two different configurations were then used to check out the equations. Based on the results of this comparison, empirical modifications were made to the equations, which were then defined as the High Angle Equation model. These equations are listed in Table 6.

4.2.4 Nominal Angle Equations

The next step in the development of the new fuselage representation was to examine the accuracy and suitability of the High Angle Equation model in simulating the forces and moments at low, or nominal, aerodynamic pitch and yaw angles (both angles less than approximately ± 15 to ± 30 degrees). Data from force and moment wind tunnel tests of five different fuselages were examined:

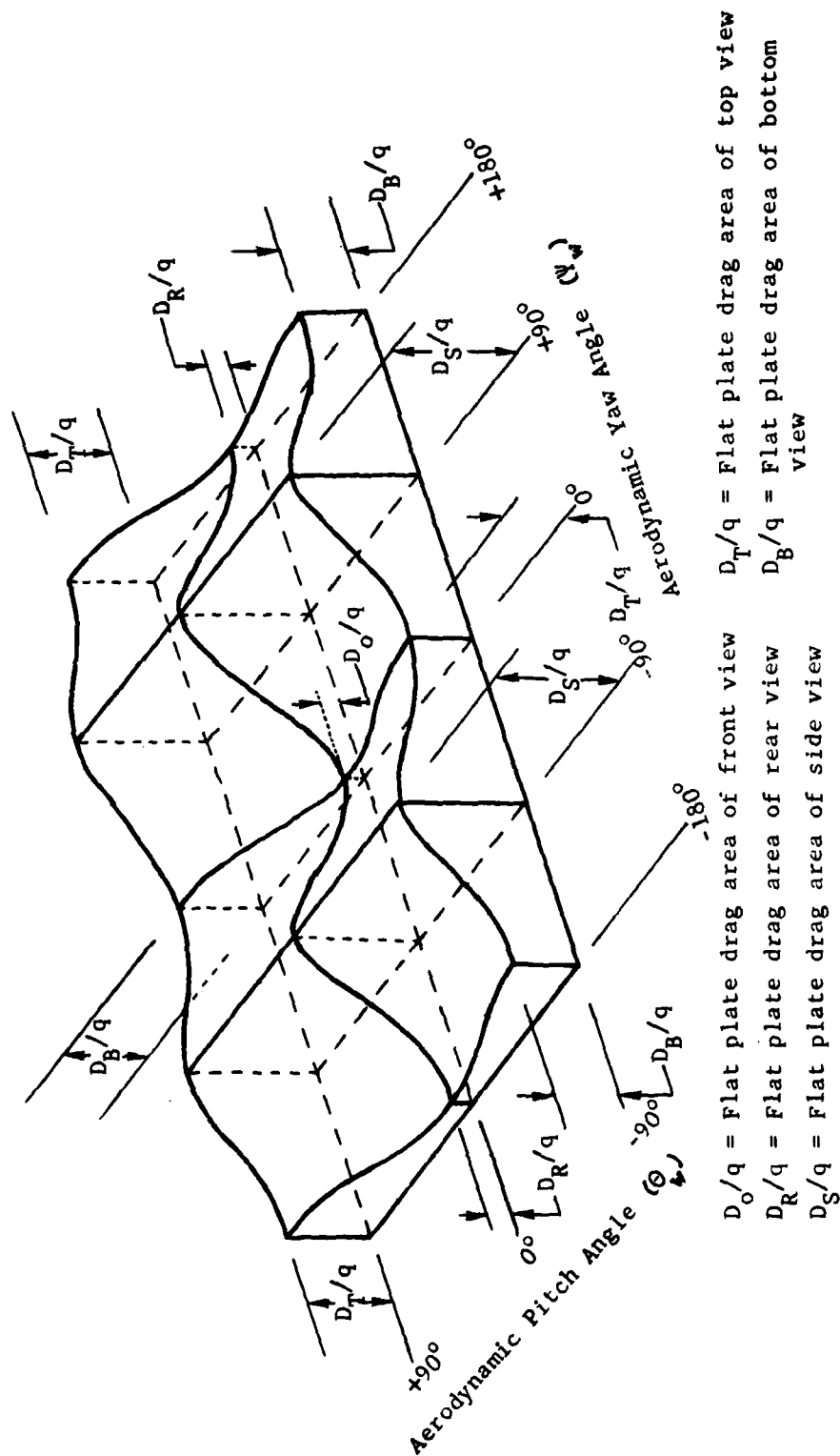


Figure 31. Sketch of Fuselage Drag as a Function of θ_w and ψ_w .

**TABLE 6. HIGH ANGLE EQUATIONS FOR FUSELAGE
AERODYNAMIC FORCES AND MOMENTS**

$$\text{Lift} = L = L_1 \cos^2 \psi_w + L_2 \sin^2 \psi_w$$

where

$$L_1 = \begin{aligned} &L(0,0) + L_3 \sin^2 \theta_w + L_4 \sin(2\theta_w) \text{ if } \psi_w \leq 90 \\ &L(180,0) - L_5 \cos^2 \theta_w - L_4 \sin(2\theta_w) \text{ if } \psi_w > 90 \end{aligned}$$

$$L_2 = L(90,0) \cos \theta_w + Y(90,0) \sin \theta_w$$

$$L_3 = L(0,90) - L(0,0)$$

$$L_4 = L(0, \theta_{wp}) - L(0,0) - L_3 \sin^2(\theta_{wp}) / \sin(2\theta_{wp})$$

$$L_5 = L(0,90) - L(180,0)$$

$$\text{Drag} = D = D_1 \cos^2 \psi_w + D(90,0) \sin^2 \psi_w$$

where

$$D_1 = D_2 \cos^2 \theta_w + D_v \sin^2 \theta_w$$

$$D_2 = \begin{aligned} &D(0,0) \text{ if } \psi_w \leq 90 \\ &D(180,0) \text{ if } \psi_w > 90 \end{aligned}$$

$$D_v = \begin{aligned} &D(0,-90) \text{ if } \theta_w \leq 0 \\ &D(0,+90) \text{ if } \theta_w > 0 \end{aligned}$$

$$\text{Pitching Moment} = M = M_1 \cos^2 \psi_w + M_2 \sin^2 \psi_w$$

where

$$M_1 = \begin{aligned} &M(0,0) + M_3 \sin^2 \theta_w + M_4 \sin(2\theta_w) \text{ if } \psi_w \leq 90 \\ &M(0,90) - M_5 \cos^2 \theta_w - M_4 \sin(2\theta_w) \text{ if } \psi_w > 90 \end{aligned}$$

$$M_2 = N(90,0) \sin \theta_w + M(90,0) \cos \theta_w$$

$$M_3 = M(0,90) - M(0,0)$$

$$M_4 = [M(0, \theta_{wp}) - M(0,0) - M_3 \sin^2(\theta_{wp})] / \sin(2\theta_{wp})$$

$$M_5 = M(0,90) - M(180,0)$$

TABLE 6. Continued

$$\text{Side Force} = Y = Y_1 \cos^2 \theta_w - L(90,0) \sin^2 \theta_w \sin \psi_w$$

where

$$Y_1 = Y(90,0) \sin \psi_w + Y_2 \sin(2\psi_w)$$

$$Y_2 = [Y(\psi_{wp},0) - Y(90,0) \sin(\psi_{wp})] / \sin(2\psi_{wp})$$

$$\text{Rolling Moment} = l = l_1 \cos^2 \theta_w + l(90,0) \sin^2 \theta_w \sin \psi_w$$

where

$$l_1 = l(90,0) \sin \psi_w + l_2 \sin(2\psi_w)$$

$$l_2 = [l(\psi_{wp},0) - l(90,0) \sin(\psi_{wp})] / \sin(2\psi_{wp})$$

$$\text{Yawing Moment} = N = N_1 \cos^2 \theta_w - M(90,0) \sin^2 \theta_w \sin \psi_w$$

where

$$N_1 = N(90,0) \sin \psi_w + N_2 \sin(2\psi_w)$$

$$N_2 = [N(\psi_{wp},0) - N(90,0) \sin(\psi_{wp})] / \sin(2\psi_{wp})$$

The force or moment symbols with double subscripts in parentheses (e.g., $D(0,-90)$, $M(90,0)$, and $N(90,0)$) indicate the orientation of the fuselage with respect to the wind for that particular force or moment. The first subscript is the aerodynamic yaw angle (ψ_w) and the second is the aerodynamic pitch angle (θ_w). For example, $D(0,-90)$ is the drag at $\psi_w = 0$ and $\theta_w = -90$.

The subscript p on ψ_w and θ_w indicates peak values. For example, $M(0,\theta_{wp})$ is the maximum pitching moment for $\theta_w < 90$ at $\psi_w = 0$ and occurs at $r_w = r_{wp}$. The peak value and angle for each force and moment are independent of the peaks for any other force or moment.

- (1) Bell Model 209 (AH-1G, or Huey Cobra) type fuselage; relatively high height-to-width ratio, low rectangular tail boom, aerodynamically clean fuselage, smooth faired pylon, pointed nose.
- (2) Bell Model 205 (UH-1H, or Huey) type fuselage: much lower height-to-width ratio than Model 209; low rectangular tail boom; bulky, aerodynamically dirty fuselage; low, blunt nose.
- (3) Bell Model 206 (OH-58A and JetRanger) type fuselage: height-to-width ratio between that of the 209 and 205; high, round tail boom; aerodynamically clean fuselage; low, pointed nose.
- (4) A proposed advanced utility helicopter type fuselage: height-to-width ratio near unity; low, round tail boom; relatively clean aerodynamically compared to Model 205; low, pointed nose.
- (5) A proposed advanced gunship type fuselage: similar to Model 209 but with twin engine pods, round tail boom, exposed tail rotor drive shaft, no pylon fairing.

The Model 205, 206, and 209 fuselages included skid gear, while the two other configurations included wheeled landing gear. In addition, data on the Model 206 with inflated pop-out float gear were examined.

Preliminary evaluation of the ability of the HAE model to simulate forces and moments in the nominal angle region showed that the HAE model could not simulate the data within the accuracy of the test data. In particular, the aerodynamic coupling was not represented as precisely as needed.

Consequently, a study was performed to determine the set of equations which could best fit the referenced test data.

The general equation chosen for the study was

$$Z = C_0 + \sum_{i=1}^N C_i [f(x)]^{I_i} [f(y)]^{J_i} \quad (236)$$

where

Z is the force or moment under consideration,

x and y are the aerodynamic angles,

I_i and J_i are the positive integer exponents for $f(x)$ and $f(y)$, and

C_i are constant coefficients

The parameters varied in the study were then

- (1) The functions of x and y , $f(x)$ and $f(y)$
- (2) The values of the exponents, I_i and J_i
- (3) The number of terms, N

The functions of x and y chosen were the angles themselves and sine functions of the angles where the sine functions had the same period as the corresponding variations in the HAE model, i.e., $\sin(\theta_w)$ or $\sin(2\theta_w)$, and $\sin(\psi_w)$ or $\sin(2\psi_w)$, as appropriate.

Initially, the values of each exponent ranged from zero to five, and up to 25 terms were considered. Judgement of the quality of the curve fit was based on the summation of the absolute values of the difference between calculated and measured values divided by the number of data points in the data set and on the root-mean-squared error per point. These parameters were then compared to the accuracy of the wind tunnel data.

Based on preliminary analysis, the general equation was reduced to 16 terms with exponents less than or equal to three because the higher order terms did not improve the fit enough to warrant their inclusion.

Hence, the baseline equation for the study was

$$\begin{aligned} Z = & C_0 + C_1 f(x) + C_2 f^2(x) + C_3 f^3(x) \\ & + [C_4 + C_5 f(x) + C_6 f^2(x) + C_7 f^3(x)] f(y) \\ & + [C_8 + C_9 f(x) + C_{10} f^2(x) + C_{11} f^3(x)] f^2(y) \\ & + [C_{12} + C_{13} f(x) + C_{14} f^2(x) + C_{15} f^3(x)] f^3(y) \end{aligned} \quad (237)$$

For lift, drag, and pitching moment, x is the pitch angle and y is the yaw angle. To obtain a physical or analytical feel for this equation and how the coefficients relate to measurable quantities, consider yawing moment. In the wind tunnel, data are generally obtained by sweeping one angle with the other held constant. If the pitch angle is constant, then Equation (237) can be rewritten for yawing moment, N , as

$$N = q[(N_0/q) + (N_1/q)f(\psi_w) + (N_2/q)f^2(\psi_w) + (N_3/q)f^3(\psi_w)] \quad (238)$$

where q is dynamic pressure on the fuselage.

where

$$N_0/q = C_0 + C_1 f(\theta_w) + C_2 f^2(\theta_w) + C_3 f^3(\theta_w) \quad (239)$$

$$N_1/q = C_4 + C_5 f(\theta_w) + C_6 f^2(\theta_w) + C_7 f^3(\theta_w) \quad (240)$$

$$N_2/q = C_8 + C_9 f(\theta_w) + C_{10} f^2(\theta_w) + C_{11} f^3(\theta_w) \quad (241)$$

$$N_3/q = C_{12} + C_{13} f(\theta_w) + C_{14} f^2(\theta_w) + C_{15} f^3(\theta_w) \quad (242)$$

N_0/q , N_1/q , N_2/q , and N_3/q are constant since pitch angle and hence $f(\theta_w)$ are constant. If N_2 and N_3 are small, and $f(\psi_w) = \sin \psi_w \doteq \psi_w$, Equation (238) can then be approximated as

$$N/q \doteq N_0/q + (N_1/q) \psi_w \quad (243)$$

which is the familiar form of the small angle, linear approximation for calculating yawing moment. Hence, N_2/q and N_3/q are simply coefficients to provide a third-order fit to the wind tunnel yaw sweep data.

Now consider that most wind tunnel tests have yaw sweeps at more than one pitch angle and that the values of N_0/q , N_1/q , N_2/q , and N_3/q will generally be different at different pitch angles. In this case their values can be curve fitted using the form of Equations (239) through (242). The resulting coefficients can then be substituted into Equation (238). Equation (238) will then simulate both the conventional variation of yawing moment with the yaw angle and the generally neglected variation of yawing moment with pitch angle, i.e., aerodynamic cross-coupling.

From further analysis of the wind tunnel data and comparison of the quality of the curve fits and accuracies of the test data, it was concluded that the terms with the coefficients C_3 , C_7 , C_{10} , C_{11} , C_{13} , C_{14} and C_{15} could be deleted from Equation (237) for the lift, drag, and pitching moment equation and that the C_7 , C_{10} , C_{11} , C_{14} , and C_{15} terms could be deleted from the side force, rolling moment, and yawing moment equations. The type of function used for $f(\theta_w)$ and $f(\psi_w)$ had a very small and random

effect on the quality of the curve fit. For some data, the polynomial form, e.g., $f(\theta) = \theta_w$, provided the best fit; for other data, the sinusoidal forms, e.g., $f(\theta) = \sin(\theta_w)$, or $\sin(2\theta_w)$, provided the best fit. Hence, for maximum compatibility with the HAE model, the sinusoidal functions were used in the baseline equation. The resulting set of equations was termed the Nominal Angle Equations (NAE) model and is given in Tables 7 and 8.

Table 9 is a summary of the effect of deleting various combinations of coefficients from the baseline equation on the quality of the curve fit for the Model 206 data. Data for the other fuselages exhibited similar trends in quality of fit relative to the test data accuracy.

From the above study it was apparent that the HAE model was not sufficiently accurate to model the forces and moments in the nominal angle case. The HAE model is convenient and desirable in that the equations are continuous, give the proper data trends at all fuselage orientations, include some cross-coupling effects, and require relatively few inputs. However, only in isolated cases was their accuracy in the nominal angle case within the accuracy of the test data.

The possibility of using the NAE model for all fuselage orientations was then investigated. The conclusion was that it could not be used to replace the HAE model because of the cross-coupling terms in the NAE model. As is typical of most curve-fit techniques, extrapolation beyond the range of data fitted gives a very poor fit. Hence, it was decided that both the HAE and NAE models should be included in the revised mathematical model of the fuselage since each model performs a function that the other cannot.

4.2.5 Logic for Phasing and Use of the High and Nominal Angle Equations

The transition from the HAE to the NAE model and vice versa should be continuous, smooth, and not cause any reversals or sharp changes in slope not actually in the data. Also, the transition should be dependent on both the pitch and yaw angle. The simplest parameter which can accomplish these objectives is the complex angle of attack, α_c .

$$\alpha_c = \cos^{-1} \frac{u}{V} \quad (244)$$

From Equation (244) and the orthogonality of the body axis velocities,

TABLE 7. NOMINAL ANGLE EQUATIONS FOR LONGITUDINAL AERODYNAMIC FORCES AND MOMENTS

$$\begin{aligned}
 FM = FM_0 &+ \frac{\partial FM}{\partial \sin \psi_w} \sin \psi_w + \frac{\partial FM}{\partial \sin^2 \psi_w} \sin^2 \psi_w \\
 &+ \left(\frac{\partial FM}{\partial \sin (ANG)} + \frac{\partial (\partial FM / \partial \sin (ANG))}{\partial \sin \psi_w} \sin \psi_w \right. \\
 &\quad \left. + \frac{\partial (\partial FM / \partial \sin (ANG))}{\partial \sin^2 \psi_w} \sin^2 \psi_w \right) \sin (ANG) \\
 &+ \left(\frac{\partial FM}{\partial \sin^2 (ANG)} + \frac{\partial (\partial FM / \partial \sin^2 (ANG))}{\partial \sin \psi_w} \sin \psi_w \right) \sin^2 (ANG) \\
 &+ \left(\frac{\partial FM}{\partial \sin^3 (ANG)} \right) \sin^3 (ANG)
 \end{aligned}$$

The above equation represents the equations for lift (L), drag (D), and pitching moment (M). To obtain the complete equation for one of the forces or the moment, substitute its corresponding symbol for the representative variable FM. For lift and pitching moment, $ANG = 2\theta_w$; for drag, $ANG = \theta_w$.

FM_0 indicates the value of FM at $\theta_w = \psi_w = 0$.

TABLE 8. NOMINAL ANGLE EQUATIONS FOR
LATERAL-DIRECTIONAL AERO-
DYNAMIC FORCES AND MOMENTS

$$\begin{aligned}
 FM = FM_0 &+ \frac{\partial FM}{\partial \sin \theta_w} \sin \theta_w \\
 &+ \frac{\partial FM}{\partial \sin^2 \theta_w} \sin^2 \theta_w + \frac{\partial FM}{\partial \sin^3 \theta_w} \sin^3 \theta_w \\
 &+ \left(\frac{\partial FM}{\partial \sin 2\psi_w} + \frac{\partial(\partial FM / \partial \sin(2\psi_w))}{\partial \sin \theta_w} \sin \theta_w \right. \\
 &\quad \left. + \frac{\partial(\partial FM / \partial \sin(2\psi_w))}{\partial \sin^2 \theta_w} \sin^2 \theta_w \right) \sin 2\psi_w \\
 &+ \left(\frac{\partial FM}{\partial \sin^2(2\psi_w)} + \frac{\partial(\partial FM / \partial \sin^2(2\psi_w))}{\partial \sin \theta_w} \sin \theta_w \right) \sin^2(2\psi_w) \\
 &+ \left(\frac{\partial FM}{\partial \sin^3(2\psi_w)} + \frac{\partial(\partial FM / \partial \sin^3(2\psi_w))}{\partial \sin \theta_w} \sin \theta_w \right) \sin^3(2\psi_w)
 \end{aligned}$$

The above equation is representative of the equations for side force (Y), rolling moment (l), and yawing moment (N). To obtain the complete equation for one of the moments or the force, substitute its corresponding symbol for the representative variable FM.

FM_0 indicates the value of FM at $\theta_w = \psi_w = 0$.

**TABLE 9. EFFECT OF DELETING TERMS FROM BASELINE
EQUATION ON ACCURACY OF CURVE FITS**

Subscript of Coefficient of Terms Deleted from Baseline Equation	Summation of Absolute Value of Errors Divided by Number of Points Fitted					
	Lift- ft ²		Drag- ft ²		Pitching Moment-ft ³	
	Case 1	Case 2	Case 1	Case 2	Case 1	Case 2
None	.4342	.2576	.2268	.0916	1.6342	.8054
15	.4362	.2579	.2267	.0940	1.6345	.8034
14, 15	.5093	.2703	.2382	.0939	2.1877	1.0667
11, 14, 15	.5186	.2709	.2381	.0942	2.1897	1.0661
10, 11, 14, 15	.5455	.3543	.2601	.1276	2.1508	1.1992
7, 10, 11, 14, 15	.5520	.3545	.2637	.1299	2.1505	1.1991
7, 10, 11, 13+15	.5522	.3545	.2651	.1299	2.1555	1.1988
3, 7, 10, 11, 13+15 *	.5566	.3544	.2650	.1308	2.1619	1.1971
3, 6, 7, 10, 11, 13+15	1.2535	.4979	.2764	.1305	2.3987	2.1779
3, 6, 7, 10+15	1.2521	.6190	.2771	.1316	2.8462	2.7814
Accuracy of test data	± 0.7 ft ²		± 0.3 ft ²		± 2.0 ft ³	

TABLE 9. Continued.						
Subscript of Coefficient of Terms Deleted from Baseline Equation	Summation of Absolute Value of Errors Divided by Number of points Fitted					
	Side Force- ft ²		Rolling Moment- ft ³		Yawing Moment- ft ³	
	Case 1	Case 2	Case 1	Case 2	Case 1	Case 2
None	.4885	.2049	1.1296	.5673	2.4860	1.2110
15	.4860	.2070	1.2955	.5675	2.4623	1.3004
14, 15	.5052	.2146	1.2957	.5685	2.7781	1.4318
11, 14, 15	.5051	.2138	1.3221	.5730	2.8010	1.4279
10, 11, 14, 15	.5121	.2661	1.3293	.5949	2.8181	1.4301
7, 10, 11, 14, 15 *	.7057	.3734	2.0218	.6988	2.9320	1.7375
7, 10, 11, 13+15	.7180	.4532	2.0621	.7337	2.9065	1.9416
Accuracy of test data	± 0.5 ft ²		± 2.0 ft ³		± 3.4 ft ³	
Units of the errors are force or moment divided by dynamic pressure per point (ft ² /point or ft ³ /point respectively). All data are for a 0.25 scale Bell Model 206 (JetRanger).						
Case 1: Basic fuselage with skid gear; 136 data points fitted; -12 ≤ θ _w < 18 ; Ψ _w ≤ 16 to 25 .						
Case 2: Basic fuselage with inflated pop-out floats; 89 data points fitted; -10 ≤ θ _w < 18 ; Ψ _w ≤ 12 .						
*Indicates the set of coefficients deleted from the baseline equation to form the programmed Nominal Angle Equation model. Baseline equation is Equation (211).						

$$\sin \alpha_c = \frac{v^2 + w^2}{V} \quad \text{sign}(u) \quad (245)$$

This parameter is the angle between the wind vector and the body X-axis. The locus of the body X-axis for a constant complex angle of attack is a conical surface of revolution about the wind vector (the positive wind X-axis).

If the angle is to be measured with respect to the positive wind Y-axis, the alternate definition of α_c is

$$\alpha_c = \cos^{-1} \frac{-v}{V} \quad (246)$$

These separate definitions are made so that the Nominal Angle Equations can be centered about either the wind X-axis (for very precise simulation in forward and rearward flight) or the wind Y-axis (for sideward flight). The choice of which axis to use as the center of the cone for these equations has been made a user option.

Three inputs to the program (LGF , α_L , and α_H) control the use and phasing together of the Nominal Angle and High Angle Equations. LGF is a logic switch, while θ_L and θ_H are boundary angles:

LGF : = 0 for the region of use of the Nominal Angle Equations to be centered about the wind X-axis.

$\neq 0$ for the region of use of the Nominal Angle Equations to be centered about the wind Y-axis.

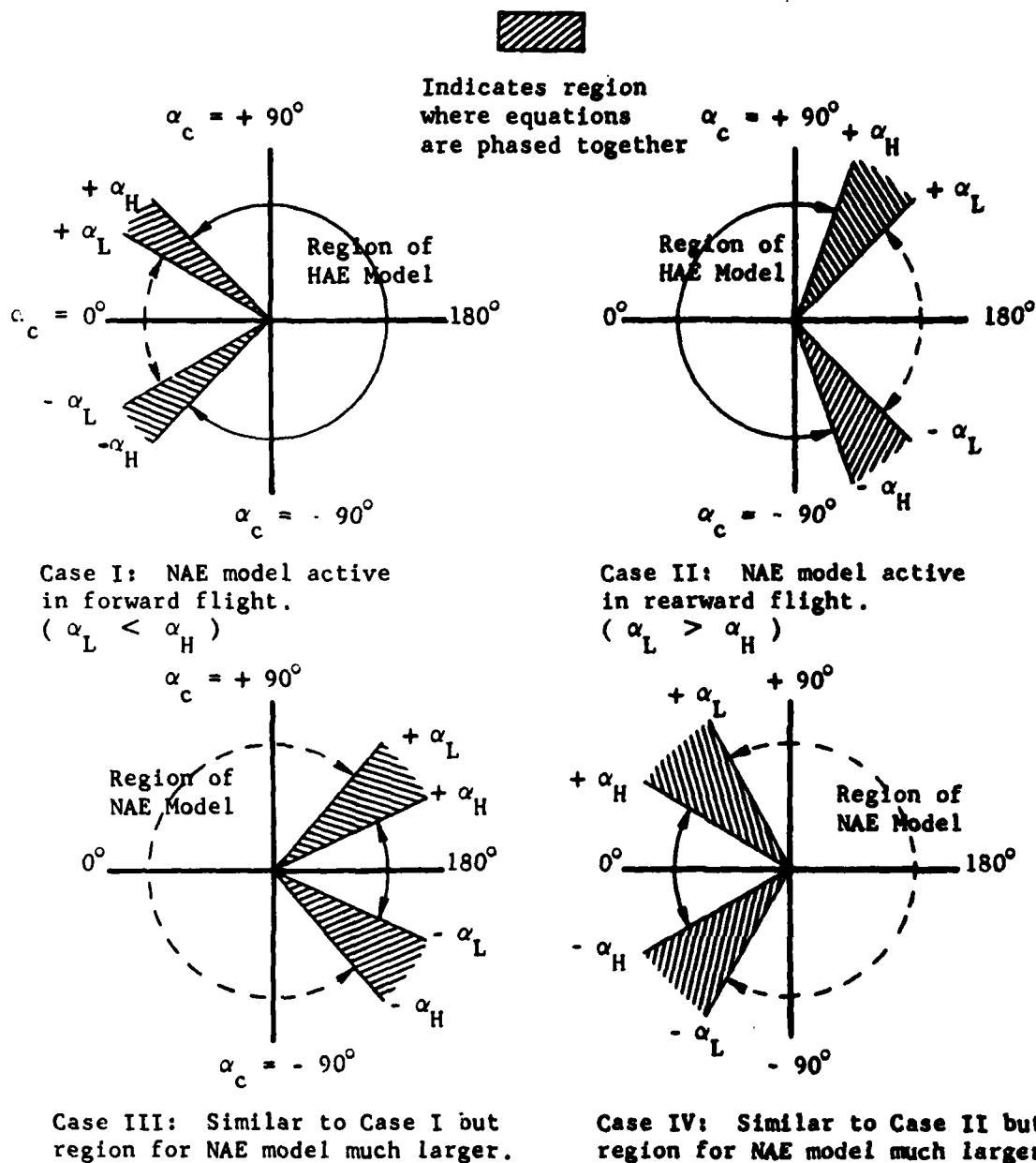
α_L : The value of α_c at the boundary between the region where the Nominal Angle Equations are used and the region where the two sets of equations are phased together.

α_H : The value of α_c at the boundary between the region where the High Angle Equations are used and the phasing region.

The logical decisions made based on these three inputs are shown in Figure 32.

Within the phasing region, the value of individual forces and moments is calculated using the phasing angle, α_{ph} ,

$$\alpha_{ph} = \frac{\alpha_c - \alpha_L}{\alpha_H - \alpha_L} \cdot 2 \quad (247)$$



Cases I and II represent likely inputs. Although Cases III and IV are possible inputs, it is improbable that the NAE model will adequately simulate the data throughout such a large region.

Figure 32. Phasing of Fuselage NAE and HAE Models.

and the following relationship.

$$FM(\theta_w, \psi_w)_{wind} = FM(\theta_w, \psi_w)_{NAE} \cos^2 \alpha_{ph} + FM(\theta_w, \psi_w)_{HAE} \sin^2 \alpha_{ph} \quad (248)$$

where

FM is a specific force or moment
wind indicates the final wind axis value
NAE indicates the value from the Nominal Angle Equation
HAE indicates the value from the High Angle Equation

4.3 EXAMPLES OF THE FUSELAGE REPRESENTATION

Figure 33 is an example of the High Angle Equation model for a medium utility helicopter. Data for drag and yawing moment are shown. Other data exhibited similar correlation. Table 10 is an example of the Nominal Angle Equation model for a light commercial helicopter. The data presented are a sample of the output of computer program AN9101 discussed in the next section and consist of the coefficients of the curve fit and a comparison of the input and calculated force or moment. The quality of the curve fit can be judged by referring to the columns labeled "DELTA" (input minus calculated value) and "REL-DEL" (DELTA divided by input value) and to the two parameters at the end of the calculations labeled "SUM OF ABS(ERRORS)/POINTS" (the summation of the absolute values of DELTA divided by the number of data points) and "RMS ERROR/POINTS" (the square root of the summation of DELTA-squared, divided by the number of points). These data and parameters indicate that the NAE model can fit the input data so closely that separate plots of the input and calculated data (e.g., contour or carpet plots) would virtually overlay each other.

4.4 AIDS TO DETERMINING THE INPUTS FOR FUSELAGE REPRESENTATION

Included with the Rotorcraft Flight Simulation Program is a separate computer program designed to aid the user in determining the inputs to the fuselage representation. This program, designated AN9101 curve-fits force and moment test data to the Nominal Angle Equations of C81. The output of the program is the set of coefficients of each equation, a comparison of the test and calculated data, and parameters for estimating the quality of the fit. At the user's option the coefficients are punched on cards. The format of the punched output is precisely that required for input to C81. See Section 7.3 of Volume II for additional information regarding this program.

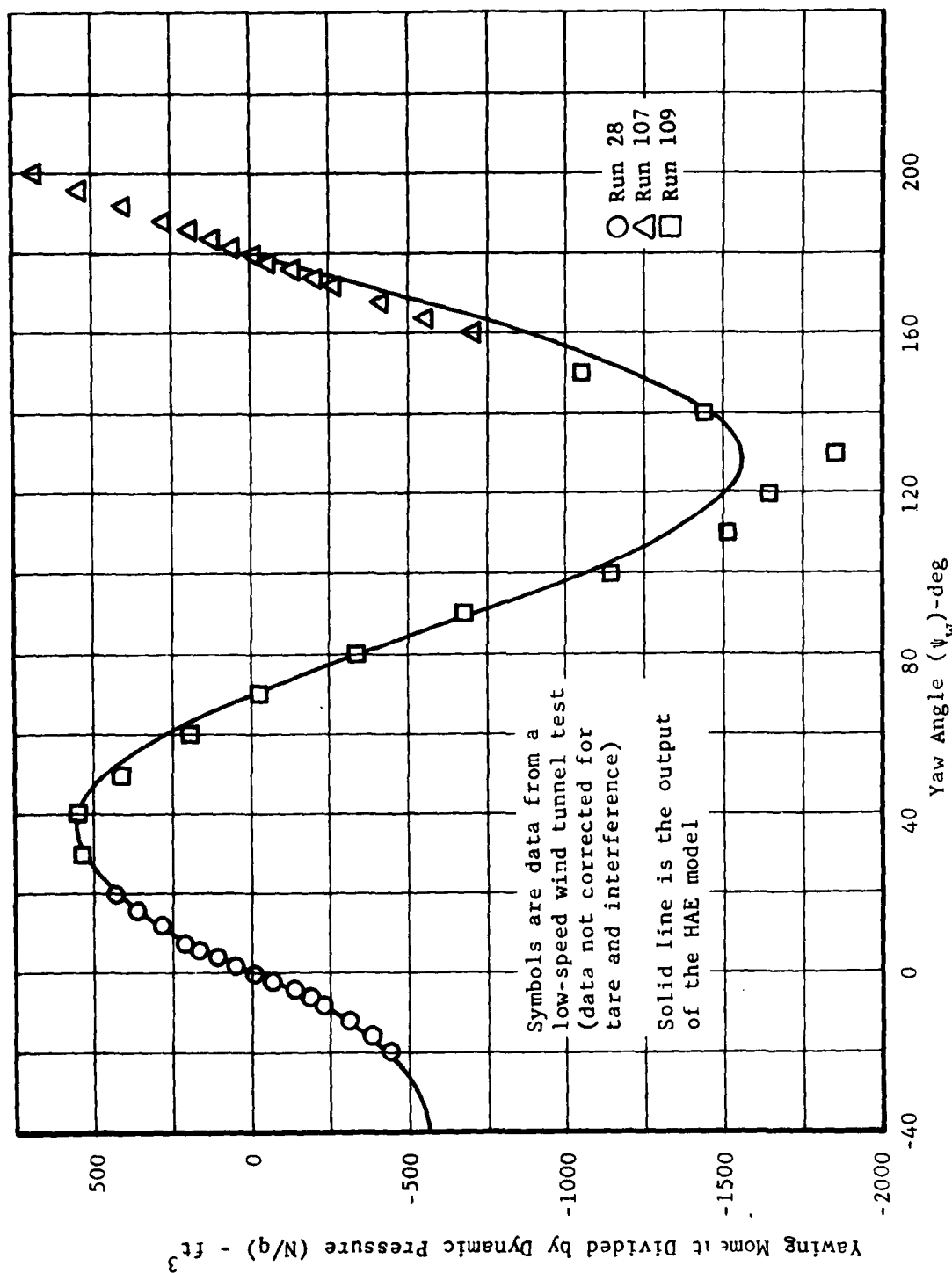


Figure 33. Examples of Fuselage Aerodynamic Representation at Large Angles for a Medium Utility Helicopter.

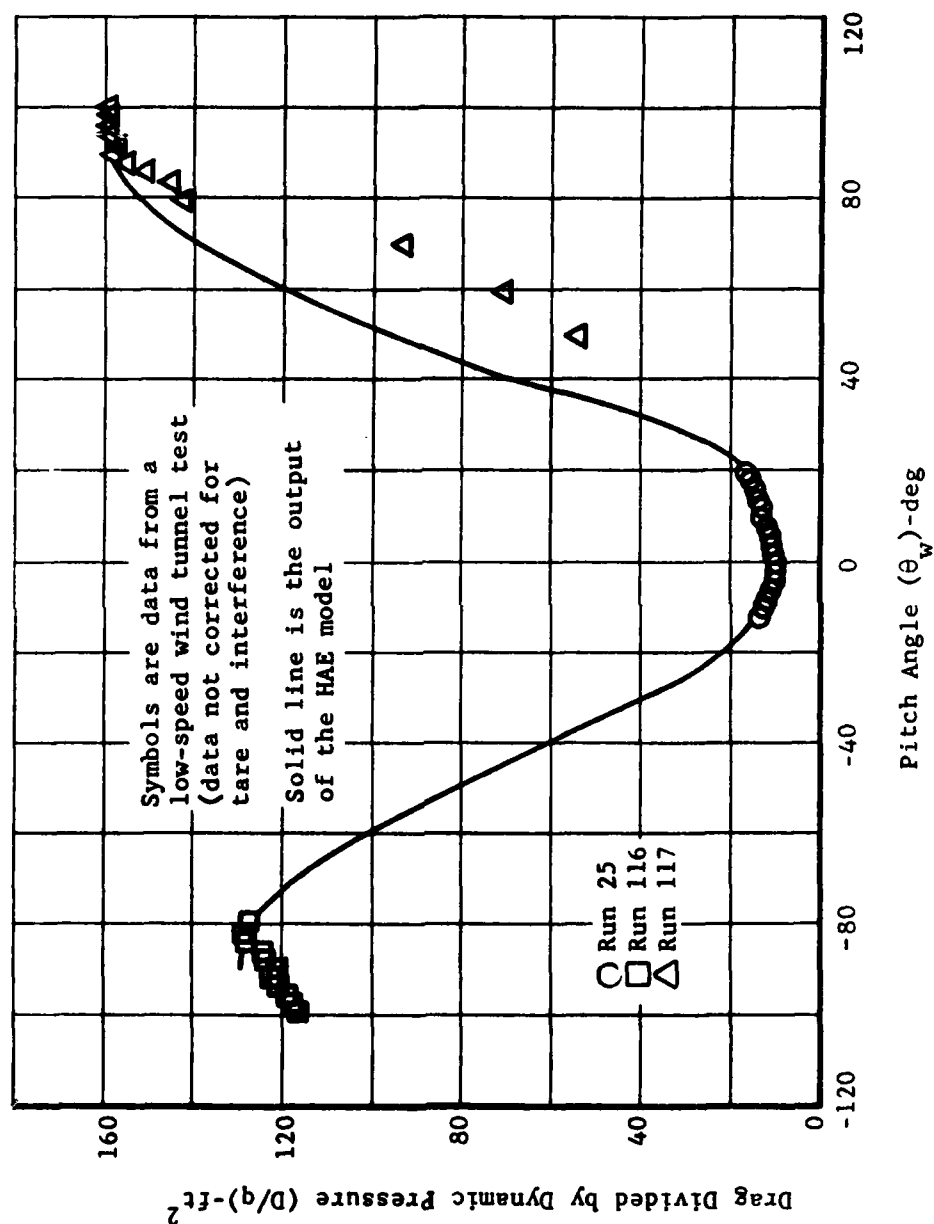


Figure 33. Concluded.

TABLE 10. EXAMPLES OF FUSELAGE AERODYNAMIC REPRESENTATION AT SMALL ANGLES FOR A LIGHT COMMERCIAL HELICOPTER

DRAG DATA			
COEFFICIENTS OF EQUATION			
SUB-SCRIPT	NON-DIMENSIONAL	DIMENSIONAL	AGA173 INPUT
00	2.10 FT**2	2.099379 FT**2/DEG**0	XFS(29)
10	-0.66 FT**2	-0.011553 FT**2/DEG**1	XFS(35)
20	07.67 FT**2	0.020613 FT**2/DEG**2	XFS(36)
01	-2.92 FT**2	-0.050906 FT**2/DEG**1	XFS(37)
11	2.32 FT**2	0.000615 FT**2/DEG**2	XFS(38)
21	0.84 FT**2	0.000004 FT**2/DEG**3	XFS(39)
32	29.93 FT**2	0.009108 FT**2/DEG**2	XFS(40)
12	-1.95 FT**2	-0.006013 FT**2/DEG**3	XFS(41)
33	-10.95 FT**2	-0.000058 FT**2/DEG**3	XFS(42)

INPUT DATA AND CALCULATIONS						
RUN/PT	PITCH	YAW	INPUT	CALCULATION	DELTA	REL-DEL
210 1	-11.74	0.00	3.8100	4.0289	-0.219	-0.05746
210 2	-10.46	-16.01	9.3000	9.1174	0.183	0.01964
210 3	-10.53	-12.01	6.6600	6.6494	-0.189	-0.02844
210 4	-10.45	-8.01	4.9300	5.1408	-0.211	-0.04276
210 5	-10.69	-8.01	4.5200	4.5950	-0.075	-0.01666
210 6	-10.76	-4.00	4.2600	4.1633	0.117	0.02726
210 7	-11.62	-1.55	4.0600	4.1110	-0.051	-0.01256
210 8	-11.36	-0.01	3.8100	4.0404	-0.230	-0.06046
210 9	-11.65	1.59	3.8800	4.0507	-0.171	-0.04359
210 10	-11.40	3.59	4.1800	4.1766	0.003	0.00081
210 11	-10.91	6.02	4.5600	4.3569	0.163	0.03577
210 12	-10.71	8.02	5.0300	4.9046	0.125	0.02493
210 13	-10.57	10.01	5.6300	5.5573	0.073	0.01291
210 14	-10.58	12.01	6.3800	6.4856	-0.026	-0.00401
210 15	-10.47	14.02	7.3500	7.3803	-0.030	-0.00612
210 16	-10.46	15.99	8.7900	8.5024	0.286	0.03272
210 17	-11.81	0.00	3.8300	4.0430	-0.213	-0.05562
211 1	-6.96	0.00	3.1300	2.9151	0.215	0.06866
211 2	-5.76	-16.00	8.2000	8.0628	0.117	0.01429
211 3	-5.76	-13.59	6.8200	6.8680	-0.048	-0.00704
211 4	-5.75	-11.99	5.5700	5.6030	-0.233	-0.06416
211 5	-5.82	-10.01	4.9100	4.9101	-0.000	-0.00002
211 6	-5.92	-8.01	4.1500	4.1607	-0.017	-0.00403
211 7	-6.05	-6.01	3.6900	3.5865	0.104	0.02805
211 8	-6.46	-4.00	3.3500	3.2178	0.132	0.03947
211 9	-6.68	-2.02	3.3400	2.9770	0.363	0.10867
211 10	-6.96	-0.01	3.1300	2.9116	0.218	0.06978
211 11	-6.97	1.59	3.1900	2.9622	0.228	0.07140
211 12	-6.59	3.59	3.4100	3.1789	0.231	0.06777
211 13	-6.85	5.59	3.6000	3.5299	0.070	0.01946
211 14	-6.31	7.59	4.1800	3.9752	0.205	0.04699
211 15	-5.86	9.59	4.6500	4.6602	0.050	0.01070
211 16	-5.76	11.59	5.4000	5.4373	-0.037	-0.00691
211 17	-5.72	13.59	6.3100	6.4345	-0.124	-0.01975
211 18	-5.61	15.59	7.5200	7.5673	-0.047	-0.00625
211 19	-6.98	0.01	3.1800	2.9149	0.265	0.08335
212 1	-1.59	-0.01	2.4800	2.2373	0.243	0.05786
212 2	-1.94	-25.00	15.5300	14.6232	0.907	0.05839
212 3	-1.95	-24.00	14.1900	13.7217	0.468	0.03301
212 4	-1.96	-22.00	11.9600	12.0010	-0.041	-0.00343
212 5	-2.00	-20.01	10.0100	10.4093	-0.399	-0.03989
212 6	-1.55	-18.01	8.3900	8.5262	-0.536	-0.06391
212 7	-2.00	-16.00	7.0600	7.5755	-0.519	-0.07358
212 8	-1.96	-14.01	5.8800	6.3763	-0.496	-0.08440
212 9	-1.87	-12.01	4.9000	5.3074	-0.407	-0.08314
212 10	-1.90	-10.01	4.1700	4.4601	-0.230	-0.05517
212 11	-1.64	-8.01	3.4600	3.6392	-0.179	-0.05178
212 12	-1.75	-6.00	3.0500	3.0350	0.015	0.00490
212 13	-1.97	-4.01	2.7900	2.6175	0.172	0.06183
212 14	-2.00	-2.00	2.6100	2.3461	0.264	0.10112
212 15	-1.94	-0.01	2.4400	2.2329	0.207	0.08486

TABLE 10. Continued.

212 16	-1.75	1.95	2.3100	2.2763	0.034	0.01458
212 17	-2.00	3.95	2.8400	2.5144	0.326	0.11465
212 18	-1.55	6.01	3.0900	2.9018	0.188	0.06092
212 19	-1.97	8.01	3.6000	3.4465	0.153	0.04263
212 20	-1.57	9.95	4.0400	4.1437	-0.104	-0.02566
212 21	-2.00	11.99	4.6600	5.0044	-0.344	-0.07391
212 22	-1.98	13.95	5.6000	6.0119	-0.412	-0.07356
212 23	-1.57	15.95	6.5800	7.1371	-0.557	-0.08466
212 24	-1.50	18.01	7.9100	8.4415	-0.532	-0.06720
212 25	-1.53	19.95	9.3600	9.8590	-0.499	-0.05331
212 26	-1.72	21.95	11.1100	11.4270	-0.317	-0.02853
212 27	-1.64	23.95	13.2300	13.0962	0.134	0.01512
212 28	-1.74	24.95	14.3900	13.9818	0.408	0.02837
212 29	-1.97	0.00	2.4100	2.2354	0.175	0.07244
213 1	8.04	-0.01	2.5800	2.2463	0.334	0.12932
213 2	8.22	-25.01	15.2400	14.5526	0.687	0.04511
213 3	8.32	-24.00	14.0500	13.6519	0.398	0.02834
213 4	8.50	-22.00	11.8900	11.9514	-0.061	-0.00517
213 5	8.73	-20.00	9.9900	10.3746	-0.385	-0.03850
213 6	8.81	-18.01	8.3700	8.9187	-0.549	-0.06556
213 7	8.79	-16.01	7.0900	7.5759	-0.490	-0.06909
213 8	8.83	-14.01	5.9400	6.3862	-0.446	-0.07513
213 9	8.60	-12.00	4.9200	5.3095	-0.390	-0.07917
213 10	8.38	-10.00	4.3100	4.3505	-0.081	-0.01868
213 11	8.25	-8.02	3.5700	3.6411	-0.071	-0.01992
213 12	8.10	-6.02	3.0900	3.0405	0.050	0.01602
213 13	8.07	-4.01	2.8700	2.6094	0.261	0.09080
213 14	8.07	-2.00	2.6900	2.3459	0.344	0.12793
213 15	8.04	0.00	2.6000	2.2463	0.354	0.13600
213 16	8.05	1.95	2.6400	2.3143	0.326	0.12130
213 17	8.07	3.95	2.8600	2.5479	0.312	0.10911
213 18	8.08	5.95	3.1000	2.9443	0.156	0.05022
213 19	8.05	8.00	3.5100	3.5118	-0.002	-0.00052
213 20	8.11	10.00	4.0000	4.2318	-0.232	-0.05796
213 21	8.11	12.01	4.7700	5.1006	-0.331	-0.06931
213 22	8.15	14.01	5.8700	6.1316	-0.262	-0.04406
213 23	8.44	15.95	7.0100	7.3126	-0.303	-0.04310
213 24	8.75	18.01	8.2600	8.6702	-0.410	-0.04500
213 25	8.83	20.02	9.8100	10.1261	-0.316	-0.03222
213 26	8.81	22.01	11.8300	11.6873	0.143	0.01200
213 27	8.71	24.02	13.9100	13.3752	0.535	0.03845
213 28	8.66	25.02	15.1000	14.2571	0.843	0.05582
213 29	8.31	-0.01	2.6400	2.2439	0.396	0.15000
214 1	18.77	0.00	4.0600	3.8904	0.170	0.04177
214 2	18.06	-20.02	12.1100	11.7792	0.331	0.02731
214 3	18.05	-18.01	10.1800	10.3020	-0.122	-0.01158
214 4	18.05	-16.01	8.7300	8.9682	-0.238	-0.02720
214 5	18.08	-14.01	7.5400	7.7807	-0.241	-0.03142
214 6	18.33	-11.95	6.6800	6.7749	-0.095	-0.01420
214 7	18.45	-10.00	5.9600	5.9174	0.043	0.00715
214 8	18.60	-8.01	5.2300	5.2036	0.026	0.00505
214 9	18.69	-6.01	4.6200	4.6407	0.039	0.00840
214 10	18.73	-4.01	4.3200	4.2292	0.091	0.02103
214 11	18.75	-2.01	4.1100	3.9773	0.133	0.03230
214 12	18.76	0.00	4.0600	3.8883	0.172	0.04225
214 13	18.76	1.95	4.1500	3.9628	0.187	0.04512
214 14	18.75	4.01	4.3000	4.2034	0.097	0.02247
214 15	18.75	5.95	4.5300	4.6036	-0.074	-0.01625
214 16	18.75	8.01	5.0700	5.1754	-0.105	-0.02079
214 17	18.67	10.01	5.7500	5.8842	-0.134	-0.02335
214 18	18.49	12.01	6.5300	6.7271	-0.197	-0.03019
214 19	18.35	13.95	7.6000	7.7187	-0.119	-0.01562
214 20	18.19	15.95	8.7100	8.8619	-0.152	-0.01744
214 21	18.05	17.95	9.9700	10.1497	-0.180	-0.01803
214 22	18.06	20.02	11.6700	11.6261	0.044	0.00376
214 23	18.78	-0.01	4.0600	3.8926	0.167	0.04123

SUM OF ABS(EPRORS)/POINTS= 0.2304
 RMS ERRGR/POINTS= 0.0267
 STANDARD DEVIATION= 0.2899

INPUTS FOR AGAJ73

2.0994
 0.020613 -0.050500 0.000615 0.000004 0.009108 -0.000010 -0.011553 CARO 25
 -0.000058 CARU 26

TABLE 10. Continued.

YAWING MOMENT DATA

COEFFICIENTS OF EQUATION

SUB-SCRIPT	NON-DIMENSIONAL	DIMENSIONAL	AGA373 INPUT
00	-3.72 FT**3	-3.724587 FT**3/DEG**0	XFS1881
10	C.45 FT**3	0.007865 FT**3/DEG**1	XFS1891
20	-8.02 FT**3	-0.002444 FT**3/DEG**2	XFS1901
30	-48.75 FT**3	-0.000259 FT**3/DEG**3	XFS1911
01	143.71 FT**3	5.016450 FT**3/DEG**1	XFS1921
11	84.34 FT**3	0.051384 FT**3/DEG**2	XFS1931
21	-220.82 FT**3	-0.002412 FT**3/DEG**3	XFS1941
02	3.29 FT**3	0.004004 FT**3/DEG**2	XFS1951
12	-21.21 FT**3	-0.000451 FT**3/DEG**3	XFS1961
03	-74.57 FT**3	-0.003189 FT**3/DEG**3	XFS1971
13	55.09 FT**3	0.000071 FT**3/DEG**4	XFS1981

INPUT DATA AND CALCULATIONS

RUN/PT	PITCH	YAW	INPUT	CALCULATION	DELTA	REL-DEL
210 1	-11.76	C.00	-5.0400	-3.7366	-1.303	C.25860
210 2	-10.46	-16.01	-52.1100	-52.1386	0.029	-C.00055
210 3	-10.53	-12.01	-45.0700	-45.5020	0.432	-C.00959
210 4	-10.45	-8.01	-39.9800	-34.6767	-5.303	C.13265
210 5	-10.65	-6.01	-34.7300	-27.6679	-7.062	C.20334
210 6	-10.70	-4.00	-26.2100	-20.0894	-6.121	C.23352
210 7	-11.04	-1.99	-15.6600	-11.6311	-3.829	C.24450
210 8	-11.80	-C.01	-5.6500	-3.7758	-1.874	C.33171
210 9	-11.69	1.99	8.6100	4.4079	4.202	C.48805
210 10	-11.40	3.99	16.4700	12.5493	3.921	C.23805
210 11	-10.81	6.02	24.3300	20.7175	3.612	C.14848
210 12	-10.71	8.02	36.5500	26.0383	6.512	C.23288
210 13	-10.57	10.01	41.4800	34.6465	6.834	C.16474
210 14	-10.58	12.01	41.1700	40.2616	0.908	C.02207
210 15	-10.47	14.02	44.8500	45.0465	-0.196	-C.00438
210 16	-10.46	15.99	49.7900	48.5635	1.227	C.02463
210 17	-11.81	C.00	-4.7700	-3.7346	-1.035	C.21706
211 1	-6.98	C.00	-4.5100	-3.6103	-0.700	C.15515
211 2	-5.76	-16.00	-58.8700	-60.1626	1.293	-C.002196
211 3	-5.76	-13.99	-55.6100	-56.2619	0.652	-C.01172
211 4	-5.75	-11.99	-50.9200	-51.2818	0.362	-C.00711
211 5	-5.82	-10.01	-42.5000	-45.2422	2.742	-C.06452
211 6	-5.92	-8.01	-30.4400	-38.1976	7.758	-C.25485
211 7	-6.05	-6.01	-24.0300	-30.3491	6.319	-C.26297
211 8	-6.48	-4.00	-24.4500	-21.7403	-2.710	C.11083
211 9	-6.68	-2.02	-15.8200	-12.9675	-2.852	C.18031
211 10	-6.96	-C.01	-5.2600	-3.8556	-1.404	C.26695
211 11	-6.57	1.99	6.5000	5.2216	1.278	C.19668
211 12	-6.55	3.99	15.2700	14.1309	1.139	C.07460
211 13	-6.65	5.99	21.2500	22.7412	-1.491	-C.07017
211 14	-6.31	7.99	23.3900	31.0945	-7.705	-C.32939
211 15	-5.86	5.99	29.8600	36.8104	-8.950	-C.29975
211 16	-5.76	11.99	41.3500	45.4572	-4.107	-C.09933
211 17	-5.72	13.99	51.0200	51.0853	-0.069	-C.00136
211 18	-5.61	15.99	58.0100	55.7823	2.228	C.03840
211 19	-6.90	C.01	-4.3700	-3.7648	-0.605	C.13848
212 1	-1.55	-C.01	-2.2600	-3.7969	1.537	-C.68005
212 2	-1.94	-25.00	-73.5800	-73.9496	0.370	-C.00502
212 3	-1.95	-24.00	-74.3300	-73.9058	-0.424	C.00571
212 4	-1.56	-22.00	-74.4200	-73.2315	-1.189	C.01597
212 5	-2.00	-20.01	-71.8400	-71.6073	-0.233	C.00324
212 6	-1.95	-18.01	-67.7600	-69.1255	1.366	-C.02015
212 7	-2.00	-16.00	-62.9100	-65.4156	2.506	-C.03983
212 8	-1.96	-14.01	-57.9200	-60.7845	2.864	-C.04946
212 9	-1.87	-12.01	-51.9300	-55.1005	3.171	-C.06105
212 10	-1.90	-10.01	-46.1100	-48.3006	2.191	-C.04751
212 11	-1.84	-8.01	-42.6900	-40.6519	-2.038	C.04774
212 12	-1.75	-6.00	-29.4400	-32.1591	2.719	-C.09236
212 13	-1.57	-4.01	-20.4400	-23.0653	2.625	-C.12844
212 14	-2.00	-2.00	-10.0400	-13.5020	3.462	-C.34482
212 15	-1.94	-C.01	-0.6100	-3.7962	3.186	-5.22330

TABLE 10. Concluded.

212 16	-1.79	1.99	7.1800	6.0244	1.156	C.16094
212 17	-2.00	3.99	13.8900	15.6241	-1.734	-C.12484
212 18	-1.99	6.01	21.1700	24.9809	-3.811	-C.18001
212 19	-1.97	8.01	29.3200	33.6997	-4.380	-C.14938
212 20	-1.97	9.99	38.1700	41.6223	-3.452	-C.09045
212 21	-2.00	11.99	46.2500	48.7592	-2.509	-C.05425
212 22	-1.98	13.99	53.1400	54.9846	-1.845	-C.03471
212 23	-1.57	15.99	58.8000	60.6161	-1.816	-C.03089
212 24	-1.50	18.01	63.2500	64.9557	-1.706	-C.02697
212 25	-1.53	19.99	64.6200	68.0746	-3.455	-C.05346
212 26	-1.72	21.99	71.3900	69.9811	1.409	C.01974
212 27	-1.64	23.99	72.8400	71.3816	1.458	C.02002
212 28	-1.74	24.99	72.5700	71.5252	1.045	C.01440
212 29	-1.97	0.00	-1.3800	-3.7476	2.368	-1.71563
213 1	8.04	-C.01	-4.2400	-4.0047	-0.235	C.05549
213 2	8.22	-25.01	-92.8300	-92.0107	-0.819	C.00883
213 3	8.32	-24.00	-91.6200	-91.0708	-0.549	C.00599
213 4	8.50	-22.00	-89.2500	-88.5453	-0.705	C.00790
213 5	8.73	-20.00	-85.9100	-85.1507	-0.759	C.00884
213 6	8.81	-18.01	-82.9100	-80.7000	-2.210	C.02666
213 7	8.79	-16.01	-78.4600	-75.2181	-3.242	C.04132
213 8	8.83	-14.01	-72.4500	-68.8383	-3.612	C.04985
213 9	8.60	-12.00	-65.1800	-61.4120	-3.768	C.05781
213 10	8.38	-10.00	-57.2900	-53.2207	-4.069	C.07103
213 11	8.25	-8.02	-46.3400	-44.4190	-1.921	C.04145
213 12	8.10	-6.02	-38.6000	-34.9018	-3.698	C.09581
213 13	8.07	-4.01	-28.2600	-24.8596	-3.400	C.12033
213 14	8.07	-2.00	-13.3500	-14.4708	1.121	-C.08396
213 15	8.04	0.00	-4.2700	-3.9520	-0.318	C.07448
213 16	8.05	1.99	9.1200	6.5139	2.606	C.28576
213 17	8.07	3.99	20.8300	16.8008	3.769	C.18271
213 18	8.08	5.99	30.6700	26.8675	3.803	C.12398
213 19	8.05	8.02	39.0200	36.5144	2.506	C.06421
213 20	8.11	10.02	49.5400	45.3763	4.164	C.08405
213 21	8.11	12.01	58.2900	53.4430	4.847	C.08315
213 22	8.19	14.01	63.5600	60.7198	2.840	C.04469
213 23	8.44	15.99	70.2400	67.0791	3.161	C.04500
213 24	8.75	18.01	74.8400	72.6823	2.158	C.02883
213 25	8.83	20.02	73.6800	77.2591	-3.579	-C.04858
213 26	8.81	22.01	81.4600	80.8724	0.528	C.00648
213 27	8.71	24.02	82.7900	83.6186	-0.829	-C.01001
213 28	8.66	25.02	83.4200	84.6799	-1.260	-C.01510
213 29	8.01	-0.01	-3.3300	-4.0023	0.672	-C.20189
214 1	18.77	C.00	-C.4500	-6.0355	-0.414	C.06426
214 2	18.06	-20.02	-88.9300	-90.3076	1.378	-C.01549
214 3	18.05	-18.01	-83.0000	-84.7615	1.762	-C.02122
214 4	18.05	-16.01	-77.1400	-78.4544	1.314	-C.01704
214 5	18.08	-14.01	-69.5600	-71.3759	1.816	-C.02611
214 6	18.33	-11.99	-50.3100	-63.4967	3.187	-C.05284
214 7	18.49	-10.00	-52.0000	-55.0519	0.052	-C.05869
214 8	18.60	-8.01	-44.3500	-46.0228	1.673	-C.03772
214 9	18.65	-6.01	-37.8700	-36.4658	-1.404	C.03708
214 10	18.73	-4.01	-29.6800	-26.5362	-3.144	C.10592
214 11	18.75	-2.01	-18.4900	-16.3634	-2.127	C.11501
214 12	18.76	C.00	-7.4600	-6.0323	-1.428	C.19139
214 13	18.76	1.99	3.1000	4.1649	-1.065	-C.34352
214 14	18.75	4.01	15.0600	14.3447	0.655	C.04369
214 15	18.75	5.99	25.1900	24.0145	1.176	C.04667
214 16	18.75	8.01	31.8400	33.4429	-1.603	-C.05034
214 17	18.67	10.01	38.9700	42.2844	-3.314	-C.08505
214 18	18.45	12.01	48.8800	50.5623	-1.682	-C.03442
214 19	18.35	13.99	57.5000	58.0364	-0.536	-C.00933
214 20	18.19	15.99	65.2700	64.8367	0.433	C.00464
214 21	18.05	17.99	72.4600	70.8208	1.639	C.02262
214 22	18.06	20.02	76.0900	75.9655	0.125	C.00164
214 23	18.78	-0.01	-5.7500	-6.0903	0.340	-C.05918

SUM OF ABSORPTION/POINTS= 2.3521
 RMS ERROR/POINTS= 0.2769
 STANDARD DEVIATION= 3.0079

INPUTS FOR 864373

-3.724587 0.007865 -0.002444 -0.006259 CARD 20
 0.000000 0.000000 -0.000000 0.000000 -0.000000 -0.000000 CARD 2E

The inputs to the High Angle Equations are stated in terms of the value of force or moments divided by dynamic pressure at specific aerodynamic angles. Provided sufficient test data are available, these inputs can be read directly from plots of the data. If test data are insufficient or not available, the inputs can be estimated by analytically determining the forces (particularly drag force or equivalent flat plate area) and the location of the fuselage center of pressure at the appropriate orientations.

Jorgensen's work (References 23 and 24) was published shortly after the development of the current fuselage representation. The engineering-type methods which are presented in the referenced reports are in general agreement with the HAE model. However, no attempts were made to incorporate Jorgensen's methods directly into C81 because of the large amount of geometric data on the body required, the high Mach number range for which the methods were derived, and the uncertainty of the validity limits of the methods. Regardless, the methods may be helpful and should be considered when estimating the inputs to the HAE.

²³Jorgensen, L. H., PREDICTION OF STATIC AERODYNAMIC CHARACTERISTICS FOR SPACE-SHUTTLE-LIKE AND OTHER BODIES AT ANGLES OF ATTACK FROM 0° TO 180°, NASA TN D-6996, January 1973.

²⁴Jorgensen, L. H., A METHOD FOR ESTIMATING STATIC AERODYNAMIC CHARACTERISTICS FOR SLENDER BODIES OF CIRCULAR AND NONCIRCULAR CROSS SECTION ALONE AND WITH LIFTING SURFACES AT ANGLES OF ATTACK FROM 0° TO 90°, NASA TN D-7228, April 1973.

5. AERODYNAMIC SURFACE MATHEMATICAL MODEL

5.1 INTRODUCTION

In the course of developing C81, mathematical models have been incorporated for aerodynamic surfaces. The earliest versions of the program contained very simple models for a wing and a horizontal stabilizer. When lateral-directional degrees of freedom were added, a vertical stabilizing surface was added. Although minor improvements were subsequently made to each of the three models, each model remained distinct and applicable only to a specific surface. The most serious shortcomings of these models was that they were restricted to simulating surfaces that were parallel to either the horizontal or vertical planes of the fuselage. Specifically, the wing and horizontal stabilizer had to be in the body X-Y plane and the vertical stabilizer in the body X-Z plane. In accordance with these restrictions, the models were referred to as the wing-elevator-fin models.

The current model for aerodynamic surfaces was developed to remove the restrictions inherent to the previous collection of models. The primary goal in the development of the current model was to provide a single model which could be used for any surface at any orientation with respect to the body. Other desirable features were:

- (1) A better representation for the flow field at each surface and the effect of surface geometry on the aerodynamic characteristics.
- (2) The inclusion of aerodynamic pitching moment characteristics for each surface.
- (3) The capability of simulating flaps or control surfaces on each aerodynamic surface.
- (4) The capability of simulating a wing and four stabilizing surfaces.

5.2 DEVELOPMENT OF THE MATHEMATICAL MODELS

The complete aerodynamic surface mathematical model was broken into four submodels for development purposes: the flow field model, the chord line orientation model, the aerodynamic angles model, and the surface aerodynamic model. The flow field and chord line models were defined to be completely independent of each other with their output being combined to define the aerodynamic angles in the third model. These three models completely replaced the comparable models which were part of the previous wing-elevator-fin models.

The current mathematical model for computing the aerodynamic force and moment coefficients is a minor update and expansion of the previous representation. The major differences include:

- (1) Changes to specific equations to improve the simulation of the effects of surface geometry.
- (2) The addition of a pitching moment coefficient to the model.
- (3) A method for modifying the coefficients computed for flap, or control surface, deflection.

5.2.1 Flow Field Model

In the development of the mathematical model, the flow field at each aerodynamic surface was considered to be dependent on the aerodynamic angles of the fuselage, the location of the surfaces with respect to the fuselage, and velocity components induced at the surface by the rotor(s). In addition, the flow field at each stabilizing surface was considered to be dependent on the wing lift coefficient and location of the surface with respect to the wing.

Although C81 has been developed exclusively for subsonic, incompressible aerodynamics of the airframe components, the incompressible flow interactions of aerodynamic surfaces on the flow fields of each other and the wing have been neglected. These interactions were neglected primarily because of the iterative procedure which would be required if each surface could affect the flow field at every other surface. Since most stabilizing surfaces are located well aft of wings, it is reasonable and justifiable to neglect the effect of the surfaces on the flow field at the wing. Neglecting the interactions between individual stabilizers was also considered justified because most stabilizing surfaces fall into one of the three following categories where mutual interference is minimal:

- (1) They are at approximately right angles to other surfaces.
- (2) If parallel, the planes of the surfaces are generally separated by distances greater than the span of either surface, or
- (3) They are separated (end plated) by major structure such as the fuselage or tail boom.

In the unusual case of two surfaces in approximately the same plane and only a few chord lengths apart, the input data used

in the aerodynamic coefficient computations can be modified to yield a reasonable simulation of the situation, e.g., reduce the lift-curve slope by the ratio of downwash to angle of attack ($d\epsilon/d\alpha$).

The flow field model computes in the following order: the effects of the fuselage, the wing (for stabilizers only), rotor wash, fuselage angular velocities, and gusts on the local flow field.

Figure 34 is a flow chart of the model as currently programmed. Most of the actual equations used are given in the User's Manual (Volume II, Sections 3.14 and 3.15). The basic inputs to the model are the body-axis components of the flight path velocity, and the outputs are the body-axis components of the local velocity. The equations were empirically derived from several rotorcraft wind tunnel tests. It was felt that none of the analytical methods were general enough to provide the necessary simulation. The first step in the model is to compute the downwash and sidewash angles due to the fuselage (ϵ_f and σ_f ,

respectively) at the surface center of pressure from program input data and the fuselage aerodynamic angles. The three body-axis components of velocity are then reduced to account for dynamic pressure loss and assumed to be acting in an axis system which is oriented by Euler rotations of σ_f degrees of yaw and ϵ_f degrees of pitch with respect to the body axis.

Next, the velocities are resolved back to body-axis. For stabilizers, these recomputed velocities are then reduced for dynamic pressure loss due to the wing and are assumed to be acting in an axis system which is pitched ϵ_{wing} degrees with respect to the body, where ϵ_{wing} is the downwash angle at the stabilizer due to the wing. Next, the velocities are resolved back to body axis and are termed the basic local velocities.

Finally, the body-axis components of linear velocity at the appropriate surface due to rotor wash, angular velocities of the surface center of pressure about the aircraft center of gravity, and those due to gusts are superimposed on the basic local velocities to yield the total local flow components in body axis: u_{SB} , v_{SB} , w_{SB} for the X, Y, and Z components, respectively. These components are then used in the aerodynamic angles model as discussed in Section 5.2.3.

5.2.2 Chord Line Orientation Model

The current surface model provides a method for specifying the orientation of the axis of incidence change and the chord line of each surface with respect to the aircraft. The initial

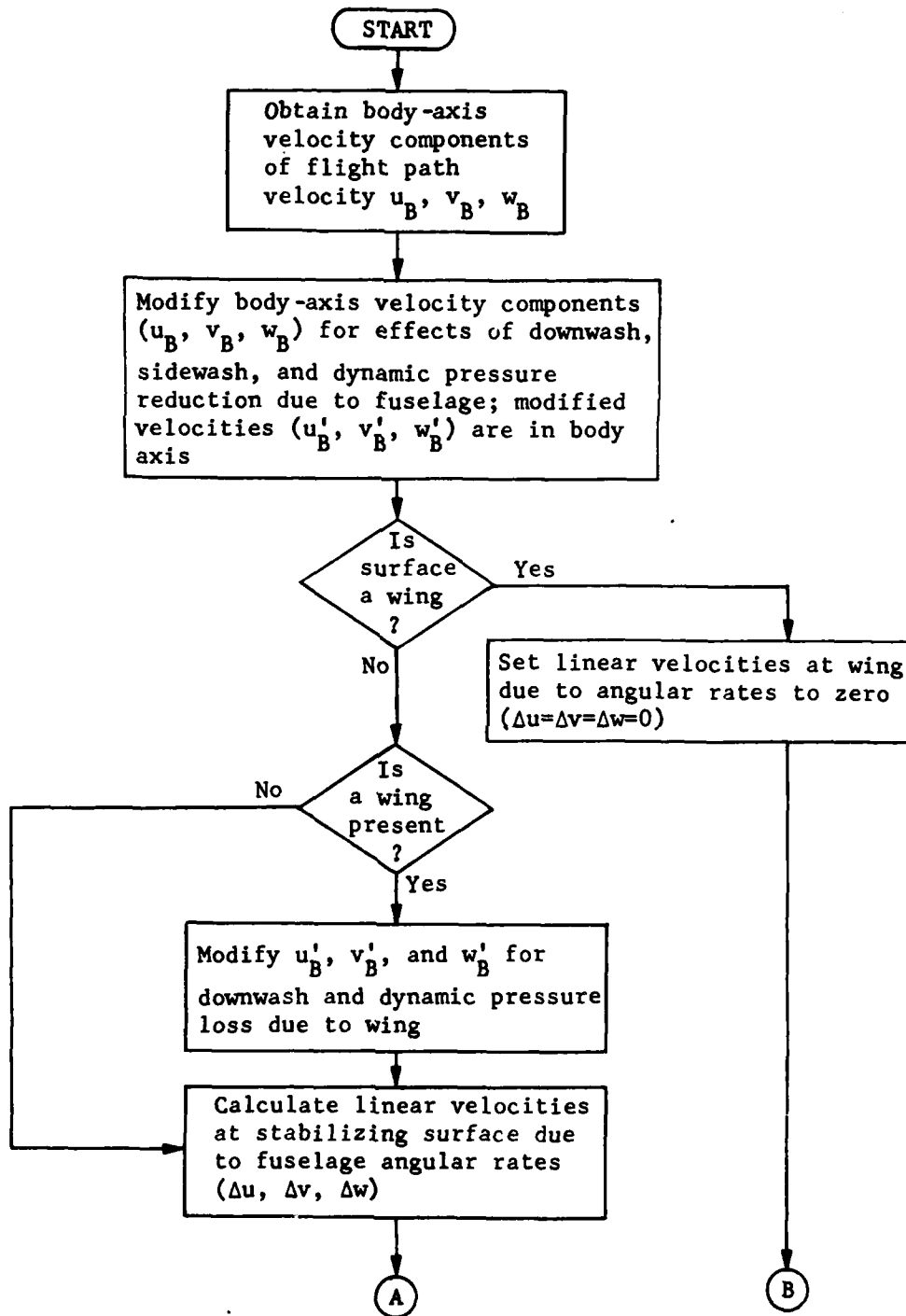


Figure 34. Flow Chart for Flow Field Model.

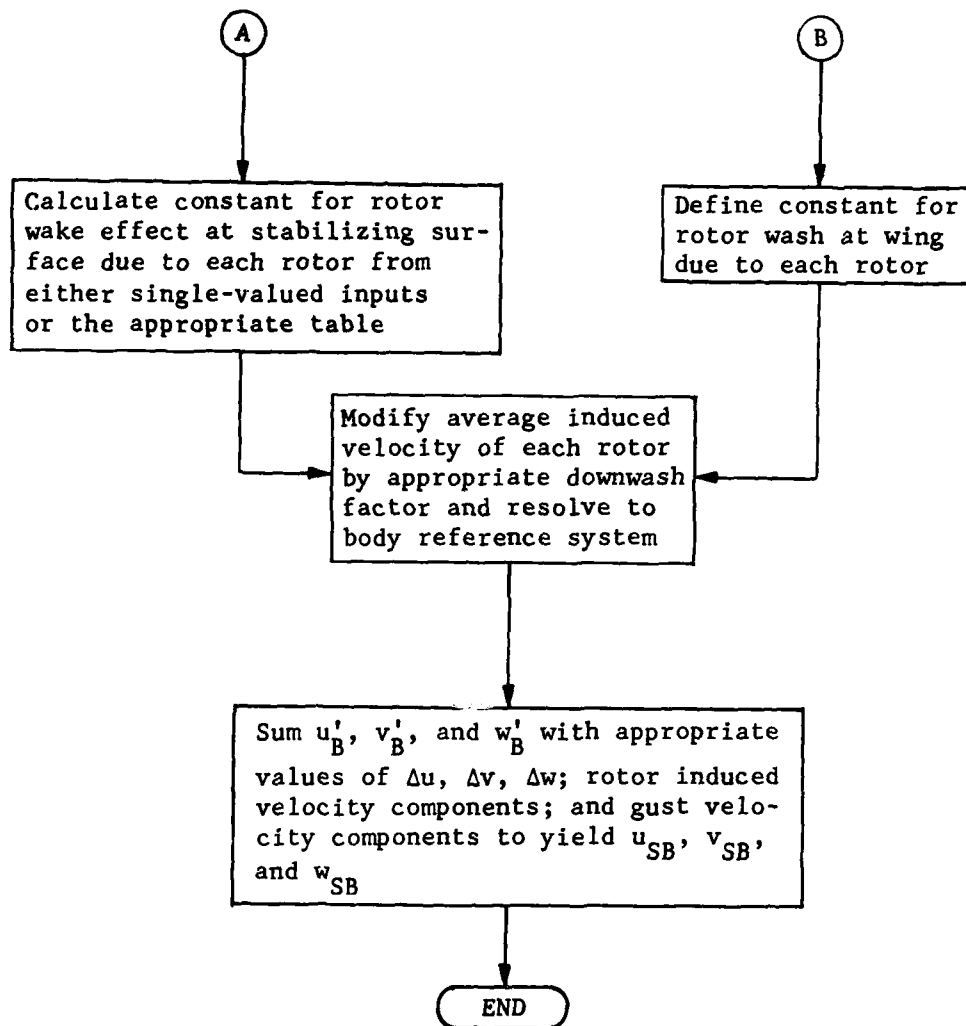


Figure 34. Concluded.

step in the development of the chordline orientation model was to define a new reference system. This system, referred to as the Aerodynamic Surface Reference System, was defined to be a right-handed coordinate system with its origin at the center of pressure of a surface and the reference airfoil section in the X-Z plane of the system. Each of the four stabilizing surfaces was assigned its own independent system while the right and left panels of the wing were assigned systems that were dependent on each other, but independent of the stabilizing surfaces. The orientation of each system was then defined with respect to the body reference system by two ordered rotations:

- (1) Γ : a positive rotation about the body X axis; a dihedral angle rotation, and
- (2) i : a positive rotation about the Y axis which has been rotated through Γ previously; an incidence rotation.

Within the model, it was most convenient to define both positive Γ and i as right-handed rotations. However, this definition would say that a surface on the right side of an airframe with its outboard tip down would have a positive dihedral angle. This definition would not be compatible with a designer's normal definition: dihedral angle is positive for the outboard tip up, whether a surface is on the right or left side of the airframe. In addition, confusion results when trying to define the dihedral angle of a vertical or ventral fin.

After considering several different conventions, it was decided to use the positive right-handed rotation within the program, but to define another convention for input purposes, i.e., a user-oriented convention. The input convention is keyed to the buttline location of the center of pressure (cp) of the surface. If the cp is at or to the left of the centerline of the airframe (Buttline ≤ 0.0), positive Γ is a right-handed rotation about the body X axis. If the cp is to the right of the centerline (Buttline > 0.0), positive dihedral is a left-handed rotation about the body X axis. Hence, to the user, positive dihedral is simply outboard tip up.

With this convention, a vertical fin with sweepback, its cp at Buttline 0.0, and its incidence defined to be positive for leading edge right would have a dihedral angle of +90 degrees. Similarly, a swept-back ventral fin with its cp at Buttline 0.0

would have a dihedral angle of -90 degrees and positive incidence would be leading edge left. This convention for input data is illustrated in Figure 35.

5.2.3 Aerodynamic Angles Model

The aerodynamic angles of attack and sideslip, respectively, used to compute the aerodynamic coefficients are measured with respect to the aerodynamic surface reference system discussed in the preceding section. The first step in defining these angles is to transform the body-axis components of the total local flow velocity determined by the flow field model into the surface reference system. These surface reference components of the total local flow are then used to define the two aerodynamic angles in the conventional manner.

$$\alpha_s = \tan^{-1} (w_s/u_s) \quad (249)$$

$$\beta_s = \tan^{-1} (v_s/V_{AS}) \quad (250)$$

where u_s , v_s , and w_s are the X, Y, and Z velocity components, respectively, in the surface reference system, and

$$\begin{aligned} V_{AS} &= \sqrt{u_s^2 + v_s^2 + w_s^2} \\ &= \sqrt{u_{SB}^2 + v_{SB}^2 + w_{SB}^2} \end{aligned} \quad (251)$$

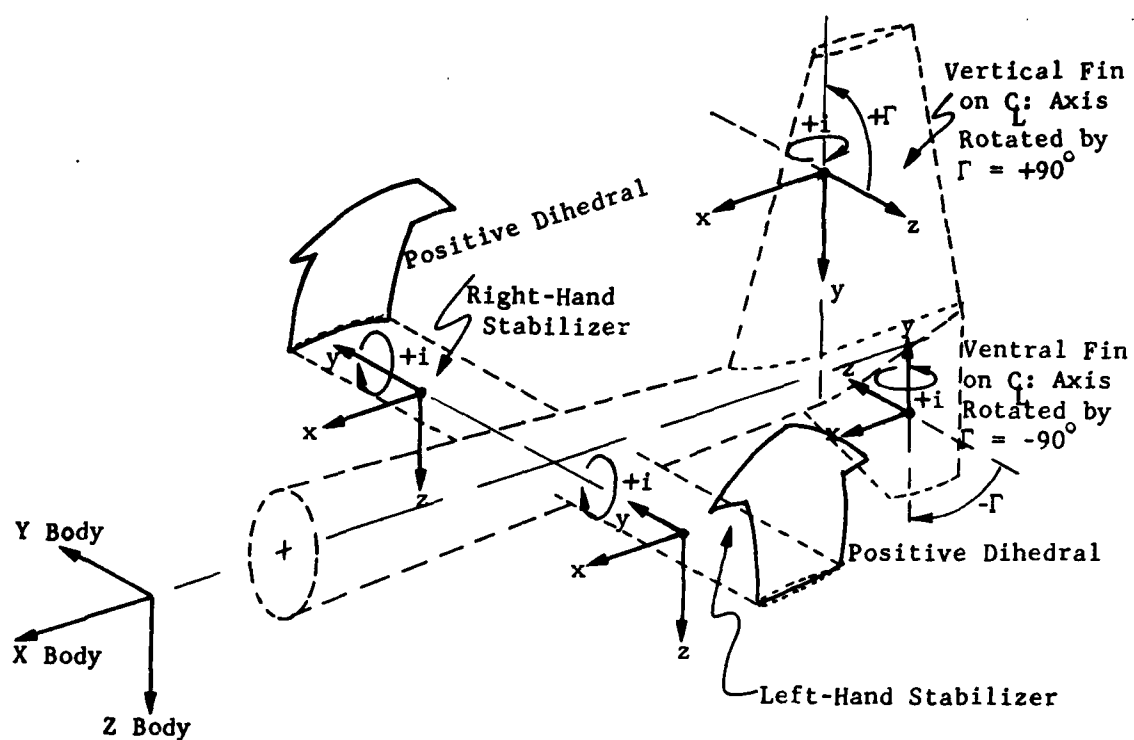
The Mach number at the aerodynamic surface is then

$$M_{AS} = V_{AS}/V_s \quad (252)$$

5.2.4 Surface Aerodynamic Model

The C81 user has the option of computing the C_L , C_D , and C_M aerodynamic coefficients of a surface from sets of data tables or from equations. Each set of data tables consists of a table for each of the three coefficients where each table is a function of the surface angle of attack and Mach number.

Although the rotor blade aerodynamics and aerodynamic surface representations have access to the same group of five sets of data tables, these sets must not be used interchangeably. Tables used for rotor aerodynamics must represent the airfoil section, or two-dimensional characteristics, while tables used for aerodynamic surfaces must represent the surface, or three-dimensional characteristics.



SURFACE	WING AND HORIZONTAL STABILIZERS		VERTICAL AND VENTRAL FINS	
	Dihedral: Γ	Incidence	Dihedral: Γ	Incidence
Buttline > 0 (Rt of C_L)	$< +90$ > -90	+ L.E. UP + L.E. UP	+90 -90	+ L.E. Left + L.E. Right
Buttline ≤ 0 (On or lt of C_L)	$< +90$ > -90	+ L.E. UP + L.E. UP	+90 -90	+ L.E. Right + L.E. Left

L. E. = Leading Edge

Figure 35. Relationship of Body and Aerodynamic Surface Reference Systems.

The mathematical model for determining the coefficients from equations is described in detail in Section 3.14.2 of Volume II of this report. The major change to the model documented in References 1 and 2 is the introduction of the concept of effective aspect ratio and effective sweep angle. Based on the work in Reference 25, the effective sweep angle is

$$\Lambda^* = \Lambda_{1/2} + \begin{cases} \beta & \text{for the trailing panel of a swept surface} \\ -\beta & \text{for the leading panel of a swept surface} \end{cases} \quad (253)$$

where $\Lambda_{1/2}$ is the sweepback of the half-chord line, and β is the sideslip angle. This effective sweep angle also impacts on the aspect ratio to yield an effective ratio

$$A^* = eA \cos^2(\Lambda^*) / \cos^2(\Lambda_{1/2}) \quad (254)$$

where A is the geometric aspect ratio, and e is the spanwise efficiency factor. The factor of one-half, which is included in the equation for A in Reference 26, is replaced here by the spanwise efficiency factor since this analysis was developed for a total surface, not a single panel (half of a surface). Also in Equation (253), the concepts of leading and trailing panels are referenced to the surface rather than to a panel. Hence,

$$\Lambda^* = \Lambda_{1/2} - \beta_s \text{ sign}(\bar{y}) \quad (255)$$

where \bar{y} is the buttline of the surface cp.

The development of the equation for the three-dimensional lift curve slope of an aerodynamic surface in Reference 25 was compared to the equivalent equation in Reference 26. Converting the nomenclature of these two references to that of this report, and introducing the effective sweep and aspect ratio

²⁵Polhamus, E. C., and Sleeman, W. C., Jr., THE ROLLING MOMENT DUE TO SIDESLIP OF SWEEPED WINGS AT SUBSONIC AND TRANSONIC SPEEDS, NASA TN D-209, February 1960.

²⁶USAF STABILITY AND CONTROL DATCOM, U.S. Air Force Flight Dynamics Laboratory, Wright-Patterson Air Force Base, Ohio, February 1972.

²⁷Etkin, Bernard, DYNAMICS OF FLIGHT, New York, N.Y., John Wiley and Sons, 1967, pp. 447-453.

parameters yielded the identical equation for three-dimensional lift curve slope:

$$C_{L_{\alpha}} = (2 A^*) / \left\{ 2 + \sqrt{(2 A^*/a_0)^2 [1 + \{\tan^2 \Lambda^*/(1-M^2)\}] + 4} \right\} \quad (256)$$

where a_0 is the experimental two-dimensional lift curve slope, and M is Mach number. Equation (256) was then evaluated over a wide range of aspect ratios and sweep angles. These results were compared to the charts in Reference 27 and showed very good agreement.

The model for the effect of control surface deflection on the aerodynamic coefficients of a surface was taken from the charts of Reference 28. Equations were empirically derived to fit the type of data presented in the referenced report. The equations compute increments which are added to the coefficients computed for zero deflection. This approach, rather than a detailed analytical model of the effects of deflection, was chosen so that test data could more easily be input to the program and so that the model would be well suited to parametric analysis.

5.3 EXAMPLES OF THE REPRESENTATION

An example of the current mathematical model for aerodynamic surfaces is shown in Figure 36. This figure is a plot of a set of level-flight trim conditions from 100 to 260 knots for the Bell Model 533 High-Performance Helicopter (HPH). Several versions of this compound research helicopter were flight tested under contract to USAAMRDL. The configuration selected for simulation was the one flown in 1968 and 1969. The significant configuration parameters were as follows:

- (1) two-bladed, teetering, low-twist main rotor (44-foot diameter)
- (2) a 78.4-ft² wing with flaps, ailerons, and spoilers
- (3) two JT12A-3 jet engines, one mounted on each wing tip

²⁸Young, A. D., THE AERODYNAMIC CHARACTERISTICS OF FLAPS, British Aeronautical Research Council RM No. 2622, February 1947 (also printed as R.A.E. Report Aero. 2185, August 1947).

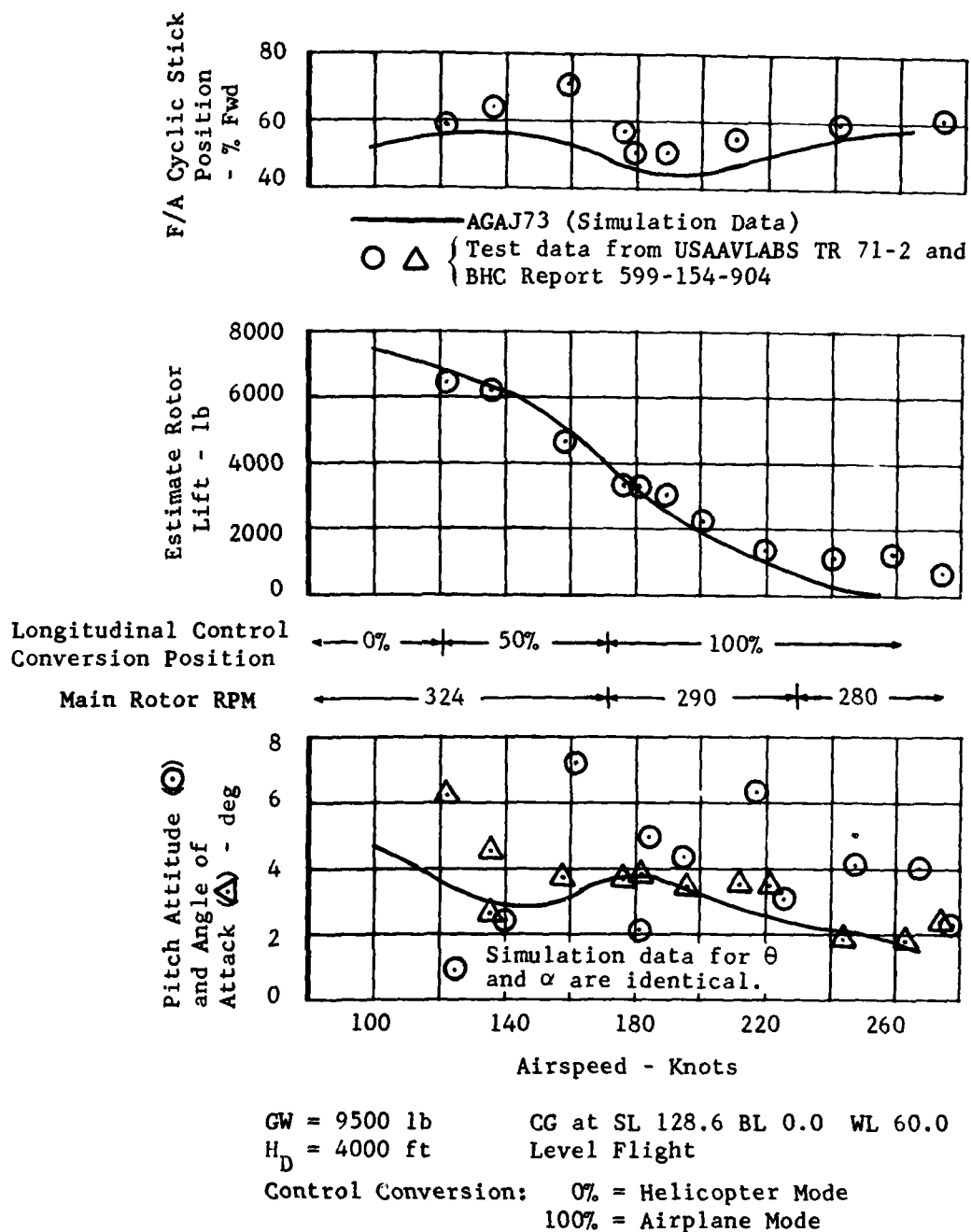


Figure 36. Comparison of Test and Simulation Data for the Bell Model 533.

- (4) A 35.0-ft² controllable stabilator mounted on the tail boom
- (5) a 5.86-ft² fixed incidence stabilizer mounted at the top of the vertical fin
- (6) a 19.95-ft² vertical fin with a sealed rudder (no ventral fin)
- (7) a convertible control system which allowed control of the aircraft using either standard rotor controls or fixed-wing type control surfaces, or a combination of both.

At the time of the HPH flight tests, the version of the Rotorcraft Flight Simulation Computer Program then in use was considerably less sophisticated than the current version. Consequently, many of the data now needed or desirable for a complete input data deck were never developed in the course of flight and wind tunnel tests and analyses of the aircraft. Regardless, the simulation data shown in Figure 36 follows the trends and magnitudes of the available test data quite well.

In level flight, the pitch attitude and angle of attack should be equal. The scatter in these data shown in Figure 36 indicates that either the test data are slightly inaccurate or the flight condition was actually a mild climb or descent rather than level flight as indicated in the flight test reports, or a combination of both. All simulation data were computed as level flight cases, and the two angles were equal. Also, the test reports emphasize that the rotor thrust data are estimates based on blade bending, not direct thrust measurements.

In the course of gathering the data for the input deck from previous C81 decks and test reports, several inconsistencies were noted in the rigging definitions for rotor controls, aerodynamics surface incidences, and the convertible control system. Average values were used as input data when such conflicts were apparent.

Consequently, in view of the absence of current data on the HPH, the fact that it is no longer on flight status (which precludes new rigging checks), and the nature of the test data, the correlation of the simulation and the test data are considered to be excellent. This situation indicates the validity of the current mathematical model for aerodynamic surfaces, as well as the accuracy of the program as a whole.

6. EXTERNAL STORES/AERODYNAMIC BRAKES MATHEMATICAL MODEL

6.1 GENERAL

The current version of C81 includes the capability of simulating the effects of external stores and aerodynamic brakes. The input group for the store/brake model consists of four subgroups where each subgroup is independent of all other subgroups and may represent either a store or a brake. The mathematical models for the stores and brakes were developed concurrently, and each requires essentially the same inputs.

The features which are common to both models are simulation of

- (1) aerodynamics lift, drag, and side force, and
- (2) the influence of dynamic pressure loss and local flow orientation on the aerodynamics forces.

In addition to the common features, the aerodynamic brake model provides for changing the brake deployment (i.e., the magnitude of the aerodynamic forces) during maneuvers, while the store model can simulate store drops or jettisons during maneuvers.

Development of the two models began by reviewing the store/brake configurations and maneuvers which had previously been simulated with artificial inputs to the jet, weapons, and other groups. Next, program users were questioned as to what features they felt were mandatory, desirable, and convenient for the store/brake models. Also, recent flying qualities design and test specifications were reviewed to assure that the models would be able to simulate the demonstrations required by them. From these discussions and investigations, the features noted above were chosen for the models.

6.2 DEVELOPMENT OF THE MATHEMATICAL MODELS

The model for the aerodynamic forces for both stores and brakes was taken directly from the High Angle Equation (HAE) model developed for the fuselage group (see Section 4.2.3 and Table 6). The HAE model equations for the aerodynamic moments of store/brakes about their own center of gravity were not included because of their small magnitude for most stores and brakes. However, inputs are provided for locating the store/brake aerodynamic center at a stationline different from its center of gravity and to move the aerodynamic center as a function of angle of attack. This feature is most applicable to large stores. It is intended that analytical inputs be used to approximate the aerodynamic moments about the store center of gravity, since test data for stores are generally limited.

Each model also includes simple approximations for the influence of nearby structure and rotor downwash on the flow field at the store/brake. The influence of nearby structure is represented by reducing the magnitude of the free-stream velocity vector at the fuselage. This reduction factor has the form of

$$\eta_v = \sqrt{1 - \Delta\eta_q}$$

where $\Delta\eta_q$ is the input for dynamic pressure loss, and η_v is then the scalar by which the velocity vector is multiplied. The value of η_v is independent of all aerodynamic angles.

The effect of rotor downwash on the local flow field is accounted for in the same manner as it is for the aerodynamic surfaces. That is, the average induced velocity at the rotor disc is multiplied by an input constant, assumed to be acting parallel to the rotor mast, and then added vectorially to the local velocity which was reduced for dynamic pressure loss. The constant which multiplies the induced velocity is independent of all aerodynamic angles. Representation of downwash and sidewash due to the fuselage and a more sophisticated model of dynamic pressure loss are not included because of the general lack of good test data or means of analytical prediction. In view of the interactions of the rotor downwash with other parts of the airframe prior to affecting the flow field at the store, the simple model of a constant times the induced velocity is considered to be adequate for the store/brake model. As the sophistication of the rotor wake analysis is enhanced in future versions of C81, it is anticipated that the representation of the effects of rotor downwash on such airframe components as stores and brakes will also be improved.

The above discussion summarizes the common features of the store and brake mathematical models. The features unique to each model are discussed below. To determine whether a subgroup represents a store or a brake, the model checks the value of the input for weight. If the weight is greater than zero, the subgroup is treated as a store; if less than zero, as a brake; and if equal to zero, the subgroup is ignored.

6.2.1 Aerodynamic Brake Model

The primary purpose of the aerodynamic brake model is to simulate an aerodynamic force whose magnitude is a function of not only the local aerodynamic angles and dynamic pressure, but also of the position of an appropriate control in the cockpit. The model incorporates a brake deployment control to accomplish this task.

The control position is input to the model as a percentage of full deployment, where full deployment of the brake results in the aerodynamic forces as calculated from the force equations using the local aerodynamic angles and dynamic pressure. The full deployment forces are then multiplied by the fraction of full control displacement, resolved to body axis, and included in the force and moment summary.

During the TRIM procedure, the control position is fixed at its input value. Then, in the maneuver section of the program, the position can be changed to simulate the deployment or retraction of the aerodynamic brake. The model does not restrict the control to being between 0 and 100 percent, nor the drag to being positive. Hence, if the need arises, negative control positions or negative drag areas (not both simultaneously) can be input to simulate propulsive forces which are proportioned to dynamic pressure and act parallel to the local flow.

6.2.2 External Store Model

The purpose of the external store model is to simulate the aerodynamic forces acting on external stores, the contribution of stores to weight, center-of-gravity location, and inertia of the total aircraft, and the reaction force caused by store jettison. The aerodynamic forces are represented in the same manner as are the forces on the aerodynamic brake except that the calculated forces are not affected by the input, or commanded, value of the deployment control position.

The first version of the store model required that the store weight and inertias be reflected in the weight, center of gravity, and inertial inputs to the fuselage group. This requirement proved very cumbersome in that the user had to locate, or in most cases, calculate, these mass properties for each store configuration of interest. Hence, the model was changed to require that mass properties input to the fuselage group must exclude the contributions of any and all stores. Consequently, during reading and initialization of the input data and prior to commencing the TRIM procedure, the mass properties of the total rotorcraft are recalculated using the inputs to the fuselage and each store subgroup. No recalculation is made if the subgroup is an aerodynamic brake, i.e., weight input less than or equal to zero.

The equations for recalculation of weight, center of gravity, and inertia were developed from conventional weight and balance equations in the following manner.

Consider that the rotorcraft is composed of K discrete parts each with weight (W_j), mass ($M_j = W_j/g$), location (x_j, y_j, z_j),

and inertia about its own cg $((I_{xx})_j, (I_{yy})_j, (I_{xz})_j)$. With K parts, the rotorcraft includes the store of interest and is termed in the new, or N, configuration. With K-1 parts, it excludes the specific store and is termed in the original, or O, configuration. Hence, the Kth part is the store with weight (W_s) , mass $(m_s = W_s/g)$, location (x_s, y_s, z_s) , and inertia $((I_{xx})_s)$. Then, the new stationline of the cg, x_N , can be determined from the known quantities.

$$W_N = W_O + W_s$$

$$W_N x_N = \sum_{j=1}^K W_j x_j$$

$$= \sum_{j=1}^{K-1} W_j x_j + W_s x_s \quad (257)$$

$$= W_O x_O + W_s x_s \quad (258)$$

Substituting Equation (257) into (258) yields

$$x_N = (W_O x_O + W_s x_s)/(W_O + W_s) \quad (259)$$

Similarly, for the buttline, y_N , and waterline, z_N ,

$$y_N = (W_O y_O + W_s y_s)/(W_O + W_s) \quad (260)$$

$$z_N = (W_O z_O + W_s z_s)/(W_O + W_s) \quad (261)$$

The new rolling moment of inertia, $(I_{xx})_N$, is then determined:

$$(I_{xx})_N = \sum_{j=1}^K m_j (y_j^2 + z_j^2) - \left(\sum_{j=1}^K m_j \right) (y_N^2 + z_N^2) + \sum_{j=1}^K (I_{xx})_j \quad (262)$$

The first term of Equation (262) can be broken down as follows:

$$\sum_{j=1}^K m_j (y_j^2 + z_j^2) = \sum_{j=1}^{K-1} [m_j (y_j^2 + z_j^2)] + m_s (y_s^2 + z_s^2) \quad (263)$$

where the first term of Equation (263) can be expressed as

$$\sum_{j=1}^{K-1} m_j (y_j^2 + z_j^2) = (I_{xx})_O + m_O (y_O^2 + z_O^2) - \sum_{j=1}^{K-1} (I_{xx})_j \quad (264)$$

The summation factor in the second term of Equation (262) can be restated as

$$\begin{aligned} \sum_{j=1}^K m_j &= \sum_{j=1}^{K-1} m_j + m_s \\ &= m_O + m_s \end{aligned} \quad (265)$$

and the third term as

$$\sum_{j=1}^K (I_{xx})_j = \sum_{j=1}^{K-1} (I_{xx})_j + (I_{xx})_s \quad (266)$$

Substituting Equation (264) into (263), and Equations (263), (264), and (265) into (262) yields

$$\begin{aligned} (I_{xx})_N &= (I_{xx})_O + (I_{xx})_s + m_O (y_O^2 - y_N^2 + z_O^2 - z_N^2) \\ &\quad + m_s (y_s^2 - y_N^2 + z_s^2 - z_N^2) \end{aligned} \quad (267)$$

Similarly, for the pitching moment of inertia, $(I_{yy})_N$, and yawing moment of inertia, $(I_{zz})_N$,

$$(I_{YY})_N = (I_{YY})_O + (I_{YY})_S + m_O (x_O^2 - x_N^2 + z_O^2 - z_N^2) + m_S (x_S^2 - x_N^2 + z_S^2 - z_N^2) \quad (268)$$

$$(I_{ZZ})_N = (I_{ZZ})_O + (I_{ZZ})_S + m_O (x_O^2 - x_N^2 + y_O^2 - y_N^2) + m_S (x_S^2 - x_N^2 + y_S^2 - y_N^2) \quad (269)$$

For the cross product of inertia, $(I_{xz})_N$,

$$(I_{xz})_N = \sum_{j=1}^K m_j x_j z_j - \left(\sum_{j=1}^K m_j \right) x_N z_N + \sum_{j=1}^K (I_{xz})_j \quad (270)$$

The first term of Equation (270) can then be written as

$$\sum_{j=1}^K m_j x_j z_j = \sum_{j=1}^{K-1} m_j x_j z_j + m_S x_S z_S \quad (271)$$

where the first term of Equation (271) can be expanded as follows.

$$\sum_{j=1}^{K-1} m_j x_j z_j = (I_{xz})_O + m_O x_O z_O - \sum_{j=1}^{K-1} (I_{xz})_j \quad (272)$$

The third term of Equation (270) expands to the following:

$$\sum_{j=1}^K (I_{xz})_j = \sum_{j=1}^{K-1} (I_{xz})_j + (I_{xz})_S \quad (273)$$

Substituting Equation (272) into (271) and Equations (265), (271), and (272) into (270) yields

$$(I_{xz})_N = (I_{xz})_O + (I_{xz})_S + m_O (x_O z_O - x_N z_N) + m_S (x_S z_S - x_N z_N) \quad (274)$$

These equations for recalculating mass properties to reflect weight added to the configuration are summarized in Table 11.

The recalculated mass properties are printed out for each recalculation prior to printout of the first trim iteration. When using the parameter sweep option (NPART = 10), the baseline mass properties input to fuselage group are used as the initial properties for each subsequent case. The recalculated values are not carried forward. The recalculations are then performed independently for each case in the sweep. This procedure prevents cumulative changes in mass properties and permits the user to change either the fuselage or store properties with NAMELIST input before starting each case.

In the maneuver section of the program, the mathematical model can simulate store jettison. Each store may be jettisoned independently of any and all other stores. The user specifies the time for jettison and the store to be jettisoned. At the instant of jettison, the aerodynamic forces of that store are set to zero for the remainder of the maneuver, and the rotorcraft weight, cg, and inertias are recalculated to reflect the loss of the store weight. Also, the moment arms of all rotorcraft components (e.g., fuselage data reference point, rotor, and aerodynamic surfaces) are recalculated using the new cg location. The equations for recalculating the mass properties to reflect weight lost from a configuration were developed in the same manner as those equations for weight added and are also summarized in Table 11. The equations are identical except for the signs on terms associated with the store.

Consideration was given to a model of the jettison reaction forces which could accurately simulate the forces caused by typical jettison mechanisms. One common mechanism is a gas-powered piston where force exerted by the piston is primarily a function of piston displacement, and piston velocity and displacement are functions of the mass being jettisoned. Since C81 requires models which are specifically functions of time, a new set of nonlinear differential equations of motion would be required to simulate such a mechanism. The added complexity of including such a model when store jettison is just one of many features of the program was not considered practical.

6.3 EXAMPLES OF THE STORE/BRAKE REPRESENTATION

To demonstrate the capabilities of the aerodynamic brake and external store representation, two cases are presented.

- (1) Application of dive brakes on the Bell Model 309 (KingCobra)

TABLE 11. EQUATIONS FOR RECALCULATION OF WEIGHT, CENTER OF GRAVITY, AND INERTIAS

$$W_N = W_O + k_s W_s$$

$$x_N = (W_O x_O + k_s W_s x_s) / W_N$$

$$y_N = (W_O y_O + k_s W_s y_s) / W_N$$

$$z_N = (W_O z_O + k_s W_s z_s) / W_N$$

$$(I_{xx})_N = (I_{xx})_O + k_s (I_{xx})_s + m_O (y_O^2 - y_N^2 + z_O^2 - z_N^2) / 144 + k_s m_s (y_s^2 - y_N^2 + z_s^2 - z_N^2) / 144$$

Roll

$$(I_{yy})_N = (I_{yy})_O + k_s (I_{yy})_s + m_O (x_O^2 - x_N^2 + z_O^2 - z_N^2) / 144 + k_s m_s (x_s^2 - x_N^2 + z_s^2 - z_N^2) / 144$$

Pitch

$$(I_{zz})_N = (I_{zz})_O + k_s (I_{zz})_s + m_O (x_O^2 - x_N^2 + y_O^2 - y_N^2) / 144 + k_s m_s (x_s^2 - x_N^2 + y_s^2 - y_N^2) / 144$$

Yaw

$$(I_{xz})_N = (I_{xz})_O + k_s (I_{xz})_s + m_O (x_O z_O - x_N z_N) / 144 + k_s m_s (x_s z_s - x_N z_N) / 144$$

Cross-Product

$k_s =$ +1.0 for adding store to a baseline configuration
-1.0 for dropping store from a baseline configuration

x = Stationline of cg, in.

W = weight, lb

y = Buttline of cg, in.

m = mass, slugs

z = Waterline of cg, in.

I = inertia, slug-ft²

O = baseline configuration

s = store parameters

N = configuration resulting from addition or drop of store

- (2) Asymmetric release of stores from an AH-1G (HueyCobra) with the Stability and Control Augmentation System off and on

6.3.1 Dive Brakes on a KingCobra

Figure 37 shows the time history of symmetrical deployment of two wing-mounted dive brakes on the KingCobra. The trim condition prior to brake application is a 3000-foot-per-minute dive at 170 KTAS. In the simulation, each brake travels from zero to full deployment in 1 second (starting at $t = 0.05$ second), and the flat plate drag area of each brake is 5.0 square feet. Since no dive brakes have been designed for the KingCobra, the inputs for the brake configuration are only meant to demonstrate the capability of the program and should not be interpreted as an optimum dive brake for any rotorcraft. In fact, during initial trial runs of the simulation it was found that with controls locked the wing location for the brakes caused a mild, but undesirable, nose-down pitching moment. To correct this situation, a control gearing was added which caused 1 degree of nose-down incidence to each horizontal stabilizer panel as the brakes went from zero to full deployment. As a result of this gearing, the helicopter pitched up less than $3/4$ of a degree (instead of 3 degrees nose down) in the 3 seconds following the start of the brake deployment. During the same period of time, changes in roll and yaw attitudes were less than 2 degrees and the airspeed decreased slightly more than 4 KTAS. The combination of these effects indicated that the aerodynamic brake model functions in the desired manner.

6.3.2 Store Drops From an AH-1G

Figures 38 and 39 show time histories for store drops from an AH-1G. The initial conditions and helicopter configuration are identical for the two examples: level flight at 100 KTAS in sea level standard atmosphere and each store location loaded to within 20 to 50 pounds of its maximum permissible loading. In both examples, the right outboard store (533 pounds) was dropped at $t = 0.05$ second maneuver time, at which time the lateral cg shifted 3.6 inches to the left. Also, the roll channel of the Automatic Pilot Simulator (see Section 8.2.2) was activated at $t = 2.05$ seconds in both cases. The only difference between the two cases is that for the simulation shown in Figure 38 the SCAS is off, while for that in Figure 39 it is on. Note that both cases used the identical autopilot gains and time constants. In particular, the rate for stick motion was limited to 25 percent per second and desirable times to achieve zero rate and zero attitude were 0.75 and 2.0 seconds respectively. This rate and these times are quite

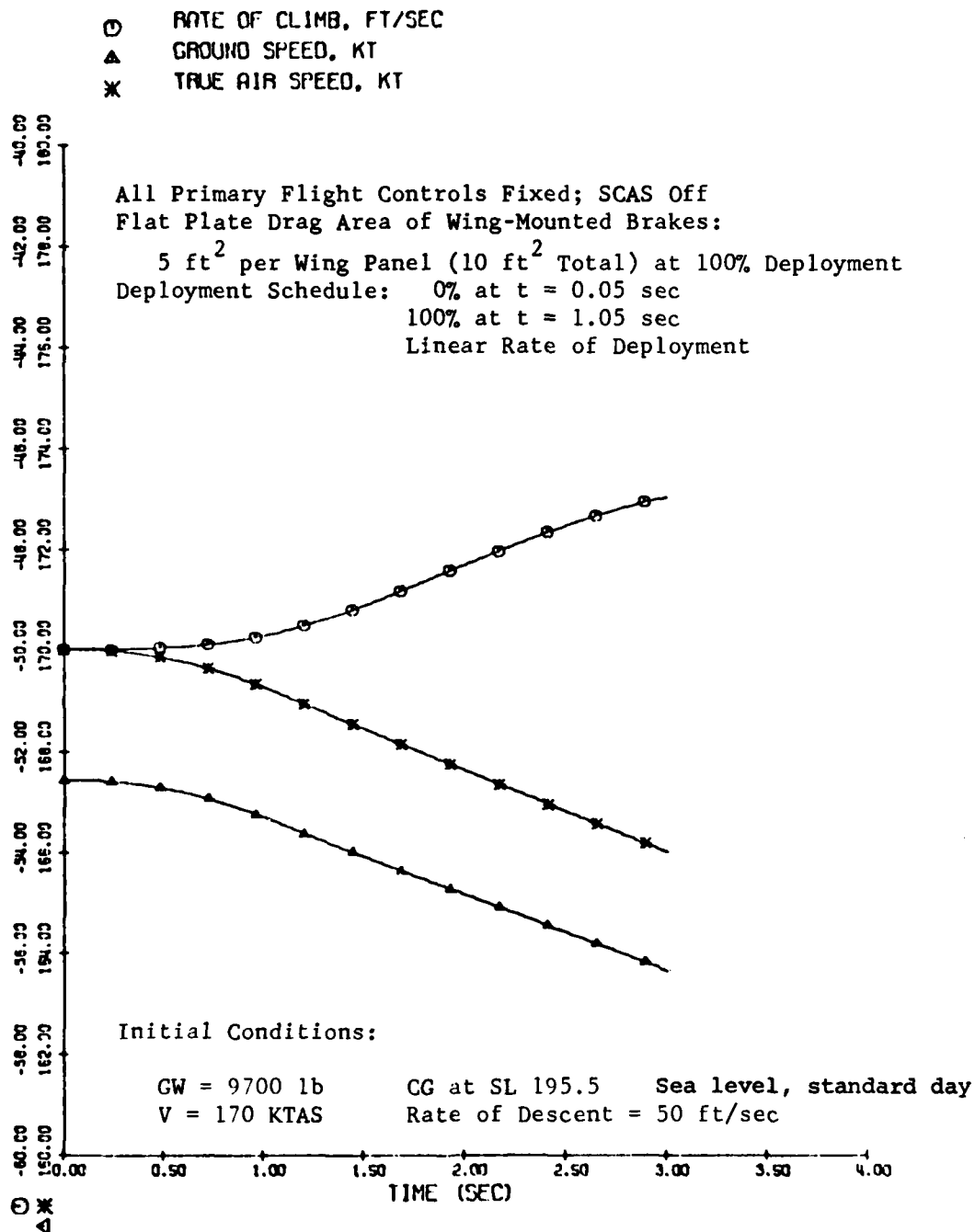


Figure 37. Time History of Dive Brake Application on a Bell Model 309.

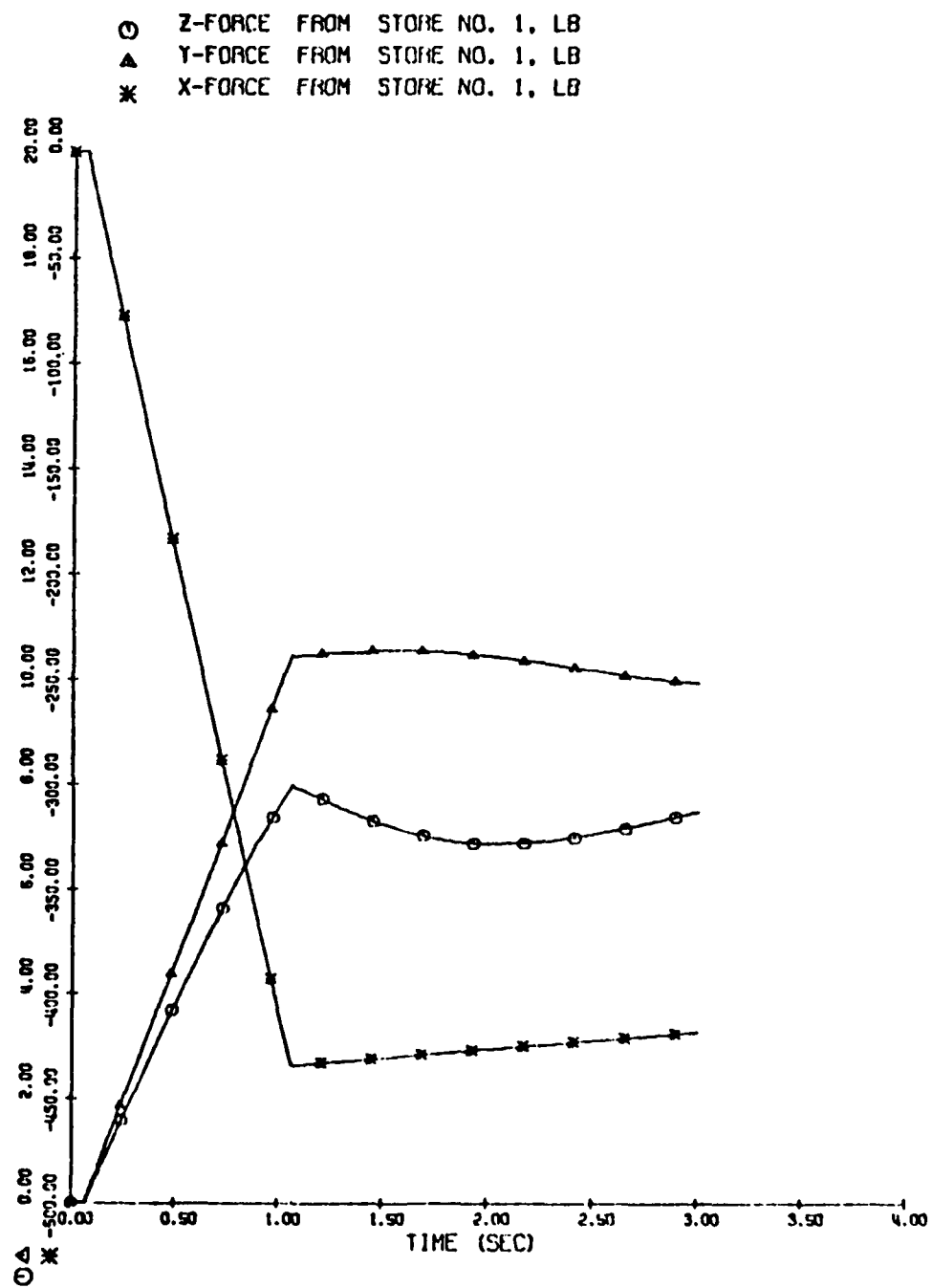


Figure 37. Continued.

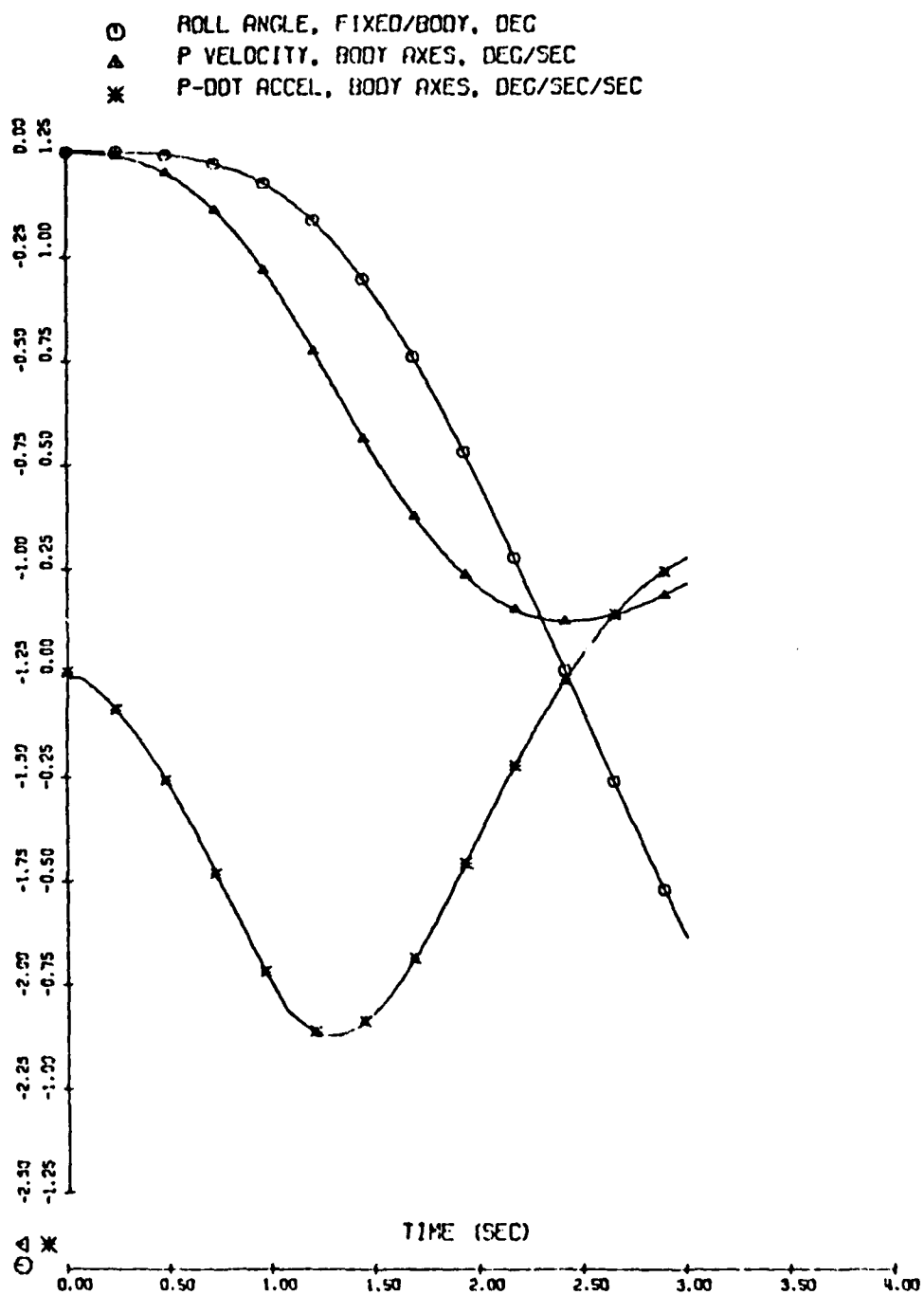


Figure 37. Continued.

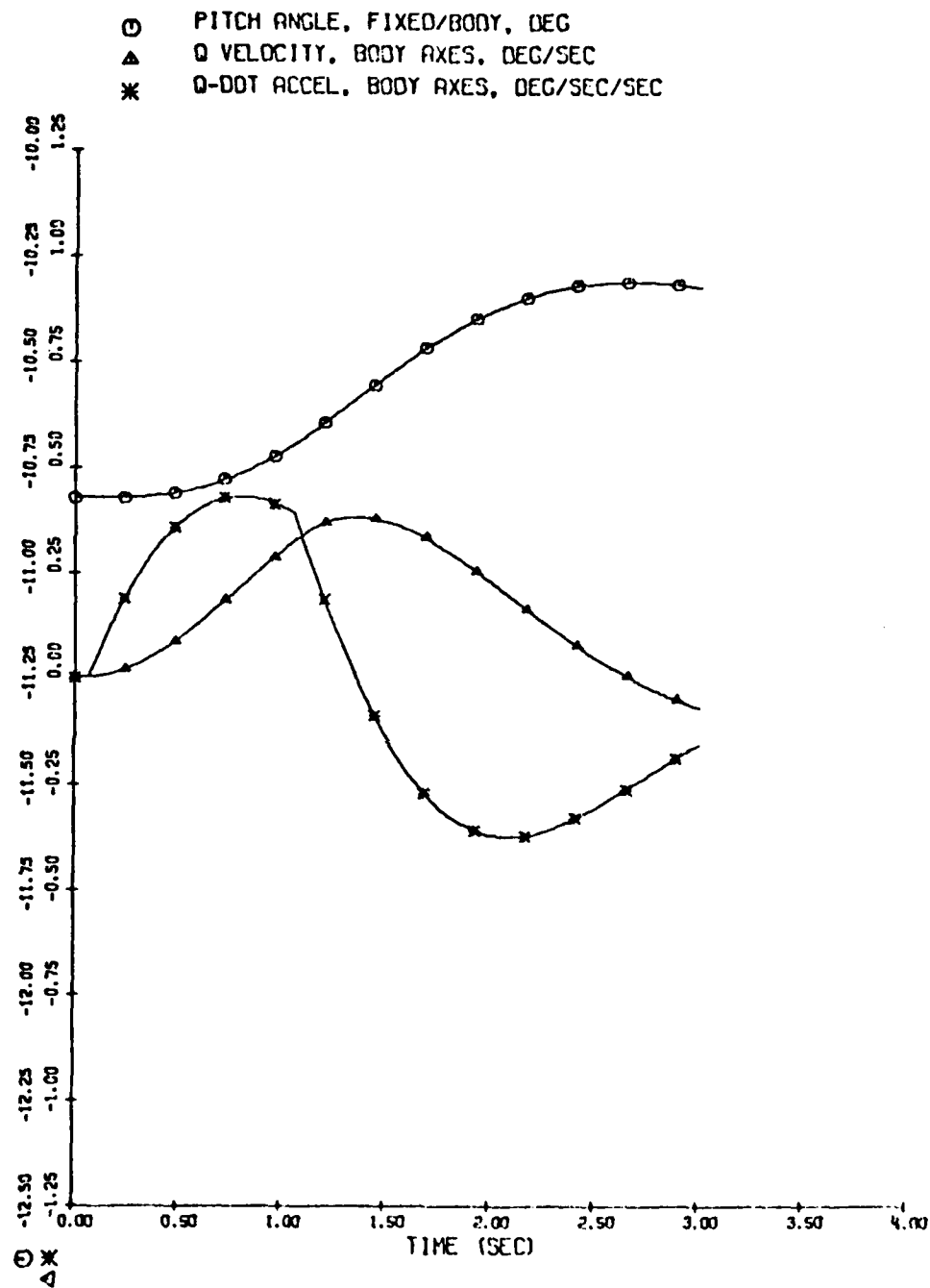
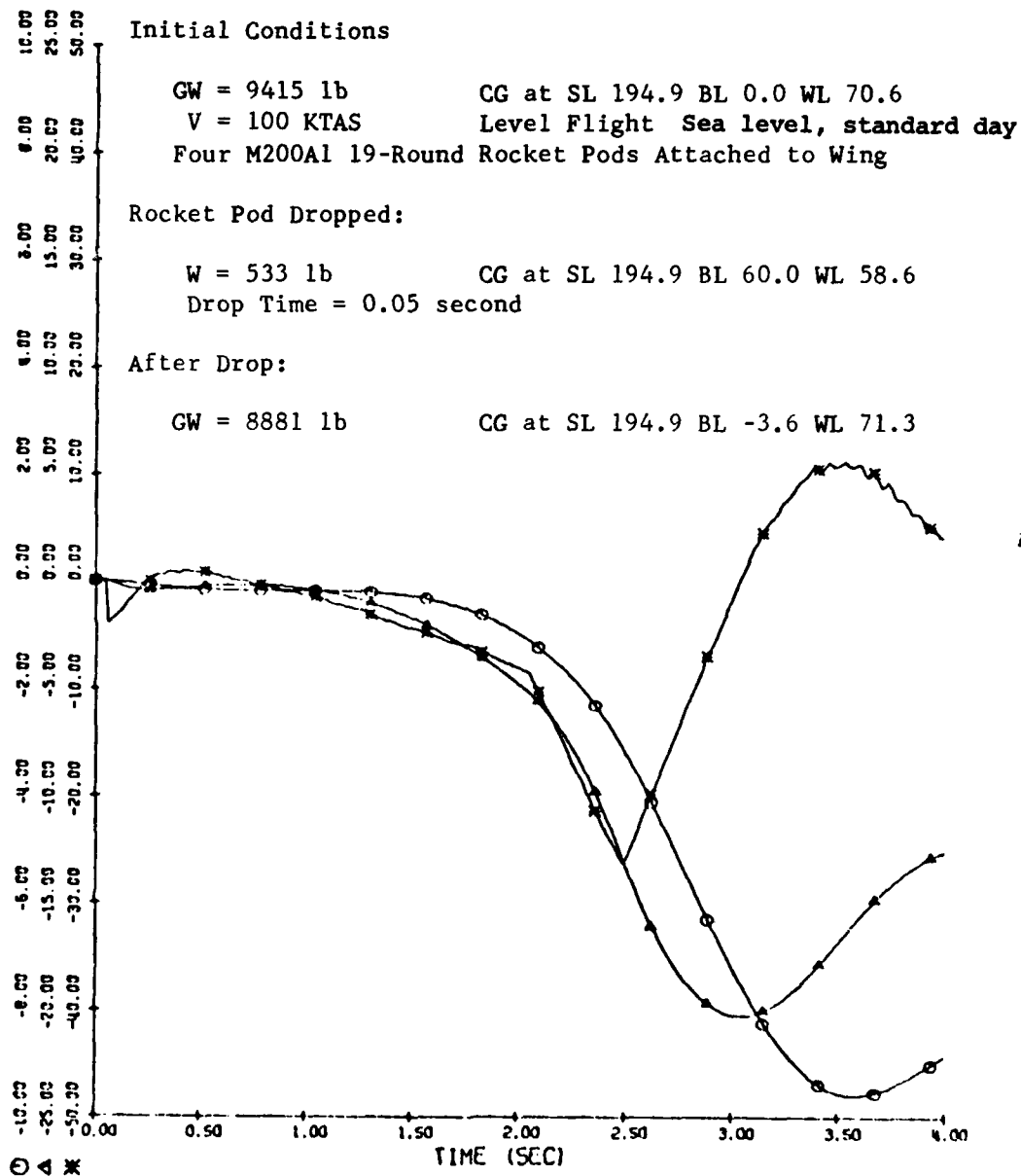


Figure 37. Concluded.

○ YAW ANGLE, FIXED/BODY, DEG
 ▲ R VELOCITY, BODY AXES, DEG/SEC
 * R-DOT ACCEL, BODY AXES, DEG/SEC/SEC



F/A cyclic, collective, and pedal position fixed for entire maneuver.
 Lateral cyclic position fixed until $t = 2.05$ sec; controlled by
 Automatic Pilot Simulator for the remainder of the maneuver.

Figure 38. Time History of an External Store Drop from a
 Bell Model 209 (SCAS Off).

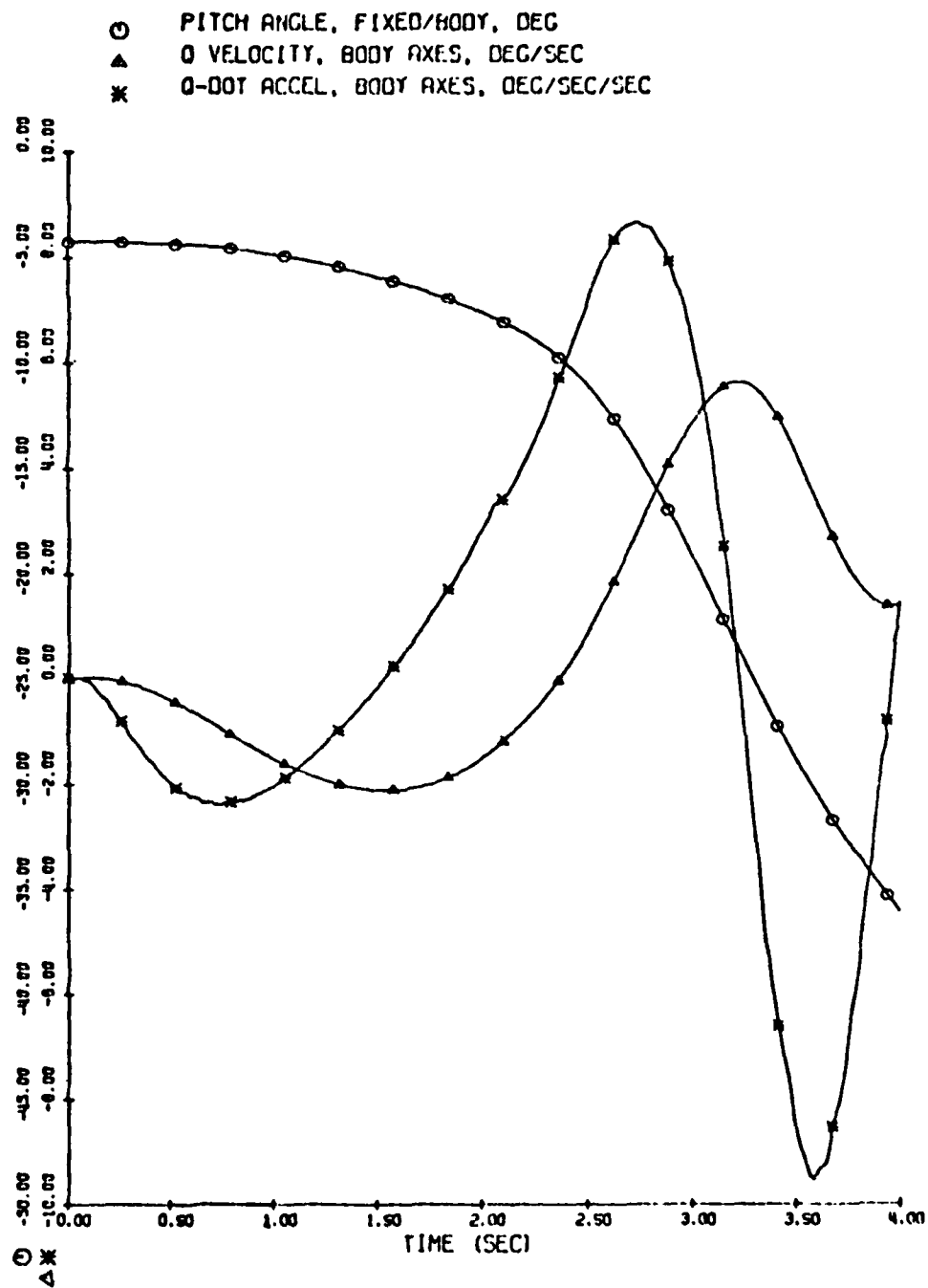


Figure 38. Continued.

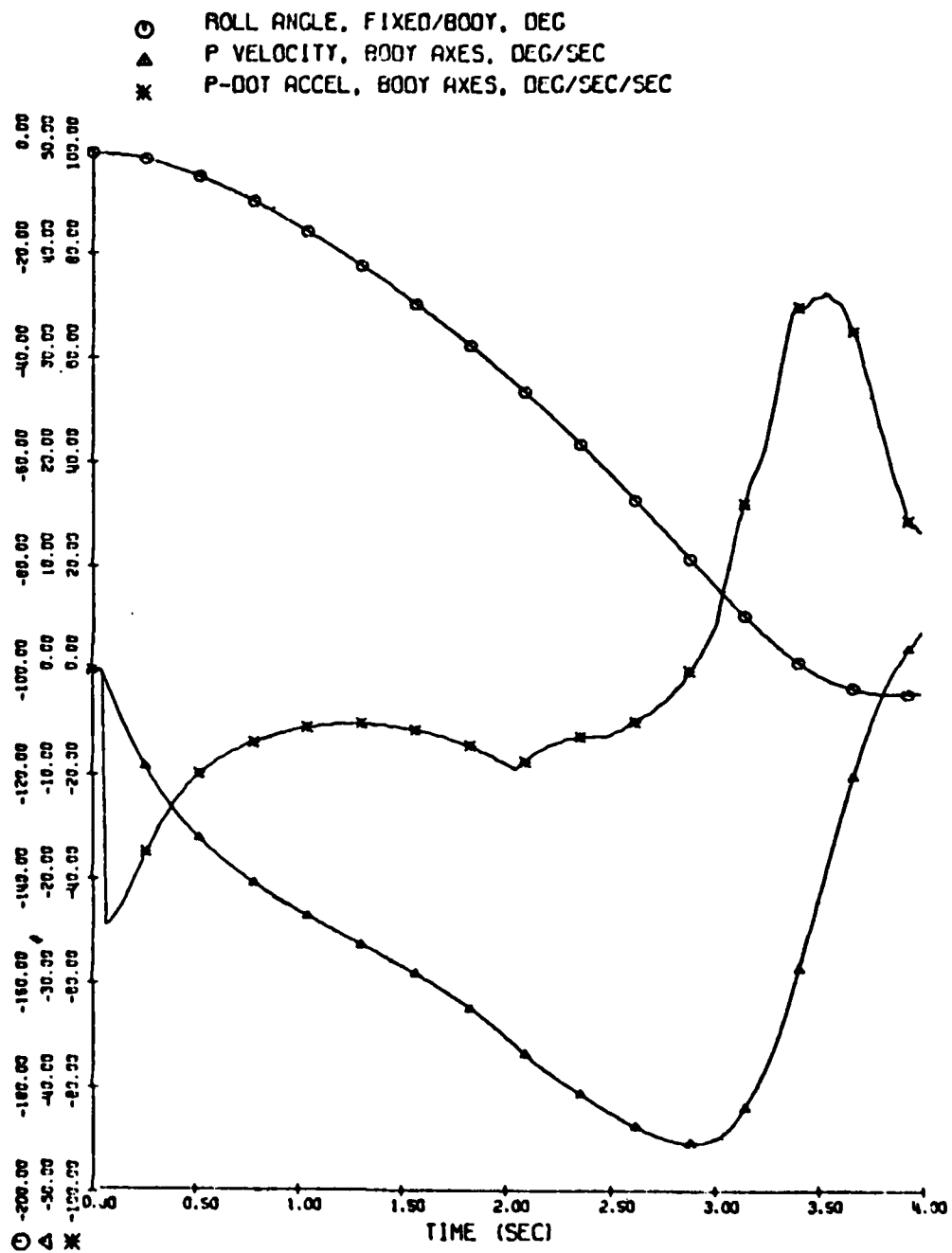
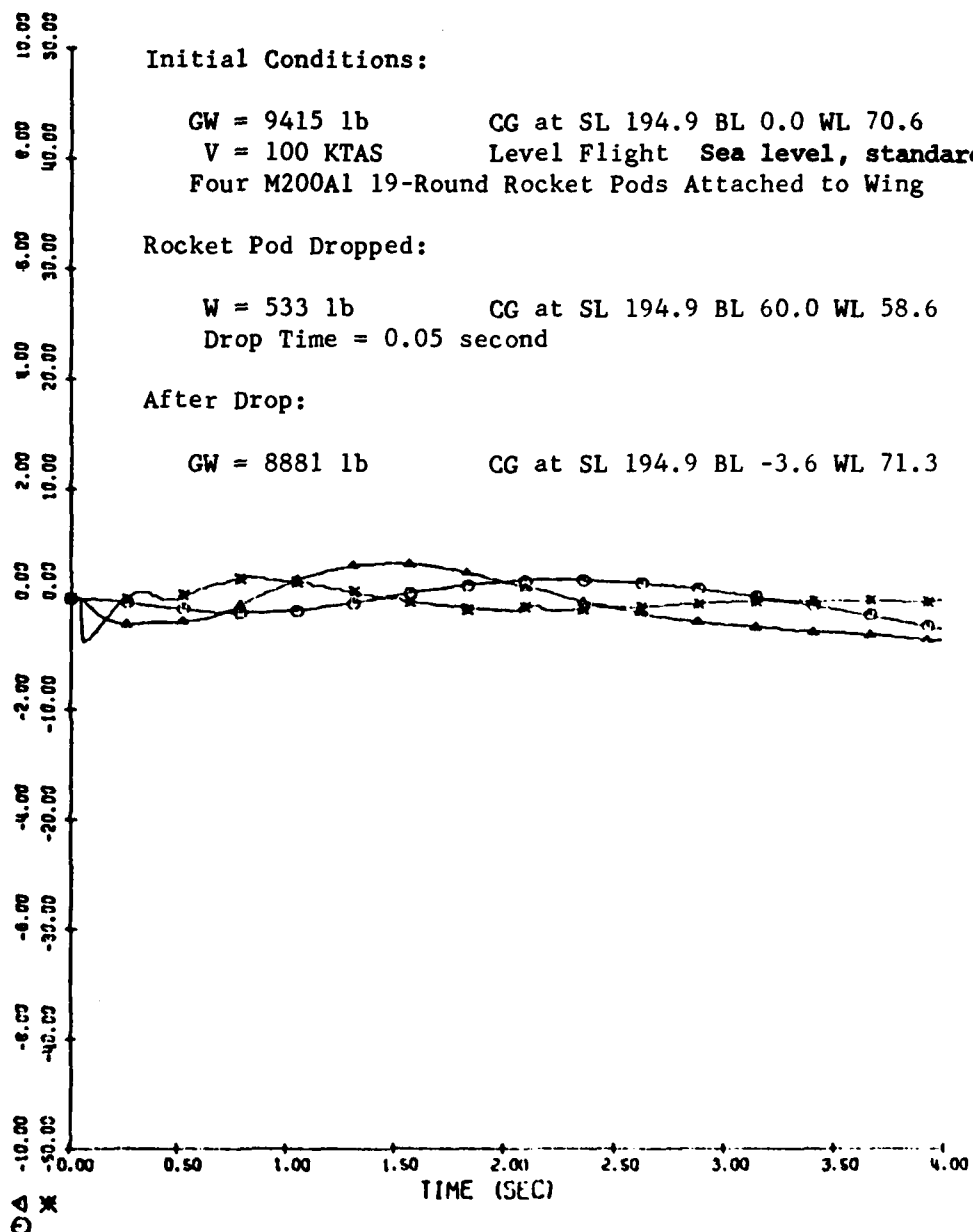


Figure 38. Concluded.

- YAW ANGLE, FIXED/BODY, DEG
- ▲ R VELOCITY, BODY AXES, DEG/SEC
- ✕ R-DOT ACCEL, BODY AXES, DEG/SEC/SEC



F/A cyclic, collective, and pedal position fixed for entire maneuver. Lateral cyclic position fixed until $t = 2.05$ sec; controlled by Automatic Pilot Simulator for the remainder of the maneuver.

Figure 39. Time History of an External Store Drop from a Bell Model 209 (SCAS On).

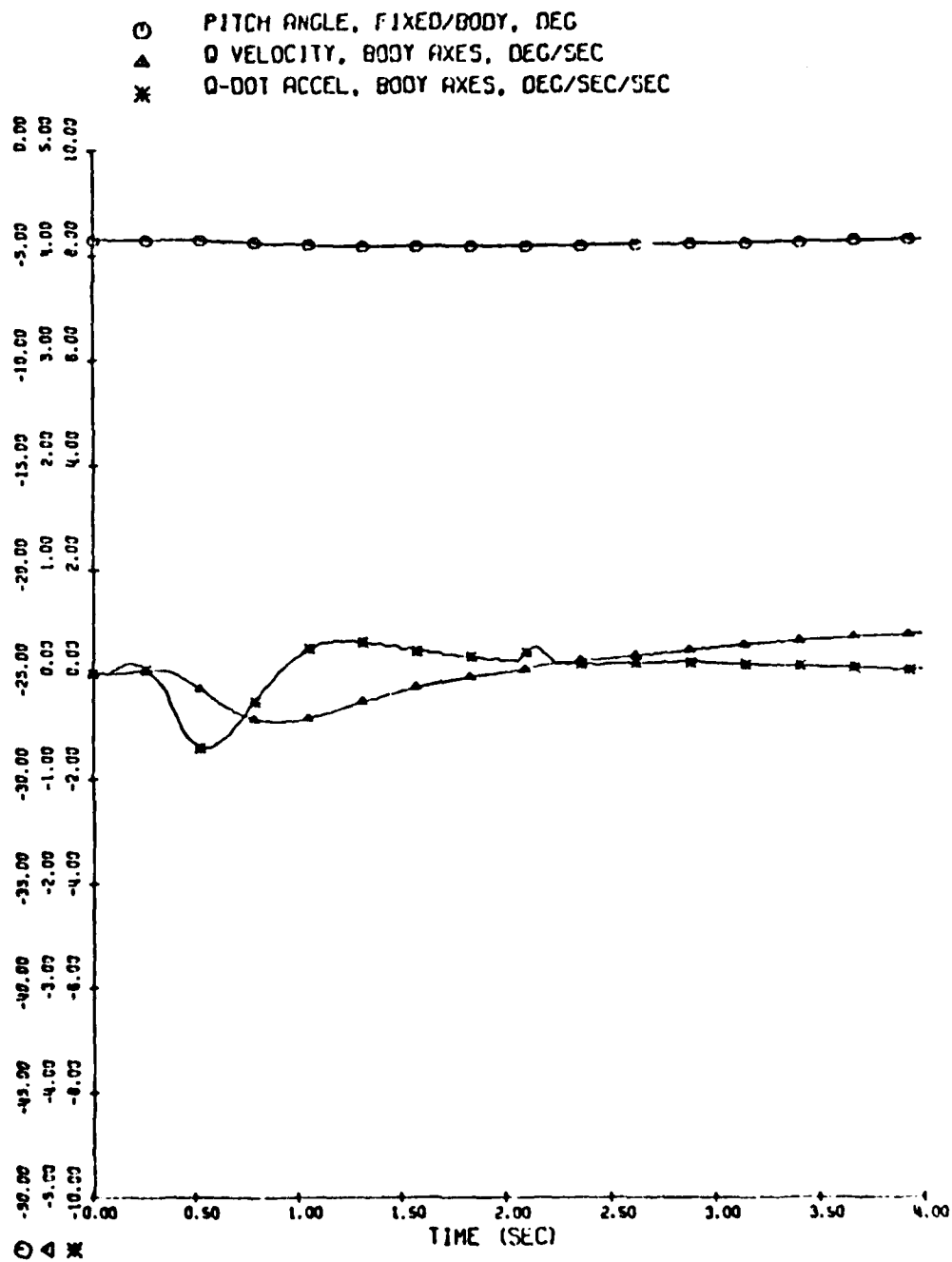


Figure 39. Continued.

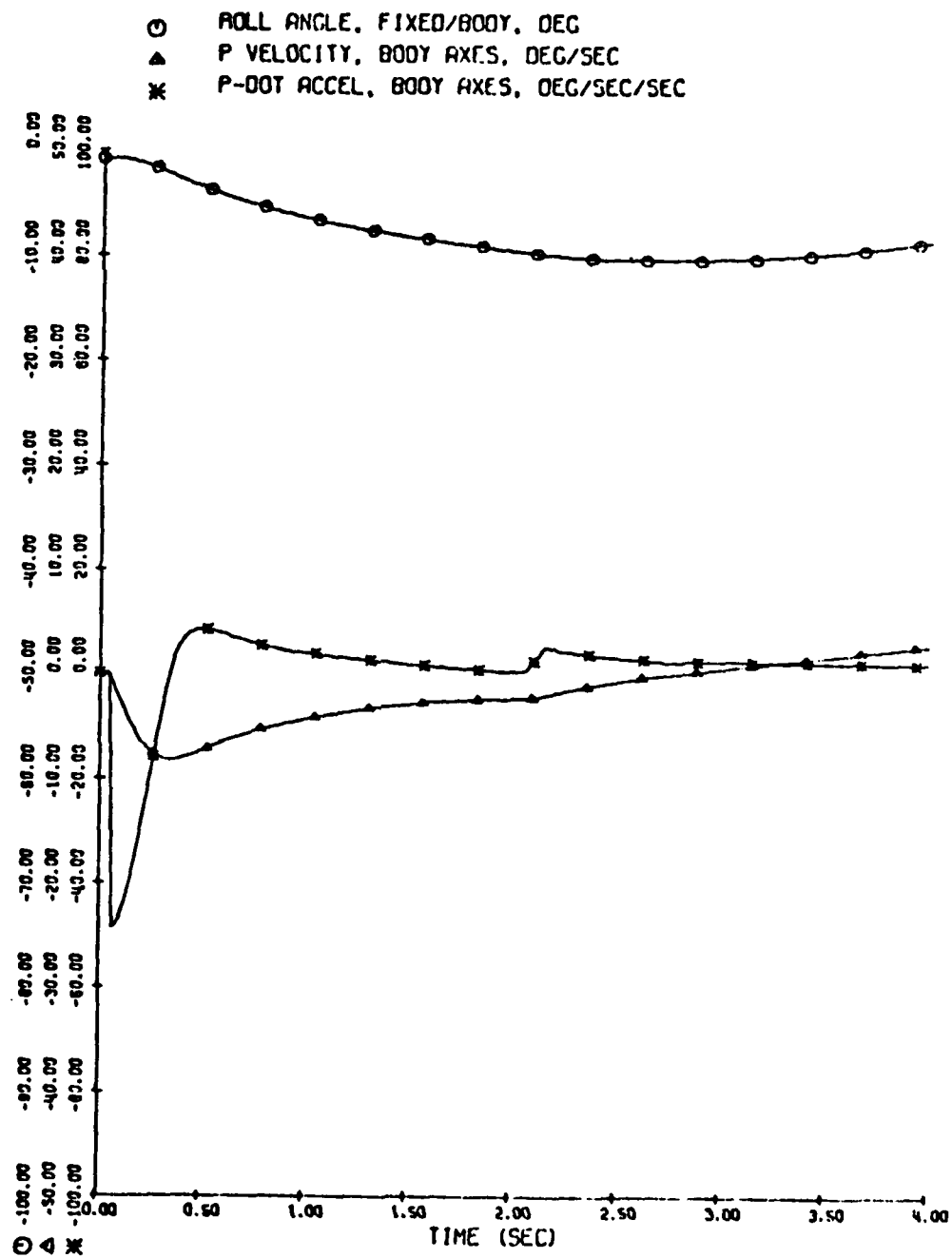


Figure 39. Continued.

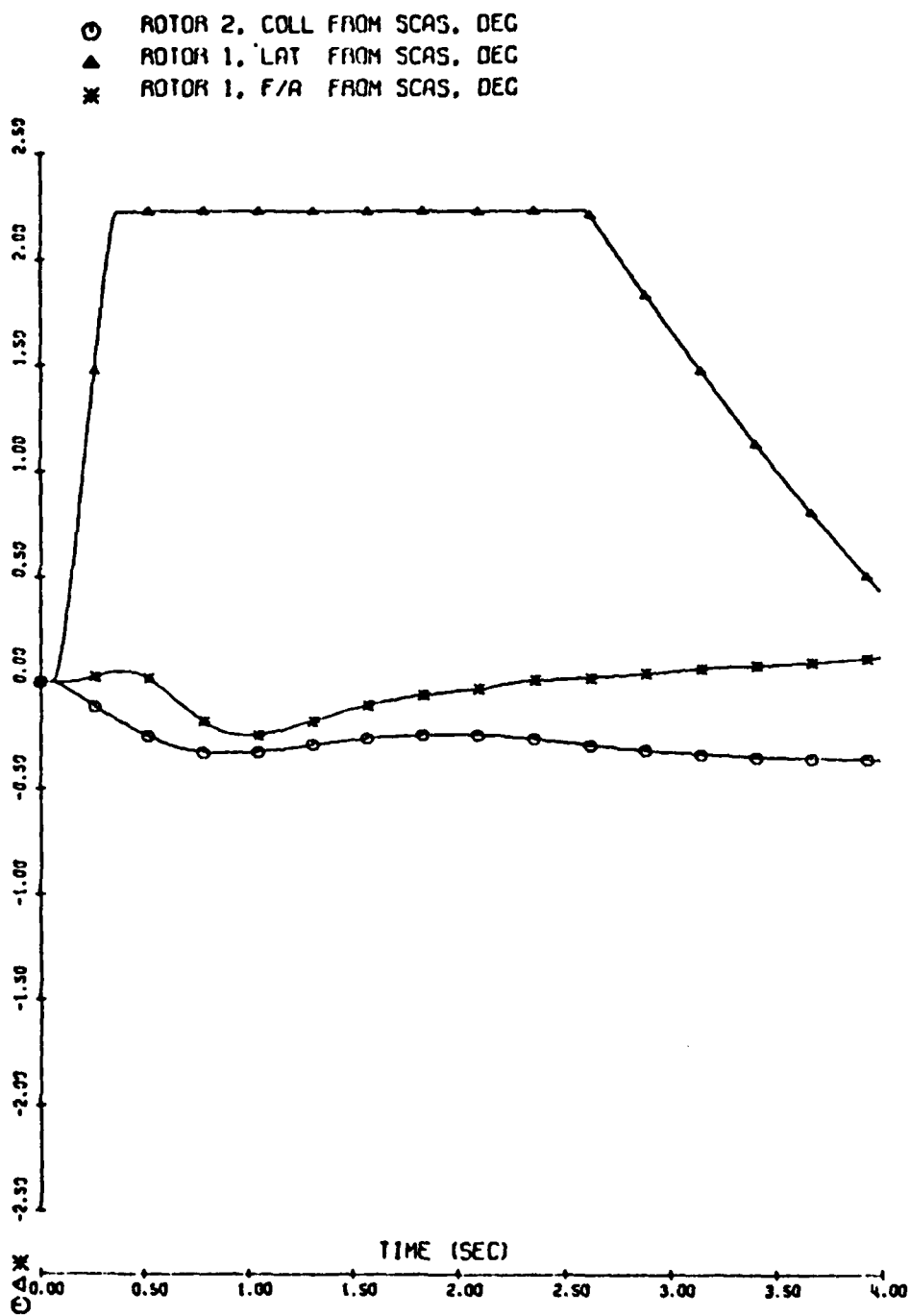


Figure 39. Concluded.

slow and long compared to pilot capability. Even though the lateral SCAS actuator saturates at 12.5 percent of lateral cyclic range within about 0.3 second, the simulation shows that SCAS can make a potentially dangerous asymmetric store drop into a relatively mild maneuver.

7. AUXILIARY PROPULSION (JETS) MATHEMATICAL MODEL

It is frequently desirable to simulate a force acting in a specific direction and at a specific point with respect to the airframe. To this end, C81 includes a very simple model for auxiliary propulsion in what is referred to as the Jet, or Jet Thrust, Group. The model is strictly a force vector acting at a point and is not in any way a mathematical model of a turbojet engine. At this time, use of turbojets for propulsion is limited to a very few research aircraft and configurations in preliminary design. Hence, the complexity of including a complete engine model for the very few cases where it is needed is not considered justifiable.

The Jet Group model currently incorporated into C81 provides for one or two jet thrusts, or, more precisely, force vectors. Inputs to the model include the point of application of the first jet; the Euler angle rotations from body axis to that vector; the magnitudes of the first and the second jets; and a logic switch to specify which jets can and cannot be controlled by the control linkages between the flight controls and jet thrust.

In the User's Guide, the first jet is defined as the right jet and the second as the left jet. However, this distribution of left and right is for input/output convenience only. The definitions define the two jets to be symmetrical in position and orientation with respect to the body X-Z plane passing through buttline zero, regardless of the signs of the buttline and the yaw angle of the first jet.

Jet thrust is controllable in TRIM and MANEUVER with the linkages discussed in Section 8. If the number of controlled jets equals one, only the first, or right, thrust vector is controlled and the second, or left, jet remains locked at its input value. If the number of controlled jets equals two, both the first and second jets are controlled. In maneuver, jet thrusts may be changed independently of the control linkages.

When both Euler angle rotations from body axis to the thrust vector are zero, the jet thrust is a positive X-force in body axis (i.e., a propulsive force). The jet thrust can be used to simulate a drag force by inputting a negative jet thrust with zero rotation angles or by inputting 180 degrees for one of the rotations (zero for the other) and a positive jet thrust.

8. CONTROL SYSTEM MATHEMATICAL MODEL

8.1 PRIMARY FLIGHT CONTROL SYSTEM REPRESENTATION

The mathematical model of the primary flight control system was developed to provide for simulation of all major rotor configurations: single main rotor, tandem, coaxial, and side-by-side (or tilt rotor). Considering the generality of the model and options within it, quite complex control systems can be represented when the model is applied to a specific configuration. These include:

- (1) Nonlinear linkages between the primary flight controls and the swashplate angles
- (2) Coupling of the swashplate angles to control angles and mast tilt
- (3) Coupling of main rotor collective pitch to load factor (g-level), i.e., a collective bobweight
- (4) Coupling of swashplate angles to pylon position
- (5) Pitch-flap coupling (δ_3 angles) and control phasing in the linkages between the swashplate and the blades
- (6) Nonlinear linkages between any or all primary flight controls and the incidence or control surface deflection of any or all aerodynamic surfaces
- (7) Linkages between the primary flight controls and jet thrust

The basic independent variables, or controlling elements, in the model are:

- (1) Collective stick position
- (2) F/A cyclic stick position
- (3) Lateral cyclic stick position
- (4) Pedal position
- (5) F/A mast tilt angle of the main rotor (Rotor 1)

In addition to the control riggings, the model also uses the following configuration-dependent inputs:

- (1) Stability and Control Augmentation System (SCAS) inputs
- (2) F/A and lateral pylon deflection angles of each rotor
- (3) Increment to collective pitch due to the collective bobweight (g-level)
- (4) Swashplate phasing angle and pitch-flap coupling
- (5) Blade motion as a function of blade azimuth
- (6) Pitch-cone coupling
- (7) Swashplate angle to feathering angle ratio

The dependent variables, or controlled elements, are then:

- (1) Blade pitch angle at the theoretical root of each rotor as a function of blade azimuth
- (2) Change in incidence or control surface deflection angle of the wing and each of the four stabilizing surfaces
- (3) Change in magnitude of the jet thrust vector

The blade pitch angles at the root computed by the control system model represent the geometric angles for a rigid blade at the centerline of the mast.

The local blade pitch angle, i.e., the angle at the outboard end of each of the 20 blade segments, is the sum of the root angle and the angle of blade twist between the root and the blade radial station of interest. This angle of blade twist is the sum of the twist built into the blade plus the change in twist resulting from blade flexibility when the aeroelastic rotor option is used. The local inflow angle is subtracted from the local blade pitch angle to give the local angle of attack used in the rotor aerodynamic computations.

The change in aerodynamic surface angle is added to the input value of incidence or control surface deflection angle of the corresponding surface. The change in the magnitude of the jet thrust vector is added to its input magnitude.

Figures 40 and 41 are schematic diagrams of the mathematical models of the Primary Flight Control System. With appropriate inputs to the programmed model, the various features of the model can be bypassed or locked out. For example, consider a

single-main-rotor helicopter with no nonlinear rigging, no mast tilt coupling, no rotor control coupling, no collective bobweight, no SCAS, no jet thrust, no pitch-flap coupling or swashplate phasing, a rigid pylon, rigid blades, and fixed aerodynamic surfaces. Then, the control system can be represented by the simple schematic in Figure 42. In this example, the collective stick is linked only to the collective pitch of the main rotor, the F/A cyclic stick only to the main rotor F/A cyclic pitch, the lateral cyclic stick only to the main rotor lateral cyclic pitch, and the pedals only to the tail rotor collective pitch. This simple control system is typical of the system definitions that are available in the very early preliminary design stage of a helicopter. As a new configuration becomes better defined, inputs for other features of the mathematical model can be added as required.

The current control system representation assumes that the system and the airframe are rigid between the pilot controls and the rotor pylon. Hence, uncommanded control inputs that result from flexing of the airframe are neglected. Recommended future improvements to C81 include development of models for an aeroelastic fuselage and elastic control system. The following two sections discuss the development of the rotor and nonrotor subsystems of the flight control system.

8.1.1 Rotor Controls Subsystem

The rotor controls subsystem uses the position of the collective and cyclic sticks, pedals, and the F/A mast tilt of the main rotor to compute the root geometric blade angle of each rotor in its respective rotating system. In the rotating system, the collective and cyclic pitch angles of a nonrotating system reduce to a single blade angle at the root, which is a function of control system geometry and blade azimuth.

Positive motions of the flight controls are defined as up collective, forward F/A cyclic, right lateral cyclic, and left pedal. In flight test, a standard definition of positive control motions is the motion required to execute a climbing righthand turn, i.e., up collective, aft F/A stick, right lateral stick, and right pedal. Hence, the C81 and flight test definitions of positive F/A stick and pedal are opposite. The C81 sign convention has not been changed to correspond to the flight test convention since the flight test convention for F/A stick is not universal and the compatibility of control motion and angular definitions can aid the programmer and user of C81 in assuring that the programmed control linkages produce the desired system characteristics.

The rotor controls subsystem was originally developed for a linear, uncoupled, single-main-rotor helicopter. In this early

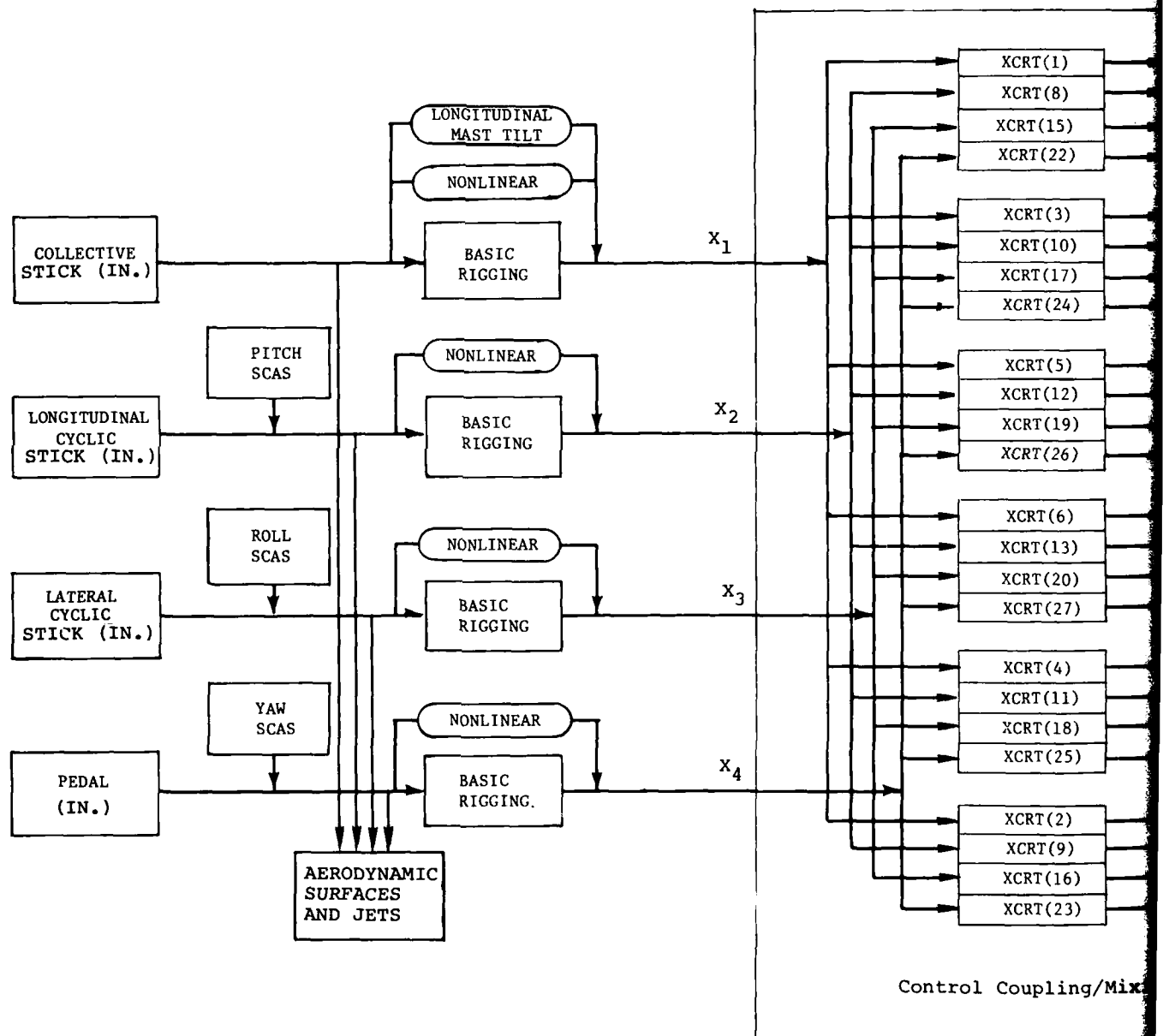


Figure 40. Schematic Diagram of Flight Control System.

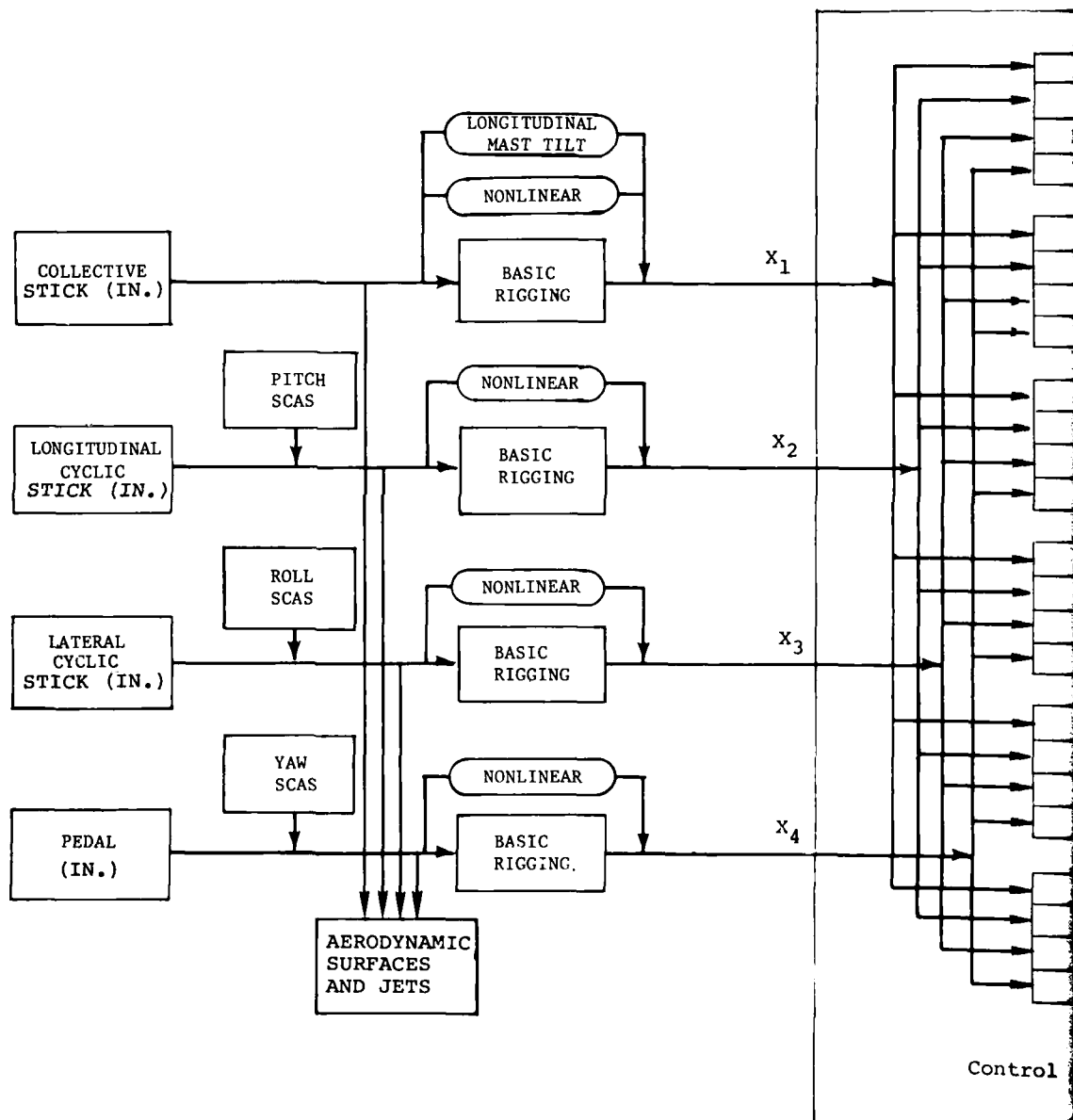
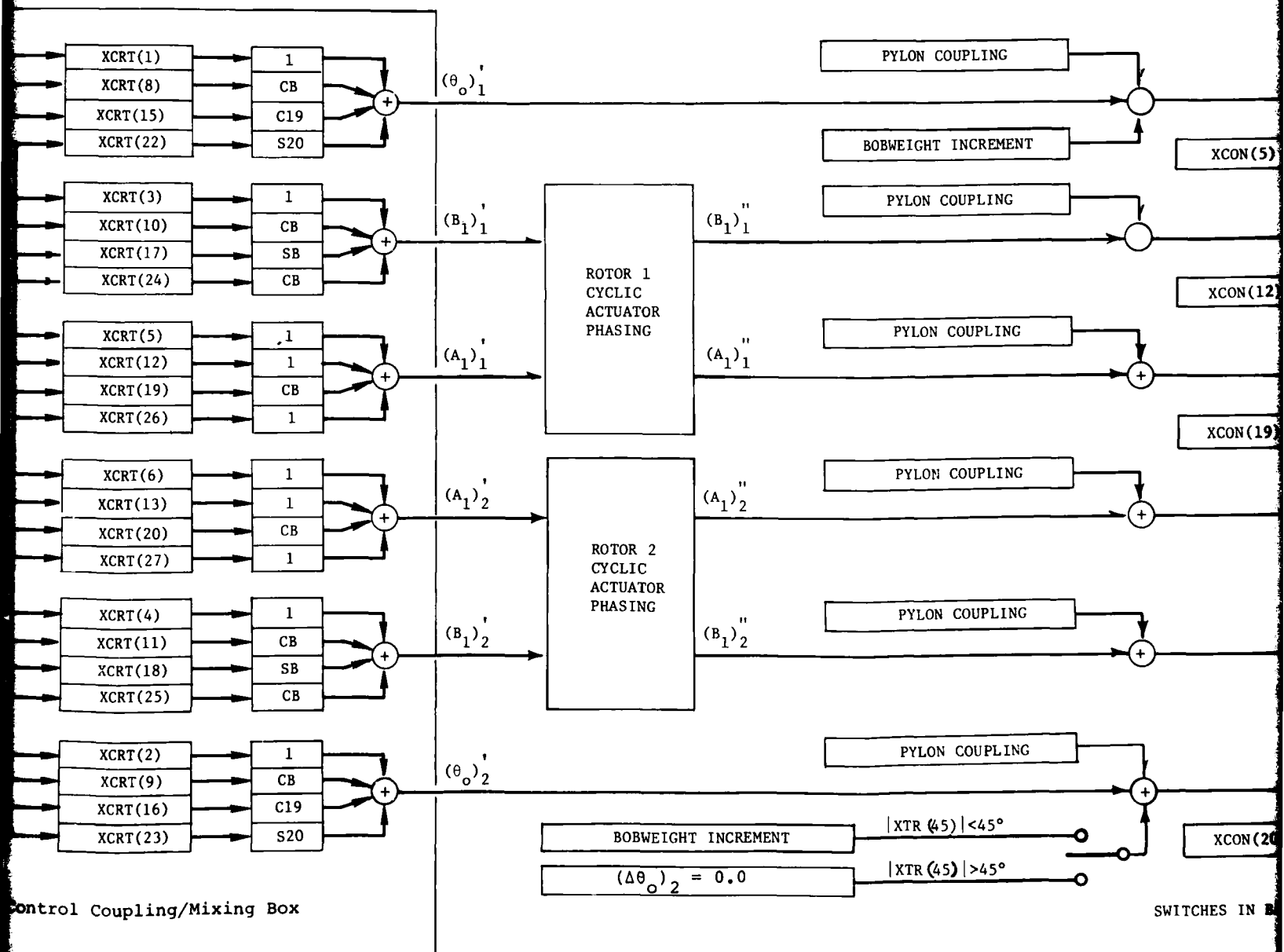
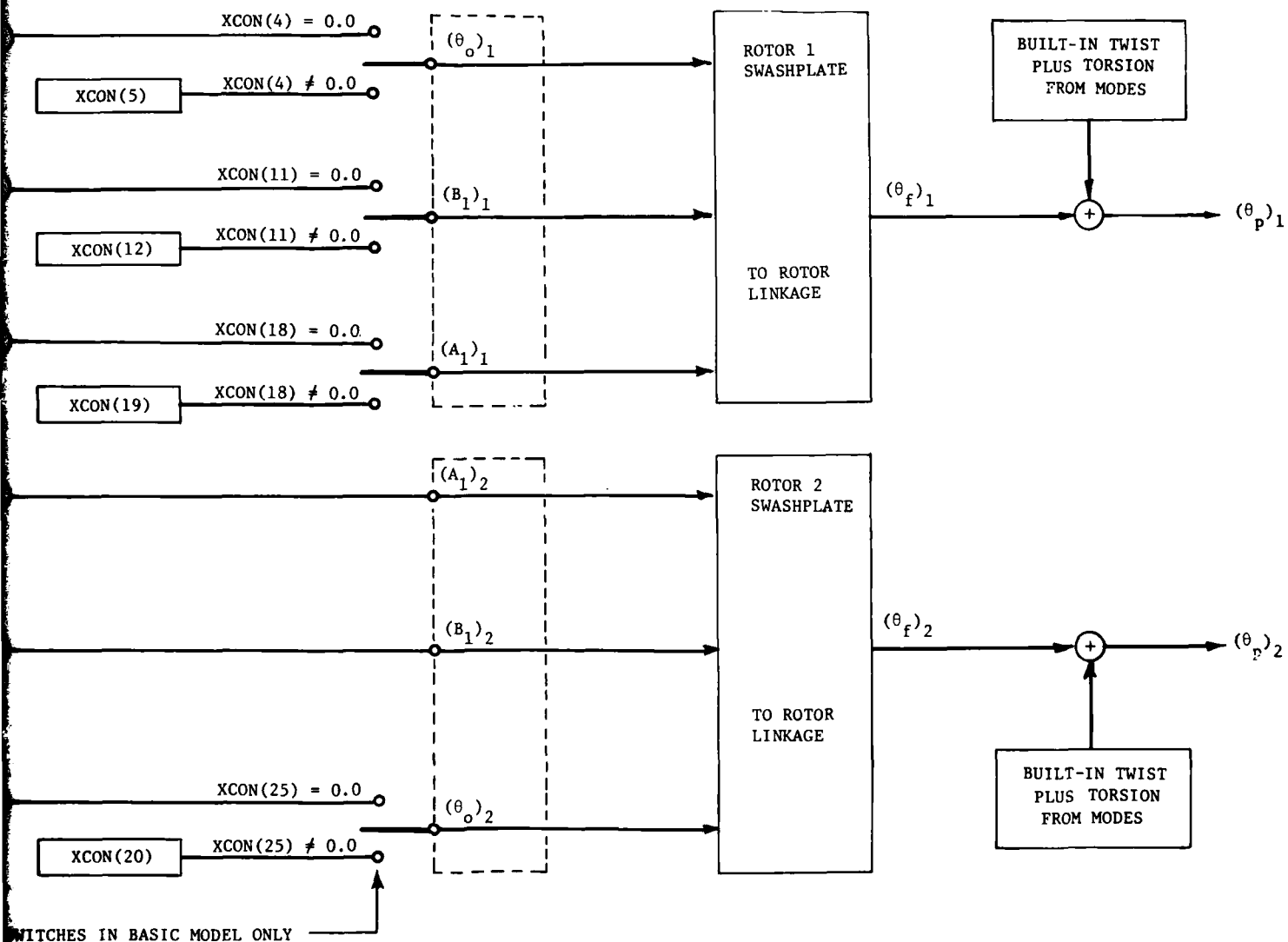


Figure 40. Schematic Diagram of Flight Control System.





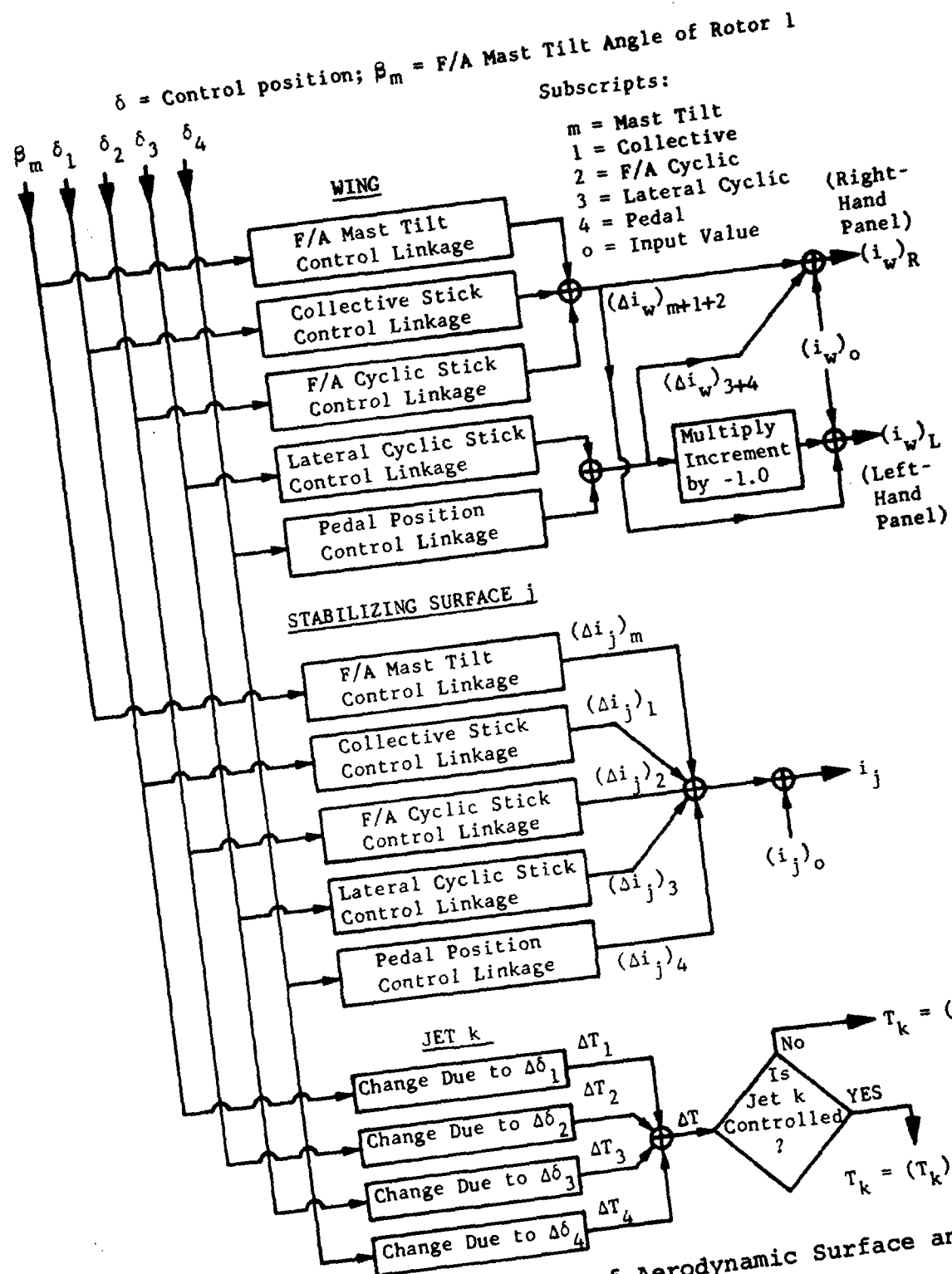


Figure 41. Schematic Diagram of Aerodynamic Surface and Jet Control Systems.

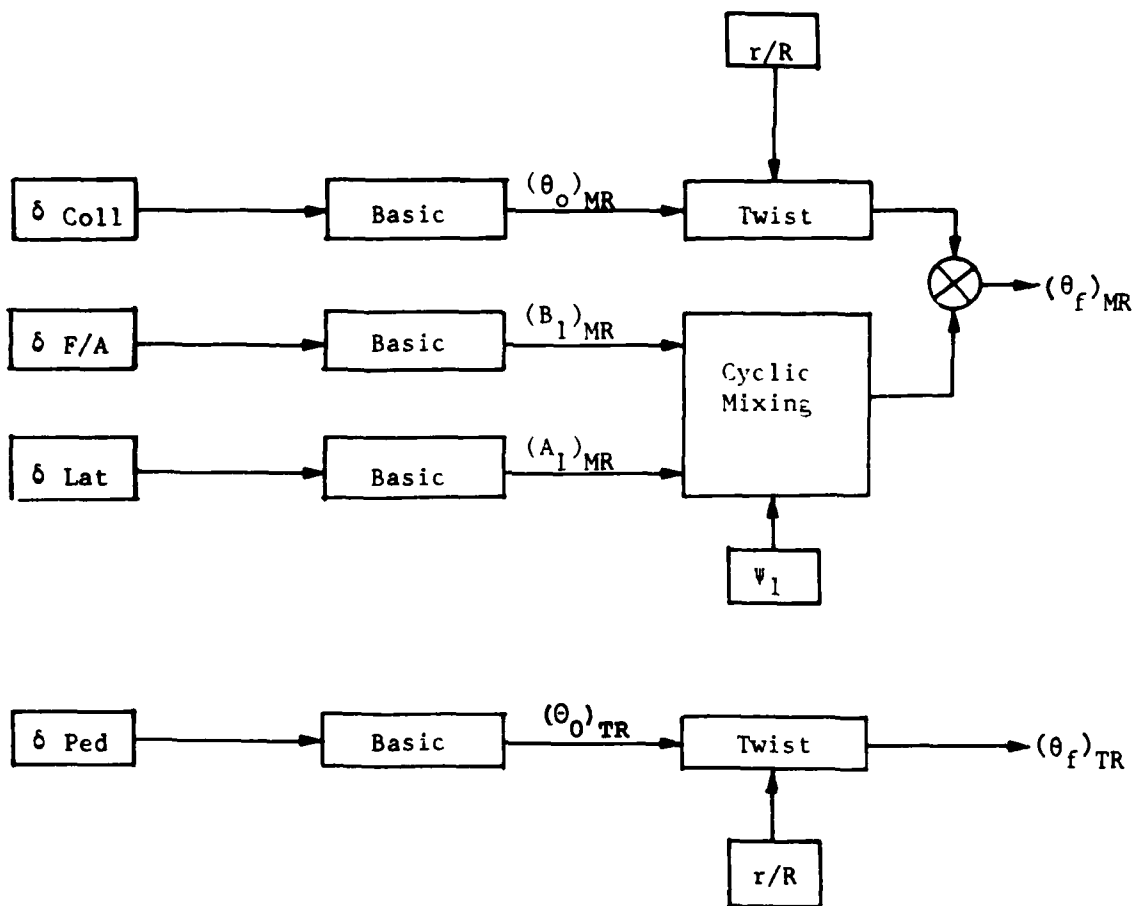


Figure 42. Control System Schematic for Simple Single-Main-Rotor Helicopter.

model, the collective stick controlled only the main rotor collective pitch, the F/A cyclic stick only the main rotor F/A cyclic, the lateral cyclic stick only the main rotor lateral cyclic, and the pedals only the tail rotor collective pitch. The linkages were defined by the value of an angle with its appropriate control at 0 percent and the range of the angle as the control was moved from 0 to 100 percent.

Subsequently, the representation was expanded to model rotor control systems of all major rotorcraft configurations. The linkages discussed above were then redefined to first compute intermediate control angles rather than collective pitch and swashplate angles specifically. Provisions were added so that these intermediate control angles could be modeled as parabolic or cubic functions of the control positions in order that the nonlinearities associated with control-tube bellcrank systems could be simulated. Also, the range and minimum value of the intermediate collective control angles were made functions of the F/A mast tilt angle of Rotor 1 to simulate the change in collective rigging needed for tilt rotor configurations during conversion.

The intermediate control angles are input to a mathematical model of a control coupling, or mixing box. This mixing box provides for linearly linking each control angle to one, or more, of the three nonrotating control angles of each rotor as indicated in Figure 40 and in Figure 43. The output of the coupling model is then six angles: the root collective pitch and the F/A and lateral cyclic swashplate angles for each rotor.

These values of collective pitch are then incremented by the output of the collective bobweight model. The bobweight is a simple spring-mass-damper system and is assumed to be mounted parallel to the body vertical, or Z, axis so that the body axis load factor (g-level) acts as the forcing function of the bobweight. The model includes a preload feature which sets the forcing function to zero at g-levels less than the value of preload. At g-levels above the preload, the forcing function equals the bobweight mass times the current g-level minus the preload. The increment added to the preliminary value of collective pitch is then proportional to the bobweight displacement. If the bobweight model is used, the increment is always added to the main rotor collective pitch; however, it is added to the collective pitch of the other rotor only if the lateral mast tilt angle of Rotor 2 is less than 45 degrees.

The six control angles, with collective modified by the bobweight input, are then modified further by the coupling of these angles to pylon angular displacements. Each rotor pylon is independent of the other pylon. Hence, increments to each

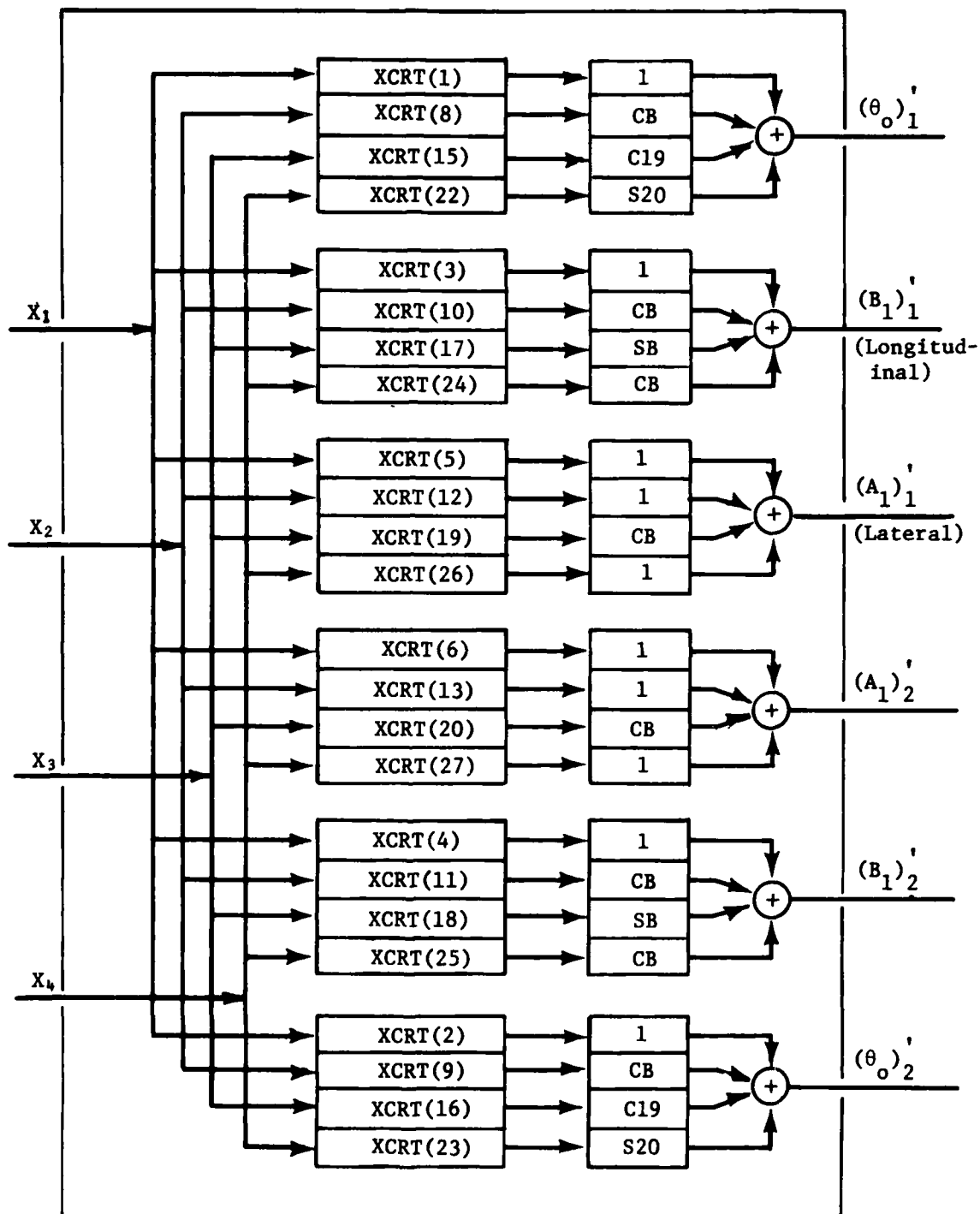


Figure 43. Schematic Diagram of Control Coupling/Mixing Box.

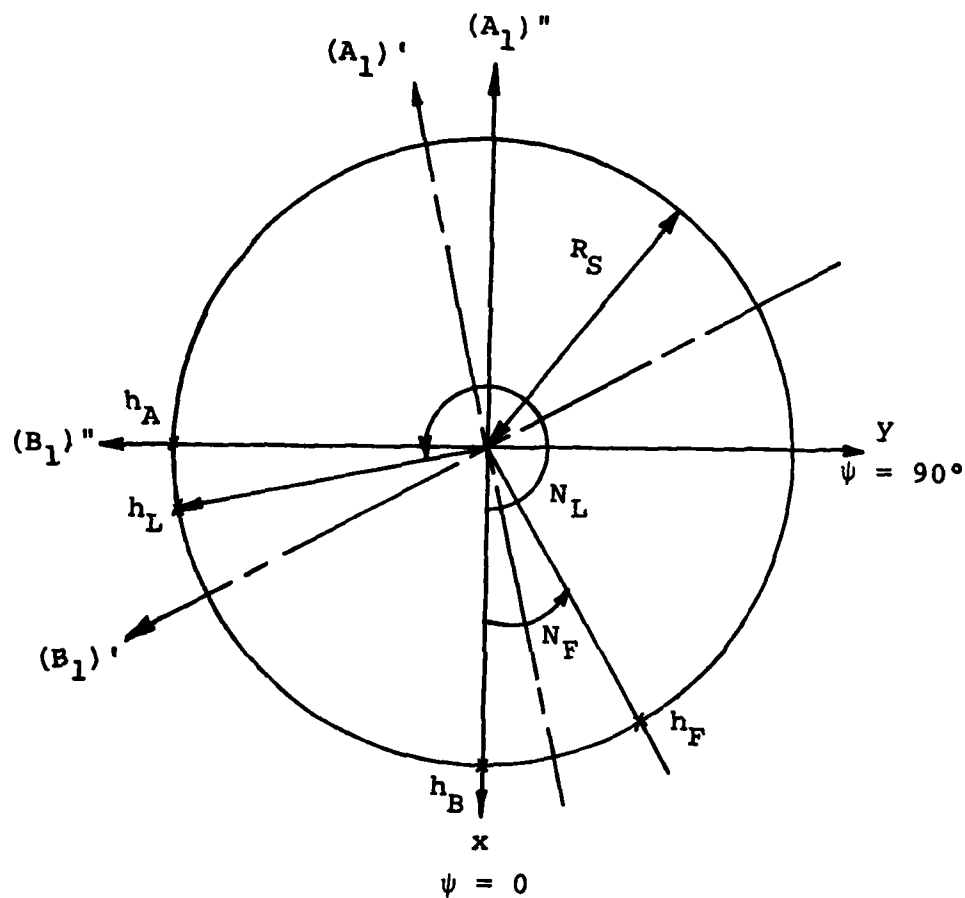
of the six preliminary angles are computed for each degree of freedom of their respective rotor. The increments are added to the appropriate angle, with the resulting six angles being the conventional collective pitch and cyclic swashplate angles.

The next step in the model is to compute the blade angle in the rotating system for each rotor from the swashplate angles and collective pitch angle. The collective pitch angle output from the pylon model is the pitch angle of the blade at its theoretical root (shaft centerline). The angle is measured with respect to the plane perpendicular to the shaft and assumes that both F/A and lateral cyclic pitch angles are zero. In the rotating systems this root collective pitch angle becomes the mean value of blade root pitch angle and is independent of blade azimuth angle. This means blade angle is then corrected at each blade radial station for the geometric and elastic twist of the blade.

A relatively simple model, which includes several small angle assumptions, is used to compute the blade feathering angle in the rotating system as a function of the swashplate tilt angles in the nonrotating system. The design and construction of most swashplate systems cause many inherent nonlinearities. These nonlinearities result primarily from the motion of the pivot points or attach points used to convert linear motion to angular motion or vice versa. To model these nonlinearities would require a very detailed geometric description of the swashplate and feathering systems. Some of the necessary parameters would be location of the pitch link attach point on the swashplate, length of the pitch link, description of any walking beams used in the system, location of the pitch link attach point on the pitch horn (blade), displacement of the pitch link attach point due to blade aeroelasticity, etc. To date, the inclusion of such a sophisticated and complex model has not been warranted because of certain small angle and rigid body assumptions in other related parts of the program and the variety of systems in use. However, as these assumptions are removed, the development of improved swashplate/feathering models becomes increasingly important. The development of such models is included in the future improvements recommended for C81.

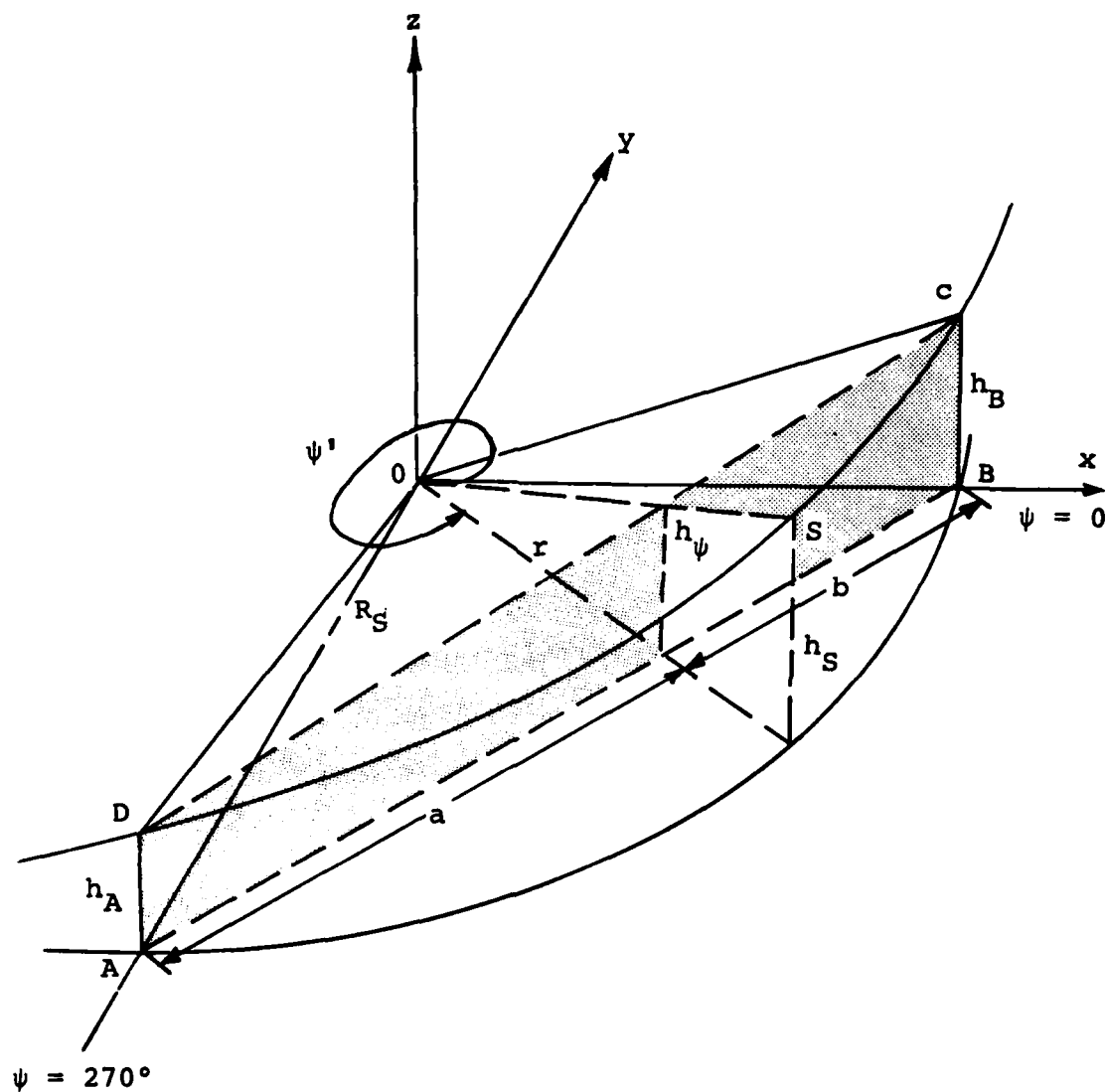
8.1.1.1 Swashplate and Blade Feathering Model

In the current swashplate/feathering system model, the first step is to determine the angle in the rotating system between an arbitrary point on the swashplate and the plane perpendicular to the mast based on the swashplate tilt angles in the nonrotating system. Figure 44 is a sketch of the swashplate model and geometry used to develop the relationship. The following quantities are defined in Figure 44 (a):



(a) Top View of Swashplate

Figure 44. Model for Swashplate in the Nonrotating System.



(b) Swashplate and Reference Plane

Figure 44. Concluded.

$(A_1)'$ is the angle of tilt for lateral stick input.

h_L is the maximum vertical displacement due to lateral stick occurring at azimuth N_L (default 270°).

$(B_1)'$ is the angle of tilt for longitudinal cyclic input. h_F is the maximum vertical displacement due to longitudinal stick occurring at azimuth N_F (default 0°).

Considering that the swashplate is normally moved by forcing vertical motion at the outside rather than by a tilting motion, trigonometric functions of the swashplate angles are unimportant. Rather, the height of a given point above some reference plane is of interest.

$$h_F = R_S (B_1)' \quad (275)$$

$$h_L = R_S (A_1)' \quad (276)$$

If

h_A = the swashplate vertical displacement at $\psi' = 270^\circ$

and

h_B = the swashplate vertical displacement at $\psi' = 0^\circ$

It can be determined from Figure 44(b) that

$$h_A = h_L \cos(N_L - 270^\circ) - h_F \sin N_F = (A_1)'' R_S \quad (277)$$

$$h_B = h_L \sin(N_L - 270^\circ) + h_F \cos N_F = (B_1)'' R_S \quad (278)$$

The quantity of interest is h_S , shown in Figure 44(b).

By proportion

$$\frac{h_S}{h_\psi} = \frac{R_S}{r} \quad (279)$$

Triangle AOB is a 45° right triangle. Therefore

$$a + b = \sqrt{2} R_S \quad (280)$$

From the law of sines

$$\frac{a}{\sin(\Psi' - 270^\circ)} = \frac{R_S}{\sin(405^\circ - \Psi')} = \frac{r}{\sin(45^\circ)} \quad (281)$$

Hence

$$a = \sqrt{2} R_S \cos \Psi' / (-\sin \Psi' + \cos \Psi') \quad (282)$$

$$r = R_S / (-\sin \Psi' + \cos \Psi') \quad (283)$$

The vertical distance from the X-Y plane to the line CD in the ABCD plane is then

$$h_\Psi = \pm(h_B - h_A) / (\sqrt{2} R_S) \pm a + h_A \quad (284)$$

Then h_S may be found by substitution as

$$h_S = h_B \cos \Psi' - h_A \sin \Psi' \quad (285)$$

where h_S is the change in height of the pitch link attachment point on the swashplate caused by cyclic inputs.

Next h_S is used to determine the cyclic blade feathering angle as a function of blade azimuth.

Figure 45 shows a top and side view of a typical swashplate-to-rotor blade linkage. The following assumptions are made for the model:

- (1) The feathering angle is computed at the theoretical blade root (mast centerline).
- (2) The pitch link is very long with respect to the radii, and the control phasing angle, γ , is a small angle; i.e., the pitch link is parallel to the mast for all swashplate and feathering angles.
- (3) The flapping hinge axis is perpendicular to the feathering axis and both axes pass through the mast centerline.
- (4) The swashplate pivots about a point on the mast centerline.
- (5) The swashplate, pitch links, and pitch horns are rigid.

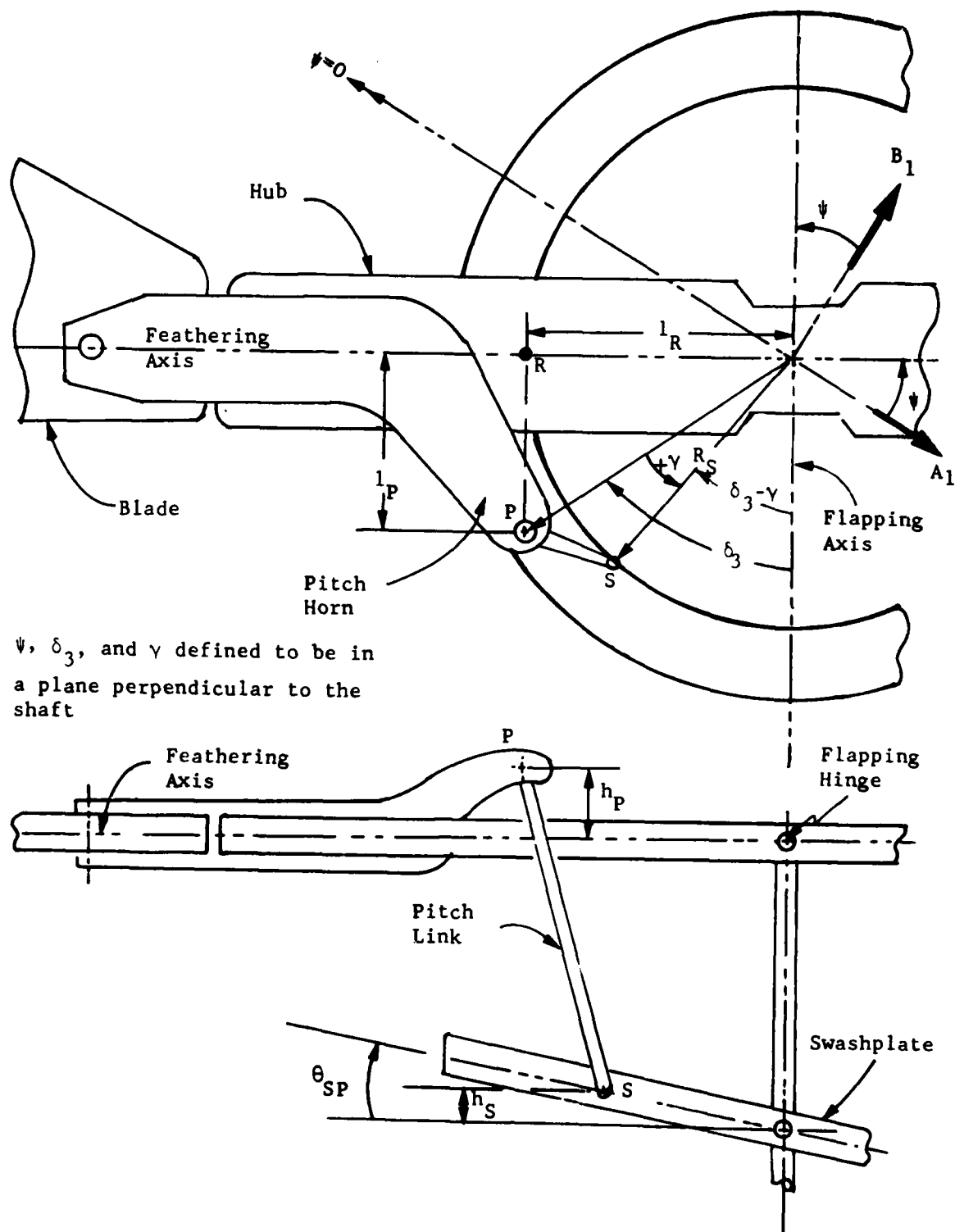


Figure 45. Rotating Control Linkages.

(6) The angles ψ , δ_3 , and γ in Figure 45 are all measured in a plane perpendicular to the mast.

From the above assumptions and the geometry shown in Figures 45 and 46, the equation for the feathering angle is derived as follows:

$$\tan \delta_3 = l_R / l_P \quad (286)$$

$$\sin \beta = h_R / l_R \quad (287)$$

and

$$\sin \theta_f = -(h_R - h_P) / l_P \quad (288)$$

From Equations (286) and (287), the vertical displacement of point R in Figures 45 and 46 is then

$$h_R = \tan \delta_3 \sin \beta l_P \quad (289)$$

and from Equations (288) and (289), the feathering angle is then

$$\sin \theta_f = -\tan \delta_3 \sin \beta + h_P / l_P \quad (290)$$

The displacement h_P , and hence θ_f , are referenced to the azimuth angle of the feathering axis while h_P is referenced to the azimuth angle of point S. Therefore, from the geometry, when the feathering axis is at an azimuth angle of ψ , point S is at an azimuth angle of $\psi + 90 - (\delta_3 - \gamma)$.

Because of the assumptions made about the pitch link geometry

$$h_P(\psi) = h_S(\psi') \quad (291)$$

$$\text{where } \psi' = \psi + 90^\circ \text{ sign } l_P - (\delta_3 - \gamma) \quad (292)$$

$$h_P(\psi) = h_B \cos \psi' - h_A \sin \psi' \quad (293)$$

By substitution from Equations (275) through (278)

$$\begin{aligned} h_P(\psi) = R_S & [(A_1)' \cos N_L + (B_1)' \cos N_F] \cos \psi' \\ & + R_S [(A_1)' \sin N_L + (B_1)' \sin N_F] \sin \psi' \end{aligned} \quad (294)$$

TPP indicates the tip path plane of a rigid blade.

Point P is the attachment point of the pitch link to the pitch horn

NFP indicates the no-feathering plane for a rotor without precone.

β is the flapping angle.

δ_3 is the pitch-flap coupling angle.

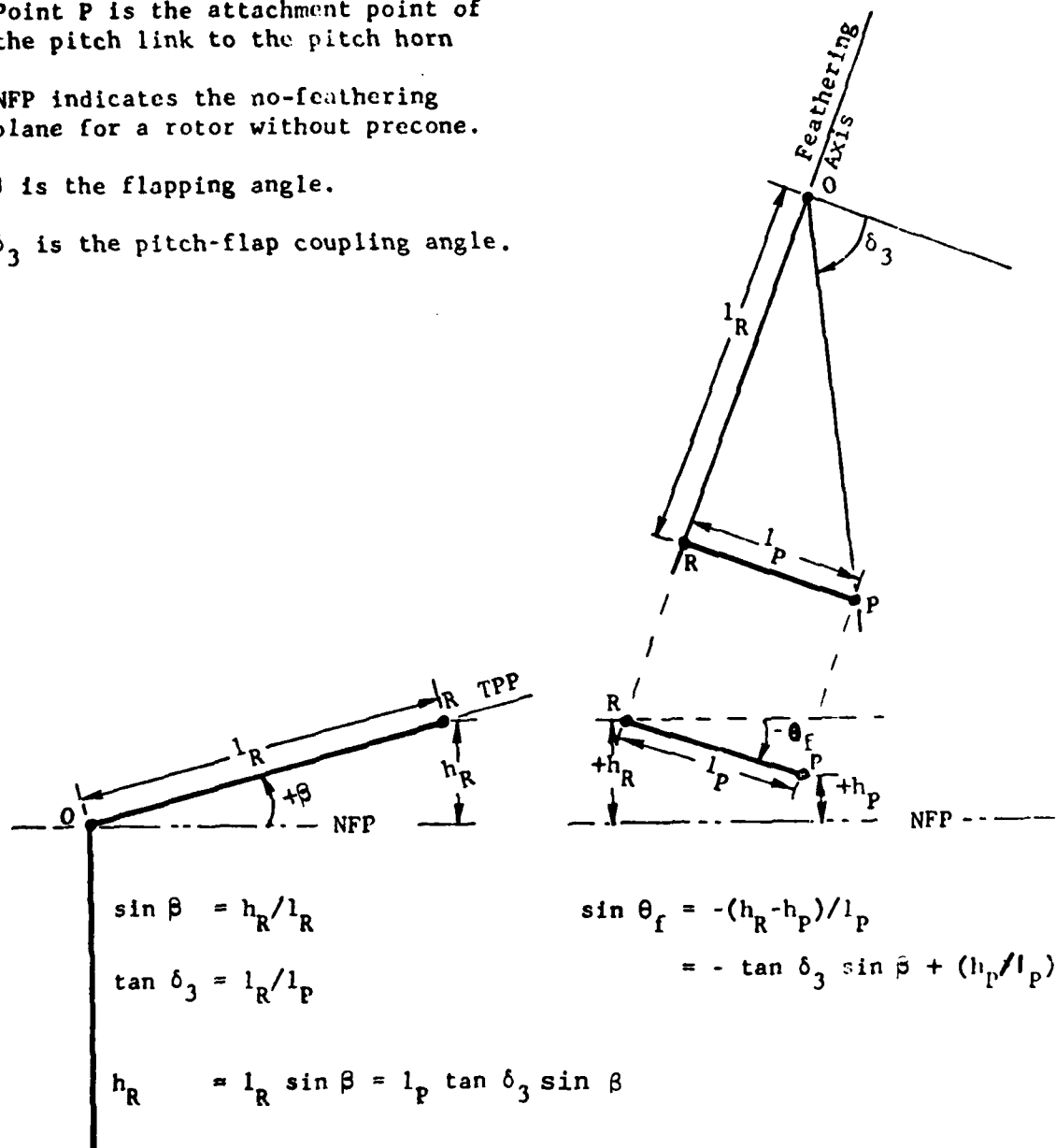


Figure 46. Blade Feathering Angle.

and

$$\begin{aligned} \sin \theta_f = & -\tan \delta_3 \sin \beta + \frac{R_S}{|1_p|} [(A_1)' \cos N_L + (B_1)' \\ & \cos N_F] \cos \psi' \\ & + \frac{R_S}{|1_p|} [(A_1)' \sin N_L + (B_1)' \sin N_F] \sin \psi' \end{aligned} \quad (295)$$

or with a small angle assumption on θ_f

$$\begin{aligned} \theta_f = & -\tan \delta_3 \sin \beta + \frac{R_S}{|1_p|} [(A_1)' \cos N_L + (B_1)' \\ & \cos N_F] \cos \psi' \\ & + \frac{R_S}{|1_p|} [(A_1)' \sin N_L + (B_1)' \sin N_F] \sin \psi' \end{aligned} \quad (296)$$

The ratio $\frac{R_S}{|1_p|}$ is an input to the program for each rotor. Adding the pitch cone coupling, $\Delta\theta_o$, and simplifying yields

$$\begin{aligned} \theta_f = & -\tan \delta_3 \sin \beta + \frac{R_S}{|1_p|} \{ [-B_1'' \cos(\delta_3 - \gamma) - A_1'' \sin(\delta_3 - \gamma)] \sin \psi \\ & + [B_1'' \sin(\delta_3 - \gamma) - A_1'' \cos(\delta_3 - \gamma)] \cos \psi \} + \Delta\theta_o \end{aligned} \quad (297)$$

where

$$A_1'' = -A_1' \sin N_L - B_1' \sin N_F$$

$$B_1'' = A_1' \cos N_L + B_1' \cos N_F$$

and $\Delta\theta_o$ is the result of pitch-cone coupling.

At the default values of $N_L = 270^\circ$ and $N_F = 0^\circ$

$$A_1'' = A_1'$$

$$B_1'' = B_1'$$

also with $\delta_3 = \gamma = \Delta\theta_0 = 0$

$$\theta_f(\psi=0) = -A_1'' = -A_1'$$

$$\theta_f(\psi=90^\circ) = -B_1'' = -B_1'$$

so that Equation (297) yields the expected results.

The two terms $\tan\delta_3 \sin\beta$ and $\Delta\theta_0$ are only used for a rotor with no input rotor modes. Both pitch-flap and pitch-cone coupling are assumed to be included in the rotor mode shapes if they are input. The δ_3 input is used in the control phasing in either case.

8.1.1.2 Pitch-Cone Coupling for Nonelastic Rotor

As stated above the pitch-cone coupling for an elastic rotor is expected to be included in the rotor mode shapes. This capability is provided in program DNAM05. In some cases pitch-cone coupling has a significant effect on stability and controllability as well. Therefore, a simplified model has been developed which requires only one user input, K_{pcc} , the pitch-cone coupling ratio in degrees of collective pitch per degree of coning. In the application of K_{pcc} the assumption is made that the lift moment and centrifugal moment are exactly in balance. This is equivalent to assuming that the rotor has zero beamwise stiffness. This is a reasonable assumption for most rotor systems.

We assume that the lift acts at the 3/4 radius. Then the lift moment is

$$M_L = 0.75R \frac{T}{b} \quad (298)$$

where b is the number of blades, and
 T is the rotor thrust

The centrifugal moment is easily defined

$$M_{CF} = - \int_0^R r \sin \beta_S \Omega^2 r m(r) dr \quad (299)$$

where

$$\beta_S = \beta_0 + \beta_e = \text{steady coning (small angle)}$$

β_o = precone (radians)

β_e = elastic coning which feeds pitch-cone coupling (radians)

$$M_{CF} = -\Omega^2 I_B (\beta_o + \beta_e) \quad (300)$$

where

I_B = flapping inertia for one blade.

Set the sum of the two moment contributions to zero.

$$0.75 \frac{RT}{b} - \Omega^2 I_B (\beta_o - \beta_e) = 0 \quad (301)$$

Then

$$\beta_e = \frac{0.75 RT}{b I_B \Omega^2} - \beta_o \quad (302)$$

The change in rotor collective pitch is then the product of β_e and the input pitch-cone coupling.

$$\Delta \theta_o = K_{pcc} \left[\frac{0.75R}{b I_B} \frac{T}{\Omega^2} - \beta_o \right] \quad (\text{radians}) \quad (303)$$

8.1.1.3 Feathering Derivatives for Unsteady Aerodynamics

In the unsteady aerodynamics equations the first and second time derivatives of θ_f are required. They may be obtained analytically by differentiating θ_f from Equation (297).

For $\ddot{\theta}_f$ and $\dot{\theta}_f$, pitch-cone and pitch-flap coupling are neglected.

$$\begin{aligned} \dot{\theta}_f = \frac{R_S}{I_p} \dot{\psi} & [-B_1'' \cos(\delta_3 - \gamma) - A_1'' \sin(\delta_3 - \gamma)] \cos \psi \\ & - \dot{\psi} [B_1'' \sin(\delta_3 - \gamma) - A_1'' \cos(\delta_3 - \gamma)] \sin \psi \\ & + [-\dot{B}_1'' \cos(\delta_3 - \gamma) - \dot{A}_1'' \sin(\delta_3 - \gamma)] \sin \psi \\ & + [\dot{B}_1'' \sin(\delta_3 - \gamma) - \dot{A}_1'' \cos(\delta_3 - \gamma)] \cos \psi \end{aligned} \quad (304)$$

$$\begin{aligned}
\ddot{\theta}_f = \frac{R_S}{|p|} \left\{ \ddot{\psi} [-B_1'' \cos(\delta_3 - \gamma) - A_1'' \sin(\delta_3 - \gamma)] \cos \psi \right. \\
- \ddot{\psi} [B_1'' \sin(\delta_3 - \gamma) - A_1'' \cos(\delta_3 - \gamma)] \sin \psi - \dot{\psi}^2 [-B_1'' \cos(\delta_3 - \gamma) \\
- A_1'' \sin(\delta_3 - \gamma)] \sin \psi \\
- \dot{\psi}^2 [B_1'' \sin(\delta_3 - \gamma) - A_1'' \cos(\delta_3 - \gamma)] \cos \psi + 2\dot{\psi} [-\dot{B}_1'' \cos(\delta_3 - \gamma) \\
- \dot{A}_1'' \sin(\delta_3 - \gamma)] \cos \psi \\
- 2\dot{\psi} [\dot{B}_1'' \sin(\delta_3 - \gamma) - \dot{A}_1'' \cos(\delta_3 - \gamma)] \sin \psi \\
\left. + [-\ddot{B}_1'' (\cos(\delta_3 - \gamma) - \dot{A}_1'' \sin(\delta_3 - \gamma))] \sin \psi + [\ddot{B}_1'' \sin(\delta_3 - \gamma) \right. \\
\left. - \ddot{A}_1'' \cos(\delta_3 - \gamma)] \cos \psi \right\} \quad (305)
\end{aligned}$$

The last four terms are neglected in C81 since they are not even calculated at this time. Sample calculations have shown that these are second- or third-order terms in any real case.

8.1.2 Nonrotating Controls Subsystems

8.1.2.1 Aerodynamic Surface Control Subsystems

Early versions of C81 contained very simple and limited linkages between the flight controls and the aerodynamic surfaces (a wing plus one horizontal and one vertical stabilizer). In the earlier model, only the zero lift line incidence was controlled (i.e., the surfaces were all moveable), the linkages were defined to be linear, and the surfaces were assumed to have symmetrical airfoil sections. The collective stick could control only wing incidence; the F/A cyclic stick only horizontal stabilizer incidence; the lateral cyclic only differential wing panel incidence; and the pedals only the vertical stabilizer incidence.

When the representation of the aerodynamic surfaces was expanded to five surfaces, the subsystem for the surface controls was also expanded. As discussed in the section on aerodynamic surfaces, the expansion from three to five surfaces included removing the restriction that the axes of incidence change for the surfaces must lie in a horizontal or vertical plane, and adding a representation for control surface (flap) deflection. Hence, in the expanded control subsystem, the capability of linking flight controls to either zero lift line incidence or flap angle was added.

In view of the infrequency of configurations where both the incidence and flap angle of one surface are variable, the current model restricts a single surface to having either incidence or flap controlled by any or all flight controls. Both angles cannot be linked simultaneously to the flight controls. However, each surface is independent of all others and one surface may have variable incidence while another has variable flap angle, e.g., an all-movable horizontal stabilizer (no elevator) and a fixed vertical stabilizer with a rudder. With the generality of the current aerodynamic surface model, the capability of linking any flight control, plus mast tilt angle for tilt-rotor configurations, to any aerodynamic surface became necessary and was added to the model. The revised linkages between the flight controls and the surfaces were then defined to be linear or parabolic, and provisions for nonlinearities were incorporated as discussed below. In view of the limited use to which mast tilt to surface linkages are put, these linkages were defined to be linear.

Although the incidence and flap angles of one surface cannot be controlled simultaneously by the flight controls, each angle is an input and, during maneuver, each can be changed regardless of which angle, if either, is linked to the flight controls. This model is capable of simulating the aerodynamic surface control systems of virtually any type of rotorcraft.

As noted above, the current model provides for linking each and every flight control to each and every surface. For the wing, a restriction is included so that lateral cyclic stick and pedal motions can cause only differential deflection of the appropriate angle. A control system where lateral and/or pedal inputs result in symmetrical angle changes to the left and right wing panels was considered too remote a possibility for inclusion.

Each linkage between a flight control and an aerodynamic surface includes a breakpoint option. This option was incorporated to help model nonlinear linkages. To use this option, a non-zero value is input for the breakpoint control position. The difference between the actual control position and the absolute value of the breakpoint input is computed. If the signs of this difference and the breakpoint input are the same, an increment to the appropriate angle of the surface is computed using the difference. If the signs are opposite, the increment is defined to be zero. That is, for a positive breakpoint input, the control linkage is only active for control positions greater than the breakpoint; while for a negative breakpoint, the linkage is only active for control positions less than the magnitude of the breakpoint. If the breakpoint input is zero, the 50-percent control position is used to compute the difference, and the linkage is active throughout the entire range

of the control. Figure 47 shows examples of the types of control linkages which may be simulated with this breakpoint option.

8.1.2.2 Auxiliary Propulsion, or Jet, Control Subsystem

Linkages are provided between each flight control and the magnitude of the left and/or right jet thrust vectors. The difference between each control position and the respective input control position is multiplied by the appropriate pounds per inch linkage, and the four values are summed and added to the input thrust values to yield the total jet thrust. See the discussion of the Jet Group mathematical model for additional information (Section 7).

8.2 AUTOMATIC FLIGHT CONTROLS

The Generalized Automatic Control Stability Package is divided into two major headings: Stability and Control Augmentation System (SCAS), and the Maneuver Autopilot (MAP). The SCAS simulation is based on the transfer functions used to design the actual system. In the maneuver portion of the program a series of differential equations is integrated numerically to define the effects of the SCAS. The MAP is an algebraic technique used to simulate the pilot's response to nonstandard flight conditions or to produce desired maneuver profiles, and is described in Section 8.3.

8.2.1 Stability and Control Augmentation

The SCAS can best be described in terms of the block diagram shown in Figure 48. In the diagram, the following definitions are applicable:

B = Pilot control input

B_G = SCAS feedforward added to pilot input to offset feedback

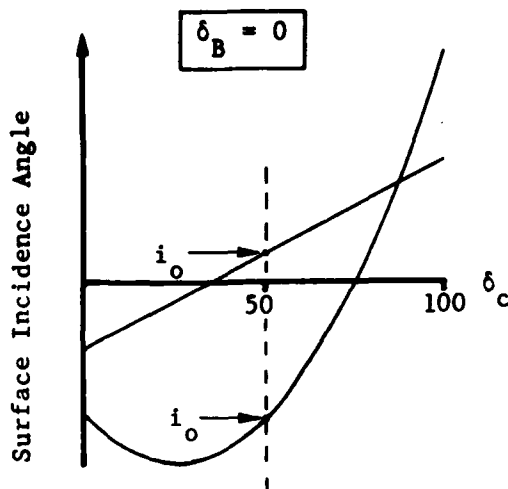
B_H = SCAS feedback dependent on ship's response

$SM = B + B_G - B_H$, total input to the swashplate

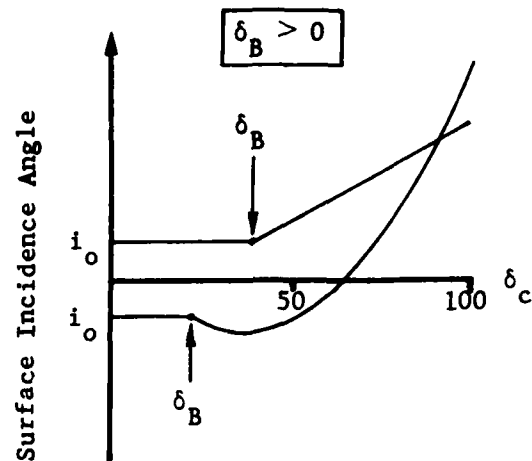
G_P = Feedforward transfer function

H = Feedback transfer function

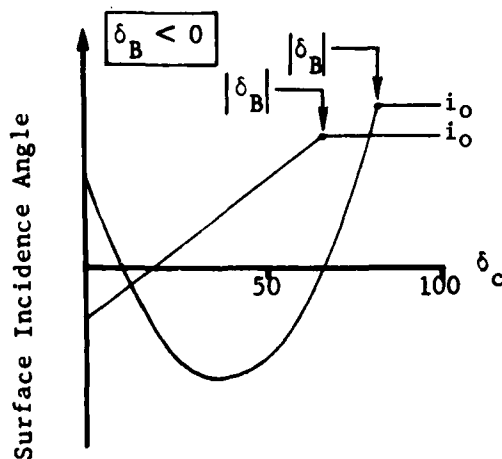
Three independent systems (roll, pitch, and yaw) are simulated in the maneuver. Only the pitch system is described below, but the other channels are based on the same principle. The symbol s is the Laplace transform variable and the τ terms are the time constants associated with the SCAS. All time constants must have nonzero values because of programming considerations.



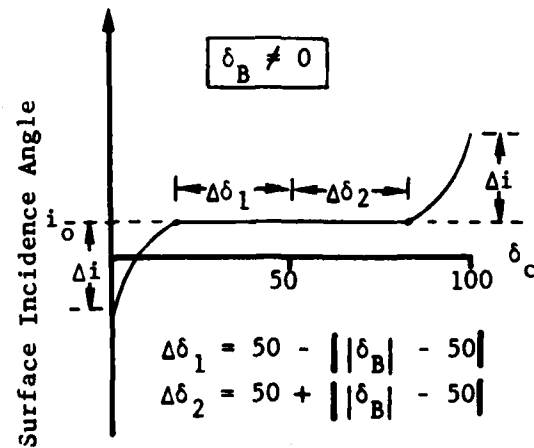
(a) Linear and parabolic linkages, no breakpoint.



(b) Linear and parabolic linkages, positive breakpoint.



(c) Linear and parabolic linkages, negative breakpoint.



(d) Parabolic linkages from pedals or lateral cyclic to wing, non-zero breakpoint.

δ_c = Control position, percent of full throw
 δ_B = Control position for breakpoint, percent
 i_o = Basic (input) incidence angle for surface, degrees

Figure 47. Aerodynamic Surface Control Linkages.

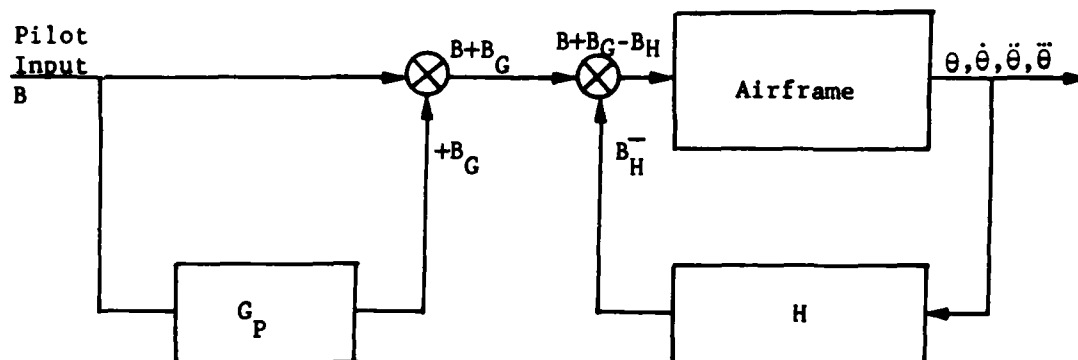


Figure 48. Schematic Diagram of SCAS.

The feedback transfer function has the form

$$H = \frac{K_H s(\tau_1 s + 1)(\tau_2 s + 1)}{(\tau_3 s + 1)(\tau_4 s + 1)(\tau_5 s + 1)} = \frac{B_H}{\theta} \quad (306)$$

The feedforward transfer function has the following form

$$G_P = \frac{K_G s}{(\tau_3 s + 1)(\tau_4 s + 1)(\tau_5 s + 1)} = \frac{B_G}{B} \quad (307)$$

where K_H and K_G are the gains associated with the feedback and feedforward transfer functions, respectively.

In the digital program, Equation (306) is written

$$C_1 B_H + C_2 \ddot{B}_H + C_3 \dot{B}_H + B_H = C_4 \theta + C_5 \ddot{\theta} + K_H \dot{\theta} \quad (308)$$

and Equation (299) is written as

$$C_1 B_G + C_2 \ddot{B}_G + C_3 \dot{B}_G + B_G = K_G \dot{B} \quad (309)$$

where

$$C_1 = \tau_3 \tau_4 \tau_5 \quad (310)$$

$$C_2 = \tau_3 \tau_4 + \tau_4 \tau_5 + \tau_3 \tau_5 \quad (311)$$

$$C_3 = \tau_3 + \tau_4 + \tau_5 \quad (312)$$

$$C_4 = \tau_1 \tau_2 K_H \quad (313)$$

$$C_5 = (\tau_1 + \tau_2) K_H \quad (314)$$

In Equations (308) and (309), all independent variables are known except the third derivative of the angular displacement with respect to time (θ). In the program, $\ddot{\theta}$ is obtained by numerically differentiating $\dot{\theta}$ with respect to time. The maneuver portion of the program has calculated θ , $\dot{\theta}$, $\ddot{\theta}$, and the stick rates B . Using those already calculated values, Equations (308) and (309) are numerically integrated in conjunction with the other differential equations which describe the motion of the rigid fuselage and the elastic rotor.

The basic feedback function, Equation (308), is written with the pitch attitude and its derivatives as the independent variables. Any other variable, and its associated derivatives that are calculated in the maneuver portion of the program, could be substituted as the independent variable with only minor changes to the program.

The maximum authority of the SCAS (in percentages of full range) is an input quantity. The third time derivative of the angular displacements is obtained from the numeric differentiation of the angular acceleration terms. This numeric differentiation can introduce "noise" into the equations of motion. The program is structured so that the product of the derivative of angular acceleration times the appropriate fuselage inertia is set to zero if it is less than the input dead band (ft-lb/sec).

8.3 MANEUVER AUTOPILOT

The second major item in the Generalized Automatic Control Stability Package is the Maneuver Autopilot (MAP). The MAP is an algebraic simulation of the pilot response required to minimize any deviation from the desired flight condition during a maneuver. The user supplies collective, cyclic and pedal gains and two time constants to activate the autopilot, and specifies desired time histories for up to five flightpath variables; roll, pitch or yaw rate, normal load factor, and rate of climb. Control motions are computed using the trim partial derivative matrix, but the control rates are limited by the maximum rate authorities input. In addition, the user may specify the motions of one or more controls, in which case the MAP will operate the remainder. Lastly, a control motion will not be commanded if there is sufficient moment imbalance to negate the rate or displacement discrepancy.

8.3.1 Digital Filter

The higher harmonic content of the \dot{W} signal is removed from the MAP input when an elastic main rotor is being used in the simulation by use of a digital filter. (This filter is also used in the rotor induced velocity calculations - see Section 3.4.2.) A single, three-pole Butterworth filter was chosen for inclusion in C81 as it gave the largest reduction in the higher harmonics with the least lag, and also required the least storage and computer time to operate. The magnitude and time lag of the transfer function are:

$$|H(if)| = \frac{1}{\sqrt{1 + \left(\frac{f}{f_u}\right)^{2N}}} \quad (315a)$$

$$T_d(f) = \frac{\sum_{m=0}^{N-1} \left(\frac{f}{f_u} \right)^{2m} \sin \left\{ (2m+1) \frac{\pi}{2N} \right\}}{2 \pi f_u \left(1 + \left(\frac{f}{f_u} \right)^{2N} \right)} \quad (315b)$$

$$T_d(0) = \frac{1}{2 \pi \sin \left(\frac{\pi}{2N} \right) f_u} \quad (315c)$$

where

f = signal frequency, Hz

f_u = upper break frequency of filter, Hz

N = number of poles of filter (three in C81)

For the three-pole filter programmed in C81, the time lag on the steady state signal (i.e., $f=0$), is

$$T_d(0) = \frac{0.31831}{f_u} \quad (316)$$

These functions for a three-pole filter with a break frequency of 5 Hz are plotted in Figure 49. Note that the time lag has been multiplied by a factor of 10 before being plotted. Assuming a 300 rpm rotor, this filter would pass all the zero frequency data, with a time lag of approximately 0.064 seconds (1/3 of a rotor revolution). 70.7 percent of the 1-per-rev would be passed with a time lag of almost 0.08 seconds (2/5 of a rotor revolution) and only 16 percent of the 2-per-rev would be passed, with a time-lag of about 0.01 seconds (1/20 of a rotor revolution). The user must adjust the break frequency input for the filter to maximize the higher harmonic attenuation while minimizing the low frequency time lag. In addition, the user must choose f_u such that

$$f_u \leq \frac{1}{2\Delta t} \quad (317)$$

where Δt is the maneuver time cut, or the filter will be ineffective.

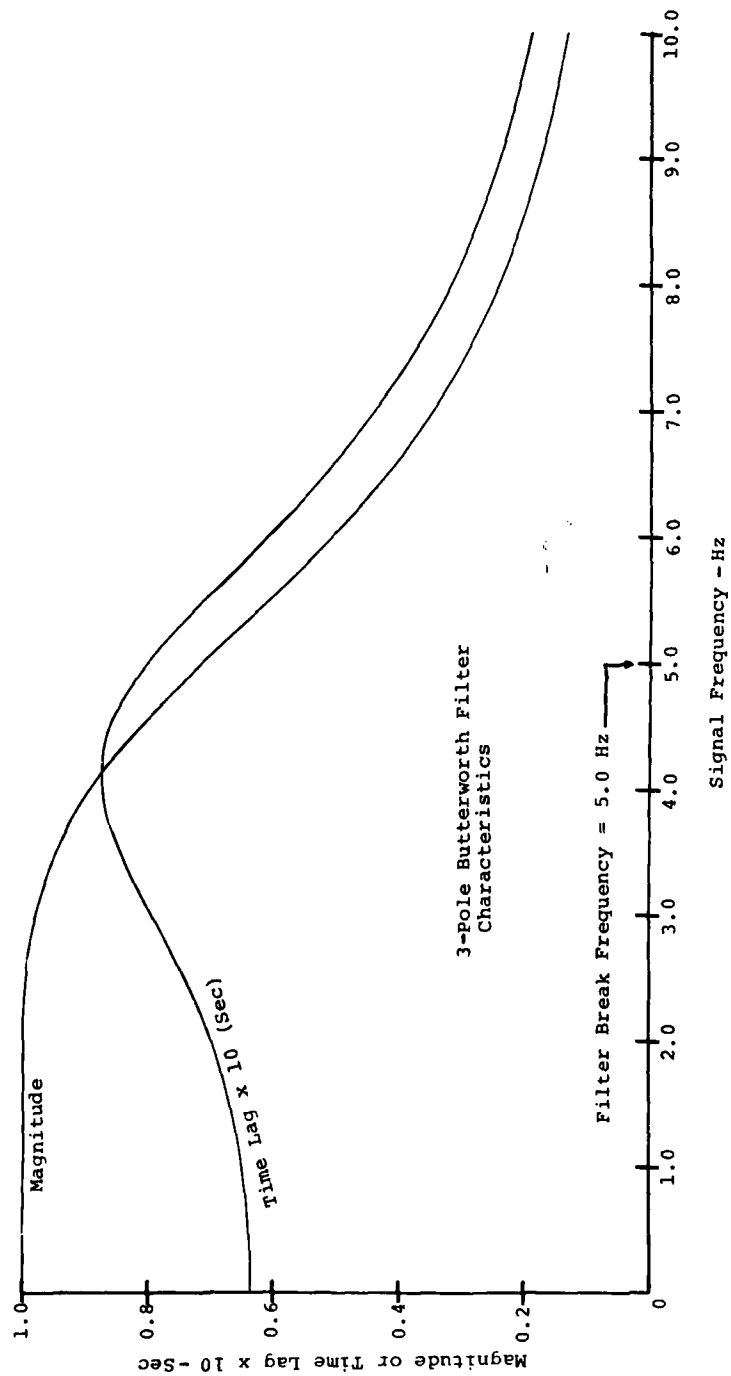


Figure 49. Magnitude and Time Lag Characteristics of a Three-Pole Butterworth Filter with a 5-Hertz Break Frequency.

8.3.2 Automatic Pilot Simulator

The Maneuver Autopilot is divided into four independent channels; roll rate, pitch rate, yaw rate and rate-of-climb. The roll and yaw rate channels are identical. The pitch rate channel is similar and accepts either a pitch rate command or converts the normal load factor command into an equivalent pitch rate command. The rate-of-climb channel is entirely different from the angular rate channels.

The algebraic equations for the autopilot have the four control increments as the independent variables. The appropriate partial derivatives of the airframe forces and moments with respect to the controls, as computed in trim, are the coefficients, and the forces and moments on the right-hand side are those required to eliminate the discrepancies between the actual and desired aircraft response. The equations are

$$\begin{array}{c} \left[\begin{array}{cccc} \frac{\delta L}{\delta \theta_o} & \frac{\delta L}{\delta F/A} & \frac{\delta L}{\delta Lat} & \frac{\delta L}{\delta Ped} \\ \frac{\delta M}{\delta \theta_o} & \frac{\delta M}{\delta F/A} & \frac{\delta M}{\delta Lat} & \frac{\delta M}{\delta Ped} \\ \frac{\delta N}{\delta \theta_o} & \frac{\delta N}{\delta F/A} & \frac{\delta N}{\delta Lat} & \frac{\delta N}{\delta Ped} \\ \frac{\delta Z}{\delta \theta_o} & \frac{\delta Z}{\delta F/A} & \frac{\delta Z}{\delta Lat} & \frac{\delta Z}{\delta Ped} \end{array} \right] \end{array} \begin{array}{c} \left\{ \begin{array}{c} \Delta \text{ Coll} \\ \Delta \text{ Long Cyc} \\ \Delta \text{ Lat Cyc} \\ \Delta \text{ Pedal} \end{array} \right\} = \begin{array}{c} \left\{ \begin{array}{c} \text{ROLL CORR.} \\ \text{PITCH CORR.} \\ \text{YAW CORR.} \\ \text{Z CORR.} \end{array} \right\} = \begin{array}{c} \left\{ \begin{array}{c} -\Delta L \\ -\Delta M \\ -\Delta N \\ -\Delta Z \end{array} \right\} \end{array} \end{array} \quad (318)$$

TRIM

This approach has the capability to eliminate accelerations directly, but cannot deal directly with rates and displacements. Any fuselage rate difference can be expressed as a moment increment by

$$\Delta \text{ Moment} = \frac{\Delta (\text{Angular rate})}{t_1} \times \text{Inertia} \quad (319a)$$

where t_1 is the user-input time to arrest a given angular rate. In like manner, fuselage angular displacements are represented as a moment increment by

$$\Delta \text{ Moment} = \frac{\Delta (\text{Angular displacement})}{t_2^2} \times \text{Inertia} \quad (319b)$$

where t_2 is the user-input time to arrest a given angular displacement. The moment increment due to angular displacement, Equation (319b), is only computed when the absolute value of

the difference between the actual and the desired angle is greater than 0.02 radian and when a desired rate trace has not been input.

At each time step in a maneuver, the desired values of the command signals are computed from the input time histories. If no time history was input for a channel, then the trim value is used as the desired value. Subroutine SUPERP then uses these values to determine the control motions, channel by channel.

8.3.2.1 Roll and Yaw Channel

These two channels are coded identically, but are independent of each other. The roll channel flow chart is given in Figure 50.

The logic first calculates the discrepancy between the current value of roll angle and the trim value, and the difference between the current rate and the trim rate plus the desired rate. It also initially sets the restoring moment required, ΔL , to the negative of the current net rolling moment at the aircraft center of gravity.

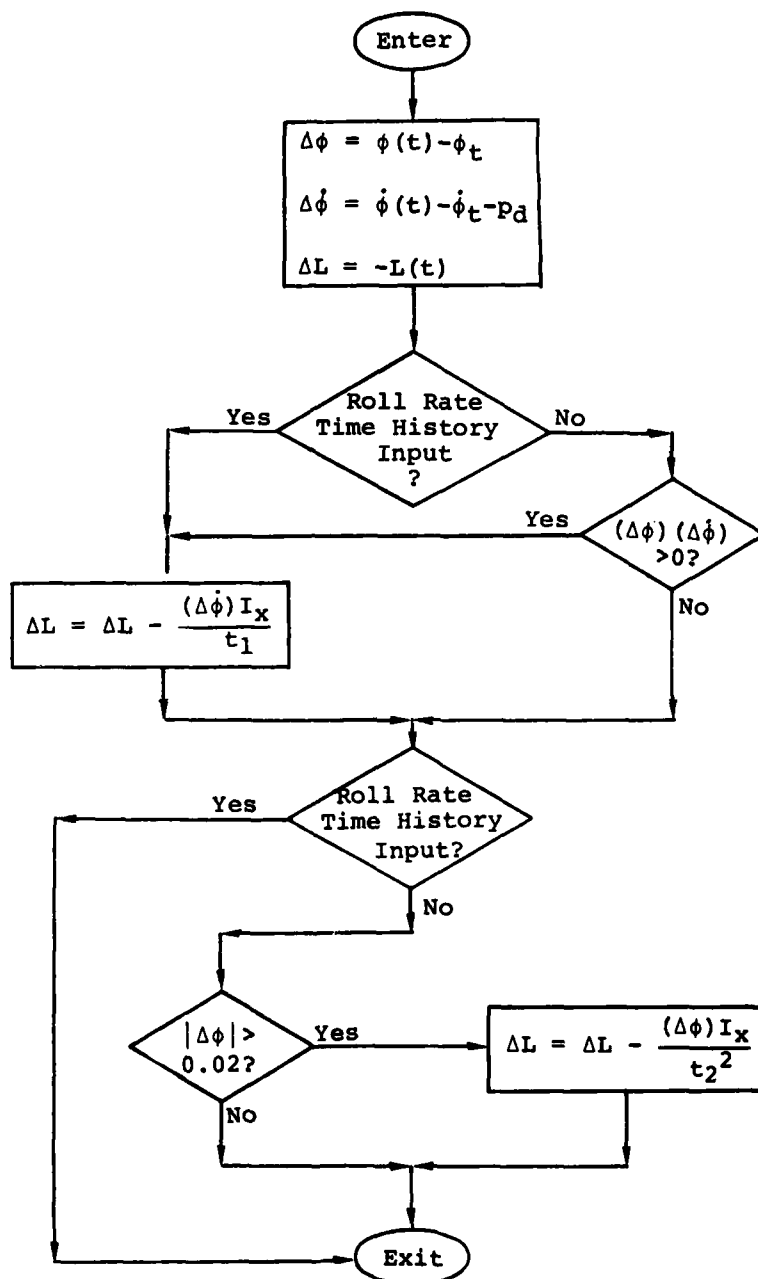
If a roll rate time history was input, then Equation (319a) is used to compute an additional increment to the restoring moment and the logic goes on to the next channel.

If a roll rate time history was not input, but the roll rate discrepancy is tending to increase the absolute value of the roll angle deviation, then Equation (319a) is also used to calculate an increment to the restoring moment.

If no roll time history was input, with the roll rate tending to decrease the roll angle deviation, then only Equation (319b) is used to compute a roll restoring moment increment, but then only if the absolute value of the angular deviation is greater than 0.02 radian.

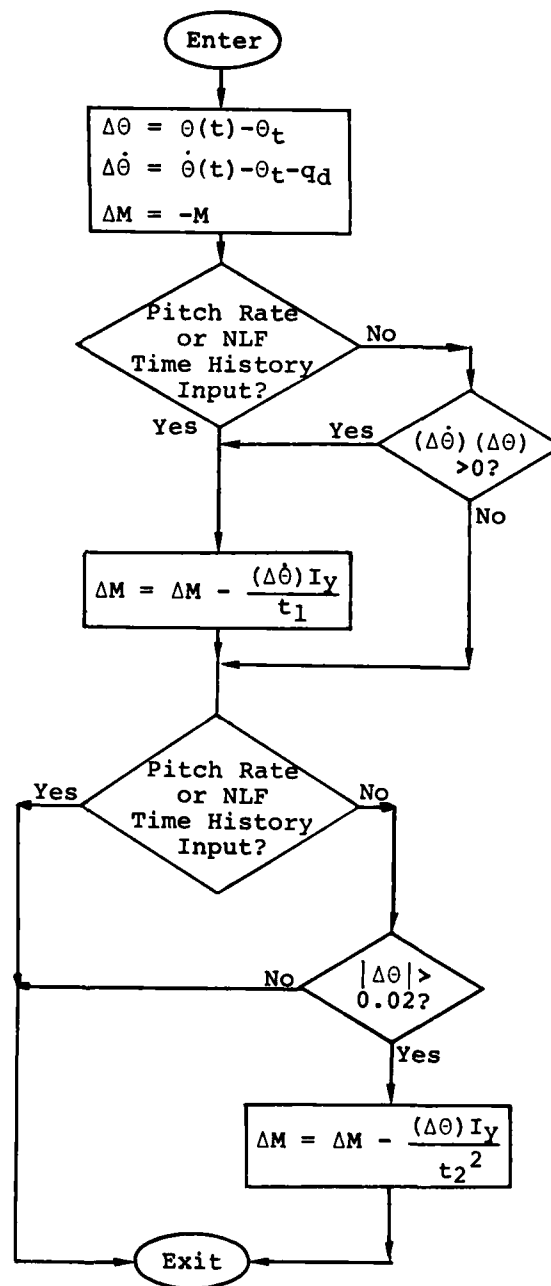
8.3.2.2 Pitch Channel

The pitch channel flow chart is given in Figure 51. It is very similar to the roll and yaw channels except that there are additional logical decisions due to the option of using either the input time history for the pitch rate, q , or of determining the desired pitch rate from the input desired normal load factor time history. If the user inputs both a desired pitch rate and a desired normal load factor time history, the latter supersedes the former.



Subscript t indicates trim value
 Subscript d indicates desired value

Figure 50. Maneuver Autopilot Roll Channel Flow Chart.



Subscript t denotes trim value
Subscript d denotes desired value

Figure 51. Maneuver Autopilot Pitch Channel Flow Chart.

In this case, the desired pitch rate, q_d , is computed as follows:

$$q_d = [(NLF_d - \cos \theta \cos \phi)g + \dot{W}_f + PV]/U \quad (320)$$

in which

NLF_d is the desired normal load factor

\dot{W}_f is the filtered value of \dot{W} , where W is the body-axis vertical velocity

P is the body-axis roll rate

V is the body-axis lateral velocity

U is the body-axis longitudinal velocity

θ is the Euler pitch angle

ϕ is the Euler roll angle

g is the acceleration due to gravity

Using \dot{W}_f instead of \dot{W} reduces the 2-per-rev and b-per-rev oscillations in the control motions experienced with previous versions of C81.

8.3.2.3 Rate-of-Climb Channel

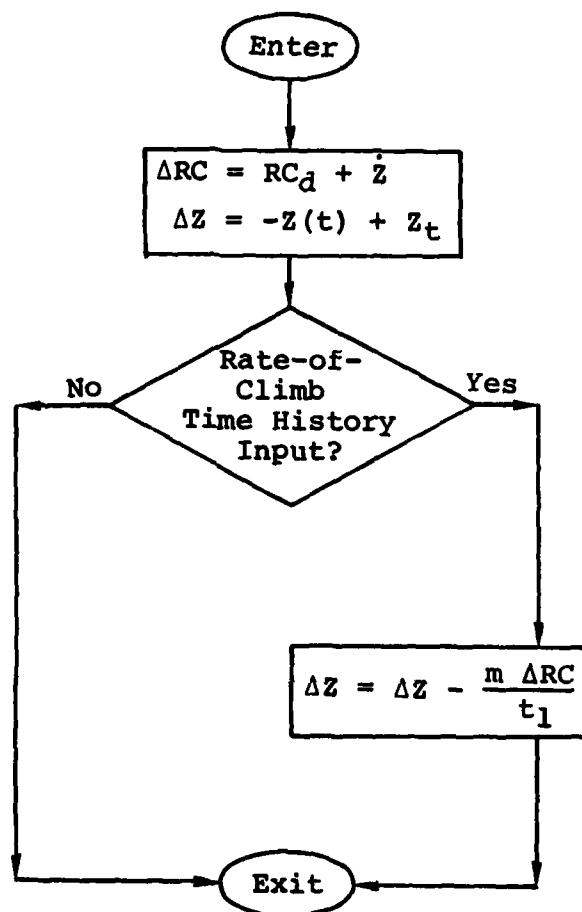
The flow chart for this channel is given in Figure 52. Note that Z is positive down and rate-of-climb is positive up. If a rate-of-climb time history was not input, then the restoring force required to null the body-axis vertical force imbalance is equal to the negative of that imbalance. If a time history was input, then the increment to the restoring force is computed from

$$\Delta Z = m \frac{\Delta RC}{t_1} \quad (321)$$

in which m is the aircraft mass and the quotient is the required change in acceleration.

8.3.2.4 Control Rate and Displacement Limitations

If one of the control motions is prescribed by a user-input time history, then the appropriate row and column are removed from Equation (318), and the order of the problem is reduced by one.



Subscript t denotes trim value
 Subscript d denotes desired value

Figure 52. Maneuver Autopilot Rate-of-Climb Channel Flow Chart.

The control increments resulting from the solution of Equation (318) are converted into control rates by dividing them by the maneuver time step, Δt . If any of the resulting rates are greater than the input allowable values, they are set equal to that value. The control increments are then recomputed by multiplying the rates by the time step, and are added to the current value of the control position. If the resulting control position exceeds the stop, the control is set on the stop; it remains there until the control rate changes sign.

9.0 ENGINE-GOVERNOR

Previous versions of C81 have had a very simple engine model in which the horsepower available was instantaneously equal to the horsepower required, up to a limit equal to 0.91 times the input maximum horsepower available. The factor of 0.91 was used to account for a 9-percent loss due to drive system inefficiency and accessory power. The modified engine-governor model installed in C81 under contract DAAJ02-77-C-0003 uses a small table to compute the maximum horsepower available for the flight condition and introduces a first-order lag in the horsepower-available response during maneuver runs.

9.1 CALCULATION OF MAXIMUM AVAILABLE HORSEPOWER

The program computes and uses the maximum continuous horsepower available, P_{MA_C} , for trim cases, and the maximum takeoff power available, $P_{MA_{TO}}$, for trim-in-maneuver and maneuver runs. The calculation is identical for both cases. The user defines a straight-line approximation of the sea level, installed power-available curves, as shown in Figure 53, by inputting T_1 , T_2 , T_3 , P_1 , P_2 , and P_3 .

The temperature for the flight condition being simulated, T , is determined from the inputs in the Flight Constants Group, and the maximum sea level, installed power available, $P_{MA_{SL}}$, is interpolated from the straight-line curve. If $T \leq T_1$, then $P_{MA_{SL}} = P_1$. Likewise, if $T \geq T_3$, then $P_{MA_{SL}} = P_3$. If the user did not input T_3 or P_3 and $T \geq T_2$, then $P_{MA_{SL}} = P_2$.

The atmospheric pressure ratio, δ , has also been computed from the Flight Constants Group inputs, and the actual maximum engine installed power available is

$$P_{MA} = \delta P_{MA_{SL}} \quad (322)$$

If P_{MA} is greater than the appropriate transmission power limit, P_{TL} , then P_{MA} is set equal to the power limit.

If no table is input for the maximum continuous horsepower calculation, then the maximum continuous transmission horsepower limit is used. The same holds true for the maximum takeoff horsepower calculations.

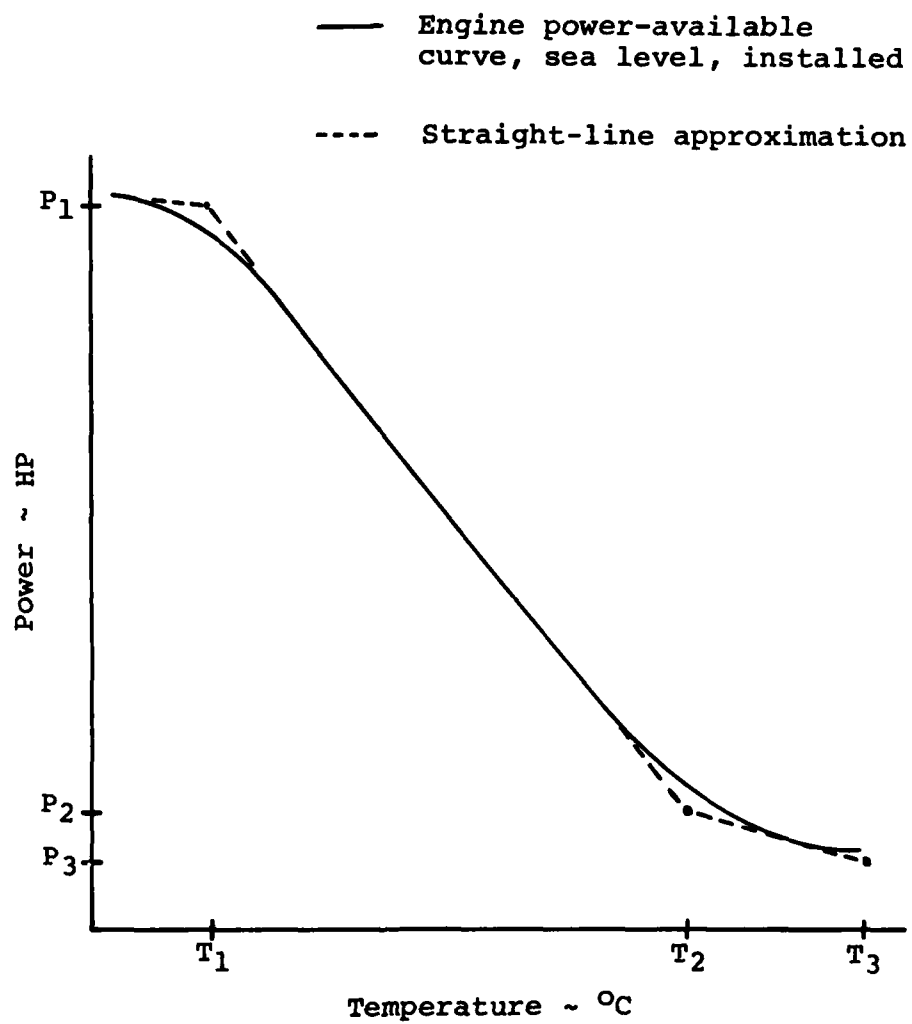


Figure 53. Straight-line Definition of Engine Power Available Curve.

9.2 CALCULATION OF HORSEPOWER REQUIRED

The total instantaneous horsepower required is

$$P_R(t) = \frac{\frac{P_{MR}(t)}{\eta_1} + \frac{P_{TR}(t)}{\eta_2} + P_{acc}}{\eta_3} \quad (323)$$

where $P_{MR}(t)$ = instantaneous horsepower required by the main rotor

$P_{TR}(t)$ = instantaneous horsepower required by the tail rotor

η_1 = main rotor gearbox efficiency ratio (input)

η_2 = tail rotor gearbox efficiency ratio (input)

η_3 = overall drive system efficiency ratio (input)

P_{acc} = accessory horsepower required (input)

This equation is used for trim, trim-in-maneuver, and maneuver cases. For the first two types of run, the number is printed out, and no RPM change is computed if P_R is greater than the appropriate available horsepower, either P_{MA_C} or $P_{MA_{TO}}$.

9.3 DRIVE SYSTEM DYNAMIC EQUATIONS

In maneuver cases, the engine RPM may vary due to differences between the instantaneous power available and power required. The first-order differential equation for rate-of-change of horsepower available is

$$\frac{dP_A(t)}{dt} = \begin{cases} \frac{1}{K_1} \Delta P & \text{for } \Delta P > 0 \\ \frac{1}{K_2} \Delta P & \text{for } \Delta P < 0 \\ 0 & \text{for } P_R > P_{MA_{TO}} \text{ or } P_R < 0 \end{cases} \quad (324)$$

where $P_A(t)$ = power available

$\Delta P = P_R(t) - P_A(t) + c(\Omega_c(t) - \Omega(t))$

c = engine-governor power gain (input)

Ω_c = commanded engine RPM (input)

Ω = current engine RPM

K_1 = time constant for engine power increase (input)

K_2 = time constant for engine power decrease (input)

The initial condition for Equation (324) is the trim horsepower required.

The rate of change of engine rpm is then

$$\frac{d\Omega}{dt} = \frac{Q_S - Q_R}{I} \quad (325)$$

where

Q_S = engine-supplied torque (derived from $P_A(t)$, at engine RPM)

Q_R = torque required from engine (derived from $P_R(t)$, at engine RPM)

I_{TE} = total engine-driven inertia

The total engine-driven inertia, I_{TE} , is

$$I_{TE} = I_{ds} + g_1^2 I_1 + g_2^2 I_2 \quad (326)$$

where

I_{ds} is the drive system inertia, at engine RPM

g_1, g_2 are the gear ratios between the rotor and engine speeds (g_1 is less than 1 for a main rotor)

I_1, I_2 are the inertias of the two rotors

10.0 TRIM PROCEDURE

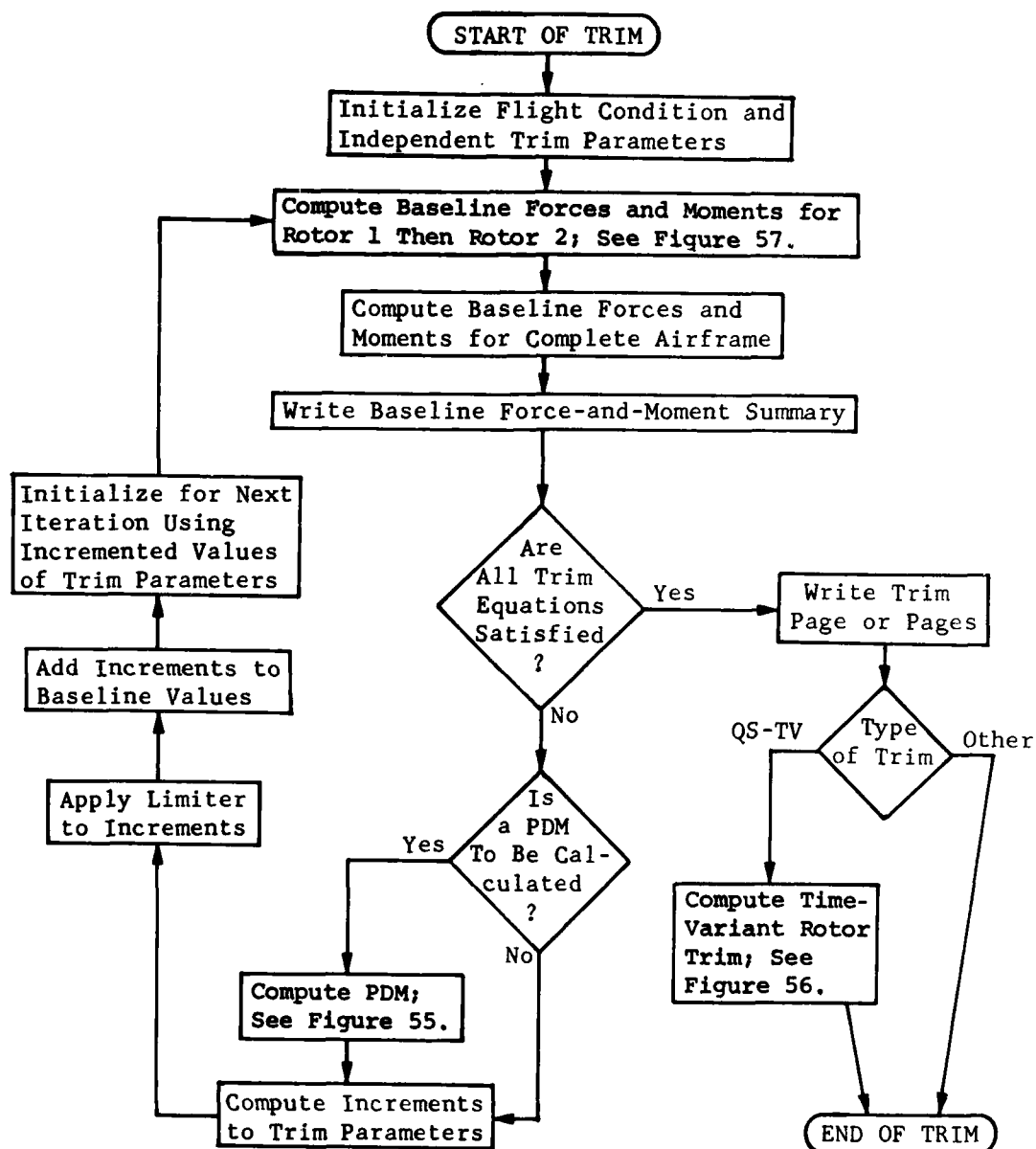
10.1 GENERAL

An essential part of any flight simulation program is its ability to define the trim attitude of the aircraft throughout the flight envelope, including accelerated as well as unaccelerated flight. AGAJ77 includes three types of trim procedure which can accomplish this task. The names given to these procedures are:

- (1) Quasi-static (QS) trim
- (2) Quasi-static followed by time-variant rotor (QS-TV) trim
- (3) Fully time-variant (FTV) trim

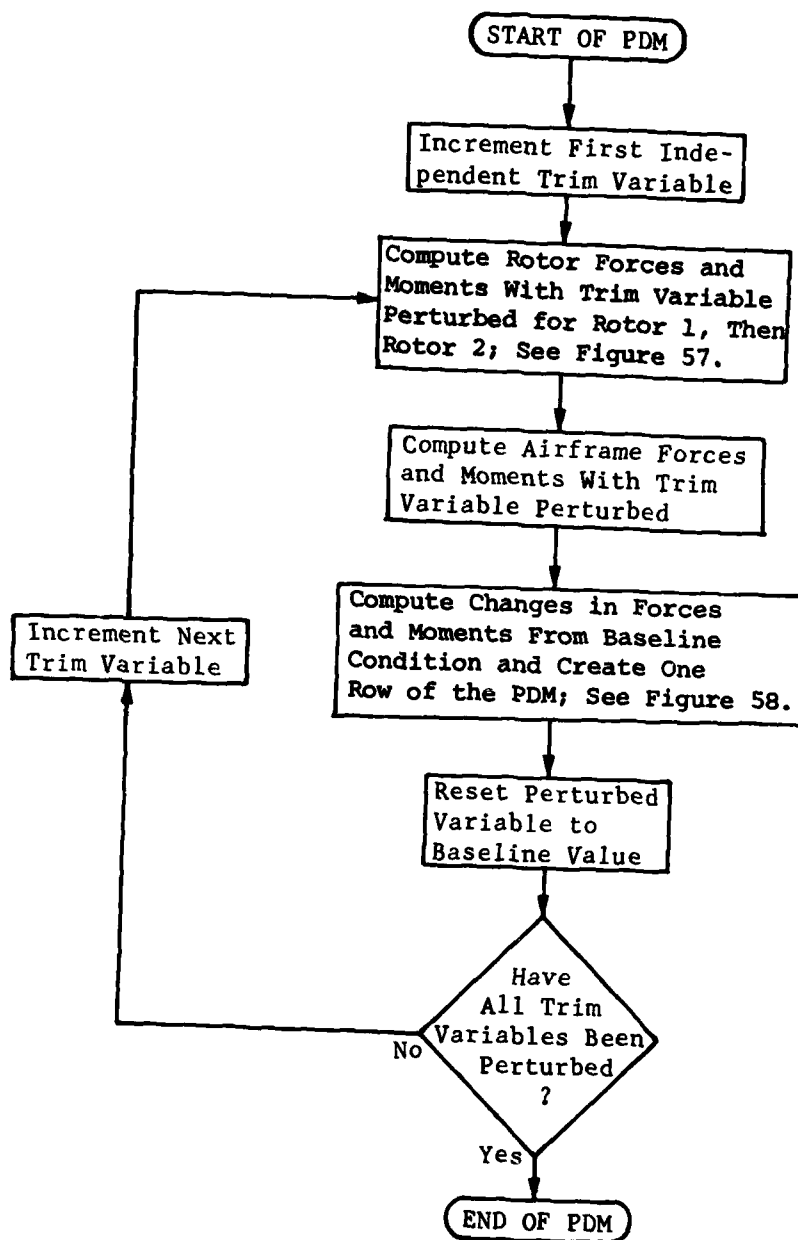
The terms quasi-static and time-variant refer to the primary rotor analyses (see Section 2.2) that are used in the procedure. Both analyses can include the effects of blade elasticity (mode shapes other than the rigid body mode shape), but only the time-variant analysis can include the interaction of the aerodynamic loads and blade elasticity, i.e., aeroelasticity. In the QS trim procedure, the quasi-static rotor analysis is used for both rotor systems. In the QS-TV trim procedure, the standard QS trim is performed first. The rotor modal equations of motion are then numerically integrated for a prescribed number of rotor revolutions using the time-variant rotor analysis with the control positions and fuselage orientation held fixed at the positions determined by the QS trim. It is assumed that after a number of revolutions, the aeroelastic effects included in the time-variant analysis will have caused the rotor either to stabilize or diverge, depending on the basic stability of the rotor system. The user may select that such time-variant trims be computed for either or both rotors. If both rotors are selected, the two time-variant trims are computed independently of each other. In the FTV trim procedure, the user specifies the rotor or rotors which use the time-variant analysis. In doing so, any reference to the QS trim procedure is deleted for the specified rotor(s). (A rotor which does not use the time-variant analysis uses the quasi-static analysis.)

The basic program flow, which is the same for all three types of trim, is shown in Figure 54. The iterative techniques represented by this figure are discussed in Section 10.3.1. The three basic blocks in the figure are the computation of the partial derivative matrix (shown in Figure 55 and discussed in Section 10.3.2), the time-variant portion of the QS-TV trim (shown in Figure 56), and the rotor force and moment computation (shown in Figure 57 and discussed in Section 10.3.3).



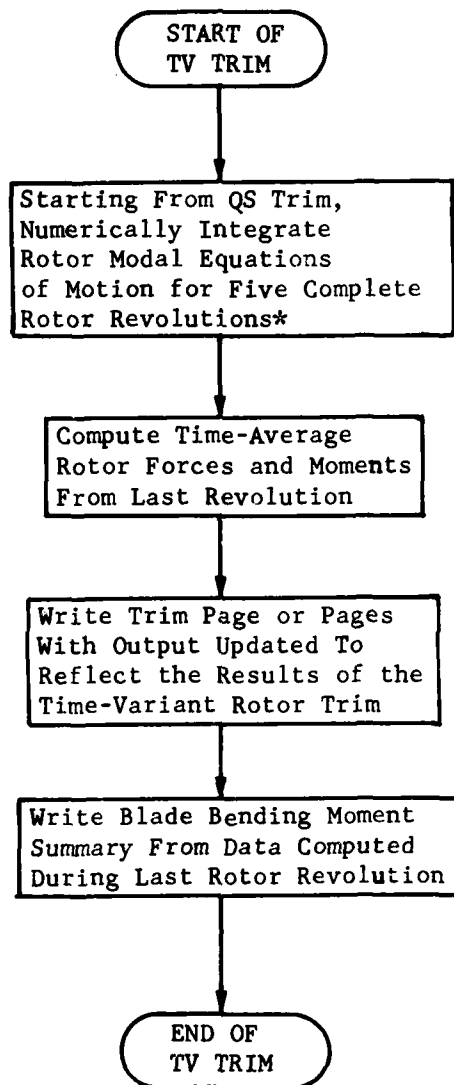
PDM = Partial Derivative Matrix
 QS-TV = Quasi-Static Trim Followed
 by Time-Variant Rotor Trim

Figure 54. Flow Chart of Trim Procedure.



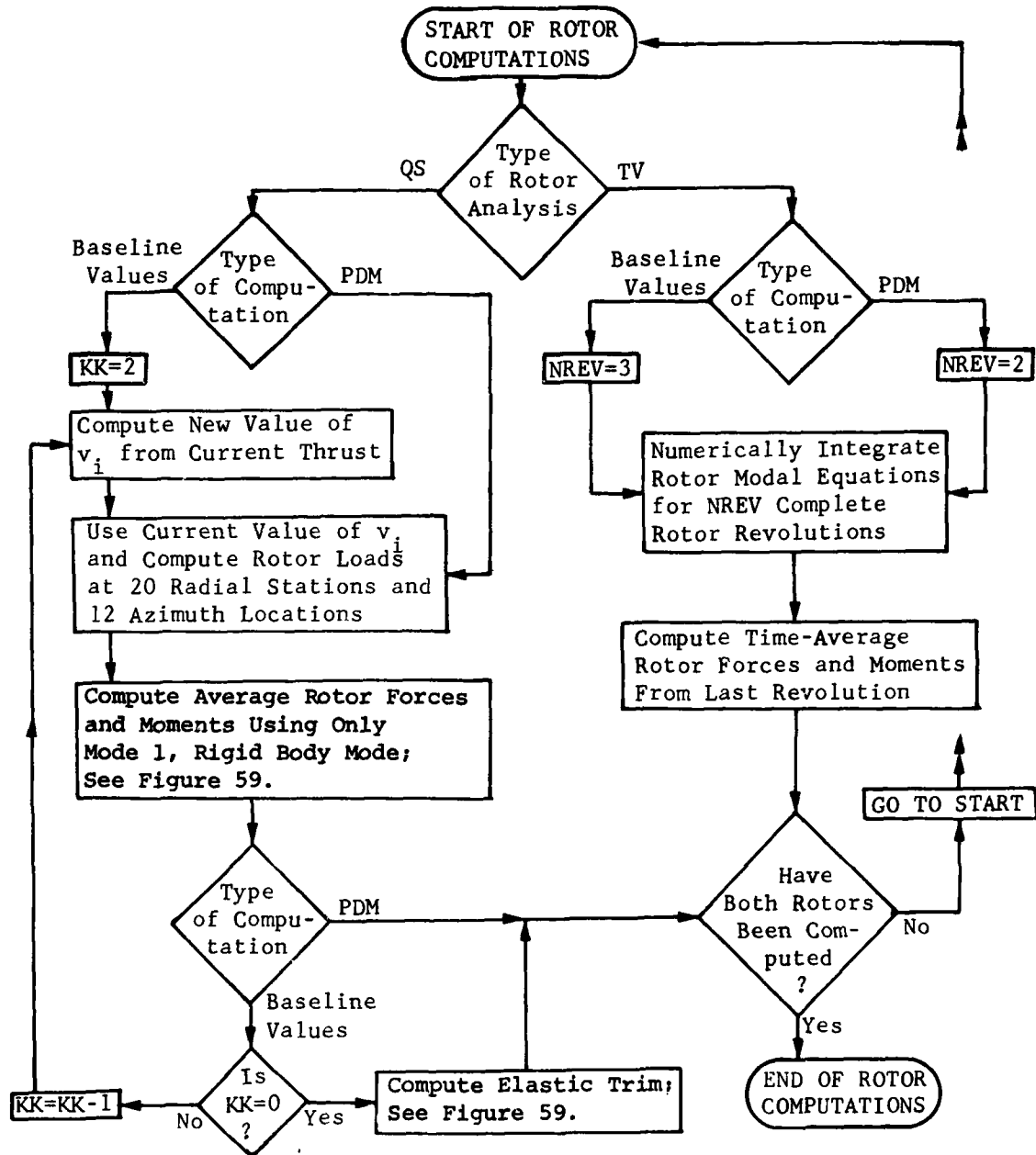
PDM = Partial Derivative Matrix

Figure 55. Flow Chart of Partial Derivative Matrix Computation.



*Control positions and fuselage degrees of freedom held fixed at the final values computed during the QS trim.

Figure 56. Flow Chart of Time-Variant Rotor Trim.



v_i = Rotor-Induced Velocity
 PDM = Partial Derivative Matrix
 KK = Thrust/ v_i Looping Variable

QS = Quasi-Static Rotor Analysis
 TV = Time-Variant Rotor Analysis
 NREV = Number of Rotor Revolutions in TV Analysis

Figure 57. Flow Chart of Rotor Force and Moment Computations During Trim Procedures.

Some of the considerations used in programming the trim procedure are discussed in Section 10.3.4.

10.2 DEFINITION OF TRIMMED FLIGHT CONDITION

The inputs to all three trim procedures are identical: rotorcraft configuration and control positions, flightpath orientation, atmospheric conditions, g-level, and type of flight (pull-up, turn, or unaccelerated). Trim is defined as that combination of appropriate independent trim parameters for which the summations of all external forces and moments (aerodynamic, gravitational, and inertial) about the center of gravity of the rotorcraft (due to both the rotor and the airframe) are less than a preassigned set of limits. For convenience the body axis has been chosen as the reference system for the force and moment summation, and the summation actually consists of six independent summations: the X, Y, and Z forces and the pitch, roll, and yaw moments.

For each rotor that uses the quasi-static rotor analysis there are two additional requirements for trim: the summations of F/A and lateral rotor moments acting at the hub (due to aerodynamic, dynamic, and gravitational forces and moments which have been averaged over the rotor disk) must also be less than a preassigned limit. These requirements are referred to, somewhat loosely, as the flapping-moment balance criteria, or equations. For a teetering or gimbaled rotor this name implies that for trim the 1-per-rev components of the flapping moment must be zero (or must balance any moment due to flapping restraint if such is present); i.e., the tip-path plane is not accelerating with respect to the rotor shaft. These moment balance equations are discussed more fully in Section 10.3.3.

Hence, the mathematical definition of trim consists of three force and three moment summation equations for all external forces and moments acting on the rotorcraft plus two rotor-moment balance equations for each rotor that uses the quasi-static analysis, i.e., 6 to 10 equations. Since the tip-path plane is not a meaningful concept in the time-variant rotor analysis, rotor-moment balance equations for a rotor which uses that analysis are not included in the trim procedure as such. Rather, the moment balances are performed by numerically integrating the modal equations of motion of the rotor for an appropriate number of rotor revolutions. All 10 possible trim equations are summarized in Table 12.

The independent trim variables that are used in all three trim procedures are the three Euler angles (which orient the body axis with respect to the fixed, or ground, reference system)

TABLE 12. DEFINITION OF TRIM CONDITION

Definition	Description
$\sum L \leq \varepsilon_1$	Total rolling moment about cg
$\sum M \leq \varepsilon_2$	Total pitching moment about cg
$\sum N \leq \varepsilon_2$	Total yawing moment about cg
$\sum F_x \leq \varepsilon_3$	Total X-force at cg
$\sum F_y \leq \varepsilon_4$	Total Y-force at cg
$\sum F_z \leq \varepsilon_5$	Total Z-force at cg
$(M_{F/A})_1 \leq \varepsilon_6$	F/A moment acting on Rotor 1 at its hub
$(M_{LAT})_1 \leq \varepsilon_6$	Lateral moment acting on Rotor 1 at its hub
$(M_{F/A})_2 \leq \varepsilon_7$	F/A moment acting on Rotor 2 at its hub
$(M_{LAT})_2 \leq \varepsilon_7$	Lateral moment acting on Rotor 2 at its hub

L, M, N, F_x , F_y , and F_z are in the Body Reference System; $(M_{F/A})_i$ and $(M_{LAT})_i$ are in the Shaft Reference System of the ith rotor ε_j ; j=1,2
 ..., 7 represent the seven allowable errors input to the program

TABLE 13. INDEPENDENT TRIM VARIABLES

Symbol	Description
ψ	Fuselage Euler Yaw Angle
θ	Fuselage Euler Pitch Angle
ϕ	Fuselage Euler Roll Angle
δ_{COLL}	Pilot's Collective Stick Position
$\delta_{F/A}$	Pilot's F/A Cyclic Stick Position
δ_{LAT}	Pilot's Lateral Cyclic Stick Position
δ_{PED}	Pilot's Pedal Position
$(a_1)_1$	F/A Flapping Angle of TPP for Rotor 1
$(b_1)_1$	Lateral Flapping Angle of TPP for Rotor 1
$(a_1)_2$	F/A Flapping Angle of TPP for Rotor 2
$(b_1)_2$	Lateral Flapping Angle TPP for Rotor 2

The flapping angles are with respect to the Rotor Shaft Reference System. For elastic blades they are based on Mode 1. TPP means tip-path plane.

and the positions of the four primary flight controls (collective, F/A cyclic, lateral cyclic, and pedals). When the quasi-static rotor analysis is used, the F/A and lateral flapping angles of the rotor that uses that analysis are also included as independent trim variables. As explained in Section 2.2.2, tip-path plane flapping angles are not independent variables in the time-variant rotor analysis; i.e., these angles cannot be included as independent trim variables for any rotor which uses this analysis. Hence, in the QS trim (or QS portion of a QS-TV trim), there are 11 independent trim variables, while in the FTV trim there will be 9 if only one rotor uses the time-variant analysis or 7 if both rotors use the time-variant analysis. These independent trim variables are summarized in Table 13.

10.3 METHODOLOGY OF THE TRIM PROCEDURE

10.3.1 Iterative Technique and Trim-Parameters

A modification of the Newton-Raphson iterative technique is used to compute the desired trim condition. This technique, which is shown in the flow chart of Figure 54, consists of the following steps:

- (1) Compute the forces and moments acting on the rotorcraft using the input (or current) values of the independent trim variables.
- (2) If all force and moment summations (imbalances) are less than the input allowable errors (ϵ_i in Table 12), the rotorcraft is considered to be trimmed and the trim procedure ends; otherwise, compute a partial derivative matrix.
- (3) Use the matrix and the imbalances to compute the increments to the values of the independent trim variables.
- (4) Add the increments to the previous values of the trim parameters, go back to step (1), and continue the iterative process until the rotorcraft is trimmed or the maximum number of iterations is exceeded.

The key feature of this technique is the computation of the partial derivative matrix (see Figure 56). The computation of this matrix requires that the mathematical model of trim consists of an equal number of trim equations and independent trim variables. However, in the definition of trim given in the previous section and in Tables 12 and 13, the number of trim variables is always one more than the number of trim

equations. Specifically, there are $7 + 2n$ variables and $6 + 2n$ equations, where n is the number of rotors which use the quasi-static analysis. Consequently, one of the independent trim variables must be eliminated (held constant) if the matrix is to be used to compute increments to the variables.

Since the flapping angles are not always included in the list of trim variables and all flight controls must normally be free to move, the choice of variables which can be held constant is limited to the Euler angles. Of these three angles, a pilot will normally be concerned with only the yaw (heading) or roll (bank) angles when trimming the rotorcraft (i.e., pitch attitude is a consequence of the desired flight condition, not a commanded condition itself). Since the mathematical procedure for computing the corrections to the trim variables is independent of the nature of the variables, the choice of which of these two angles is held constant has been made a user option. The user should consider the flight condition being simulated when specifying the angle to be held constant. For example, pilots normally fly rotorcraft at constant heading, particularly at low airspeeds. However, at high airspeeds the pilot may be more apt to command a particular roll angle, such as zero in unaccelerated flight (or in a pullup or push-over) or the bank angle associated with a desired g-level in a turn. In practice, a fixed yaw angle trim works well and is basically representative of actual flight at all airspeeds, while a fixed roll angle trim is only really suitable for flight above the speed for minimum power.

10.3.2 Computation of the Partial Derivative Matrix Increments

The procedure for computing a partial derivative matrix (PDM) is shown in Figure 55 and can be described as follows:

- (1) Perturb one of the independent trim variables from its baseline value.
- (2) Compute the imbalance in each of the trim equations.
- (3) Subtract the imbalances in the baseline condition from those in the perturbed condition.
- (4) Divide each of the differences by the perturbation.

The complete PDM is generated by performing the above procedure for each independent trim variable.

The complete PDM is then used in conjunction with the force and moment imbalances of the baseline condition to compute increments to the independent trim variables. Each increment is

compared to a maximum allowable change. The initial limit is an input; however, the limit is reduced as the imbalances get closer to the allowable errors. If any increment is larger than the limit, all increments are ratioed by the same factor with the result being that the largest increment is equal to the limit. The increments are subsequently added to their corresponding value at the baseline condition.

If the system of equations in C81 were linear, the new values of the variables would trim the rotorcraft, i.e., reduce the imbalance to zero. However, the equations in C81 are non-linear, and the program generally must repeat the above operations several times to reduce the imbalances to less than the allowable errors.

The algebraic formulation of this trim procedure is shown in Figure 58 for the QS trim, i.e., 10 equations and 10 trim variables. However, the method of computation is the same for the 8 by 8, or the 6 by 6, system of equations used in the FTV trim. The formulation can be expressed by the following matrix equation:

$$[PDM_{ij}] \times [\Delta Y_j] = [-(x_i)_B] \quad (327)$$

where

$[PDM_{ij}]$ is the square partial derivative matrix (a 10 by 10 matrix for the QS trim),

$[\Delta y_j]$ is the matrix of increments to the independent trim variables, y_j (a 10 by 1 matrix for the QS trim), and

$[-(x_i)_B]$ is the matrix of the negatives of the force and moment imbalances, x_i , at the baseline flight condition (a 10 by 1 matrix for the QS trim).

The value of each element in PDM_{ij} is computed as follows:

$$PDM_{ij} = [(x_i)_p - (x_i)_B] / [(y_j)_p - (y_j)_B] \quad (328)$$

where the subscript B indicates the baseline condition and P, the perturbed condition. Hence, each time one of the values of y_j is perturbed, the resulting calculations generate one row of the partial derivative matrix. If the perturbations are small and the equations are nearly linear over the range of the perturbation, then

***Alternatively Yaw or ΔYaw**

In matrix notation:

$$[\text{PDM}_{ij}] \times [\Delta y_j] = [- (x_i)_B]$$

$$\left\{ \begin{array}{l} \text{PDM}_{ij} = [(x_i)_P - (x_i)_B] / [(y_j)_P - (y_j)_B] \\ B = \text{Baseline condition} \\ P = \text{Perturbed condition} \\ i \text{ and } j \text{ range in value from 1 to 10} \end{array} \right.$$

Figure 58. Algebraic Formulation of Trim Procedure.

$$PDM_{ij} \quad \partial x_i / \partial y_j \quad (329)$$

The 10 equations in 10 unknowns represented by Equation (327) are then solved for the values of Δy_j by Gauss reduction (Reference 22, Chapter 10.3). Subject to the limiting technique discussed earlier, the values of Δy_j are then added to the previous values of the trim variables to obtain a better approximation of the final trim condition to be used for the next trim iteration. The iterative process is continued until all trim requirements are satisfied.

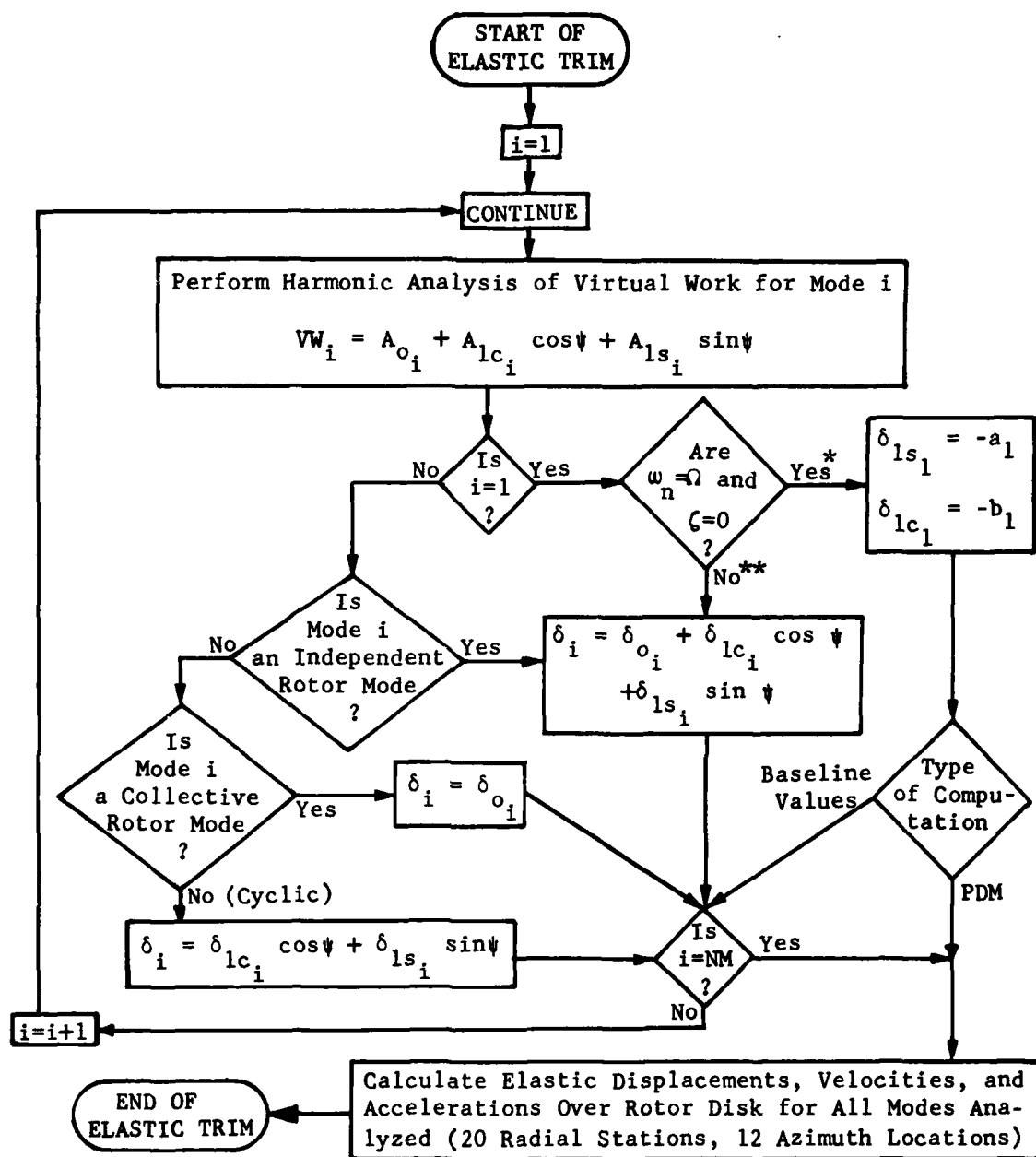
10.3.3 Rotor Force and Moment Computations

The flow charts in both Figures 54 and 55 include a block for computing the rotor forces and moments. Details of the computations within this block are shown in Figure 57. The primary factor affecting the path of the program through the rotor computations is the type of rotor analysis which is to be used. For the QS trim (and QS portion of a QS-TV trim), the QS path in Figure 57 is followed for both rotors. For the FTV trim, the TV path is followed only if the rotor in question is to use the time-variant rotor analysis. When only one rotor is to be time-variant in the FTV trim, the other rotor follows the QS path.

Regardless of the path chosen, the next decision is whether the forces and moments to be computed are for the baseline values of an iteration or for a PDM. In the QS path this decision determines whether or not the thrust/induced-velocity iteration loop and the elastic trim routine are to be used. (They are used for baseline values; they are not used for the PDM.) In the TV path the decision determines the number of rotor revolutions to be made in the numerical integration of the modal equations. (3 revolutions are used to compute the baseline values; 2 are used to compute a PDM.)

A flow chart of the elastic trim technique is shown in Figure 59. This technique is used to include the steady and 1-per-rev components of blade elasticity in the quasi-static analysis. The procedure consists of performing a harmonic analysis of the virtual work done by the airloads on the mode shapes. The virtual work for the i^{th} mode shape is defined as

$$VW_i(\psi) = \int_0^R F(x, \psi) MS_i(x) dx / I_i \quad (330)$$



* Gimbale Rotor

** Rigid or Articulated Rotor

NM = Number of Modes

PDM = Partial Derivative Matrix

ζ = Damping Ratio

a_1 = F/A Flapping Angle

ω_n = Natural Frequency

b_1 = Lateral Flapping Angle

δ_{o_i} , δ_{lc_i} , δ_{ls_i} : See Equations (334), (335) and (336), respectively.

Figure 59. Elastic Trim Technique.

where $F(x, \psi)$ is the summation of the aerodynamic, dynamic, and gravitational forces,

x is the blade station,

ψ is the blade azimuth location,

$MS_i(x)$ is the mode shape of the i^{th} mode, and

I_i is the generalized inertia of the i^{th} mode.

From the harmonic analysis of the virtual work parameters, only the steady and 1-per-rev components are retained, such that

$$VW_i(\psi) = A_{o_i} + A_{lc_i} \cos\psi + A_{ls_i} \sin\psi \quad (331)$$

where A_{o_i} , A_{lc_i} , and A_{ls_i} are the coefficients generated by the analysis.

The modal participation factor is then truncated to a first-harmonic series:

$$\delta_i(\psi) = \delta_{o_i} + \delta_{lc_i} \cos\psi + \delta_{ls_i} \sin\psi \quad (332)$$

Substituting Equations (331) and (332) into the modal equations of motion,

$$\delta_i + 2 \zeta \omega_{n_i} \dot{\delta}_i + \omega_{n_i}^2 \delta_i = VW_i \quad (333)$$

yields the following:

$$\delta_{o_i} = A_{o_i} / \omega_{n_i}^2 \quad (334)$$

$$\delta_{lc_i} = [A_{lc_i} (\omega_{n_i}^2 - \Omega^2) - A_{ls_i} (2 \zeta \omega_{n_i} \Omega)] / \text{Denom} \quad (335)$$

$$\delta_{ls_i} = [A_{ls_i} (\omega_{n_i}^2 - \Omega^2) + A_{lc_i} (2 \zeta \omega_{n_i} \Omega)] / \text{Denom} \quad (336)$$

$$\text{Denom} = (\omega_{n_i}^2 - \Omega^2)^2 + (2 \zeta \omega_{n_i} \Omega)^2 \quad (337)$$

where

ω_{n_i} is the natural frequency of the i th mode (rad/sec),

Ω is the rotor speed (rad/sec), and

ζ is the nondimensional damping ratio of the mode.

Finally, the elastic displacements, velocities, and accelerations over the rotor disk due to these participation factors are computed and used. This routine provides reasonable starting values for all modal participation factors when a time-variant rotor trim (the TV portion of a QS-TV trim) or a time-variant maneuver follows a QS trim. Without the elastic trim routine these participation factors would have to be assumed to be zero, which would increase the magnitude of the transient rotor motion that occurs when the program switches from the quasi-static to the time-variant rotor analysis.

The participation factors output from the elastic trim routine are also used in the computation of the rotor moments which must be balanced as part of the QS trim procedure (see Section 10.2). The rotor moments computed at each of the 12 azimuth locations of the quasi-static rotor analysis are subjected to a harmonic analysis like that performed on the virtual work in the elastic trim routine. Discarding the higher harmonics, the moment is expressed as

$$M(\Psi) = M_0 + M_{lc} \cos\Psi + M_{ls} \sin\Psi \quad (338)$$

Equating like harmonics then yields the following expressions for the F/A and lateral rotor moments about the hub:

$$M_{F/A} = M_{lc} - \sum_{i=1}^{NM} (BBMC_i \delta_{lc_i}) - (M_H)_{F/A} \quad (339)$$

$$M_{LAT} = M_{ls} - \sum_{i=1}^{NM} (BBMC_i \delta_{ls_i}) - (M_H)_{LAT} \quad (340)$$

where

$BBMC_i$ is the blade bending moment coefficient at the hub for the i^{th} mode,

NM is the number of modes, and

M_H is the moment (F/A and lateral) at the hub due to flapping restraint and/or stops.

In the QS trim procedure it is these two moments which must be less than the input limits (ϵ_6 or ϵ_7 in Table 12) for the rotor to be considered trimmed.

For a teetering or gimbaled rotor without flapping restraint (hub spring), there is no moment transfer from the hub to the rotor shaft. Hence, $BBMC$ is zero, and $M_{F/A}$ and M_{LAT} can properly be termed flapping moments. For a rigid or articulated rotor, $BBMC$ is normally nonzero and the restraint at the hub is included in the mode shapes, not as a hub spring (i.e., $(M_H)_{F/A}$ and $(M_H)_{LAT}$ both equal zero).

One of the implications of Equations (339) and (340) is that with appropriate inputs to the QS trim a rigid or articulated rotor can be modeled as a gimbaled rotor with rigid blades and a hub spring that simulates the rotor mode shapes. Obviously, this approximation is not suitable for dynamic analyses where blade loads, etc., are required; however, it can be useful in performance and stability analyses when complete mode shape data are not available.

10.3.4 Programming and Running Considerations

The overall trim procedure has been developed to iterate to a trimmed flight condition in a minimum amount of computer time. Since the rotor calculations are the most time-consuming operation of the procedure, the number of times that these calculations must be performed is held to a minimum. For example, in a QS trim, the computation of the PDM does not include the thrust/induced-velocity iteration loop or the elastic trim routine used in the computation of the baseline forces and moments of the rotor. Although their inclusion would create a more accurate PDM, the increased accuracy does not necessarily reduce the number of iterations required to trim and generally increases rather than decreases the overall run time. Similarly, the usual number of rotor revolutions used with the time-variant rotor analysis is 5 in the TV portion of the QS-TV trim, but only 3 in the computation of the baseline values, and only 2 in the computation of the PDM in the FTV trim because the increased number of revolutions does not shorten the run time in the FTV trim.

In terms of computer time required to achieve trim, the QS trim is always the fastest procedure. Since the TV portion of a QS-TV trim is essentially a post-processor to a QS trim, a QS-TV trim will obviously take longer than a QS trim. The FTV trim will take the longest of all. Because of the marked differences in the QS and FTV trim procedures and the many rotorcraft configuration variables, it is impossible to estimate the relative run times of the two procedures, even for the same configuration starting at the same point. However, it is strongly recommended that all the inputs for the trim variables in FTV trims be obtained from previously computed QS or QS-TV trims for the identical flight conditions and rotorcraft configuration.

Although past use of the program has shown that the trim procedure can generally iterate to a trimmed flight condition from most any reasonable combination of guessed inputs, the user should choose inputs that are as close to the trim condition as possible to insure a successful trim and to minimize the computer time required to trim. One of the more common reasons for failure of the program to trim is starting with too high a collective stick position, i.e., with the rotor in a stalled condition. If the rotor is stalled, the partial derivative matrix is likely to indicate that up collective will reduce rotor thrust (which it could well do in a stalled condition) while also increasing rotor torque. The result of this apparent control reversal may be a fictitious trim at a very high power level (somewhat equivalent to trimming on the backside of the power curve) or more likely, no trim at all. Hence, while the trim procedure is basically forgiving, it can run into problems when gross nonlinearities are encountered.

10.4 ROTOR-ONLY TRIM PROCEDURE

It is not mandatory that C81 simulate an entire rotorcraft system. Frequently, it is desirable to simulate an isolated rotor, e.g., a wind tunnel simulation. A special path has been included in the general trim procedure to provide for such rotor-only simulations in conjunction with the quasi-static rotor analysis. For a rotor-only trim, all references to the fuselage force and moment balances are deleted. That is, the user sets ϵ_1 through ϵ_5 in Table 12 so large that the first six (total rotorcraft) trim equations are effectively deleted from the trim procedure. The allowable errors for the flapping moment imbalances (ϵ_6 for Rotor 1, ϵ_7 for Rotor 2) are kept at realistic values. Also, the two rotors are decoupled from each other, which in effect reduces the single 10 by 10 matrix in Figure 56 to a pair of 2 by 2 matrices. It is not necessary or normal, that both rotors be included in a rotor-only trim. Assuming the second rotor is deleted, the 10 by 10 matrix then

reduces to a single 2 by 2 matrix. The independent variables for reducing the flapping moments may then be either the fore-and-aft and lateral shaft-axis flapping angles or the fore-and-aft and lateral blade feathering angles. When the flapping angles are the independent variables, the case is equivalent to letting the rotor seek a new equilibrium flapping condition for a prescribed set of blade feathering angles. When the feathering angles are the independent variables, the case is equivalent to letting the rotor control seek the values which will cause a prescribed set of flapping angles. The latter case is particularly useful in simulating wind tunnel tests where data are measured at specified flapping angles rather than control positions. The former case can also be useful during a total rotorcraft trim when difficulty is encountered in trimming the entire rotorcraft system with the 10 by 10 matrix. Either or both sets of rotor equations may be decoupled and allowed to trim within one conventional trim iteration.

It should be emphasized that the rotor-only procedure described here cannot be used for a time-variant rotor since the flapping angles and rotor moments on which it is based do not exist in the time-variant analysis. However, the equivalent of the trim at specified blade feathering angles can be performed with the QS-TV or FTV trim by using appropriate dummy inputs for the fuselage and aerodynamic surfaces. As another alternative, the allowable errors can be set very large so that the program will immediately "drop through" the trim procedure, and a time-variant maneuver with an appropriate number of rotor revolutions can be performed at fixed feathering angles.

A second (optional) trim page has been added to the program to present significant rotor performance data that are useful in analyzing wind tunnel simulations and are not printed as part of the standard trim page. The data are in both dimensional and nondimensional forms. A summary of the rotor and tunnel parameters, and the rotor bending moments are also printed. This optional page may be printed following either a total rotorcraft or rotor-only trim.

11.0 ROTORCRAFT STABILITY ANALYSIS

11.1 INTRODUCTION

The principal objective of this section is to present a basis for evaluating each element in an 18-degree-of-freedom system characteristic determinant. The application of perturbation theory as presented herein follows the development given in Reference 27.

The first form of the stability analysis programmed as a subroutine in C81 was based on six rigid-body degrees of freedom of the fuselage with rotor effects introduced as additional terms. The original analysis was performed assuming two decoupled systems of three equations each and then combining these six equations into a representation of a single coupled system. Later, 12 more equations which are representative of rotor and pylon degrees of freedom were introduced. The system discussed herein consists of the six fuselage degrees of freedom and the additional rotor and pylon degrees of freedom. The resulting set of 18 equations (see Table 14) of rigid body motion are presented herein, associated symbols are defined, and the procedure of analysis is delineated.

11.2 STABILITY ANALYSIS EQUATIONS

The basic stability analysis equations correspond to the equations of motion used in the calculations of maneuver time histories. However, it is convenient in the stability analysis to represent the rotors with two equations each, one for fore-and-aft flapping and one for lateral flapping.

The equations in Table 14 reduce to the usual equations of motion, except for the aerodynamic terms involving W in the fuselage group, if

$$G_i = 0 \quad i = 1, 2, \dots, 18 \quad (341)$$

For $i = 1, 2, \dots, 6, 11, 12, 17$ and 18 , the equations are the same as given for the rigid body fuselage and the rotor flapping components developed in Reference 1, except as noted above. The fuselage equations are ordered so that the first three reduce to the traditional "longitudinal" equations when decoupled from the rest of the system. Similarly, the next three equations reduce to the "lateral" equations. For $i = 7-10$ and $13-16$ the equations are the same as the pylon equations developed in Section 3.3. The inertia coupling terms in the pylon equations may be found by observing Equations (125), (126), (133), and (134).

TABLE 14. STABILITY ANALYSIS EQUATIONS

FUSELAGE

$$G_1 = m(\dot{U} + Q W - R V) - F_x - W_x$$

$$G_2 = m(\dot{W} + P V - Q U) - F_z - W_z - Z \dot{W}$$

$$G_3 = I_y \dot{Q} + R P (I_x - I_z) + I_{xz} (P^2 - R^2) - M - M_w \dot{W}$$

$$G_4 = m(\dot{V} + R U - P W) - F_y - W_y - Y \dot{W}$$

$$G_5 = I_x \dot{P} - I_{xz} \dot{R} + Q R (I_z - I_y) - I_{xz} P Q - L - L_w \dot{W}$$

$$G_6 = I_z \dot{R} - I_{xz} \dot{P} + P Q (I_y - I_x) + I_{xz} Q R - N - N_w \dot{W}$$

MAIN (FIRST) PYLON - j = 1, 2, 3, 4

$$\begin{aligned} G_{j+6} = & \sum_{i=1}^4 I_{jiM} \ddot{P}_{iM} + 2\zeta_{jM} \omega_{jM} \dot{P}_{jM} + \omega_{jM}^2 P_{jM} \\ & - F_{ojM}/G I_{jM} - I_{xjM} \dot{U} - I_{yjM} \dot{V} - I_{zjM} \dot{W} \\ & - I_{pjM} \dot{P} - I_{qjM} \dot{Q} - I_{rjM} \dot{R} \end{aligned}$$

MAIN (FIRST) ROTOR FLAPPING

$$G_{11} = I_{RM} [(-\ddot{A}_{1M} - \dot{Q}_{SM}) - 2 \Omega_M (\dot{B}_{1M} + P_{SM})] - M_{RM}$$

$$G_{12} = I_{RM} [(-\ddot{B}_{1M} - \dot{P}_{SM}) + 2 \Omega_M (\dot{A}_{1M} + Q_{SM})] - L_{RM}$$

TABLE 14. CONCLUDED

TAIL (SECOND) PYLON - j = 1, 2, 3, 4

$$\begin{aligned}
 G_{j+12} = & \sum_{i=1}^4 I_{jiT} \ddot{P}_{jT} + 2 \zeta_{jT} \omega_{jT} \dot{P}_{jT} + \omega_{jT}^2 P_{jT} \\
 & - F_{ojT}/G I_{jT} - I_{xjT} \dot{U} - I_{yjT} \dot{V} - I_{zjT} \dot{W} \\
 & - I_{pjT} \dot{P} - I_{qjT} \dot{Q} - I_{rjT} \dot{R}
 \end{aligned}$$

TAIL (SECOND) ROTOR FLAPPING

$$G_{17} = I_{RT} [(-\ddot{A}_{1T} - \dot{Q}_{ST}) - 2 \Omega_T (\dot{B}_{1T} + P_{ST})] - M_{RT}$$

$$G_{18} = I_{RT} [(-\ddot{B}_{1T} - \dot{P}_{SM}) + 2 \Omega_T (\dot{A}_{1T} + Q_{ST})] - L_{RT}$$

The perturbation method requires representation of the partial derivatives of the G_i with respect to the 18 base variables and their first and second derivatives. Some of these derivatives can be evaluated only by way of auxiliary equations relating the base variables to secondary variables. The weight components, W_x , W_y , and W_z , are denoted explicitly so that their partial derivatives can be evaluated analytically. The effects of rate of change of angle of attack are also included explicitly as coefficients of \dot{W} in G_2 , G_3 , G_4 , G_5 , and G_6 . It is assumed that, except for these five terms, the aerodynamic forces and moments are not functions of the acceleration variables.

11.3 AUXILIARY EQUATIONS

Five reference systems involved in the stability analysis are

Ground, or Fixed
 Body, or Fuselage
 Main (First) Pylon Mast or Shaft
 Tail (Second) Pylon Mast or Shaft
 Wind (Section 11.6.3)

An ordered set of angular rotations (Ψ , θ , ϕ) relating the body reference system to the fixed reference as described in Reference 27 is called the "fuselage Euler angles." Note that in the following discussions, body reference and fuselage reference are used synonymously. Similar sets are used to relate each pylon mast reference system to the fuselage. The rotor tip-path plane flapping components (A_{1M} , B_{1M} for the main rotor and A_{1T} , B_{1T} for the tail rotor) are represented as rotations about the mast axes. The Euler angle velocities are functions of fuselage rotation velocity components (P , Q , R) and the transformations of components from one reference frame to another require the following group of auxiliary relationships.

11.3.1 Fuselage Euler Angle Velocities in Body Reference System

$$\dot{\Psi} = (Q \sin \phi + R \cos \phi) \sec \theta \quad (342)$$

$$\dot{\theta} = Q \cos \phi - R \sin \phi \quad (343)$$

$$\dot{\phi} = P + (Q \sin \phi + R \cos \phi) \tan \theta \quad (344)$$

11.3.2 Weight Components in Body Reference System

The fuselage Euler angle transformation matrix, T , given in Reference 1, is used to evaluate the components of the weight vector in the fuselage body reference system. Since $\psi = 0$ in this case,

$$[T(0, \theta, \phi)] = \begin{bmatrix} \cos \theta & \sin \theta \sin \phi & \sin \theta \cos \phi \\ 0 & \cos \phi & -\sin \phi \\ -\sin \theta & \cos \theta \sin \phi & \cos \theta \cos \phi \end{bmatrix} \quad (345)$$

Then

$$[W_x \ W_y \ W_z] = [0 \ 0 \ mg][T(0, \theta, \phi)] \quad (346)$$

11.3.3 Body Angular Velocity and Acceleration Components in Pylon (Rotor) Mast Reference Systems

Let θ_M = the main rotor shaft tilt fore-and-aft, positive forward

ϕ_M = the main rotor shaft tilt lateral, positive right

and similarly θ_T and ϕ_T for the tail rotor. Then

$$[P_{SM} \ Q_{SM} \ R_{SM}] = [P \ Q \ R][T(0, -\theta_M, \phi_M)] \quad (347)$$

$$[\dot{P}_{SM} \ \dot{Q}_{SM} \ \dot{R}_{SM}] = [\dot{P} \ \dot{Q} \ \dot{R}][T(0, -\theta_M, \phi_M)] \quad (348)$$

$$[P_{ST} \ Q_{ST} \ R_{ST}] = [P \ Q \ R][T(0, -\theta_T, -\phi_T)] \quad (349)$$

$$[\dot{P}_{ST} \ \dot{Q}_{ST} \ \dot{R}_{ST}] = [\dot{P} \ \dot{Q} \ \dot{R}][T(0, -\theta_T, -\phi_T)] \quad (350)$$

Elements of $T(0, -\theta_M, \phi_M)$ are denoted $T_{M_{ij}}$, so that, for example,

$$P_{SM} = PT_{M_{11}} + RT_{M_{31}} \quad (351)$$

11.4 INDEXED NOTATION

For convenience in developing the stability analysis, an indexed notation is introduced. Body displacement variables are supplied in the form of velocity integrals.

11.4.1 Basic Variables

$\bar{x}_1 = \int U dt$	$\dot{\bar{x}}_1 = U$	$\ddot{\bar{x}}_1 = \dot{U}$
$\bar{x}_2 = \int W dt$	$\dot{\bar{x}}_2 = W$	$\ddot{\bar{x}}_2 = \dot{W}$
$\bar{x}_3 = \int Q dt$	$\dot{\bar{x}}_3 = Q$	$\ddot{\bar{x}}_3 = \dot{Q}$
$\bar{x}_4 = \int V dt$	$\dot{\bar{x}}_4 = V$	$\ddot{\bar{x}}_4 = \dot{V}$
$\bar{x}_5 = \int P dt$	$\dot{\bar{x}}_5 = P$	$\ddot{\bar{x}}_5 = \dot{P}$
$\bar{x}_6 = \int R dt$	$\dot{\bar{x}}_6 = R$	$\ddot{\bar{x}}_6 = \dot{R}$
$\bar{x}_7 = P_{1M}$	$\dot{\bar{x}}_7 = \dot{P}_{1M}$	$\ddot{\bar{x}}_7 = \ddot{P}_{1M}$
$\bar{x}_8 = P_{2M}$	$\dot{\bar{x}}_8 = \dot{P}_{2M}$	$\ddot{\bar{x}}_8 = \ddot{P}_{2M}$
$\bar{x}_9 = P_{3M}$	$\dot{\bar{x}}_9 = \dot{P}_{3M}$	$\ddot{\bar{x}}_9 = \ddot{P}_{3M}$
$\bar{x}_{10} = P_{4M}$	$\dot{\bar{x}}_{10} = \dot{P}_{4M}$	$\ddot{\bar{x}}_{10} = \ddot{P}_{4M}$
$\bar{x}_{11} = A_{1M}$	$\dot{\bar{x}}_{11} = \dot{A}_{1M}$	$\ddot{\bar{x}}_{11} = \ddot{A}_{1M}$
$\bar{x}_{12} = B_{1M}$	$\dot{\bar{x}}_{12} = \dot{B}_{1M}$	$\ddot{\bar{x}}_{12} = \ddot{B}_{1M}$
$\bar{x}_{13} = P_{1T}$	$\dot{\bar{x}}_{13} = \dot{P}_{1T}$	$\ddot{\bar{x}}_{13} = \ddot{P}_{1T}$
$\bar{x}_{14} = P_{2T}$	$\dot{\bar{x}}_{14} = \dot{P}_{2T}$	$\ddot{\bar{x}}_{14} = \ddot{P}_{2T}$
$\bar{x}_{15} = P_{3T}$	$\dot{\bar{x}}_{15} = \dot{P}_{3T}$	$\ddot{\bar{x}}_{15} = \ddot{P}_{3T}$
$\bar{x}_{16} = P_{4T}$	$\dot{\bar{x}}_{16} = \dot{P}_{4T}$	$\ddot{\bar{x}}_{16} = \ddot{P}_{4T}$
$\bar{x}_{17} = A_{1T}$	$\dot{\bar{x}}_{17} = \dot{A}_{1T}$	$\ddot{\bar{x}}_{17} = \ddot{A}_{1T}$
$\bar{x}_{18} = B_{1T}$	$\dot{\bar{x}}_{18} = \dot{B}_{1T}$	$\ddot{\bar{x}}_{18} = \ddot{B}_{1T}$

(352)

11.4.2 Auxiliary Variables

$$\begin{array}{llll}
 \bar{y}_1 = \psi & \dot{\bar{y}}_1 = \dot{\psi} & \dot{\bar{y}}_4 = P_{SM} & \ddot{\bar{y}}_4 = \dot{P}_{SM} \\
 \bar{y}_2 = \theta & \dot{\bar{y}}_2 = \dot{\theta} & \dot{\bar{y}}_5 = Q_{SM} & \ddot{\bar{y}}_5 = \dot{Q}_{SM} \\
 \bar{y}_3 = \phi & \dot{\bar{y}}_3 = \dot{\phi} & \dot{\bar{y}}_6 = R_{SM} & \ddot{\bar{y}}_6 = \dot{R}_{SM}
 \end{array} \quad (353)$$

11.4.3 Applied Forces and Moments

$$\begin{array}{llll}
 F_1 = F_x & F_6 = N & F_{11} = M_{RM} & F_{16} = F_{04T} \\
 F_2 = F_z & F_7 = F_{01M} & F_{12} = L_{RM} & F_{17} = M_{RT} \\
 F_3 = M & F_8 = F_{02M} & F_{13} = F_{01T} & F_{18} = L_{RT} \\
 F_4 = F_y & F_9 = F_{03M} & F_{14} = F_{02T} & \\
 F_5 = L & F_{10} = F_{04M} & F_{15} = F_{03T} &
 \end{array} \quad (354)$$

11.4.4 The Perturbation Variables

Each base variable is represented as the sum of the initial value, x_{i_0} , and an increment, $\Delta \bar{x}_i$. Denote \bar{x}_{i_0} as x_{i_0} and $\Delta \bar{x}_i$ as x_i . Then

$$\bar{x}_i = x_{i_0} + x_i ; \quad \dot{\bar{x}} = \dot{x}_{i_0} + \dot{x}_i ; \quad \ddot{\bar{x}} = \ddot{x}_{i_0} + \ddot{x}_i \quad (355)$$

The x_i , \dot{x}_i , and \ddot{x}_i are the basic perturbation variables.

Similarly, for the auxiliary variables,

$$\bar{y}_i = y_{i_0} + y_i ; \quad \dot{\bar{y}}_i = \dot{y}_{i_0} + \dot{y}_i ; \quad \ddot{\bar{y}}_i = \ddot{y}_{i_0} + \ddot{y}_i \quad (356)$$

In the notation of Table 14, the uppercase symbols correspond to the \bar{x} 's and \bar{y} 's. Lowercase symbols are used elsewhere for the initial incremental parts. Thus,

$$U = u_0 + u, \quad V = v_0 + v, \quad \text{etc.} \quad (357)$$

11.5 THE EIGENVALUE SOLUTION

11.5.1 Formulation

The equations of motion are nonlinear in the basic variables and thus do not admit of a direct eigenvalue solution. They are linearized by considering a perturbation about an initial condition specified by x_j , \dot{x}_j , and \ddot{x}_j . The equations of motion can be written

$$G_i(\bar{x}_j, \dot{\bar{x}}_j, \ddot{\bar{x}}_j, \bar{y}_k, \dot{\bar{y}}_k, \ddot{\bar{y}}_k) = 0, \quad (358)$$

where

$$i = 1, 2, \dots, 18$$

$$j = 1, 2, \dots, 18$$

$$k = 1, 2, \dots, 6$$

or, since the \bar{y} variables are functions of the \bar{x} variables, the equations can be specified as

$$G_i(\bar{x}_j, \dot{\bar{x}}_j, \ddot{\bar{x}}_j) = 0 \quad (359)$$

The total differential of G_i , with controls fixed, can be expressed in terms of the base variables as

$$dG_i = \sum_j \left. \frac{\partial G_i}{\partial x_j} \right|_0 x_j + \sum_j \left. \frac{\partial G_i}{\partial \dot{x}_j} \right|_0 \dot{x}_j + \sum_j \left. \frac{\partial G_i}{\partial \ddot{x}_j} \right|_0 \ddot{x}_j = 0 \quad (360)$$

in which the partial derivatives are evaluated at the initial values, x_{j0} .

Assume $x_j = x_{j0} e^{\lambda t}$. Then the equation represented by Equation (360) can be written as

$$\sum_j \left(\left. \frac{\partial G_i}{\partial \ddot{x}_j} \right|_0 \lambda^2 + \left. \frac{\partial G_i}{\partial \dot{x}_j} \right|_0 \lambda + \left. \frac{\partial G_i}{\partial x_j} \right|_0 \right) x_j = 0 \quad (361)$$

The determinant of the coefficients is the characteristic determinant for fixed controls.

11.5.2 Solution Procedure

The eigenvalue problem is characterized by a set of simultaneous equations which can be expressed in matrix form as

$$[A]\{X\} = \lambda\{X\} \quad (362)$$

where $[A]$ is a square matrix, $\{X\}$ is a vector of unknowns, and λ is a scalar quantity. Equation (362) can be rewritten as a homogenous equation:

$$([A] - \lambda[I])\{X\} = 0 \quad (363)$$

where $[I]$ is the identity matrix having the same order as $[A]$. However, Equation (363) is linear in λ whereas Equation (361) is quadratic, and the two equations are of somewhat different form. Hence, the following procedure is used to transform Equation (360) to the standard eigenvalue form. First, the coefficients of x in Equation (360) are defined as

$$M_{ij} = \left. \frac{G_i}{\ddot{x}_j} \right|_0 \quad (364)$$

$$C_{ij} = \left. \frac{G_i}{\dot{x}_j} \right|_0 \quad (365)$$

$$K_{ij} = \left. \frac{G_i}{x_j} \right|_0 \quad (366)$$

These coefficients then become the elements of mass, damping, and stiffness matrices, respectively, when Equation (360) is rewritten in matrix form as

$$[M]\{\ddot{X}\} + [C]\{\dot{x}\} + [K]\{x\} = 0 \quad (367)$$

where $[M]$, $[C]$, and $[K]$ are square matrices (N by N) and $\{\ddot{x}\}$, $\{\dot{x}\}$, and $\{x\}$ are column matrices (of length N). At this point, a substitution variable (y) is defined:

$$y = \dot{x} \quad (368)$$

and Equation (367) becomes

$$[M]\{\dot{y}\} + [C]\{y\} + [K]\{x\} = 0 \quad (369)$$

Equation (368) is then multiplied by the identity matrix and added to Equation (369) to yield

$$[M]\{\dot{y}\} + ([I]\{\dot{x}\} - [I]\{y\}) + [C]\{y\} + [K]\{x\} = 0$$

which can be rewritten as

$$\begin{bmatrix} [M] & [0] \\ [0] & [I] \end{bmatrix} \begin{Bmatrix} \{\dot{y}\} \\ \{\dot{x}\} \end{Bmatrix} + \begin{bmatrix} [C] & [K] \\ -[I] & [0] \end{bmatrix} \begin{Bmatrix} \{y\} \\ \{x\} \end{Bmatrix} = \begin{Bmatrix} 0 \\ 0 \end{Bmatrix} \quad (370)$$

where [0] is an N by N matrix of zeroes and the matrices which contain [0] are 2N by 2N.

Next, the x and y variables are replaced with another substitution variable z, such that

$$\{z\} = \begin{Bmatrix} \{y\} \\ \{x\} \end{Bmatrix} \quad (371)$$

Then, it is assumed that

$$\{z_k\} = \{z_{k_0}\} e^{\lambda t} \quad (372)$$

where k ranges from 1 to 2N.

Equation (370) can then be written as

$$\begin{bmatrix} [M] & [0] \\ [0] & [I] \end{bmatrix} \{\dot{z}_k\} + \begin{bmatrix} [C] & [K] \\ -[I] & [0] \end{bmatrix} \{z_k\} = 0 \quad (373)$$

or

$$\begin{bmatrix} [M] & [0] \\ [0] & [I] \end{bmatrix} \lambda + \begin{bmatrix} [C] & [K] \\ -[I] & [0] \end{bmatrix} \{z_{k_0}\} e^{\lambda t} = 0 \quad (374)$$

or

$$\begin{bmatrix} [M] & [0] \\ [0] & [I] \end{bmatrix}^{-1} \begin{bmatrix} [C] & [K] \\ -[I] & [0] \end{bmatrix} - \lambda [I] \{z_{k_0}\} e^{\lambda t} = 0 \quad (375)$$

Comparing Equation (375) to Equation (363) shows that they have the identical format. Specifically, the A and X arrays are formulated as follows

$$\begin{aligned}
 [A] &= - \begin{bmatrix} [M] & [0] \\ [0] & [I] \end{bmatrix}^{-1} \begin{bmatrix} [C] & [K] \\ -[I] & [0] \end{bmatrix} \\
 &= - \begin{bmatrix} [M]^{-1} & [0] \\ [0] & [I] \end{bmatrix} \begin{bmatrix} [C] & [K] \\ -[I] & [0] \end{bmatrix} \\
 &= \begin{bmatrix} -[M]^{-1} & [C] & -[M]^{-1} & [K] \\ \hline & [I] & & [0] \end{bmatrix}
 \end{aligned} \tag{376a}$$

and

$$\{X\} = \left\{ z_k \right\}_o e^{\lambda t} \tag{376b}$$

where [A] is dimensioned 2N by 2N and [X] is 1 by 2N.

The A matrix is then input to the ALLMAT subroutine (Reference 29) which returns the eigenvalues of the A matrix (λ , the roots to the characteristic equation). A second entry to the same routine can be used to compute the eigenvectors (the X array for the corresponding values of λ ; the mode shapes).

11.6 EVALUATION OF THE PARTIAL DERIVATIVES

The partial derivatives in Equation (361) are to be evaluated at the initial condition as indicated by the subscript o. There are

$$3 \times 18 \times 18 = 972$$

elements in the full set of partial derivatives. The discussion of their evaluation, which follows, is intended to be illustrative rather than exhaustive.

²⁹Fiar, Gale, ALLMAT: A TSS/360 FORTRAN IV SUBROUTINE FOR EIGENVALUES AND EIGENVECTORS OF A GENERAL COMPLEX MATRIX, NASA TND-7032, January 1971.

11.6.1 The Euler Angle Relationships

The relationships between the set of Euler angle perturbations, Ψ , θ , and ϕ , and the base perturbations, x_3 , x_5 , and x_6 , are developed from Equations (342), (343), and (344).

In terms of the perturbation variables, the total differential of $\dot{\theta}$ is, from Equation (343),

$$d\dot{\theta} = \frac{\partial \dot{\theta}}{\partial Q} dQ + \frac{\partial \dot{\theta}}{\partial R} dR + \frac{\partial \dot{\theta}}{\partial \phi} d\phi \quad (377)$$

or

$$d\dot{\theta} = \cos \phi dQ - \sin \phi dR - (Q \sin \phi + R \cos \phi) d\phi \quad (378)$$

In the perturbation notation,

$$\begin{aligned} \dot{\theta} &= q \cos (\phi_0 + \phi) - r \sin (\phi_0 + \phi) \\ &\quad - [(q_0 + q) \sin (\phi_0 + \phi) \\ &\quad + (r_0 + r) \cos (\phi_0 + \phi)] \phi \end{aligned} \quad (379)$$

The following approximations are used:

$$\left. \begin{aligned} \cos (\phi_0 + \phi) &\sim \cos \phi_0 - \phi \sin \phi_0 \\ \sin (\phi_0 + \phi) &\sim \sin \phi_0 + \phi \cos \phi_0 \end{aligned} \right\} \quad (380)$$

Omitting the terms containing products of perturbation variables,

$$\dot{\theta} = q \cos \phi_0 - r \sin \phi_0 - (q_0 \sin \phi_0 + r_0 \cos \phi_0) \phi \quad (381)$$

Whence

$$\begin{aligned} \theta &= \cos \phi_0 \int q dt - \sin \phi_0 \int r dt \\ &\quad - (q_0 \sin \phi_0 + r_0 \cos \phi_0) \int \phi dt \end{aligned} \quad (382)$$

Then

$$\frac{\partial \theta}{\partial x_3} = \cos \phi_0; \quad \frac{\partial \theta}{\partial x_6} = -\sin \phi_0 \quad (383)$$

Similarly,

$$\frac{\partial \psi}{\partial x_3} = \sin \phi_0 \sec \theta_0; \quad \frac{\partial \psi}{\partial x_6} = \cos \phi_0 \sec \phi_0 \quad (384)$$

$$\frac{\partial \phi}{\partial x_3} = \sin \phi_0 \tan \theta_0; \quad \frac{\partial \phi}{\partial x_5} = 1; \quad \frac{\partial \phi}{\partial x_6} = \cos \phi_0 \tan \theta_0 \quad (385)$$

11.6.2 The Partial Derivatives of G_1

The partial derivatives of G_1 are developed in detail. The same procedure is applicable to the remaining G_i .

Consider the first fuselage rigid-body equation.

$$G_1 = m (\dot{U} + QW - RV) - F_x - W_x \quad (386)$$

In the perturbation notation,

$$\begin{aligned} G_1 = m & \left[\ddot{x}_{1_0} + \ddot{x}_1 + (\dot{x}_{3_0} + \dot{x}_3)(\dot{x}_{2_0} + \dot{x}_2) \right. \\ & \left. - (\dot{x}_{6_0} + \dot{x}_6)(\dot{x}_{4_0} + \dot{x}_4) \right] - F_x - W_x \end{aligned} \quad (387)$$

or, dropping perturbation variable product terms,

$$\begin{aligned} G_1 = m & (\ddot{x}_{1_0} + \dot{x}_{3_0} \dot{x}_{2_0} - \dot{x}_{6_0} \dot{x}_{4_0}) \\ & + m(\ddot{x}_1 + \dot{x}_{3_0} \dot{x}_2 + \dot{x}_{2_0} \dot{x}_3 - \dot{x}_{6_0} \dot{x}_4 - \dot{x}_{4_0} \dot{x}_6) \\ & - F_x - W_x \end{aligned} \quad (388)$$

Then the M_{1j} are

$$\frac{\partial G_1}{\partial \ddot{x}_1} = m, \quad \frac{\partial G_1}{\partial \ddot{x}_j} = 0, \quad j \neq 1 \quad (389)$$

Since from Equation (346)

$$\frac{\partial W_x}{\partial x_j} = \frac{\partial W_y}{\partial x_j} = \frac{\partial W_z}{\partial x_j} = 0 \quad (390)$$

and from Equation (388), the G_{1j} are

$$\frac{\partial G_1}{\partial \dot{x}_1} = - \frac{\partial F_x}{\partial \dot{x}_1}; \quad \frac{\partial G_1}{\partial \dot{x}_2} = m x_{3_0} - \frac{\partial F_x}{\partial \dot{x}_2} \quad (391)$$

$$\left. \begin{aligned} \frac{\partial G_1}{\partial \dot{x}_3} &= m\dot{x}_{2_0} - \frac{\partial F_x}{\partial \dot{x}_3} ; \quad \frac{\partial G_1}{\partial \dot{x}_4} = -m\dot{x}_{6_0} - \frac{\partial F_x}{\partial \dot{x}_4} \\ \frac{\partial G_1}{\partial \dot{x}_5} &= -\frac{\partial F_x}{\partial \dot{x}_5} ; \quad \frac{\partial G_1}{\partial \dot{x}_6} = m\dot{x}_{4_0} - \frac{\partial F_x}{\partial \dot{x}_6} \end{aligned} \right\} \quad \begin{array}{l} (391 \\ \text{Contd.}) \end{array}$$

and

$$\frac{\partial G_1}{\partial \dot{x}_j} = -\frac{\partial F_x}{\partial \dot{x}_j}, \quad j = 7, 8, \dots, 18 \quad (392)$$

Finally, the K_{1j} are derived from

$$\frac{\partial G_1}{\partial x_j} = -\frac{\partial F_x}{\partial x_j} - \frac{\partial W_x}{\partial x_j}, \quad j = 1, 2, \dots, 18 \quad (393)$$

as follows.

By Equation (346)

$$W_x = -mg \sin (\theta_0 + \theta) \quad (394)$$

Then

$$\frac{\partial W_x}{\partial x_j} = \frac{\partial W_x}{\partial \theta} \frac{\partial \theta}{\partial x_j} \quad (395)$$

From Equation (394)

$$\frac{\partial W_x}{\partial \theta} = -mg \cos \theta_0 \quad (396)$$

According to Equation (382)

$$\frac{\partial \theta}{\partial x_j} = 0, \quad j = 1, 2, 4, 5, 7, 8, \dots, 18 \quad (397)$$

and therefore

$$\frac{\partial W_x}{\partial x_j} = 0, \quad j = 1, 2, 4, 5, 7, 8, \dots, 18 \quad (398)$$

The nonzero partial derivatives of θ are found from equation (383).

Thus

$$\frac{\partial W_x}{\partial x_3} = -mg \cos \theta_0 \cos \phi_0 \quad (399)$$

Since F_x is not a function of x_3 ,

$$\frac{\partial G_1}{\partial x_3} = mg \cos \theta_0 \cos \phi_0 \quad (400)$$

or, comparing with Equation (346)

$$\frac{\partial G_1}{\partial x_3} = W_z \quad (401)$$

Similarly,

$$\frac{\partial G_1}{\partial x_6} = -mg \cos \theta_0 \sin \phi_0 \quad (402)$$

or,

$$\frac{\partial G_1}{\partial x_6} = -W_y \quad (403)$$

For the remainder of the first row of the K-matrix,

$$\frac{\partial G_i}{\partial x_i} = - \frac{\partial F_x}{\partial x_i}, \quad i = 7, 8, \dots, 18 \quad (404)$$

The derivatives of F_x are computed numerically. The approximation is

$$\frac{\partial F_x}{\partial x_i} = \frac{F_x(x_{i0} + \Delta_i) - F_x(x_{i0})}{\Delta_i} \quad (405)$$

where the Δ_i are constants controlled by user input.

11.6.3 Aerodynamic Coefficients in the M Matrix

Effects of rate of change of wing angle of attack on the lift coefficients of each stabilizing surface are included in the M matrix as \dot{W} , or acceleration, derivative in accordance with the analysis in Section 5.5 of Reference 27. As stated in the reference,

The $\dot{\alpha}$ derivatives owe their existence to the fact that the pressure distribution on a wing or tail does not adjust itself instantaneously to its equilibrium value when angle of attack is suddenly changed.

The $\dot{\alpha}$ derivatives discussed in Reference 27 are $C_{Z_{\dot{\alpha}}}$ and $C_{M_{\dot{\alpha}}}$

which correspond to $Z_{\dot{w}}$ and $M_{\dot{w}}$ in C81. In the referenced analysis, the spans of both the wing and tail are assumed to be parallel to a body X-Y plane; consequently, the contributions of $\dot{\alpha}$ to lift affect only the vertical force and the pitching moment. In C81 the $\dot{\alpha}$ derivative is replaced by the \dot{W} derivative, and the stabilizing surface does not necessarily lie in a body X-Y plane; i.e., the surface may have a large dihedral angle. Therefore, the \dot{W} increment is resolved from the body to the wind axis reference system, the change in lift is calculated, and the force is resolved back to the body axis, which yields both a Z and a Y force. The result is that in addition to the conventional $Z_{\dot{w}}$ and $M_{\dot{w}}$ derivatives, side force, rolling moment, and yawing moment derivatives ($Y_{\dot{w}}$, $L_{\dot{w}}$, and $N_{\dot{w}}$) are also included.

11.6.4 Tabulation of the Partial Derivatives

The entire set of partial derivatives is given in Figures 60, 61, and 62. Figure 60 is the M matrix. The elements in this matrix are all determined analytically, and the elements are zero where not otherwise indicated.

The C matrix, Figure 61, contains analytical terms as well as derivatives of the applied forces and moments. The symbol $-\partial$ indicates that

$-\frac{\partial F_i}{\partial x_j}$ is included in the element in the i th row, j th column.

In the K matrix, Figure 62,

$-\frac{\partial F_i}{\partial x_j}$ is indicated in the same manner.

INERTIAL MATRIX

$\frac{\partial}{\partial}$	\ddot{u}	\dot{u}	\ddot{q}	\dot{q}	\ddot{v}	\dot{v}	\ddot{p}	\dot{p}	\ddot{f}	\dot{f}	\ddot{p}_{1H}	\dot{p}_{1H}	\ddot{p}_{2H}	\dot{p}_{2H}	\ddot{p}_{3H}	\dot{p}_{3H}	\ddot{p}_{4H}	\dot{p}_{4H}	\ddot{b}_{1H}	\dot{b}_{1H}	\ddot{p}_{1T}	\dot{p}_{1T}	\ddot{p}_{2T}	\dot{p}_{2T}	\ddot{p}_{3T}	\dot{p}_{3T}	\ddot{p}_{4T}	\dot{p}_{4T}	\ddot{a}_{1T}	\dot{a}_{1T}	\ddot{b}_{1T}	\dot{b}_{1T}	
1	m																																
2		$m \cdot z_0$																															
3		$-I_y$																															
4		$-I_y$																															
5		$-I_y$																															
6		$-I_y$																															
7		$I_{1H} \dot{u}$		$I_{1H} \ddot{u}$		$I_{1H} \dot{v}$		$I_{1H} \ddot{v}$		$I_{1H} \dot{p}$		$I_{1H} \ddot{p}$		$I_{1H} \dot{f}$		$I_{1H} \ddot{f}$		$I_{1H} \dot{p}_{1H}$		$I_{1H} \ddot{p}_{1H}$		$I_{1H} \dot{p}_{2H}$		$I_{1H} \ddot{p}_{2H}$		$I_{1H} \dot{p}_{3H}$		$I_{1H} \ddot{p}_{3H}$		$I_{1H} \dot{p}_{4H}$		$I_{1H} \ddot{p}_{4H}$	
8		$I_{2H} \dot{u}$		$I_{2H} \ddot{u}$		$I_{2H} \dot{v}$		$I_{2H} \ddot{v}$		$I_{2H} \dot{p}$		$I_{2H} \ddot{p}$		$I_{2H} \dot{f}$		$I_{2H} \ddot{f}$		$I_{2H} \dot{p}_{1H}$		$I_{2H} \ddot{p}_{1H}$		$I_{2H} \dot{p}_{2H}$		$I_{2H} \ddot{p}_{2H}$		$I_{2H} \dot{p}_{3H}$		$I_{2H} \ddot{p}_{3H}$		$I_{2H} \dot{p}_{4H}$		$I_{2H} \ddot{p}_{4H}$	
9		$I_{3H} \dot{u}$		$I_{3H} \ddot{u}$		$I_{3H} \dot{v}$		$I_{3H} \ddot{v}$		$I_{3H} \dot{p}$		$I_{3H} \ddot{p}$		$I_{3H} \dot{f}$		$I_{3H} \ddot{f}$		$I_{3H} \dot{p}_{1H}$		$I_{3H} \ddot{p}_{1H}$		$I_{3H} \dot{p}_{2H}$		$I_{3H} \ddot{p}_{2H}$		$I_{3H} \dot{p}_{3H}$		$I_{3H} \ddot{p}_{3H}$		$I_{3H} \dot{p}_{4H}$		$I_{3H} \ddot{p}_{4H}$	
10		$I_{4H} \dot{u}$		$I_{4H} \ddot{u}$		$I_{4H} \dot{v}$		$I_{4H} \ddot{v}$		$I_{4H} \dot{p}$		$I_{4H} \ddot{p}$		$I_{4H} \dot{f}$		$I_{4H} \ddot{f}$		$I_{4H} \dot{p}_{1H}$		$I_{4H} \ddot{p}_{1H}$		$I_{4H} \dot{p}_{2H}$		$I_{4H} \ddot{p}_{2H}$		$I_{4H} \dot{p}_{3H}$		$I_{4H} \ddot{p}_{3H}$		$I_{4H} \dot{p}_{4H}$		$I_{4H} \ddot{p}_{4H}$	
11				$-I_{RM} \ddot{u}$				$-I_{RM} \ddot{v}$		$-I_{RM} \ddot{p}$		$-I_{RM} \ddot{f}$		$-I_{RM} \ddot{p}_{1H}$		$-I_{RM} \ddot{p}_{2H}$		$-I_{RM} \ddot{p}_{3H}$		$-I_{RM} \ddot{p}_{4H}$													
12				$-I_{RM} \ddot{u}$				$-I_{RM} \ddot{v}$		$-I_{RM} \ddot{p}$		$-I_{RM} \ddot{f}$		$-I_{RM} \ddot{p}_{1H}$		$-I_{RM} \ddot{p}_{2H}$		$-I_{RM} \ddot{p}_{3H}$		$-I_{RM} \ddot{p}_{4H}$													
13		$I_{1T} \dot{u}$		$I_{1T} \ddot{u}$		$I_{1T} \dot{v}$		$I_{1T} \ddot{v}$		$I_{1T} \dot{p}$		$I_{1T} \ddot{p}$		$I_{1T} \dot{f}$		$I_{1T} \ddot{f}$		$I_{1T} \dot{p}_{1H}$		$I_{1T} \ddot{p}_{1H}$		$I_{1T} \dot{p}_{2H}$		$I_{1T} \ddot{p}_{2H}$		$I_{1T} \dot{p}_{3H}$		$I_{1T} \ddot{p}_{3H}$		$I_{1T} \dot{p}_{4H}$		$I_{1T} \ddot{p}_{4H}$	
14		$I_{2T} \dot{u}$		$I_{2T} \ddot{u}$		$I_{2T} \dot{v}$		$I_{2T} \ddot{v}$		$I_{2T} \dot{p}$		$I_{2T} \ddot{p}$		$I_{2T} \dot{f}$		$I_{2T} \ddot{f}$		$I_{2T} \dot{p}_{1H}$		$I_{2T} \ddot{p}_{1H}$		$I_{2T} \dot{p}_{2H}$		$I_{2T} \ddot{p}_{2H}$		$I_{2T} \dot{p}_{3H}$		$I_{2T} \ddot{p}_{3H}$		$I_{2T} \dot{p}_{4H}$		$I_{2T} \ddot{p}_{4H}$	
15		$I_{3T} \dot{u}$		$I_{3T} \ddot{u}$		$I_{3T} \dot{v}$		$I_{3T} \ddot{v}$		$I_{3T} \dot{p}$		$I_{3T} \ddot{p}$		$I_{3T} \dot{f}$		$I_{3T} \ddot{f}$		$I_{3T} \dot{p}_{1H}$		$I_{3T} \ddot{p}_{1H}$		$I_{3T} \dot{p}_{2H}$		$I_{3T} \ddot{p}_{2H}$		$I_{3T} \dot{p}_{3H}$		$I_{3T} \ddot{p}_{3H}$		$I_{3T} \dot{p}_{4H}$		$I_{3T} \ddot{p}_{4H}$	
16		$I_{4T} \dot{u}$		$I_{4T} \ddot{u}$		$I_{4T} \dot{v}$		$I_{4T} \ddot{v}$		$I_{4T} \dot{p}$		$I_{4T} \ddot{p}$		$I_{4T} \dot{f}$		$I_{4T} \ddot{f}$		$I_{4T} \dot{p}_{1H}$		$I_{4T} \ddot{p}_{1H}$		$I_{4T} \dot{p}_{2H}$		$I_{4T} \ddot{p}_{2H}$		$I_{4T} \dot{p}_{3H}$		$I_{4T} \ddot{p}_{3H}$		$I_{4T} \dot{p}_{4H}$		$I_{4T} \ddot{p}_{4H}$	
17				$-I_{RT} \ddot{u}$				$-I_{RT} \ddot{v}$		$-I_{RT} \ddot{p}$		$-I_{RT} \ddot{f}$		$-I_{RT} \ddot{p}_{1H}$		$-I_{RT} \ddot{p}_{2H}$		$-I_{RT} \ddot{p}_{3H}$		$-I_{RT} \ddot{p}_{4H}$													
18				$-I_{RT} \ddot{u}$				$-I_{RT} \ddot{v}$		$-I_{RT} \ddot{p}$		$-I_{RT} \ddot{f}$		$-I_{RT} \ddot{p}_{1H}$		$-I_{RT} \ddot{p}_{2H}$		$-I_{RT} \ddot{p}_{3H}$		$-I_{RT} \ddot{p}_{4H}$													

Figure 60. Inertial Matrix.

DAMPING MATRIX														
$\frac{x}{c}$	u	w	q	v	p	r	\dot{p}_{11}	\dot{p}_{21}	\dot{p}_{31}	\dot{p}_{41}	\dot{p}_{12}	\dot{p}_{22}	\dot{p}_{32}	\dot{p}_{42}
1	-0	$m_{00} \cdot 0$	$m_{00} \cdot 0$	$m_{00} \cdot 0$	-0	$-m_{00} \cdot 0$	-0	-0	-0	-0	-0	-0	-0	-0
2	$-m_{00} \cdot 0$	-0	$-m_{00} \cdot 0$	$m_{00} \cdot 0$	$m_{00} \cdot 0$	-0	-0	-0	-0	-0	-0	-0	-0	-0
3	-0	-0	-0	-0	$(1_x - 1_z) \cdot 0 \cdot 21 \cdot xz \cdot 0$	$(1_x - 1_z) \cdot 0 \cdot 21 \cdot xz \cdot 0$	-0	-0	-0	-0	-0	-0	-0	-0
4	$m_{00} \cdot 0$	$-m_{00} \cdot 0$	-0	-0	$-m_{00} \cdot 0$	$m_{00} \cdot 0$	-0	-0	-0	-0	-0	-0	-0	-0
5	-0	-0	$(1_z - 1_y) \cdot 0 \cdot 1 \cdot xz \cdot 0$	-0	$-1 \cdot xz \cdot 0$	$(1_z - 1_y) \cdot 0 \cdot 0$	-0	-0	-0	-0	-0	-0	-0	-0
6	-0	-0	$(1_y - 1_x) \cdot 0 \cdot 1 \cdot xz \cdot 0$	-0	$(1_y - 1_x) \cdot 0 \cdot 0$	$1 \cdot xz \cdot 0$	-0	-0	-0	-0	-0	-0	-0	-0
7	-0	-0	-0	-0	-0	-0	$2 \cdot (1_y \cdot 0 \cdot 0)$	-0	-0	-0	-0	-0	-0	-0
8	-0	-0	-0	-0	-0	-0	-0	$2 \cdot (1_x \cdot 0 \cdot 0)$	-0	-0	-0	-0	-0	-0
9	-0	-0	-0	-0	-0	-0	-0	-0	$2 \cdot (1_y \cdot 0 \cdot 0)$	-0	-0	-0	-0	-0
10	-0	-0	-0	-0	-0	-0	-0	-0	-0	$2 \cdot (1_x \cdot 0 \cdot 0)$	-0	-0	-0	-0
11	-0	-0	-0	-0	$-2 \cdot 0 \cdot 0 \cdot 0 \cdot 1 \cdot 1 \cdot 0$	$-2 \cdot 0 \cdot 0 \cdot 0 \cdot 1 \cdot 0 \cdot 1 \cdot 0$	-0	-0	-0	-0	-0	-0	-0	-0
12	-0	-0	$2 \cdot 0 \cdot 0 \cdot 0 \cdot 1 \cdot 0 \cdot 2 \cdot 0$	-0	$2 \cdot 0 \cdot 0 \cdot 0 \cdot 1 \cdot 0 \cdot 2 \cdot 0$	$2 \cdot 0 \cdot 0 \cdot 0 \cdot 1 \cdot 0 \cdot 2 \cdot 0$	-0	-0	-0	-0	-0	-0	-0	-0
13	-0	-0	-0	-0	-0	-0	-0	-0	-0	-0	$2 \cdot (1_y \cdot 0 \cdot 0)$	-0	-0	-0
14	-0	-0	-0	-0	-0	-0	-0	-0	-0	-0	-0	$2 \cdot (1_x \cdot 0 \cdot 0)$	-0	-0
15	-0	-0	-0	-0	-0	-0	-0	-0	-0	-0	-0	-0	$2 \cdot (1_y \cdot 0 \cdot 0)$	-0
16	-0	-0	-0	-0	-0	-0	-0	-0	-0	-0	-0	-0	-0	$2 \cdot (1_x \cdot 0 \cdot 0)$
17	-0	-0	-0	-0	$-2 \cdot 0 \cdot 0 \cdot 0 \cdot 1 \cdot 1 \cdot 1 \cdot 0$	$-2 \cdot 0 \cdot 0 \cdot 0 \cdot 1 \cdot 1 \cdot 1 \cdot 0$	-0	-0	-0	-0	-0	-0	-0	$-2 \cdot 0 \cdot 0 \cdot 0 \cdot 1 \cdot 1 \cdot 1 \cdot 0$
18	-0	-0	$2 \cdot 0 \cdot 0 \cdot 0 \cdot 1 \cdot 0 \cdot 2 \cdot 0$	-0	$2 \cdot 0 \cdot 0 \cdot 0 \cdot 1 \cdot 0 \cdot 2 \cdot 0$	$2 \cdot 0 \cdot 0 \cdot 0 \cdot 1 \cdot 0 \cdot 2 \cdot 0$	-0	-0	-0	-0	-0	-0	-0	-0

Figure 61. Damping Matrix.

STIFFNESS MATRIX

X	f_{uat}	f_{wat}	f_{vot}	f_{rot}	P_{JM}	P_{2M}	P_{3M}	P_{4M}	θ_{JM}	b_{JM}	P_{1I}	P_{2I}	P_{3I}	P_{4I}	θ_{1I}	b_{1I}
6																
1	W_z			$-W_y$							-0	-0	-0	-0	-0	-0
2	$-W_x$			W_y							-0	-0	-0	-0	-0	-0
3											-0	-0	-0	-0	-0	-0
4				$-W_z$							-0	-0	-0	-0	-0	-0
5				W_x							-0	-0	-0	-0	-0	-0
6											-0	-0	-0	-0	-0	-0
7					w_{1I}^2-0	-0	-0	-0		-0						
8					-0	w_{2I}^2-0	-0	-0		-0						
9					-0	-0	w_{3I}^2-0	-0		-0						
10					-0	-0	-0	w_{4I}^2-0		-0						
11					-0	-0	-0	-0		-0						
12					-0	-0	-0	-0		-0						
13											w_{1I}^2-0	-0	-0	-0	-0	-0
14											-0	w_{2I}^2-0	-0	-0	-0	-0
15											-0	-0	w_{3I}^2-0	-0	-0	-0
16											-0	-0	-0	w_{4I}^2-0	-0	-0
17											-0	-0	-0	-0	-0	-0
18											-0	-0	-0	-0	-0	-0

Note: -0 indicates $-\partial F_i / \partial X_j$

Figure 62. Stiffness Matrix.

11.7 CONTROL POWER DERIVATIVES AND TRANSFER FUNCTIONS

Once the stick-fixed-stability frequencies and mode shapes are determined, transfer functions and frequency response for the three attitude controls are found. The transfer functions of primary interest are pitch response to longitudinal cyclic, roll response to lateral cyclic, and yaw response to pedal. Transfer functions for other combinations of fuselage degrees of freedom and rotor flapping may be obtained by selection of appropriate values of IPL(93). Define the four control inputs for which control power derivatives are determined as

C_1 = disturbance of collective stick from trim position

C_2 = disturbance of longitudinal cyclic stick from trim position

C_3 = disturbance of lateral cyclic stick from trim position

C_4 = disturbance of pedal from trim position

Then the set of equations represented by (360) becomes the set of equations for forced motion.

$$\sum_j \left. \frac{\partial G_i}{\partial x_j} \right|_0 x_j + \sum_j \left. \frac{\partial G_i}{\partial \dot{x}_j} \right|_0 \dot{x}_j + \sum_j \left. \frac{\partial G_i}{\partial \ddot{x}_j} \right|_0 \ddot{x}_j = \sum_k \frac{\partial G_i}{\partial C_k} C_k \quad (406)$$

The solution of these equations to obtain the transfer functions is done by the use of Cramer's rule. The denominator is already available from the stick fixed stability analysis. The numerator is obtained by replacing one column of the stiffness matrix with one column from the control power matrix. For the pitch response to longitudinal cyclic, the third column of the stiffness matrix ($\int Q dt$) is replaced by the second column of the control matrix (longitudinal cyclic). The solution procedure is the same as described in Section 11.5.2. The same procedure is used for each transfer function.

By making use of the transfer functions, the frequency response is found for the three variables of interest. The frequency response calculations are described by the following equation:

$$F(\omega) = \left. \frac{\text{Gain}(S+Z_1)(S+Z_2)\dots(S+Z_m)}{(S+P_1)(S+P_2)\dots(S+P_n)} \right|_{S = j\omega} \quad (407)$$

where

z_1, z_2 , etc., are the roots of the forced response equations

p_1, p_2 , etc., are the roots of the stick fixed equations
and $j = \sqrt{-1}$

$F(\omega)$ is evaluated for a number of values of ω between 0.01 and 100 radian/second for the C81 output.

11.8 THE OUTPUT

The Stability Analysis section in C81 produces output in the form of eigenvalues and eigenvectors which is immediately useful to the user. Also, the control power derivatives are computed and listed. With these values, complete information for control transfer function parameters is listed. A detailed explanation of the STAB output is given in Section 4.11 of Volume II.

12.0 MANEUVER SIMULATION

12.1 INTRODUCTION

Since the capability of simulating maneuvers was first added to C81, the four-cycle Runge-Kutta method has been used to integrate numerically the equations of motion during such simulations. Over the years, several new methods of numerical integration have been developed and some previously existing methods have come into more prevalent use. Consequently, a study was conducted in 1973 under Contract DAAJ02-72-C-0098, to determine which of the available techniques of numerical integration is most suitable to the system of differential equations used in C81.

Four criteria were used to assess each method:

- (1) Compatibility with the type of differential equations in C81
- (2) Accuracy of the integration
- (3) Computer time required to perform the integration
- (4) Computer storage requirements for the algorithm

With regard to the first criterion, certain techniques of numerical integration are unstable or otherwise unsuitable when applied to certain types of differential equations. For example, the system of equations in C81 includes many differential equations, some of which have little harmonic content and some of which have relatively high harmonics. This situation automatically eliminated from consideration several techniques which are known to have difficulty when simultaneously integrating both types of equations.

The second and third criteria had to be considered as trade-offs and in most cases as a single criterion. That is, given an unlimited amount of computer time, almost any method could meet any prescribed accuracy requirement. However, given a limited or specified amount of computer time, the accuracy of a method could be adversely affected. In view of the historical use of the Runge-Kutta method, its accuracy and time requirements were taken as baseline values for evaluating other methods.

Only minor emphasis was placed on the fourth criterion. The reasoning was (1) that the Runge-Kutta technique was only responsible for about 5 percent of the total program storage for the AGAJ72 version of C81 and would account for an even

smaller percentage of the storage requirements for later versions, and (2) that the advent of larger computers and virtual memory systems reduces the importance of storage requirements. Hence, numerical techniques which would require up to twice the storage of the Runge-Kutta method were still considered acceptable.

12.2 EVALUATION OF TECHNIQUES OF NUMERICAL INTEGRATION

Ten methods of numerical integration were examined during the study. The following procedure was used to evaluate the methods. The fore-and-aft and lateral flapping rate equations from C81 were chosen as a typical set of equations which any method would need to solve.

$$\frac{dp}{dt} = -\Omega q - F_A \quad (408)$$

$$\frac{dq}{dt} = \Omega p - F_B \quad (409)$$

where F_B and F_A are forcing functions,

Ω is rotor speed, and
 p and q are rotor roll and pitch rates, respectively.

These equations were programmed on an analog computer, and the responses to several forcing functions such as those shown in Figure 63 were computed. Response data to the same forcing functions were also computed with a very small error tolerance on the Runge-Kutta numerical method. The resulting analog and digital data (which were within the accuracy limitations of the respective computations) were then defined to be the baseline against which the remaining nine methods of numerical integration would be compared.

Where possible, existing computer subroutines for the methods studied were used to compute the response of Equations (408) and (409) to the same forcing functions used in the baseline case. Some of the simpler methods for which programming did not exist were programmed and evaluated in a similar manner.

This initial phase of the study indicated that, of the methods which were examined and are currently available, Hamming's predictor-corrector method was the best with respect to the four criteria stated above. The current Runge-Kutta method was judged to be the next best. Seven other methods were deemed not suitable. The tenth technique (the Adams-Krogh method) was judged to show much promise but was considered to be too experimental, not yet checked out thoroughly enough by the originator of the method, and not sufficiently documented to be

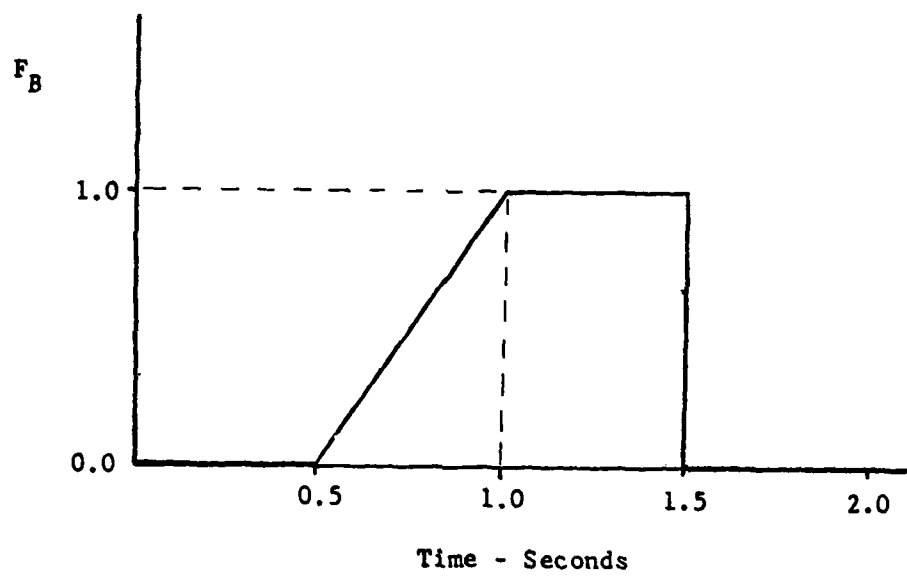
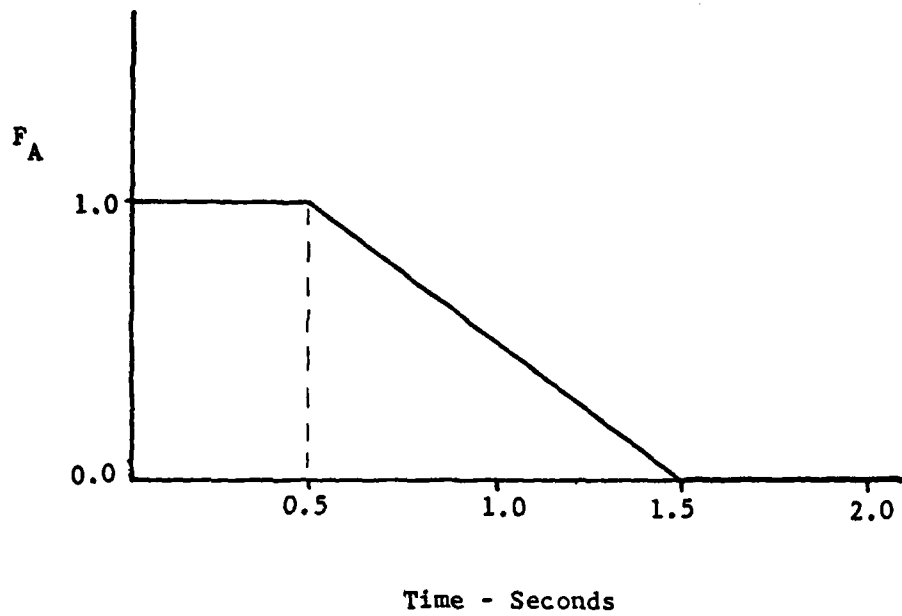


Figure 63. Forcing Functions Used in Study of Techniques.

included as one of the two best methods. However, it was felt that the Adams-Krogh method should be reconsidered in the future.

A brief description (including some equations) and a few remarks about each of the 10 methods evaluated follow. The sources for most of the methods can be found in the selected bibliography given in Section 16.

12.2.1 Runge-Kutta Method

Consider a first-order differential equation

$$\frac{dy}{dt} = f(t, y) \quad (410)$$

with initial values t_0 and y_0 . The increment for advancing the dependent variable is given in

$$\Delta y = \frac{\Delta t}{6} (f_1 + 2f_2 + 2f_3 + f_4) \quad (411)$$

where Δt is the time step (independent variable) and

$$f_1 = f(t_0, y_0) \quad (412)$$

$$f_2 = f(t_0 + \frac{\Delta t}{2}, y_0 + \frac{\Delta t}{2}f_1) \quad (413)$$

$$f_3 = f(t_0 + \frac{\Delta t}{2}, y_0 + \frac{\Delta t}{2}f_2) \quad (414)$$

$$f_4 = f(t_0 + \Delta t, y_0 + \Delta t f_3) \quad (415)$$

The values at (t_1, y_1) are then given by

$$t_1 = t_0 + \Delta t \quad (416)$$

and

$$y_1 = y_0 + \Delta y. \quad (417)$$

The value of Δy for the second interval is computed by the same formulas with (t_0, y_0) replaced by (t_1, y_1) .

This is one of the most widely used methods of numerical integration. It is stable and self-starting, step size is easy to change at any step in the calculations, its computational routine has fewer formulas, and the routine is easily programmed. It requires four function evaluations per time step. This method was judged to be the second best of the methods studied.

12.2.2 Treanor's Method

This method, in general, is similar to the Runge-Kutta method with the exception that evaluation of f_4 in Equation (415) is modified as shown below.

$$f_4 = f(t_0 + \frac{\Delta t}{2}, y_0 + \Delta t f_m) \quad (418)$$

where

$$f_m = 2f_3g_2 + (g_1 - 2g_2)f_1 + pf_2g_2\Delta t \quad (419)$$

$$P = \text{Max} \begin{cases} \frac{2(f_2 - f_3)}{\Delta t(f_2 - f_1)} \\ 0 \end{cases} \quad (420)$$

$$g_1 = \frac{-1}{p\Delta t} e^{-p\Delta t} \quad (421)$$

$$g_2 = \frac{g_1 - 1}{-p\Delta t} \quad (422)$$

By using this method to solve a set of stiff equations, larger step size can be applied and more accurate results can be obtained than those from the Runge-Kutta method. However, for harmonic functions it can lead to dividing by zero. In view of the harmonic nature of many parameters in C81, this method was rejected.

12.2.3 Hamming's Predictor-Corrector Method

This is a stable fourth-order integration procedure that requires the function evaluation only twice per time step. This is a great advantage compared with other methods of the same order of accuracy. Another advantage is that at each step the calculation procedure gives an estimate for the local truncation error. Thus, the procedure is able to automatically change the step size. However, this is not a self-starting method. To obtain the starting values, a special Runge-Kutta procedure followed by one iteration step is added to the predictor-corrector method. This special procedure is also used to take care of any discontinuities which may cause trouble to the predictor-corrector method.

To evaluate the function at $(n+1)^{\text{th}}$ time point, it is necessary to go through the formulas below.

$$\text{Predictor: } P_{n+1} = y_{n-3} + \frac{4\Delta t}{3}(2y'_n - y'_{n-1} + 2y'_{n-2}) \quad (423)$$

$$\text{Modifier: } M_{n+1} = P_{n+1} - \frac{112}{121}(P_n - C_n) \quad (424)$$

$$M'_{n+1} = f(t_{n+1}, M_{n+1}) \quad (425)$$

$$\text{Corrector: } C_{n+1} = \frac{1}{8} [9y_n - y_{n-2} + 3\Delta t(M'_{n+1} - 2y'_n - y'_{n-1})] \quad (426)$$

$$\text{Final Values: } y_{n+1} = C_{n+1} + \frac{9}{121}(P_{n+1} - C_{n+1}) \quad (427)$$

$$y'_{n+1} = f(t_{n+1}, y_{n+1}) \quad (428)$$

Note that

$$y' = dy/dt = f(t, y) \text{ with } y(t_0) = y_0 \quad (429)$$

Hamming's method was selected and programmed in C81, but it was later deleted due to unsatisfactory performance. As a predictor-corrector method it could not handle the discontinuous forcing functions found in the rotor equations.

12.2.4 Finite Difference Method

This is one of the most stable methods. It is self-starting and it is easy to change step size.

For a system of this form,

$$a\ddot{y} \pm b\dot{y} \pm cy = f(t) \quad (430)$$

The first step is to define an estimated value for the second time derivative of y , $y_g(t)$.

Next, initial values of $y(0)$, $\dot{y}(0)$, and $\ddot{y}(0)$ are used to solve for estimated values of $y(t)$ and $\dot{y}(t)$:

$$\dot{y}_g(t) = \dot{y}(0) + \frac{\Delta t}{2} [\ddot{y}(0) + \ddot{y}_g(t)] \quad (431)$$

$$y_g(t) = y(0) + \frac{\Delta t}{2} [\dot{y}_g(t) + \dot{y}(0)] \quad (432)$$

$$+ \frac{(\Delta t)^2}{6} [\ddot{y}_g(t) - \ddot{y}(0)] \quad (433)$$

where Δt is the step size.

Equation (430) can then be solved for a computed value of \ddot{y} , i.e., $\ddot{y}_c(t)$:

$$\ddot{y}_c(t) = [f(t) - b\dot{y}_g(t) - cy_g(t)] / a. \quad (434)$$

Finally, if

$$\left| \frac{\ddot{y}_c(t) - \ddot{y}_g(t)}{\ddot{y}_c(t)} \right| = \left| \frac{\Delta \ddot{y}(t)}{\ddot{y}_c(t)} \right| \leq \varepsilon \quad (435)$$

where ε is some preassigned accuracy limit, the system can be regarded as solved at the time point t . If the above convergence criterion is not met, a new estimated value of $y_g(t)$ is provided by a procedure which uses previous $\Delta \ddot{y}$ and \ddot{y}_g values to find a solution which minimizes $\Delta \ddot{y}$. The process repeats itself until the convergence criterion is met. Since this is an iterative procedure, it may take considerable computer time to solve a large system of equations. Considering the size of the system of equations in C81, this method was also rejected.

12.2.5 Milne Method

This is a predictor-corrector type method. It uses

$$y_{n+1} = y_{n-3} + \frac{4}{3}\Delta t(2y'_n - y'_{n-1} + 2y'_{n-2}) \quad (436)$$

as a predictor and

$$y_{n+1} = y_{n-1} + \frac{\Delta t}{3}(y'_{n+1} + 4y'_n + y'_{n-1}) \quad (437)$$

as a corrector. It requires four previous values to start the method. For systems with positive damping, equations solved by this method are unstable because each single error is magnified exponentially, while the exact solution decays. Since nothing precludes positive damping in C81, this method was rejected.

12.2.6 Adam's Method

This is also a predictor-corrector type method. It uses

$$y_{n+1} = y_n + \frac{\Delta t}{24}(55y'_n - 59y'_{n-1} + 37y'_{n-2} - 9y'_{n-3}) \quad (438)$$

as a predictor and

$$Y_{n+1} = Y_n + \frac{\Delta t}{24}(9y'_{n+1} + 19y'_n - 5y'_{n-1} + y'_{n-2}) \quad (439)$$

as a corrector. Although it needs four previous values to start, the method is stable. This method was programmed for comparison to the analog-digital baseline response data discussed previously. Based on time and accuracy criteria, Adam's method was inferior to Runge-Kutta and was consequently rejected.

12.2.7 Gear's Method

This is a multistep predictor-corrector method. The step size may be specified by the user, but is changed by the subroutine DIFSUB (Reference 30) to limit the estimated error to a specified tolerance. The orders of the predictor-corrector formulas are automatically chosen by the subroutine as the integration proceeds. Up to three corrector iterations can be taken.

In highly damped systems, this method can use large time steps through most of the integration region, as shown in Reference 30, where this method is compared with Adam's. When forcing functions are of harmonic forms, which are typical helicopter equations, test runs of subroutine DIFSUB indicated that Adam's method, discussed in the previous section, is more efficient. Since Adam's method was inferior to Runge-Kutta, Gear's method being inferior to Adam's method was considered sufficient grounds for rejecting Gear's method.

12.2.8 A Predictor-Corrector Method

In Hamming's method, the predictor is calculated first, then modifier, corrector, and final value. Before proceeding to the next time point, it evaluates derivatives. In the type of predictor-corrector method considered here, the concept is to try to replace derivative evaluation by numerical differentiation. Thus, at each time point only one function value is needed. Unfortunately, the numerical differentiation is unstable and its result is not accurate enough. Hence, this method was also rejected.

³⁰Gear, C. William, NUMERICAL INITIAL VALUE PROBLEMS IN ORDINARY DIFFERENTIAL EQUATIONS, Prentice-Hall, New York, 1971, pp. 83-84.

12.2.9 Forward Method

This is one of the simplest predictor-corrector type methods. The predictor formula is

$$y_{n+1} = y_n + \Delta t y'_n \quad (440)$$

and the corrector formula is

$$y_{n+1} = y_n + \frac{\Delta t}{2}(y'_n + y'_{n+1}) \quad (441)$$

It requires only one previous function value. Therefore, it is easier to incorporate into any system. Unfortunately, the step size must be kept small to assure sufficient accuracy. To match the accuracy of Runge-Kutta, the required time step is so small that the computation time becomes too great with respect to Runge-Kutta computation time. Hence, this method was rejected.

12.2.10 Adams-Krogh Method

This method is a self-starting, predictor corrector type method with variable order and variable step size. The change in step size is carried out by using modified divided differences.

Although this method appeared to combine some of the better features of several of the techniques examined, it is a very new technique and not yet thoroughly checked out. Hence, this method was rejected primarily because of its unknown characteristics rather than for any adverse qualities. It is felt that the method shows considerable promise and should be reconsidered as a new or alternate technique for numerical integration in C81 when the method is better known and more thoroughly documented.

12.3 CURRENT PROGRAM OPTIONS

As a result of the study discussed in the previous section, Hamming's predictor-corrector method of numerical integration was programmed into C81. The test cases during the study had indicated that Hamming's method required fewer function evaluations than the Runge-Kutta method and that it should reduce the run time of a maneuver by 25 to 40 percent as compared to runs with Runge-Kutta.

When Hamming's method was chosen for incorporation into C81, the decision was also made to retain the Runge-Kutta method in the program until the checkout of Hamming's method was

complete. Hence, Hamming's method was installed as a programmer option. The logic was structured such that the two methods of numerical integration were completely independent of each other. Although this parallel logic was originally intended to simplify the removal of the second best method at the end of the comparison phase of the study, it greatly facilitated switching from one method to the other during checkout.

The comparison phase of the study concluded that Hamming's method did not live up to expectation. In particular, run times with Hamming's method were 20 to 30 percent longer than the corresponding Runge-Kutta runs. Curiously enough, the cause of the longer than anticipated run time with Hamming's method was traced to the integration of the rotor flapping equations given by Equations (408) and (409) in this report. Specifically, the C81 program found it necessary to halve the time increment more often than in the test case run outside of C81. The reason for the increased number of step size reductions was apparently the presence of aerodynamic damping in the C81 equation and lack of it in the external test cases. Efforts to reduce the run time of Hamming's method to less than those with Runge-Kutta failed. Hamming's method was retained in C81 until 1976, when its lack of use and high core storage requirements caused it to be removed.

13.0 COUPLED ROTOR STABILITY ANALYSIS

13.1 GENERAL

Rotor stability has been recognized for many years as a prime requirement for safe rotary wing aircraft flight. A number of analyses have been developed to examine rotor dynamic characteristics. These analyses have been characterized by simplification in some portions of the coupled rotor/fuselage representation. A restriction in the number of degrees of freedom, simplifying assumptions in the aerodynamics, or restrictions in the types of rotor systems treated were the primary limitations of existing methods.

As a part of Contract DAAJ02-75-C-0025, a study was conducted to find a rotor stability analysis method which could be applied to C81. Several constraints were placed on any method considered to fulfill this function. It had to fit into the form of the existing C81 program so that all of the C81 equations would not have to be rewritten. That is, it had to be able to handle equations in an implicit rather than explicit form. The stability method would have to be general enough to employ the same mathematical model used by the rest of C81 in order to provide a fully coupled, general analysis which requires only the standard C81 input deck. Finally, some consideration had

³¹Kinnen, Edwin and Chen, Chiou Shiun, LYAPUNOV FUNCTIONS FOR A CLASS OF nth ORDER NONLINEAR DIFFERENTIAL EQUATIONS, NASA CR-687, January 1967.

³²Crimi, Peter, A METHOD FOR ANALYZING THE AEROELASTIC STABILITY OF A HELICOPTER ROTOR IN FORWARD FLIGHT, NASA CR-1332, 1968.

³³Piarulli, V. J., and White, R. P., Jr., A METHOD FOR DETERMINING THE CHARACTERISTIC FUNCTIONS ASSOCIATED WITH THE AEROELASTIC INSTABILITIES OF HELICOPTER ROTORS IN FORWARD FLIGHT, NASA CR-1577, June 1970.

³⁴Peters, D. A., and Hohenemser, K. H., APPLICATION OF THE FLOQUET TRANSITION MATRIX TO PROBLEMS OF LIFTING ROTOR STABILITY, Journal of the American Helicopter Society, Volume 16, Number 2, 1971, pp. 25-33.

³⁵Friedman, Peretz, and Silverthorn, Louis J., AEROELASTIC STABILITY OF COUPLED FLAP-LAG MOTION OF HINGELESS HELICOPTER BLADES AT ARBITRARY ADVANCE RATIOS, NASA CR-132,431, February 1974.

³⁶Hsu, C. S., and Cheng, W. H., APPLICATIONS OF THE THEORY OF IMPULSIVE PARAMETRIC EXCITATION AND NEW TREATMENTS OF GENERAL PARAMETRIC EXCITATION PROBLEMS, Transactions of the ASME, Paper Number 73-WA/APM-6, March 1973.

to be given to computer run time in order to try to keep the computer usage within practical limits. It was thought that C81 should be used to check the stability boundaries which had already been defined by some simpler and cheaper program so that computer usage would not be a strictly confining restraint.

During the investigation of stability methods, several different approaches were found described in the literature. A purely mathematical approach to the general problem of determining stability of nonlinear differential equations by use of the Lyapunov method, as found in Reference 31, was rapidly discarded because of the uncertainty of obtaining any answer at all. In References 32 and 33, we found typical simplified methods where linearized perturbation equations are developed strictly for the purpose of obtaining stability data for helicopters. The methods used by these analysts could not be applied to C81. The methods which were deemed to be worth further study were either based on Floquet theory or the numerical analysis of time-history data. A straightforward application of Floquet theory was found in Reference 34, and a more efficient method was shown in References 35 and 36. The Floquet technique showed much promise initially, but as it was tried on more complex systems it became unreliable. The remaining stability analysis methods were based on the numerical analysis of the time-history data. One description of the moving-block technique is given in Reference 37. The randomdec method of Reference 38 and the combination moving block/randomdec of Reference 37 were considered and discarded because they were not applicable to helicopter problems. Prony's method, as described in References 39 and 40, was found to be one of the best numerical techniques.

13.2 STUDY OF FLOQUET TECHNIQUE

The Floquet theory is a valid method for determining the stability of linear, homogeneous, differential equations with

³⁷Hammond, C. E., and Doggett, R. V., Jr., DETERMINATION OF SUBCRITICAL DAMPING BY MOVING BLOCK/RANDOMDEC APPLICATIONS, Proceedings of the NASA Symposium on Flutter Testing Techniques, Flight Research Center, Edwards Air Force Base, California, October 1975.

³⁸Cole, Henry A., Jr., ON-LINE FAILURE DETECTION AND DAMPING MEASUREMENT OF AEROSPACE STRUCTURES BY RANDOM DECREMENT SIGNATURES, NASA CR-2205, March 1973.

³⁹Kelly, Louis G., HANDBOOK OF NUMERICAL METHODS AND APPLICATIONS, Addison-Wesley, Reading, Massachusetts, 1967, p. 80.

⁴⁰Myhill, J., and Gaal, P. H., ANALYSIS FOR EXPONENTIALS, Proceedings of the AIAA/AICHE/AMS/ISA/SCI/SHARE Summer Computer Conference, San Diego, California, June 1972.

periodic coefficients. The development of the theory is shown in detail in References 34 and 35. Here it is sufficient to describe the application of the theory as a two-step process. First, the Floquet Transition Matrix is generated by methods we will describe shortly. Then, the eigenvalues of the Floquet Transition Matrix are found to give the stability and damping of the equations. Actually, the largest eigenvalue, Λ_L , is the least stable, and the real part of the response associated with this root is given by

$$\lambda_L = \frac{1}{2} T \ln[(\text{Re } \Lambda_L)^2 + (\text{Im } \Lambda_L)^2] \quad (442)$$

There were two basic problems in the application of Floquet theory to the equations in C81. First, the general rotorcraft equations are not homogeneous, and because of their implicit form, they could only be made homogeneous by use of some numerical technique. Second, the C81 differential equations are nonlinear, in some cases highly nonlinear, so the validity of the Floquet theory is then open to question.

In order to address these equations in an economical fashion, a small computer program, SIMFLO, was written as a time-history generator. SIMFLO uses a paddle blade element for a single blade on an isolated rotor. It uses a single mode with beamwise, chordwise, and torsional degrees of freedom. The aerodynamic calculations ignore the induced velocity, but include the effects of forward speed, shaft tilt, rotational speed, collective pitch, and cyclic pitch as well as the dynamic response of the blade mode. The lift, drag, and moment coefficients were obtained from a table for a NACA 0012 as a function of angle of attack only. For some special cases, a Mach number squared term was added to the drag coefficient to provide a simple approximation to the Mach number effects. As a means of checking the implementation of the Floquet methods, the Mathieu equation was programmed as an alternate differential equation with known stability boundaries. A discussion of the Mathieu equation may be found in any text on nonlinear differential equations or nonlinear systems even though it is a linear equation.

The Floquet method of References 35 and 36 appeared to be quite attractive when first studied because of the greatly reduced computer time for large systems of equations as compared to Reference 34. The problem with using this method is that it requires an explicit form of the equations at each time point. In matrix notation, the form required is

$$\{\dot{y}\} = [A]\{y\} \quad (443)$$

For a program such as C81 or even SIMFLO, [A] is not available, but it was thought that it might be possible to make some assumption about the form of [A] and still obtain a solution. If [A] is viewed as a transfer function, then any [A] which yields the same results should be valid for use in generating the Floquet Transition Matrix. To begin this study, the procedure was tried for the Mathieu equation for which the actual [A] and the stability results are known. Even on this simplest case the synthesis [A] from {y} and {ẏ} would not produce a valid transition matrix so the method was abandoned.

The application of the Floquet method presented in Reference 34 is fairly simple. A perturbation method has to be used in order to eliminate the nonhomogeneous part of the problem solution. First, a base time history is run for one revolution. Then each state variable is perturbed, one at a time, and a one-revolution time history is run. The differences between the perturbed and the base values of the state variables then determine the Floquet Transition Matrix.

This method worked beautifully on the Mathieu equation. It also worked well for the first cases run with the SIMFLO rotor, which were aimed at finding the value of damping for flapping motion under various conditions. It is known that the Floquet method will work for linear systems, and it is certain that some extreme degree of nonlinearity will make it fail to properly predict the stability. The questions remaining then are how much nonlinearity can the Floquet stand, and is a realistic helicopter equation inside or outside of this limit?

As a first step in finding the nonlinearity limit, an artificial displacement squared spring term was added to the equation so that a known amount of nonlinearity could be added. The coefficient of this term was increased to quite large values without hurting the Floquet results too badly. Even when the response was driven unstable by the spring term, the Floquet method showed the stability boundary. Although these results were encouraging, the nature of the time-history curves as shown in Figure 64 were not typical of the modal response time histories obtained from C81. C81 responses show two or three harmonic functions superimposed rather than the pure 1-per-rev of Figure 64. In order to obtain more realistic response curves, several changes in data and program were made for SIMFLO. First, the study was shifted to look at response of an inplane mode. Then, the natural frequency of the inplane mode was changed to be well above 1-per-rev. Finally, the Mach number squared term was added to the drag coefficient to simulate drag divergence on the advancing blade tip. A typical time history resulting from these changes is shown in Figure

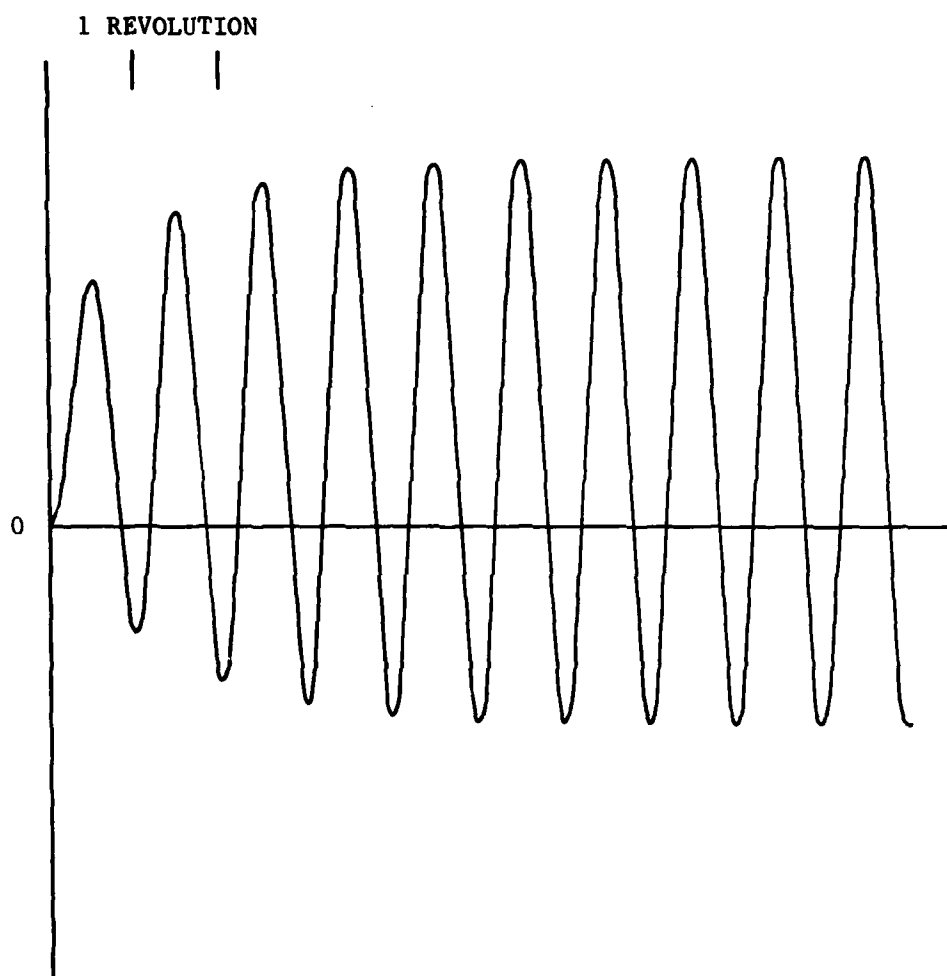


Figure 64. SIMFLO Time History with Dominant One-Per-Rev.

64. This is a much more realistic case than Figure 64. The trace shown in Figure 65 is obviously stable; however, the Floquet method results may well indicate that it is unstable. The Floquet results for this case and several cases vary over a wide range depending on which rotor revolution shown is used as the base revolution. When these results were found, there was no choice but to discard the Floquet theory from consideration for a rotor stability analysis in C81. Any method used in C81 would have to handle even the most extreme cases without raising questions such as those shown here.

13.3 THE MOVING BLOCK FAST FOURIER TRANSFORM

The Moving Block Fast Fourier Transform (or simply moving block) is a well-known method for analyzing test data. The moving block extracts the frequency and damping in the vicinity of an assumed frequency from a time-history record. The moving block is quite fast, but it does require advance knowledge about the frequency of interest. This method was selected and is now functional in C81.

The basic component of the moving block is quite simple. The response amplitude is found for a given block of data at the selected frequency. Then the amplitude is found for the same length block of data starting at a slightly later time point. Hence, the name moving block. The logarithm of the amplitude versus starting time then determines the damping indicated in the response at the selected frequency. The same process is carried out for a number of frequencies on either side of the selected frequency. The amplitude function that gives the lowest least square error function is then chosen for the true frequency and damping of the response.

13.4 PRONY'S METHOD CURVE FIT

Prony's method was investigated as a more economical alternative to the moving block. As described in Reference 39, Prony's method fits a curve of the form

$$f(x) = \sum_{i=1}^n A_i e^{a_i x} \quad (444)$$

to a given set of data points. The a_i coefficients are complex. Using at least $2n$ data points, a set of n difference equations are set up and solved simultaneously. The characteristic equation is then solved for the characteristic roots

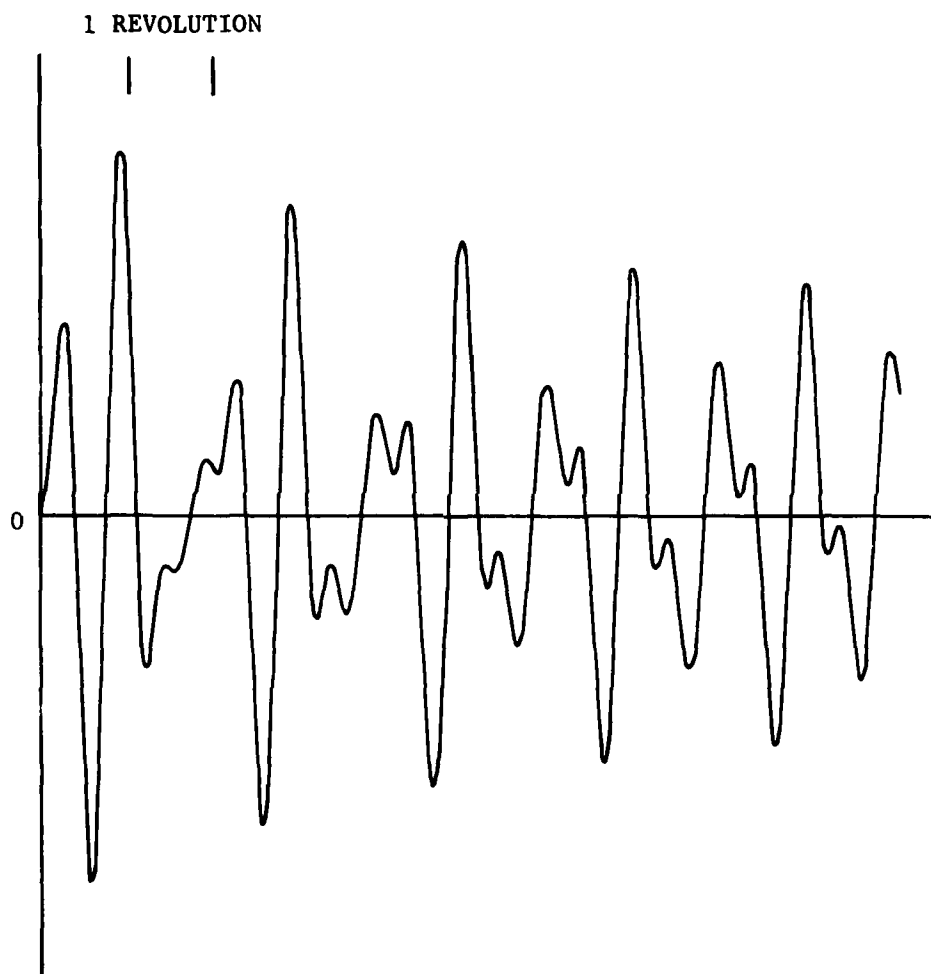


Figure 65. SIMFLO Time History Showing Several Harmonic Components.

$$r_i = e^{a_i}$$

(445)

Finally, a set of simultaneous equations is used to determine the A_i coefficients. Thus it can be seen that Prony's method gives frequency and damping information for all of the frequencies contained in the data analyzed. The penalty associated with all of this extra information is that Prony's method takes considerably more computer time than the moving block. In relationship to the computer time used by the rest of C81, Prony's method was not too large. Therefore, Prony's method was also selected to be programmed in C81.

The numerical properties of Prony's method are not well defined, but several points of interest were determined in this study.

1. n should be at least three times as large as the number of roots of interest.
2. If two frequencies are close together, there is a tendency for damping coefficients to cross over from one frequency to the other. The extent of this crossover is controlled by the frequency separation and the record length.
3. For an isolated frequency, a one-cycle record provides an adequate resolution by the method.
4. For a pair of nearby frequencies, two or more cycles are required for a reasonable resolution.
5. If n is too large, the solution procedure will fail and the case will have to be rerun with a smaller n .

Table 15 shows the basis for most of these conclusions. The results shown were based on a generated record so that the true solution was known. When 200 points were used ($N=200$), the record length was just over one cycle of the lowest frequency (1.3 radian/second).

The time history shown in Figure 65 was also analyzed using Prony's method. For this case the 1-per-rev frequency was 30 radian/second, and the input natural frequency of the blade mode was 45 radian/second. The four terms of significance obtained by Prony's method are shown in Table 16. It has not been possible to verify the amplitudes, but the frequency content is correct and the damping appears to be correct as well.

TABLE 15. PRONY'S METHOD TEST CASES

$$f(t) = \sum_{i=1}^5 A_i e^{\zeta_i t} \sin(\omega_i t + \phi_i)$$

Input Function All $\phi_i = 0$

$A_1 = 10$	$A_2 = 3$	$A_3 = 20$	$A_4 = 5$	$A_5 = 1$
$\zeta_1 = 0$	$\zeta_2 = -0.2$	$\zeta_3 = 0$	$\zeta_4 = 0$	$\zeta_5 = 0.05$
$\omega_1 = 20$	$\omega_2 = 15$	$\omega_3 = 10$	$\omega_4 = 1.3$	$\omega_5 = C$

For $i = 1, 2, 3$: the maximum error in amplitude was 3%
the maximum error in damping was 0.1%
and the maximum error in frequency was 0.001%.

Other results below:

N	C	A_4	ζ_4	ω_4	A_5	ζ_5	ω_5
200	1.5	5.96	-0.017	1.347			
300	1.5	6.2	-0.016	1.348			
400	1.5	6.43	-0.028	1.35	0.1567	0.091	0.683
200	1.75	5.37	-0.043	1.46	0.3	0.45	1.03
300	1.75	7.48	-0.18	1.387	2.197	-0.044	0.608
400	1.75	4.25	0.029	1.292	1.765	-0.013	1.668
200	2.0	2.51	0.178	1.24	3.07	-0.075	1.748
300	2.0	4.71	0.0031	1.285	2.44	-0.192	1.958
400	2.0	4.91	0.0039	1.296	1.01	0.042	1.992
200	2.25	4.43	0.045	1.29	1.38	-0.031	2.184
300	2.25	5.32	-0.011	1.31	1.52	-0.035	2.24
400	2.25	4.79	0.0084	1.291	1.06	0.035	2.217
200	2.5	4.85	0.0118	1.299	1.07	0.022	2.49
300	2.5	5.10	-0.0048	1.299	1.222	0.0217	2.506
400	2.5	4.91	0.0035	1.298	1.06	0.0403	2.497

TABLE 16. PRONY'S METHOD RESULTS FOR TIME HISTORY

i	A_i	ζ_i	$\omega_i \left(\frac{\text{radian}}{\text{sec}} \right)$	$\phi_i \text{ (radian)}$
1	18.8	-1.13	44.9	-.939
2	9.8	- .0055	60.0	3.11
3	14.0	- .0060	29.95	1.61
4	1.06	- .5	89.94	1.78

13.5 MANEUVER PERTURBATIONS

In order to apply any of the rotor stability techniques studied, a method had to be incorporated into C81 to provide a small perturbation to each of the state variables followed by a time history of the whole system. The specifications for the maneuver perturbation option are as follows:

1. An unperturbed maneuver of N rotor revolutions will be run and saved on magnetic disk. N will be determined by the standard C81 maneuver time inputs.
2. One at a time, all of the variables of interest will be perturbed by a small amount, and a maneuver of N rotor revolutions will be run and saved.
3. No other maneuver type inputs will be allowed with the perturbation maneuver.
4. The variables of interest will consist of three sets with the sets used to be selected by the user. One set will include all of the rotor modes, the second set will include all the pylon modes, and the third set will include the fuselage motions.
 - a. The fuselage variables are the Euler angles, the linear velocity components, and the angular velocity components.
 - b. The pylon variables are the displacement and velocity of each pylon modal participation factor.
 - c. The rotor variables are the modal participation factor displacements and velocities in combinations depending on hub type and mode type.
 - (1) For a gimbaled or teetering rotor
 - (a) Increment all blades equally on a collective mode
 - (b) Cyclic mode
 - {1} For two blades, increment blade one plus and blade two minus.
 - {2} For a multiblade rotor, first increment blade i by $\cos \psi_i$ function and then by $\sin \psi_i$ function.

- (c) For a scissor mode, alternate increments--one plus, one minus, one plus, etc.
- (d) Increment one blade at a time for an independent mode.
- (2) For the rigid hub type (articulated or hingeless rotor), increment one blade at a time for each mode.

The inputs that activate the maneuver perturbation option and the data sequence required to apply the moving block or Prony's method to the perturbed time histories are given in Appendix C.

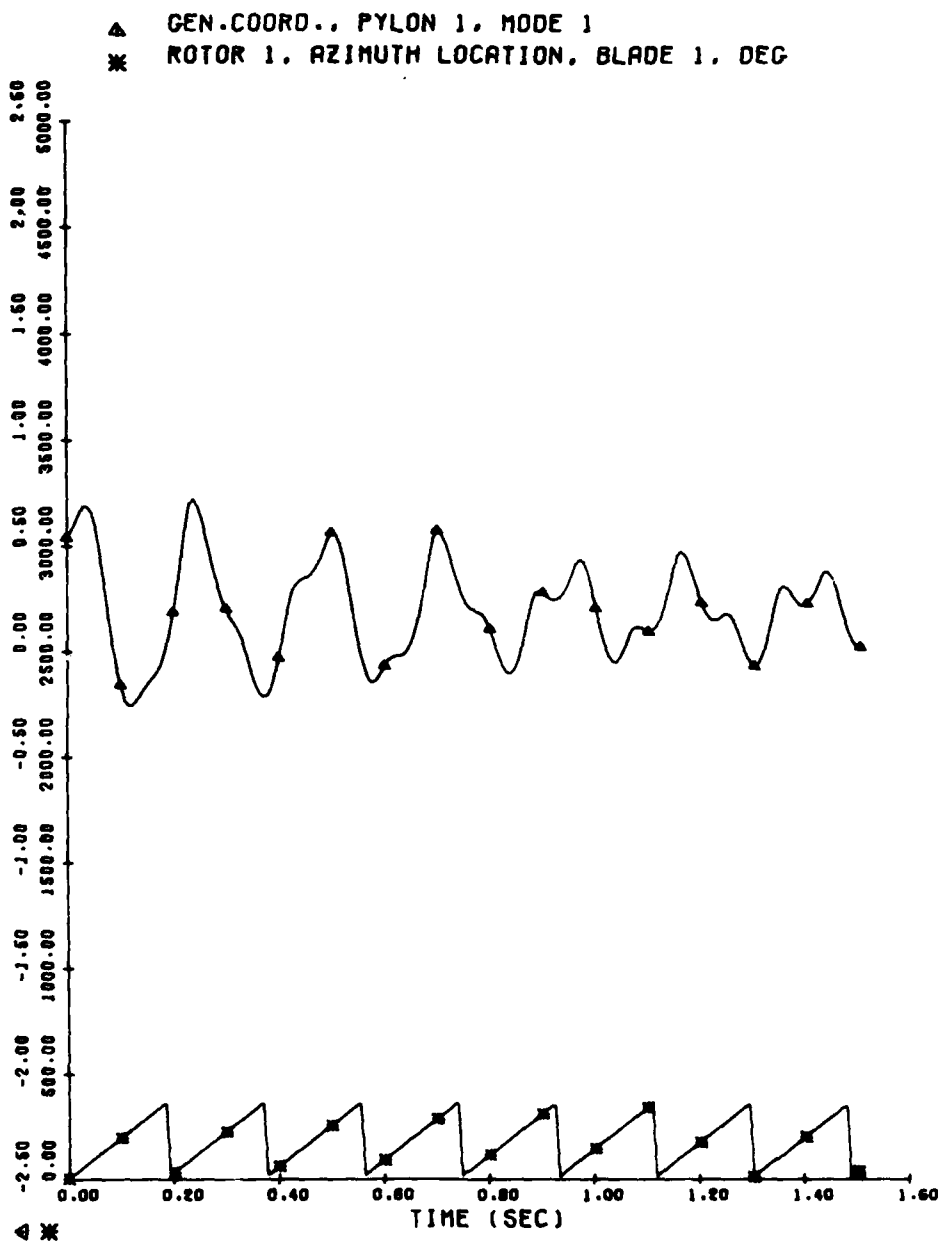
13.6 DEMONSTRATION OF ROTOR STABILITY ANALYSES

13.6.1 Pylon Stability for the Huey Cobra

To demonstrate the stability analysis for a realistic helicopter case, a Huey Cobra deck was trimmed in a 150-knot dive. The case used three rotor modes obtained from DNAM05 DN9100 and three pylon modes obtained from a NASTRAN model. The pylon modes were of special interest for this case because the Huey Cobra was known to have a lightly damped pylon mode at high speed before this was corrected by adjusting the SCAS. The pylon perturbation case was run with zero structural damping to obtain conservative results.

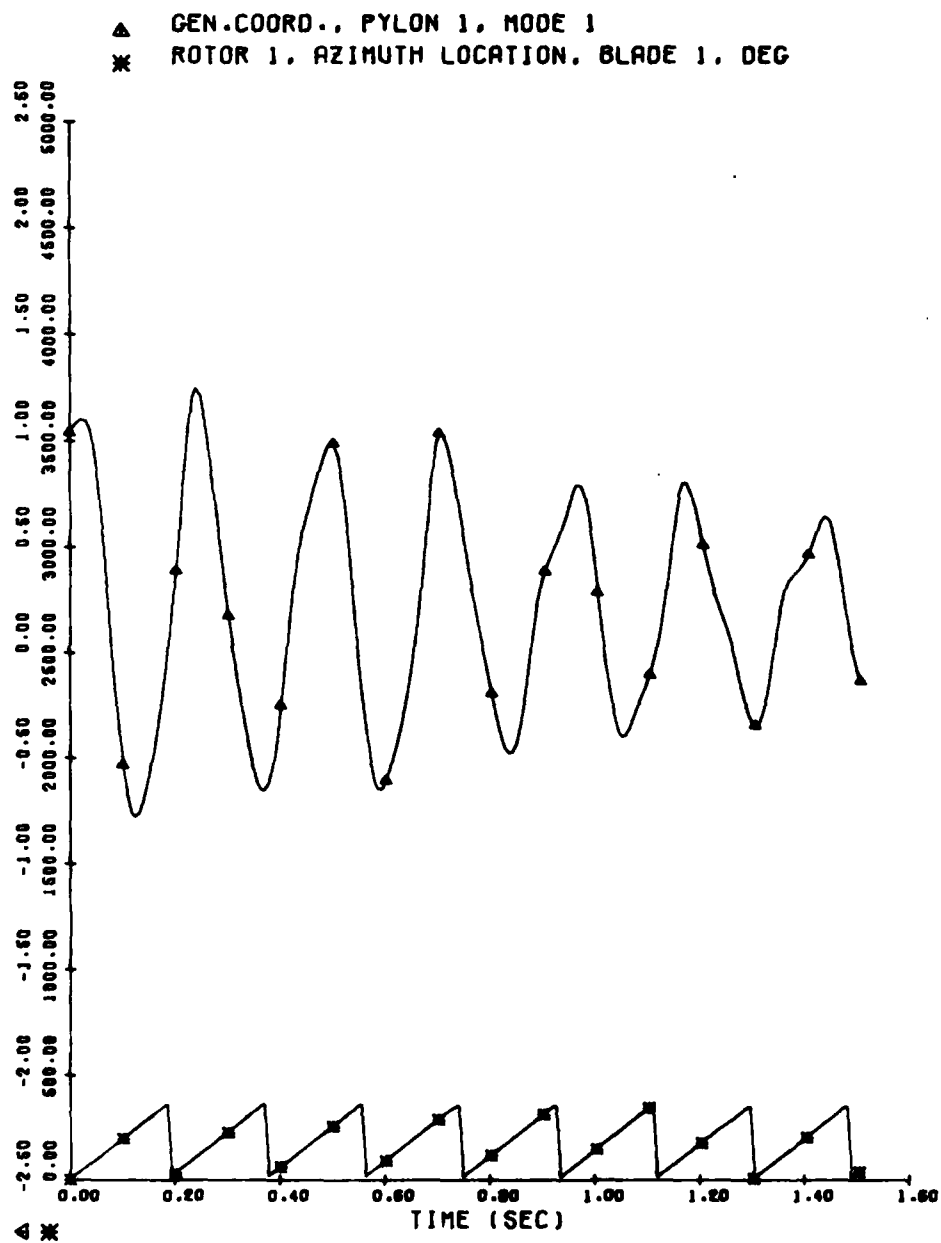
The time-history traces for both the base and perturbed conditions for each pylon mode are shown in Figures 66 through 71. Both moving block and Prony analyses were made of each perturbed condition. The actual results of these analyses are shown in Figures 72, 73, and 74. The input natural frequency of the first pylon mode was very near 3 Hz, so 3 Hz was the estimated frequency for the moving block. Since the actual frequency reported is at the top of the allowed band, we might suspect that the true coupled frequency is even higher than 3.5 Hz. The Prony's method results show this to be the case with the response frequency closest to 3 Hz being 4.25 Hz. The damping obtained by the two methods is in good agreement considering the separation of the frequencies.

When we look at the second pylon mode we see very good agreement between the moving block and Prony methods for both frequency and damping. The third pylon mode, a predominantly vertical mode, appears to be the one of interest. Its input natural frequency was 7.9 Hz. The moving block results show the mode to be slightly unstable, and Prony's method shows it to be barely stable. From the time history, we might guess that mode three is neutrally stable because the general



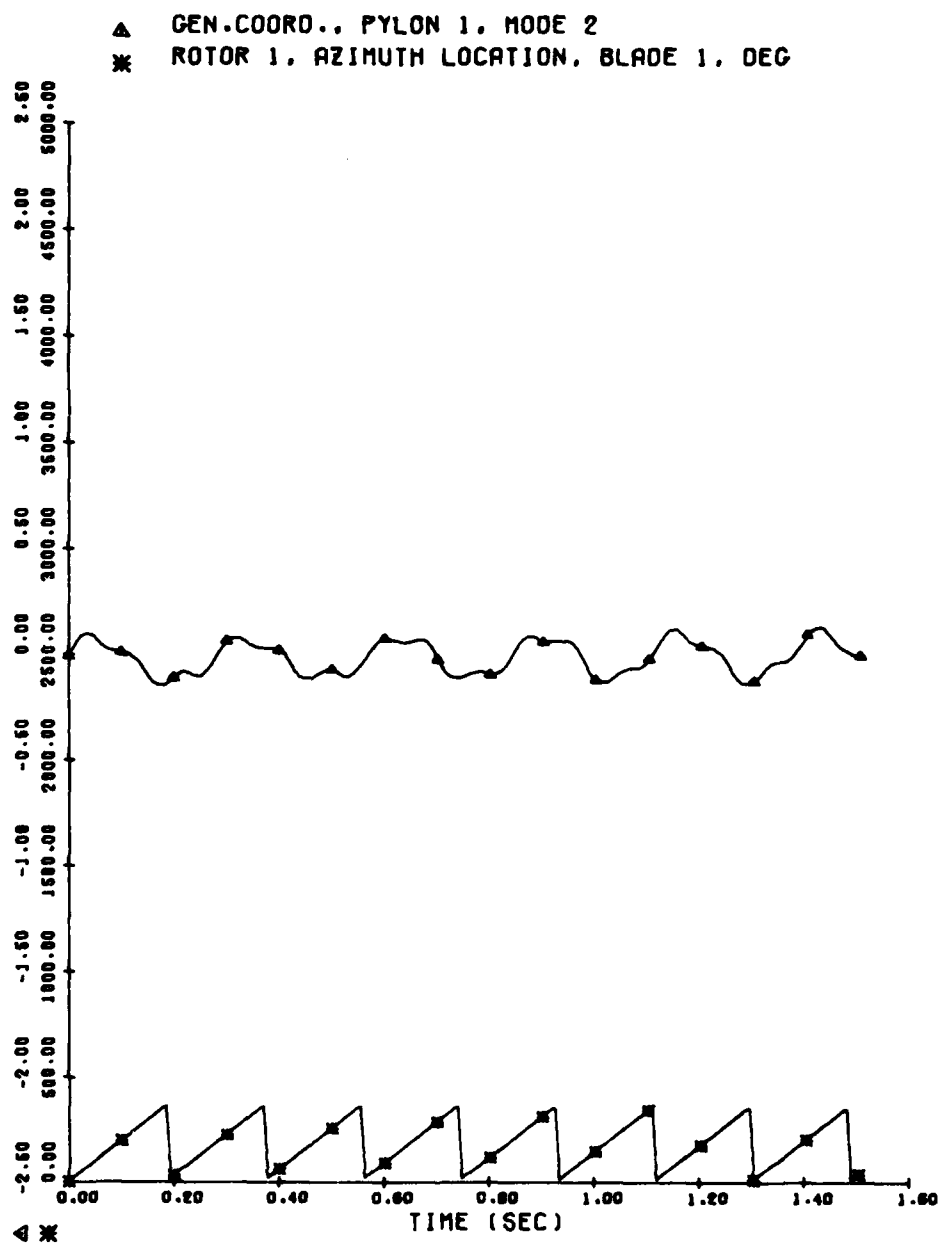
IPEN 0

Figure 66. Huey Cobra Time History for Pylon Mode One, Unperturbed.



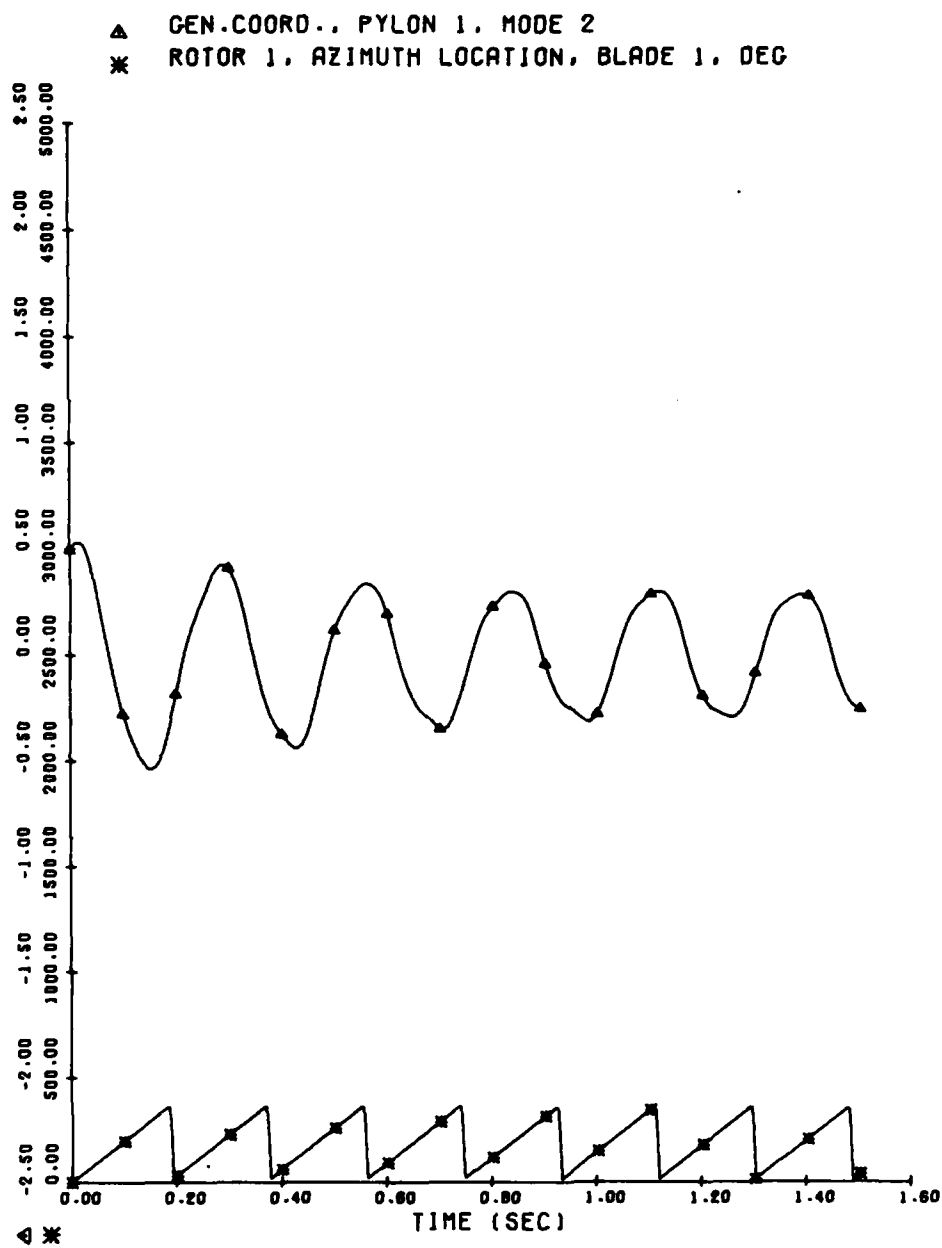
IPSN 0

Figure 67. Huey Cobra Time History for Pylon Mode One, Perturbed.



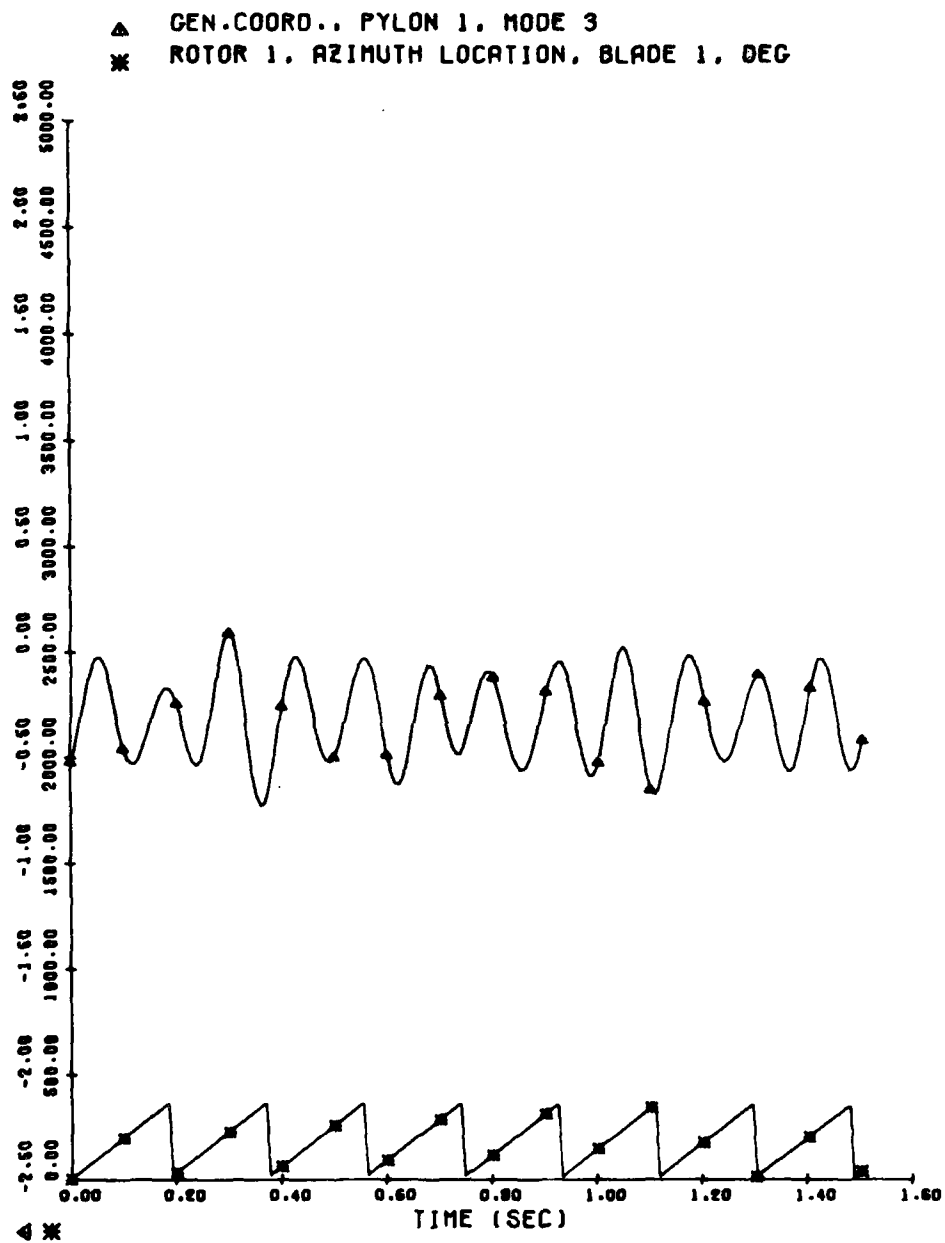
IPEN 0

Figure 68. Huey Cobra Time History for Pylon Mode Two, Unperturbed.



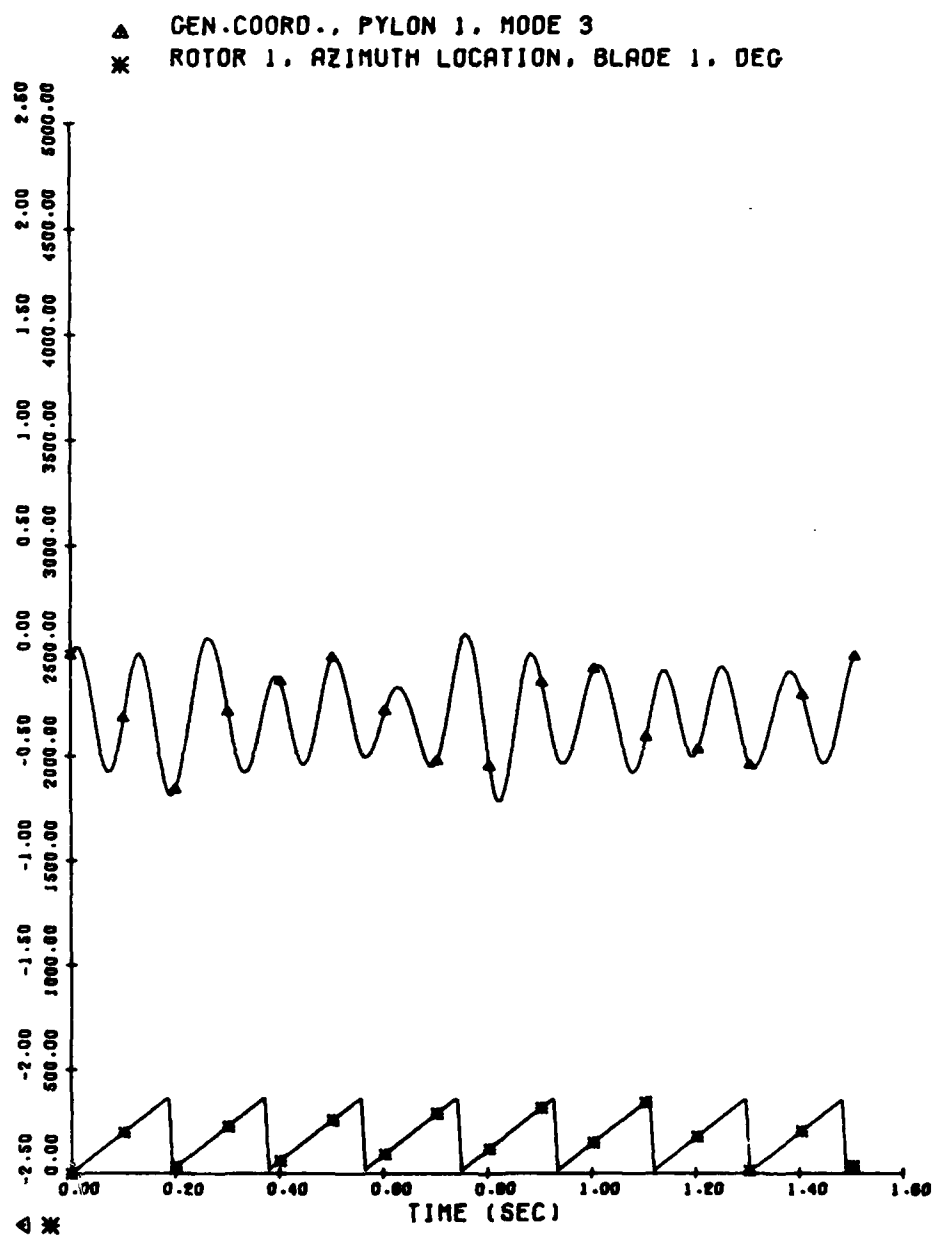
IPSN 0

Figure 69. Huey Cobra Time History for Pylon Mode Two, Perturbed.



IPSN 0

Figure 70. Huey Cobra Time History for Pylon Mode Three, Unperturbed.



IP6N 0

Figure 71. Huey Cobra Time History for Pylon Mode Three, Perturbed.

DAMPING DETERMINED BY MOVING BLOCK FFT FOR GEN.COORD.. PYLON 1. MODE 1
 TIME INTERVAL ANALYZED: START: 0.0 SECONDS STOP: 0.856 SECONDS
 FREQUENCY RANGE ANALYZED: 2.500 HERTZ TO 3.500 HERTZ
 NUMBER OF CYCLES ANALYZED IS 2
 ACTUAL FREQUENCY IS 3.503 HERTZ
 DAMPING EXPONENT IS -0.24768 /SECOND (NEGATIVE STABLE) AND THE DAMPING IS 1.12517 % CRITICAL (POSITIVE STABLE).
 VARIABLE CODE = 1466

VARIABLE CODE = 1466

STABILITY ANALYSIS BY PRONY CURVE FIT METHOD FOR: GEN.COORD.. PYLON 1. MODE 1
 TIME INTERVAL ANALYZED: START: 0.0 SECONDS STOP: 0.987 SECONDS
 30 TERMS USED FOR THE CURVE FIT

ROOT NUMBER J	ABSOLUTE AMPLITUDE B(J)	REAL PART (/SEC)	IMAGINARY PART (RAD/SEC)	IMAGINARY PART (HZ)	(PER REV)	PERCENT DAMPING	PHASE ANGLE (DEG)
1	0.04155	-3.33	0.0	0.0	0.0	100.00	180.00
2	0.04247	-62.55	24.81	4.27	0.79	100.00	70.83
3	0.04284	-3.55	24.81	4.27	0.79	2.02	-86.18
4	0.09548	-4.07	40.99	6.52	1.21	0.17	-113.65
5	0.10502	-4.12	67.65	10.77	1.99	1.33	-97.01
6	0.15380	-1.26	95.14	15.14	2.80	7.40	-1.80
7	0.01612	-8.43	113.61	18.08	3.35	0.09	67.26
8	0.00796	-0.12	135.46	21.56	3.99	44.42	13.63
11	0.01511	-102.61	206.95	32.94	6.10		

Figure 72. Huey Cobra Pylon Mode One Stability Results.

VARIABLE CODE = 1467

DAMPING DETERMINED BY MOVING BLOCK FFT FOR GEN.COORD.. PYLON 1. MODE 2

TIME INTERVAL ANALYZED: START: 0.0 SECONDS STOP: 0.833 SECONDS

FREQUENCY BAND ANALYZED: 2.800 HERTZ TO 3.800 HERTZ

NUMBER OF CYCLES ANALYZED IS 2

ACTUAL FREQUENCY IS 3.601 HERTZ

DAMPING EXPONENT IS -0.73437 /SECOND (NEGATIVE STABLE) AND THE DAMPING IS 3.24601 X CRITICAL (POSITIVE STABLE).

VARIABLE CODE = 1467

STABILITY ANALYSIS BY PRONY CURVE FIT METHOD FOR: GEN.COORD.. PYLON 1. MODE 2

TIME INTERVAL ANALYZED: START: 0.0 SECONDS STOP: 0.987 SECONDS

30 TERMS USED FOR THE CURVE FIT

ROOT NUMBER	ABSOLUTE AMPLITUDE S(J)	REAL PART (/SEC)	IMAGINARY PART (RAD/SEC)	IMAGINARY PART (HZ)	(PER REV)	PERCENT DAMPING	PHASE ANGLE (DEG)
1	0.07306	-3.27	0.0	0.0	0.0	100.00	180.00
2	0.12294	-234.92	0.0	0.0	0.0	100.00	180.00
3	0.11349	-0.65	22.92	0.0	0.68	102.00	76.84
4	0.50859	-0.34	36.51	3.65	1.00	11.60	-134.01
5	0.03107	-0.09	67.57	5.81	1.99	10.14	-19.95
6	0.10710	-1.72	94.37	10.75	2.78	1.62	20.90
7	0.01245	-11.12	121.21	15.02	3.57	9.13	149.69
8	0.00262	-0.13	135.25	21.53	3.99	0.10	176.01
9	0.00262	-0.13	135.25	21.53	3.99	0.10	176.01
10	0.00262	-0.13	135.25	21.53	3.99	0.10	176.01
11	0.00262	-0.13	135.25	21.53	3.99	0.10	176.01
12	0.00262	-0.13	135.25	21.53	3.99	0.10	176.01
13	0.00262	-0.13	135.25	21.53	3.99	0.10	176.01
14	0.00262	-0.13	135.25	21.53	3.99	0.10	176.01
15	0.00262	-0.13	135.25	21.53	3.99	0.10	176.01
16	0.00262	-0.13	135.25	21.53	3.99	0.10	176.01
17	0.00262	-0.13	135.25	21.53	3.99	0.10	176.01
18	0.00262	-0.13	135.25	21.53	3.99	0.10	176.01
19	0.00262	-0.13	135.25	21.53	3.99	0.10	176.01
20	0.00262	-0.13	135.25	21.53	3.99	0.10	176.01
21	0.00262	-0.13	135.25	21.53	3.99	0.10	176.01
22	0.00262	-0.13	135.25	21.53	3.99	0.10	176.01
23	0.00262	-0.13	135.25	21.53	3.99	0.10	176.01
24	0.00262	-0.13	135.25	21.53	3.99	0.10	176.01
25	0.00262	-0.13	135.25	21.53	3.99	0.10	176.01
26	0.00262	-0.13	135.25	21.53	3.99	0.10	176.01
27	0.00262	-0.13	135.25	21.53	3.99	0.10	176.01
28	0.00262	-0.13	135.25	21.53	3.99	0.10	176.01
29	0.00262	-0.13	135.25	21.53	3.99	0.10	176.01
30	0.00262	-0.13	135.25	21.53	3.99	0.10	176.01

Figure 73. Huey Cobra Pylon Mode Two Stability Results.

VARIABLE CODE = 1468

DAMPING DETERMINED BY MOVING BLOCK FFT FOR GEN.COORD., PYLON 1, MODE 3
 TIME INTERVAL ANALYZED: START: 0.0 SECONDS STOP: 0.393 SECONDS
 FREQUENCY BAND ANALYZED: 7.000 HERTZ TO 8.400 HERTZ
 NUMBER OF CYCLES ANALYZED IS 2
 ACTUAL FREQUENCY IS 7.625 HERTZ
 DAMPING COEFFICIENT IS 0.12247 /SECOND (NEGATIVE STABLE) AND THE DAMPING IS -0.25564 X CRITICAL (POSITIVE STABLE).

VARIABLE CODE = 1468

STABILITY ANALYSIS BY HADNY CURVE FIT METHOD FOR: GEN.COORD., PYLON 1, MODE 3
 TIME INTERVAL ANALYZED: START: 0.0 SECONDS STOP: 0.987 SECONDS

3. TERMS USED FOR THE CURVE FIT

MODE NUMBER	AMPLITUDE (IN)	REAL PART (/SEC)	IMAGINARY PART (/SEC)	PERCENT DAMPING	PHASE ANGLE (DEG)
1	0.11952	-0.03012	0.0	100.00	180.00
2	0.10507	-0.073	0.23	2.74	38.17
3	0.0624	-0.36	0.52	0.90	156.46
4	0.07532	-0.01	0.47	0.03	88.16
5	0.07760	0.57	0.68	-0.15	-28.26
6	0.08066	-1.79	1.77	1.85	46.82
7	0.0871	-1.79	2.00	12.10	77.56
8	0.06161	-0.14	21.69	0.11	-111.44

Figure 74. Huey Cobra Pylon Mode Three Stability Results.

character of the response is not changed by changing the initial conditions. The presence of structural damping would, of course, increase the damping present in the response of all three pylon modes. In this example, the advantage of having two methods available to find the stability can be seen.

13.6.2 Stability of Simplified Rotor Model

A paper by D. A. Peters (Reference 41) was selected as being typical of the simplified rotor stability analyses in existence. His analysis is based on a centrally hinged, rigid blade with uncoupled flapping and lagging motion. The aerodynamics feature a constant lift curve slope and a constant drag coefficient with no stall or Mach number effects. He assumes uniform inflow with a slow time constant so that only long-term changes in induced velocity are accounted for. Most of these assumptions were matched using C81. The fast changes in induced velocity could not be stopped. Also, the rotor dynamics could not be simplified quite to the same level. The C81 cases were run using a 20-foot-radius rotor with three blades of 12.5-inch chord. The rotor rpm was 315, which gives 660 ft/sec tip speed. With these variables chosen, all of Peters' given data can be converted from nondimensional form into real numbers.

The cases run attempted to match the results of Figure 4 from Reference 41. This figure and the C81 results are shown in Figure 75. The C81 results do not correlate with Peters' results. The main reason for this is thought to be the rapid following time for the induced velocity in C81. The fact that the moving block and Prony's method do not agree indicates that the actual time histories have close to neutral stability. Possibly the use of longer records would yield more definite results.

⁴¹Peters, D. A. FLAP-LAG STABILITY OF HELICOPTER ROTOR BLADES IN FORWARD FLIGHT, Journal of the American Helicopter Society, Volume 20, Number 4, October 1975, pp. 2-13.

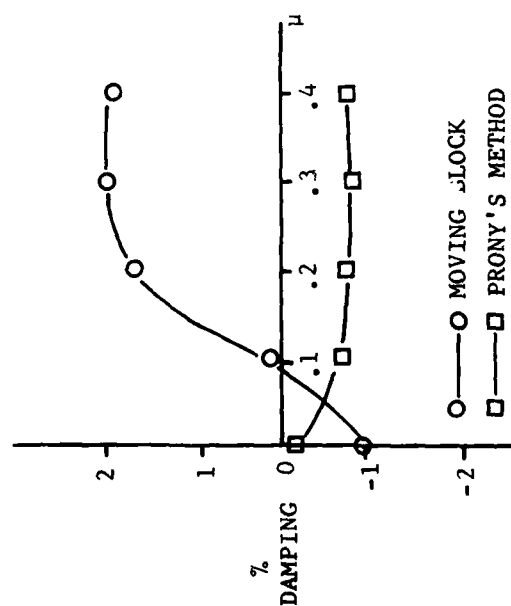


Figure 75. Comparison of Stability Results for Simple Check Case.

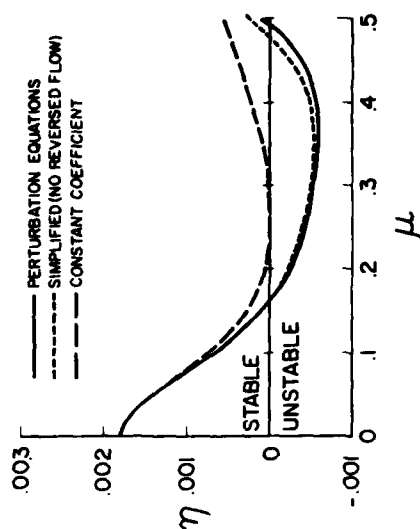


Figure 4. Effect of mathematical approximations on blade damping. $b = 1.15$, $\omega_t = 1.4$, $R = 0$, $\gamma = 5$, $\sigma = 0.05$, $c_{d_0} = 0.01$, $C_T/\sigma = 0.2$, trimmed, $\bar{f} = 0$.

Reprinted with the permission of the American Helicopter Society. This article, "Flap-Lag Stability of Helicopter Rotor Blades in Forward Flight," by D. A. Peters, appeared in the JOURNAL OF THE AMERICAN HELICOPTER SOCIETY, Volume 20, Number 4, October, 1975. (Reference 41)

According to Dr. Peters,

In principle, the analysis of flap-lag stability in forward flight could be performed by analyzing the time history traces from any of the so-called global rotor response programs. In practice, however, these programs are not satisfactory for obtaining blade damping characteristics over a wide range of configuration parameters. First, the computation time required for these programs is considerable and prohibits a detailed and systematic variation of all significant parameters. Second, the blade transient response is obscured by the blade forced response, which often drifts considerably during one or two rotor revolutions. Third, traditional log-decrement methods of damping determination are not applicable to forward flight because of the effect of the periodic coefficients. Thus, most investigations of blade stability in forward flight treat simplified sets of equations that can be systematically analyzed.

These comments are in part correct, but may also be misleading. Use of "so-called global rotor response programs" such as C81 is necessary in the aircraft design process. While it is true that these "global" programs are not practical for parametric studies during conceptual design of novel rotors, neither are linear models adequate for the detailed analysis of either model or full-scale hardware where the cost of design, fabrication, and testing as well as personal safety factors outweigh the cost of long-running computer programs. Although linear models may be useful for parametric studies, they are unable to model many of the detailed differences in design which may distinguish a stable configuration from an unstable one and may only be applicable to a limited range of flight conditions. Rotor blade stiffness distribution, inertia weights, and stall and Mach number effects are all local phenomena which cannot be represented by a single parameter. When papers such as Peters' are presented, they should point out all of the assumptions made and the limits of applicability, along with any conclusions.

With regard to Dr. Peters' second comment, it is acknowledged that calculation of a true equilibrium state is a difficult problem for C81 and other global programs, especially with the introduction of the blade torsional degree of freedom. Available numerical techniques are not adequate to guarantee finding a near-equilibrium condition even if the rotor is stable. It is suspected that neutral or negative rotor stability compounds this problem. However, it is always possible to run a time-variant rotor simulation in a wind tunnel mode to ascertain the rotor stability. If fuselage drift is a problem, the same thing may be done following a trim solution.

The traditional log-decrement methods of damping determination may not be applied to forward flight. However, there are numerical techniques available that may be applied to helicopter forward flight, as shown in Section 13.6.1. Such applications do demand that the engineer exercise some judgement in interpreting the results. For example, see Figure 72. The Prony's method results show frequencies at 1.99- and 4.00-per-rev, with damping of -0.11 and 0.11 percent, respectively. Since the system is an elastic pylon supporting a two-blade rotor, some steady forced response at 2- and 4-per-rev would be experienced. The calculated damping coefficients of nearly zero indicate that the steady forced response maintained an almost constant amplitude and hence was not affected by perturbing the pylon mode. Therefore, these harmonics may be disregarded for stability considerations.

14.0 CONCLUSIONS AND RECOMMENDATIONS

Prior to 1971, the Rotorcraft Flight Simulation Program C81 was used primarily as a handling qualities program to obtain flight-path stability and performance data. Since that time it has been increasingly used to calculate rotor loads using the aeroelastic rotor analysis. With the completion of Contract DAAJ02-75-C-0025, C81 has also been tailored to determine rotor stability characteristics. The program modifications made under this contract were directed at improving the capability to predict rotor stability. However, the improved control system model, the revised input for rotor modes, and the modal form of the pylon equations all yield better bending moment calculations as well. Also, the inclusion of the Rotor Frequency Program DN9100 ensures that the equations used to calculate the rotor modes are compatible with the equations used in C81. The ability to use less than 20 segments, which was coded into the program as part of the variable segment length option, permits the user to reduce the run time. For example, by using a five-segment tail rotor, up to a 50-percent reduction in computer time may be obtained with no penalty in the accuracy of the main rotor simulation. For many applications, greater savings may be achieved by also reducing the number of main rotor segments.

The modifications to C81 performed under the current contract, DAAJ02-77-C-0003, were suggested in the final report of the previous contract. The dynamic model of the rotor has been improved by including pitch-change axis and cg offsets in both DNAM05 and C81. A first-order lag was introduced in the horsepower-available calculations to provide a more accurate rpm time history during maneuver. The maneuver autopilot has been modified to allow the user to specify several more commands, and the inclusion of a digital filter has eliminated many of the difficulties formerly experienced in simulating a maneuver with an elastic main rotor.

The filter is also used in the rotor induced velocity calculations. The independent variables of the RIVD tables were changed to facilitate their use, and program AR9102 was modified to remain compatible with C81. Finally, the amount of data post-processing previously required has been reduced by adding the ability to time-history plot selected rotor variables after TVT and by adding a rotor contour-plot feature to the program.

Although C81 is the best general rotorcraft flight simulation in existence, there are several items of improvement needed for a unified and useful design tool. These items can be separated into two classes: those which improve the accuracy of the simulation, and those which provide increased user capability and convenience. The items of most importance are as follows:

1. The program should allow for the use of a data table for the fuselage nominal angle aerodynamics. A 20 x 20 table for each of the six aerodynamic forces and moments would require 2.5K additional storage; a significant improvement in the accuracy of the fuselage aerodynamics in the normal flight regime would result.
2. The wing and stabilizing surface aerodynamic models should be modified to allow the user to input a two-dimensional airfoil table, with the three-dimensional modifications being performed by C81 based on geometric inputs.
3. Modify the RWAS table model to be similar to the RIVD tables; i.e., to have μ and α_{WP} as the independent variables and to use an input average induced velocity table. Program AR9102 should be modified to calculate these RWAS tables.
4. Modify the store/brake aerodynamics model to include a pitching moment equation.
5. For a user to obtain a trim in autorotation or a maximum power climb, it is currently necessary first to compute trims at several rates of climb (or descent), then to interpolate or extrapolate the data to determine the rate which gives the desired power condition, and finally to run another trim to verify the predicted results. An option should be provided for trimming at a prescribed power level, with rate of climb being added to the trim procedure as an independent variable.
6. Rotor segment aerodynamic quantities should be added to the list of plot codes, and the vector analysis, harmonic analysis, and stability analysis options of GDAJ07 should be made available after TVT as well as after maneuver.

In view of the number of revisions made in developing the AGAJ77 version of C81, it would be very desirable to recheck some of the validation cases which were run on the AGAJ74 version by Boeing Vertol (Contract DAAJ02-74-C-0051) and by Sikorsky (Contract DAAJ02-74-C-0046).

15.0 REFERENCES

1. Harvey, K. W., Blankenship, B. L., and Drees, J. M., ANALYTICAL STUDY OF HELICOPTER GUST RESPONSE AT HIGH FORWARD SPEED, Bell Helicopter Company, USAAVLABS Technical Report 69-1, U.S. Army Aviation Materiel Laboratories, Fort Eustis, Virginia, September 1969, AD862594.
2. Livingston, C. L., A STABILITY AND CONTROL PREDICTION METHOD FOR HELICOPTER AND STOPPABLE ROTOR AIRCRAFT, Bell Helicopter Company Technical Report AFFDL-TR-69-123, Volumes I - IV, Air Force Flight Dynamics Laboratory, Air Force Systems Command, Wright-Patterson AFB, Ohio, 1970.
3. Crimi, P., THEORETICAL PREDICTION OF THE FLOW IN THE WAKE OF A HELICOPTER ROTOR, Cornell Aeronautical Laboratory Report BB-1994-S-1, Buffalo, New York, September 1965, AD 629782.
4. McLarty, Tyce T., Van Gaasbeek, James R., and Hsieh, P. Y., ROTORCRAFT FLIGHT SIMULATION WITH COUPLED ROTOR AEROELASTIC STABILITY ANALYSIS, Bell Helicopter Textron, USAAMRDL Technical Report 76-41A, -41B, -41C, U.S. Army Air Mobility Research and Development Laboratory, Fort Eustis, Virginia, June 1977.
5. Houbolt, John C., and Brooks, George W., DIFFERENTIAL EQUATIONS OF MOTION FOR COMBINED FLAPWISE BENDING, CHORDWISE BENDING AND TORSION OF TWISTED NONUNIFORM ROTOR BLADES, NACA Report 1346, 1958.
6. Myklestad, N. O., FUNDAMENTALS OF VIBRATION ANALYSIS, New York, N.Y., McGraw-Hill, 1956.
7. Oette, H., BERECHNUNG DER SCHLAGBRIEGE-, SCHWENKBIEGE-UND TORSIONSSCHWINGUNGEN VON ROTORBLÄTTERN MIT GEKOPPELTEN EIGENFORMEN UND -FREQUENZEN, Deutsche Luft-und Raumfahrt, DLR - Forschungsbericht 71-108, 1971.
8. Mil, M. L., et al, HELICOPTERS: CALCULATION AND DESIGN, NASA TTF-494, 1967.
9. Gessow, Alfred and Myers, Garry C., Jr., AERODYNAMICS OF THE HELICOPTER, New York, N.Y., The Macmillan Company.

10. Livingston, C. L., ROTOR INDUCED VELOCITY, Bell Helicopter Company Inter-Office Memo 81:CLL:am-838, October 7, 1966.
11. Drees, J. M., A THEORY OF AIRFLOW THROUGH ROTORS AND ITS APPLICATIONS TO SOME HELICOPTER PROBLEMS, The Journal of The Helicopter Society of Great Britain, Vol. 3, No. 2, 1949.
12. Harris, F. D., Tarzanin, F. J., Jr., and Fisher, R. D., Jr., ROTOR HIGH SPEED PERFORMANCE, THEORY VS. TEST, Journal of the American Helicopter Society, Volume 15, No. 3, July 1970.
13. Hoerner, Signard F., FLUID-DYNAMIC DRAG, New York, N.Y., Published by the author, 1958.
14. Loewy, R. G., A TWO-DIMENSIONAL APPROXIMATION TO THE UNSTEADY AERODYNAMICS OF ROTARY WINGS, J. Aeron. Sci. 24(2), 1957.
15. Timman, R., and Van de Vooren, A. I., FLUTTER OF A HELICOPTER ROTOR ROTATING IN ITS OWN WAKE, J. Aeron. Sci., 1957.
16. Drees, J. M., AEROELASTIC ROTOR PHENOMENA AND NONSTEADY ROTOR AERODYNAMICS, Annals of the New York Academy of Sciences, Volume 154, Art. 2., pp. 481-504, New York, N.Y., 1968.
17. Carta, F. O., Casellini, L. M., Arcidiacono, P. J., and Elman, H. L., ANALYTICAL STUDY OF HELICOPTER ROTOR STALL FLUTTER, Paper presented at the 26th Annual National Forum of the American Helicopter Society, Washington, D.C., 1970.
18. Arcidiacono, P. J., Carta, F. O., Casellini, L. M., and Elman, H. L., INVESTIGATION OF HELICOPTER CONTROL LOADS INDUCED BY STALL FLUTTER, USAAVLABS Technical Report 70-2. U.S. Army Air Mobility Research and Development Laboratory, Fort Eustis, Virginia, March 1970, AD869823.
19. Bisplinghoff, R. L., Ashley, H., and Halfman, R. L., AEROELASTICITY, Cambridge, Massachusetts, Addison-Wesley Publishing Company, 1955.
20. Scanlan, R. H., and Rosenbaum, R., AIRCRAFT VIBRATION AND FLUTTER, New York, N.Y., Macmillan Co., 1951.

21. Gormont, R. E., A MATHEMATICAL MODEL OF UNSTEADY AERODYNAMICS AND RADIAL FLOW FOR APPLICATION TO HELICOPTER ROTORS, Boeing-Vertol, USAAMRDL Technical Report 72-67, U.S. Army Air Mobility Research and Development Laboratory, Fort Eustis, Virginia, May 1973, AD767240.
22. Hildebrand, F. B., INTRODUCTION TO NUMERICAL ANALYSIS, New York, McGraw-Hill, 1956.
23. Jorgensen, L. H., PREDICTION OF STATIC AERODYNAMIC CHARACTERISTICS FOR SPACE-SHUTTLE-LIKE AND OTHER BODIES AT ANGLES OF ATTACK FROM 0° TO 180° , NASA TN D-6996, January 1973.
24. Jorgensen, L. H., A METHOD FOR ESTIMATING STATIC AERODYNAMIC CHARACTERISTICS FOR SLENDER BODIES OF CIRCULAR AND NONCIRCULAR CROSS SECTION ALONE AND WITH LIFTING SURFACES AT ANGLES OF ATTACK FROM 0° TO 90° , NASA TN D-7228, April 1973.
25. Polhamus, E. C., and Sleeman, W. C., Jr., THE ROLLING MOMENT DUE TO SIDESLIP OF SWEEPED WINGS AT SUBSONIC AND TRANSONIC SPEEDS, NASA TN D-209, February 1960.
26. USAF STABILITY AND CONTROL DATCOM, U.S. Air Force Flight Dynamics Laboratory, Wright-Patterson Air Force Base, Ohio, February 1972.
27. Etkin, Bernard, DYNAMICS OF FLIGHT, New York, N.Y., John Wiley and Sons, 1967.
28. Young, A. D., THE AERODYNAMIC CHARACTERISTICS OF FLAPS, British Aeronautical Research Council RM No. 2622, February 1947 (also printed as R.A.E. Report Aero. 2185, August 1947).
29. Fair, Gale, ALLMAT: A TSS/360 FORTRAN IV SUBROUTINE FOR EIGENVALUES AND EIGENVECTORS OF A GENERAL COMPLEX MATRIX, NASA TN-7032, January 1971.
30. Gear, C. William, NUMERICAL INITIAL VALUE PROBLEMS IN ORDINARY DIFFERENTIAL EQUATIONS, Prentice-Hall, New York, 1971.
31. Kinnen, Edwin and Chen, Chiou Shiun, LYAPUNOV FUNCTIONS FOR A CLASS OF n th ORDER NONLINEAR DIFFERENTIAL EQUATIONS, NASA CR-687, January 1967.
32. Crimi, Peter, A METHOD FOR ANALYZING THE AEROELASTIC STABILITY OF A HELICOPTER ROTOR IN FORWARD FLIGHT, NASA CR-1332, 1968.

33. Piarulli, V. J., and White, R. P., Jr., A METHOD FOR DETERMINING THE CHARACTERISTIC FUNCTIONS ASSOCIATED WITH THE AEROELASTIC INSTABILITIES OF HELICOPTER ROTORS IN FORWARD FLIGHT, NASA CR-1577, June 1970.
34. Peters, D. A., and Hohenemser, K. H., APPLICATION OF THE FLOQUET TRANSITION MATRIX TO PROBLEMS OF LIFTING ROTOR STABILITY, Journal of the American Helicopter Society, Volume 16, Number 2, 1971.
35. Friedman, Peretz, and Silverthorn, Louis J., AEROELASTIC STABILITY OF COUPLED FLAP-LAG MOTION OF HINGELESS HELICOPTER BLADES AT ARBITRARY ADVANCE RATIOS, NASA CR-132,431 February 1974.
36. Hsu, C. S., and Cheng, W. H., APPLICATIONS OF THE THEORY OF IMPULSIVE PARAMETRIC EXCITATION AND NEW TREATMENTS OF GENERAL PARAMETRIC EXCITATION PROBLEMS, Transactions of the ASME, Paper Number 72-WA/APM-6, March 1973.
37. Hammond, C. E., and Doggett, R. V., Jr., DETERMINATION OF SUBCRITICAL DAMPING BY MOVING BLOCK/RANDOMDEC APPLICATIONS, Proceedings of the NASA Symposium on Flutter Testing Techniques, Flight Research Center, Edwards Air Force Base, California, October 1975.
38. Cole, Henry A., Jr., ON-LINE FAILURE DETECTION AND DAMPING MEASUREMENT OF AEROSPACE STRUCTURES BY RANDOM DECREMENT SIGNATURES, NASA CR-2205, March 1973.
39. Kelly, Louis G., HANDBOOK OF NUMERICAL METHODS AND APPLICATIONS, Addison-Wesley, Reading, Massachusetts, 1967.
40. Myhill, J., and Gaal, P. H., ANALYSIS FOR EXPONENTIALS, Proceedings of the Summer Computer Conference AIAA/AICHE/AMS/ISA/SCI/SHARE, San Diego, California, June 1972.
41. Peters, D. A., FLAP-LAG STABILITY OF HELICOPTER ROTOR BLADES IN FORWARD FLIGHT, Journal of the American Helicopter Society, Volume 20, Number 4, October 1975.

16.0 SELECTED BIBLIOGRAPHY

1. Ralston, Anthony, and Wilf, Herbert S., MATHEMATICAL METHODS FOR DIGITAL COMPUTERS, New York, Wiley, 1967, pp. 95-120.
2. Treanor, Charles E., A METHOD FOR THE NUMERICAL INTEGRATION OF COUPLED FIRST-ORDER DIFFERENTIAL EQUATIONS WITH GREATLY DIFFERENT TIME CONSTANTS, Mathematics of Computing No. 20, January 1966, pp. 39-45.
3. Losey, H. E., and Hsieh, P. Y., A STUDY OF FOLDING PROP-ROTOR VTOL AIRCRAFT DYNAMICS, Vol. II, Bell Helicopter Company; AFFDL Technical Report 71-7, U.S. Air Force Flight Dynamics Laboratory, Wright-Patterson Air Force Base, Ohio, September 1971, pp. 63-65.
4. Gear, C. W., THE AUTOMATIC INTEGRATION OF ORDINARY DIFFERENTIAL EQUATIONS, Communications of the Association of Computing Machinery, Vol. 14, No. 3, March 1971, pp. 176-179.
5. Gear, C. W., DIFSUB FOR SOLUTION OF ORDINARY DIFFERENTIAL EQUATIONS, Communications of the Association of Computing Machinery, Vol. 14, No. 3, March 1971, pp. 185-190.
6. Hamming, R. W., NUMERICAL METHODS FOR SCIENTISTS AND ENGINEERS, New York, N. Y., McGraw-Hill, 1962, pp. 202-204.
7. Krogh, Fred T., CHANGING STEPSIZE IN THE INTEGRATION OF DIFFERENTIAL EQUATIONS USING MODIFIED DIVIDED DIFFERENCES, California Institute of Technology; JPL Internal Document, Section 914 TM No. 312, Jet Propulsion Laboratory, Pasadena, California, October 1972.

APPENDIX A

ROTOR DIFFERENTIAL EQUATIONS

The purpose of this appendix is to present the development of the differential equations for a rotor blade. This development closely parallels that of Houbolt and Brooks (H&B) (Reference 5). An attempt has been made to remove as many of the simplifying assumptions of H&B as possible. The assumptions made here that differ from those of H&B include the following:

- (1) Rotor blade cross sections are not symmetric.
- (2) The elastic axis is not a straight line.
- (3) Structural principal axes and mass principal axes are not parallel.

Derivation of Longitudinal Strains

The derivation of the longitudinal strain will be carried out in a manner similar to H&B. The coordinate system has been changed and a nonsymmetric cross section is assumed. Also, the pitch change axis of the undeformed blade is used as the reference axis rather than the elastic axis so that the elastic axis is not required to be straight.

Figure A-1 shows an undeformed cross section of the beam. An elemental fiber for which the strain will be derived is indicated by f . The origin, O , is located on the pitch-change axis in the undeformed position. The distance η is measured parallel to the major structural axis of the section, and ζ parallel to the minor structural axis. The angle θ_s is then the structural twist, which is not necessarily the same as the aerodynamic twist or the twist of the principal axes of inertia. The position and rate of change of position of f with respect to radial location y may be written in x - z coordinates as

$$\left. \begin{aligned} x &= \eta \cos \theta_s + \zeta \sin \theta_s \\ z &= -\eta \sin \theta_s + \zeta \cos \theta_s \end{aligned} \right\} \quad (A-1)$$

$$\left. \begin{aligned} x' &= -\eta \theta'_s \sin \theta_s + \zeta \theta'_s \cos \theta_s = \theta'_s z \\ z' &= -\eta \theta'_s \cos \theta_s - \zeta \theta'_s \sin \theta_s = -\theta'_s x \end{aligned} \right\} \quad (A-2)$$

Now allow beam displacements to occur so that the point O , on the reference axis, moves through the distances u , v , and w in the x , y , and z directions respectively, and so that the cutting

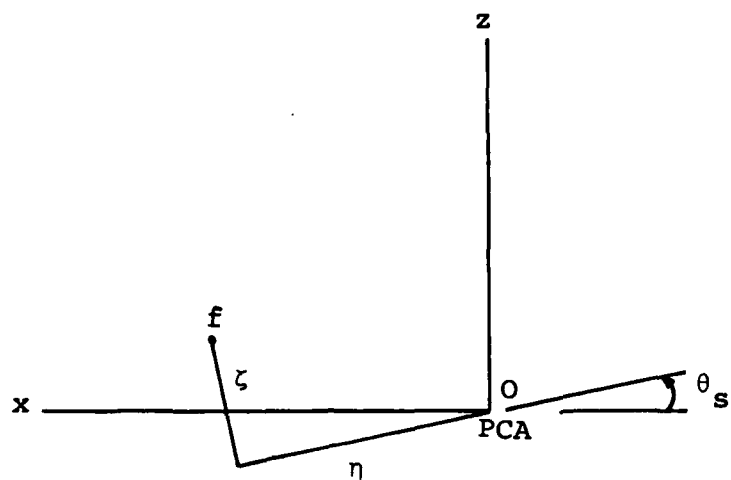


Figure A-1. Undisplaced Blade Coordinate System.

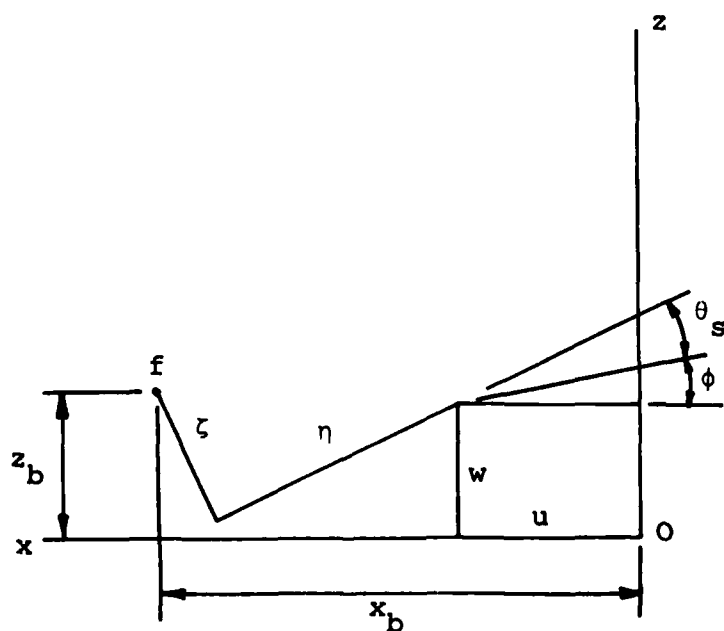


Figure A-2. Displaced Blade Coordinate System.

plane remains perpendicular to the reference axis and rotates around it by an angle ϕ . At this point, H&B apply a small angle assumption on ϕ and eliminate several terms. Here, delay the small angle assumptions until the equations are complete in order to be sure that no significant terms are lost. The deformed section is shown in Figure A-2. Using this figure, the new position of the fiber f is defined by the following:

$$\left. \begin{aligned} x_b &= u + x \cos \phi + z \sin \phi \\ y_b &= y + v - u'(x_b - u) - w'(z_b - w) \\ y_b &= y + v + u'(x \cos \phi + z \sin \phi) + w'(z \cos \phi - x \sin \phi) \\ z_b &= w + z \cos \phi - x \sin \phi \end{aligned} \right\} \quad (A-3)$$

The derivatives of x_b , y_b , and z_b with respect to y , denoted by x'_b , y'_b , z'_b , are given below.

$$\left. \begin{aligned} x'_b &= u' + x' \cos \phi + z' \sin \phi - x\phi' \sin \phi + z\phi' \cos \phi \\ x'_b &= u' + (z \cos \phi - x \sin \phi)(\phi' + \theta'_s) \\ y'_b &= 1 + v' - u''(x \cos \phi + z \sin \phi) - w''(z \cos \phi - x \sin \phi) - u'(x' \cos \phi + z' \sin \phi - x\phi' \sin \phi + z\phi' \cos \phi) - w'(z' \cos \phi - x' \sin \phi - z\phi' \sin \phi - x\phi' \cos \phi) \\ y'_b &= 1 + v' - u''(x \cos \phi + z \sin \phi) - w''(z \cos \phi - x \sin \phi) - u'(z \cos \phi - x \sin \phi)(\phi' + \theta'_s) + w'(+ x \cos \phi + z \sin \phi)(\phi' + \theta'_s) \\ z'_b &= w' + z' \cos \phi - x' \sin \phi - z\phi' \sin \phi - x\phi' \cos \phi \end{aligned} \right\} \quad (A-4)$$

$$z'_b = w' - (x \cos \phi + z \sin \phi)(\phi' + \theta'_s) \quad (A-4)$$

The longitudinal strain that is developed in a fiber may be found from these equations by considering the amount an elemental fiber of length ds changes in length. In terms of the differential components of length in the x -, y -, and z -directions, the final length ds_b of a fiber is given by the following equation:

$$ds_b^2 = dx_b^2 + dy_b^2 + dz_b^2 \quad (A-5)$$

Thus

$$\left(\frac{ds_b}{dy}\right)^2 = (x'_b)^2 + (y'_b)^2 + (z'_b)^2 \quad (A-6)$$

Substituting Equation (A-4) into (A-6) and neglecting the many higher order terms in the deformations and their derivatives,

$$\begin{aligned} \left(\frac{ds_b}{dy}\right)^2 &= 1 + 2 v' + (x^2 + z^2)(\theta_s'^2 + 2\theta_s' \phi') \\ &\quad - 2 u'' (x \cos \phi + z \sin \phi) \\ &\quad - 2 w'' (z \cos \phi - x \sin \phi) \end{aligned} \quad (A-7)$$

At this point a small angle assumption on ϕ may be used without danger of losing any terms. Then several more higher order terms may be thrown out, leaving

$$\begin{aligned} \frac{ds_b}{dy} &= \{1 + 2 v' + (x^2 + z^2)(\theta_s'^2 + 2 \theta_s' \phi') \\ &\quad - 2 u'' x - 2 w'' z\}^{1/2} \end{aligned} \quad (A-8)$$

This expression may be compared exactly with the expression obtained by H&B. Similarly, the equation for the original length ds is determined by setting $u=v=w=\phi=0$ in equation (A-8).

$$\frac{ds}{dy} = \{1 + (x^2 + z^2) \theta_s'^2\}^{1/2}$$

The tensile strain in the fiber can now be written

$$\begin{aligned}
\varepsilon &= (ds_p - ds)/ds \\
\varepsilon &= (ds_p/ds) - 1 \\
\varepsilon &= \{1 + (2/[1 + \theta_2^2(x^2 + z^2)]) \\
&\quad [v' + \theta_s' \phi'(x^2 + z^2) - u'x - w'z])\}
\end{aligned}
\tag{A-9}$$

In order to simplify further we apply the binomial expansion through the first-order term to give

$$\begin{aligned}
\varepsilon &= (1/[1 + \theta_s'^2(x^2 + z^2)])[v' + \theta_s' \phi'(x^2 + z^2) \\
&\quad - u''x - w''z]
\end{aligned}
\tag{A-10}$$

At this point H&B assume that the denominator term is close to one. That may not be a good assumption for some of today's rotor designs with high twist or wide chord, so such an assumption should be delayed as long as possible.

Now the strain equation may be written in terms of the cross-sectional coordinates η and ζ .

$$\begin{aligned}
\varepsilon &= (1/[1 + \theta_s'^2(\eta^2 + \zeta^2)])[v' + \theta_s' \phi'(\eta^2 + \zeta^2) \\
&\quad - u''(\eta \cos \theta_s + \zeta \sin \theta_s) - w''(\zeta \cos \theta_s \\
&\quad - \eta \sin \theta_s)]
\end{aligned}
\tag{A-11}$$

At this point, H&B eliminate the equivalent of the v' strain component by integrating the tensile stress over the structural area and by equating the centrifugal tension in the beam. In their equation we see the assumption of a homogeneous cross section since they have written Young's Modulus, E , on the outside of the integral. The basic equation should be

$$\begin{aligned}
T &= \int_{\eta_{1e}}^{\eta_{te}} \int_{\zeta_1}^{\zeta_u} E \varepsilon d\zeta d\eta \\
\text{or} \quad T &= \int_{\eta_{1e}}^{\eta_{te}} \int_{\zeta_1}^{\zeta_u} D E [v' + \theta_s' \phi'(\eta^2 + \zeta^2) \\
&\quad - u''(\eta \cos \theta_s + \zeta \sin \theta_s) \\
&\quad - w''(\zeta \cos \theta_s - \eta \sin \theta_s)] d\zeta d\eta
\end{aligned}
\tag{A-12}$$

where

$$D = 1/[1 + \theta_s'^2(\eta^2 + \zeta^2)]$$

Note also that the limits on ζ have been changed to reflect a nonsymmetric cross section integrating from the lower surface to the upper surface. For evaluation of this integral the quantities w'' , u'' , v' , ϕ' , θ_s' , and θ_s are all constant. If the integration is performed one term at a time, there are four integrals of interest.

$$\int_{\eta_{1e}}^{\eta_{te}} \int_{\zeta_1}^{\zeta_u} D E \, d\zeta \, d\eta \quad (A-13)$$

$$\int_{\eta_{1e}}^{\eta_{te}} \int_{\zeta_1}^{\zeta_u} D E (\eta^2 + \zeta^2) \, d\zeta \, d\eta \quad (A-14)$$

$$\int_{\eta_{1e}}^{\eta_{te}} \int_{\zeta_1}^{\zeta_u} D E \, \eta \, d\zeta \, d\eta \quad (A-15)$$

$$\int_{\eta_{1e}}^{\eta_{te}} \int_{\zeta_1}^{\zeta_u} D E \, \zeta \, d\zeta \, d\eta \quad (A-16)$$

None of these integrals can be evaluated in general in this form, In practice these integrals must be performed piecewise and usually numerically because of the construction of modern rotor blades, even if the same assumptions as H&B are made. However, some insight can be gained by making the same assumptions as H&B except for the symmetric cross section. If this is done

(A-13) is the section modulus times the area = EA.

(A-14) is the section modulus times the polar second area moment about the reference axis = EA k_A^2 .

(A-15) is the section modulus times the first area moment chordwise about the reference axis or the section modulus times the area times the chordwise offset of the section neutral axis = EA e_{AC} .

(A-16) is the section modulus times the first area moment beamwise about the reference axis or the section

modulus times the area times the beamwise offset
of the section neutral axis = $EA e_{AB}$.

It is apparent that effective values of A , k_A , e_{AC} , and e_{AB}
may be defined such that the true integrals are satisfied.
In integrated form, Equation (A-12) then becomes

$$T = EA \{ v' + \theta'_S \phi' k_A^2 - u'' (e_{AC} \cos \theta_S + e_{AB} \sin \theta_S) \\ - w'' (e_{AB} \cos \theta_S - e_{AC} \sin \theta_S) \} \quad (A-17)$$

Solving for v' yields

$$v' = T/EA - \theta'_S \phi' k_A^2 + u'' (e_{AC} \cos \theta_S + e_{AB} \sin \theta_S) \\ + w'' (e_{AB} \cos \theta_S - e_{AC} \sin \theta_S) \quad (A-18)$$

If T/EA is denoted by the tensile strain, ϵ_T , then equation
(A-18) may be combined with (A-11) to yield^T

$$\epsilon = D \{ \epsilon_T + \theta'_S \phi' (\eta^2 + \zeta^2 - k_A^2) \\ - (\eta - e_{AC})(u'' \cos \theta_S - w'' \sin \theta_S) \\ - (\zeta - e_{AB})(u'' \sin \theta_S + w'' \cos \theta_S) \} \quad (A-19)$$

This is the complete expression for the longitudinal strain
of any fiber in the cross section. The only apparent differ-
ence between Equation (A-19) and the H&B equation (A-12) is
the additional term for the beamwise first area moment because
of the nonsymmetric cross section. It should also be noted
here that η and ζ are relative to a different reference axis
than are H&B's.

Derivation of Elastic Moments

The longitudinal stress follows directly from the strain equa-
tion.

$$\sigma = DE [\epsilon_T + \theta'_S \phi' (\eta^2 + \zeta^2 - k_A^2) \\ - (\eta - e_{AC})(u'' \cos \theta_S - w'' \sin \theta_S) \\ - (\zeta - e_{AB})(u'' \sin \theta_S + w'' \cos \theta_S)] \quad (A-20)$$

No further development of cross-sectional stresses or strains
is necessary. The shearing stresses associated with the longi-
tudinal stresses integrate to zero about the section shear cen-
ter by definition. The twisting moments about the reference
axis are simply the moments of the net shear forces times the

beamwise and chordwise offsets of the shear center from the reference axis. The St. Venant moment for twisting deformation is the same as in H&B.

The net integral resisting moments are obtained by integrating the moments of the longitudinal stress components about the reference axes over the cross section.

The beamwise bending moment (about the η axis) is

$$M_B = - \int_{\eta_{1e}}^{\eta_{te}} \int_{\zeta_1}^{\zeta_u} \sigma \zeta d\zeta d\eta \quad (A-21)$$

The chordwise bending moment (about the ζ axis) is

$$M_C = - \int_{\eta_{1e}}^{\eta_{te}} \int_{\zeta_1}^{\zeta_u} \sigma \eta d\zeta d\eta \quad (A-22)$$

Note that M_B is positive for compression in the upper surface as for H&B. M_C is positive for tension in the leading edge, which is opposite to H&B.

The component of the stress in the plane normal to the reference axis leads to an effective resisting torque. The addition of this term to the St. Venant torque and the torque caused by the net shear forces acting about the reference axis gives the equation of the total resisting torque.

$$Q = GJ \phi' + \int_{\eta_{1e}}^{\eta_{te}} \int_{\zeta_1}^{\zeta_u} \sigma (\theta_s + \phi)' (\eta^2 + \zeta^2) d\zeta d\eta - V_\zeta s_C + V_\eta s_B \quad (A-23)$$

The problem of actually locating the shear center has been dealt with in great detail in a number of places in the literature so that exercise is deleted from the current discussion.

The elastic moments expressed as a function of the blade displacements are obtained by substitution of Equation (A-20) into Equations (A-21), (A-22), and (A-23).

By use of the same argument that was used with regard to expressions (A-13), (A-14), (A-15), and (A-16), effective values of I_B and I_C may be defined such that the following equations are satisfied.

$$\int_{\eta_{1e}}^{\eta_{te}} \int_{\zeta_1}^{\zeta_u} D E \zeta^2 d\zeta d\eta = E(I_B + A e_{AB}^2) \quad (A-24)$$

$$\int_{\eta_{1e}}^{\eta_{te}} \int_{\zeta_1}^{\zeta_u} D E \eta^2 d\zeta d\eta = E(I_C + A e_{AC}^2) \quad (A-25)$$

also

$$\int_{\eta_{1e}}^{\eta_{te}} \int_{\zeta_1}^{\zeta_u} D E \zeta \eta d\zeta d\eta = E A e_{AB} e_{AC} \quad (A-26)$$

These expressions are easier to understand if it is recalled that I_B and I_C are the effective second-area moments about the principal axes of the section, and the other terms are added to transfer to the reference axis. If

$$B_1 = \int_{\eta_{1e}}^{\eta_{te}} \int_{\zeta_1}^{\zeta_u} D E \zeta (\eta^2 + \zeta^2 - k_A^2) d\zeta d\eta \quad (A-27)$$

$$B_2 = \int_{\eta_{1e}}^{\eta_{te}} \int_{\zeta_1}^{\zeta_u} D E \eta (\eta^2 + \zeta^2 - k_A^2) d\zeta d\eta \quad (A-28)$$

$$B_3 = \int_{\eta_{1e}}^{\eta_{te}} \int_{\zeta_1}^{\zeta_u} D E (\eta^2 + \zeta^2) (\eta^2 + \zeta^2 - k_A^2) d\zeta d\eta \quad (A-29)$$

$$B_4 = \int_{\eta_{1e}}^{\eta_{te}} \int_{\zeta_1}^{\zeta_u} D E (\eta - e_{AC}) (\eta^2 + \zeta^2) d\zeta d\eta \quad (A-30)$$

$$B_5 = \int_{\eta_{1e}}^{\eta_{te}} \int_{\zeta_1}^{\zeta_u} D E (\zeta - e_{AB}) (\eta^2 + \zeta^2) d\zeta d\eta \quad (A-31)$$

then the moment equations may be written.

$$M_B = -T e_{AB} - \theta'_s \phi' B_1 + E I_B (u'' \sin \theta_s + w'' \cos \theta_s) \quad (A-32)$$

$$M_C = -T e_{AC} - \theta'_s \phi' B_2 + E I_C (u'' \cos \theta_s - w'' \sin \theta_s) \quad (A-33)$$

$$\begin{aligned} Q = & G J \phi' - V_\zeta s_C + V_\eta s_B + T k_A^2 (\theta_s + \phi)' \\ & + B_3 \theta_s'^2 \phi' - B_4 \theta'_s (u'' \cos \theta_s - w'' \sin \theta_s) \\ & - B_5 \theta'_s (u'' \sin \theta_s + w'' \cos \theta_s) \end{aligned} \quad (A-34)$$

Moments in x_b, y_b, z_b Reference

In the consideration of the equilibrium between moments and forces, it is more convenient to deal with moments that are aligned with the x_b, y_b, z_b coordinate system. These moments are labeled M_x, M_y , and M_z in Figure A-3. Note that M_z is opposite the z_b axis. With a small angle assumption on ϕ , the transformation of M_B, M_C , and Q to M_x, M_y , and M_z may be written as follows:

$$\begin{aligned} M_x = & M_B (\cos \theta_s - \phi \sin \theta_s) - M_C (\sin \theta_s + \phi \cos \theta_s) \\ & + Q u' \\ M_y = & Q + w' [M_C (\cos \theta_s - \phi \sin \theta_s) + M_B (\sin \theta_s \\ & + \phi \cos \theta_s)] + u' [-M_B (\cos \theta_s - \phi \sin \theta_s) \\ & + M_C (\sin \theta_s + \phi \cos \theta_s)] \\ M_z = & M_B (\sin \theta_s + \phi \cos \theta_s) + M_C (\cos \theta_s - \phi \sin \theta_s) \\ & - Q w' \end{aligned} \quad (A-35)$$

Now Equations (A-32), (A-33), and (A-34) may be substituted into Equation (A-35). When the resulting second-order terms are dropped the following are obtained:

$$\begin{aligned} M_x = & T(e_{AC} \sin \theta_s - e_{AB} \cos \theta_s) + \theta'_s \phi' (B_2 \sin \theta_s \\ & - B_1 \cos \theta_s) + T \phi (e_{AC} \cos \theta_s + e_{AB} \sin \theta_s) \\ & + u'' (E I_B - E I_C) \sin \theta_s \cos \theta_s \\ & + w'' (E I_B \cos^2 \theta_s + E I_C \sin^2 \theta_s) \end{aligned} \quad (A-36)$$

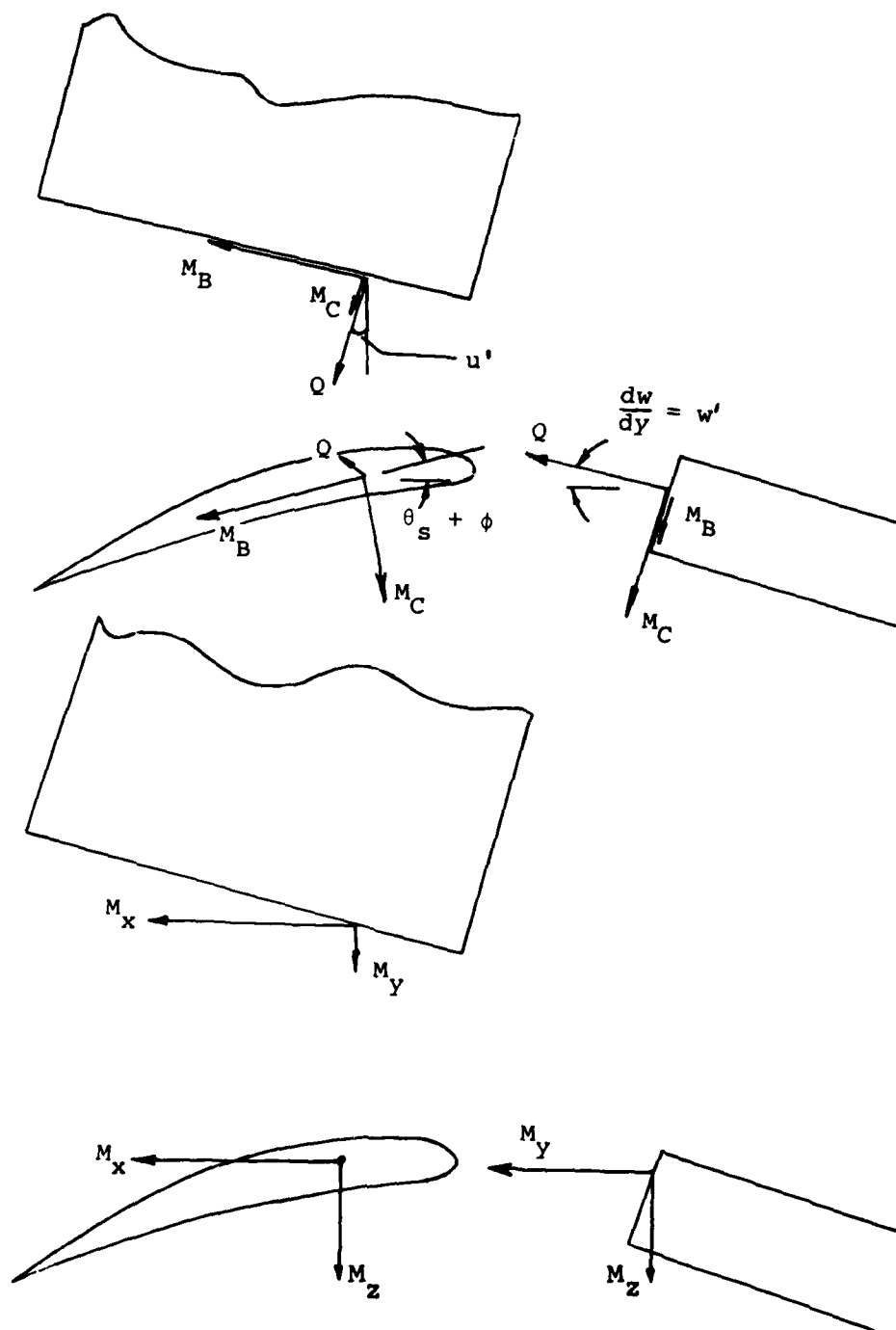


Figure A-3. Transformation to X, Y, Z Coordinates.

$$\begin{aligned}
M_Y = & \phi' (G J + T k_A^2 + B_2 \theta_s'^2) - V_\zeta s_C + V_\eta s_B \\
& + \theta_s' [T k_A^2 - u'' (B_4 \cos \theta_s + B_5 \sin \theta_s) \\
& - w'' (B_5 \cos \theta_s - B_4 \sin \theta_s)] \\
& + T u' (e_{AB} \cos \theta_s - e_{AC} \sin \theta_s) \\
& - T w' (e_{AC} \cos \theta_s + e_{AB} \sin \theta_s)
\end{aligned} \tag{A-37}$$

$$\begin{aligned}
M_Z = & -T (e_{AB} \sin \theta_s + e_{AC} \cos \theta_s) - \theta_s' \phi' (B_1 \sin \theta_s \\
& + B_2 \cos \theta_s) - T \phi (e_{AB} \cos \theta_s - e_{AC} \sin \theta_s) \\
& - u'' (E I_B \sin^2 \theta_s - E I_C \cos^2 \theta_s) \\
& - w'' (E I_B + E I_C) \sin \theta_s \cos \theta_s
\end{aligned} \tag{A-38}$$

Blade Element Forces and Moments

The next step in the development is consideration of the dynamic equilibrium of forces and moments acting on a differential element of the blade as shown in Figure A-4. Two slices are made parallel to the xz plane and a distance dy apart. The forces acting on the blade segment are shown in Figure A-4(a); the moments, in Figure A-4(b). The quantities F_x , F_y , F_z , Q_x , Q_y , and Q_z are resultant force and moment loadings which include both the acceleration body forces and the applied aerodynamic loading. The acceleration body forces will be developed next.

Accelerations

In the development of the equation for the acceleration of an arbitrary point on the blade we will begin at ground reference (inertial system) and progress logically through the various systems of interest to the blade. Five coordinate systems to handle all moving components will be defined. The transformation from one system to another will be discussed later.

1. Ground Reference - The ground reference system is taken to be the inertial reference system. Variables associated with the ground reference system will be denoted by the subscript or superscript g. The x_g axis is pointed north; y_g axis, east; and z_g axis, down.

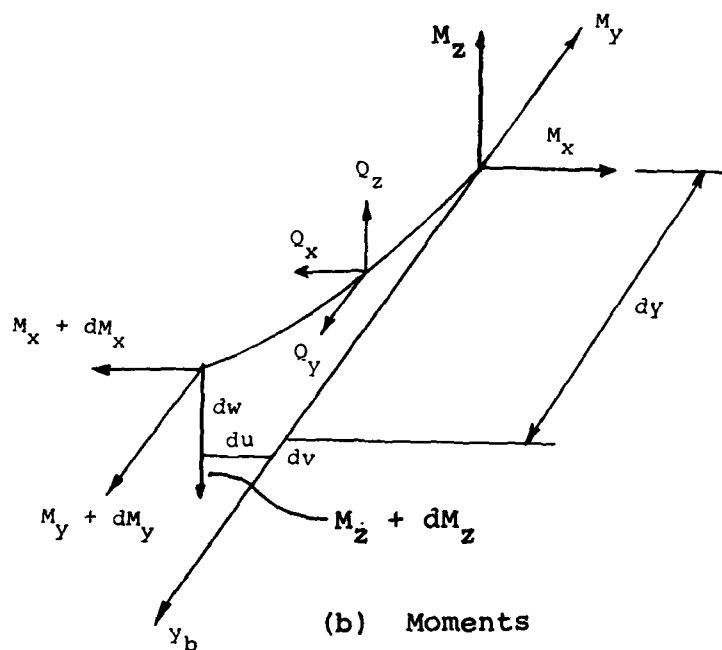
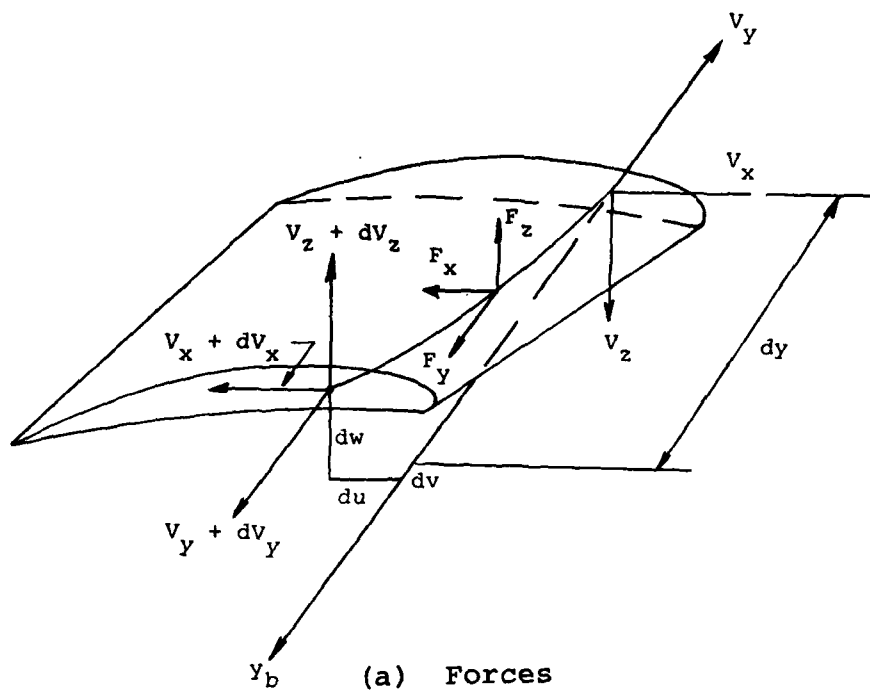


Figure A-4. Equilibrium of Forces and Moments.

2. Fuselage Reference - The fuselage coordinate system is centered at the fuselage center of gravity. Fuselage variables are denoted by the letter f. The x_f axis is forward; y_f , to the right; and z_f , down.
3. Mast Reference - The mast reference system is centered at the rotor flapping hinge or at the intersection of the blade radial axes if there is no central flapping hinge. This system does not rotate with the rotor. Mast referenced quantities will be identified by the letter m. The orientation of the mast reference system for zero mast tilt angles and no pylon motion has the x_m , y_m , and z_m axes parallel to the x_f , y_f , and z_f axes, respectively, and in the same directions. The mast reference system moves with the longitudinal and lateral mast tilt angles and with any angles introduced by pylon motion.
4. Hub Reference - The hub coordinate system is a rotating coordinate system which shares the same origin as the mast reference system. The letter h is used to indicate variables associated with the hub reference system. The y_h axis extends radially outward from the center of rotation. The z_h axis is parallel to the z_m axis but directed upward rather than downward. The x_h axis is directed as required to make a right-handed coordinate system, generally toward the trailing edge of the blade.

The hub coordinate system experiences motion due to flapping of the hub relative to the mast caused by cyclic rotor modes and due to "mast wind-up" which is reflected in the collective rotor modes rather than pylon modes. A description of cyclic and collective modes is found in Section 3.2.10.

5. Blade Reference - The origin of the blade coordinate system is at the inboard end of the feathering bearings. Variables associated with the blade reference are marked with the letter b. The y_b axis is aligned with the feathering bearings. The x_b axis is aft, parallel to the major principal axis of inertia. The z_b axis is upward, parallel to the minor principal axis of inertia.

The need for this coordinate system is to account for the flap-lag and twisting motion of the pitch change axis. Therefore in the case of rotors without feathering bearings, the origin of the blade coordinate system is at the radius where the pitch horn or other pitch mechanism applies the feathering control to the blade.

Notation

To get from one system to another a general Euler angle transformation is defined from system 1 to system 2 through the angles α_1 , α_2 , and α_3 .

$$\bar{A}^{(2)} = [T_{2/1}] \bar{A}^{(1)}$$

indicates the transformation of vector \bar{A} from system 1 to system 2 coordinates. The actual Euler angle transformation and the angles relating to the five defined systems are discussed in Appendix B.

In the development that follows, the symbols \bar{r} and \bar{R} are used to denote a displacement vector. The symbols $\dot{\bar{r}}$, $\dot{\bar{R}}$, and $\dot{\bar{V}}$ are used to indicate velocities. The symbols $\ddot{\bar{r}}$, $\ddot{\bar{R}}$, and $\ddot{\bar{a}}$ are used for accelerations. The symbols $\bar{\Omega}$ and $\dot{\bar{\Omega}}$ are used for angular velocity and acceleration, respectively. A superscript in parentheses is used to indicate in which coordinate system a quantity is expressed. A subscript such as 1/2 indicates motion of system 1 relative to system 2. A single subscript with the symbols \bar{R} , $\dot{\bar{R}}$, or $\ddot{\bar{R}}$ indicates the motion of the origin of that coordinate system. The symbols $\dot{\bar{V}}$ and $\ddot{\bar{a}}$ with a single subscript indicate absolute velocity or acceleration of some point relative to the ground.

The following equations may be used to find the velocity and acceleration of a point in system 2 relative to system 1:

$$\left. \begin{aligned} \dot{\bar{V}}_2^{(2)} &= \dot{\bar{R}}_1^{(2)} + \dot{\bar{r}}_2^{(2)} + \bar{\Omega}_{2/1}^{(2)} \times \bar{r}_2^{(2)} \\ \ddot{\bar{a}}_2^{(2)} &= \ddot{\bar{R}}_1^{(2)} + \ddot{\bar{r}}_2^{(2)} + \bar{\Omega}_{2/1}^{(2)} \times (\bar{\Omega}_{2/1}^{(2)} \times \bar{r}_2^{(2)}) \\ &\quad + 2 \bar{\Omega}_{2/1}^{(2)} \times \dot{\bar{r}}_2^{(2)} + \dot{\bar{\Omega}}_{2/1}^{(2)} \times \bar{r}_2^{(2)} \end{aligned} \right\} \quad (A-39)$$

where

$\bar{R}^{(2)}$ is the location of the system 2 origin relative to system 1 in system 2 coordinates.

$\bar{r}_2^{(2)}$ is the location of the point in question within system 2.

$\bar{\Omega}_{2/1}^{(2)}$ is the angular velocity of system 2 relative to system 1.

Velocities and Accelerations

The rigid body fuselage equations that are developed by Etkin (Reference 27) are written in fuselage reference. This makes the velocities and accelerations relative to ground directly available: $\dot{\bar{R}}_f^{(f)}$, $\ddot{\bar{R}}_f^{(f)}$, $\dot{\bar{\Omega}}_f^{(f)}$, and $\ddot{\bar{\Omega}}_f^{(f)}$.

These values are used to define the velocity and acceleration of the origin of the mast coordinate system. For the general problem, assume fully elastic fuselage modes adding to the motion at the top of the mast. Fuselage modes from NASTRAN or some other structural analysis program will be in fuselage reference. Therefore, the pylon equations will be formulated to fit this convention.

The velocity and acceleration of the origin of the mast coordinate system are given by the following:

$$\left. \begin{aligned} \dot{\bar{v}}_m^{(f)} &= \dot{\bar{R}}_f^{(f)} + \dot{\bar{r}}_{m/f}^{(f)} + \dot{\bar{\Omega}}_f^{(f)} \times \bar{r}_{m/f}^{(f)} \\ \ddot{\bar{a}}_m^{(f)} &= \ddot{\bar{R}}_f^{(f)} + \ddot{\bar{r}}_{m/f}^{(f)} + \dot{\bar{\Omega}}_f^{(f)} \times (\bar{\Omega}_f^{(f)} \times \bar{r}_{m/f}^{(f)}) \\ &\quad + 2 \bar{\Omega}_f^{(f)} \times \dot{\bar{r}}_{m/f}^{(f)} + \ddot{\bar{\Omega}}_f^{(f)} \times \bar{r}_{m/f}^{(f)} \\ \dot{\bar{\Omega}}_m^{(f)} &= \dot{\bar{\Omega}}_f^{(f)} + \dot{\bar{\Omega}}_{m/f}^{(f)} \\ \ddot{\bar{\Omega}}_m^{(f)} &= \ddot{\bar{\Omega}}_f^{(f)} + \ddot{\bar{\Omega}}_{m/f}^{(f)} \end{aligned} \right\} \quad (A-40)$$

These quantities are expressed in fuselage coordinates as indicated. The variables $\ddot{\bar{R}}_f^{(f)}$ and $\ddot{\bar{\Omega}}_f^{(f)}$ will be unknowns in the final system of equations. $\ddot{\bar{r}}_{m/f}^{(f)}$ and $\ddot{\bar{\Omega}}_{m/f}^{(f)}$ will appear implicitly in the acceleration of the fuselage modal coordinates.

The next step is to transform the necessary quantities from fuselage coordinates to mast coordinates.

$$\left. \begin{aligned} \dot{\bar{R}}_m^{(m)} &= [T_{m/f}] \dot{\bar{v}}_m^{(f)} \\ \ddot{\bar{R}}_m^{(m)} &= [T_{m/f}] \ddot{\bar{a}}_m^{(f)} \end{aligned} \right\} \quad (A-41)$$

$$\left. \begin{aligned} \bar{\Omega}_m^{(m)} &= [T_{m/f}] \bar{\Omega}_m^{(f)} \\ \dot{\bar{\Omega}}_m^{(m)} &= [T_{m/f}] \dot{\bar{\Omega}}_m^{(f)} + \bar{\Omega}_m^{(m)} \times [T_{m/f}] \bar{\Omega}_f^{(f)} \end{aligned} \right\} \quad \begin{array}{l} (A-41) \\ \text{Cont'd} \end{array}$$

The next item of interest is the velocity and acceleration of the origin of the hub reference system which is coincident with the origin of the mast reference system.

$$\left. \begin{aligned} \bar{R}_h^{(h)} &= [T_{h/m}] \bar{R}_m^{(m)} = [T_{h/m}] [T_{m/f}] \bar{V}_m^{(f)} \\ \ddot{\bar{R}}_h^{(h)} &= [T_{h/m}] \ddot{\bar{R}}_m^{(m)} = [T_{h/m}] [T_{m/f}] \bar{a}_m^{(f)} \end{aligned} \right\} \quad (A-42)$$

For the angular velocity and acceleration, the rpm component must be added.

$$\left. \begin{aligned} \bar{\Omega}_h^{(h)} &= \dot{\bar{\Psi}}^{(h)} + [T_{h/m}] \bar{\Omega}_m^{(m)} \\ &= \dot{\bar{\Psi}}^{(h)} + [T_{h/m}] [T_{m/f}] \bar{\Omega}_m^{(m)} \\ \dot{\bar{\Omega}}_h^{(h)} &= \ddot{\bar{\Psi}}^{(h)} + [T_{h/m}] \dot{\bar{\Omega}}_m^{(m)} + \dot{\bar{\Psi}}^{(h)} \times [T_{h/m}] \bar{\Omega}_m^{(m)} \\ &= \ddot{\bar{\Psi}}^{(h)} + [T_{h/m}] [T_{m/f}] \dot{\bar{\Omega}}_m^{(m)} \\ &\quad + \dot{\bar{\Psi}}^{(h)} \times [T_{h/m}] [T_{m/f}] \bar{\Omega}_m^{(f)} \end{aligned} \right\} \quad (A-43)$$

The next step is to find the velocity and acceleration of the origin of the blade reference. This origin will be at the interface between the hub and the blade. It will normally be at the feathering bearings.

$$\left. \begin{aligned} \bar{R}_b^{(b)} &= [T_{b/h}] \{ \bar{R}_h^{(h)} + \bar{r}_{b/h}^{(h)} + \bar{\Omega}_h^{(h)} \times \bar{r}_{b/h}^{(h)} \} \\ \ddot{\bar{R}}_b^{(b)} &= [T_{b/h}] \{ \ddot{\bar{R}}_h^{(h)} + \ddot{\bar{r}}_{b/h}^{(h)} + \bar{\Omega}_h^{(h)} \times (\bar{\Omega}_h^{(h)} \times \bar{r}_{b/h}^{(h)}) \\ &\quad + 2 \bar{\Omega}_h^{(h)} \times \dot{\bar{r}}_{b/h}^{(h)} + \dot{\bar{\Omega}}_h^{(h)} \times \bar{r}_{b/h}^{(h)} \} \end{aligned} \right\} \quad (A-44)$$

These quantities are in local blade reference and are relative to the blade.

Now the velocity and acceleration of any point on the blade may be written.

$$\left. \begin{aligned} \bar{v}_b^{(b)} &= \dot{\bar{R}}_b^{(b)} + \dot{\bar{r}}_b^{(b)} + \bar{\Omega}_b^{(b)} \times \bar{r}_b^{(b)} \\ \bar{a}_b^{(b)} &= \ddot{\bar{R}}_b^{(b)} + \ddot{\bar{r}}_b^{(b)} + \bar{\Omega}_b^{(b)} \times (\bar{\Omega}_b^{(b)} \times \bar{r}_b^{(b)}) \\ &\quad + 2 \bar{\Omega}_b^{(b)} \times \dot{\bar{r}}_b^{(b)} + \dot{\bar{\Omega}}_b^{(b)} \times \bar{r}_b^{(b)} \end{aligned} \right\} \quad (A-45)$$

where

$$\left. \begin{aligned} \bar{\Omega}_b^{(b)} &= [T_{b/h}] \bar{\Omega}_h^{(h)} + \bar{\Omega}_{b/h}^{(b)} \\ \dot{\bar{\Omega}}_b^{(b)} &= [T_{b/h}] \dot{\bar{\Omega}}_h^{(h)} + \dot{\bar{\Omega}}_{b/h}^{(b)} + \bar{\Omega}_{b/h}^{(b)} \times [T_{b/h}] \bar{\Omega}_h^{(h)} \end{aligned} \right\} \quad (A-46)$$

In dealing with the rotor blade, Equation (A-45) is the only equation of interest. In this equation

$\ddot{\bar{R}}_b^{(b)}$ represents the total acceleration of the origin of the blade coordinate system.

$\bar{\Omega}_b^{(b)}$ represents the total angular velocity of the blade including feathering motion.

$\dot{\bar{\Omega}}_b^{(b)}$ represents the total angular acceleration of the blade including feathering motion.

$\bar{r}_b^{(b)}$, $\dot{\bar{r}}_b^{(b)}$, and $\ddot{\bar{r}}_b^{(b)}$ represent the motion of a mass particle within the blade coordinate system; includes static location plus elastic motion. They are expressed in a form similar to H&B equation (B3) or (B4).

The blade coordinates used to develop the strain equation are related to the system used for the acceleration equation as follows:

$$\bar{r}_b^{(b)} = x_b i + y_b j + z_b k \quad (A-47)$$

By substitution from Equations (A-1) and (A-3) we obtain the following expressions. Superscripts have been deleted because all quantities are in blade reference.

$$\left. \begin{aligned} x_b &= u + \eta \cos (\theta_s + \phi) + \zeta \sin (\theta_s + \phi) \\ y_b &= y + v - u'[\eta \cos (\theta_s + \phi) + \zeta \sin (\theta_s + \phi)] \\ &\quad + w'[\eta \sin (\theta_s + \phi) - \zeta \cos (\theta_s + \phi)] \\ z_b &= w - \eta \sin (\theta_s + \phi) + \zeta \cos (\theta_s + \phi) \end{aligned} \right\} \quad (A-48)$$

$$\left. \begin{aligned} \dot{x}_b &= \dot{u} + \dot{\phi}[\zeta \cos (\theta_s + \phi) - \eta \sin (\theta_s + \phi)] \\ \dot{y}_b &= \dot{v} - \dot{u}'[\eta \cos (\theta_s + \phi) + \zeta \sin (\theta_s + \phi)] \\ &\quad - \dot{w}'[\zeta \cos (\theta_s + \phi) - \eta \sin (\theta_s + \phi)] \\ &\quad + u' \dot{\phi}[\eta \sin (\theta_s + \phi) - \zeta \cos (\theta_s + \phi)] \\ &\quad + w' \dot{\phi}[\zeta \sin (\theta_s + \phi) + \eta \cos (\theta_s + \phi)] \\ \dot{z}_b &= \dot{w} - \dot{\phi}[\zeta \sin (\theta_s + \phi) + \eta \cos (\theta_s + \phi)] \end{aligned} \right\} \quad (A-49)$$

$$\left. \begin{aligned} \ddot{x}_b &= \ddot{u} + \ddot{\phi}[\zeta \cos (\theta_s + \phi) - \eta \sin (\theta_s + \phi)] \\ &\quad - \dot{\phi}^2[\zeta \sin (\theta_s + \phi) + \eta \cos (\theta_s + \phi)] \\ \ddot{y}_b &= \ddot{v} - \ddot{u}'[\eta \cos (\theta_s + \phi) + \zeta \sin (\theta_s + \phi)] \\ &\quad - \ddot{w}'[\zeta \cos (\theta_s + \phi) - \eta \sin (\theta_s + \phi)] \\ &\quad + 2 \dot{u}' \dot{\phi}[\eta \sin (\theta_s + \phi) - \zeta \cos (\theta_s + \phi)] \\ &\quad + 2 \dot{w}' \dot{\phi}[\zeta \sin (\theta_s + \phi) + \eta \cos (\theta_s + \phi)] \\ &\quad + u' \dot{\phi}^2[\eta \cos (\theta_s + \phi) + \zeta \sin (\theta_s + \phi)] \\ &\quad + w' \dot{\phi}^2[\zeta \cos (\theta_s + \phi) - \eta \sin (\theta_s + \phi)] \end{aligned} \right\} \quad (A-50)$$

$$\left. \begin{aligned}
& + u' \ddot{\phi} [\eta \sin (\theta_s + \phi) - \zeta \cos (\theta_s + \phi)] \\
& + w' \ddot{\phi} [\zeta \sin (\theta_s + \phi) + \eta \cos (\theta_s + \phi)] \\
\ddot{z}_b &= \ddot{w} - \ddot{\phi} [\zeta \sin (\theta_s + \phi) + \eta \cos (\theta_s + \phi)] \\
& - \dot{\phi}^2 [\zeta \cos (\theta_s + \phi) - \eta \sin (\theta_s + \phi)]
\end{aligned} \right\} \quad \begin{array}{l} \text{(A-50)} \\ \text{Cont'd} \end{array}$$

By substitution of Equations (A-48), (A-49), and (A-50) into (A-45) the three components of $\bar{a}_b^{(b)}$ may be found. The small angle assumption on ϕ may also be made at this time.

Let

$$\left. \begin{aligned}
\bar{a}_b^{(b)} &= a_{bx} i + a_{by} j + a_{bz} k \\
\bar{R}_b^{(b)} &= \bar{R}_{bx} i + \bar{R}_{by} j + \bar{R}_{bz} k \\
\text{and} \quad \bar{\Omega}_b^{(b)} &= \Omega_{bx} i + \Omega_{by} j + \Omega_{bz} k
\end{aligned} \right\} \quad \text{(A-51)}$$

in Equation (A-45). Then as one intermediate step

$$\left. \begin{aligned}
a_{bx} &= \bar{R}_{bx} + \ddot{x}_b - x_b (\Omega_{by}^2 + \Omega_{bz}^2) + \Omega_{by} \Omega_{bx} y_b \\
&+ \Omega_{bx} \Omega_{bz} z_b + 2(\Omega_{by} \dot{z}_b - \Omega_{bz} \dot{y}_b) \\
&+ \dot{\Omega}_{by} z_b - \dot{\Omega}_{bz} y_b \\
a_{by} &= \bar{R}_{by} + \ddot{y}_b + \Omega_{by} \Omega_{bx} x_b + \Omega_{by} \Omega_{bz} z_b \\
&- (\Omega_{bx}^2 + \Omega_{bz}^2) y_b + 2(\Omega_{bz} \dot{x}_b - \Omega_{bx} \dot{z}_b) \\
&+ \dot{\Omega}_{bz} x_b - \dot{\Omega}_{bx} z_b \\
a_{bz} &= \bar{R}_{bz} + \ddot{z}_b + \Omega_{bx} \Omega_{bz} x_b + \Omega_{by} \Omega_{bz} y_b \\
&- (\Omega_{bx}^2 + \Omega_{by}^2) z_b + 2(\Omega_{bx} \dot{y}_b - \Omega_{by} \dot{x}_b) \\
&+ \dot{\Omega}_{bx} y_b - \dot{\Omega}_{by} x_b
\end{aligned} \right\} \quad \text{(A-52)}$$

The final expression for the acceleration components is as follows:

$$\begin{aligned}
 a_{bx} = & \ddot{R}_{bx} + \ddot{u} - u(\Omega_{by}^2 + \Omega_{bz}^2) + \Omega_{by} \Omega_{bx}(y + v) \\
 & + \Omega_{bx} \Omega_{bz} w + 2 \Omega_{by} \dot{w} - 2 \Omega_{bz} \dot{v} + \dot{\Omega}_{by} w \\
 & - \dot{\Omega}_{bz}(y + v) \\
 & + \eta(\cos \theta_s - \phi \sin \theta_s) \{-\dot{\phi}^2 - (\Omega_{by}^2 + \Omega_{bz}^2) \\
 & - \Omega_{by} \Omega_{bx} u' - 2 \Omega_{by} \dot{\phi} + 2 \Omega_{bz} (\dot{u}' - w' \dot{\phi}) \\
 & + \dot{\Omega}_{bz} u'\} + \eta(\sin \theta_s + \phi \cos \theta_s) \{-\ddot{\phi} \\
 & + \Omega_{by} \Omega_{bx} w' - \Omega_{bx} \Omega_{bz} - 2 \Omega_{bz} (\dot{w}' + u' \dot{\phi}) \\
 & - \dot{\Omega}_{by} - \dot{\Omega}_{bz} w'\} + \zeta(\cos \theta_s - \phi \sin \theta_s) \{\ddot{\phi} \\
 & - \Omega_{by} \Omega_{bx} w' + \Omega_{bx} \Omega_{bz} + 2 \Omega_{bz} (\dot{w}' + u' \dot{\phi}) \\
 & + \dot{\Omega}_{by} + \dot{\Omega}_{bz} w'\} + \zeta(\sin \theta_s + \phi \cos \theta_s) \{-\dot{\phi}^2 \\
 & - \Omega_{by} \Omega_{bx} u' - 2 \Omega_{by} \dot{\phi} + 2 \Omega_{bz} (\dot{u}' - w' \dot{\phi}) \\
 & + \dot{\Omega}_{bz} u' - (\Omega_{by}^2 + \Omega_{bz}^2)\} \quad (A-53)
 \end{aligned}$$

$$\begin{aligned}
 a_{by} = & \ddot{R}_{by} + \ddot{v} + u(\Omega_{by} \Omega_{bx} + \dot{\Omega}_{bz}) - w(\Omega_{by} \Omega_{bz} - \dot{\Omega}_{bx}) \\
 & - (y + v)(\Omega_{bx}^2 + \Omega_{bz}^2) + 2 \Omega_{bz} \dot{u} - 2 \Omega_{bx} \dot{w} \\
 & + \eta(\cos \theta_s - \phi \sin \theta_s) \{-\ddot{u}' + 2 \dot{\phi} \dot{w}' + u' \dot{\phi}^2 \\
 & + w' \ddot{\phi} + \Omega_{by} \Omega_{bx} + \dot{\Omega}_{bz} + u'(\Omega_{bx}^2 + \Omega_{bz}^2) \\
 & + 2 \Omega_{bx} \dot{\phi}\} + \eta(\sin \theta_s + \phi \cos \theta_s) \{2 \dot{\phi} \dot{u}' \\
 & + \dot{w}' + u' \ddot{\phi} - w' \dot{\phi}^2 - 2 \Omega_{bz} \dot{\phi} - \Omega_{by} \Omega_{bz} \\
 & + \dot{\Omega}_{bx} - w'(\Omega_{bx}^2 + \Omega_{bz}^2)\} + \zeta(\cos \theta_s - \phi \sin \theta_s) \\
 & \{-2 \dot{\phi} \dot{u}' - \dot{w}' + w' \dot{\phi}^2 + \Omega_{by} \Omega_{bz} - u' \ddot{\phi} - \dot{\Omega}_{bx} \} \quad (A-54)
 \end{aligned}$$

$$\begin{aligned}
& + 2 \Omega_{bz} \dot{\phi} + w'(\Omega_{bx}^2 + \Omega_{bz}^2) \} + \zeta(\sin \theta_s \\
& + \phi \cos \theta_s) \{ -\ddot{u}' + 2 \dot{\phi} \dot{w}' + u' \dot{\phi}^2 + w' \ddot{\phi} \\
& + \Omega_{by} \Omega_{bx} + \dot{\Omega}_{bz} + u'(\Omega_{bx}^2 + \Omega_{bz}^2) + 2 \Omega_{bx} \dot{\phi} \} \quad (A-54) \\
a_{bz} = & \ddot{R}_{bz} + \ddot{w} + u(\Omega_{bx} \Omega_{bz} - \dot{\Omega}_{by}) + \\
& + (y + v)(\Omega_{by} \Omega_{bz} + \dot{\Omega}_{bx}) - w(\Omega_{bx}^2 + \Omega_{by}^2) \\
& + 2 \Omega_{bx} \dot{v} - 2 \Omega_{by} \dot{u} + \eta(\cos \theta_s - \phi \sin \theta_s) \{ -\ddot{\phi} \\
& + \Omega_{bx} \Omega_{bz} - \dot{\Omega}_{by} - u'(\Omega_{by} \Omega_{bz} + \dot{\Omega}_{bx}) \\
& - 2 \Omega_{bx}(\dot{u}' - w' \dot{\phi}) \} - \eta(\sin \theta_s + \phi \cos \theta_s) \{ -\dot{\phi}^2 \\
& - w'(\Omega_{by} \Omega_{bz} + \dot{\Omega}_{bx}) - (\Omega_{bx}^2 + \Omega_{by}^2) \\
& - 2 \Omega_{bx}(\dot{w}' + u' \dot{\phi}) - 2 \Omega_{by} \dot{\phi} \} + \zeta(\cos \theta_s \\
& - \phi \sin \theta_s) \{ -\dot{\phi}^2 - w'(\Omega_{by} \Omega_{bz} + \dot{\Omega}_{bx}) \\
& - (\Omega_{bx}^2 + \Omega_{by}^2) - 2 \Omega_{bx}(\dot{w}' + u' \dot{\phi}) - 2 \Omega_{by} \dot{\phi} \} \\
& + \zeta(\sin \theta_s + \phi \cos \theta_s) \{ -\ddot{\phi} + \Omega_{bx} \Omega_{bz} - \dot{\Omega}_{by} \\
& - u'(\Omega_{by} \Omega_{bz} + \dot{\Omega}_{bx}) - 2 \Omega_{bx}(\dot{u}' - w' \dot{\phi}) \} \quad (A-55)
\end{aligned}$$

The inertia loadings on the beam may now be derived from these acceleration equations by appropriate integrations over the cross section. The total or resultant loadings desired in the analysis are the sum of the inertia loadings and the applied loadings. The moment loadings are found by taking moments about point 0* of Figure A-2. The resulting force and moment loadings are given by the following equations:

$$\left. \begin{aligned}
F_x &= L_x - \int_{\eta_{le}}^{\eta_{te}} \int_{\xi_u}^{\xi_1} a_{bx} \rho d\xi d\eta \\
F_y &= L_y - \int_{\eta_{le}}^{\eta_{te}} \int_{\xi_u}^{\xi_1} a_{by} \rho d\xi d\eta \\
F_z &= L_z - \int_{\eta_{le}}^{\eta_{te}} \int_{\xi_u}^{\xi_1} a_{bz} \rho d\xi d\eta
\end{aligned} \right\} \quad (A-56)$$

$$\begin{aligned}
Q_x &= M_{Ax} - \int_{\eta_{le}}^{\eta_{te}} \int_{\zeta_u}^{\zeta_l} [a_{bz}(y_b - v) \\
&\quad - a_{by}(z_b - w)] \rho \, d\zeta \, d\eta \\
Q_y &= M_{Ay} + \int_{\eta_{le}}^{\eta_{te}} \int_{\zeta_u}^{\zeta_l} [a_{bz}(x_b - u) \\
&\quad - a_{bx}(z_b - w)] \rho \, d\zeta \, d\eta \\
Q_z &= M_{Az} - \int_{\eta_{le}}^{\eta_{te}} \int_{\zeta_u}^{\zeta_l} [a_{by}(x_b - u) \\
&\quad - a_{bx}(y_b - v)] \rho \, d\zeta \, d\eta
\end{aligned}
\tag{A-56}$$

Cont'd

where

ρ is the density of the structural material and may be a function of ζ and η .

L_x , L_y , and L_z are three components of airload force.

and

M_{Ax} , M_{Ay} , and M_{Az} are three components of airload moment (M_{Ax} and M_{Az} normally zero).

Let

m = mass per unit length of beam section

e_{mB} = beamwise cg offset from reference axis for a section. For positive e_{mB} , the cg is above the reference axis.

e_{mC} = chordwise cg offset from reference axis for a section. For positive e_{mC} , the cg is aft of the reference axis.

Then

$$\int_{\eta_{le}}^{\eta_{te}} \int_{\zeta_u}^{\zeta_l} \rho \, \eta \, d\zeta \, d\eta = m \, e_{mC}
\tag{A-57}$$

$$\left. \begin{aligned} \int_{\eta_{1e}}^{\eta_{te}} \int_{\xi_u}^{\xi_1} \rho \xi d\xi d\eta &= m e_{mB} \\ \int_{\eta_{1e}}^{\eta_{te}} \int_{\xi_u}^{\xi_1} \rho d\xi d\eta &= m \end{aligned} \right\} \quad \begin{array}{l} (A-57) \\ \text{Cont'd} \end{array}$$

Making use of Equations (A-57) write the three integrated force components.

$$\begin{aligned} F_x = L_x - m[& \ddot{R}_{bx} + \ddot{u} - u(\Omega_{by}^2 + \Omega_{bz}^2) + \Omega_{by} \Omega_{bx}(Y + v) \\ & + \Omega_{bx} \Omega_{bz} w + 2 \Omega_{by} \dot{w} - 2 \Omega_{bz} \dot{v} - \dot{\Omega}_{by} w \\ & - \dot{\Omega}_{bz}(Y + v) + e_{mC}(\cos \theta_s - \phi \sin \theta_s)\{-\dot{\phi}^2 \\ & - (\Omega_{by}^2 + \Omega_{bz}^2) - \Omega_{by} \Omega_{bx} u' - 2 \Omega_{by} \dot{\phi} \\ & + 2 \Omega_{bz}(\dot{u}' - w' \dot{\phi}) + \dot{\Omega}_{bz} u'\} + e_{mC}(\sin \theta_s \\ & + \phi \cos \theta_s)\{-\ddot{\phi} + \Omega_{by} \Omega_{bx} w' - \Omega_{bx} \Omega_{bz} \\ & - 2 \Omega_{bz}(\dot{w}' + u' \dot{\phi}) - \dot{\Omega}_{by} - \dot{\Omega}_{bz} w'\} \\ & + e_{mB}(\cos \theta_s - \phi \sin \theta_s)\{\ddot{\phi} - \Omega_{by} \Omega_{bx} w' \\ & + \Omega_{bx} \Omega_{bz} + 2 \Omega_{bz}(\dot{w}' + u' \dot{\phi}) + \dot{\Omega}_{by} + \dot{\Omega}_{bz} w'\} \\ & + e_{mB}(\sin \theta_s + \phi \cos \theta_s)\{-\dot{\phi}^2 - \Omega_{by} \Omega_{bx} u' \\ & - 2 \Omega_{by} \dot{\phi} + 2 \Omega_{bz}(\dot{u}' - w' \dot{\phi}) + \dot{\Omega}_{bz} u' \\ & - (\Omega_{by}^2 + \Omega_{bz}^2)\}] \end{aligned} \quad (A-58)$$

$$\begin{aligned} F_y = L_y - m[& \ddot{R}_{by} + \ddot{v} + u(\Omega_{by} \Omega_{bx} + \dot{\Omega}_{bz}) \\ & - w(\Omega_{by} \Omega_{bz} - \dot{\Omega}_{bx}) - (Y + v)(\Omega_{bx}^2 + \Omega_{bz}^2) \\ & + 2 \Omega_{bz} \dot{u} - 2 \Omega_{bx} \dot{w} + e_{mC}(\cos \theta_s \\ & - \phi \sin \theta_s)\{-\ddot{u}' + 2 \dot{\phi} \dot{w}' + u' \dot{\phi}^2 + w' \ddot{\phi} \\ & + \Omega_{by} \Omega_{bx} + \dot{\Omega}_{bz} + u'(\Omega_{bx}^2 + \Omega_{bz}^2) + 2 \Omega_{bx} \dot{\phi}\} \\ & + e_{mC}(\sin \theta_s + \phi \cos \theta_s)\{2 \dot{\phi} \dot{u}' + \dot{w}' + u' \ddot{\phi} \end{aligned} \quad (A-59)$$

$$\begin{aligned}
& -w' \dot{\phi}^2 - 2 \Omega_{bz} \dot{\phi} - \Omega_{by} \Omega_{bz} + \dot{\Omega}_{bx} - w' (\Omega_{bx}^2 \\
& + \Omega_{bz}^2) \} + e_{mB} (\cos \theta_s - \phi \sin \theta_s) \{ -2 \dot{\phi} \dot{u}' \\
& - \dot{w}' + w' \dot{\phi}^2 + \Omega_{by} \Omega_{bz} - u' \ddot{\phi} - \dot{\Omega}_{bx} + 2 \Omega_{bz} \dot{\phi} \\
& + w' (\Omega_{bx}^2 + \Omega_{bz}^2) \} + e_{mB} (\sin \theta_s + \phi \cos \theta_s) \{ -\dot{u}' \\
& + 2 \dot{\phi} \dot{w}' + u' \dot{\phi}^2 + w' \ddot{\phi} + \Omega_{by} \Omega_{bx} + \dot{\Omega}_{bz} \\
& + u' (\Omega_{bx}^2 + \Omega_{bz}^2) + 2 \Omega_{bx} \dot{\phi} \}] \quad (A-59)
\end{aligned}$$

$$\begin{aligned}
F_z = & L_z - m[\ddot{R}_{bz} + \ddot{w} + u(\Omega_{bx} \Omega_{bz} - \dot{\Omega}_{by}) \\
& + (y + v)(\Omega_{by} \Omega_{bz} + \dot{\Omega}_{bx}) - w(\Omega_{bx}^2 + \Omega_{by}^2) \\
& + 2 \Omega_{bx} \dot{v} - 2 \Omega_{by} \dot{u} + e_{mC} (\cos \theta_s \\
& - \phi \sin \theta_s) \{ -\ddot{\phi} + \Omega_{bx} \Omega_{bz} - \dot{\Omega}_{by} - u' (\Omega_{by} \Omega_{bz} \\
& + \dot{\Omega}_{bx}) - 2 \Omega_{bx} (\dot{u}' - w' \dot{\phi}) \} - e_{mC} (\sin \theta_s \\
& + \phi \cos \theta_s) \{ -\dot{\phi}^2 - w' (\Omega_{by} \Omega_{bz} + \dot{\Omega}_{bx}) - (\Omega_{bx}^2 \\
& + \Omega_{by}^2) - 2 \Omega_{bx} (\dot{w}' + u' \dot{\phi}) - 2 \Omega_{by} \dot{\phi} \} \\
& + e_{mB} (\cos \theta_s - \phi \sin \theta_s) \{ -\dot{\phi}^2 - w' (\Omega_{by} \Omega_{bz} \\
& + \dot{\Omega}_{bx}) - (\Omega_{bx}^2 + \Omega_{by}^2) - 2 \Omega_{bx} (\dot{w}' + u' \dot{\phi}) \\
& - 2 \Omega_{by} \dot{\phi} \} + e_{mB} (\sin \theta_s + \phi \cos \theta_s) \{ -\ddot{\phi} \\
& + \Omega_{bx} \Omega_{bz} - \dot{\Omega}_{by} - u' (\Omega_{by} \Omega_{bz} + \dot{\Omega}_{bx}) \\
& - 2 \Omega_{bx} (\dot{u}' - w' \dot{\phi}) \}] \quad (A-60)
\end{aligned}$$

In order to write the moment equations, three other integrals must be evaluated.

Let

$$I_{\eta\eta} = \int_{\eta_{1e}}^{\eta_{te}} \int_{\xi_1}^{\xi_u} \rho \eta^2 d\xi d\eta \quad (A-61)$$

$$I_{\zeta\zeta} = \int_{\eta_{le}}^{\eta_{te}} \int_{\zeta_u}^{\zeta_l} \rho \zeta^2 d\zeta d\eta$$

(A-61)
Cont'd

$$I_{\eta\zeta} = \int_{\eta_{le}}^{\eta_{te}} \int_{\zeta_u}^{\zeta_l} \rho \eta \zeta d\zeta d\eta$$

In order to refer these inertia terms to more readily available quantities, first allow for a translation from the reference axis to the section cg and then account for the possibility that the principal axes for mass moments of inertia are not at the same angle as the structural principal axes. Thus

$$\begin{aligned} I_{\zeta\zeta} &= m e_{mB}^2 \cos^2(\theta_m - \theta_s) + m e_{mC}^2 \sin^2(\theta_m - \theta_s) \\ &\quad + I_{CC} \sin^2(\theta_m - \theta_s) + I_{BB} \cos^2(\theta_m - \theta_s) \\ I_{\eta\eta} &= m e_{mC}^2 \cos^2(\theta_m - \theta_s) + m e_{mB}^2 \sin^2(\theta_m - \theta_s) \\ &\quad + I_{CC} \cos^2(\theta_m - \theta_s) + I_{BB} \sin^2(\theta_m - \theta_s) \\ I_{\eta\zeta} &= [m e_{mB} e_{mC} + (I_{CC} - I_{BB})] \sin(\theta_m - \theta_s) \cos(\theta_m - \theta_s) \end{aligned} \quad (A-62)$$

where

I_{BB} = minor principal mass moment of inertia of the section. (Mass moment about chordwise axis.)

I_{CC} = major principal mass moment of inertia of the section. (Mass moment about beamwise axis.)

θ_m = angle between mass principal axis and x_b axis, positive for leading edge upward.

Then the airload and inertial loading moments may be written.

$$\begin{aligned} Q_x &= M_{AX} - \int_{\eta_{le}}^{\eta_{te}} \int_{\zeta_l}^{\zeta_u} -a_{by} (-\eta [\sin \theta_s + \phi \cos \theta_x] \\ &\quad + \zeta [\cos \theta_s - \phi \sin \theta_s]) \rho d\zeta d\eta \end{aligned}$$

$$\begin{aligned}
Q_y = M_{Ay} + \int_{\eta_{le}}^{\eta_{te}} \int_{\zeta_1}^{\zeta_u} \{ & a_{bz}(\eta[\cos \theta_s - \phi \sin \theta_s] \\
& + \zeta[\sin \theta_s + \phi \cos \theta_s]) + a_{bx}(\eta[\sin \theta_s \\
& + \phi \cos \theta_s] - \zeta[\cos \theta_s - \phi \sin \theta_s]) \} \rho \, d\zeta \, d\eta \\
Q_z = M_{Az} - \int_{\eta_{le}}^{\eta_{te}} \int_{\zeta_1}^{\zeta_u} & a_{by}(\eta[\cos \theta_s - \phi \sin \theta_s] \\
& + \zeta[\sin \theta_s + \phi \cos \theta_s])
\end{aligned}
\tag{A-63}$$

Cont'd

Substitution of a_{bx} , a_{by} , and a_{bz} from equations (A-53), (A-54), and (A-55) into Equation (A-63) yields the complete form of the loading moments.

$$\begin{aligned}
Q_x = M_{Ax} - I_{\eta\eta} [& \sin \theta_s \\
& + \phi \cos \theta_s \{ (\cos \theta_s - \phi \sin \theta_s) [-\ddot{u}' + 2 \dot{\phi} \dot{w}' \\
& + u' \dot{\phi}^2 + w' \ddot{\phi} + \Omega_{by} \Omega_{bx} + \dot{\Omega}_{bz} + u' (\Omega_{bx}^2 + \Omega_{bz}^2) \\
& + 2 \Omega_{bx} \dot{\phi}] + (\sin \theta_s + \phi \cos \theta_s) \{ 2 \dot{\phi} \dot{u}' + \ddot{w}' \\
& + u' \ddot{\phi} - w' \dot{\phi}^2 - 2 \Omega_{bz} \dot{\phi} - \Omega_{by} \Omega_{bz} + \dot{\Omega}_{bx} \\
& - w' (\Omega_{bx}^2 + \Omega_{bz}^2) \}] + I_{\zeta\zeta} [\cos \theta_s - \phi \sin \theta_s \{ (\cos \theta_s \\
& - \phi \sin \theta_s) \{ -2 \dot{\phi} \dot{u}' - \ddot{w}' + w' \dot{\phi}^2 + \Omega_{by} \Omega_{bz} \\
& - u' \ddot{\phi} - \dot{\Omega}_{bx} + 2 \Omega_{bz} \dot{\phi} + w' (\Omega_{bx}^2 + \Omega_{bz}^2) \} \\
& + [\sin \theta_s + \phi \cos \theta_s] [-\ddot{u}' + 2 \dot{\phi} \dot{w}' + u' \dot{\phi}^2
\end{aligned}
\tag{A-64}$$

$$\begin{aligned}
& + w' \dot{\phi} + \Omega_{by} \Omega_{bx} + \dot{\Omega}_{bz} + u'(\Omega_{bx}^2 + \Omega_{bz}^2) \\
& + 2 \Omega_{bx} \dot{\phi}] - I_{\eta\zeta} \{ (\sin \theta_s + \phi \cos \theta_s)^2 [-\ddot{u}' \\
& + 2 \dot{\phi} \dot{w}' + u' \dot{\phi}^2 + w' \dot{\phi} + \Omega_{by} \Omega_{bx} + \dot{\Omega}_{bz} \\
& + u'(\Omega_{bx}^2 + \Omega_{bz}^2) + 2 \Omega_{bx} \dot{\phi}] + (\sin \theta_s \\
& + \phi \cos \theta_s)(\cos \theta_s - \phi \sin \theta_s)[-2 \dot{\phi} \dot{u}' - \ddot{w}' \\
& + w' \dot{\phi}^2 + \Omega_{by} \Omega_{bz} - u' \dot{\phi} - \dot{\Omega}_{bx} + 2 \Omega_{bz} \dot{\phi} \\
& + w'(\Omega_{bx}^2 + \Omega_{bz}^2)] - (\cos \theta_s - \phi \sin \theta_s)^2 [-\ddot{u}' \\
& + 2 \dot{\phi} \dot{w}' + u' \dot{\phi}^2 + w' \dot{\phi} + \Omega_{by} \Omega_{bx} + \dot{\Omega}_{bz} \\
& + u'(\Omega_{bx}^2 + \Omega_{bz}^2) + 2 \Omega_{bx} \dot{\phi}] - (\cos \theta_s \\
& - \phi \sin \theta_s)(\sin \theta_s + \phi \cos \theta_s)[2 \dot{\phi} \dot{u}' + \ddot{w}' + u' \dot{\phi} \\
& - w' \dot{\phi}^2 - 2 \Omega_{bz} \dot{\phi} - \Omega_{by} \Omega_{bz} + \dot{\Omega}_{bx} - w'(\Omega_{bx}^2 \\
& + \Omega_{bz}^2)] \} - m[e_{mC}(\sin \theta_s + \phi \cos \theta_s) \\
& - e_{mB}(\cos \theta_s - \phi \sin \theta_s)][\ddot{R}_{by} + \ddot{v} \\
& + u(\Omega_{by} \Omega_{bx} + \dot{\Omega}_{bz}) - w(\Omega_{by} \Omega_{bz} - \dot{\Omega}_{bx} \\
& - (y + v)(\Omega_{bx}^2 + \Omega_{bz}^2) + 2 \Omega_{bz} \dot{u} - 2 \Omega_{bx} \dot{w}]
\end{aligned}$$

(A-64)
Concluded

$$\begin{aligned}
Q_y = & M_{Ay} + m[e_{mC}(\cos \theta_s - \phi \sin \theta_s) + e_{mB}(\sin \theta_s \\
& + \phi \cos \theta_s)][\ddot{R}_{bz} + \ddot{w} + u(\Omega_{bx} \Omega_{bz} - \dot{\Omega}_{by}) \\
& + (y + v)(\Omega_{by} \Omega_{bz} + \dot{\Omega}_{bx}) - w(\Omega_{bx}^2 + \Omega_{by}^2) \\
& + 2 \Omega_{bx} \dot{v} - 2 \Omega_{by} \dot{u}] + m[e_{mC}(\sin \theta_s + \phi \cos \theta_s) \\
& - e_{mB}(\cos \theta_s - \phi \sin \theta_s)][\ddot{R}_{bx} + \ddot{u} \\
& - u(\Omega_{by}^2 + \Omega_{bz}^2) + \Omega_{by} \Omega_{bx}(y + v) + \Omega_{bx} \Omega_{bz} w \\
& + 2 \Omega_{by} \dot{w} - 2 \Omega_{bz} \dot{v} + \dot{\Omega}_{by} w - \dot{\Omega}_{bz}(y + v)] \\
& + I_{\eta\eta}[\cos \theta_s - \phi \sin \theta_s]\{(\cos \theta_s - \phi \sin \theta_s)[- \ddot{\phi} \\
& + \Omega_{bx} \Omega_{bz} - \dot{\Omega}_{by} - u'(\Omega_{by} \Omega_{bz} + \dot{\Omega}_{bx}) - 2 \Omega_{bx}(\dot{u}'
\end{aligned}$$

(A-65)

$$\begin{aligned}
& - w' \dot{\phi}] - (\sin \theta_s + \phi \cos \theta_s) [-\dot{\phi}^2 - w' \Omega_{by} \Omega_{bz} \\
& + \dot{\Omega}_{bx}] - (\Omega_{bx}^2 + \Omega_{by}^2) - 2 \Omega_{bx} (\dot{w}' + u' \dot{\phi}) \\
& - 2 \Omega_{by} \dot{\phi}] + I_{\zeta\zeta} [\sin \theta_s + \phi \cos \theta_s] \{ (\cos \theta_s \\
& - \phi \sin \theta_s) [-\dot{\phi}^2 - w' (\Omega_{by} \Omega_{bz} + \dot{\Omega}_{bx}) - (\Omega_{bx}^2 \\
& + \Omega_{by}^2) - 2 \Omega_{bx} (\dot{w}' + u' \dot{\phi}) - 2 \Omega_{by} \dot{\phi}] \\
& + (\sin \theta_s + \phi \cos \theta_s) [-\dot{\phi} + \Omega_{bx} \Omega_{bz} - \dot{\Omega}_{by} \\
& - u' (\Omega_{by} \Omega_{bz} + \dot{\Omega}_{bx}) - 2 \Omega_{bx} (\dot{u}' - w' \dot{\phi})] \} \\
& + I_{\eta\zeta} \{ (\cos \theta_s - \phi \sin \theta_s) [(\cos \theta_s \\
& - \phi \sin \theta_s) (-\dot{\phi}^2 - w' [\Omega_{by} \Omega_{bz} + \dot{\Omega}_{bx}] - [\Omega_{bx}^2 \\
& + \Omega_{by}^2] - 2 \Omega_{bx} [\dot{w}' + u' \dot{\phi}] - 2 \Omega_{by} \dot{\phi}) + (\sin \theta_s \\
& + \phi \cos \theta_s) (-\dot{\phi} + \Omega_{bx} \Omega_{bz} - \dot{\Omega}_{by} - u' [\Omega_{by} \Omega_{bz} \\
& + \dot{\Omega}_{bx}] - 2 \Omega_{bx} [\dot{u}' - w' \dot{\phi}]) + (\sin \theta_s \\
& + \phi \cos \theta_s) [(\cos \theta_s - \phi \sin \theta_s) (-\dot{\phi} + \Omega_{bx} \Omega_{bz} \\
& - \dot{\Omega}_{by} - u' [\Omega_{by} \Omega_{bz} + \dot{\Omega}_{bx}] - 2 \Omega_{bx} [\dot{u}' - w' \dot{\phi}]) \\
& - (\sin \theta_s + \phi \cos \theta_s) (-\dot{\phi}^2 - w' [\Omega_{by} \Omega_{bz} + \dot{\Omega}_{bx}] \\
& - [\Omega_{bx}^2 + \Omega_{by}^2] - 2 \Omega_{bx} [\dot{w}' + u' \dot{\phi}] - 2 \Omega_{by} \dot{\phi})] \} \\
& + I_{\eta\eta} [\sin \theta_s + \phi \cos \theta_s] \{ (\cos \theta_s \\
& - \phi \sin \theta_s) [-\dot{\phi}^2 - (\Omega_{by}^2 + \Omega_{bz}^2) - \Omega_{by} \Omega_{bx} u' \\
& - 2 \Omega_{by} \dot{\phi} + 2 \Omega_{bz} (\dot{u}' - w' \dot{\phi}) + \dot{\Omega}_{bz} u'] \\
& + (\sin \theta_s + \phi \cos \theta_s) [-\dot{\phi} + \Omega_{by} \Omega_{bx} w' \\
& - \Omega_{bx} \Omega_{bz} - 2 \Omega_{bz} (\dot{w}' + u' \dot{\phi}) - \dot{\Omega}_{by} - \dot{\Omega}_{bz} w'] \} \\
& - I_{\zeta\zeta} (\cos \theta_s - \phi \sin \theta_s) \{ (\cos \theta_s \\
& - \phi \sin \theta_s) [\dot{\phi} - \Omega_{by} \Omega_{bx} w' + \Omega_{bx} \Omega_{bz} \\
& + 2 \Omega_{bz} (\dot{w}' + u' \dot{\phi}) + \dot{\Omega}_{by} + \dot{\Omega}_{bz} w'] \\
& + (\sin \theta_s + \phi \cos \theta_s) [-\dot{\phi}^2 - \Omega_{by} \Omega_{bx} u' - 2 \Omega_{by} \dot{\phi}
\end{aligned}$$

(A-65)
Cont'd

$$\begin{aligned}
& + 2 \Omega_{bz} (\dot{u}' - w' \dot{\phi}) + \dot{\Omega}_{bz} u' - (\Omega_{by}^2 + \Omega_{bz}^2)] \} \\
& + I_{\eta\zeta} \{ (\sin \theta_s + \phi \cos \theta_s) [(\cos \theta_s - \phi \sin \theta_s) \{ \ddot{\phi} \\
& - \Omega_{by} \Omega_{bx} w' + \Omega_{bx} \Omega_{bz} + 2 \Omega_{bz} (\dot{w}' + u' \dot{\phi}) \\
& + \dot{\Omega}_{by} + \dot{\Omega}_{bz} w' \} + (\sin \theta_s + \phi \cos \theta_s) \{ -\dot{\phi}^2 \\
& - \Omega_{by} \Omega_{bx} u' - 2 \Omega_{by} \dot{\phi} + 2 \Omega_{bz} (\dot{u}' - w' \dot{\phi}) \\
& + \dot{\Omega}_{bz} u' - (\Omega_{by}^2 + \Omega_{bz}^2) \}] - (\cos \theta_s \\
& - \phi \sin \theta_s) [(\cos \theta_s - \phi \sin \theta_s) \{ -\dot{\phi}^2 - (\Omega_{by}^2 \\
& + \Omega_{bz}^2) - \Omega_{by} \Omega_{bx} u' - 2 \Omega_{by} \dot{\phi} + 2 \Omega_{bz} (\dot{u}' \\
& - w' \dot{\phi}) + \dot{\Omega}_{bz} u' \} + (\sin \theta_s + \phi \cos \theta_s) \{ -\ddot{\phi} \\
& + \Omega_{by} \Omega_{bx} w' - \Omega_{bx} \Omega_{bz} - 2 \Omega_{bz} (\dot{w}' + u' \dot{\phi}) \\
& - \dot{\Omega}_{by} - \dot{\Omega}_{bz} w' \}] \}
\end{aligned}$$

(A-65)
Cont'd

$$\begin{aligned}
Q_z = M_{Az} - m[& e_{mC} (\cos \theta_s - \phi \sin \theta_s) + e_{mB} (\sin \theta_s \\
& + \phi \cos \theta_s)] [\ddot{R}_{by} + \ddot{v} + u (\Omega_{by} \Omega_{bx} + \dot{\Omega}_{bz}) \\
& - w (\Omega_{by} \Omega_{bz} - \dot{\Omega}_{bx}) - (y + v) (\Omega_{bx}^2 + \Omega_{bz}^2) \\
& + 2 \Omega_{bz} \dot{u} - 2 \Omega_{bx} \dot{w}] - I_{\eta\eta} (\cos \theta_s \\
& - \phi \sin \theta_s) \{ (\cos \theta_s - \phi \sin \theta_s) [-\ddot{u}' + 2 \dot{\phi} \dot{w}' \\
& + u' \dot{\phi}^2 + w' \ddot{\phi} + \Omega_{by} \Omega_{bx} + \dot{\Omega}_{bz} + u' (\Omega_{bx}^2 + \Omega_{bz}^2) \\
& + 2 \Omega_{bx} \dot{\phi}] + (\sin \theta_s + \phi \cos \theta_s) [2 \dot{\phi} \dot{u}' \\
& + \ddot{w}' + u' \ddot{\phi} - w' \dot{\phi}^2 - 2 \Omega_{bz} \dot{\phi} - \Omega_{by} \Omega_{bz} \\
& + \dot{\Omega}_{bx} - w' (\Omega_{bx}^2 + \Omega_{bz}^2)] \} - I_{\zeta\zeta} (\sin \theta_s \\
& + \phi \cos \theta_s) \{ (\cos \theta_s - \phi \sin \theta_s) [-2 \dot{\phi} \dot{u}' - \ddot{w}' \\
& + w' \dot{\phi}^2 + \Omega_{by} \Omega_{bz} - u' \ddot{\phi} - \dot{\Omega}_{bx} + 2 \Omega_{bz} \dot{\phi} \\
& + w' (\Omega_{bx}^2 + \Omega_{bz}^2)] + (\sin \theta_s + \phi \cos \theta_s) [-\ddot{u}'
\end{aligned}$$

(A-66)

$$\begin{aligned}
& + 2 \dot{\phi} \dot{w}' + u' \dot{\phi}^2 + w' \ddot{\phi} + \Omega_{by} \Omega_{bx} + \dot{\Omega}_{bz} \\
& + u'(\Omega_{bx}^2 + \Omega_{bz}^2) + 2 \Omega_{bx} \dot{\phi} \} - I_{\eta\zeta} \{ [\cos \theta_s \\
& - \phi \sin \theta_s] (\cos \theta_s - \phi \sin \theta_s) \{ -2 \dot{\phi} \dot{u}' - \dot{w}' \\
& + w' \dot{\phi}^2 + \Omega_{by} \Omega_{bz} - u' \ddot{\phi} - \dot{\Omega}_{bx} + 2 \Omega_{bz} \dot{\phi} \\
& + w'(\Omega_{bx}^2 + \Omega_{bz}^2) \} + (\sin \theta_s + \phi \cos \theta_s) \{ -\ddot{u}' \\
& + 2 \dot{\phi} \dot{w}' + u' \dot{\phi}^2 + w' \ddot{\phi} + \Omega_{by} \Omega_{bx} + \dot{\Omega}_{bz} \\
& + u'(\Omega_{bx}^2 + \Omega_{bz}^2) + 2 \Omega_{bx} \dot{\phi} \} + [\sin \theta_s \\
& + \phi \cos \theta_s] [(\cos \theta_s - \phi \sin \theta_s) \{ -\ddot{u}' \\
& + 2 \dot{\phi} \dot{w}' + u' \dot{\phi}^2 + w' \ddot{\phi} + \Omega_{by} \Omega_{bx} + \dot{\Omega}_{bz} \\
& + u'(\Omega_{bx}^2 + \Omega_{bz}^2) + 2 \Omega_{bx} \dot{\phi} \} + (\sin \theta_s \\
& + \phi \cos \theta_s) \{ 2 \dot{\phi} \dot{u}' + \dot{w}' + u' \ddot{\phi} - w' \dot{\phi}^2 \\
& - 2 \Omega_{bz} \dot{\phi} - \Omega_{by} \Omega_{bz} + \dot{\Omega}_{bx} - w'(\Omega_{bx}^2 + \Omega_{bz}^2) \} \} \}
\end{aligned}$$

(A-66)
Contd.

Equilibrium of Forces and Moments

Now consider the equilibrium of the blade element which was shown in Figure A-4. Summation of the forces in the x_b , y_b , and z_b directions, and summation of the moments about the x_b , y_b , z_b axes yield the equilibrium conditions for shear and moment.

$$\left. \begin{aligned} dV_x + F_x dy &= 0 \\ dV_y + F_y dy &= 0 \\ dV_z + F_z dy &= 0 \end{aligned} \right\} \quad (A-67)$$

$$\left. \begin{aligned} dM_x + V_z(dy + dv) - V_y dw + Q_x dy &= 0 \\ dM_y + V_x dw - V_z du + Q_y dy &= 0 \\ dM_z + V_x(dy + dv) V_y du - Q_z dy &= 0 \end{aligned} \right\} \quad (A-68)$$

It is these six equations that form the basis for the analysis in DNAM05 and C81. It is unnecessary to make the substitutions for forces and moments because that does not add to the understanding of the equations or physical phenomena.

APPENDIX B

EULER ANGLE TRANSFORMATION

In this appendix the relationships needed for the Euler angle transformations from one coordinate system to another are described. As stated in Appendix A, the general Euler angle transformation from system 1 to system 2 is an ordered rotation through the angles α_1 , α_2 , and α_3 . The transformation of vector \bar{A} from system 1 to system 2 coordinates is indicated by

$$\bar{A}^{(2)} = [T_{2/1}] \bar{A}^{(1)} \quad (B-1)$$

This transformation is made by first rotating about the z axis of system 1 through the angle α_1 . Then a rotation is made about the new y axis through the angle α_2 . Finally, a rotation is made about the new x axis through the angle α_3 to reach the system 2 coordinates. The resulting general transformation is shown in Figure B-1.

The items remaining to complete the angular transformations are the angles themselves that are used to get from one system to the next. These are

- (1) Ground Reference to Fuselage Reference - $[T_{f/g}]$
 α_1 is the yaw angle, ψ_f ; α_2 is the pitch angle, θ_f ; and α_3 is the roll angle, ϕ_f .
- (2) Fuselage Reference to Mast Reference - $[T_{m/f}]$
The α_1 rotation about z_f axis is always zero. α_2 is equal to the negative of the rotor longitudinal mast tilt angle ($-\xi_{F/A}$). α_3 is the lateral mast tilt angle (ξ_{Lat}).
- (3) Mast Reference to Hub Reference (one for each blade) - $[T_{h/m}]$ α_1 is 180 degrees plus the blade azimuth angle ($180^\circ + \psi$). α_2 is always zero. α_3 is upward through the blade feathering angle for this blade.

(4) Hub reference to Blade Reference - $[T_{b/h}]$

α_1 is the negative of the lag angle at the feathering bearings. α_2 is the geometric pitch angle at the feathering bearings (or pitch change axis origin) including kinematic inputs plus dynamic effects of the rotor modes. α_3 is the flapping angle at the pitch change axis origin, including coning.

$$[T_{2/1}] =$$

$$\begin{bmatrix} \cos \alpha_1 \cos \alpha_2 & \sin \alpha_1 \cos \alpha_2 & -\sin \alpha_2 \\ \cos \alpha_1 \sin \alpha_2 \sin \alpha_3 & \sin \alpha_1 \sin \alpha_2 \sin \alpha_3 & \cos \alpha_2 \sin \alpha_3 \\ -\sin \alpha_1 \cos \alpha_3 & +\cos \alpha_1 \cos \alpha_3 & \\ \cos \alpha_1 \sin \alpha_2 \cos \alpha_3 & \sin \alpha_1 \sin \alpha_2 \cos \alpha_3 & \cos \alpha_2 \cos \alpha_3 \\ +\sin \alpha_1 \sin \alpha_3 & -\cos \alpha_1 \sin \alpha_3 & \end{bmatrix}$$

Figure B-1. General Euler Angle Transformation Matrix.

APPENDIX C

USE OF THE MANEUVER PERTURBATION OPTION IN C81

ACTIVATING THE MANEUVER PERTURBATION OPTION

The purpose of this appendix is to explain the input for and operation of the maneuver perturbation option of C81. In order to activate the maneuver perturbation option, a special value of J on card 311 is required. The usual card 311, as discussed in Sections 2.27 and 3.27 of Volume II, contains data indicating what type of maneuver inputs are to be used. The special card 311 has only three inputs as follows:

Column 1 NEXTJ = 0 for last card 311

NEXTJ \neq 0 if another card 311 follows

Columns 3 - 5 J

J = 101 for the maneuver perturbation of the fuselage degrees of freedom. The increment used is based on input XIT(4) as discussed in Section 3.19 of Volume II. The order of the maneuver cases run is

- (1) Base - no perturbations
- (2) ϕ_f - fuselage Euler angle roll
- (3) θ_f - fuselage Euler angle pitch
- (4) ψ_f - fuselage Euler angle yaw
- (5) V_{xf} - fuselage reference x velocity
- (6) V_{yf} - fuselage reference y velocity
- (7) V_{zf} - fuselage reference z velocity
- (8) p - fuselage reference roll rate
- (9) q - fuselage reference pitch rate
- (10) r - fuselage reference yaw rate

J = 102 for perturbation of pylon modes

Columns 11 - 20 contain the increment to pylon modal displacement; the increment to the pylon velocities is

the displacement increment
times the natural frequency of
the mode in question (rad/sec)

The maneuver cases are run in the following order:

- (1) Base conditions (if not already run for fuselage)
- (2) Perturb each pylon displacement for rotor 1
- (3) Perturb each pylon displacement for rotor 2
- (4) Perturb each pylon velocity for rotor 1
- (5) Perturb each pylon velocity for rotor 2

J = 103 for perturbation of rotor modes

Columns 11 - 20 contain the increment to rotor modal displacements

For the rotor perturbations the base case is run first, then all of rotor 1 followed by rotor 2.

Because of the differences in the methods of incrementing gimbaled hub rotors and rigid hub rotors, two separate sequences are needed.

For a gimbaled rotor the sequence is strictly by mode number with all of the displacements first and then all of the velocities.

For a nongimbaled hub (hingeless or articulated rotor), each mode on each blade must be incremented separately.

- (1) Increment each mode for blade 1.
- (2) Increment each mode for blade 2.
- (3) Continue through all blades.
- (4) Then increment all velocities in same order.

USE OF PERTURBATION MANEUVERS IN THE POST-PROCESSOR

One additional input parameter has been added to help the user process the maneuver perturbation results for plots, rotor stability data, etc., as described in Sections 3.28 through 3.34 of Volume II. The new input is a special value of the NOP variable which goes in columns 1 and 2 of a card following the 311 cards.

Initially, the post-processor is set to process the base case maneuver data. Any number of processing steps may be carried out on this data, or none. In order to advance to the first perturbation case, a card with NOP = 14 must be entered. Then any amount of processing may be carried out on these data until another NOP = 14 is encountered. Each time an NOP = 14 is encountered, the program advances to the next set of maneuver data so that some sets of data may be skipped entirely if the user desires. It is permissible to stop the job at any point so it is not necessary to advance the data to the last perturbation case.

LIST OF SYMBOLS

A	unsteady pitching moment parameter proportional to $\bar{\alpha}$ used with Carta's tables
\bar{A}	unit vector defining intersection of aircraft plane of symmetry and plane perpendicular to the resultant force vector
A_1, \dots, A_5	constants used to calculate the aerodynamic pitching moment coefficient
A_{1M}	main (first) rotor fore-and-aft flapping displacement, positive down aft with respect to vertical shaft, rad
A_{1T}	tail (second) rotor fore-and-aft flapping displacement, positive down aft with respect to vertical shaft, rad
A_u	component of aerodynamic force in the x_b direction, lb
A_w	component of aerodynamic force in the z_b direction, lb
A_ϕ	component of aerodynamic pitching moment about the y_b direction axis, right hand positive, ft-lb
a	distance from midchord to elastic axis divided by semichord
\bar{a}	absolute acceleration of a point relative to ground (with various subscripts), ft/sec ²
\underline{a}	slope of lift curve
a_{1WP}	longitudinal flapping angle of the wake plane, deg
a_m	total mast tilt angle, rad
B	unsteady pitching moment parameter proportional to $\bar{\theta}$ used with Carta's tables

B	tip loss factor
\bar{B}	vector equal to the cross-product of the rotor resultant force vector and the velocity vector, $\frac{\text{ft-lb}}{\text{sec}}$
B_1, \dots, B_5	Integrals in rotor blade bending equations
B_{1M}	main (first) rotor lateral flapping displacement, positive down right with respect to vertical shaft, rad
B_{1T}	tail (second) rotor lateral flapping displacement, positive down left with respect to vertical shaft, rad
b	as subscript, indicates blade reference system
b	blade semichord, ft
b_{1WP}	lateral flapping angle of the wake-plane, deg
$[C]$	velocity coefficient matrix in the stability analysis
C_B	corrected thrust coefficient
C_d	aerodynamic drag coefficient
C_{d_N}	aerodynamic coefficient for determining drag force in the y_b direction
C_{d_R}	aerodynamic drag coefficient for determining drag force in the x_b direction
C_{ij}	element of the velocity coefficient matrix in the stability analysis
C_l	aerodynamic lift coefficient
$C_{L_{\max}}$	maximum lift coefficient
C_{l_s}	steady state aerodynamic lift coefficient
C_{l_T}	lift coefficient with unsteady effects included

C_m	aerodynamic pitching moment coefficient
C_T	thrust coefficient
$C(k)$	Theodorsen circulation function
c	blade chord, ft
c	lead-lag damper coefficient, ft-lb-sec/rad
D	intermediate variable in blade bending analysis-Equation (A-12)
d	length dependent on the blade chord and pitch axis location
\bar{d}	constant used to calculate the aerodynamic pitching moment coefficient
E	Young's modulus for rotor blade section, lb/in ²
E	expression involving the Theodorsen circulation function
e_{AB}	beamwise neutral axis offset from pitch-change axis, positive up, in.
e_{AC}	chordwise neutral axis offset from pitch-change axis, positive aft, in.
e_{mB}	beamwise center of gravity offset from pitch-change axis, positive up, in.
e_{mC}	chordwise center of gravity offset from pitch-change axis, positive aft, in.
F_{C81}	magnitude of the average or filtered resultant force vector computed by C81, lb
F_N	function for determining the value of induced velocity, normalized by \bar{V}_i
F_R	magnitude of resultant force vector used to calculate the RIVD table, lb
F_i	i^{th} applied force or moment in the stability analysis

F_n	forcing function for the n^{th} blade mode, ft-lb
F_u	inplane component of F_n , ft-lb
F_w	out-of-plane component of F_n , ft-lb
F_x	total applied load in x_b direction at a point on the blade, lb
F_x	fore-and-aft (X) component of applied force in fuselage body reference, lb
F_y	total applied load in y_b direction at a point on the blade, lb
F_y	lateral (Y) component of applied force in fuselage body reference, lb
F_z	total applied load in z_b direction at a point on the blade, lb
F_z	vertical (Z) component of applied force in fuselage body reference, lb
$F(k)$	real component of $C(k)$
f	elemental fiber in development of strain equation
f	as subscript, indicates fuselage reference system
f	frequency, Hz
f_1	induced velocity distribution function
f_2	nondimensional function used to modify the induced velocity distribution to account for tip-vortex effects
f_u	upper break frequency of the digital filter, Hz
G	ground effect factor
G	shear modulus for rotor blade section, lb/in. ²
G_i	functional notation used in representing the equations of motion in the stability analysis

$\left. \frac{\partial G_i}{\partial x_j} \right _0$	partial derivative of the i^{th} motion expression with respect to the j^{th} perturbation variable, evaluated at the initial condition
$G(k)$	imaginary component of $C(k)$
g	as subscript, indicates ground reference system
g_1	gear ratio, rotor 1 to engine
g_2	gear ratio, rotor 2 to engine
$H(if)$	digital filter transfer function
HTC	hub transfer coefficient matrix
h	as subscript, indicates hub reference system
h	undersling distance, ft
\dot{h}	vertical (heaving) velocity of blade segment, positive down, ft/sec
\ddot{h}	vertical (heaving) acceleration, positive down, ft/sec ²
\dot{h}_o	"steady" (frequency less than Ω) part of the inflow velocity, positive down, ft/sec
\dot{h}_v	vibratory part of the inflow velocity, positive down, ft/sec
I_1	rotor 1 rotary inertia, slug-ft ²
I_2	rotor 2 rotary inertia, slug-ft ²
I_B	blade beamwise area moment of inertia about neutral axis, in. ⁴
I_{BB}	blade beamwise mass moment of inertia about center of gravity, in.-lb-sec ² /in.
I_C	blade beamwise area moment of inertia about neutral axis, in. ⁴
I_{CC}	blade chordwise mass moment of inertia about center of gravity, in.-lb-sec ² /in.

I_{TE}	total inertia driven by the engine, slug-ft ²
I_n	generalized inertia of n th blade mode, ft-lb-sec ²
I_u	inplane inertial force distribution, lb/ft
I_w	out-of-plane inertial force distribution, lb/ft
I_ϕ	inertial pitching moment distribution, ft-lb/ft
$I_{\eta\eta}$	chordwise mass moment of inertia about pitch change axis, in.-lb-sec ² /in.
$I_{\eta\zeta}$	mass product of inertia about pitch change axis, in.-lb-sec ² /in.
$I_{\zeta\zeta}$	beamwise mass moment of inertia about pitch change axis, in.-lb-sec ² /in.
i, j, k	unit vectors in the blade reference system
J	area polar moment of inertia of blade cross section, in. ⁴
$[K]$	displacement coefficient matrix in the stability analysis
K_1	time constant for engine power increase, sec
K_2	time constant for engine power decrease, sec
K_{ij}	element of the displacement coefficient matrix in the stability analysis
K_{27}	multiplier on $f_2(\mu)$
k	reduced frequency in the Theodorsen circulation function
k_A	area radius of gyration of blade section, in.
k_S	flapping stop spring rate, ft-lb/rad
k_β	flapping spring rate, ft-lb/rad
L	roll component of applied moment in fuselage reference, ft-lb

L' lift per unit span, positive down, lb/ft
 L_{RM} roll component of applied moment in main (first) rotor reference, ft-lb
 L_{RT} roll component of applied moment in tail (second) rotor reference, ft-lb
 L_w roll component of aerodynamic moment caused by vertical acceleration of the fuselage, (ft-lb)/(ft/sec)
 L_x, L_y, L_z components of aerodynamic force in blade reference, lb/in.
 M Mach number
 M pitch component of applied moment in fuselage reference, ft-lb
 $[M]$ acceleration coefficient matrix in the stability analysis
 M_{Ax}, M_{Ay}, M_{Az} component of aerodynamic moment in blade reference, in.-lb/in.
 M_{blade} three-dimensional Mach number with yawed flow effect
 M_B internal blade beamwise bending moment, in.-lb
 M_C internal blade chordwise bending moment, in.-lb
 M_{ij} element of the acceleration coefficient matrix in the stability analysis
 M_{RM} roll component of applied moment in main (first) rotor reference, ft-lb
 M_{RT} roll component of applied moment in tail (second) rotor reference, ft-lb
 M_s flapping moment due to flapping spring, ft-lb
 M_w pitch component of aerodynamic moment caused by vertical acceleration of the fuselage, (ft-lb)/(ft/sec)
 M_x, M_y, M_z components of internal blade bending moment, in.-lb

MM	Mach number parameter
m	mass per unit length on blade, lb-sec ² /in. ²
m	as subscript, indicates mast reference
N	yaw component of applied moment in fuselage reference, ft/lb
N	order of digital filter
N _w	yaw component of aerodynamic moment caused by vertical acceleration of the fuselage, (ft-lb)/(ft/sec)
NB	number of blades
NM	total number of modes used in elastic rotor representation
O	origin of blade coordinate system
P	roll component of fuselage angular velocity in fuselage body reference, rad/sec
P ₁ , P ₂ , P ₃	input powers used to compute maximum power available, hp
P _A	power available, HP
P _{ACC}	accessory power, HP
P _{MA_C}	maximum continuous power available, HP
P _{MA_{SL}}	maximum sea level power available, HP
P _{MA_{TO}}	maximum takeoff power available, HP
P _{MR}	main rotor power required, HP
P _R	power required from engine, HP •
P _{SM}	roll component of fuselage angular velocity in main (first) rotor shaft reference, rad/sec

P_{ST}	roll component of fuselage angular velocity in tail (second) rotor shaft reference, rad/sec
P_{TR}	tail rotor power required, HP
PA	location of pitch axis, normalized on the chord length, positive aft of the leading edge (Reference 18)
PMOM	pitch moment at top of shaft, ft-lb
p_n	value of a polynomial p at time point t_n
$p_n^{(r)}$	value of the r^{th} derivative of the polynomial p at t_n
p_o	initial value of the fuselage roll angular velocity in the stability analysis, rad/sec
Q	pitch component of the fuselage angular velocity in fuselage body reference, rad/sec
Q	blade reference internal torsional moment, in.-lb
Q_R	torque required by aircraft, at engine rpm, ft-lb
Q_S	torque supplied by engine, at engine rpm, ft-lb
Q_{SM}	pitch component of fuselage angular velocity in main (first) rotor shaft reference, rad/sec
Q_{ST}	pitch component of fuselage angular velocity in tail (second) rotor shaft reference, rad/sec
Q_x, Q_y, Q_z	components of applied moment on blade including airloads and inertia loads, in.-lb/in.
q	dynamic pressure, lb/ft ²
\bar{q}	dynamic pressure with vibratory velocity included, lb/ft ²
q_o	initial value of the fuselage pitch angular velocity (q) in the stability analysis, rad/sec
q_1, q_2	constants used to calculate Mach number with yawed flow effect

R	components of the fuselage angular velocity in fuselage body reference, rad/sec
R	rotor radius
\bar{R}	radius vector to origin of a coordinate system
RC	rate of climb, ft/sec
$\bar{r}_{m/f}$	radius vector from fuselage cg to top of mast, ft
$RMOM$	rolling moment at top of shaft, ft-lb
R_{SM}	yaw component of fuselage angular velocity in main (first) rotor shaft reference, rad/sec
R_{ST}	yaw component of fuselage angular velocity in tail (second) rotor shaft reference, rad/sec
\bar{r}	radius vector to a point within a coordinate system
r_o	initial value of fuselage yaw angular velocity (r) in the stability analysis, rad/sec
s	as subscript, indicates structural principal axes
s_B	beamwise shear center offset from pitch change axis positive up, in.
s_C	chordwise shear center offset from pitch change axis, positive aft, in.
T	tension in blade, local blade reference, lb
T	thrust, lb
T_1, T_2, T_3	input temperatures used to compute engine power available, °C
$T_d(f)$	time delay of digital filter, sec
$T_{M_{ij}}$	element of the Euler angle transformation matrix relating fuselage body reference to main (first) rotor shaft reference
$T_{T_{ij}}$	element of the Euler angle transformation matrix relating fuselage body reference to tail (second) rotor shaft reference

$T[\psi, \theta, \phi]$	Euler angle transformation matrix in rotorcraft stability analysis
t_1	time constant to null rates, sec
t_2	time constant to null displacements, sec
U	magnitude of relative wind, ft/sec
U	fore-and-aft (X) component of fuselage linear velocity in fuselage body reference, ft/sec
\bar{U}	magnitude of relative wind with vibratory velocity included, ft/sec
U_P	component of relative wind velocity perpendicular to U_T and U_R , positive up, ft/sec
U_R	component of relative wind velocity in radial direction, positive outboard, ft/sec
U_T	component of relative wind velocity perpendicular to blade-span axis and shaft axis, positive toward trailing edge, ft/sec
$\bar{U}_T, \bar{U}_R, \bar{U}_P$	components of relative wind with blade vibration velocity included, ft/sec
u, v, w	components of blade elastic displacement, inplane/out-of-plane reference
u_0	initial value of the fuselage fore-and-aft velocity (u) in the stability analysis, ft/sec
V	lateral (y) component of fuselage linear velocity in fuselage body reference, ft/sec
V	flight path velocity, ft/sec
\bar{V}	vector indicating absolute velocity of a point relative to ground
V_h	magnitude of inplane component of the free stream velocity at the rotor hub, ft/sec
\bar{V}_i	average value of induced velocity, ft/sec
$\bar{V}_i(\mu, \alpha_{WP})$	average induced velocity input as part of RIVD table

\bar{V}_i _{avC81}	average induced velocity computed by subroutine VIND, ft/sec
(\bar{V}_i) _{IGE}	average induced velocity in ground effect, ft/sec
\bar{V}_i _N	average induced velocity divided by 1.0 ft/sec
(\bar{V}_i) _{OGE}	average induced velocity out of ground effect, ft/sec
V_N	free stream airspeed divided by 1.0 ft/sec
V_x, V_y, V_z	components of shear in inplane/out-of-plane reference, lb
V_z	magnitude of out-of-plane component of the free stream velocity at the rotor hub, ft/sec
V_η	local blade chordwise shear, lb
V_ξ	local blade beamwise shear, lb
v	resultant wind velocity
\vec{V}_i	induced velocity at a point on the rotor blades, ft/sec
v_i	magnitude of the induced velocity, ft/sec
v_o	initial value of the fuselage lateral velocity (v) in the stability analysis, ft/sec
v_{sound}	velocity of sound, ft/sec
$VBM(y, t)$	total out-of-plane bending moment distribution, ft-lb
W	virtual work, ft-lb
W	vertical component of fuselage linear velocity in fuselage body reference, ft/sec
W_x	fore-and-aft component of the weight vector in fuselage body reference, lb

w_y	lateral component of the weight vector in fuselage body reference, lb
w_z	vertical component of the weight vector in fuselage body reference, lb
w_o	initial value of the fuselage vertical velocity (w) in the stability analysis, ft/sec
x,y,z	blade coordinates used to develop the strain equation
x_i	i^{th} basic perturbation variable in the stability analysis
\bar{x}_i	i^{th} basic variable in the stability analysis
x_{i_o}	i^{th} basic variable initial value in the stability analysis
y_w	side force component of aerodynamic force caused by vertical acceleration of the fuselage, lb/(ft/sec)
y_i	i^{th} auxiliary perturbation variable in the stability analysis
\bar{y}_i	i^{th} auxiliary variable in the stability analysis
y_{i_o}	initial value of i^{th} auxiliary variable in the stability analysis
z_w	vertical component of aerodynamic force caused by vertical acceleration of the fuselage, lb/(ft/sec)
α	angle of attack, rad
$\bar{\alpha}$	angle of attack with vibratory velocity included, rad
$\underline{\alpha}$	angle of attack excluding the effect of vertical velocity, rad
α_B	angle of attack at which the aerodynamic pitching moment coefficient curve breaks sharply, rad
α_{Carta}	angle of attack modified for Mach number effect before entering Carta tables
α_{EQU}	the equivalent angle of attack including effects from the circulation function (Reference 18), rad

α_{mod}	angle of attack modified for yawed flow, rad
α_{RD}	reference angle of attack for drag
α_{RL}	reference angle of attack for lift
α_{WP}	wake-plane angle of attack, deg
$\alpha_1, \alpha_2, \alpha_3$	general set of Euler angles in definition of coordinate transformations
α'	$90 - \alpha_{\text{WP}}$, deg
β	flapping angle, positive up, rad
β_o	"steady" (frequency less than Ω) part of β , rad
β_v	vibratory part of the flapping angle, rad
γ	blade tip sweep angle, rad
$\Delta \text{ a.c.}$	offset of blade segment aerodynamic center, ft
ΔC_l	increment in lift coefficient due to unsteady aerodynamic effects
ΔC_m	increment in pitching moment coefficient due to unsteady effects
ΔD_N	normal drag vector for a blade segment, lb
ΔD_R	radial drag vector for a blade segment, lb
Δ_i	i^{th} constant in numerical evaluation of partial derivatives
ΔL	incremental lift, lb
$\Delta \vec{L}$	lift vector for a blade segment, lb
$\Delta \vec{M}$	pitching moment vector for a blade segment, ft-lb
Δr	blade segment length, ft

Δt	increment of time, sec
$\Delta \alpha$	angle of attack increment for stall hysteresis, rad
δ	atmospheric pressure ratio
ϵ	strain in blade differential equations
ϵ_T	strain due to steady centrifugal force
ζ	beamwise coordinate in blade differential equations
ζ_l	lower surface value of ζ
ζ_u	upper surface value of ζ
η	chordwise coordinate in blade differential equations
η_1	rotor 1 gearbox efficiency ratio
η_2	rotor 2 gearbox efficiency ratio
η_3	overall gearbox efficiency ratio
$\eta_{\cos}(r,n)$	n^{th} harmonic cosine component of the induced velocity distribution at radius r
η_{le}	leading edge value of η
$\eta_{\sin}(r,n)$	n^{th} harmonic sine component of the induced velocity distribution at radius r
η_{te}	trailing edge value of η
η_{le}	leading edge value of η
θ	Euler pitch angle relating the fuselage body axis system to an inertial axis system, rad
θ_M	main (first) rotor fore-and-aft tilt angle, positive forward, rad
θ_T	tail (second) rotor fore-and-aft tilt angle, positive forward, rad
θ	fuselage Euler pitch angle perturbation in the stability analysis, rad

$\bar{\theta}$	geometric pitch with blade vibration velocity included, rad
θ_c	total blade cyclic pitch, rad
$\theta_{F/A}$	fore-and-aft cyclic pitch angle, rad
θ_{LAT}	lateral cyclic pitch angle, rad
θ_m	angle of mass principal axis relative to shaft plane
θ_o	collective pitch angle, rad
θ_o	initial value of the fuselage Euler pitch angle in the stability analysis, rad
θ_o	steady (frequency = 0) part of the pitch angle, rad
θ_s	angle of structural principal axis relative to shaft plane
θ_{tw}	total twist angle, rad
θ_v	vibratory part of the pitch angle, rad
Λ	angle of the relative wind to blade-span axis (yawed flow angle), rad
$\bar{\Lambda}$	Λ with vibratory velocity included, rad
λ	local flow ratio
λ	eigenvalue of the stability determinant
$\bar{\lambda}$	average inflow ratio
$\bar{\lambda}_i$	average induced velocity divided by the blade tip tangential speed
μ	advance ratio
$\bar{\mu}$	average advance ratio
ρ	mass density
σ	local blade stress, lb/in. ²

ϕ	Euler roll angle relating the fuselage body axis system to an inertial axis system, rad
ϕ_M	main (first) rotor lateral tilt angle, positive right, rad
ϕ_T	tail (second) rotor lateral tilt angle, positive right, rad
ϕ	fuselage Euler roll angle perturbation in the stability analysis, rad
ϕ	blade elastic twist angle, positive leading edge up
ϕ_A	inflow angle, rad
$\bar{\phi}_A$	inflow angle with blade vibration velocity included, rad
ϕ_0	initial value of the fuselage Euler roll angle in the stability analysis, rad
ϕ_{WP}	wake plane phase angle, deg
ϕ'	$90 - \phi_{WP}$, deg
ψ	Euler yaw angle relating the fuselage body axis system to an inertial axis system, rad
ψ	azimuth of blade-span axis, rad
ψ	fuselage Euler yaw angle perturbation in the stability analysis, rad
ψ_0	initial value of the fuselage Euler yaw angle in the stability analysis, rad
Ω	rotor angular velocity, rad/sec
$\bar{\Omega}$	angular velocity vector, used with several subscripts
Ω_k	response frequency used in computing the reduced frequency argument for the circulation function, rad/sec
ω	frequency of oscillation, rad/sec
∇	backward difference operator

- ∇^r operator indicating the r^{th} backward difference
- ' operator indicating derivatives with respect to radial distance, y
- operator indicating a vector variable

DEPARTMENT OF THE ARMY

Applied Technology Laboratory
U.S. Army Research and Technology
Laboratories (AVRADCOM)
DAVDL-ATL-TSD
Fort Eustis, Virginia 23604

OFFICIAL BUSINESS
PENALTY FOR PRIVATE USE, \$300

POSTAGE AND FEES PAID
DEPARTMENT OF THE ARMY
DOD-314



FOURTH CLASS